FATIGUE ENHANCEMENT OF UNDERSIZED, DRILLED CRACK-ARREST HOLES

BY

Gary G. Simmons

Submitted to the graduate degree program in Civil, Environmental, and Architectural Engineering and the Graduate Faculty of the University of Kansas in partial fulfillment of the requirements for the degree of Doctor of Philosophy

Chairperson Dr Caroline R. Bennett

Dr Stanley T. Rolfe

Dr Adolfo B. Matamoros

Dr Ron M. Barrett-Gonzalez

Dr William J. Hall

Date Defended: August 19, 2013

المنارة للاستشارات

www.manaraa.com

UMI Number: 3604779

All rights reserved

INFORMATION TO ALL USERS
The quality of this reproduction is dependent upon the quality of the copy submitted.

In the unlikely event that the author did not send a complete manuscript
and there are missing pages, these will be noted. Also, if material had to be removed,
a note will indicate the deletion.

UMI Dissertation Publishing

UMI 3604779

Published by ProQuest LLC (2013). Copyright in the Dissertation held by the Author.

Microform Edition © ProQuest LLC.
All rights reserved. This work is protected against
unauthorized copying under Title 17, United States Code

ProQuest LLC.
789 East Eisenhower Parkway
P.O. Box 1346
Ann Arbor, MI 48106 - 1346

المنارة للاستشارات

www.manaraa.com

The Dissertation Committee for Gary G. Simmons certifies that this is the approved version of the following dissertation:

FATIGUE ENHANCEMENT OF UNDERSIZED, DRILLED CRACK-ARREST HOLES

____

Chairperson: Dr. Caroline R. Bennett

Date approved: ______________

المنارة للاستشارات

www.manaraa.com

EXECUTIVE SUMMARY

Fatigue cracks occur in steel bridges from repeated loads. If allowed to continue to grow, eventually the fatigue cracks will require either expensive repairs or reduction of traffic loads on the bridge, or they may lead to the failure of the bridge. The exact number of bridges susceptible to fatigue cracking is difficult to evaluate, but the problem is widespread. In addition, many current repair options are expensive or marginally effective.

The objective of this research was to develop a new, cost-effective technique that can be used to arrest the growth of fatigue cracks before they develop to an extent that more expensive repairs are required. It is well known that drilling a hole (crack-stop hole) at each end of a fatigue crack can arrest the growth of the fatigue crack. The diameter of the hole required to arrest crack growth can be calculated from a formula developed by Rolfe and Barsom (1977) and by Fisher et al (1980, 1990). Unfortunately, the required diameter of the hole is usually so large that it is either impractical or does not fit in the space available.

This new technique consisted of cold-expanding a crack-arrest hole thereby cold-working the material around the hole and subjecting the cold-worked material to ultrasonic vibration. It was hypothesized that this process would increase fatigue crack initiation life three ways. First, the compressive force used to cold-expand the hole would result in residual compressive stress fields around the hole when the radial force was removed. Second, the cold-expansion would cause strain-hardening and cold-working with a concomitant increase in the yield and ultimate strengths of the steel. Third, the ultrasonic vibration from the PICK treatment would further increase the resistance to fatigue propagation by increasing the yield and ultimate strengths and

www.manaraa.com

increasing the radial extent of the residual compressive stress field. These expected results and their effects on fatigue crack initiation were investigated through a proof-of-concept testing program using reduced-scale, laboratory models and by mathematical modeling.

Fatigue testing was the primary method of demonstrating the effectiveness of this PICK treatment, but analytical techniques and other experimental techniques were used to investigate how the PICK process modified the material to enhance the effectiveness of the crack-arrest holes. The fatigue testing program demonstrated that the PICK process improved the fatigue initiation life of a small-scale, Gr. A36 steel specimen. The brittle coating showed that a plastic region was formed as a result of the PICK treatment. Metallurgical testing, i.e., grain size analysis, indicated that cold-working had modified the grain sizes of the steel in the cold-expanded specimens and in the PICK-treated specimens about the same. The increase in hardness between the cold-expanded specimens and the PICK treated specimens was the result of acoustic hardening. Although they proved to not be totally adequate, analyses using closed-form techniques by Nadai (1943) and Ball (1995) show that a compressive, residual stress field was imposed tangentially around the hole by cold-expansion. Neutron diffraction measurements of strain made evident that the PICK process produced a radial extent of the plastic strain and of the residual compressive stress which exceeded that predicted by the closed-form analyses.

This increase in the extent of the tangential compressive stress field resulting from the PICK process contributed to the increase in fatigue initiation life. While the cold-expansion increased fatigue initiation life by a factor of 1.8 over specimens not cold-expanded, the total effect of PICK treatment was to improve the fatigue initiation life by a factor of 2.6 over specimens not

المنارة للاستشارات
www.manaraa.com

cold-expanded. From these it is apparent that the PICK treatment was successful in providing a method of improving the capacity of crack-arrest holes to stop fatigue crack initiation in reduced-scale, laboratory models.

www.manaraa.com

ACKNOWLEDGMENTS

The successful completion of this research project was only possible with the assistance from numerous people, groups, and organizations. I am deeply indebted for their direction, advice, support and encouragement. Drs. Caroline R. Bennett, Adolfo B. Matamoros, Ron Barrett-Gonzales, Stanley T. Rolfe, and William J. Hall provided essential engineering direction, advice, and assistance. Jim Weaver, former Laboratory Supervisor, Department of Civil, Environmental, and Architectural Engineering, and Wes Ellison, Laboratory Director, Aerospace Engineering Department, provided much needed assistance in the experimental portions of the research. Brian Rice, Rice Precision Manufacturing, Inc. 401 E. High Street, Baldwin City, KS 66006 provided expertise and advice on fabricating the PICK tool and fatigue specimens. Clifford C. Biglow and Steve A. Sanders of Engineering Systems Inc. 923-A Terra Lane, O'Fallon, MO 63366 were particularly helpful with the metallurgical analysis and in explaining the results. Drs Camden R. Hubbard and Thomas R. Watkins of the Diffraction and Thermal Physical Properties Group, Oak Ridge National Laboratory, enthusiastically shared their expertise and guided me through the neutron diffraction and X-ray diffraction research on residual stress.

The author would like to gratefully acknowledge support from participants in Transportation Pooled Fund Study TPF-5 (189), which included the following Stat DOTs and entities: KS, CA, FHWA, IA, IL, LA, NJ, NY, OR, PA, TN, WA, WisDOT, and WY. As cosponsors of this work, these entities may claim exemptions for intellectual property royalties on US Pat. 8,343,294. The author is also grateful for support from the KU Transportation Research Institute, under Project TRI KAN42839.

www.manaraa.com

The author is also grateful for funding provided by the University of Kansas Transportation Research Institute (KU TRI) and to its Director, Dr. Robert B. Honea for his assistance in gaining access to Oak Ridge National Laboratory.

Research at the 2nd Generation Neutron Residual Stress Mapping Facility at the High Flux Isotope Reactor was partially sponsored by the U.S. Department of Energy, Office of Energy Efficiency and Renewable Energy, Vehicle Technologies Program, through the Oak Ridge National Laboratory's High Temperature Materials Laboratory User Program and by the Scientific User Facilities Division, Office of Basic Energy Sciences, U.S. Department of Energy.

www.manaraa.com

DISCLAIMER NOTICE:

This document was prepared by Gary G. Simmons as a result of the use of facilities of the U. S. Department of Energy (DOE) that are managed by UT-BATTELLE, LLC. Neither UT-BATTELLE, LLC, DOE or the U. S. government, nor any person acting on their behalf: (a) makes any warranty or representation, express or implied, with respect to the information contained in this document; or (b) assumes any liabilities with respect to the use of, or damages resulting from the use of, any information contained in the document.

المنارة للاستشارات
www.manaraa.com

TABLE OF CONTENTS

المنارة للاستشارات

www.manaraa.com

المنارة للاستشارات

www.manaraa.com

www.manaraa.com

المنارة للاستشارات

www.manaraa.com

CHAPTER 5: DEVELOPMENT OF A TECHNIQUE TO IMPROVE FATIGUE LIVES OF CRACK-ARREST HOLES IN STEEL BRIDGES – ANALYTICAL AND EXPERIMENTAL STRESS AND STRAIN

المنارة للاستشارات

www.manaraa.com

www.manaraa.com

CHAPTER 6: SUMMARY, CONCLUSIONS AND RECOMMENDATIONS

المنارة للاستشارات
www.manaraa.com

المنارة للاستشارات

www.manaraa.com

LIST OF FIGURES

CHAPTER 1: INTRODUCTION

www.manaraa.com

CHAPTER 2: SIZING CRACK-ARREST HOLES

المنارة للاستشارات
www.manaraa.com

www.manaraa.com

المنارة للاستشارات
www.manaraa.com

المنارة للاستشارات

www.manaraa.com

CHAPTER 5: DEVELOPMENT OF A TECHNIQUE TO IMPROVE FATIGUE LIVES OF CRACK-ARREST HOLES IN STEEL BRIDGES – ANALYTICAL AND EXPERIMENTAL STRESS AND STRAIN

المنارة للاستشارات

www.manaraa.com

المنارة للاستشارات

www.manaraa.com

LIST OF TABLES

CHAPTER 1: INTRODUCTION

CHAPTER 2: SIZING CRACK-ARREST HOLES

CHAPTER 3: DEVELOPMENT OF A TECHNIQUE TO IMPROVE FATIGUE LIVES OF CRACK-STOP HOLES IN STEEL BRIDGES

CHAPTER 4: DEVELOPMENT OF A TECHNIQUE TO IMPROVE FATIGUE LIVES OF CRACK-ARREST HOLES IN STEEL BRIDGES – FATIGUE AND METALLURGICAL RESULTS

المنارة للاستشارات
www.manaraa.com

CHAPTER 5: DEVELOPMENT OF A TECHNIQUE TO IMPROVE FATIGUE LIVES OF CRACK-ARREST HOLES IN STEEL BRIDGES – ANALYTICAL AND EXPERIMENTAL STRESS AND STRAIN

www.manaraa.com

LIST OF ACRONYMS

2D, 3D – two dimension(al) and three-dimension(al)

AASHTO – American Association of State Highway and Transportation Officials

ASTM – American Society for Testing Materials

Be – beryllium

CRFP – Carbon fiber reinforced polymer

DIFC - distortion-induced fatigue crack(ing)

ER – expansion ratio

FEA – Finite Element Analysis

FHWA – Federal Highway Administration

Gr.- Grade of steel

HIFR - High Flux Isotope Reactor

KDOT – Kansas Department of Transportation

NCHRP – National Cooperative Highway Research Program

ND – Neutron diffraction

NRSF2 - Second Generation Neutron Residual Stress Mapping Facility

ORNL- Oak Ridge National Laboratory

PICK – Piezoelectric Induced Compressive Kinetics

PICK-Piezoelectric Induced Compressive Kinetics

R – Stress Ratio

SEM – Scanning electron microscope

Si - silcon

R – Stress Ratio – the ratio of minimum stress to maximum stress, $\sigma_{min}/\sigma_{max}$

المنارة للاستشارات

www.manaraa.com

UTS – Universal testing machine

XRD –X-Ray diffraction

المنارة للاستشارات

www.manaraa.com

LIST OF SYMBOLS

ΔK – range of stress intensity

ρ – radius of crack-arrest hole

C – Constant for determining radius of crack-arrest hole

σ_{ys} – yield strength of material

$\Delta\sigma$ – stress range of the cyclical load

a – length of edge crack or half length of internal crack

D_f of D_o – initial or final diameter of cold-expanded hole

ε – strain

n – hardening exponent

H – strength coefficient

E – modulus of elasticity

β - Bauschinger parameter

λ = wavelength of X-ray beam

d_{hkl} = distance between hkl lattice planes inside the material

$2\theta_{hkl}$ = angle between the incident and the diffracted beams – Bragg's diffraction angle

κ - Electromechanical coupling coefficient for piezoelectric material

ζ - Piezoelectric transfer efficiency piezoelectric material

d33 - Activation constant for strain in the 3-direction for current in the 3-direction

YE33 - Short circuit Young's modulus of piezoelectric material piezoelectric material

ν - Poission's ratio

$\sigma 1$ and $\sigma 2$ are principle stresses in the plane of the surface

ϕ is the angle from a principle stress in the plane of the surface

المنارة للاستشارات
www.manaraa.com

ψ is the tilt angle of the X-ray tube of the neutron diffraction

www.manaraa.com

CHAPTER 1: INTRODUCTION

OBJECTIVE

Fatigue cracks occur in steel bridges from repeated loads. If allowed to continue to grow, eventually the fatigue cracks will require either expensive repairs or reduction of traffic loads on the bridge, or they may lead to the failure of the bridge. The exact number of bridges susceptible to fatigue cracking is difficult to evaluate, but the problem is widespread. In addition, many current repair options are expensive or marginally effective.

The objective of this research is to develop a new, cost-effective technique that can be used to arrest the growth of fatigue cracks before they develop to an extent that more expensive repairs are required. It is well known that drilling a hole (crack-stop hole) at each end of a fatigue crack can arrest the growth of the fatigue crack. Unfortunately, the required diameter of the hole is usually so large that it is either impractical or does not fit in the space available. This research has aimed to develop a new technique to treat the inside surface of the crack-stop hole so that a practical-sized hole can be drilled that will fit within the space limitations yet prevent crack re-initiation and thus stop further crack growth.

BACKGROUND

Fatigue Cracks in Bridges

The principal loads on bridges are dead loads from the self-weight of the bridge and live loads from vehicular traffic across the bridge. Depending on span length, the ratio of live to dead load can vary from approximately 1 to 3 with the lower ratio applying to bridges with spans greater than 100 ft (30.5m) and the higher ratio for bridges with spans less than 50 ft (15.25m) (McGuire1968). As the live loads are transient, live load stresses fluctuate with time. From

المنارة للاستشارات
www.manaraa.com

these live / dead load ratios, the time-varying live load stresses could approach 50-80% of the allowable stress in the steel. Such high fluctuating stresses may cause fatigue cracks to initiate in steel bridges if fatigue was not properly accounted for in the design of the bridge members, connections, and details.

Fatigue cracks, in fact, currently exist in numerous highway bridges in the United States. The Federal Highway Administration (FHWA) has governmental oversight responsibility for the maintenance of 592,000 bridges. Of this total, more than 120,000 are steel highway bridges with welded details. According to the 2001 National Bridge Inventory, more that 83,000 of the 592,000 (14%) are structurally deficient (FHWA 2001). Applying the 14% structurally deficient figure to 120,000 welded-steel highway bridges implies that approximately 16,800 welded-steel bridges in the United States are structurally deficient. The major problems causing the bridges to be labeled as structurally deficient are fatigue sensitive details, need to increase service loads, corrosion, and lack of proper maintenance (Tavakkolizadeh and Saadatmanesh 2003). Therefore, there is a significant need in the Nation's steel bridge infrastructure to address damage due to fatigue.

Several common steel bridge details have proven to be susceptible to fatigue cracking. A survey of 20 states and the Province of Ontario conducted between 1978 and 1981 collected information on fatigue cracking that had occurred in 142 bridges (Fisher 1984). From this data set, the location of the crack in the bridge and proximate cause of the cracking was tabulated. The details and/or causes of the fatigue cracking were grouped into categories; the top categories were distortion-induced fatigue, problems associated with sub-standard welds, and over-

المنارة للاستشارات
www.manaraa.com

constraint at connections of multiple members. The most common fatigue prone detail was distortion-induced fatigue in web gaps, with at least 60 of the 142 bridges (42%) developing fatigue cracks as a result of this detail. Given these percentages, the number of welded steel highway bridges with potential for fatigue cracking from distortion-induced fatigue cracking is quite significant.

Distortion-Induced Fatigue Cracking (DIFC)

DIFC is one of the most common conditions to produce fatigue cracks. To understand the extent of the problem of fatigue cracking in bridges, it is instructive to trace the history behind the engineering which lead to fatigue sensitive details that result in DIFC. Distortion-induced fatigue cracking occurs primarily in the webs of plate girders bridges as a result of significant secondary stresses under the application of cyclic traffic loads. For many years, normal practice was to not weld transverse and connection stiffeners to the flanges of web girders, instead, leaving a gap between the end of the connection stiffeners and the girder flanges. At connection stiffeners, transverse members or cross-frames connect adjacent girders, providing lateral bracing during erection and aiding in load distribution under traffic loads after the concrete deck is in place. However, girders are loaded differentially even under normal traffic loads due to non-symmetric traffic loads in adjacent traffic lanes. As a result of these non-symmetric loads, girders do not deflect together uniformly and the cross-frames induce moments in the girder about the longitudinal axis of the girder. Since the top of the flange of the girder is constrained by the bridge deck while the bottom flange is unrestrained, the bottom flange tends to move laterally, bending the cross-section about its longitudinal axis. Because the vertical connection stiffener stiffens the web and the deck restrains the top flange, the lateral force is resisted by bending induced in the girder web at the gap left between the flange(s) and the vertical stiffener.

المنارة للاستشارات
www.manaraa.com

This results in high secondary bending stresses in this web gap (Fig. 1). One measurement of these secondary bending stresses has estimated stresses of 35 ksi (241 MPa) in a bridge constructed with Gr. A36 steel (Anderson 2008). This stress of 35 ksi (241 MPa) was determined from strain gages placed on the bridge girder after the bridge had been in service for several years and was developed from a test truck traveling across the bridge. Therefore, the stress of 35 ksi (241 MPa) represents the total stress range. This magnitude of stress is consistent with results from finite element analyses (Zhao and Roddis 2007). Since this mode of deformation may occur with every non-symmetric traffic load, the resulting high loading cycles may cause fatigue cracks to develop and propagate in the web at the end of the connection plates and at the weld between the girder web and flange (Fig. 2). The cracks develop initially along the axis of the girder but often propagate into a "horseshoe" shape (Fig. 2).

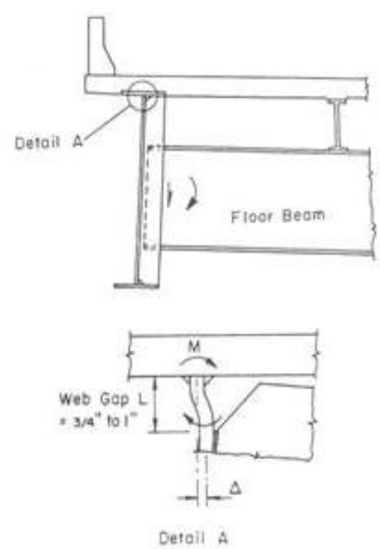

Figure 1 Distortion in the Web Gap (Fisher Et Al 1990)

المنارة للاستشارات
www.manaraa.com

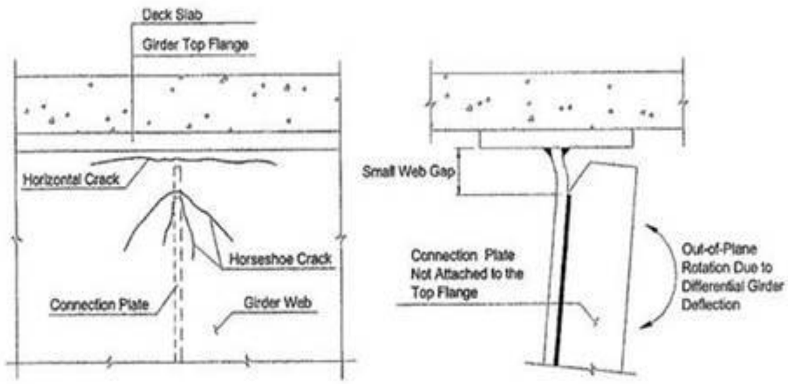

Figure 2 Typical Distortion-Induced Cracks in the Web Gap (Roddis And Zhao 2001)

History

Fisher and Keating (1989) state that the practice of not welding to the tension flange and leaving the gap between the connection stiffener and the tension flange was the result of bridge failures in Europe in the late 1930s; these failures occurred in some of the first all-welded steel bridges and the failures were partially attributed to transverse welds on the tension flanges. The reference list from Fisher and Keating's work (1989) cites the Hasselt Bridge. The Hasselt Bridge was one of approximately fifty Vierendeel truss bridges constructed across the Albert Canal in Belgium. A Vierendeel truss does not have diagonals like normal trusses but instead has stiff connections between vertical members and chords that enable it to carry loads as a rigid frame. The Vierendeel trusses in the Hasselt Bridge (Fig. 3) were shaped like a tied arch in that the top chords were in the shape an arch and the bottom chords were in tension and acted like tie members. Vertical hangers carried the load between the top and bottom chords. However, unlike a normal truss, where the verticals attach to the chords with pin connections, the cross sections of the vertical members flared at their ends to provide a smooth transition from the vertical members to the flanges of the horizontal members comprising the chords (Fig 4).

www.manaraa.com

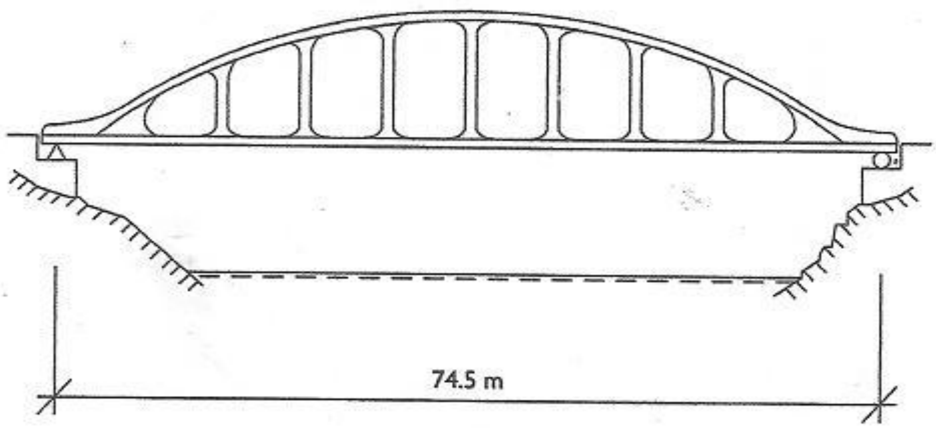

Figure 3. Hasselt Bridge in Profile (Akesson 2008)

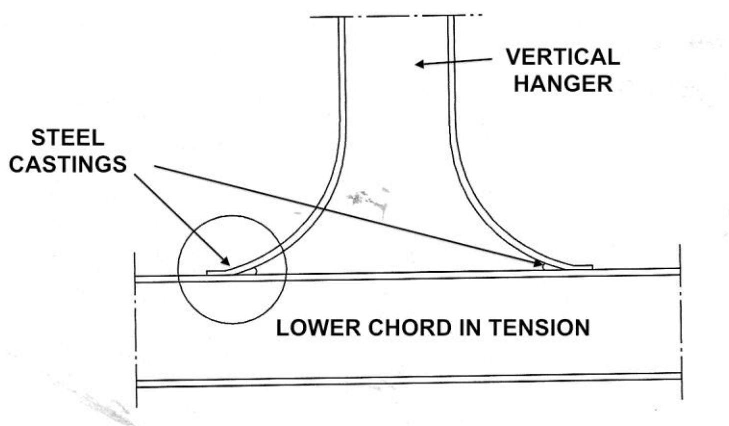

Figure 4. Flared End of Vertical Hangers at Connection to Lower Chord on Hasselt Bridge (Akesson 2008)

The Hasselt Bridge had a span of 75 m (245 ft), was designed for road and light rail traffic, was erected between 1935 and 1936, and was commissioned in January 1937 (Hayes 1996). The bridge failed at 8:20 am on March 14, 1938 (Maranian 2010). The temperature was –20 ^{o}C (-4 ^{o}F) and a tramcar and several pedestrians were on the bridge when a crack opened in the lower chord of the bridge. Then the third and forth verticals fractured and load was transferred to the top chord. The top chord held for approximately six minutes. Then the bridge (Fig. 5) broke into three pieces and fell into the canal (Maranian 2010) taking the tramcar and pedestrians with it. All the people survived (Hayes 1996). Since this was the first major failure of an all-welded

www.manaraa.com

steel structure, an extensive investigation was conducted.

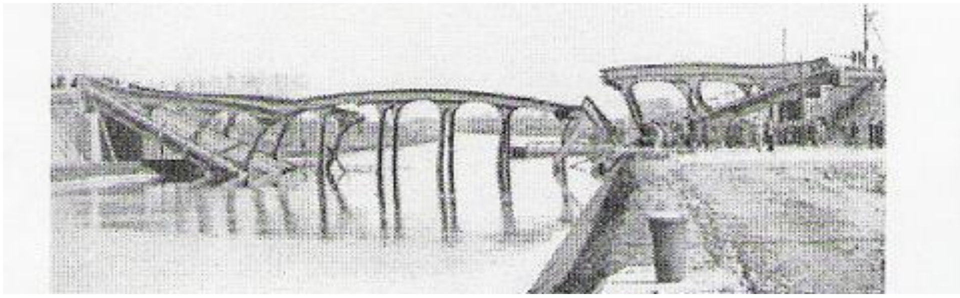

Figure 5. Collapse of the Hasselt Bridge (Kuhn 2008)

The initial crack started at a butt weld between a vertical and the lower chord (Fig 6). At the lower chord, the flared end of the vertical was welded to a steel casting that had been welded to the top flange of the horizontal tie beam to provide for smooth stress flow from the vertical hanger to the tie beam (Reeve 1940), as shown in Fig 6. This casting contained sulphur and phosphorus concentrations higher than the limits considered acceptable for welding (Reeve 1940). In addition, an examination of a similar butt weld showed lack of fusion at the bottom and the absence of a sealing pass (back weld) along the back of the weld (Reeve 1940). The lack of a back weld on the bottom side was probably the result of construction sequencing (Reeve 1940). In addition, Reeve (1940) found some indications that some of the welds might have been made using bare (unshielded) electrodes.

www.manaraa.com

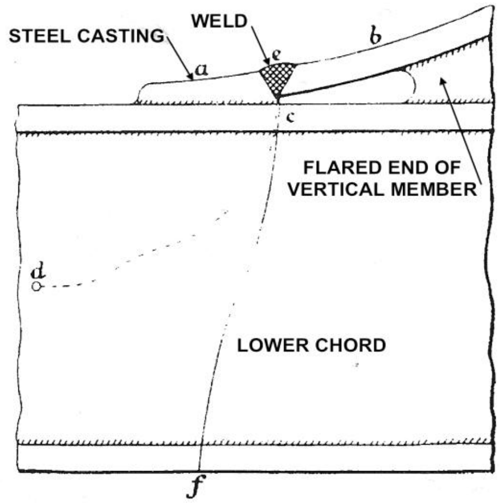

Figure 6. Details of Brittle Fracture at Hasselt Bridge (Hayes 1996)

Shortly after the failure of the Hasselt Bridge, two other Vierendeel truss bridges failed in Belgium in 1940. Both the Herentals-Oolen and the Kaulille bridges experienced extensive cracking but did not collapse (Akesson 2008). From the sketches available, some of the cracks in these bridges appeared in the same location as the crack which initiated the failure of the Hasselt Bridge (Akesson 2008). Two more welded-steel bridges in Berlin, Germany, failed: a welded I-beam railway viaduct and a continuous welded-steel road bridge. Both failed in wintertime by brittle fracture, but no details on these bridges are available. Details for the other bridges in Belgium and those in Germany were probably lost due to the beginning of World War II which started in early 1940.

Recommended Practices and Codes

As a result of the failure of the Hasselt Bridge, it became standard practice in the United States to not weld stiffeners to tension flanges of primary bridge members. A steel design text used at a major university in 1972 recommended leaving a gap between the connection stiffener and the tension flange of a girder with a height 4.3 times the web thickness (McGuire 1968); a steel

المنارة للاستشارات
www.manaraa.com

designer's handbook published in 1972 (Merritt 1972) contained the same recommended practice.

Roddis and Zhao (2001) presented a concise history of the detailing of the connection plates in the codes. According to Roddis and Zhao (2001), the 1981 Interim to the AASHTO Standard Specification for Highway Bridges stated that intermediate stiffeners:

> "when in pairs …fit tight to the compression flange" and "When used only one side of the web, … shall be fastened to the compression flange". "Transverse intermediate stiffeners need not be in bearing with the tension flange." (Roddis and Zhao 2001)

Since distortion-induced fatigue was not yet recognized as a problem in 1981, the Specification was interpreted as having the stiffener detail requirements apply to connection stiffeners. The 1982 Interim mentioned connection plates separately but only in connection with the compression flange. It stated that, *"consideration shall be given to the need for this attachment"* to the compression flange if a stiffener is used as a connection plate and *"will produce out of plane movements in a welded web to flange connection."* (Roddis and Zhao 2001) This seems to allow but not require attachment to the compression flange, and it is completely silent about an attachment to the tension flange. In 1983, the 13th edition of the AASHTO Standard Specification for Highway Bridges changed its format, addressing the stiffener-compression-flange detail in one section and the stiffener-tension-flange detail in another. The requirements for both were, however, unchanged from the 1982 Interim. The 1985 Interim was the first to require that "*Vertical connection plates… shall be rigidly connected to the top and bottom flanges*" (Roddis and Zhao 2001). As with all changes in the Specifications, it took several years

المنارة للاستشارات
www.manaraa.com

for these details to become accepted practice. For example, the Kansas Department of Transportation (KDOT) did not begin to weld or bolt connection plates to both top and bottom flanges of plate girders until 1989 (Roddis and Zhao 2001). In 1995, the connection stiffener detail was revised in the code to clearly state that a rigid connection was required to both top and bottom flanges for connection of diaphragms and cross-frames. (AASHTO 1995)

In summary, from 1940 until the late 1980s, welded steel bridges constructed in the United States were designed and constructed with connection and stiffener plates not connected to the tension flanges. This includes all the welded steel bridges in the extensive Interstate Highway System constructed from the 1950s into the 1980s. The result is that a large number of welded-steel bridges with fatigue prone details exist and may require some form of repair for fatigue cracking.

Current Solutions to Fatigue Cracking / DIFC

Once fatigue cracks occur, they must be repaired or at least prevented from growing; several different approaches have been used to repair fatigue cracking (Roddis and Zhao 2001). If the fatigue cracks need to be removed, repair options consist of replacing the affected member or re-welding the crack. Replacing a cracked member may be difficult as the bridge may have to be taken out of service, the bridge deck removed, the member replaced, and the deck reinstalled. This may be prohibitively expensive. Re-welding or filling the fatigue crack with weld material requires grinding out the crack and any associated welds, filling the crack with weld material, and grinding the new weld surfaces smooth. When doing this, it is essential that the crack tips are within the area included in the grinding and re-welding; if they inadvertently extend outside

المنارة للاستشارات
www.manaraa.com

this area, the crack may reinitiate. If access to the fatigue crack is limited or difficult, which is often the case, considerable effort may also be required to ensure adequate weld quality and a smooth surface finish. Also any surface irregularities in the finished weld may provide a location for future fatigue crack initiation and subsequent propagation.

If the decision is made to repair the crack in place without replacing the member or re-welding the crack, crack-stop holes can be drilled at both ends of the fatigue crack; this may prevent crack reinitiation and propagation. For locations where the cracking is caused by distortion-induced fatigue, stiffening the web gaps, softening the web gaps, removing or repositioning lateral bracing and diaphragms, or even loosening bolts at the cross frame to web connections have all been implemented to prevent continued crack growth – with varying outcomes in the various case studies. Another alternative is to install bolted connections between the connection stiffeners and adjacent flange.

Crack Stop Holes

Crack-stop holes are more easily drilled in locations where a crack is propagating in a plate girder not at a weld joint formed by the intersection of two members such as a web to flange joint; away from such joints the hole can be drilled perpendicular to a flat surface without intersecting or being tangent to another surface. Where the crack forms in a fillet weld, such as at a web to flange weld, drilling a hole will be difficult because of the interference formed by the two perpendicular surfaces, and the crack-stop hole may be ineffective. When or if the crack propagates away from the intersection of the two members into the underlying plate, the crack-stop hole is an attractive repair.

المنارة للاستشارات
www.manaraa.com

Crack Stop Hole Formulae

Drilling a hole at the tip of a fatigue crack increases the radius of the crack tip from infinitely small to the radius of the hole; this blunts the crack tip to an extent that crack growth may be stopped. There are two formulae in the literature that may be used to determine the radius required for the hole to effectively stop crack growth. Both formulae relate the radius of the hole to the yield strength of the steel, stress intensity factor range, and the half-length of the crack; but use different experimentally derived constants. The first is from Rolfe and Barsom (1977) and Barsom and Rolfe (1999) while the second is found in Fisher et al (1980), Fisher et al (1990), and Dexter (2004). Both formulae follow the general form first presented by Barsom and Rolfe (1977):

$$\frac{\Delta K}{\sqrt{\rho}} = C\sqrt{\sigma_{ys}}$$

Equation 1

Where:
C = constant developed from testing. Barsom and Rolfe (1977) recommend a value of 10 from their testing; while Fisher et al (1980) recommend a value of 4 from their work.

ρ = required radius of the crack stop hole (in).

σys = the yield strength of the steelksi)

ΔK = the range of the stress intensity factor for an infinite plate that contains an edge crack of a length a and that is subjected to fatigue loading of uniaxial, fluctuating tensile stresses. These conditions constitute a Mode I type fracture and, for Mode I,

$\Delta K = \Delta\sigma\sqrt{\pi a}$ ksi√in) where:

a = the length of the edge crack (in)

It is important to note that both equations are unit sensitive and, therefore, only US customary units are used in this section since both values of *C* were generated in US customary units.

المنارة للاستشارات
www.manaraa.com

When $\Delta K = \Delta\sigma\sqrt{\pi a}$ and the values for C are substituted into Eqn. 1, Eqn. 2a and 2b result:

$$\frac{\Delta\sigma\sqrt{\pi a}}{\sqrt{\rho}} = 10\sqrt{\sigma_{ys}}$$ Rolfe and Barsom (1977) Equation 2a

$$\frac{\Delta\sigma\sqrt{\pi a}}{\sqrt{\rho}} = 4\sqrt{\sigma_{ys}}$$ Fisher et al (1980) Equation 2b

The Eqn 2a was developed from cyclic tension loading of various notched plate specimens with different radii and with yield strengths varying between 36 and 110 ksi with stress ratios ($\sigma_{max}/\sigma_{min}$) of –1.0, 0.1, and 0.5. The specimens experienced Mode I failure.

The Eqn. 2b was developed from tests on rolled sections (Fisher et al 1980) and plate girders (Fisher et al 1990) both with in-plane and out-of-plane bending where out-of-plane bending was imposed on the section at cross frame connections to the side of the web to develop distortion-induced fatigue cracking. Tests were conducted on steels with 36-ksi-yield strength. After cracking developed, either a ¾-in. or a 1-in. diameter hole was drilled at the tip of the crack and testing continued until failure in Mode III shear or complex Mode III shear combined with beam bending. If failure did not occur within a reasonable time, the testing was terminated. The differences in the testing leading to the different constants '*C*' are summarized in Table 1.

المنارة للاستشارات
www.manaraa.com

Table 1 Comparison of the Parameters in the Development of the Crack-Arrest Hole Equations

	Equation 2a	Equation 2b
Yield strength of the steel	Measured yield strength between 36 and 110 ksi	Measured yield strength of 36 ksi
Loading	Tension	Both in-plane bending and out-of plane bending at cross-frame connections
ρ radius of crack stop hole	Constant radius; $\frac{\Delta K}{\sqrt{\rho}}$ varied by changing the tension stress	¾ -in and 1-in diameters
Section geometry	Wide plates	Rolled wide flanges and built-up plate girders
Failure Mode	Mode 1 (tension opening crack)	Mode III (shear in a plane perpendicular to the direction of crack growth) or Mode III combined with bending
Stress	Stress controlled by controlling the Stress Ratio (R) (σmin/σmax) with R varying between –1.0, 0.1, and 0.5 based on nominal stress away from the notch	Stress controlled at specified points developed from finite element analysis (FEA). Bending strain measured at tension flange and out-of-plane strain measured on the web at location selected from FEA
Resulting constant, C	10	4
Stress limits to equation	None as long as the equation is satisfied	<15 ksi from out-of-plane bending at the weld toe & <6 ksi in in-plane bending

Both Fisher et al (1980) and Rolfe and Barsom (1977) noted that, if a stop-crack-hole is used, it is important to identify the crack tip and locate the crack-stop hole such that the center of the hole is located at the tip of the hole. For typical crack sizes, hole diameters, and stresses, the hole diameter is significant with respect to the crack length and should be added to the crack length. If the holes are is located as shown in Figure 7 and if the hole diameter is included with the crack length, Eqn. 2a and 2b become:

www.manaraa.com

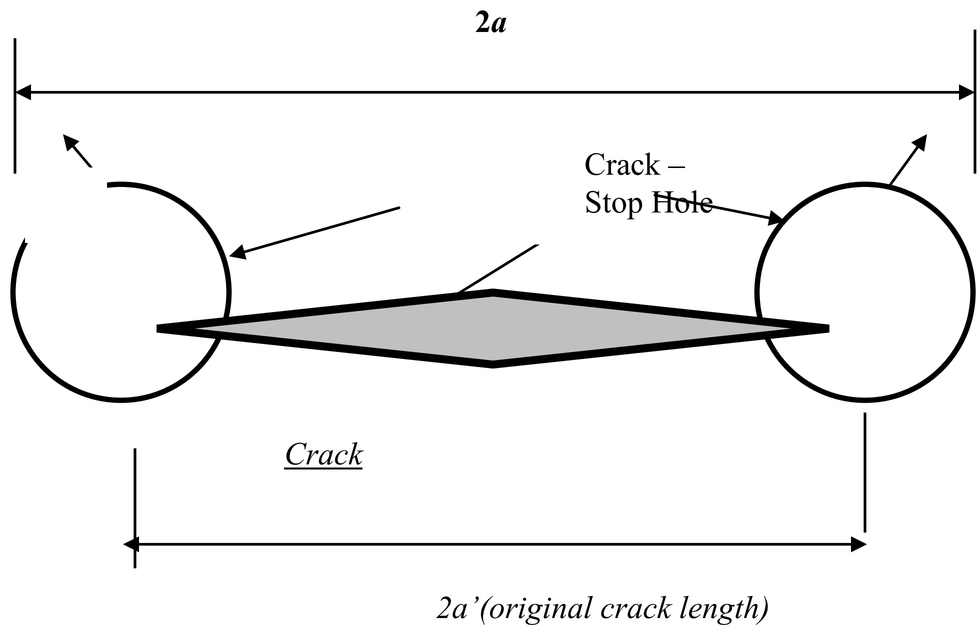

Figure 7. Recommended Location of Crack Stop Holes

$$\frac{\Delta\sigma\sqrt{\pi(a' + \rho)}}{\sqrt{\rho}} = C\sqrt{\sigma_{ys}}$$ Equation 3

re-arranged, Eqn. 3 may be re-written as:

$$\rho = \left(\frac{\Delta\sigma^2\pi}{C^2\sigma_{ys} - \Delta\sigma^2\pi}\right) * a'$$ Equation 4

Where C = either 10 or 4

A comparison of Eqn. 4 determined with two different values for the constant, C=10 and C=4, shows that C=4 requires a crack-stop hole radius significantly larger than Eqn. 4 with C=10. Using arbitrary but reasonable values for a bridge with a crack in the main girder ($2a'$ = 8 in., σ_y = 36 ksi, and $\Delta\sigma$ = 10 ksi), Eqn. 4 with C = 10 requires a hole diameter of approximately $^7/_8$ -in.

المنارة للاستشارات
www.manaraa.com

to halt crack propagation while Eqn. 4 with *C*=4 requires a diameter of approximately $9^{5}/_{8}$ -in. Depending on the location of the crack in the bridge, the larger hole may be noticeable and could cause consternation. Also, due to physical dimensional constraints and obstructions, it may not be possible to fit a hole of this size at the crack tips at each end of the crack.

Further comparison of the constants, *C*, may be made by plotting both values on the graph of experimental data from Fisher et al. (1989) as shown in Fig. 8. It appears that the original location on the graph for $4\sqrt{\sigma_y}$ may not be plotted correctly; therefore, the correct location of $4\sqrt{\sigma_y}$ as well as the location of $10\sqrt{\sigma_y}$ have been plotted as shown in Fig. 8. From the graph it appears that using *C*=10 is a reasonable average of the data, and *C*=4 is representative of a conservative lower bound.

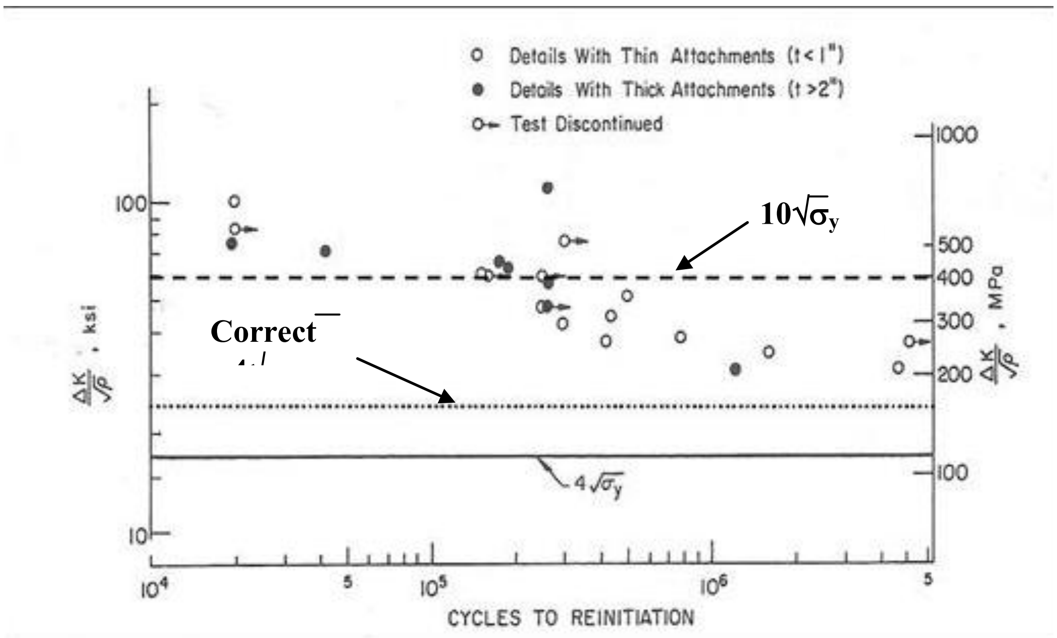

Figure 8. Development of Constant C for Crack Stop Hole Formula (Fisher 1980)

Typical practice seems to be to drill a reduced-size hole, with diameters from ¾-in to 1-in being

المنارة للاستشارات
www.manaraa.com

typical (Fig. 9). Unfortunately, when reduced-size holes are used, the fatigue crack eventually re-initiates and continues to propagate on the other side of the hole (Fig. 10).

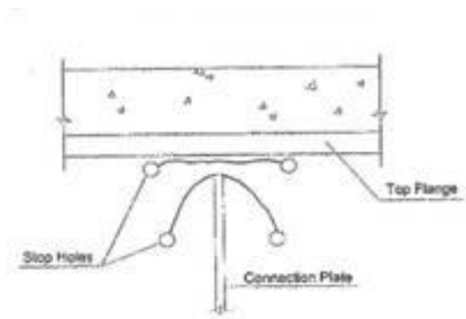

Figure 9. Crack-Stop Holes at Fatigue Cracks (Roddis and Zhao 2001)

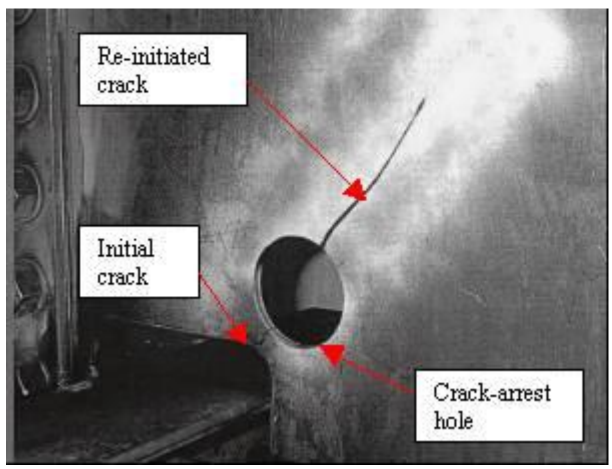

Figure 10. Fatigue Crack Re-Initiating through Stop Crack Hole (Dexter 2004)

Reinforcing Crack Stop Holes

If a reduced-diameter hole is drilled, two techniques have been developed in the aerospace industry which could be used to attempt to make an undersized hole perform in stopping crack growth as well as a full sized hole. These are mechanical expansion of the hole and installing over-sized bolts (i.e., bolt interference). The degree of mechanical expansion for both is reported in terms of the Expansion Ratio (E.R) or Retained Expansion. Both are calculated as in Eqn. 5:

www.manaraa.com

$$E.R. = \frac{D_f - D_o}{D_o} \% \qquad \text{Equation 5}$$

Where:
D_f = final diameter of cold-expanded hole
D_o = initial diameter

Mechanical expansion is a widely accepted technique to reinforce bolt and/or rivet holes in aluminum aircraft members both during manufacturing and maintenance to keep fatigue cracks from developing or to extend fatigue life in the presence of existing cracks. A literature review did not produce any example where mechanical expansion has been used outside the aircraft industry but, from a personal conversation with L. Reid of Fatigue Technology, mechanical expansion has recently been used on railroads and bridges (Reid 2011). This technique was expanded to railroads to improve the fatigue performance of the bolt holes in connections joining rail sections and has only been used on one bridge structure, an elevated section of a highway in California (Reid 2011). The Fatigue Technology mechanical expansion process utilizes a split-sleeve-mandrel system that consists of an oversized, solid, and tapered mandrel and an internally lubricated split sleeve (Figs. 11-14). The split sleeve is placed on the small end of the tapered mandrel and the mandrel-split sleeve placed in the in the hole with the large end of the mandrel going in first. An external force is then applied to the small end of the mandrel and the large end of the mandrel is pulled through the split sleeve causing the hole to expand by plastically deforming the inside of the hole in a radial direction. The sleeve is then withdrawn. This results in cold working the inside diameter of the hole and inducing a residual compressive stress field tangentially and radially around the hole; both of these act to retard crack initiation and crack propagation (Fig. 15).

المنارة للاستشارات
www.manaraa.com

Figure 11. **Cold Expansion Process. Pre-Lubricated Split Sleeve, Mandrel, and Hydraulic Puller (Fatigue Technology 2011)**

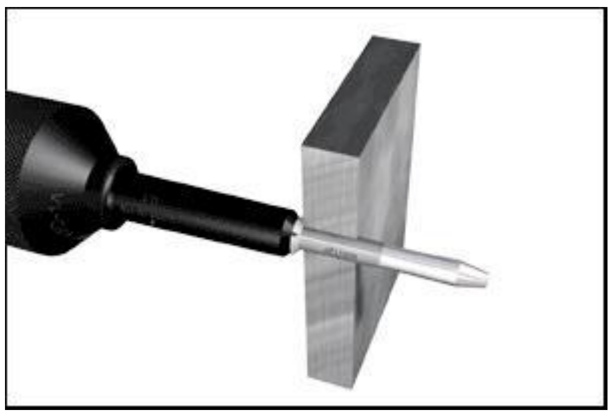

Figure 12. Cold Expansion Process. Mandrel and Sleeve Inserted in the Hole (Fatigue Technology 2011)

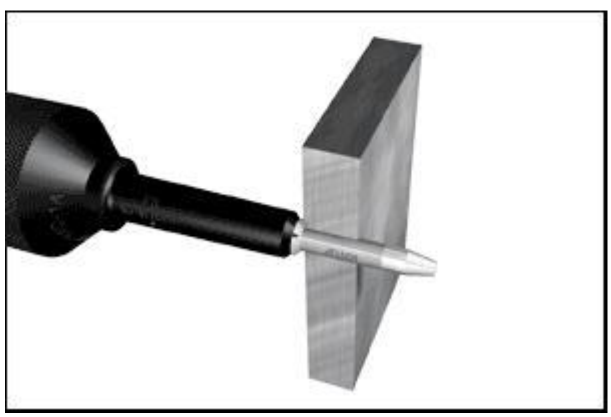

Figure 13. Cold Expansion Process. Mandrel Being Drawn through the Sleeve and the Hole (Fatigue Technology 2011)

www.manaraa.com

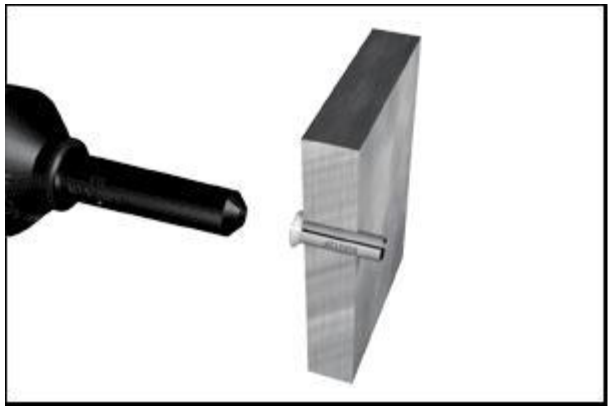

Figure 14. Cold Expansion Process. Remove and Discard Sleeve (Fatigue Technology 2011)

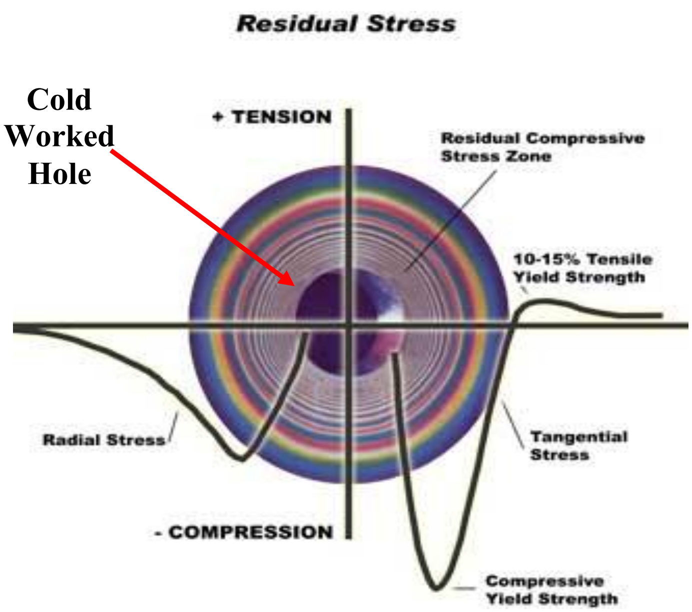

Figure 15. Residual Stress Field Resulting from Cold Expansion (Fatigue Technology 2011)

Interference fit fasteners are currently limited to the aircraft industry where they are used to improve fatigue performance of drilled holes; their use has not translated to bridges or other civil structures (Bontillo 2011). Interference-fit fasteners consist of a tapered bolt and an internally tapered and flanged outer-sleeve, which is ground straight externally for use in a straight-sided hole. The interference fit is achieved by tightening the bolt, forcing the taper of the bolt to work

المنارة للاستشارات
www.manaraa.com

against the taper of the sleeve (Fig. 16). Fatigue tests have shown an increase in fatigue life with Expansion Ratios of up to 2.5% with fatigue life being improved roughly by a factor of 10 (10^5 cycles to 10^6 cycles) (Lanciotti and Polese 2005). Above this interference level, further increases had little effect on fatigue resistance (Lanciotti and Polese 2005).

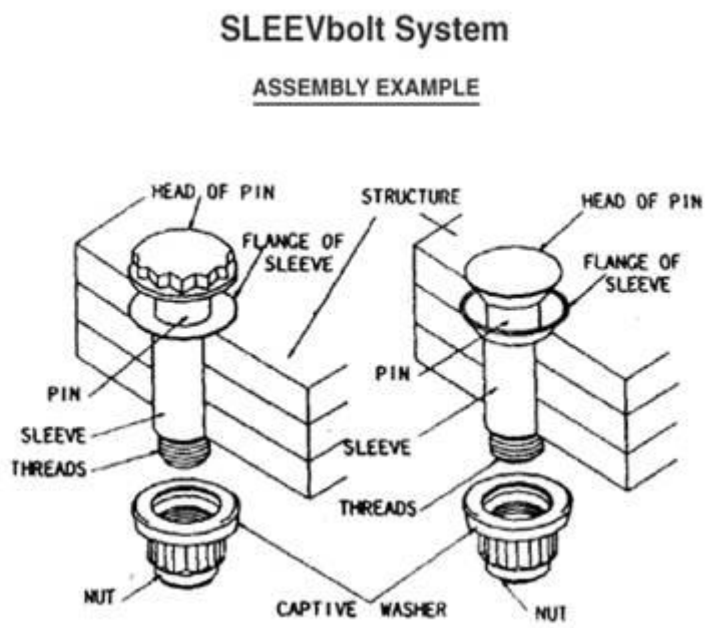

Figure 16. Interference Fit Fastener (PBFasteners 2011)

Strain Hardening, Cold Working, and Hardness Testing

If point σ_{ot} in Fig. 17 depicts the yield stress in tension, strain hardening occurs when stress exceeds σ_{ot}, with increasing deformations and stress. The stress – strain behavior beyond σ_{ot} may be non-linear and can be described with some type of power-law relationship, such as the Ramberg-Osgood equation (Eqn. 6) (Ramberg and Osgood 1943). The Ramberg-Osgood equation provides a single, continuous, and smooth curve that does not exhibit a distinct yield point. H and n are experimentally-derived constants unique to each material. H is similar to the

www.manaraa.com

strength coefficient and n to the strain-hardening exponent used in the normal power law (Dowling 2007).

$$\varepsilon = \frac{\sigma}{E} + \left(\frac{\sigma}{H}\right)^{\frac{1}{n}}$$

Equation 6

If stress is reduced after the onset of strain hardening at σ_{ot} (Fig. 17), the stress-strain relationship unloads with the same slope as the elastic portion of the stress-strain curve (Point B to Point C). If unloading does not progress beyond Point C to yielding in compression, reloading follows back along the same path as unloading until the previous high stress, Point B, is reached. Further loading beyond Point B continues with the same strain hardening behavior as previously. The stress at which strain hardening begins after unloading and reloading is approximately the same value which was reached before unloading occurred, Point B.

However, if stress in tension has exceeded the yield stress, σ_{ot}, and if the stress is reversed to an extent along b-c such that yielding occurs in compression at Point A, the yield stress in compression at Point A will be less than that produced from monotonic compressive loading, σ_{oc}. This effect, called the Bauschinger effect, occurs with subsequent reversals if the stress in a previous load step went beyond yield stress in the opposite direction. For example, yielding in tension will cause a lower yield stress in compression than if yielding in tension had not occurred. The opposite also holds, i.e. yielding in compression will result in a subsequent lower yield stress in tension. In summary, strain hardening extends the linear stress – strain range above yielding if any previous stress reversals have not progressed to yielding in the opposite sense; however, for cyclical loading yielding occurs before the yield strength is reached if

المنارة للاستشارات
www.manaraa.com

yielding in a previous load step occurred in the reverse direction.

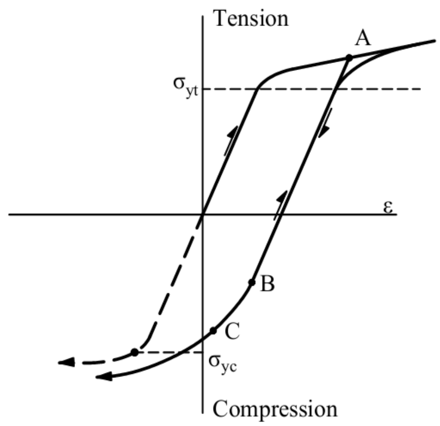

Figure 17. Stress / Strain with Strain Hardening and Bauschinger Effect (Dowling 2007)

Cold working is severe plastic deformation by a controlled mechanical operation (e.g. rolling or drawing) performed at ambient temperature for the purpose of shaping a product. Cold working reduces one or two dimensions of the object while increasing the other corresponding dimension(s). Cold working elongates the grains of the material in the direction of working, while flattening the grains perpendicular to the direction of working (Figs 17 and 18). Cold working may increase dislocation density, vacancies, stacking faults, and twin faults; most of the energy from cold working appear to be expended in increasing the dislocation density which is primarily responsible for the changes in material properties (Dieter 1989). An annealed metal has a density of dislocations of $10^6 – 10^8$ dislocations per cm^2 (Dieter 1989). After cold working with severe plastic deformation of ~10%, the dislocation density increases to 10^{12} dislocations/cm^2 (Dieter 1989). These dislocations form dense tangles concentrated at the grain walls resulting in cell-like structures with the tangles being the cell walls (Fig 18). The tangles act as obstacles to further slip along slip planes. The cold working with grain deformation and

www.manaraa.com

formation of dislocation tangles increases the yield stress, ultimate stress, and hardness while decreasing elongation and reduction in area (Dieter 1989), as depicted in Fig 19. Cold working also causes strain hardening.

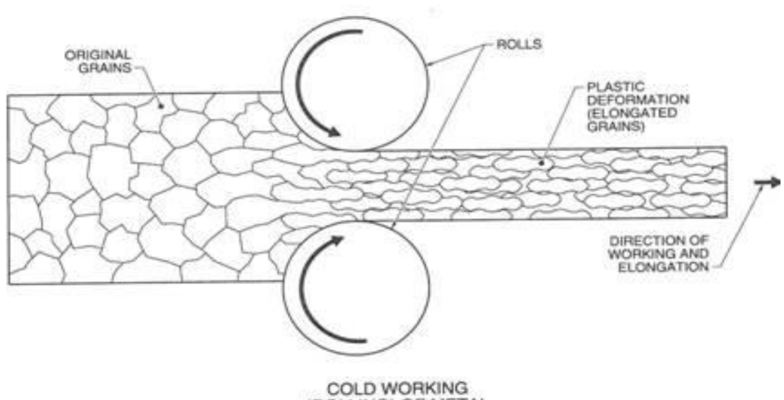

Figure 18. Cold working by Rolling (Moniz 1994)

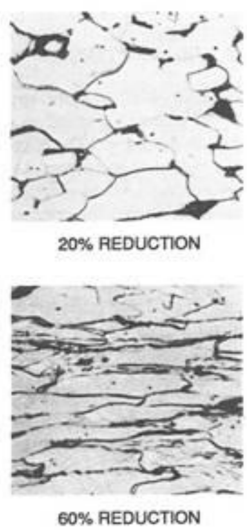

Figure 19. Cold working of Grains Showing Elongation in the Direction of Working (at 20% and 60% reduction in area) (Moniz 1994)

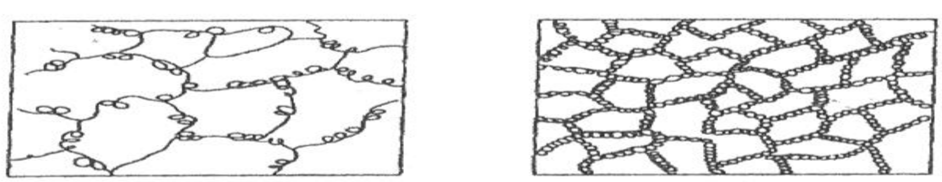

Figure 20. Cold Working with Dislocations Tangled into Cellular Structure. (a) deformed to 10% and (b) deformed to 50% (Dieter 1989)

www.manaraa.com

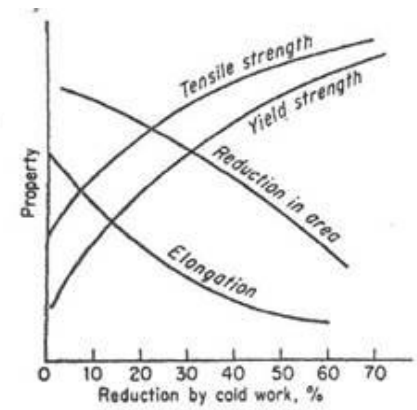

Figure 21. Variation of Tensile Properties with Amount of Cold working (Dieter 1989)

Hardness can be measured with an indenter; several types are available but all measure the depth and /or width of an indention with a ball-, pyramid-, or a diamond-shaped indenter into the surface of the metal object. The indenter only disturbs the top few grain layers but these indentations impose a triaxial state of stress and plastic deformation in the range of 30% or more strain (Richards 1961). Empirical relationships exist to relate the hardness values of the different indenters to each other (ASTM E140), and to the ultimate strength (F_u) of the metal (Moniz 1994). Because the indenter readings are related to plastic deformation of the material, the hardness readings can only be related to the ultimate strength; no empirical relationships exist between the indenter hardness values and the yield stress.

Piezoelectric Materials and the Effects of Ultrasonic Waves on Metals

Pierre and Jacques Curie first identified the direct piezoelectric effect in 1881 when they showed that a quartz crystal produced an electric current when subjected to a pressure. The converse piezoelectric effect, that a voltage applied to a quartz crystal would produce expansion in the crystal, was reported the next year. The effect can be introduced into certain other materials containing dipole elements by 'poling'. Poling consists of raising the material above the Curie

المنارة للاستشارات
www.manaraa.com

temperature, applying a strong electric field across it, and cooling the material below the Curie temperature while maintaining the electrical field. This process changes the dipoles which are arrayed in a random direction before poling and fixes them so that they are aligned in the direction of the electrical field. After poling, if an external circuit is connected to electrodes on the surfaces of the piezoelectric material in the poling direction and if pressure is applied, a proportional transient electric current flows in the circuit while the pressure is changing (direct effect). If an external electric field is applied to the circuit, proportional strain occurs (converse effect). The poling can be eliminated by raising the temperature above the Curie temperature without the presence of an electric current or by applying high pressures. In addition, the piezoelectric effect decays over time, usually in terms of decades. Hard piezoelectric materials have Curie temperatures above 300 ^{o}C and soft piezoelectric material have a Curie temperature below 200 ^{0}C and are readily depoled at room temperature with a strong electric field (Srinivasan and McFarland 2001).

Blaha and Langenecker (1955) reported the first results of imposing ultrasonic vibration on metals when they ultrasonically vibrated zinc crystals while the zinc crystals were being tested in tension. Langenecker (1966) reported that ultrasonic waves can both soften and harden metals. At energy levels below 5 W/cm^2, acoustic softening occurred when zinc crystals were subjected to ultrasonic irradiation during static tension testing conducted under displacement control. The static stress required to continue straining dropped abruptly when the ultrasound radiation was switched on and returned to the original elastic stress-strain curve when it was turned off. See *a – a'* in Fig. 20. At energy levels between 15 W/cm^2 to 25 W/cm^2, the softening occurred during irradiation but, when it was turned off, acoustic hardening occurred, i.e. the stress to produce

www.manaraa.com

additional strain rose above the original elastic stress-strain curve, as shown with *b –b'* and *c – c'* in Fig. 20. Above 25 W/cm^2 plastic deformation occurred in the zinc. Langenecker (1966) hypothesized that the ultrasonic waves increased dislocation density and that the dislocations migrated to form sub-boundaries composed of dislocation networks. The softening occurred during application of the ultrasound which unlocked dislocation pile-ups; when the ultrasonic radiation is removed, an increased number of dislocations are fixed in locations that require higher stresses to produce additional slip. This resulted in hardening in the metal.

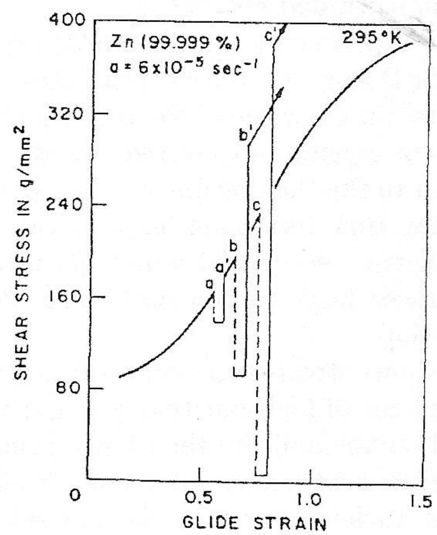

Figure 22. Acoustic Softening and Hardening in Zinc Crystals Under Deformation Control (Langenecker 1966). Dotted lines show were ultrasonic vibration was applied

Nevill and Brotzen (1957) subjected low-carbon steel to ultrasonic vibration while testing the steel in tension. They used annealed, 20-gage (.035-in.) (0.889-mm) wire in a small tension-testing machine under displacement control. The wire was tensioned and ultrasonic vibration applied in short intervals along the axis of the wire. The effect of the frequency was investigated by changing the length of the wire until standing waves were obtained over the range of frequencies being used. Nevill and Brotzen (1957) reported that the stress necessary to initiate plastic deformation was reduced by the introduction of the ultrasonic vibration. The reduction in

المنارة للاستشارات
www.manaraa.com

stress was proportional the amplitude of the vibration, but independent of frequency within the range of 15 kHz to 80 kHz, of temperature between 30 ^{0}C and 500^{0}C, and of prior strain for values of average permanent elongation of up to 15%. See Fig. 21 and Fig. 22.

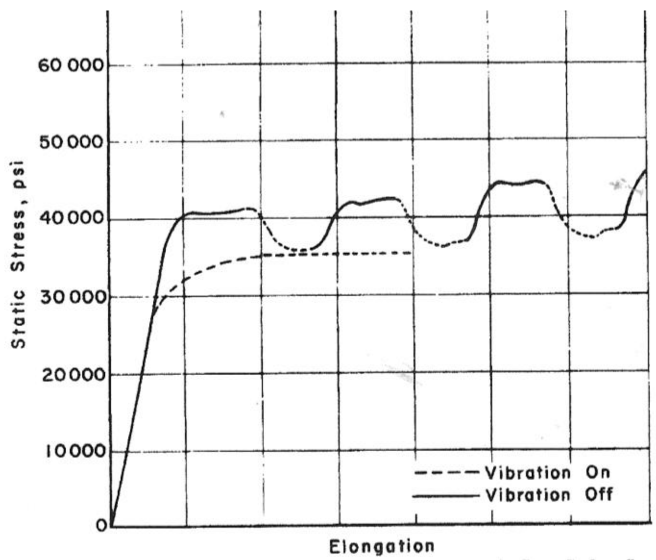

Figure 23. Effect of Ultrasonic Vibration on Static Yield Stress of Low-Carbon Steel (Nevill and Brotzen 1957)

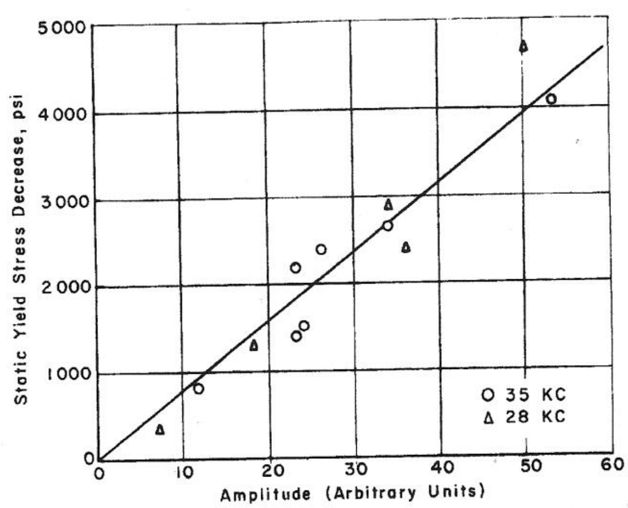

Figure 24. Effect of Amplitude of Vibration on Static Yield Stress of Low-Carbon Steel at Room Temperature (Nevill and Brotzen 1957)

www.manaraa.com

Residual Stress and Strain around Cold-Expanded Holes

A substantial body of work exists on determining the stress / strain relationship resulting from cold-expanding bolt and rivet holes in aluminum members in aircraft and the residual stress / strain remaining at the end of cold working. These papers can be classified into those providing results from analytical, numerical, and experimental techniques. The analytical techniques report development of closed-form solutions that provide acceptable results with low computational effort and are amenable to parametric studies. The closed-form solutions were developed over time from the formulae for thick shells with different analysts using different yield criteria (i.e., Tresca or von Mises), different stress-state assumptions (i.e., plane stress or plane strain), different material models (varying between elastic-perfectly plastic to elastic, nonlinear strain-hardening), and different unloading models (from elastic to elastic with non-linear reverse yielding). Numerical techniques, primarily finite element analysis (FEA), are efficient for determining residual stresses after cold working, modeling nonlinear material behavior, and accommodating large deflections. However, each FEA is limited to a unique geometric configuration and material model, and any change in initial geometry or material model requires a new FEA. In addition, a sophisticated FEA program is required for the problem of coldworking around a hole producing residual stress. Several experimental techniques have been attempted in previous studies (Arora et al. 1992, Polosook and Sharp 1978, Sharp 1978, Gracia-Granda 2001, Rowlands 1993, Ozdemir and Edwards 2004, and Cheng et al 2003) to measure the strain in both circumferential and radial directions around the hole during and after coldworking. Ball and Lowery (1998) provide a summary and evaluation of the all these different experimentally techniques. Because of the small dimensions, high strain gradients, and large strain magnitudes involved, measuring the strains is a difficult task and requires skill,

المنارة للاستشارات
www.manaraa.com

patience, and, sometimes, sophisticated equipment for success.

Nadai (1943) reported the first analytical work concerning coldworking around a hole. He was concerned with copper boiler tubing, which was fitted into holes in steel drums or steel head plates in industrial water heaters, steam boilers, and turbine condensers. These connections had to remain tight under high pressure and high temperatures; consequentially, high pressures need to be developed between the copper tubing and the steel boiler head / plate. Tight fit was achieved by revolving hardened rollers around a tapered pin such that the tube material and the steel in the drums or headers were deformed into the plastic range in both the radial and circumferential directions. When the expanding operation was completed and the rollers removed, residual stresses remained (compressive in both the circumferential and the radial direction) which kept the joint tight. Nadai (1943) assumed an elastic-perfectly plastic stress-strain relationship for the steel and both elastic–perfectly plastic and elastic with a strain-hardening component for the tube material. His equations for the tubes and holes in the plates were further developments of his previous work solving for stresses and deflections in thick tubes but, with the plane stress assumptions, were also applicable to this instance (Nadai 1931, Nadai 1943 and Nadai 1950).

Later analytical work was primarily undertaken to understand the residual stress around cold worked holes in aluminum for the aerospace industry. Hsu and Forman (1975) extended the work from Nadai (1943) using a modified Ramberg-Osgood (1943) type strain-hardening model but still used elastic unloading. Rich and Impellizzeri (1977) used formulas for thick tubes from Hoffman and Sachs (1953) and developed different formulas using plane strain assumptions. On

المنارة للاستشارات
www.manaraa.com

unloading, they also allowed the material to yield in compression near the edge of the hole to comply with the von Mises yield criteria. Guo (1993) extended the Hsu and Forman (1975) analysis by including kinematic hardening (Bauschinger effect) and by investigating the effect of a finite thin plate; however, he provided only a minimal explanation on how to determine residual stress. Ball (1995) also extended the Hsu and Forman (1975) analysis by including elastic – plastic unloading but provided an explicit solution for elastic, nonlinear-plastic unloading for residual stress that provided for a zone of reverse yielding in compression near the hole edge. Zhang et al. (2005) used Ball's (1995) approach but developed the solution for a finite-sized plate with appropriate boundary conditions. Wang and Zhang (2003) compared the results of the most promising of these closed-form solutions with accepted tangential and radial stress profiles and found that they provided adequate results when using an appropriate strain hardening exponent, n, and Bauschinger parameters, β. Table 2 presents a summary of these different analyses.

المنارة للاستشارات
www.manaraa.com

Table 2 Comparison of Assumptions for Various Closed-Form Analytical Methods

	Material	Plate Size	Stress State	Failure Criterion	Stress - Strain Curve for Loading	Stress – Strain Curve for Unloading	Compressive Yielding on Unloading
Nadai	Steel	Thin Infinite	Plane Stress	von Mises	Elastic – Perfectly plastic	Elastic	No
Hsu-Forman	Aluminum	Thin Infinite	Plane Stress	von Mises	Modified Ramberg-Osgood	Elastic	No
Rich / Impellizzeri	Aluminum	Thick Finite	Plane Strain	von Mises	Elastic - Perfectly Plastic	Elastic with approximation for reverse yielding	Yes
Guo	Aluminum and high strength steel	Thin Finite	Plane Stress	von Mises	Modified Ramberg-Osgood	Elastic non-linear strain hardening with Bauschinger parameter	Yes
Ball	Aluminum	Thin Infinite	Plane Stress	von Mises	Modified Ramberg-Osgood	Elastic non-linear strain hardening with Bauschinger parameter	Yes
Zhang	Medium Carbon Steel	Thin Finite	Plane Stress	von Mises	Modified Ramberg-Osgood	Elastic non-linear strain hardening with Bauschinger parameter	Yes

Various papers report the details of FEA of cold expanded holes (Forgues et al. 1993; Poussard et al. 1994; Poussard et al. 1995; Zhang et al. 2005; and Nigrelli and Pasta 2008). The FEA models in these analyses consisted of 2D, 3D, or axisymmetric models, with axisymmetric and 2D being the predominate approaches. The material properties were input mostly as the actual stress-strain curves developed from unixial tension testing. One paper (Nigrelli and Pasta 2008) used a power hardening law. The effects of plane stress and plane strain assumptions were both investigated by using different element formulations. For example, Zhang et al. (2005) used 8-node, biquadratic plane stress quadrilaterals and 8-node, biquadratic plane strain quadrilaterals to investigate the differences between plane stress and plane strain assumptions. The von Mises yield criteria was invoked to determine yielding. Tension stress into the plastic range coupled with unloading and compressive residual stresses approaching compressive yielding were

المنارة للاستشارات
www.manaraa.com

modeled with both isotropic (no Bauschinger effect) and kinematic behavior (full Bauschinger effect). A Bauschinger parameter, β, was used to investigate the effects of isotropic and kinematic models on reverse yielding and behavior varying between isotropic and kinematic. $\beta = 0$ simulates isotropic behavior, $\beta = 1$ produces kinematic hardening, and $0 < \beta < 1$ provides for a mixed-mode type hardening model with a partial Bauschinger effect. The models were typically loaded with a specified displacement imposed in steps on the hole wall. Results from the FEA were compared with other papers which used the finite element method, and with papers using closed-form solutions. Both the closed-form solutions and the finite element analyses produced similar results when the same assumptions were used in the modeling as used in the closed-form approaches (Zhang et al 2005). There does not appear to be a significant advantage between either of the approaches, closed-form or FEA, with respect to accuracy when the appropriate assumptions are used.

Accurate experimental determination of strain around a cold-expanded hole requires precise measurements to obtain reliable results. Several techniques have been tried with reported success but each has some limitations. These included using strain gages, Sach's boring method, x-ray diffraction, neutron diffraction, and imposing a microgrid around the cold worked hole.

Arora et al. (1992) and Polosook and Sharp (1978) both used strain gages to determine the boundary between the plastic region and the elastic region of a cold worked hole. Arora et al. (1992) placed 12 gages in a spiral pattern around the hole with gages spaced from 1.5 mm (0.059 in) to 14.0 mm (0.551 in) and measured the strain both before and after coldworking.

المنارة للاستشارات
www.manaraa.com

Sharp (1978) used a Vickers hardness tester to place a microgrid around a hole before cold working. The Vickers hardness tester was used to form pyramidal indentions approximately 10μm (0.00039 in) square and in a pattern at 200 μm (0.00787 in) spacing. The distance between the indentations was measured both before and after cold working, and could be measured to within 0.1μm (0.000004 in) allowing for accurate measurement of strain greater than 2%. Sharp (1978) reported that this was a "tedious but reliable technique."

Sach's boring method was developed to determine axisymmetric residual stresses in autofrettaged tubes (Gracia-Granda 2001), where autofrettage describes a process where an outer thick tube is heated, in inner thick tube inserted, and the outer tube allowed to cool. The inner tube has an outer diameter slightly greater than the inner diameter of the outer tube, and after cooling compressive residual stresses exist in the inner tube and tensile residual stresses remain in the outer tube. It can be adapted to coldworked holes by machining the specimen after cold working into a disk with the hole at the center of the disk. The interior residual compressive stress in the tangential direction is balanced by tension stress in the tangential direction on the outer edge of the disk. Strain gages are placed on the edge of the disk at specific angles around the disk with the vertices of the angles being at the center of the disk. These gages are used to measure tangential strain around the circumference of the disk. The inner hole is then bored out in small increments (0.06 mm) (0.00236 in) and the change in tangential strain in the strain gages on the outer edge of the disk is measured after each boring increment. Gracia-Granda (2001) developed the use of a Fourier expansion to project the strain between values at the end of each boring increments and back to the hole edge.

المنارة للاستشارات
www.manaraa.com

X-ray diffraction is an experimental technique for determining surface strains in the plane of the surface; it assumes a plane stress condition with the stresses perpendicular to the surface either constant or zero. X-rays are part of the electromagnetic spectrum and exhibit interference, reflection, and diffraction. Their short wavelength enables them to penetrate metals which reflect visible light. Strain is determined from measuring inter-atomic spacing and changes in this spacing using certain lattice planes as the gage length. Bragg's Law relates the angle of diffraction to the length of the lattice planes. Changes in the length of the lattice planes change the angle of diffraction. Strain is determined by impinging x-rays on the surface and measuring the intensity of the diffracted x-rays at different angles. Penetration can be 30-40 μm (0.00118 in - 0.00157 in) and stress can be determine within 3-5 ksi (20.7 MPa - 34.48 MPa) compared to ~2 ksi (13.79 MPa) for strain gages on metal (Rowlands 1993). If strain at greater depth is required, the surface layers must be removed without inducing residual strain with the removal process. One problem with X-ray diffraction is that all residual stresses from manufacturing processes such as rolling or forming must be removed in such a manner that does not itself induce residual surface stresses.

Neutron diffraction is analogous to X-ray diffraction in that neutrons bombard the material and are scattered from lattice planes in the crystal. The diffracted beam is collected and peak intensities occur when Bragg's law relating the length of the lattice planes and the angle of diffraction is satisfied. Changes in the length of the lattice plane change the angle of diffraction and the residual strain is determined by comparing the length of the undeformed lattice with the deformed lattice. Neutron diffraction is a volumetric measurement with the strain averaged within a cube, whose dimensions can be as small as 0.5 x 0.5 x 1.0 mm (0.0197 x 0.197 x 0.0394

المنارة للاستشارات
www.manaraa.com

in) in steel (Cheng et al 2003). Due to the greater penetrating power of the neutrons, neutron diffraction can measure strain to a depth of 50 mm (1.97 in). Discrete strains in a specified direction can be measured along a line with spacing so close as to make the measurements almost continuous. By using different orientations of the specimen, strains in all three orthogonal directions can be obtained. Unlike X-ray diffraction, surface preparation to eliminate surface residual stresses is not required.

SCOPE OF PROPOSED RESEARCH

The scope of this research is to develop a new technique to cold expand and work harden the inside surface of an undersized hole and to treat the work hardened surface with ultrasonic waves. Further, this research will investigate whether this treated, undersized hole will provide longer fatigue initiation life than an untreated hole. The smaller size of the hole will permit the hole to be drilled in areas with limited access and will minimize concerns about removing excessive material from a structural member. In addition, it is expected that application of this procedure will be less expensive than current repair methods.

1. The technique to work harden and treat the undersized hole is termed Piezoelectric Induced Compressive Kinetics (PICK) and will consist in general of:

2. Drilling a hole in a fatigue specimen made from steel plate,

3. Driving a slightly oversized aluminum plug into the hole,

4. Loading the plug in compression into the plastic range of the aluminum plug causing plastic deformation in the steel plate,

المنارة للاستشارات
www.manaraa.com

5. Using multiple piezoelectric elements to further load and deform the plug while subjecting the steel around the hole to ultrasonic vibration,

6. Removing the plug, and

7. Testing to evaluate the results of the PICK treatment.

It is hypothesized that this process will produce three separate results; all of which will act to prevent crack initiation. First, the compression force on the plug during cold expansion will introduce tensile stresses in the circumferential direction around the hole in the steel plate; these tensile stresses will become compressive residual stresses when the plug is removed. Secondly, due to cold expansion and the repeated loading by the piezoelectric actuators, Cold working will increase the tensile yield and ultimate strength of the steel. Thirdly, energy input from the piezoelectric actuators will increase dislocation density which will further increase the yield strength and the ultimate strength. These expected results and their affects on fatigue crack initiation will be investigated with laboratory testing and mathematical modeling.

REFERENCES

1. Akesson, Bjorn (2008). Understanding Bridge Collapses. Taylor & Francis Group, London, England

2. American Association of State Highway and Transportation Officials (AASHTO), (1995) "Standard Specification for Highway Bridges". 16th Edition, Washington, D.C.

3. American Association of State Highway and Transportation Officials (AASHTO), (1983) "Standard Specification for Highway Bridges". 13th Edition, Washington, D.C.

4. Anderson, Benjamin, Rolfe, S. T., Matamoros, A. B., Bennett, C., and Bonetti, S. (2008). Post-Retrofit Analysis of the Tuttle Creek Bridge (Bridge NO 16-81-2.24). Report No. K-TRAN: KU-06-2, Final Report.

المنارة للاستشارات
www.manaraa.com

5. Arora, P. R, Dattagaguru, B., and Subramanya Hande, H. S., (1992) "A Method of Estimation of the Radius of Elastic-Plastic Boundary Around Cold-Worked Holes" Journal of Testing and Evaluation vol 20, no. 5 Sept 1992.

6. ASTM E140 - 07 (2007)"Standard Hardness Conversion Tables for Metals Relationship Among Brinell Hardness, Vickers Hardness, Rockwell Hardness, Superficial Hardness, Knoop Hardness, and Scleroscope Hardness" American Society for Testing and Materials, West Conshohocken, Pa.

7. Ball, D. L. (1995) "Elastic-Plastic Stress Analysis of Cold Expanded Fastener Holes", Fatigue and Fracture of Engineering Materials and Structures, vol 18, issue 1.

8. Ball, D. L. and Lowry, D. R. (1998). "Experimental Investigation on the Effects of Cold Expansion of Fastener Holes". Fatigue and Fracture of Engineering Materials and Structures, vol 12, pp 17-33.

9. Barsom, John M. and Rolfe, S. T. (1999). Fracture and Fatigue Control in Structures: Applications of Fracture Mechanics. Third Edition. American Society for Testing and Materials, West Conshohocken, Pa.

10. Blaha, F. and Langenecker, B. (1955). "Tensile Deformation of Zinc Crystals Under Ultrasonic Vibration", Naturwissenschaften vol 42, p. 556.

11. Bontillo, Robert, PBFasteners, personal communications, 2011.

12. Cheng, Xiaohua, Fisher, John W., Prask, Henry J., Gnaupel-Herold, Thomas, Yen, Ben T., and Roy, Saugata (2003) "Residual stress modification of post-weld treatment and its beneficial effect on fatigue strength of welded structures" International Journal of Fatigue 25.

13. Dexter, Robert J. (2004). "Signs, Signals, Light Support Structures and Manual for Repair of Fatigue and Fracture" Third Annual Bridge Workshop: Fatigue and Fracture. Available on the Internet.

14. Dieter, George (1989), Mechanical Metallurgy, McGraw-Hill, New York, New York

15. Dowling, Norman E. (2007). Mechanical Behavior of Materials, 3rd edition, Pearson / Prentice Hall, New Jersey.

16. Fatigue Technology (2011). "Split Sleeve Cold Expansion", Fatigue Technology, <www.fatiguetech.com> (Feb. 27, 2011).

17. Federal Highway Administration (FHWA) Bridge Program Group. (2001). "Count of deficient bridges by state non federal-aid highway." (http://www.fhwa.dot.gov/bridges/britab.htm) (March 20,2002) The Office of Bridge Technology, Washington, D.C.

المنارة للاستشارات

www.manaraa.com

18. Federal Highway Administration (FWHA) Bridge Program Group. (2001). Count of deficient bridges by state non-federal aid highway http://www.fhwa.dot.gov./bridges/britab/.htm (March 20,2002). The Office of Bridge Technology, Washington, D. C.

19. Fisher, John (1984). Fatigue and Fracture in Steel Bridges. John Wiley and Sons, New York.

20. Fisher, John W. and Keating, P. B. (1989). "Distortion-Induced Fatigue Cracking of Bridge Details in Web Gaps". Journal of Construction Steel Research, 12.

21. Fisher, John W., Barthelemy, B. M., Mertz, D. R., and Edinger, J. A. (1980). "Fatigue Behavior of Full-Scale Welded Bridge Attachments". National Cooperative Highway Research Program (NCHRP) Report 227, National Transportation Research Board, Washington, D. C.

22. Fisher, John W., Jin, Jain, Wagner, David C., and Yen, Ben T. (1990). "Distortion-Induced Fatigue Cracking in Steel Bridges". National Cooperative Highway Research Program (NCHRP) Report 336, National Transportation Research Board, Washington, D. C.

23. Forgues, S. A., Bernard, M., and Bui-Quoc, T. (1993) "3-d axisymmetric numerical analysis and experimental study of the fastener hole coldworking process" Transactions of Engineering Sciences vol 2 WIT Press.

24. Garcia-Granda, A. A., Lacarac, V. D., Smith, D. J., and Parier, M. J., (2001) "A new procedure based on Sachs' boring method for measuring non-axisymmetric residual stress: experimental application", International Journal of Mechanical Application 43.

25. Guo, Wanlin (1993), "Elastic Plastic Analysis of a Finite Sheet with a Cold-Worked Hole", Engineering Fracture Mechanics, vol 46, Issue 3.

26. Hayes, B. (1996). "Classic Brittle Failures in Large Welded Structures". Engineering Failure Analysis, Vol 3 (2).

27. Hoffman, Oscar and Sachs, George (1953), Introduction to the Theory of Plasticity for Engineers, McGraw-Hill, New York, New York.

28. Hsu, Y.C. and Forman, R. G. (1975), "Elastic-Plastic Analysis of an Infinite Sheet Having a Circular Hole Under Pressure", The American Society of Mechanical Engineers Journal of Applied Mechanics 42.

29. Kuhn, B., Lukic, M., Naussbaumer, A., Gunther, H. P., Helmerich, R., Herion, S., Kolstein, M. H., Walbridge, S., Androic, B., Dijkstra, O., and Bucak O. (2008). "Assessment of Existing Steel Structures: Recommendations for Estimation of Remaining Fatigue Life". JRC Scientific and Technical Reports, EUR 23252EN-2008.

www.manaraa.com

30. Lanciotti, A. and Polese, C. (2005). "The effect of interference-fit fasteners on the fatigue life of central hole specimens". Fatigue and Fracture in Engineering Materials and Structures 28 (2005).

31. Langenecker, Bertwin (1966) "Effects of Ultrasound on Deformation Characteristics of Metals", Transaction on Sonics and Ultrasound, vol su-13, no 1.

32. Maranian, Peter (2010). Reducing Brittle and Fatigue Failures in Steel Structures. American Society of Civil Engineers, Reston, VA.

33. McGuire, William (1968). Steel Structures. Prentice-Hall, Inc. Englewood Cliffs, NJ.

34. Merritt, Frederick S., Editor, (1972). Structural Steel Designers' Handbook. McGraw-Hill Book Company, New York, NY.

35. Moniz, B. J. (1994), Metallurgy, Second Edition, American Technical Publishers, Inc., Homewood, Illinois.

36. Nadai, A. (1931), Plasticity, McGraw-Hill, New York, New York.

37. Nadai, A. (1943) "Theory of Expanding of Boiler and Condenser Tube Joints Through Rolling", Transaction of the American Society of Mechanical Engineers, vol 65, issue 8.

38. Nadai, A. (1950) Theory of Flow and Fracture in Solids, McGraw-Hill, New York, New York.

39. Nevill, G. F., Jr. and Brotzen, Franz R., (1957) "The Effect of Vibration on the Static Yield Strength of Low-Carbon Steel" Proceedings of American Society of Testing Materials, vol 57.

40. Nigrelli, V. and Pasta, S. (2008) "Finite element simulation of residual stress induced by split-sleeve cold-expansion process of holes" Journal of Material Processing Technology 205.

41. Ozdemir, A. T. and Edwards, L. (2004). "An Assessment of the Complete Through Thickness Residual Stress Distribution after the Split Sleeve Cold Expansion of Fastener Holes" Canadian Metallurgical Quarterly, vol. 43, no. 2.

42. PBFasteners (2011). "SLEEvbolt Interference Fastening System" PBFasteners <www.pbfasteners.com> (Feb. 27, 2011).

43. Poolsuk, S. and Sharpe, W. N., Jr, (1978) "Measurement of the Elastic Plastic Boundary and Coldworked Fastener Holes", Winter Annual Meeting Dec 1978, American Society of Mechanical Engineers.

44. Poussard, C. G. C., Pavier, M. J., and Smith (1994) Prediction of Residual Stress in Clod Worked Fastener Holes Using the Finite Element Method" Proceedings of the 2nd

المنارة للاستشارات

www.manaraa.com

Biennial European Joint Conference on Engineering System Design and Analysis vol 8, part A (American Society of Mechanical Engineers, New York).

45. Poussard, C., Pavier, M.J., and Smith, D. J. (1995) “Analytical and Finite Element Predictions of Residual Stress in Cold Worked Faster Holes” Journal of Strain Analysis vol 30 no 4.

46. Ramberg, W. and Osgood, W. R. (1943) Description of Stress-Strain Curves by Three Parameters, NCAA TN 902.

47. Reeve, L. (1940). “Examination of Welded Steel Specimens from the Hasselt Bridge”. Transaction of the Institute of Welding, vol 3 (1).

48. Reid, Len, Fatigue Technology, personal communications, 2011

49. Rich, D. L. and Impellizzeri, L. F., (1977) “Fatigue Analysis of Cold-Worked and Interference Fit Fastener Holes”, Cyclic Stress-Strain and Plastic Deformation Aspects of Fatigue Crack Growth ASTM 637, American Society of Testing Materials Philadelphia, PA.

50. Richards, Cedric W. (1961) Engineering Materials Science, Wadsworth Publishing Co, Belmont, California.

51. Roddis, W. M. Kim and Zhao, Yuan (2001). “Out-of-Plane Fatigue Cracking in Welding Steel Bridges”. Welding Innovations, 27(2).

52. Rolfe, S. T. and Barsom, John M. (1977). Fracture and Fatigue Control in Structures: Applications of Fracture Mechanics. First Edition. Prentice Hall.

53. Rowlands, Robert E. (1993) “Residual Stress” Chap 18 Handbook on Experimental Mechanics, Kobayoshi, Albert S. ed, Society for Experimental Mechanics, Bethel CT.

54. Sharpe, W.N. Jr., (1978) “Residual Stress around Coldworked Fastener Holes”, Journal of Engineering Materials and Technology, Vol 100, July 1978.

55. Sirnivasan, A. V. and McFarland, D. Michael, (2001) Smart Structures, Cambridge University Press, Cambridge, UK.

56. Tavakkolizadeh, M. and Saadatmanesh, H. (2003). “Fatigue Strength of Steel Girders Strengthened with Carbon Fiber Reinforced Polymer Patch”. American Society of Civil Engineers Journal of Structural Engineering, 129(2).

57. Wang, Z. and Zang, X. (2003) “Predicting Fatigue Crack Growth Life for Cold-Worked Holes Based on Existing Closed-Form Residual Stress Models” International Journal of Fatigue, vol 25 issue 9-11.

58. Zhang, Y., Fitzpatrick, M. E., and Edwards, L., (2005) “Analysis of Residual Stress Around a Cold-Expanded Fastener Hole in a Finite Plate” Strain vol 41.

المنارة للاستشارات

www.manaraa.com

59. Zhao, Y., and Roddis, W. M. Kim (2007). "Fatigue Behavior and Retrofit Investigation of Distortion-Induced Web Gap Cracking". Journal of Bridge Engineering, 12(6).

المنارة للاستشارات

www.manaraa.com

CHAPTER 2: SIZING CRACK-ARREST HOLES

ABSTRACT

Through an examination of the literature on this topic, this paper discusses how to determine the required diameter of a crack-arrest hole to ensure that the crack-arrest hole will effectively halt crack propagation. Two different experimental programs were the basis for the formula that may be used to calculate the required diameter of the crack-arrest hole. As a result, each experimental program recommended different constants for use in the formula. Both of the experimental programs are discussed in detail and the development of the each constant is provided. The effect of each constant on the required diameter is presented, the impact of several critical terms in the formula is discussed, and an extension to the formula adding the size of the hole diameter into the formula is provided. In addition, one recommended 'rule-of-thumb' for sizing a crack-arrest hole is presented.

INTRODUCTION

Crack-arrest holes are a time-honored, simple solution for stopping fatigue crack propagation. They stop fatigue crack propagation by blunting the crack tip and reducing the stress concentration at the crack tip. The radius of the crack tip is very small, approaching zero, and the curvature (*1/radius*) approaches infinite. Correspondingly, the stress concentration factor (Eqn 1) at the crack tip approaches infinite. The crack-arrest hole changes the radius and curvature to that of the crack-arrest hole and reduces the stress concentration factor substantially.

$$k_t = \frac{\sigma_{max}}{\sigma_{nominal}}$$

Equation 1 (Barsom and Rolfe 1997)

المنارة للاستشارات

www.manaraa.com

Where:
kt is the stress concentration factor,
σmax is the maximum at the edge of the crack, and
σnominal is the stress sufficiently far away from the crack that it
is not influenced by the crack

For example, the stress concentration factor at the edge of an ellipse is Eqn. 2 (Barsom and Rolfe 1997):

$$k_t = \left(1 + 2\frac{a}{b}\right)$$

Equation 2 (Barsom and Rolfe 1997)

Where:
k_t is the stress concentration factor
2a is the length of the major axis of the ellipse and
2b is the length of the minor axis of the ellipse

For sharp cracks *b* approaches *0* and *a/b* becomes very large; then k_t also becomes very large. By placing a crack-arrest hole of radius *r* at the tip of the crack, *r* replaces *b* and the stress concentration factor reduces from infinite to a relatively small finite number.

OBJECTIVE

This paper is based on an examination of the available literature on crack-arrest holes. The objective of this paper is to discuss how to determine the required diameter of a crack-arrest hole using the formula and recommendations from the literature. The required diameter to ensure that the crack-arrest hole will effectively halt crack propagation is based on two different experimental programs. The differences between the experimental programs resulted in two different constants for use in the formula. The effect of each constant on the required diameter is presented, the impacts of several critical terms in the formula are discussed, and an extension to

المنارة للاستشارات
www.manaraa.com

the formula for including the size of the hole into the calculation for determining the required diameter is provided.

BACKGROUND

The principal loads on bridges are dead loads from the weight of the bridge materials and live loads from traffic occurring on the bridge. Depending on span length (McGuire 1968), the ratio of live-to-dead loads varies from less than 1 to approximately 3. From the live-to-dead load ratios, the time-varying stresses for the higher ratio could approach 50-80% of the allowable stress in the steel and may cause fatigue cracks to initiate in welded-steel bridges if fatigue was not properly accounted for in the design. According to the 2001 National Bridge Inventory update, more than 85,000 highway bridges may be structurally deficient (FHWA Bridge Program Group 2001). Steel bridges make up 43% of the highway bridges in the United States; more than 120,000 of these are steel highway bridges with welded details (Tavakkolizadeh and Saadatmanesh 2003). The major problems causing bridges to be labeled structurally deficient are the presence of fatigue-sensitive details, out-dated service loads, corrosion, and lack of proper maintenance (Tavakkolizadeh and Saadatmanesh 2003). In fact, fatigue cracks currently exist or will form in numerous steel highway bridges in the United States. From this discussion it is obvious that fatigue cracking is a major infrastructure issue in the U.S.

One detail which produces a large percentage of the fatigue cracks in steel girder bridges occurs at the gap left between a connection plate and adjacent girder flanges when the connection plate is welded to the girder web but not to the flanges. This particular detail is often referred to as a web-gap. Asymmetric loads from normal traffic cause torsion to develop about the longitudinal

المنارة للاستشارات
www.manaraa.com

axis of the girder. This torsion results in bending in the girder webs at these gaps and eventually in distortion-induced fatigue cracking (DIFC) in the girder webs (Fig. 1).

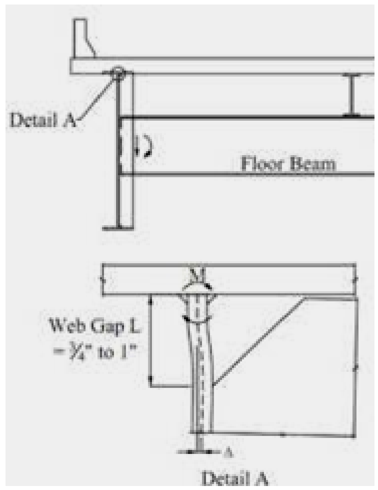

Figure 1. Distortion in the web gap

Once fatigue cracks occur, they must be repaired or closely monitored for crack growth. Numerous approaches have been used to repair fatigue cracks (Roddis and Zhao 2001), and the chosen repair generally depends on the type of fatigue loading (in-plane vs. out-of-plane) and the location and severity of the crack. Replacing a structural member may be difficult and cost-prohibitive, as the bridge may have to be taken out of service, the bridge deck removed, the member replaced, and the deck reinstalled. Re-welding or filling the fatigue crack with weld material requires grinding out the crack and any associated welds, filling the crack with weld material, and grinding the new weld surfaces smooth. Access and quality field welding often present difficult problems with welded solutions. Crack-arrest holes may be an appropriate solution if the holes are drilled large enough to effectively prevent crack reinitiating.

Because of its simplicity, one of the first techniques often considered for arresting fatigue crack

المنارة للاستشارات
www.manaraa.com

propagation is to drill a crack-arrest hole at each end of the fatigue crack (Fig 2). Unfortunately, the diameter required to arrest crack propagation may be so large that the hole does not fit within available spacing because of interference with a connection plate, stiffener, flange, or other details. In addition, a hole with the "correct" diameter may remove so much material that the hole becomes noticeable causing concern. In Kansas, common practice is to drill crack-arrest holes with a diameter ranging from 19 mm (¾ in) to 38.1 mm (1½ in). Experience has shown that if the diameter of the hole is not large enough, the crack will eventually grow through the hole and continue propagating (Fig 3).

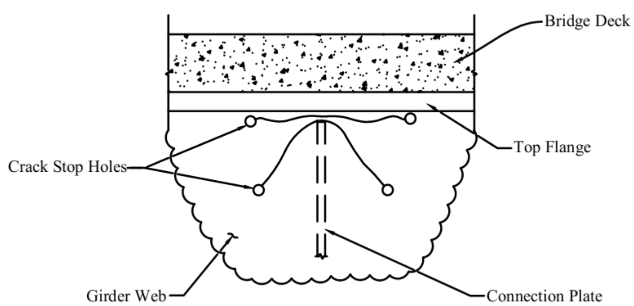

Figure 2. Crack-arrest holes at fatigue cracks (Roddis and Zhao 200

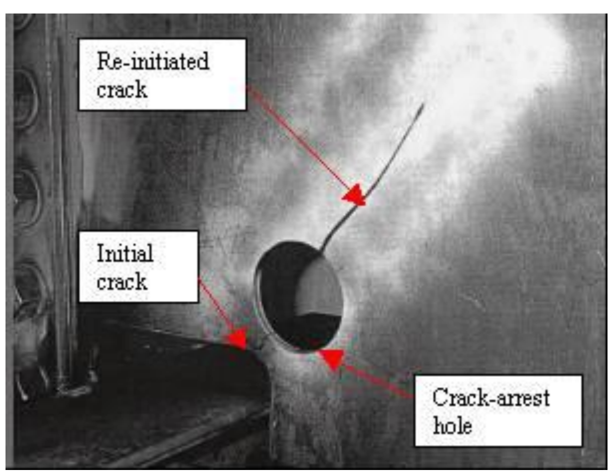

Figure 3. Fatigue crack reinitiating through crack-arrest hole (Dexter 2004)

المنارة للاستشارات
www.manaraa.com

CRACK-ARREST HOLE FORMULA

The formula for determining the diameter of the crack-arrest hole to stop fatigue crack propagation was first presented in Rolfe and Barsom (1977) and is in the latest edition of Barsom and Rolfe (1999). Fisher et al. (1980; 1990) used the same formula but developed a different constant from different experimental testing. The formula (Eqn. 3) relates the required radius of the crack-arrest hole to the yield strength of the steel, the range of the stress intensity factor, and the half-length of the crack along with a constant from experimentation.

Rolfe and Barsom (1977) Formula

The formula was presented in the following form (Rolfe and Barsom 1977):

$$\frac{\Delta K}{\sqrt{\rho}} = C\sqrt{\sigma_{ys}}$$

Equation 3

Where:

C = constant derived from experimental testing,
ρ = required radius of the crack-arrest-hole,
σ_{ys} = the yield strength of the steel,
ΔK = the range of the stress intensity factor.

and was based on a series of experiments on several identical sets of steel plates with edge notches. Within each identical set, the edge notch radii were different for each plate but the edge notch lengths were all the same. The yield strengths of the each set of steel plates was different and varied between 248 MPa (36 ksi) to 758 MPa (110 ksi). The loading, which consisted of uniaxial, cyclical loads, was varied to provide stress ratios ($R = \sigma_{max}/\sigma_{min}$) of –1.0 (full stress reversal), 0.1, and 0.5. This plate geometry with the uniaxial, tension-compression loading resulted in Mode I type fracture, where Mode I fracture is a tension-opening crack (Fig. 5). For

www.manaraa.com

this edge notch configuration, the range of the stress intensity factor can be determined by:

$$\Delta K = \Delta\sigma \sqrt{\pi \cdot a} \qquad \text{Equation 4}$$

Where:

ΔK = range of the stress intensity factor
$\Delta\sigma$ = cyclic stress range (σ_{max} - σ_{min}) for the fluctuating stresses, and
a = the length of the edge crack ($^1/_2$ the length of the crack for an interior crack).

When $\Delta K = \Delta\sigma\sqrt{\pi \cdot a}$ is substituted into Eqn. 3, Eqn. 5 results:

$$\frac{\Delta\sigma\sqrt{\pi \cdot a}}{\sqrt{\rho}} = C\sqrt{\sigma_{ys}} \qquad \text{Equation 5}$$

This can be rearranged in terms of ρ and a and becomes:

$$\rho = \left(\frac{\pi \cdot \Delta\sigma}{C^2 \cdot \sigma_{ys}}\right) \cdot a \qquad \text{Equation 6}$$

المنارة للاستشارات
www.manaraa.com

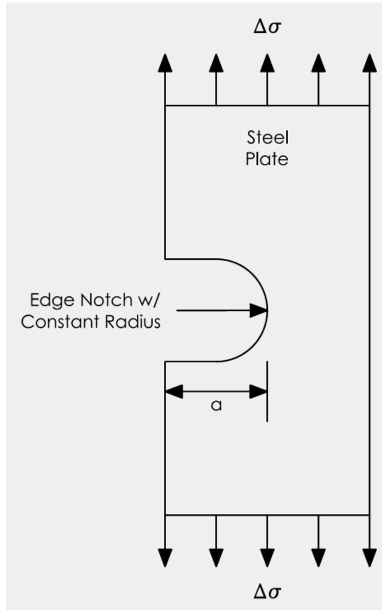

Figure 4. Plate Configuration for Crack-Arrest Hole Testing (Barsom and Rolfe 1999)

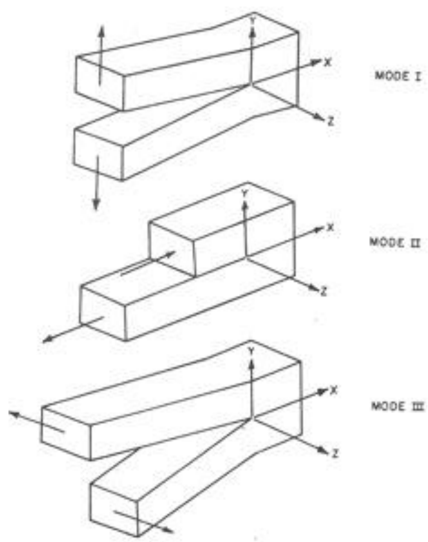

Figure 5. Fracture Modes (Barsom and Rolfe 1999)

Fisher et al. (1980; 1990) Formula

The crack-arrest formula is also found in Fisher et al. (1980; 1990). Fisher et al. conducted a series of experiments on rolled, wide-flange shapes (Fisher et al. 1980) and welded-plate girders (Fisher et al. 1990) where the full-scale members were configured and loaded in such a manner

المنارة للاستشارات
www.manaraa.com

that they were subjected to both in-plane bending stresses and out-of plane distortion stresses (Fig. 6). This combination resulted in distortion-induced fatigue cracking at locations where cross-bracing attached to the connection plates, which were in turn welded to the girder webs as depicted in Figs. 2, 7, & 8.

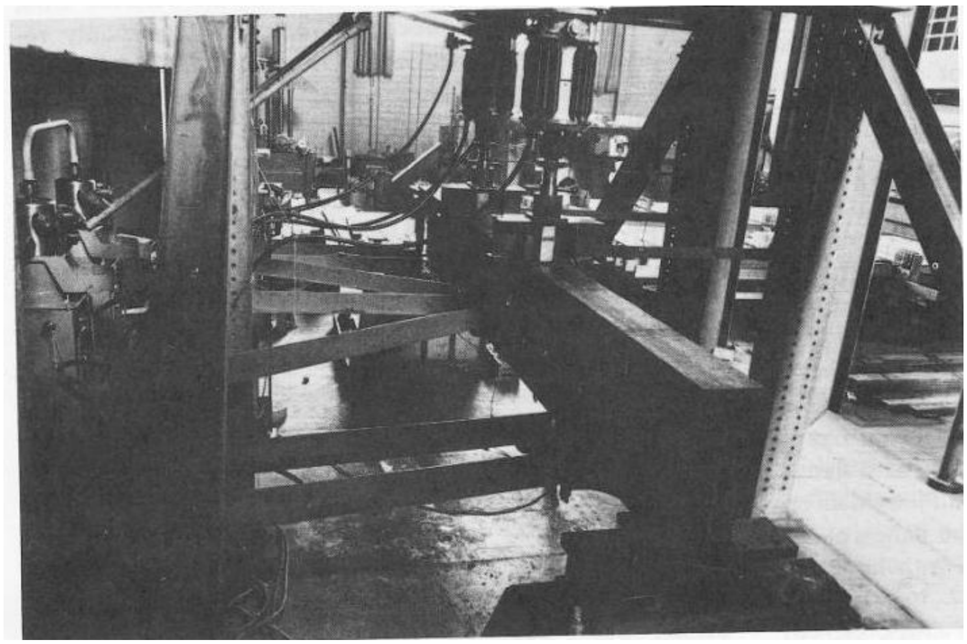

Figure 6. Fisher et al. (1980) Crack-Arrest Experimental Arrangement

The steel was limited to Gr. A370 steel, which had measured yield strength of 248 MPa (36 ksi). The fatigue cracking was caused by a complex, triaxial stress field and resulted in a Mode III failure (shear in a plane perpendicular to direction of crack growth) (Fig. 5) or in a complex mode with both Mode III and bending stress components. When fatigue cracks developed in the members, holes were drilled at the ends of the crack tips; these holes typically had diameters of 19mm (¾ in), 25.4mm (1in), or 31.75mm (1¼ in). The test were restarted and continued until the cracks reinitiated or the test was stopped. For the tests on the rolled shapes, the control stress variable was the stress range in the normal flexural bending stresses as measured in the beam

المنارة للاستشارات
www.manaraa.com

web at the bottom of the gusset at midspan (Fig. 7). The stress ranges were 41.4, 62.0, 82.7, or 103.4 MPa (6, 9, 12, or 15 ksi). For tests on the plate girders, testing was controlled by limiting the in-plane bending stress to either 41.4 or 82.7 MPa (6 or 12 ksi) and inducing out-of-plane distortion stress of either low, medium, or high values. The out-of-plane distortion stress was calculated from strains measured in the web gap with strain gages and then extrapolated back to the edge of the transverse stiffener (Fig. 8). The crack length, *a*, was defined as in Fig. 7 for the lateral gusset plate and Fig. 8 for the transverse stiffener. Cracks as depicted in Fig. 8 often extended to the other side of the transverse stiffener as shown in Fig. 2; when they extend to the other side, the distance shown in Fig. 8 should more properly be labeled as *a* instead of *2a*.

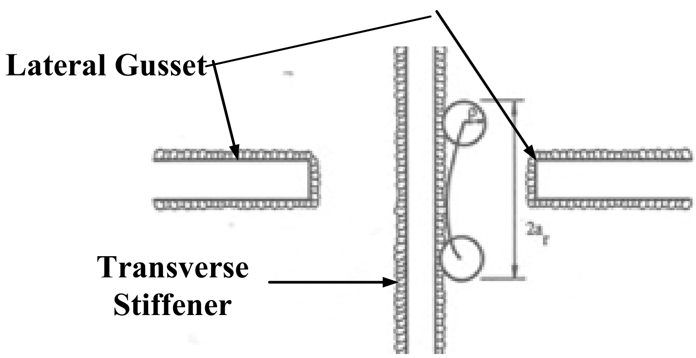

Figure 7. Crack -Arrest Holes at the Ends of a Crack at Lateral Stiffener (Fisher et al. 1990)

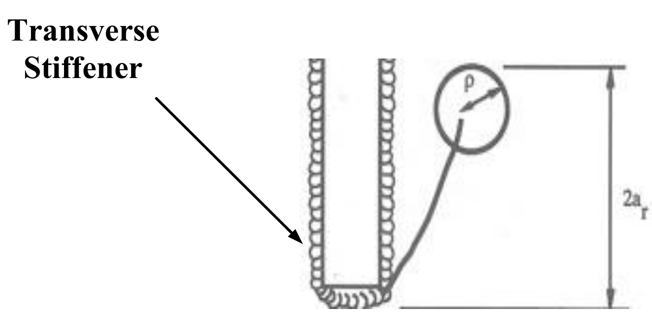

Figure 8. Crack-Arrest Hole at End of Crack in Transverse Stiffener (Fisher et al. 1990)

'Rule of Thumb'

In a PowerPont presentation available on the Internet with minimal written explanation, Dexter (2004) provided the following recommendations:

المنارة للاستشارات
www.manaraa.com

1. Diameter of the crack-arrest hole should be one third the length of the crack

2. The crack-arrest hole must be 4-in in diameter and can be permanently effective if the crack is less that 6-in long on each side of the transverse stiffener

Constant, *C*

Despite the differences in the testing methodology, Fisher et al. (1980) used Eqns. 3 & 4 for determining the required radius of the crack-arrest hole but developed a different constant *C*. Using Eqns. 3 and 4 resulted in Eqn. 5 for both Rolfe and Barsom (1977) and Fisher et al. (1980, 1990). Since *C* was derived from different testing methodologies, the values for *C* depend on using consistent units. Table 1 provides the consistent units and the corresponding values for *C* from Rolfe and Barsom (1977) and from Fisher et al. (1980, 1990) in both SI and US Customary units.

Table 1. Values for C and Units for Crack -Arrest Hole Equations

Units	*C* – Rolfe and Barsom (1977)	*C* – Fisher et al. (1980)	$\Delta\sigma$	σ_{ys}	a	ρ
SI	26.3	10.5	MPa	MPa	mm	mm
US	10	4	ksi	ksi	in	in

Further comparison of the constants, *C*, may be made by plotting the recommended value from Rolfe and Barsom (1977) on the graph of experimental data from Fisher et al. (1980) as shown in Fig. 9. To be consistent with Fisher et al. (1980), $10\sqrt{\sigma_y}$, from Rolfe and Barsom (1977) has been plotted with σ_y = 248 MPa (36 ksi). It appears that the original location on the graph for

المنارة للاستشارات
www.manaraa.com

$4\sqrt{\sigma_y}$ from Fisher et al. (1980) was not plotted at the correct value of $\frac{\Delta k}{\sqrt{\sigma_y}}$; therefore, the correct location for $4\sqrt{\sigma_y}$, as well as the location for $10\sqrt{\sigma_y}$, have been plotted as shown in Fig. 9. From Fisher et al.'s data in Fig 9, it appears that using $C = 10$ is an approximate average of the data and $C = 4$, when correctly plotted, is a lower bound.

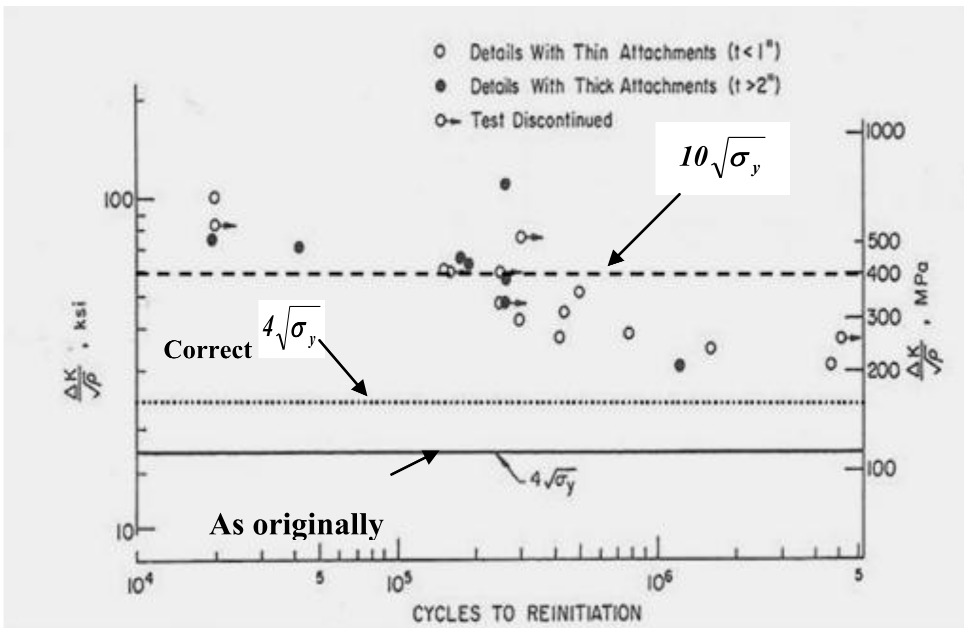

Figure 9. Development of Constant, *C*, for Crack-Arrest Hole Formula (Fisher 1980)

Effect of Hole Radius on Formula

Both Fisher et al. (1980) and Barsom and Rolfe (1999) noted that, if a crack-arrest hole is used, it is important to identify the crack tip and drill the crack-arrest hole such that the crack tip is located within the circumference of the hole. Out of the infinite locations for the crack tip within the hole, four distinct positions are depicted in Fig. 10. The first position is with the crack tip extending beyond the circumference on the far side of the hole (Fig 10a). This is the worst possible location as the crack-arrest hole will be totally ineffective at this location. The second

www.manaraa.com

position is with crack tip just inside the hole circumference at the far side of the hole (Fig. 10b). The concern about this geometry is that the tip may not have been identified accurately and the crack tip may actually extend beyond the hole as in Fig 10a. The third position, (Fig. 10c), is with the crack tip located at the center of the hole. The fourth position of the hole with respect to the crack tip is with the crack tip at the near side of the hole circumference (Fig. 10d). Fisher et al. (1980) states that this (Fig. 10d) is the optimum location with the hole positioned such that the crack tip just touches the circumference of the crack-arrest hole.

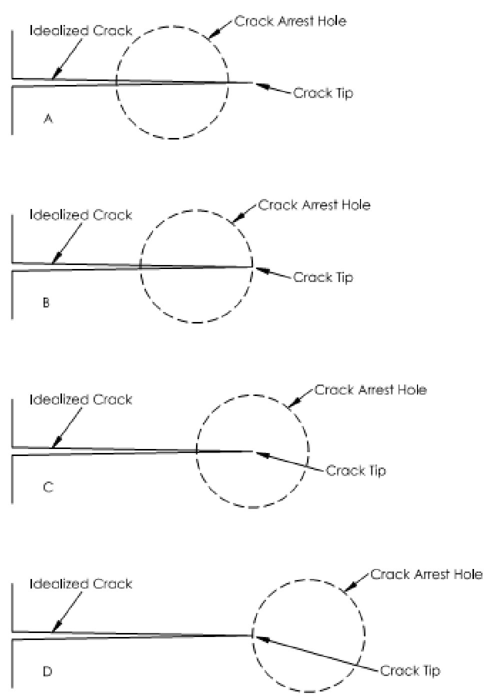

Figure 10. Location of Crack-Arrest Hole with Respect to the Crack Tip

For typical crack sizes, hole diameters, and stresses, the size of the hole diameter may be significant with respect to the crack length. Since the length of the hole diameter that extends beyond the crack tip effectively makes the crack longer, that portion of the diameter should be added to the crack length. If the hole is located as in Fig. 10b, no portion of the diameter needs

www.manaraa.com

to be added to the crack length. However, if the hole is located as shown in Fig. 10c and if the hole radius, ρ, is included with the crack length, a, Eqn. 5 becomes:

$$\frac{\Delta\sigma\sqrt{\pi(a+\rho)}}{\sqrt{\rho}} = C\sqrt{\sigma_{ys}}$$

Equation 7

Re-arranged so that the hole radius, ρ, is the dependent variable and the ½ -length of the crack, a, is the independent variable, Eqn. 7 may be re-written as:

$$\rho = \left(\frac{\pi\cdot(\Delta\sigma)^2}{C^2\sigma_{ys} - \pi\cdot(\Delta\sigma)^2}\right)\cdot a$$

Equation 8

If the holes are located as in Fig. 10d and, if the hole diameter, ρ, is included with the crack length, a, Eqn. 5 becomes:

$$\frac{\Delta\sigma\sqrt{\pi(a+2\rho)}}{\sqrt{\rho}} = C\sqrt{\sigma_{ys}}$$

Equation 9

Re-arranged, so that the hole radius, ρ, is the dependent variable and the ½ -length of the crack, a, is the independent variable, Eqn. 9 may be re-written as:

$$\rho = \left(\frac{\pi\cdot(\Delta\sigma)^2}{C^2\sigma_{ys} - 2\cdot\pi\cdot(\Delta\sigma)^2}\right)\cdot a$$

Equation 10

Limitation of the Formula

المنارة للاستشارات
www.manaraa.com

Fisher et al. (1990) states that, if the out-of-plane bending stress at the transverse stiffener is greater than 103 MPa (15 ksi) or if the in-plane bending stress in the web at the web to flange weld is greater than 41 MPa (6 ksi), the crack-arrest hole with a radius as calculated from the Eqn. 6 using the constant $C = 4$ will not prevent the crack from reinitiating on the other side of the hole. Rolfe and Barsom (1977) did not specify a restriction on load in their discussion of the formula.

DISCUSSION

This discussion is limited to a comparison of the behavior of the three crack-arrest hole formulae, Eqns. 6, 8, & 10. No additional testing has been done to the knowledge of the author to provide additional insight beyond that reported in Rolfe and Barsom (1977) and Fisher et al. (1980; 1990).

Figs. 11 and 12 demonstrate the differences resulting from including the crack-arrest hole radius in the formula to determine the correct radius and doing this with two different stress ranges. Fisher et al. (1980, 1990) used both 41 MPa (6 ksi) in-plane bending stress and 110 MPa (16 ksi) out-of-plane stress, $\Delta\sigma$, as criteria for the limits of the applicability of their formula. In an example calculation for determining the correct hole radius, Fisher et al. (1980) used 41 MPa (6 ksi) as the stress range without any explanation on why this was used rather than the 110 MPa (16 ksi). Fig. 11 uses as constants 248 MPa (36 ksi) for yield stress and 41 MPa (6 ksi) stress range and shows the effect of using C as either 4 or 10 with either equation 6, 8, or 10. Fig. 12 shows the same but uses 110 MPa (16 ksi) as the stress range, $\Delta\sigma$. Using C equal to 10 and σ_{ys} = 248 MPa (36 ksi), the difference between using any of the three equation was found to be slight

المنارة للاستشارات
www.manaraa.com

for the stress range for 41 MPa (6 ksi) (Fig 11) but more significant for the stress range of 110 MPa (16 ksi) (Fig 12). Using $C = 4$ and with the same conditions, large differences appear in the results from using the three equations. Note that Eqns. 8 and 10 are discontinuous; both are positive and increasing as long as the denominator is positive but experience a singularity when the denominator becomes 0. When the denominator becomes negative, the crack-arrest hole diameter becomes negative (Fig 12). These characteristics are also illustrated in Fig. 15.

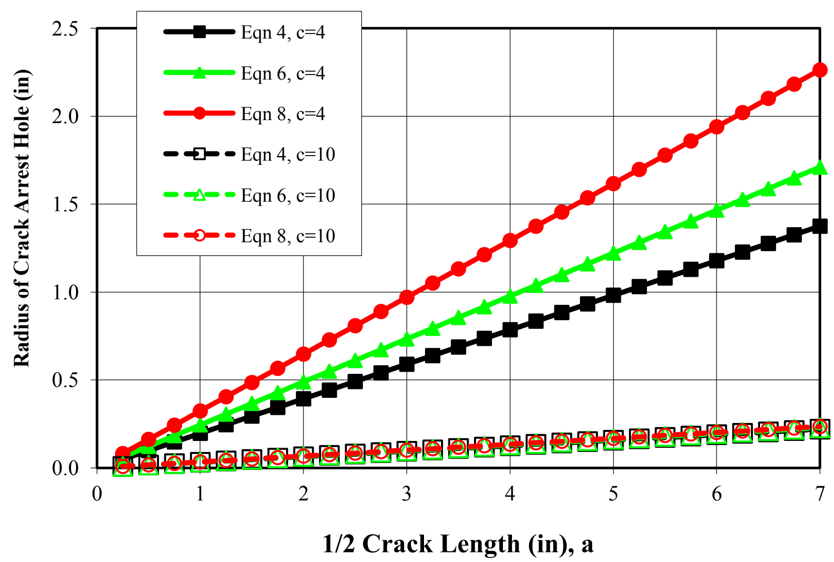

Figure 11. Radius of Crack-Arrest Hole as Determined by Eqns. 6, 8, & 10 as a Function of the ½-Crack Length and the Constant, *C*, with Yield Strength and Stress Range Held Constant at 248 MPa(36 ksi) and 41 MPa (6 ksi) In-Plane Stress Respectively

www.manaraa.com

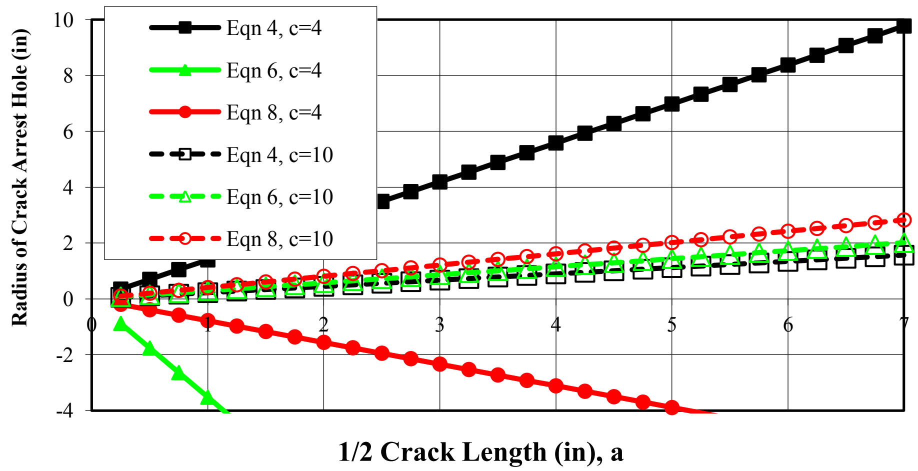

Figure 12. Radius of Crack-Arrest Hole as Determined by Eqns. 6, 8, & 10 as a Function of the ½-Crack Length and the Constant, *C*, with Yield Strength and Stress Range Held Constant at 248 MPa (36 ksi) and 110 MPa (16 ksi) Out-of-Plane Stress Respectively

Fig. 13 shows the results of calculating the required radius using Eqn 8 with the stress range at a constant 88 MPa (12 ksi) and with *C* either 4 or 10 while the yield stress varies as either 248 MPa (36 ksi), 290 MPa (42 ksi), 345 MPa (50 ksi), or 414 MPa (60 ksi). This shows that the three equations are insensitive to yield stress with $C = 10$ but are sensitive to yield stress with $C = 4$.

www.manaraa.com

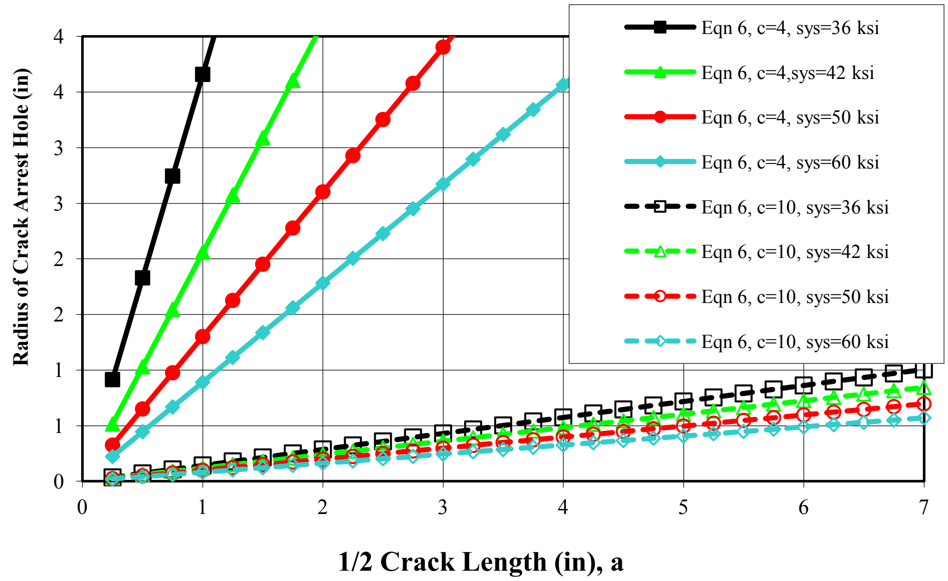

Figure 13. Radius of Crack-Arrest Hole as Determined by Eqn. 8 as a Function of the ½-Crack Length and the Yield Strength with the Constant, *C,* Being Either 4 or 10 and the Stress Range Held Constant at 83 MPa (12 ksi)

Fig. 14 shows the change in calculated radius using Eqn 8 with constant yield stress of 248 MPa (36 ksi) with different stress ranges, *Ds*, and with *C* as either 4 or 10. Comparing Figs. 11, 12, 13, and 14 indicate that the stress range is the dominant variable and has the most effect on the magnitude of the calculate radius. This effect is more dramatic with $C = 4$ but is still significant with $C = 10$.

www.manaraa.com

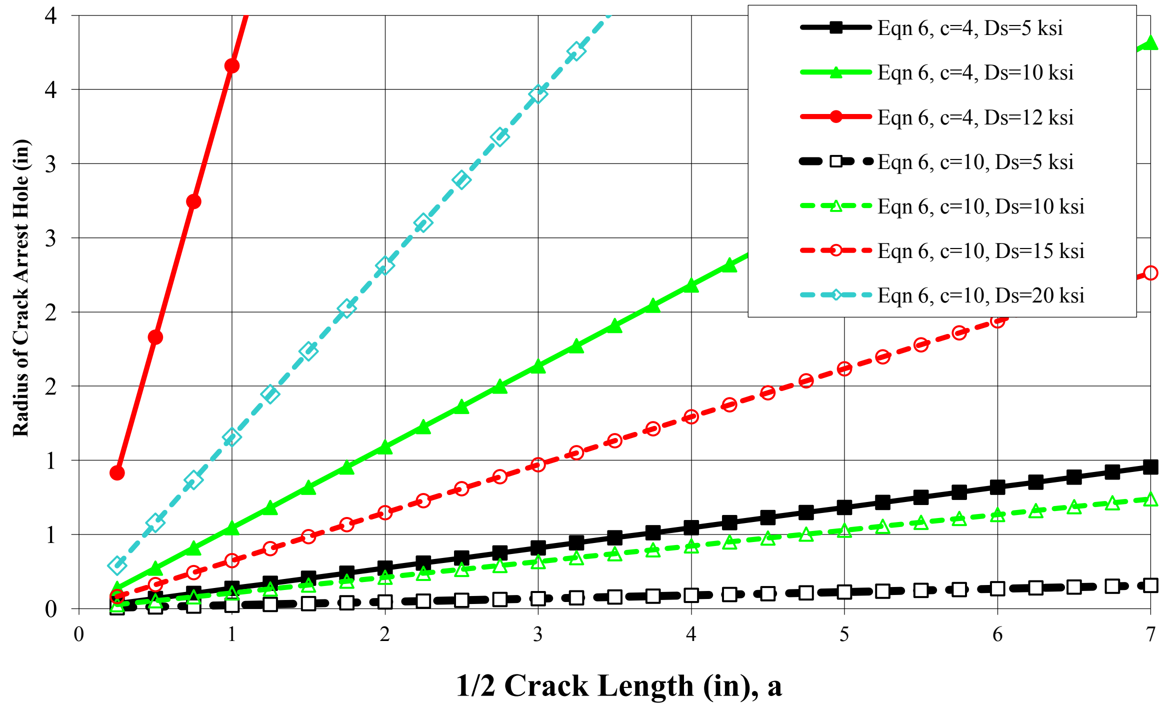

Figure 14. Radius of Crack-Arrest Hole as Determined by Eqn. 8 as a Function of the ½-Crack Length and the Stress Range with the Constant, *C,* Being Either 4 or 10 and the Yield Stress Held Constant at 248 MPa (36 ksi)

On a specific crack in a specific bridge, the crack half-length, *a*, could be measured and the yield strength of the steel may be available from the construction documents. The location of the hole with respect to the crack tip could be selected depending on the confidence in being able to accurately locate the crack tip. *C* could be chosen between 4 and 10 depending on the desired factor of safety. This leaves only the stress range as an unknown in applying one of the three crack-arrest formulae. At this time, whether to use the in-plane or out-of-plane stress range is not clear. In addition, it may be difficult to arrive at even an approximate value for either the in-plane or out-of-plane bending stress range.

To further investigate the effect of stress range variations on the crack-arrest hole equation, Eqn. 8 was reordered to provide the normalized crack-arrest-hole radius as a function of the

المنارة للاستشارات
www.manaraa.com

normalized stress range and the results plotted in Fig. 15. Dividing by the half-length of the crack normalized the crack-arrest-hole radii and dividing by the yield stress normalized the stress range. The results were then plotted using four values of yield stress and two values of *C*. Fig. 15 shows both the positive and negative values of Eqn. 8 illustrating the discontinuous nature of the equation and the singularity when the denominator equals 0.

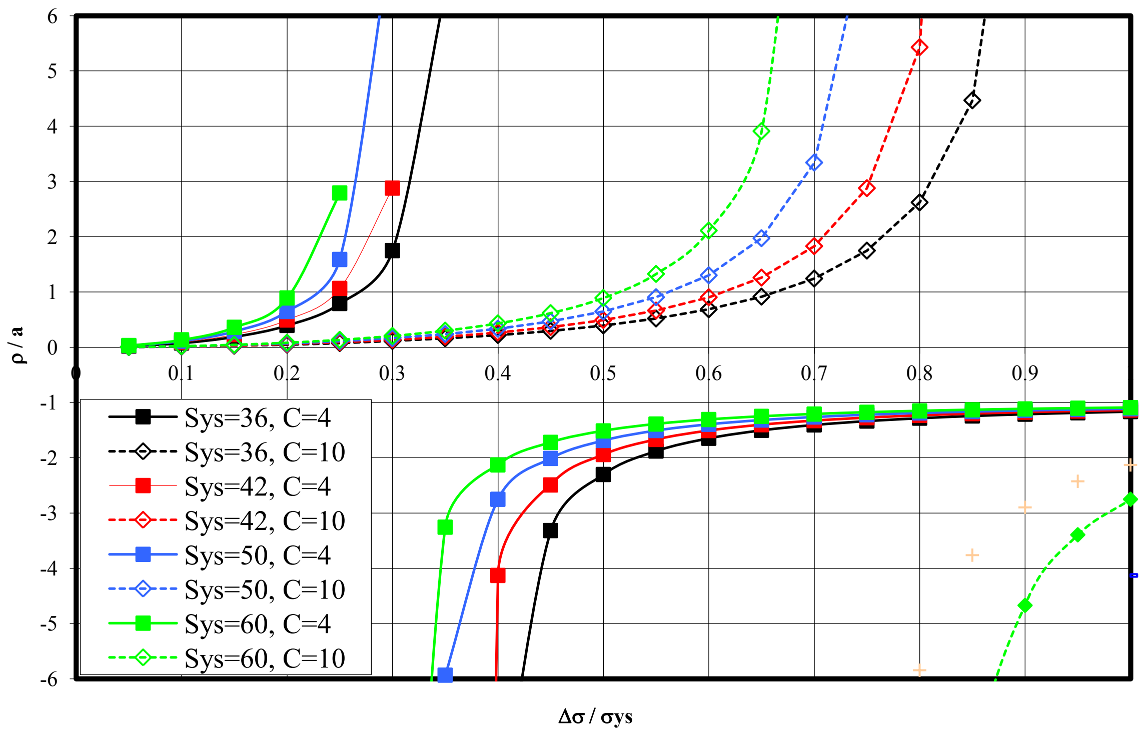

Figure 15. Normalized Radius of the Crack-Arrest Hole Compared to Normalized Stress Using Eqn. 8 with the Constant, *C*, Being Either 4 or 10 and Vary Stresses Showing Negative Values

Fig. 16 presents only the positive values of Eqn. 8 shown at an expanded scale. Fig. 16 seems to show that with $C = 4$, crack-arrest hole will only be effective for stress ranges approximately 20 to 30 percent of yield stress and that the radii of the crack-arrest hole increase quickly. The plot of $C = 4$ also does not support Dexter's (2004) recommendations.

www.manaraa.com

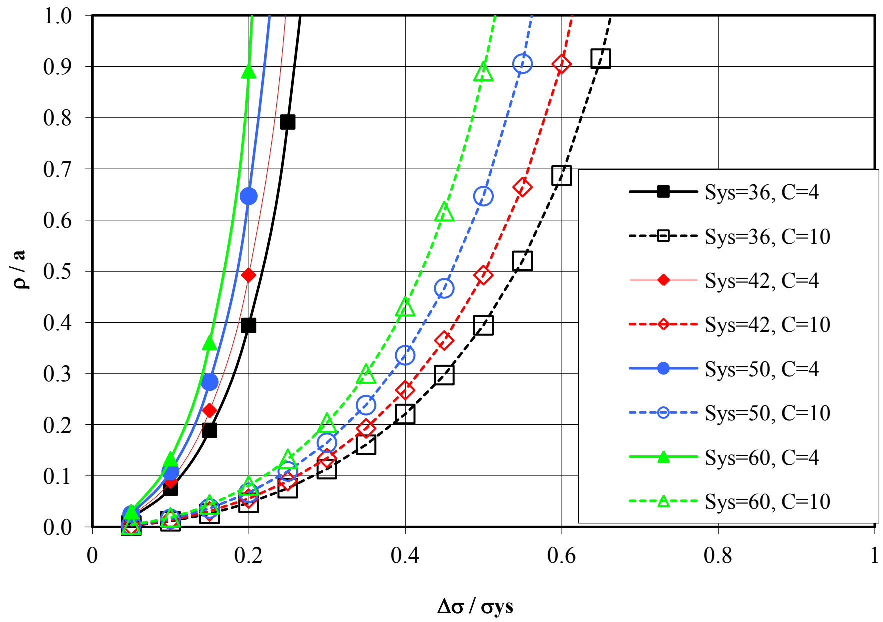

Figure 16. Normalized Radius of the Crack-Arrest Hole Compared to Normalized Stress Using Eqn. 8 with the Constant, *C*, Being Either 4 or 10 and Varying Yield Stresses Showing Only Positive Values

CONCLUSIONS

1. The location of the crack-arrest hole with respect to the crack tip is an important consideration with regard to preventing crack reinitiation. Depending on the location of the crack-arrest hole, some portion of the radius of the crack-arrest hole needs to be added to the half-length of the crack when calculating the required radius. This can be accomplished with some algebraic manipulations.

2. The stress range is the critical unknown quantity and dominates the calculation for the required diameter for the crack-arrest hole. The location and sense for the controlling value of the stress range is not clear when addressing DIFC and determining the in situ value for this stress range on an actual bridge will be difficult.

المنارة للاستشارات
www.manaraa.com

3. The values for C are supported by experimentation. C =4 is was a lower bound and C = 10 was an average value. Both must be used with engineering judgment with due consideration to the experimental parameters used in their development.

4. The crack-arrest hole diameter may be so large that it is impractical or it may not be physically possible to drill the size of hole required due to interference with connection plates, stiffeners, flanges, etc.

Therefore, in conclusion, crack-arrest hole should be used as a practical matter with a reasonable radius. Calculating an exact radius for the crack-arrest hole is probably not feasible

REFERENCES

1. Barsom, John M. and Rolfe, S. T. (1999). Fracture and Fatigue Control in Structures: Applications of Fracture Mechanics. Third Edition. American Society of Testing Materials, Philadelphia, PA, 182-192.

2. Dexter, Robert J. (2004). "Signs, Signals, Light Support Structures and Manual for Repair of Fatigue and Fracture" Third Annual Bridge Workshop: Fatigue and Fracture. Available on the Internet.

3. Federal Highway Administration (FHWA) Bridge Program Group. (2001). "Count of deficient bridges by state non federal-aid highway." (http://www.fhwa.dot.gov/bridges/britab.htm) (March 20,2002) The Office of Bridge Technology, Washington, D.C.

4. Fisher, John W., Barthelemy, B. M., Mertz, D. R., and Edinger, J. A. (1980). "Fatigue Behavior of Full-Scale Welded Bridge Attachments". National Cooperative Highway Research Program (NCHRP) Report 227, National Transportation Research Board, Washington, D. C.

5. Fisher, John W., Jin, Jain, Wagner, David C., and Yen, Ben T. (1990). "Distortion-Induced Fatigue Cracking in Steel Bridges". National Cooperative Highway Research Program (NCHRP) Report 336, National Transportation Research Board, Washington, D. C.

6. McGuire, William (1968). Steel Structures. Prentice-Hall, Inc. Englewood Cliffs, NJ, 208-220.

المنارة للاستشارات
www.manaraa.com

7. Roddis, W. M. Kim and Zhao, Yuan (2001). "Out-of-Plane Fatigue Cracking in Welding Steel Bridges". Welding Innovations, 27(2).

8. Rolfe, S. T. and Barsom, John M. (1977). Fracture and Fatigue Control in Structures: Applications of Fracture Mechanics. First Edition. Prentice Hall.

9. Tavakkolizadeh, M. and Saadatmanesh, H. (2003). "Fatigue Strength of Steel Girders Strengthened with Carbon Fiber Reinforced Polymer Patch". American Society of Civil Engineers Journal of Structural Engineering, 129(2).

www.manaraa.com

CHAPTER 3: DEVELOPMENT OF A TECHNIQUE TO IMPROVE FATIGUE LIVES OF CRACK-STOP HOLES IN STEEL BRIDGES

Josh S. Crain[1], Gary G. Simmons[2], Caroline R. Bennett[3], Ron Barrett-Gonzalez[4], Adolfo Matamoros[5], and Stanley T. Rolfe[6]

ABSTRACT

A common technique used to prevent the propagation of fatigue cracks in bridge girders is the drilling of crack-stop holes at crack tips. By doing so, stress concentrations at the crack tips are reduced and fatigue life of the bridge is extended. The size of the crack-stop hole needed to prevent any further crack growth is determined by utilizing known material properties and relationships developed through experimentation. However, these equations often result in a crack-stop hole diameter larger than can be practically drilled; physical limitations force crack-stop holes to be undersized in the field. To improve effectiveness of undersized holes to that of full-sized holes, a method is needed to strengthen undersized crack-stop holes.

The purpose of this study was to investigate the potential of a new technique to improve the fatigue life of undersized, crack-stop holes. The technique uses piezoelectric actuators.

operated at ultrasonic frequencies to convert electrical signals into mechanical work . This technique produced residual compressive stresses of the same order of magnitude as those produced by static cold expansion. A suite of finite element models was created to quantify and

University of Kansas, 1530 W. 15th St., 2150 Learned Hall, Lawrence, KS 66045
1 Josh S. Crain, Graduate Research Assistant,
2 Gary G. Simmons, P.E., Graduate Research Assistant, University of Kansas
3 Caroline R. Bennett, PhD, Assistant Professor, University of Kansas
4 Ron Barrett-Gonzalez, PhD, Associate Professor, University of Kansas
5 Adolfo B. Matamoros, PhD, Associate Professor, University of Kansas
6 Stanley T. Rolfe, PhD, PE, Learned Distinguished Professor, University of Kansas

www.manaraa.com

characterize the residual stresses surrounding the cold-expanded, undersized, crack-stop holes. Results were compared with analyses found in past literature.

INTRODUCTION

As a result of the relatively long propagation life between initiation of a fatigue crack and eventual failure, measures can be taken to retrofit and preserve existing cracked bridge members if fatigue cracks are detected early. There are several existing methods that can retard or stop the propagation of fatigue cracks. These methods include: repair welding or grinding of shallow cracks; metal reinforcements; adhesive CRFP patching; altering connection details; and drilling stop holes at crack tips [1-5]. These methods are attractive considering that the alternatives are either complete replacement of the cracked structural member or reducing external loads coupled with careful monitoring.

The technique of drilling a hole at a crack tip is a well-known procedure used in everyday practice to enhance fatigue life of steel structures [2]. The primary challenges associated with correctly applying this technique are that the theoretical size of the crack-stop hole is often too large for practical implementation in the field or the location is blocked by other members. To overcome these issues, crack-stop holes are often drilled undersized and left unreinforced. While undersized holes do improve fatigue life of a cracked structural member, it has been shown that varying levels of cold expansion can increase fatigue life of an unreinforced crack-stop hole by an order of magnitude [6-14]. The increase in fatigue life provided by cold expansion is a result of the three principal residual stresses induced by cold expansion: tangential, radial and transverse. Among these, compressive tangential stresses (also referred to as hoop or circumferential stress) is the major contributor to significant gains in fatigue life [9].

المنارة للاستشارات
www.manaraa.com

Several techniques have been developed to cold expand holes in metal structures, each having the common feature of inducing a layer of residual compressive stress around the outside of the hole. These compressive residual stresses are the direct result of forced, inelastic deformation of material around the circumference of a crack- stop hole. As a crack-stop hole is forced to expand through a mechanical process, yielding will first initiate along the edges of the hole where stresses are highest. As further expansion is mechanically induced, the zone of plasticity spreads further outward from the hole. Material that lies beyond this plastically-deformed region will deform elastically under applied stress. After the mechanically-applied pressure or displacement is removed from the system, residual compressive stresses around the hole are created from the elastic rebounding, or "springback," of the unyielded material surrounding the permanently-deformed plastic zone [15]. Figure 1 shows the level of residual tangential compressive stress that can be expected to develop around a mechanically expanded hole.

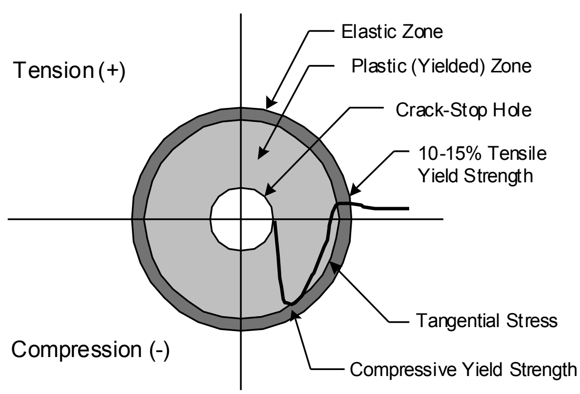

Figure 1. Residual Tangential (i.e., Circumferential or Hoop) Stress Surrounding Cold-Expanded Hole

A different technique, examined by Reemsnyder [16], involved the installation of high-strength bolts in crack-stop holes used to enhance fatigue performance. While the main focus of the

www.manaraa.com

study by Reemsnyder [16] was the potential fatigue life improvement of previously cracked holes in riveted bridge connections, the study mentioned that high-strength bolts were installed in drilled crack-stop holes located a predetermined distance away from the riveted connections. Cracks did not reinitiate from the crack-stop holes with the installed high-strength bolts; however, because fatigue life improvement of crack-stop holes was not the main focus of the study, no quantified fatigue life improvement was provided.

In separate studies performed by Huhn et. al. [17] and Brown et. al. [18], the influence of fully-tensioned high-strength bolts on the fatigue life of bolt holes in slip critical connections was examined. According to both studies, tensioned high-strength bolts significantly increased fatigue life of the bolt hole plate. According the authors, “this was due to the high pressure under the washers of the bolts. This high pressure gives a certain protection of the area around the hole, so that the stress distribution in the net section became much more favorable, even after the slip of the connections.” [17]

The method of installing high-strength bolts does not appear to improve fatigue performance as a result of cold working. No study [16-18] reported mechanical expansion occurring at the edges of the holes as a result of tensioning the high-strength bolts. Installing tensioned high-strength bolts is a separate technique and is one that could potentially be coupled with cold working to produce even larger improvements in fatigue life.

The technique described in this article used piezoelectric actuators to dynamically work and cold-expand the volume of steel plate surrounding the inner surface of a crack-stop hole.

المنارة للاستشارات
www.manaraa.com

Dynamically working steel through impact at high frequencies is a proven method for refining coarse grained steel into finer grained material [19], which can translate into improved fatigue performance. Plastic strains induced by the cold-expansion from the piezoelectric transducers were intended to create a residual compressive stress field similar to that achieved through existing techniques. The technique discussed in this paper has been termed Piezoelectric Impact Compressive Kinetics (PICK).

BACKGROUND

Existing Cold Working Techniques

While development of the PICK technique has focused solely on improving the fatigue performance of steel bridges, similar challenges are commonly encountered in the aerospace industry. Fastener holes in aircraft structures are sources of large stress concentrations and, as a result, are potential sites for cracks to initiate and propagate. It is common practice in the aerospace industry to cold-expand fastener holes, often resulting in a fatigue life improvement of three to ten times that of an untreated hole [11]. Most of the development of cold expansion has been performed within the aerospace field. As a result, the majority of existing studies involve numerical modeling and testing with various grades of aluminum, titanium, and high strength steel [20]. Benefits obtained from cold expansion of mild grade steel are expected to be similar to those found in aerospace-industry materials as a result of the similarity in the stress-strain relationship of the two types of materials when stressed beyond yield.

The most common technique currently used to cold-work fastener holes in aerospace applications is the split sleeve mandrel process [21]. While a thorough review of literature on this topic did not expose any application of this technique to bridges, it has been used extensively

المنارة للاستشارات
www.manaraa.com

in other structural applications. The process utilizes a solid, tapered mandrel and an internally lubricated steel split sleeve. Application of this technique begins by positioning the sleeve over the mandrel and inserting the mandrel into the hole. The hole is then expanded as the mandrel is drawn back through the sleeve. The expanded sleeve remains in the hole and can be discarded. It should be noted that it is common practice to remove existing damage by reaming and/or drilling the inside of the fastener hole [22].

Crack-Stop Holes

Current methods used to determine the size of crack-stop holes needed to prevent crack reinitiation are based on linear-elastic fracture-mechanic theory [23]. Analytical methods involving linear-elastic fracture mechanics are based on the procedure that relates magnitude of the stress-field near the tip of a crack to nominal applied stress, as described by Eqn. 1:

$$\sigma_{max} = k_t \sigma_{nom}$$

Equation 1

Parameters that affect the magnitude of the stress amplification factor, k_t, are: size, shape, and orientation of the crack or crack-like imperfections. The elastic-stress field at the edge of an imperfection, as described in Eqn. 2, is derived under the assumption that the shape of the imperfection is either elliptical or hyperbolic (see Figure 2) and the nominal applied stress is normal to the plane of the imperfection. In Eqn. 2, the stress intensity factor, ΔK_I, is determined assuming a zero radius crack tip and an initial crack length, $a = a_o + \rho$, where ρ is the radius of the hole.

$$\Delta\sigma_{max} = \frac{2\Delta K_I}{\sqrt{\pi\rho}}$$

Equation 2

المنارة للاستشارات
www.manaraa.com

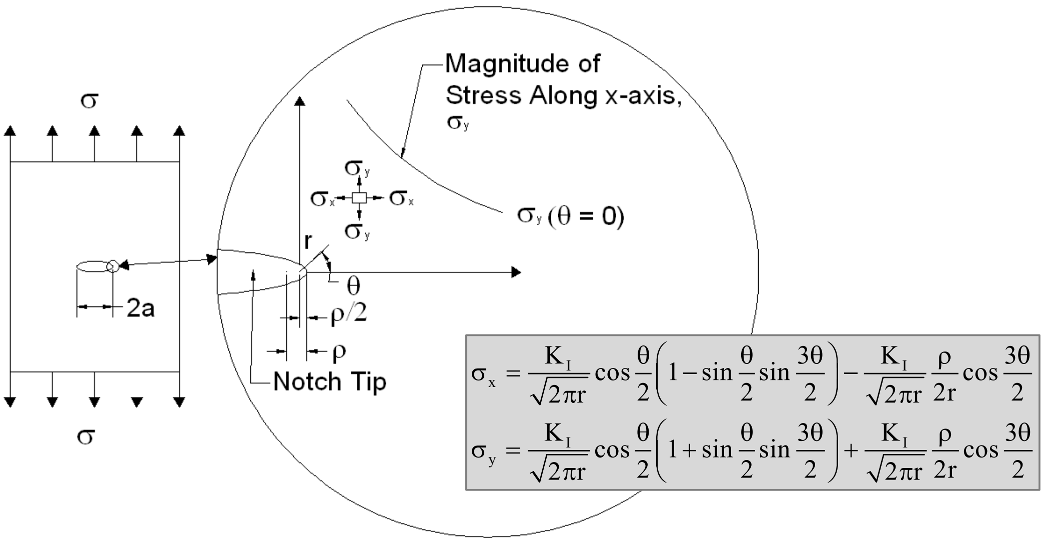

Figure 2. Schematic of Elastic-Stress Distribution Near Tip of an Elliptical Crack

From Eqn. 2, it is observed that both ΔK_I and the square root of the radius of the notch tip, $\sqrt{\rho}$, have an effect on the magnitude of maximum stress at the edge of the notch. Eqn. 2, which is valid for relatively sharp notches, is only exact when the notch tip radius is equal to zero. However, finite element analyses have shown that Eqn. 2 provides a fairly accurate relationship for imperfections with notch tip radii small compared with the crack length, 2*a* [24]. The theoretical relationship between terms $(\Delta K_I/\sqrt{\rho})$ and maximum stress, $\Delta\sigma_{max}$, led to further laboratory investigation to study its significance to fatigue crack initiation life. Thus, through basic fracture mechanic theory and extensive laboratory testing, Eqn. 3 was derived in [23], and can be used for determining the minimum crack-stop hole radii needed to prevent crack reinitiation in steel bridges:

المنارة للاستشارات
www.manaraa.com

$$\rho = \left(\frac{\Delta K_{total}}{10\sqrt{\sigma_{ys}}} \right)^2$$ Equation. 3

As an illustrative example of how Eqn. 3 may be used in a practical application is presented in the following. A fatigue crack is found during an inspection in the web of a bridge girder, near the top flange. The crack runs longitudinal to the girder, as shown in Figure 3, and is 216 mm (8.50 in.) long, offset 12.7 mm (0.500 in.) from the top flange. Therefore, there is sufficient space for a crack-stop hole with an approximate diameter of 25.4 mm (1.00 in).

For the fatigue crack scenario presented, the steel in the girder web is Gr. A36 with a yield strength under static loading, σ_{ys} = 248 MPa (36.0 ksi). For the 216 mm (8.50 in.) length crack, the stress intensity factor, ΔK_{total}, can be determined as follows (note that the following calculations are provided in US standard units as Eqn. 3 is not dimensionally independent):

$$\Delta K_{total} = \Delta\sigma\sqrt{\pi a}$$ Equation. 4

$$\Delta K_{total} = \left(26.0^{ksi}\right)\sqrt{(\pi)\left(\frac{8.50^{in.}}{2}\right)} = 95.0 \text{ ksi}\sqrt{\text{in.}}$$

The value of 179 MPa (26.0 ksi) assumed for the nominally applied stress was taken from previous finite element studies [3-4] which quantified the nominal stress demand at web gaps of details similar to that shown in Figure 3. The required radius to prevent further crack propagation can then be directly solved for from Eqn. 3:

المنارة للاستشارات
www.manaraa.com

$$\rho = \left(\frac{95.0^{\mathrm{ksi}\sqrt{\mathrm{in.}}}}{10\sqrt{36.0^{\mathrm{ksi}}}} \right)^2 = 2.51 \text{ in.}$$

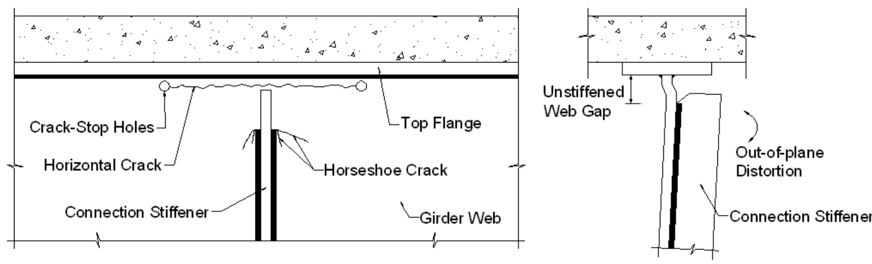

Figure 3. Fatigue Crack with Drilled-Crack-Stop Holes

Therefore, the required crack-stop hole diameter for the 216 mm (8.50 in.) long crack is approximately 127 mm (5.00 in). For this crack length, there is not enough space to install a properly-sized crack-stop hole, and even if there was, the 127 mm (5.00 in.) diameter seems excessive. Given the dimensional constraints the hole would have to be undersized. The 25.4 mm (1.00 in.) diameter hole could serve as a temporary aid to retard the crack from propagating. However, eventually the fatigue crack would reinitiate and propagate away from the edge of the undersized hole until eventual failure of the structural member or additional repair. This situation is often typical for crack-stop hole design scenarios, where the hole diameter needed to completely prevent crack reinitiation is simply too large to be practically implemented.

OBJECTIVE

The objective of this study was to explore the potential for inducing residual compressive stresses in undersized, drilled crack stop holes to extend the fatigue life of steel bridges. The residual stresses are induced through use of a PICK tool. A significant body of work with cold expansion has been developed in the aerospace field over the past three decades, and one of the

www.manaraa.com

goals of this paper was to provide a meaningful link between existing technologies developed for application in the aerospace industry and practical needs within the steel bridge industry.

DEVELOPMENT OF PICK TOOL

A proof-of-concept prototype tool was developed for the laboratory, which utilized ultrasonic piezoelectric actuators. The PICK tool was used to treat Gr. A36 steel fatigue specimens, which consisted of a 3.18 mm (0.125 in.) thick x 760 mm (30.0in.) long plate fabricated with varying width. The minimum width of the cross section was 31.7 mm (1.25 in.), at the center of the plate. A 3.18 mm (0.125 in.) diameter hole was precisely drilled at the center of the specimen and an aluminum plug pressed into the hole. The PICK tool utilizes piezoelectric actuators, which deform proportionally to a harmonic electric signal, inducing a harmonic load large enough to plastically deform the aluminum plug inside the hole, causing the hole to expand. After the hole was plastically expanded, the plug was carefully removed from the hole exploiting the thermal mismatch between steel and aluminum.

The PICK device was powered by a signal generator supplying a sine wave and an amplifier circuit. A strip of piezoelectric material was attached to the rear of the tool to measure the acceleration response of the tool. A strain gage was attached to the inside surface of the vertical element of the PICK tool to measure the strain induced by tightening the bolt and from the sine wave excitation. A calibration curve was developed to establish a relationship between the load applied to the aluminum plug and the strain measured on the PICK tool. This allowed the load imparted from the transducers during application to be directly evaluated. Figure 4 shows the PICK tool and a steel specimen being treated.

المنارة للاستشارات
www.manaraa.com

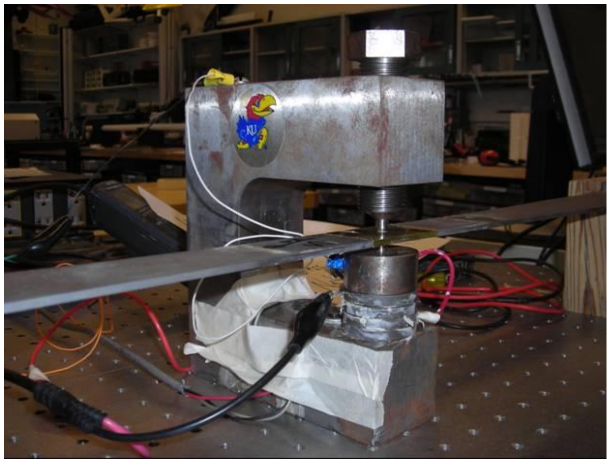

Figure 4 Photograph showing PICK too being used to treat a crack-stop hole is a steel fatigue specimen

The aluminum plug used as expansion media within the crack-stop hole was 3.18 mm (0.125 in.) tall x 3.18 mm (0.125 in.) diameter 6061-T6 aluminum with 276 MPa (40.0 ksi) nominal yield strength. In operation, the plug was pressed into the specimen and the integral bolt tightened on the PICK device until the load was large enough to cause yielding of the aluminum plug. Because the amount of strain energy in the steel is proportional to the strain, a frequency sweep was performed until the measured strain was maximized, at a frequency corresponding to a natural frequency of the PICK device. Operating the tool at this frequency maximizes the distortional energy applied to the steel specimen being treated. Typically, the frequency ranged between 30 – 34 kHz (outside the audible range) and the strain ranged between approximately 220 $\mu\varepsilon$ and 320 $\mu\varepsilon$. The strain values corresponded to loads of 9.56 kN (2.15) kips and 13.9 kN (3.12 kips) on the aluminum plug.

The effect of the deformation on the inside of the hole was evaluated analytically, and compared with results from 2-D and 3-D finite element analyses that examined the performance of uniformly-expanded crack stop holes. The 2-D and 3-D uniform expansion finite element

المنارة للاستشارات
www.manaraa.com

analyses were validated through comparison with similar uniform expansion models performed on aluminum plates, reported in aerospace engineering literature and replicated in this study to serve as a basis for comparison. It should be noted that an ongoing experimental thrust aimed at evaluating the fatigue performance of PICK-treated crack-stop holes is not described in this article. This article has focused instead on the feasibility of achieving sufficient residual stresses and the characteristics of the necessary expansion to have a beneficial effect on fatigue life of steel bridges.

METHODOLOGY

Closed-Form Solutions

Previous analytical investigations of cold expansion [3-4, 11, 13, and 22] have been based largely on two-dimensional approximations. These closed-formed solutions have been applied to both the plain-strain condition of the thick-walled cylinder and the plain-stress condition of holes in infinitely wide plates. These analytical simplifications used both Tresca and von Mises yield criterion with assumptions of either elastic-perfectly-plastic or strain-hardening material properties. An extensive review of these closed-form solution techniques has been performed [14].

Each method reported attempted to quantify and characterize the level of residual stress that could be achieved through cold expansion. Each method of analysis was consistent in showing that a level of residual compressive stress approximately equal to the yield strength of the material could be achieved in the tangential direction near the edge of a hole. These methods have also shown that the residual compressive stresses decay rapidly in the radial direction and ultimately change to tensile stresses at a point referred to as the elastic-plastic boundary, r_p.

المنارة للاستشارات
www.manaraa.com

From these studies, the maximum r_p is shown to occur at approximately one hole diameter away from the hole edge and has been shown to be a function of the varying levels of expansion.

Uniform Expansion of Crack-Stop Holes

A significant body of literature exists describing numerical simulation studies that have been performed with the intent of comparing uniform levels of expansion with existing cold expansion techniques. Most of these studies have simulated the process of split sleeve mandrel cold expansion in aluminum plates, a common application in the aerospace field. For the study described in this article, a similar analysis approach was used to compare uniform expansion of mild steel with expansion created using the PICK tool technique.

The material properties of the aluminum and mild steel uniform expansion models are shown in Table 1. Values reported for the mild steel are from tensile tests performed as part of this study, while the values used for aluminum are from the existing body of literature.

Table 1 Material properties used for models simulating uniform expansion

Material	Modulus of Elasticity, MPa (ksi)	Yield Strength, MPa (ksi)	Ultimate Strength, MPa (ksi)	Poisson's Ratio
Aluminum	77,220 (11,200)	312 (45.2)	440 (63.8)	0.35
Mild Steel	200,000 (29,000)	319 (46.3)	463 (67.2)	0.30

ABAQUS, a general-purpose finite element program capable of nonlinear, large-deflection, plastic analysis, was used as the analytical engine. The first task was to create a 2-D model in ABAQUS with aluminum material properties, with the purpose of corroborating results with

المنارة للاستشارات
www.manaraa.com

those from published studies. After results from the 2-D aluminum model were confirmed, a similar 2-D model was created using material properties for mild steel as determined from standard tension tests.

Previous research has shown that an optimum level of cold expansion of a fastener hole using presently-accepted cold expansion techniques is approximately 4% larger than the original hole size [9,26-27]. The general equation governing the degree of expansion, *i*, is:

$$i = \frac{D_e - D_0}{D_0} \times 100\% \qquad \text{Equation 5.}$$

where D_e is equal to the hole diameter after expansion has occurred, and D_0 is hole diameter prior to expansion. This optimum level of expansion, 4%, is the level at which minimal additional benefit is gained with increased levels of expansion. 2-D mild steel and aluminum models created for this study examined four uniform levels of expansion: 3%, 4%, 5% and 6%.

The uniform expansion ABAQUS models were created using a two step process. To obtain the desired level of uniform expansion in each of the four 2D models, an outward displacement was induced and the inside of the hole was expanded to the levels described previously. Then, the uniform displacement was removed, and a permanently deformed surface with residual stresses remained.

After general behavior was confirmed for the 2-D models, four 3-D models were created to analyze the change in residual stress through the thickness of the specimens under uniform expansion using the same levels of expansion as studied in the 2-D models. The 3-D models were created to have the exact same dimensions and thickness of the 3.18 mm (0.125 in.) thick

المنارة للاستشارات
www.manaraa.com

mild steel fatigue specimens used in axial fatigue tests. Figure 5a shows the mesh geometry in the 3D models, as well the residual stress field around a hole in mild steel plate after 6% uniform expansion.

Plug-Plate-Tool Interaction Model

A 3-D finite element (FE) model was created to examine the plug-plate-tool interaction behavior specific to the PICK method of treatment. The model required the large-displacement, nonlinear, plastic-material capabilities of ABAQUS to perform the analysis and included the aluminum plug and a 50.8 mm (2.00 in) length of the plate. Material properties used were from tension tests of the Gr. A36 plate and from published typical curves [29]. Load was applied as a non-following surface traction to the top and bottom of the plug, and the plate was simply constrained in all directions at discrete locations along the edges. Eight-node, 3-D, hybrid continuum elements with incompatible modes were used in all plug and plate parts. The surfaces between the plug and the plate were modeled as frictionless contact surfaces. To achieve convergence of the highly nonlinear analysis, automatic stabilization was included in all steps by specifying a dissipated energy fraction of 0.004.

The analysis was performed through a series of steps, first loading the plug on its exposed surfaces so that it expanded inside the plate. The restart feature in ABAQUS allowed the converged configuration to become the new base model for the step to remove the plug. In this step, the plug was removed by specifying a linear displacement of both top and bottom surfaces of the plug. After the plug was removed, residual stresses were examined. Figure 5b shows the permanently deformed shapes of the crack-stop hole and plug.

المنارة للاستشارات
www.manaraa.com

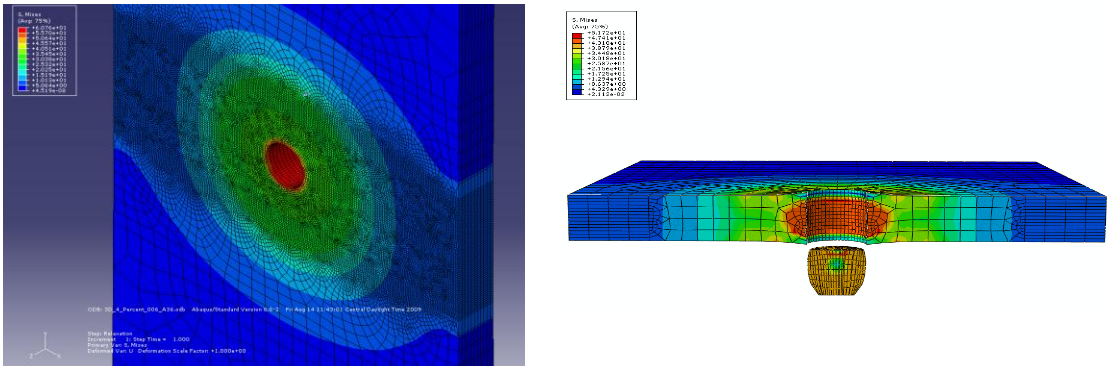

Figure 5 Screen Shots from (a) Three-Dimensional Modeling of Uniform Expansion and Resulting Residual Stresses in a Crack-Stop Hole and (b) Cross-Section View of Plug-Plate-Tool Interaction Model Showing Residual Stresses After Plug Was Loaded and Removed

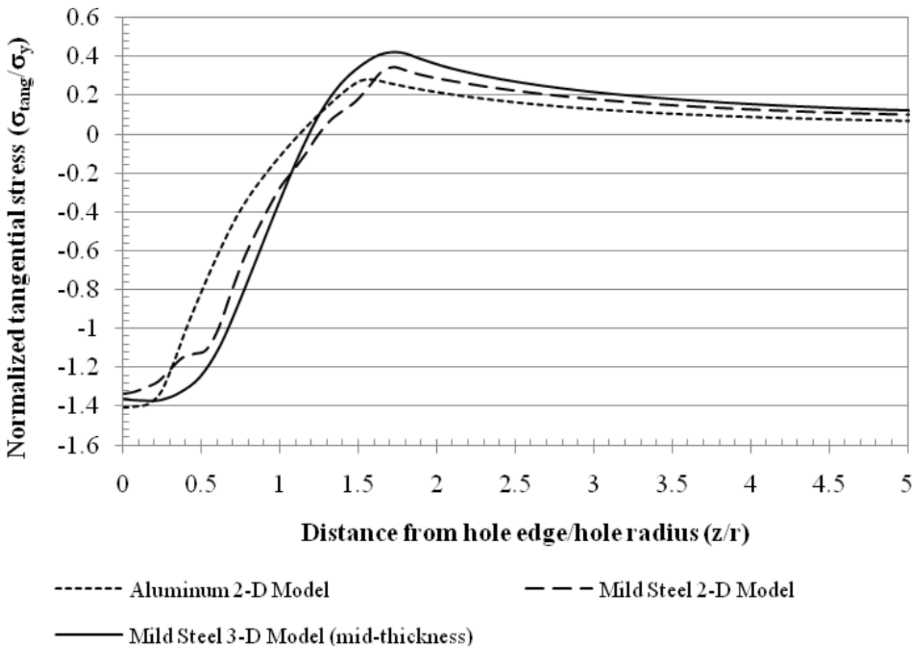

Figure 6. Tangential Residual Stress Normalized with Respect to Material Yield Strength Comparing Model Results for Aluminum and Mild Steel at 4% Uniform Expansion Results and Discussion

RESULTS AND DISCUSSION

Uniform Expansion of Crack-Stop Holes

www.manaraa.com

The results for the 2-D aluminum models were comparable in both shape and magnitude with previously published finite element studies [9,28]. The level of tangential residual stress was shown to be approximately equal to the yield strength of the material and the transition between compressive to tensile stresses was shown to occur at approximately the diameter of the hole away from the edge of the hole. There was a slight difference between the 2-D mild steel and aluminum model results in the shape of the residual tangential stress fields, as highlighted in Figure 6. Results for the 2-D mild steel model showed a slight discontinuity in the curve after the level of residual stress reached a value approximately equal to the yield strength, which was not observed with the aluminum models. This difference is thought mostly to be a result of the yield plateau implemented in the mild steel model. Tangential residual stresses induced by 3%, 4%, 5%, and 6% expansion in the 3-D mild steel model are presented in Figure 7.

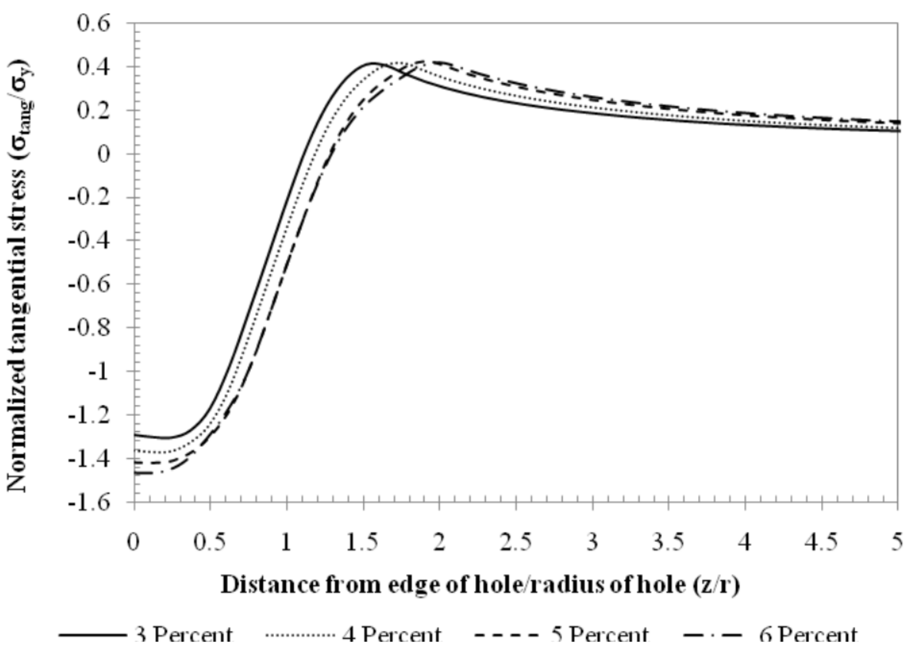

Figure 7. Tangential Residual Compressive Stress Fields Resulting from Uniform Expansion in Mild Steel Three-Dimensional Models

www.manaraa.com

The 3-D model for a uniform 4% expansion in a 3.18 mm (0.125 in.) thick mild steel plate displayed similar results to the 2-D mild steel models at mid-thickness of the plate, as can be noted in Figure 8. However, the level of tangential residual stress achieved at mid-thickness, -437 MPa (-63.4 ksi), was greater than that found at the edges of the plate, -370 MPa (-53.7 ksi). This finding was consistent with results from previous studies [9, 28]. The higher level of tangential stress found at mid-thickness was thought to be a result of the constraint provided by the thickness of the plate.

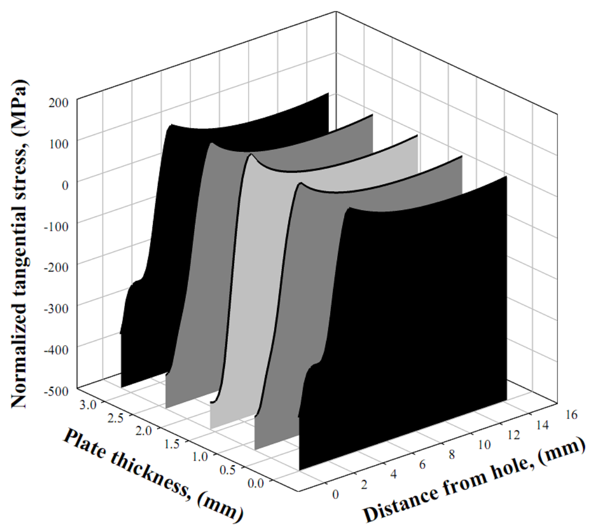

Figure 8 Through-Thickness Residual Stress Distribution 3-D Model with Uniform 4% Expansion

Plug-Plate-Tool Interaction Model

FE analyses of the plug-plate-tool model showed that the PICK device deformed the aluminum plug well into the plastic range causing the plug to develop a barrel shape. As the top and bottom of the plug were compressed, the top and bottom surfaces of the plug deformed inside the corresponding surfaces of the plate, losing contact with the edges of the hole. This resulted in non-uniform expansion of the inner surface of the crack-stop hole. In addition, the analyses also showed that the inside of the hole was expanded well into the plastic range, although not

المنارة للاستشارات
www.manaraa.com

uniformly.

Residual tangential stresses on the inside of the hole in the uniform expansion model were found to vary uniformly through the plate thickness, however, the 3-D plug-plate-tool model showed that the residual tangential stresses were in tension at the surfaces (90 MPa (13 ksi)) and compressive (-270 MPa to -349 MPa (-41.0 ksi to -53.0 ksi)) through the center as a result of the deflected shape of the plug, as detailed in Figure 9.

The expansion from the 3-D plug-plate-tool model analyses was found to be in agreement with the measured expansion for the treated specimen; in the center of the hole, the model and physical measurements both showed approximately 7% expansion. The analyses showed that the maximum expansion was similar to that required to obtain maximum benefit for an undersized hole. However, the analyses also highlighted that the expansion at the plate surfaces was less than that at the center. The measured expansion at the plate surfaces was found to be much less than that needed to significantly improve the fatigue performance of an undersized hole. The difference between the analyses and the measured expansion was likely due to difficulties in perfectly aligning the tool with the plug, and indicates that further refinement of the tool geometry is necessary. Figure 10 presents the amount of expansion determined numerically through the thickness of the plug, as well as measured expansion amounts at top, mid-thickness, and bottom of a treated crack stop hole.

المنارة للاستشارات
www.manaraa.com

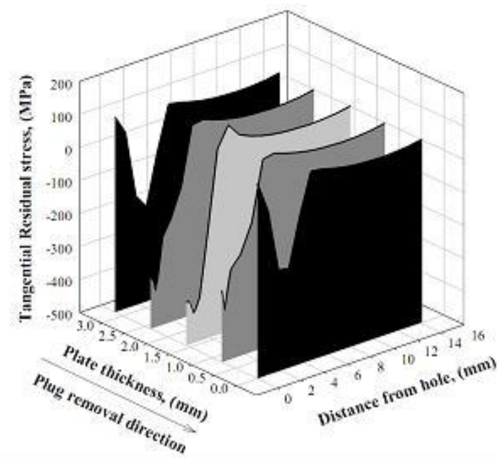

Figure 9 Through-thickness residual stress distribution 3-D plug-plate-tool interaction model

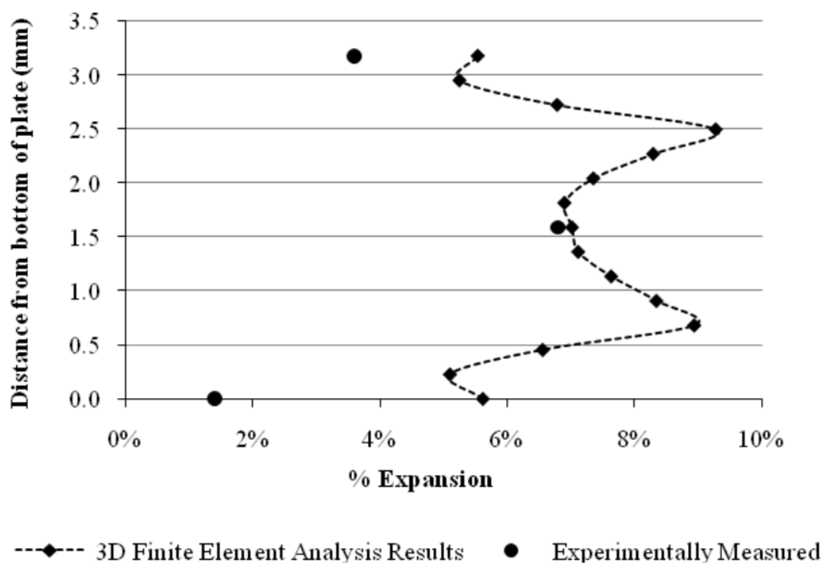

Figure 10 Percent expansion from finite element analysis compared to measured expansion at top, bottom, and mid-depth of treated crack-stop hole

CONCLUSIONS

The results of a study exploring the potential of inducing compressive residual stresses in drilled crack stop holes using an ultrasonic piezoelectric transducer has led to the following conclusions:

المنارة للاستشارات
www.manaraa.com

1. A 4% expansion of crack stop holes in steel plates was found to have a very similar effect to that observed in aluminum plates. This conclusion is based on the similarity of normalized tangential residual stress for both materials. This was an important finding, because it helps to provide a meaningful link between existing research performed in the aerospace engineering literature and current needs within the field of bridge engineering. Results from the 2-D and 3-D uniform expansion modeling can be interpreted to be independent from the particular technique chosen to cold-expand undersized crack stop holes, and can be used in future studies to corroborate detailed finite element analyses and experimental findings for specific techniques applicable to steel bridges.

2. It has previously been shown that the levels of residual stress corresponding to 4% expansion of crack stop holes in aluminum have been sufficient to improve the fatigue performance of fatigue specimens by an order of magnitude. Because of the general overall similarity in behavior of metals subjected to fatigue loading, it is expected that steel specimens will respond similarly to aluminum when crack-stop holes are treated with 4% or more expansion. Therefore, based on the results of this study, it is concluded that significant gains in fatigue capacity may be realized in mild steel when expansion on the order of 4% or more is achieved in crack stop holes.

3. Finite element analyses and physical measurements of treated specimens showed that the prototype PICK device was capable of expanding an undersized, 3.18 mm (0.125 in.) diameter crack stop hole in 3.18 mm (0.125 in.) thick plate between 5% and 9% at the interior of the hole. These levels of expansion in the steel plates modeled are similar to or greater than levels of expansion noted in identical models performed on aluminum plates.

المنارة للاستشارات
www.manaraa.com

4. Detailed 3D Plug-Plate-Tool interaction numerical analyses showed that tensile residual stresses were imparted in the treated crack stop hole at the outer faces of the hole. This was an important finding, because it represents a need to refine the treatment process such that more uniform compressive residual stresses result from treatment. It is also important because great care was taken in the physical development of this technique to produce uniform compressive stresses in the crack-stop hole; therefore, detailed analyses should be performed on all new techniques that may be developed in the future to perform a similar task to ensure that undesirable consequences are not being realized.

5. Although the crack-stop hole examined was "bench-sized," results of this study lend confidence to the ability of the device to be scaled up to treat thicker plate material and larger diameter crack-stop holes, and lend credence to the plug-plate interaction treatment approach chosen.

The technique of cold expansion of holes in metallic structures has already been proven as a highly effective retrofitting technique in the aerospace industry. A suite of 2D and 3D uniform expansion and detailed 3D Plug-Plate-Tool interaction numerical analyses have shown that a new treatment technique was capable of inducing normalized compressive residual stresses of the same order of magnitude in steel structures as those achievable with current techniques used on aluminum structures. Additionally, 2D and 3D uniform expansion models performed as part of this study may be useful to future researchers attempting to achieve compressive residual stresses in steel crack-stop holes using new treatment techniques. Given the success of this technique in the aerospace industry, the potential benefits of using a similar process to improve the fatigue life of existing steel bridges with fatigue cracks are very significant.

www.manaraa.com

ACKNOWLEDGEMENTS:

The authors are grateful for support from the Kansas Department of Transportation (KDOT) and the University of Kansas Transportation Research Institute (KU TRI). The authors would also like to appreciatively acknowledge support provided though Pooled Fund Study TPF-5(189), which includes the following participating State DOTs: Kansas, California, Iowa, Illinois, New Jersey, New York, Oregon, Pennsylvania, Tennessee, Wisconsin, and Wyoming, as well as the Federal Highway Administration.

REFERENCES:

1. Domazet, Z. (1996). "Comparison of fatigue crack retardation methods." Engineering Failure Analysis, 3(2), 137-147.

2. Vulić, N., Jecić, S., and Grubišić, V. (1997). "Validation of crack arrest technique by numerical modeling." International Journal of Fatigue, 19(4), 283-291.

3. Kim Roddis, W.M. & Zhao, Y. (2003). "Finite-element analysis of steel bridge distortion-induced fatigue." Journal of Bridge Engineering, 8(5), 259-266.

4. Zhao, Y. & Kim Roddis, W.M. (2007). "Fatigue behavior and retrofit investigation of distortion-induced web gap cracking." Journal of Bridge Engineering, 12(6), 737-745.

5. Hu, Y., Shield, C.K. and Dexter, R.J. (2005). "Use of adhesives to retrofit out-of-plane distortion at connection plates." Journal of the Transportation Research Board., CD 11-S, 419-427.

6. Amrouche, A., Ghfiri, R., Imad, A., & Mesmacque, G. (2000). "Fatigue life estimation after crack repair in 6005 A-T6 aluminum alloy using the cold expansion hole technique." Fatigue Fract. Engr. Mater. Struct., 23, 991-916.

7. de Matos, P. F. P., McEvily, A. J., Moreira, P. M. G. P., and de Castro, P. M. S. T. (2007). "Analysis of the effect of cold-working of rivet holes on the fatigue life of an aluminum alloy." International Journal of Fatigue, 29(3), 575-586.

8. Forgues, S. A., Bernard, M., and Bui-Quoc, T. (1993). "3-d axisymmetric numerical analysis and experimental study of the fastener hole coldworking process." Computer Methods and Experimental Measurements for Surface Treatments Effects, edited by C. A. Brebbia and M. H. Aliabadi, Engineering Sciences, (2), Computational Mechanics Publications, Southampton, UK, 61-70.

المنارة للاستشارات

www.manaraa.com

9. Herman, R. & Ozdemir, A.T. (1999). “Effect of expansion techniques and plate thickness on near-hole residual stresses and fatigue life of cold expanded holes.” Journal of Material Science. 34, 1243-1252.

10. Landry, M. A., Armen, H. Jr., and Eidinoff, H. L. (1986). "Enhanced Stop-Drill Repair Procedure for Cracked Structures." Fatigue in Mechanically Fastened Composite and Metallic Joints, ASTM STP 927, edited by J. M. Potter, American Society for Testing and Materials, Philadelphia, PA, 190-220.

11. Pavier, M. J., Poussard, C. G. C., and Smith, D. J. (1999). "Effect of residual stress around cold worked holes on fracture under superimposed mechanical load." Engineering Fracture Mechanics, 63(6), 751-773.

12. Shin, C.S., Song, P.S., & Wang, C.M. (1996). “Fatigue damage repair: a comparison of some possible methods.” International Journal of Fatigue, 18(8), 535-546.

13. Zhang, Y., Fitzpatrick, M. E., and Edwards, L. (2005). "Analysis of the Residual Stress around a Cold-expanded Fastener Hole in a Finite Plate." Strain, 41(2), 59-70.

14. Ball, D. & Lowry, D.R. (1998). “Experimental investigation on the effects of cold expansion of fastener holes.” Fatigue Fract. Engr. Mater. Struct., 21(1), 17-34.

15. Poolsuk, Saravut. (1977). "Measurement of the elastic-plastic boundary around coldworked fastener holes," thesis, presented to Michigan State University at East Lancing, MI, in partial fulfillment of the requirements for the degree of Doctor of Applied Mechanics.

16. Reemsnyder, H.S. (1975). “Fatigue life extension of riveted connections.” ASCE Journal of the Structural Division, 101(12), 2591-2608.

17. Huhn, H. and Valtinat, G. (2004). “Bolted connections with hot dipped galvanized steel members with punched holes.” Proceedings of the ECCS/AISC Workshop, Connection in Steel Structures V: Innovative Steel Connections, June 3-5,2004. Amsterdam: European Convention for Construction Steelwork/American Institute of Steel Construction.

18. Brown, J.D., Lubitz, D.J., Cekov, Y.C., Frank, K.H., and Keating, P.B. (2007). “Evaluation of influence of hole making upon the performance of structural steel plates and connections.” Center for Transportation Research, Texas, Project: 0-4624, CTR Technical Report:0-4624-1. 236 p. Sponsored by the Texas Department of Transportation.

19. Statnikov, E.S. (2004). “Physics and mechanisms of ultrasonic impact treatment.” IIV Document XIII-2004-04, International Institute of Welding, Paris, France.

20. Phillips, J.L. (1974). “Sleeve cold working fastener holes, Vol. 1.” AFML-TR-74-10, Air Force Materials Laboratory, Wright-Patterson AFB OH.

21. Engineering manager. Fatigue Technology, Inc., Seattle, WA, 98188.

المنارة للاستشارات
www.manaraa.com

22. Leon, A. (1998). "Benefits of split mandrel coldworking." International Journal of Fatigue, 20(1), 1-8.

23. Barsom, J.M & Rolfe, S.T. (2006). Fracture and Fatigue Control in Structures: Application of Fracture Mechanics Third Edition. ASTM, West Conshohocken, PA.

24. Creager, M. (1966). "The elastic stress field near the tip of a blunt crack," Measter Science thesis, Lehigh University, Bethlehem, PA.

25. Poussard, C., Pavier, M. J., and Smith, D. J. (1995). "Analytical and finite element predictions of residual stresses in cold worked fastener holes." Journal of Strain Analysis for Engineering Design, 30(4), 291-304.

26. Poussard, C. G. C., Pavier, M. J., and Smith, D. J. (1994). "Prediction of residual stresses in cold worked fastener holes using the finite element method." Proceedings of the 2nd Biennial European Joint Conference on Engineering Systems Design and Analysis, 8(A) ASME, New York, N.Y., 47-53.

27. Ozelton, M. W., and Coyle, T. G. (1986). "Fatigue Life Improvement by Cold Working Fastener Holes in 7050 Aluminum." Fatigue in Mechanically Fastened Composite and Metallic Joints, ASTM STP 927, edited by J. M. Potter, American Society for Testing and Materials, Philadelphia, PA, 53-71.

28. de Matos, P. F. P, Moreira, P. M. G. P., Camanho, P. P., and de Castro, P. M. S. T. (2005). "Numerical simulation of cold working of rivet holes." Finite Elements in Analysis and Design, 41(9-10), 989-1007.

29. Boyer, H. E. (1987). Atlas of Stress Strain Curves. ASM International(OH).

المنارة للاستشارات
www.manaraa.com

CHAPTER 4: DEVELOPMENT OF A TECHNIQUE TO IMPROVE FATIGUE LIVES OF CRACK-ARREST HOLES IN STEEL BRIDGES – FATIGUE AND METALLURGICAL RESULTS

ABSTRACT

A new technique to improve the performance of crack-arrest holes to stop fatigue crack propagation is presented. The historical background for one detail that is susceptible to fatigue cracking is provided as an example of the seriousness of the problem. Repair options for fatigue cracks are discussed including crack-arrest holes. The new technique consists of cold expanding the inside of the crack-arrest hole and subjecting the inside of the hole to ultrasonic vibration using piezoelectric elements. This procedure was termed Piezoelectric Induced Compressive Kinetics (PICK) and was conducted as a proof-of-concept, laboratory study using 3.2 mm (1/8-in) thick steel bars. The effectiveness of this technique was assessed by comparing the result of fatigue testing; three types of fatigue specimens were tested: untreated specimens were used as control specimens; some were only mechanically expanded, and others were PICK treated. In addition to the fatigue testing, metallurgical examination, measuring retained expansion, and monitoring load decay were used to determine the physical changes caused by the PICK process that resulted in the improved fatigue performance. The metallurgical examination consisted of grain size analysis and hardness testing. The compressive residual stresses resulting from the PICK treatment are discussed in detail in Simmons 2013. The conclusion of this study was that the PICK treatment would increase the fatigue initiation life of reduced-scale, laboratory specimens.

www.manaraa.com

INTRODUCTION

The principal loads on bridges are dead loads from the weight of the bridge materials and live loads from traffic across the bridge. Depending on span length, the ratio of live-to-dead loads can be determined from McGuire (1968) to be approximately 1 to 3. From these live-to-dead load ratios, the time-varying stresses from live loads could approach 50-80% of the allowable stress in the steel. Such fluctuating stresses may cause fatigue cracks to initiate in steel bridges if fatigue was not properly accounted for in the design. Fatigue cracks, in fact, currently exist or will form in numerous highway bridges in the United States. The Federal Highway Administration (FHWA) has governmental oversight responsibility for the maintenance for more than 120,000 steel highway bridges with welded details. According to the 2001 National Bridge Inventory, approximately 14% of the inventory, or 16,800 bridge structures, may be structurally deficient (FHWA 2001). The major problems causing bridges to be labeled structurally deficient are the presence of fatigue-sensitive details, the need to increase service loads, corrosion, and lack of proper maintenance (Tavakkolizadeh and Saadatmanesh 2003). There is significant need in the nations steel bridge infrastructure to address damage due to fatigue.

One technique to arrest fatigue crack propagation is to drill a hole (crack-arrest hole) at each end of the fatigue crack. Separate expressions have been developed by Rolfe and Barsom (1977) and Fisher et al. (1980; 1990) which describe crack-arrest hole diameters large enough to arrest further crack propagation. In Kansas, common practice is to drill crack-arrest holes having diameters ranging from 19 mm (¾ in) to 38.1 mm (1½ in). Unfortunately, the crack-arrest hole diameter determined though the Rolfe and Barsom (1977) or Fisher et al. (1980; 1990) expressions may be so large that a hole with the "correct" diameter may not be practical or fit in

المنارة للاستشارات
www.manaraa.com

the space available.

OBJECTIVE

The objective of this research was to develop a new technique to cold-expand and treat crack-arrest holes such that a hole with a smaller-than-required diameter would gain effectiveness in halting further crack propagation. The technique investigated to expand and treat the undersized hole has been termed Piezoelectric Induced Compressive Kinetics (referred to herein as PICK) and, in general, consists of the following steps in the laboratory:

1. Drilling a hole in a fatigue specimen made from steel plate,
2. Driving an oversized aluminum plug into the hole,
3. Compressively loading the aluminum plug to develop plastic stresses in the aluminum plug and in the adjacent steel specimen,
4. Using multiple piezoelectric elements to further load and deform the plug while subjecting the aluminum plug and the steel around the hole to ultrasonic vibration, and
5. Removing the aluminum plug from the steel specimen.

It was hypothesized that this process would produce three separate results, all of which would contribute to prevention of crack reinitiation and propagation. First, the compressive force on the plug during cold-expansion was expected to induce tensile stresses in the circumferential direction around the hole; these tensile stresses would become compressive residual stresses when the plug is removed. Second, cold-expansion causes work-hardening, which increase both

المنارة للاستشارات
www.manaraa.com

the yield and ultimate strength of the steel. Third, energy input in the form of ultrasonic vibration from the piezoelectric elements may also increase the yield strength of the steel. This paper focuses on the design, fabrication, operation, and results of the tool (PICK tool) used to produce an improvement in fatigue life from cold-expansion, work-hardening, and ultrasonic vibration. This paper describes the PICK process and evaluates the effectiveness of the PICK tool by assessing the results from fatigue testing, measured retained expansion, hardness testing, and metallurgical examination. The stresses / strains induced by the PICK tool and the resulting residual stresses / strains are discussed in another paper (Simmons 2013)

BACKGROUND

One reason that fatigue cracks are an issue with bridges is that the conditions which lead to fatigue cracks were not addressed by codes or adopted in practice until recently. For example, one detail which produces a large percentage of the fatigue cracks in steel plate-girder bridges is the gaps left between connection stiffeners and the girder flanges when the connection stiffeners are welded to the girder web but not to the flanges. When asymmetric loading is applied to adjacent girders, torsion develops about the longitudinal axis of the girders resulting in bending in the girder webs at these gaps. This bending from the cyclic, asymmetric loading results in distortion-induced fatigue cracking (DIFC) in the girder webs (Fig. 1).

المنارة للاستشارات
www.manaraa.com

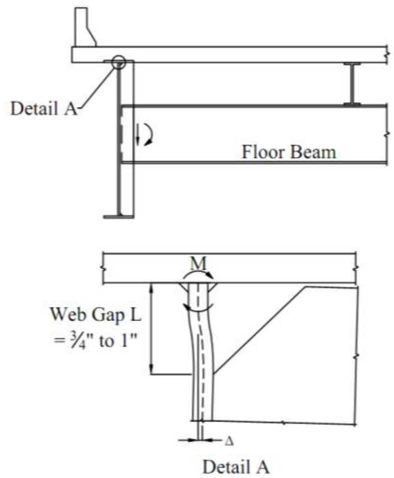

Figure 1. Distortion in the Web Gap

Fisher and Keating (1989) state that the practice of leaving a gap between the connection stiffener and flanges was the result of bridge failures in Europe in the late 1930s and further cite as an example the Hasselt Bridge. The Hasselt Bridge was composed of Vierendeel trusses shaped like a tied arch, in that the top chords were arched and the bottom chords served as tie members (Akesson 2008). The vertical members between the top and bottom chords were welded to the respective chords instead of having pinned connections as in a true truss. The bridge was commissioned in January, 1937, and collapsed at 8:20 am on March 14, 1938, when the temperature was –20 ^{o}C (-4 ^{o}F) and a tramcar and several pedestrians were on the bridge (Maranian 2010). The initial crack started in the tension flange of the lower chord at a butt-weld between a vertical member and the lower chord (Hayes 1996). Shortly thereafter the bridge broke into three pieces and fell into the Albert Canal.

As a result of the failure of the Hasselt Bridge, it became standard practice in the United States to not weld connection stiffeners to the tension flanges of the main girders. Steel design texts and design guides recommended leaving a gap between the connection stiffeners and the tension

www.manaraa.com

flange as late as 1972 (McGuire 1968 and Merritt 1972). Roddis and Zhao (2001) presented a concise history of the detailing of the connection plates in which they described that the *AASHTO Standard Specification for Highway Bridges* did not require welding connection stiffeners to the girder flanges until the 1985 Interim (AASHTO 1985). Even with this change, it took several years for these details to become accepted practice; for example, the Kansas Department of Transportation (KDOT) did not begin to weld or bolt connection plates to both top and bottom flanges of plate girders until 1989 (Roddis and Zhao 2001). The result was that, from approximately 1940-1990, a fatigue-prone detail (DIFC) was often used in welded bridges and, as a result, these bridges were and are susceptible to fatigue cracking.

Once fatigue cracks occur, they should be repaired or monitored for crack growth. Numerous approaches have been used to repair fatigue cracks (Roddis and Zhao 2001). Repair options have included replacing the affected member or re-welding the crack. Replacing a member may be difficult, as the bridge may have to be taken out of service, the bridge deck removed, the member replaced, and the deck reinstalled. Re-welding or filling the fatigue crack with weld material requires grinding out the crack and any associated welds, filling the crack with weld material, and grinding the new weld surfaces smooth. Access and quality field welding often present difficult problems with these welded solutions. Crack-arrest holes are also an appropriate solution if the holes are drilled large enough to effectively prevent crack reinitiation. At locations where cracking is caused by DIFC, techniques that have been used include stiffening web gap regions, softening web gap regions, removing or repositioning lateral bracing and diaphragms, or even loosening bolts at the cross frame to web connections (Roddis and Zhao 2001). Another alternative for repairing DIFC-related fatigue cracks that has been used is to

المنارة للاستشارات
www.manaraa.com

install splice plates connecting the connection stiffeners to the flanges and/or the girder web.

Crack-Arrest Hole Formulae

Drilling a hole at the tip of a fatigue crack increases the radius of the crack tip from infinitely small to the radius of the hole; this may blunt the crack tip to an extent that crack growth is stopped. There are two formulae in the literature that may be used to determine the required radius for the hole to effectively arrest crack growth. Both formulae relate the radius of the hole to: the yield strength of the steel; the range of the stress intensity factor; and the half-length of the crack, but use a different experimentally derived constant (Eqn. 1). This equation was originally developed in Rolfe and Barsom (1977) and is also found in Barsom and Rolfe (1999). They performed multiple, uniaxial, cyclic-tension tests on several identical sets of steel plates with edge notches. Within each identical set, the edge notch radii were different for each plate but the edge notch lengths were all the same. The yield strengths of the each set of steel plates was different and varied between 248 MPa (36 ksi) to 758 MPa (110 ksi). This plate geometry with the uniaxial loading results in Mode I type fracture, where Mode I fracture is a tension-opening crack. The second is found in Fisher et al. (1980; 1990). Fisher et al. (1980; 1990) conducted a series of full-scale tests on steel wide flanges and plate girders, all with 248 MPa (36 ksi) yield strength. These tests subjected the wide flanges and plate girders to both in-plane bending stresses and out-of-plane distortion stresses; the combination resulted in DIFC.

The equation developed by Rolfe and Barsom (1977) from testing is:

$$\frac{\Delta K}{\sqrt{\rho}} = C\sqrt{\sigma_{ys}}$$

Equation 1

Where:

المنارة للاستشارات
www.manaraa.com

C = constant from testing with Rolfe and Barsom (1977) and Fisher et al. (1980) developing different values for C (seeTable 1),
ρ = required radius of the hole to arrest crack reinitiation,
σ_{ys} = yield strength of the steel,
ΔK = the range of the stress intensity factor. For the edge-notch configuration used by Rolfe and Barsom (1977), the range of the stress intensity factor can be determine by:

$$\Delta K = \Delta\sigma\sqrt{\pi a}$$

where

$\Delta\sigma$ = stress range (σ_{max}-σ_{min}) for the fluctuating stresses,
a = the length of the edge crack.

When $\Delta K = \Delta\sigma\sqrt{\pi a}$ is substituted into Eqn. 1, Eqn. 2 results:

$$\frac{\Delta\sigma\sqrt{\pi a}}{\sqrt{\rho}} = C\sqrt{\sigma_{ys}}$$

Equation 2

This can be re-arranged in terms of ρ and a as presented in Eqn. 3:

$$\rho = \frac{\pi \cdot \Delta\sigma^2}{\sigma_{ys} \cdot C^2}(a)$$

Equation 3

Even though using different testing programs, Fisher et al. (1980; 1990) used the same formula but developed different values for C. Since C was derived from testing, the values for C depend on using consistent units. Table 1 provides the appropriate units and the corresponding values for C from Rolfe and Barsom (1977) and from Fisher et al (1980; 1990), and Dexter (2004).

Table 1. Values for *C* and Units for Crack-Arrest Hole Equations

Units	C – Rolfe and Barsom (1977)	C – Fisher et al. (1980)	□□	□ys	a	□
SI	26.3	10.5	MPa	MPa	mm	mm
US	10	4	ksi	ksi	in	in

www.manaraa.com

The differences in the parameters used in development of the two values of *C* between Rolfe and Barsom (1977) and Fisher et al. (1980; 1990) are presented and discussed in Simmons (2013). An extension to the formula to include the diameter of the crack-arrest hole with the crack length is also included in Simmons (2013).

As previously discussed, typical practice in Kansas is to drill a hole with diameters from 19 mm (¾ in) to 38 mm (1½ in) (Fig. 2); unfortunately, these hole diameters are often not large enough to arrest crack propagation, and the fatigue crack eventually reinitiates and continues to propagate on the other side of the hole (Fig. 3).

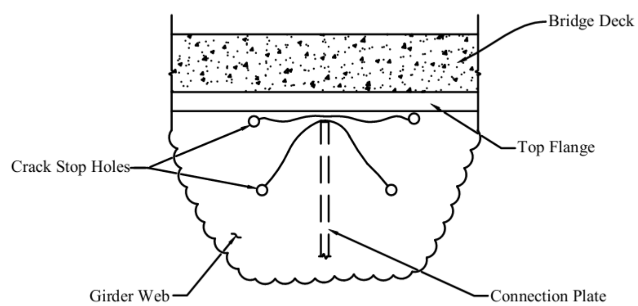

Figure 2. Crack-Arrest Holes at Fatigue Cracks (Roddis and Zhao 2001)

المنارة للاستشارات
www.manaraa.com

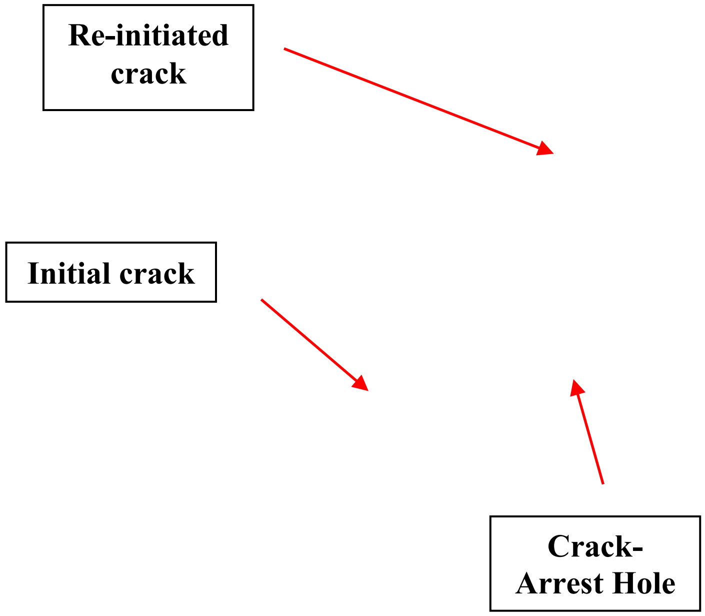

Figure 3. Fatigue Crack Reinitiating through Crack-Arrest Hole (Dexter 2004)

Reinforcing Crack-Arrest Holes

Two techniques, mechanical expansion of the hole and installation of interference fit fasteners, have been developed in the aerospace industry to be used to make an undersized hole perform as well as a full sized hole with respect to limiting fatigue propagation. Mechanical expansion is an accepted technique to reinforce bolt and/or rivet holes in aluminum aircraft members during both manufacturing and maintenance to keep fatigue cracks from developing or to extend fatigue life in the presence of existing cracks. A literature review did not produce any examples in which mechanical expansion has been used outside the aircraft industry but, from a personal conversation with L. Reid of Fatigue Technology, mechanical expansion has recently been used on railroad tracks and bridges (Reid 2011). This technique is being used by railroads to improve the fatigue performance of the bolt holes in connections joining rail sections and it has been used on one bridge structure, an elevated section of a highway in California (Reid 2011). The Fatigue

www.manaraa.com

Technology mechanical expansion process utilizes a split-sleeve with a tapered mandrel system that consists of a solid, tapered mandrel and an internally lubricated split sleeve. The split sleeve is placed on the small end of the tapered mandrel and the tapered mandrel with split-sleeve one it are placed in the hole with the large end of the tapered mandrel going in first. An external force is then applied to the small end of the tapered mandrel and the large end of the mandrel is pulled through the split-sleeve causing the sleeve and hole to expand and plastically deform the inside of the hole in both the radial and tangential directions. The sleeve is then withdrawn. This results in cold-working the inside diameter of the hole and induces residual, compressive stresses tangentially and radially around the hole. Both the cold-working and the residual compressive stresses act to retard crack initiation and crack propagation.

Use of interference fit fasteners is currently limited to the aircraft industry where they are applied to improve fatigue performance of drilled holes; their use has not translated to bridges or other civil structures (Bontillo 2011). Interference fit fasteners consist of a tapered bolt and an internally tapered and flanged outer-sleeve, which is ground straight externally for use in a straight-sided hole. The interference fit is achieved by tightening the bolt, forcing the taper of the bolt to work against the taper of the sleeve. Fatigue tests have shown an increase in fatigue life with interference fit fasteners by a factor of 10 ($1x10^5$ cycles to $1x10^6$ cycles) (Lanciotti and Polese 2005).

Strain Hardening, Work-Hardening, and Hardness Testing

Strain hardening is depicted in Fig. 4, which represents a portion of an idealized stress-strain curve for a strain-hardening steel. If point □yt in Fig. 4 is the yield stress in tension, strain hardening occurs with increasing deformation and stress beyond □yt. If stress is reduced after

المنارة للاستشارات
www.manaraa.com

the onset of strain hardening at □yt, the stress-strain relationship unloads with the same slope as the elastic portion of the stress-strain curve (Point A to Point B). If unloading does not progress beyond Point B to yielding in compression at Point C, reloading follows back along the same path as unloading until the previous high stress, Point A, is reached. Further loading beyond Point A continues with the same strain hardening behavior as previously. The stress at which strain hardening begins after unloading and reloading is approximately the same value that was reached before unloading occurred, Point A, and is higher than initial yielding, □yt.

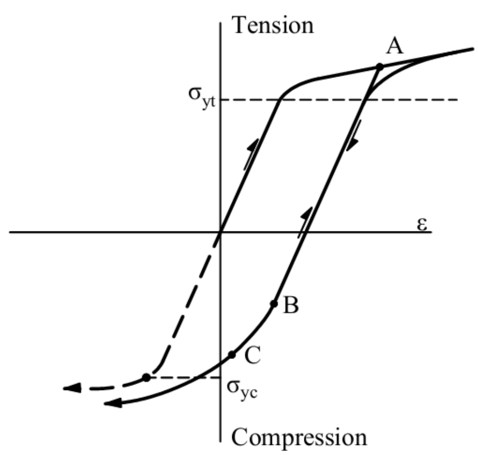

Figure 4. Stress / Strain with strain hardening for a strain hardening steel

Work-hardening (also called cold-working) is severe plastic deformation by a controlled mechanical operation (e.g. rolling or drawing) performed at ambient temperature for the purpose of shaping a product. Work-hardening elongates the grains of the material in the direction of working, while flattening the grains perpendicular to the direction of working (see Fig. 5). Work-hardening increases dislocation density, vacancies, stacking faults, and twin faults; however, most of the energy from work-hardening appears to be expended in increasing the dislocation density (Dieter 1989). An annealed metal has a dislocation density of $1x10^6 – 1x10^8$

المنارة للاستشارات
www.manaraa.com

dislocations per cm^2 (Dieter 1989). After work-hardening with severe plastic deformation of ~10%, the dislocation density increases to $1x10^{12}$ dislocations per cm^2 (Dieter 1989). Work-hardening with grain deformation and increase in dislocation density raises the yield stress, ultimate stress, and hardness while reducing elongation and reduction in area (Dieter 1989), as depicted in Fig. 6. The plastic deformation associated with work-hardening also results in strain hardening.

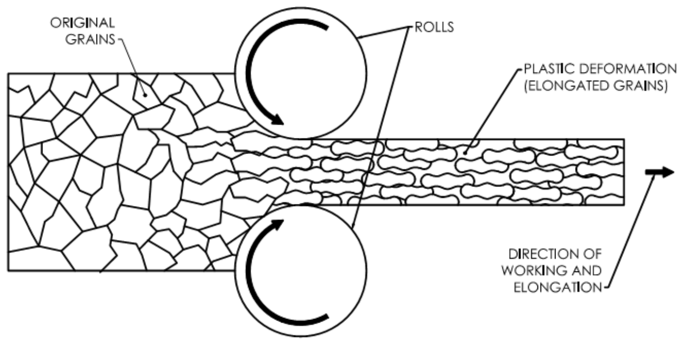

Figure 5. Work-Hardening by rolling (Moniz 1994)

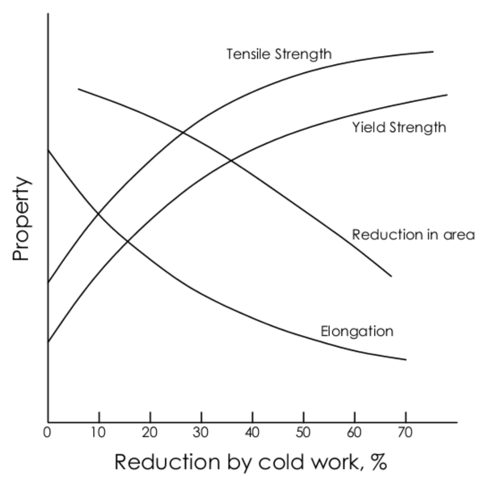

Figure 6. Variation of Tensile Properties with Amount of Work-Hardening (Dieter 1989)

Because of the small volume affected, measuring work-hardening on the inside surface of a crack-arrest hole is not possible with standard testing techniques such as reduced-size tension

www.manaraa.com

tests. One method to qualitatively assess the existence and extent of any work-hardening is with hardness measurements. Hardness can be measured with an indenter; several types are available but all measure the depth and/or width of an indention with a ball-, pyramid-, or a diamond-shaped indenter into the surface of an object. In steel specimens, the indenter only disturbs the top few grain layers but, for these top few grain layers, the indentations impose a triaxial state of stress and plastic deformation with strains in the range of 30% or more (Richards 1961). Empirical relationships exist to relate the hardness values of the different indenters to each other (ASTM E140) and to the ultimate strength (F_u) of the metal (Moniz 1994). Because the indenter readings are physically related to plastic deformation of the material, the hardness readings can only be related to the ultimate strength; no empirical relationship exists between the indenter hardness values and the yield stress.

Piezoelectric Material and the Effects of Ultrasonic Waves on Metals

Pierre and Jacques Curie first identified the direct piezoelectric effect in 1881 when they showed that a quartz crystal produced an electric current when subjected to pressure. The converse piezoelectric effect, that a voltage applied to a quartz crystal would produce expansion in the crystal, was reported the next year. This property can be introduced into certain other materials containing dipole elements by 'poling', which consists of raising the material above the Curie temperature, applying a strong electric field across it, and cooling the material below the Curie temperature while maintaining the electrical field. This process changes the dipoles which are arrayed in a random direction before poling and fixes them so that they are aligned in the direction of the electrical field. After poling to align and fix the dipoles, the material will act as a piezoelectric material and exhibit both the direct and converse piezoelectric effects (Srinivasan and McFarland 2001).

المنارة للاستشارات
www.manaraa.com

Various researchers have reported changes in yield strength and tensile strength when metals are subjected to ultrasonic vibration while under tensile loads. Langenecker (1966) reported that ultrasonic vibration can both soften and harden metals. He documented that softening, which he termed acoustic softening, occurred immediately when zinc crystals were subjected to ultrasonic vibration above certain minimum energy levels during static tension testing under deformation control. The tension stress required for continued straining dropped abruptly when the ultrasonic vibration was applied and returned to the original linear-elastic stress-strain curve when it was removed. Above higher energy inputs, softening occurred during ultrasonic vibration but, when it was turned off, the stress required to produce additional strain was above the original elastic stress-strain curve. Langenecker labeled this effect acoustic hardening.

Nevill and Brotzen (1957) subjected low-carbon steel to ultrasonic vibration while testing the steel in tension. They used annealed, 0.9 mm (20-gage) (0.04-in) diameter wire in a small tension testing machine under deformation control. The wire was tensioned and ultrasonic vibration applied along the axis of the wire for short time intervals. Nevill and Brotzen (1957) reported that the stress necessary to initiate plastic deformation was reduced by the introduction of the ultrasonic vibration. The reduction in stress was proportional the amplitude of the vibration, but independent of frequency within the range of 15 kHz to 80 kHz, of temperature between 30^0C (86^oF) and 500^0C (932^oF), and of prior strain for values of average permanent elongation up to 15%.

المنارة للاستشارات
www.manaraa.com

METHODOLOGY

It was decided to focus the current research on a proof-of-concept study using a reduced-scale, laboratory-compatible PICK tool and fatigue specimens to determine viability of the technique. While multiple techniques would be used to evaluate the PICK tool performance, the most conclusive way to evaluate changes in fatigue performance as a result of treatment by the PICK tool would be fatigue testing treated specimens. The desired measurement was an improvement in fatigue performance of undersized, crack-arrest holes; however, it was thought that inducing a controlled crack and drilling holes at the crack tips would be a complex, time-consuming operation and would increase the size of the specimen and time-to-failure of the fatigue testing. Since the objective was to study crack initiation from a hole at the tip of an existing crack, it was decided that the same effect could be evaluated without inducing a crack but by drilling a hole in a location that would be designed to be susceptible to fatigue cracking and counting the load cycles for fatigue cracks to initiate at the either edge of the hole. This also eliminated the length of the crack as a variable. The specimen was designed to incorporate these details and to fit the universal testing machine (UTM) available for the fatigue testing. When the details for the fatigue specimens were fixed, the PICK tool was designed to be compatible.

Hardware Description

Fatigue Specimens

As the majority of plate girder bridges susceptible to fatigue cracking are older structures, it was decided to use Gr. A36 steel with yield strength of approximately 250 MPa (36 ksi) for the fatigue specimens. The actual material properties were determined for the steel per standard tension testing requirements for flat bars (ASTM E8-04), but the material properties used for the

www.manaraa.com

aluminum plug, which was 60601-T6, were from the literature (Boyer 1987). Both were reported in Crain et al. 2010 and are reproduced in Table 2.

Table 2. Material Properties for A-36 Steel and 6061-T6 Aluminum (Crain et al 2010)

Material	Modulus of Elasticity, MPa (ksi)	Yield Strength, MPa (ksi)	Ultimate Strength, MPa (ksi)	Poisson's Ratio
Aluminum	77,220 (11,200)	312 (45.2)	440 (63.8)	0.35
Mild Steel	200,000 (29,000)	319 (46.3)	463 (67.2)	0.30

The test specimens were fabricated from a 3.2 mm (1/8-in) thick steel bar and, to ensure the fatigue cracking occurred at the center of the specimen, the width of the specimens narrowed from 53 mm (2 in) at the ends to 32 mm (1-1/8 in) at the center (Fig. 7). Holes with diameters of 3.2 mm (1/8 in) were drilled and reamed at the center of each specimen at the minimum width with the expectation that fatigue cracking would initiate at this location first with the cracks oriented perpendicular to the long axis of the specimen and initiating at the inside edges of the hole. The ends of the specimens were reinforced to prevent bearing or fatigue failure at the ends rather than fatigue cracking at the center.

Aluminum Plug

The aluminum plug was cut from aluminum dowel stock with a slightly larger diameter than the 3.2 mm (1/8-in) diameter holes with the length slightly longer than the 3.2 mm (1/8-in) thickness of the bar

المنارة للاستشارات
www.manaraa.com

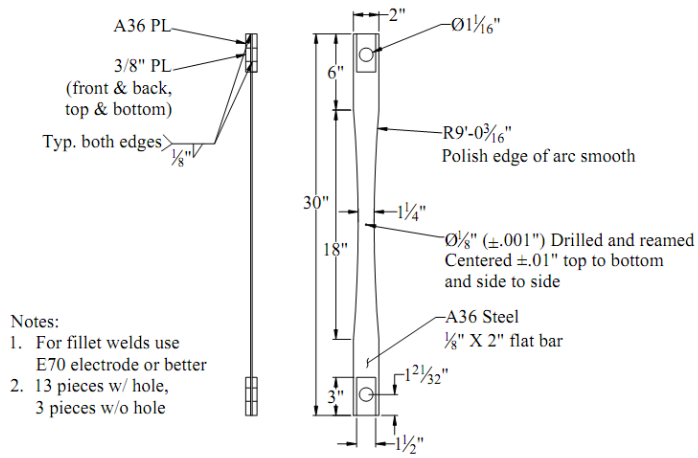

Figure 7. Fatigue test specimen

PICK Tool

The PICK tool was designed to compress the aluminum plug, hold this force on the plug, and provide a stiff reaction platform to focus the ultrasonic vibration into the aluminum plug and the steel fatigue specimen. The tool needed to be stiff to ensure that most of the energy went into the specimen and was not absorbed by the tool. The tool was bench mounted with its major features being the C-shaped base, threaded bolt, piezoelectric elements, and a round, load-transfer plate (shown in Figs. 8 and 9). The base and the other steel components were machined from 4140 annealed steel with yield strength of 412 MPa (60 ksi) and with dimensions as shown in Fig. 8. The end of the bolt was machined to form a 3.2 mm (1/8-in) diameter tip to match the 3.2 mm (1/8-in) plug; force was applied to the plug by tightening the bolt at the top of the tool thereby pressing the tip into the aluminum plug. The tip of the bolt proved to be too soft and deformed excessively; therefore, the tip was replaced with a hardened dowel pin which was pressed into a hole drilled into the tip of the bolt. The tip of the dowel pin was machined into a truncated-cone shape with the smaller end fitting on the end of the aluminum plug. Underneath the fatigue

www.manaraa.com

specimen was a round, load-transfer plate, which was machined to fit on top of a nylon rod and to fit tight with the top of the piezoelectric stack beneath it. A hardened steel rod with a tip also machined to 3.2 mm (1/8-in) diameter was pressed into the top of the round, load-transfer plate and completed the load path through the aluminum plug. The piezoelectric elements were stacked and held in place with the nylon rod. The ultrasonic force developed by the piezoelectric elements was transmitted through the round, load-transfer plate and focused into the aluminum plug and steel fatigue specimen.

A Micro-Measurements strain gage (EA-06-062AQ-350) and a small strip of piezoelectric material (7.5-mil thick strip of PZT-5A from Piezo Systems) were attached to the PICK tool. The strain gage was glued to the flat section on the inside surface of the vertical upright of the PICK tool so that the gage measured bending strain. The piezoelectric strip was aligned vertically and glued to the vertical leg of the tool on the back surface opposite the strain gage, as shown in Fig. 8.

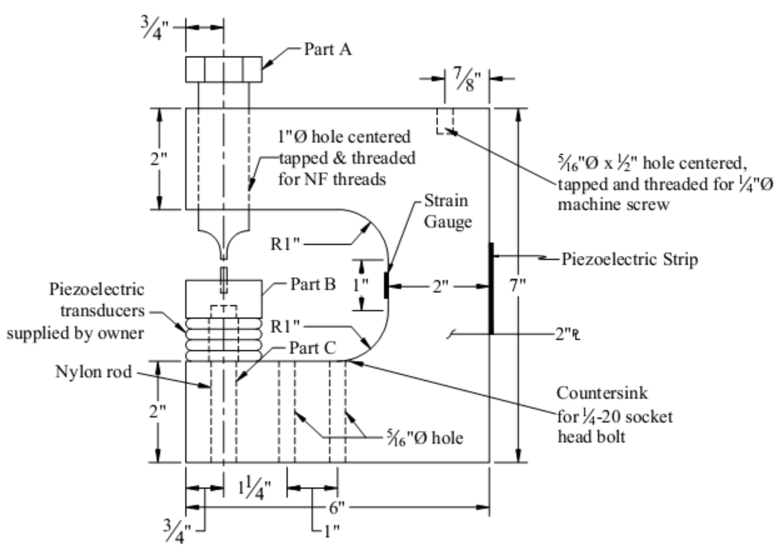

Figure 8. PICK tool schematic

المنارة للاستشارات
www.manaraa.com

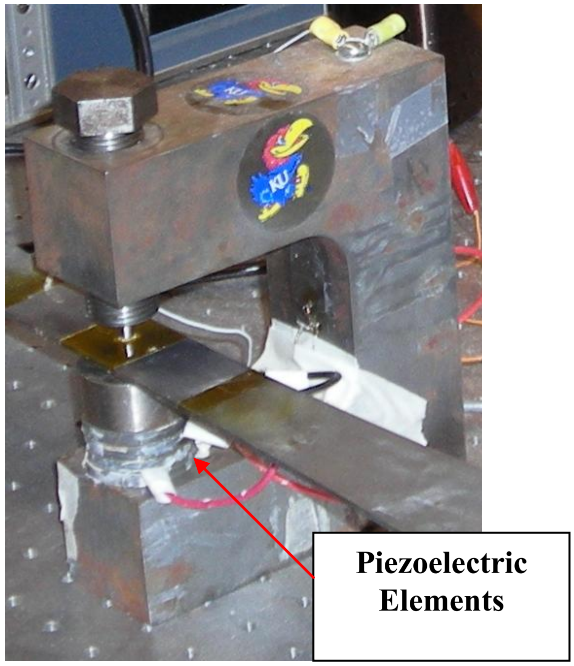

Figure 9. Fatigue specimen during PICK treatment

Piezoelectric Elements

The piezoelectric elements were obtained by disassembling a commercial ultrasonic cleaner; the piezoelectric elements were assumed to be PZT-4 material, which is the commonly used piezoelectric element in these cleaners. The properties for PZT-4 are shown in Table 3.

Table 3. Assumed Properties for Piezoelectric Elements

Electromechanical coupling coefficient - □	Piezoelectric transfer efficiency - □	Activation constant for strain in the 3-direction for current in the 3-direction - d33	Short circuit Young's modulus of piezoelectric material - YE33
0.700	0.837	285x10-12 m/volt	6.6x1010 N/m2

Piezoelectric elements have a positive and a negative side; these can be identified by placing an element on a conductive surface and connecting a volt meter between the conductive surface and the upper face of the piezoelectric element. If the voltmeter shows positive when the positive

المنارة للاستشارات
www.manaraa.com

probe is pressed against the surface of the piezoelectric element, that face of the piezoelectric element is the positive side and the other side is the negative side. This can be checked by reversing the probes and the faces of the piezoelectric element and applying force through the negative probe. Once the positive and negative faces were identified, the four piezoelectric elements were assembled as shown in Figs. 8 and 9 such that direction of current was the same across each element. With the piezoelectric elements stacked in this a manner, expansion and contraction deformations obtained by applying an electric field across the elements (converse effect) were additive in all the elements.

The piezoelectric elements are brittle and must be handled with care. They are susceptible to cracking if dropped from only a couple of inches. Fortunately, they can be repaired by gluing the parts back together with compatible glue. This did not seem to affect their performance.

Electronics

Electronics powering the PICK tool consisted of a sine wave generator and an amplifier. The sine wave generator was a Hewlett Packard 3300A Function Generator with a variable-sweep-frequency capability and adjustable voltage output. The amplifier was a Piezo Systems Inc. Linear Amplifier Model EPA-104 with adjustable gain, as shown in Fig. 10.

المنارة للاستشارات
www.manaraa.com

Figure 10 Electronics used with PICK tool

Data Acquisition

While fatigue testing of the treated specimens is the most direct method to demonstrate any improvement in fatigue performance achieved by the PICK tool, multiple techniques besides fatigue testing were used to evaluate PICK tool performance.

Retained expansion (*RE*) as defined by Eqn. 4 is used by the aerospace industry as a measure of the amount of the expansion remaining after mechanically expanding a hole (Ball and Lowery 1998).

$$RE = \left(\frac{R_{final} - R_{initial}}{R_{initial}} * 100 \right) \% \qquad \text{Equation 4}$$

Where

المنارة للاستشارات
www.manaraa.com

R_{final} = the final radius of the hole and
$R_{initial}$ = the initial radius before cold-expansion

Cold-expansion imposes tangential tensile stresses and radial compressive stresses around the hole. After completion of cold-expansion and after the plug has been removed, the tangential tensile stresses become compressive residual stresses while the radial compressive stresses remain compressive but change distribution. By considering the change in the circumference with expansion, it can be shown that *RE* also provides a measure of the amount of permanent plastic strain / permanent set remaining after the elastic strain is recovered and compressive residual strain is imposed, as presented in Eqn. 5. Some elastic strain is included with this plastic strain but, at retained expansion ratios normally achieved (3-8%), it is small compared to the amount of plastic strain. *RE* was obtained by measuring the hole diameter with a digital caliper before and after treatment by the PICK tool. Ten measurements were taken at different diametric locations around the hole and the values averaged both before and after treatment. Retained expansion was then computed using Eqn. 4.

$$RE = \left(\frac{2 * \pi * R_{final} - 2 * \pi * R_{initial}}{2 * \pi * R_{initial}} * 100 \right)$$

Equation 5

$$= \left(\frac{R_{final} - R_{initial}}{R_{initial}} * 100 \right) = \varepsilon_{plastic}$$

A brittle coating with a layer of undercoat was applied to the specimens after the plug was pressed into the hole but before treatment by the PICK tool. The brittle coating and undercoat were Stresscoat ST-70F/21C and Stresscoat ST-850 Undercoat and were applied following the

www.manaraa.com

manufacturer's directions. These were applied to provide an immediate indication of whether the PICK tool was actually plastically deforming the steel in the vicinity of the hole. The brittle coating is formulated to crack at a specified level of elastic strain; however, where the steel plastically deforms, the brittle coating debonds and flakes off. This flaking provides a clear delineation of the extent of plastic deformation and the location of the elastic-plastic interface. The results from the brittle coating and a discussion of these results are presented in Simmons (2013).

The strain gage that was installed on the PICK tool was used to monitor static loading when the bolt was tightened on the aluminum plug; this was to ensure the loading on the plug from the PICK tool was consistent with every specimen treated. Another gage (MicroMeasurements WK-06-250BG-350) was glued to a piece of scrap steel that was separate from the tool but in close vicinity to the tool. This gage was used to monitor for signal drift and random electrical noise. A National Instruments (NI) NI ENET-9219 Ethernet DAQ device with a NI cDAQ 9172 USB Data Acquisition System was used to power both of these gages and to collect both of their output signals. NI LabView on a desktop computer was used to process the signals and to provide the results for real time monitoring and evaluation.

The piezoelectric elements of the PICK tool were excited with a sine wave from the signal generator and amplifier. The converse effect of these piezoelectric elements subjected the aluminum plug and the surrounding steel to ultrasonic vibration and imposed a sine wave bending deformation mode on the PICK tool. The bending response of the PICK tool to this imposed deflection caused bending in the piezoelectric strip on the back of the PICK tool which

www.manaraa.com

generated another electrical signal by the direct effect. This signal was monitored with a Telequipment Type D54 oscilloscope (Fig. 9) which provided a measurement of the strength and frequency of the PICK tool response.

An Extech True RMS Multimeter was used to measure the frequency output from the signal generator to the amplifier and to measure current output from the amplifier to the piezoelectric elements in the PICK tool. As the input frequency to the piezoelectric elements was in the kilohertz range and the multimeter was not capable of measuring voltage output at this frequency range, the Telequipment Type D54 oscilloscope was used to measure voltage from the signal generator to the amplifier, from the amplifier to the piezoelectric elements, and the output from the piezoelectric strip.

Fatigue specimens were also instrumented. Two Micro-Measurement strain gages (WK-06-250BG-350) were attached to opposite faces of each of the fatigue specimens. These two gages were aligned on the fatigue specimen to measure axial strain at corresponding locations on the opposite faces of the fatigue specimen for the purpose of monitoring bending of the specimen during fatigue testing. In addition, another of strain gage was placed on an unrelated piece of scrap steel and used to monitor electrical / background noise. These three gages were powered and the output signal collected by a NI ENET-9219 Ethernet DAQ device with a NI cDAQ 9172 USB Data Acquisition System, which provided the results to a desktop computer. A MTS Model 312.31 Load Frame with a MTS Model 661.21, 345-MPa (50-kip) Load Cell was used to perform the fatigue testing. During fatigue testing, movement of the crosshead of the MTS and load from the load cell of the MTS were provided to the same NI data acquisition devices as the

المنارة للاستشارات
www.manaraa.com

strain gage values. NI LabView was used to process and display the strain gage data, cross head movement, and load from the UTS.

Other Evaluation Techniques

Metallurgical Evaluation

One fatigue specimen was sent to a metallurgical lab for evaluation after being treated by the PICK tool but before being subjected to fatigue testing. The metallurgical evaluation consisted of both grain size analysis and hardness testing. The specimens were cut with a slow-speed diamond saw such that the cuts were perpendicular to the surface and perpendicular to the long axis to obtain cross sections through the treated hole. These cross sections were mounted and then polished with progressively finer grits up to 1 micron, then lightly etched with a 3% Nital solution (3% nitric acid and methanol). Grain size analyses and Vicker's microhardness testing were then conducted on these cross sections. After reviewing the results, three new specimens approximately 51 mm x 51 mm (2 in x 2 in) from the same bar stock were fabricated with a 3.2-mm (1/8-in) diameter hole at the center. One of these was a control specimen not treated by the PICK tool. The second was only mechanically expanded by applying force with the PICK tool to plastically deform the steel in the vicinity around the hole but not using the piezoelectric elements to apply ultrasonic vibration. The third was fully PICK-treated. These three specimens were also sent to the metallurgical lab for evaluation where they were prepared like the first specimen.

X-Ray Diffraction and Neutron Diffraction

Two more 51 mm x 51 mm (2 in x 2 in) plates were fabricated from the same bar stock with a

www.manaraa.com

hole as previously described, and were treated with the PICK tool. X-ray diffraction was used to measure the value and distribution of the residual strain produced by the PICK tool on one of these and neutron diffraction was used to measure the same on the other. These tests and the ensuing results are presented and discussed in Simmons (2013).

Testing Protocol

PICK Treatment

Before using the PICK tool to treat fatigue specimens, the strain gage on the PICK tool was calibrated using a calibrated load cell to establish a load versus strain curve for the PICK tool (Simmons 2013); this calibration provided a direct reading of the load applied to the aluminum plug.

In preparing fatigue specimens for PICK treatment, an area approximately 51 mm (2 in) in length and centered on the fatigue specimen was cleaned of mill scale. Then, the width and thickness at the center as well as the hole diameter were measured with digital calipers. The alignment of the PICK tool was adjusted so that the tips of the bolt and the round, load-transfer plate would be aligned with the hole in the fatigue specimen; then the aluminum plug was pressed into the hole. The undercoat and brittle coating were applied to the cleaned area and cured per manufacturer's instructions. The specimen was placed in the PICK tool, alignment checked, and bolt tightened carefully to ensure the tips aligned with the plug. Once suitable alignment was achieved, the bolt was tightened until a strain value of 224 microstrain was read from the strain gage on the inside of the PICK tool. This equated to a force of 9.2 kN (2.1 kips), or an approximate stress of 1.2 GPa (170 ksi), on the aluminum plug. The electronics were energized and supplied power as a

المنارة للاستشارات
www.manaraa.com

sine wave voltage to the piezoelectric elements in the PICK tool. A sweep of frequencies was then conducted to identify the resonant frequency of the tool with the sine wave excitation of the piezoelectric elements. This was accomplished by observing the magnitude of the voltage coming back into the oscilloscope from the piezoelectric strip on the back of the PICK tool. The tool deformed in bending as a result of the expansion and contraction of the piezoelectric elements and the piezoelectric strip on the back of the tool flexed with the bending of the tool - the larger the bending in the tool, the higher the voltage from the piezoelectric strip displayed on the oscilloscope. Resonant frequency, which was in the ultrasonic range and always at the upper end or above the audible range, was the input frequency to the tool that produced the largest output voltage from the piezoelectric strip on the back of the tool. Once the resonance frequency was determined, the strain gage for the tool was checked and the bolt tightened until the 224 microstrain was re-established. The treatment was left with the 224 microstrain and the frequency set at the resonance frequency for 114.5 hours. Both of these values, 224 microstrain and 114.5 hours, were known to be arbitrary, but they were used consistently to maintain a basis for comparing results. Once the time period was reached, the specimen was taken out of the tool, photographed, and the extent of the area where the brittle coating had flaked off measured with a circle template. Next, the aluminum plug was gently pressed out of the specimen. The remnants of the brittle coating were then removed, and dimensions of the hole were measured along 10 different diametric locations and the diameters averaged and the retained expansion calculated using Eqn. 4.

Fatigue Testing

Due to several causes which could not be totally eliminated (slight misalignment of the grips of

المنارة للاستشارات

www.manaraa.com

the UTS, slight initial imperfections in specimen straightness, the holes in the ends of the fatigue specimen not being entirely parallel and/or perpendicular to the axis of the fatigue specimens, etc.), some bending was induced in the tensile fatigue specimen during fatigue testing. To eliminate or minimize this bending, cable ferrules were pressed on the ends of two small wire cables and one end of each cable threaded through the hole of the fatigue specimen. The other ends of the cables were attached to turnbuckles which were in turn attached through other small cables to the columns of the MTS (Fig. 11). The tension in the cables could be adjusted using the turnbuckles and the center of the fatigue specimen held in an aligned position to minimize induced bending strain. To measure the bending strain, strain from the two strain gages attached to the fatigue specimen were collected and processed with LabView to separate bending and tension strains. The wire cables connected to the center of the fatigue specimens were tightened or loosened as required to minimize bending strain as much as possible. This was an improvement, but bending strain existed to some extent in all the fatigue specimens.

After completing several fatigue tests to establish the testing protocol, a stress range was selected that would provide a basis for comparison yet limit testing time to a reasonable value. The lower value of the stress range was selected to be as low as possible while ensuring that the specimen remained completely in tension during each load cycle. Specifying the load corresponding to this stress range for the fatigue testing produced a range of cross-head displacement once the testing started. A crack-initiation indicator was established by choosing a crosshead displacement several thousandths of an inch larger than the highest displacement being experienced and setting this value as a displacement limit for the test. Reaching this limit was an indication that a crack had initiated. Once this limit was reached, the test was immediately

المنارة للاستشارات
www.manaraa.com

halted and the specimen checked to determine if a fatigue crack had actually initiated. Dye penetrant was applied and fatigue testing restarted. The combination of dye penetrant and an ongoing fatigue test made even small fatigue cracks visible. If fatigue cracking had initiated, the stress range and the number of cycles to failure were recorded. If not, the test was re-started with new displacement limits established and was allowed to continue until the new displacement limit was reached. This cycle was repeated until a fatigue crack was observed.

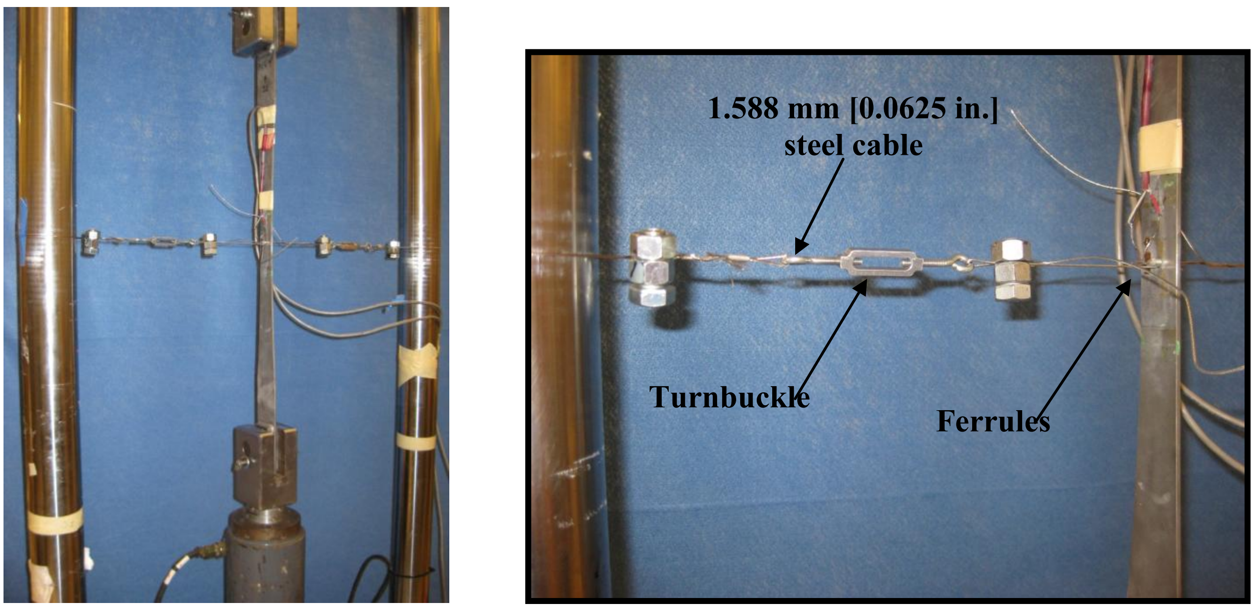

Figure 11. Fatigue specimen mounted in UTS (Crain 2010)

RESULTS

Fatigue Testing

The stress range used in the fatigue testing was established as 221 MPa (32 ksi) with 14 MPa (2 ksi) being the lower limit and 234 MPa (34 ksi) being the upper limit. Bending of the fatigue specimens during fatigue testing was a significant problem. ASTM E 466-07 stipulates that the bending stress should be less than 5% of the maximum stress; several tests were discounted

المنارة للاستشارات
www.manaraa.com

because the bending was beyond this limit and could not be reduced using the wire-cable system discussed above. Three sets of fatigue testing specimens were fabricated: the first set of five was used as control specimens with no mechanical expansion of the aluminum plug or treatment by the PICK tool; the second set consisted of four specimens subjected to mechanical expansion only with no PICK treatment; and the third set consisted of six specimens that were subject to mechanical expansion and were the full PICK-treated with piezoelectric vibration. The fatigue testing protocol and results are presented in Table 4. Results have also been plotted on an S-N graph in Fig. 12. The averages, standard deviation, coefficient of variation for the results of each category are presented in Table 4. The results in Table 4 show a difference in the fatigue life between the three different testing protocols. The result for PICK 9 was well above the rest of the specimens that were only mechanically expanded, and was considered anomalous to the extent that it is thought that it should be discarded. With the result discarded for PICK 9, a 95% confidence level was established using Student's t-distribution for small sample sets. This confidence level provides a statistical estimate for fatigue life for crack initiation which will be exceeded by 95% of test specimens; only 5% of the fatigue specimens will have fatigue life for crack initiate below this number of cycles-to-failure. The 95% confidence limits have been included on Fig. 12. Using the 95% confidence levels and including test specimen PICK 9, treatment with pressure-only increased the expected fatigue life only 6%; if PICK 9 is excluded and comparing the 95% confidence levels, pressure-only increased fatigue life by 84%. Comparing the 95% confidence levels of fatigue life between specimens with no treatment and those fully treated with the PICK tool shows an increase in fatigue live of 160%.

المنارة للاستشارات
www.manaraa.com

Table 4. Fatigue Testing Results

Control Specimens		Tool w/ pressure only		Tool w/ pressure only & w/ PICK 9 deleted		Tool w/ pressure & Ultrasonic Vibration	
Specimen	**Cycles to failure**	**Specimen**	**Cycles to failure**	**Specimen**	**Cycles to failure**	**Specimen**	**Cycles to failure**
F9	234,824	PICK 6	426,302	PICK 6	426,302	PICK 3	818,635
F10	177,106	PICK 7	397,595	PICK 7	397,595	PICK 4	743,725
F11	169,222	PICK 8	338,557	PICK 8	338,557	PICK 10	532,310
F12	195,220	PICK 9	992,108			PICK 11	744,767
F13	194,449					PICK 12	350,026
						PICK 13	412,814
AVE	194,164		538,641		387,485		600,380
Std Dev	25,335		304,511		44,738		195,715
Coefficient of Variation	13%		57%		12%		33%
95% confidence level	170,000		180,328		312,000		439,000

المنارة للاستشارات

www.manaraa.com

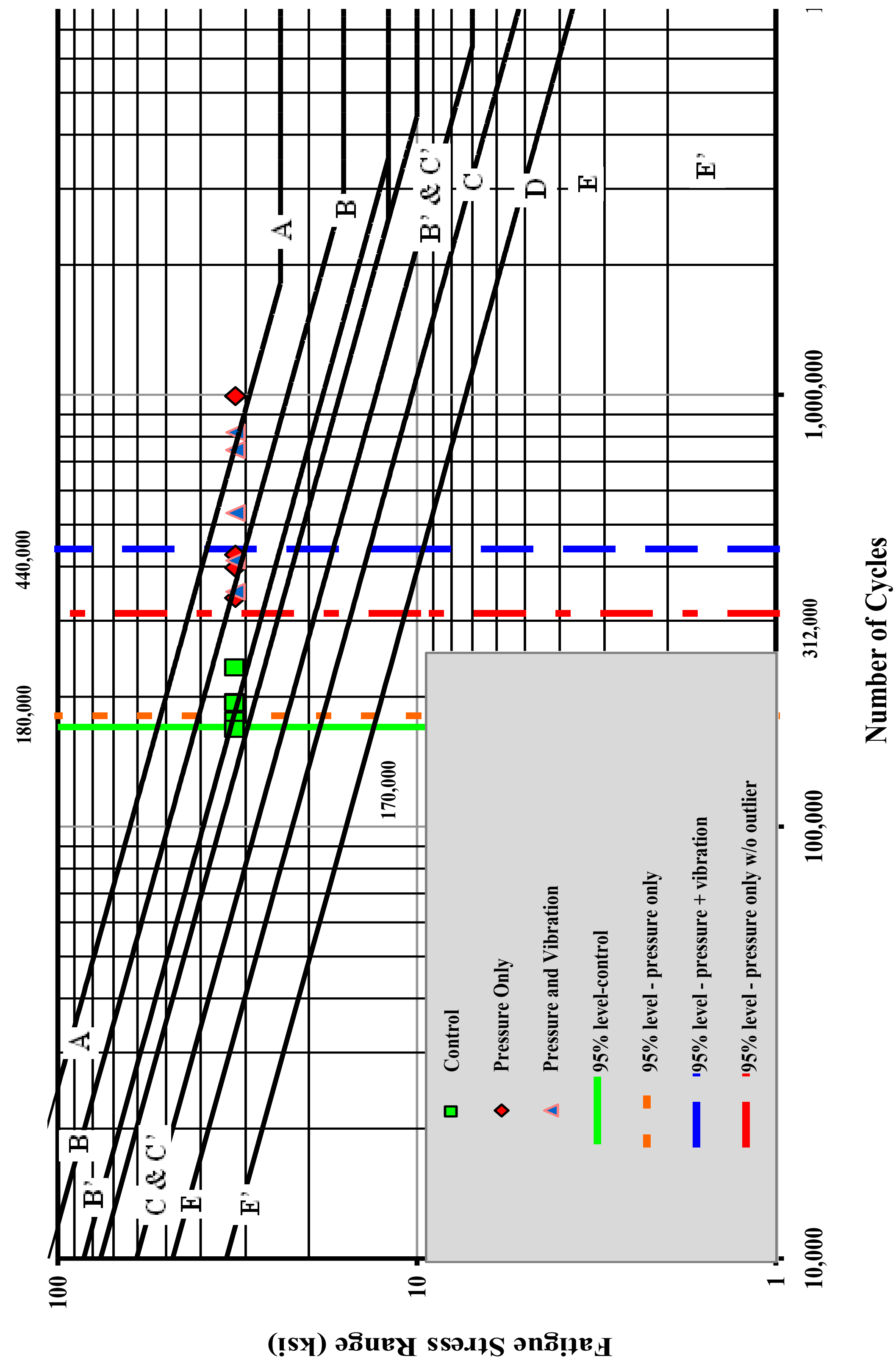

Figure 12 Fatigue Initiation for 1/8 – in Specimens at Stress Ratio = 32 ksi

www.manaraa.com

Metallurgical Testing Results

Four specimens were sent to Engineering Systems, Inc. in St Louis, MO, for metallurgical testing. This testing consisted of microhardness test and grain size analysis as previously discussed.

Hardness Testing

Microhardness readings were taken along several paths on different cut surfaces of the first sample (fully PICK treated) sent to the metallurgical lab. One slice was made well away from the hole and the area affected by the PICK treatment around the hole to provide an untreated cut surface; microhardness readings were taken along the centerline of this surface and used to establish a baseline hardness for untreated steel. Two sets of microhardness readings were taken along a section which was through the specimen along a diametric line through the center of the hole. One set of readings was taken along a line at mid-plane and the other was taken along a line near the surface. The other three specimens (untreated, mechanically expanded only, and fully PICK-treated) had microhardness readings taken only along the midplane of the cuts, which was through the specimen along a diametric line through the center of the hole. The microhardness readings were converted from the Vicker's hardness scale to the Rockwell hardness B scale using tables in ASTM E140. The metallurgical report with all the details are presented in Simmons 2013. The hardness values were further converted from Rockwell hardness B to ultimate tensile strength using a conversion table in Moniz (1994).

The results of the hardness testing are presented in Fig. 13. The trendlines for the midplane hardness readings are third degree polynomials and provided the best fit for the data. All the

المنارة للاستشارات
www.manaraa.com

trend lines for both the mechanically expanded and the fully PICK-treated data showed an increase in harden ss and ultimate strength over the control specimen. The trend line for the near-surface traverse shows an approximate linear reduction in hardness and ultimate tensile strength with distance from the hole. These readings may have been affected by residual surface stresses induced by the rolling process used to form the flat bar. In addition, while the midplane section may exhibit plane strain behavior because the material at the midplane may be constrained by the steel between the midplane and the surfaces of the bar, the material near the surface may be in a plane stress condition. The hardness readings for the midplane traverses for the two fully PICK-treated specimens were taken at different distances from the hole and were combined together and plotted as one set of data. Hardness values for the fully PICK-treated specimens were found to be consistently higher than those for the pressure-only treated specimens. The hardness readings for the fully PICK-treated specimens were approximately 22% higher than those for the untreated specimens; while those for the mechanically expanded were roughly 15% higher than for the untreated specimens. These differences between the untreated and the mechanically expanded specimens may be the result of the cold-working from the mechanical expansion. The differences between the mechanically expanded and the fully PICK treated may be the result of acoustic hardening from the piezoelectric vibration during the PICK treatment. Some of the differences are probably accounted for by the normal variation in hardness readings. However, the trendlines seem to show an increase in hardness / ultimate strength was achieved with the PICK treatment near the hole and that this increase in hardness / ultimate strength decreased with distance from the hole. Furthermore, the trendlines approached the value for the untreated steel at about the same distance from the hole as the estimated limit of plastic deformation, the elastic/plastic interface. This elastic/plastic boundary was estimated

المنارة للاستشارات

www.manaraa.com

from the brittle coating results and is fully discussed in Simmons 2013.

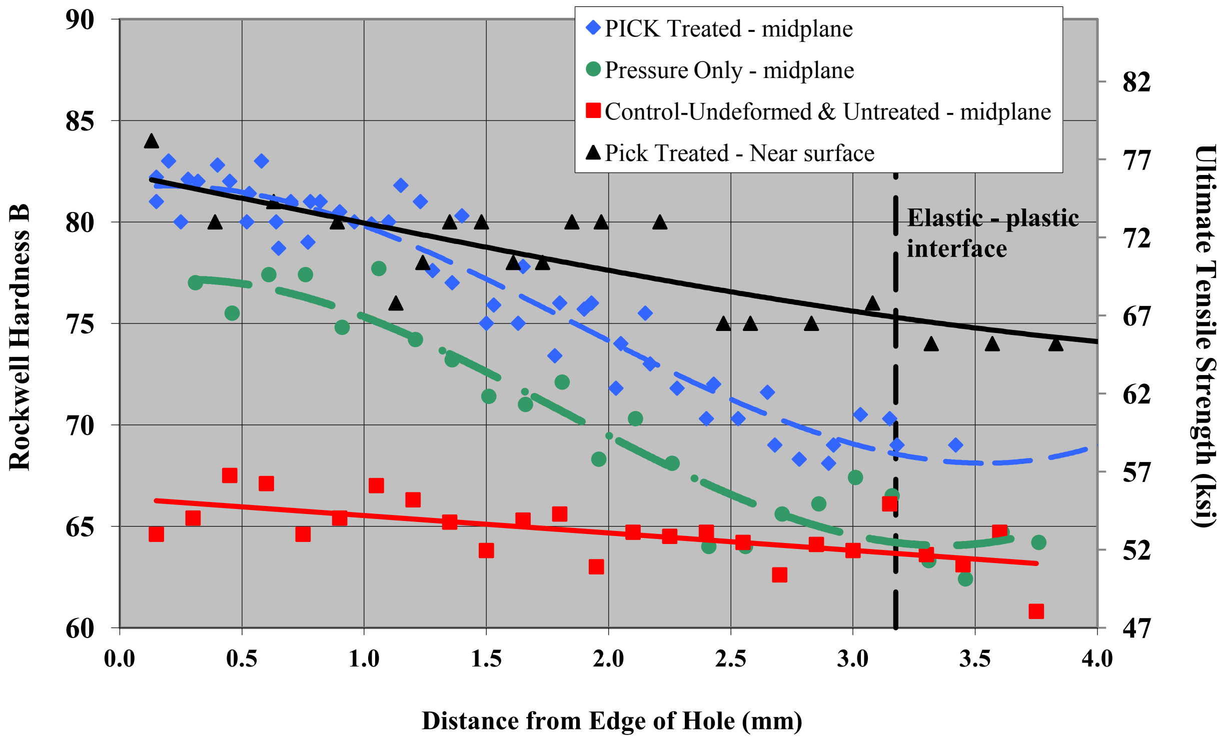

Figure 13 Increase in hardness and ultimate strength with different cold-expansion treatments

Grain Size Analysis

Grain size analyses consisted of using both an optical microscope and a scanning electron microscope (SEM). The optical microscope provided a view of the grain size with magnification up to 550X while the SEM was capable of magnification up to 5000X. Typical microstructure of the untreated metal is shown in Fig. 14 and was found to consist of ferrite grains with small islands of dark-etching pearlite; this is consistent with low-carbon steel such as Gr. A36. Grain sizes were mixed, averaging between 13.3 and 15.9 microns.

For the untreated specimen (Fig. 15), which was only subjected to drilling and reaming of the

www.manaraa.com

hole, the optical microscope revealed shallow grain deformation of the grains at the surface of the hole as expected. This deformation was limited to those grains immediately next to the hole surface.

For the mechanically expanded specimen, a layer around the surface the hole exhibited grain deformations to a depth of approximately 0.008 to 0.009 mm (0.0003- 0.0035 in), and may be viewed in Fig. 16.

For the PICK-treated specimen, the optical microscope revealed a layer of grain deformation to a depth of approximately 0.001 mm (0.004 in) from the edge of the hole, as shown in Fig. 17. One sample displayed semi-circular regions immediately adjacent to the edge of the hole where grain deformations extended to a distance of 0.038 mm (0.0015 in). Within these regions, the grains appeared to be flattened and elongated. The SEM also revealed an unresolved structure where the grain size and shape could not be discerned, which can be seen in Fig. 18.

المنارة للاستشارات
www.manaraa.com

Figure 14. Sample 1-P (PICK treated). Microstructure of base metal away from the hole, showing light-etching ferrite matrix with small, dark-etching pearlite colonies. (~550x)

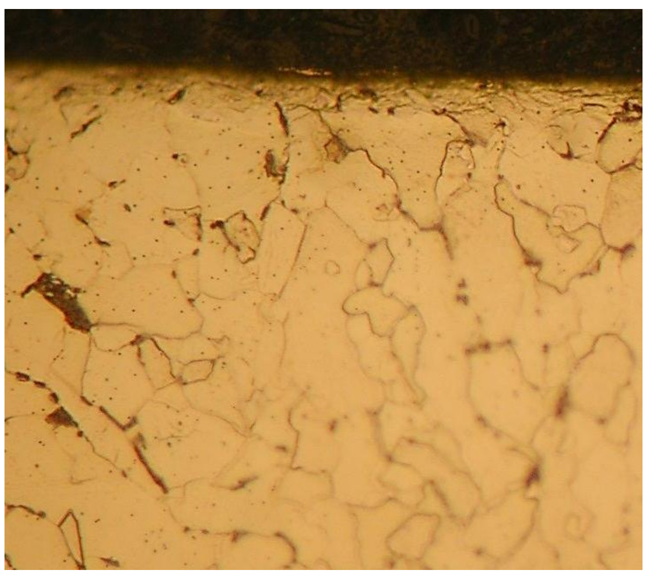

Figure 15. Sample 9-U (Drilled and Reamed Only). Microstructure, showing shallow depth of grain deformation at the surface of the hole, shown at top. (~500X)

www.manaraa.com

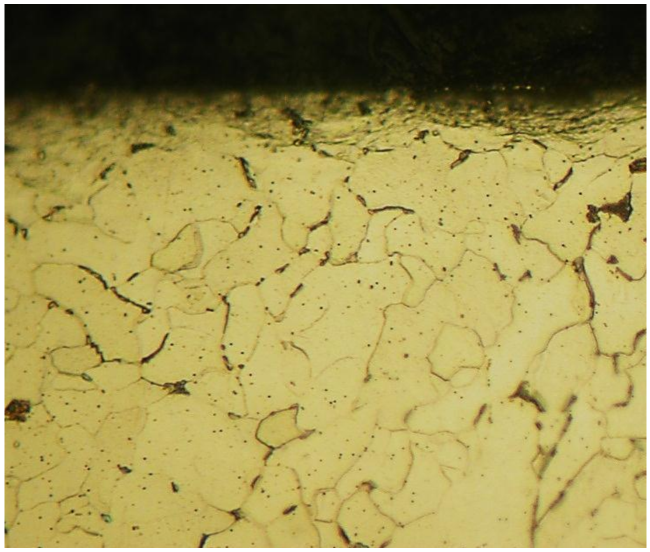

Figure 16. Sample 10-D (Mechanically Expanded Only). Microstructure at the surface of the hole (top), showing shallow zone of grain deformation. (~500X)

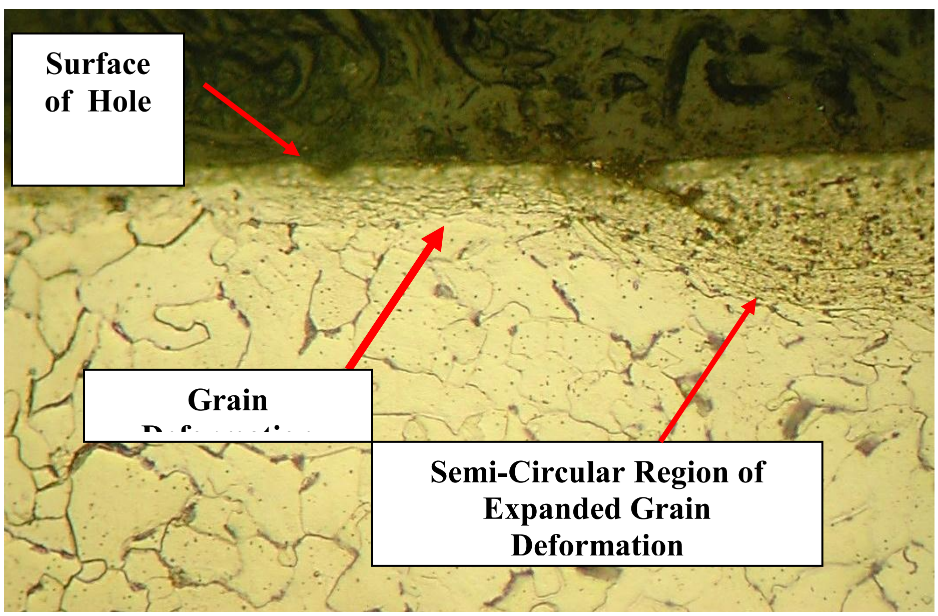

Figure 17. Sample 4-P (PICK-Treated). Microstructure at the inside cylindrical surface of the hole showing shallow zone of grain deformation (arrow) and semi-circular region of additional deformation. (~500 X).

المنارة للاستشارات
www.manaraa.com

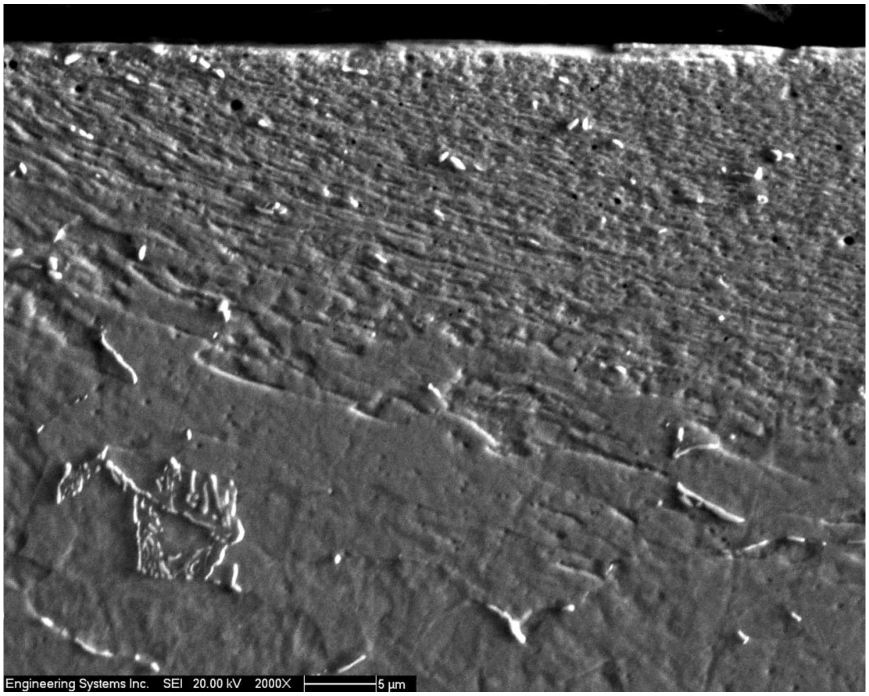

Figure 18. Sample 4-P (PICK-Treated). SEM photo of semi-circular region at the hole surface near the outer plate surface, showing localized grain deformation, and unresolved structure closer to the hole surface (top). Note small pits within this region (~2000 X).

Retained Expansion

The diametric measurements before and after treatment and Retained Expansion (*RE*) as calculated using Eqn 5 are shown in Table 5 and plotted in Fig. 19. Table 5 and Fig. 19 show that the PICK treatment produced a RE ratio 24% higher than the mechanically expansion for fatigue specimens (specimens P-4 through P-15M). For the plate specimens, the PICK treatment produced a RE ratio 66.3% higher than for plate specimens (PL-2 through PL10).

During treatment of the fatigue specimens, the load on the plug from the tool was set at a level to produce 224 microstrain in the tool as previously explained. This tool strain was allowed to decay with time and was not adjusted unless the data acquisition had to be re-initialized. However, the data acquisition system during this series of treatment was not stable and often had to re-initialized. When re-initialized, the load was reset to the value producing 224 microstrain.

المنارة للاستشارات
www.manaraa.com

During treatment of the plate specimens it was decided to keep the strain in the tool as close as possible to a constant 224 microstrain. To this end, the load was reset several times a day to maintain 224 microstrain in the PICK tool. It is believed that this change in methodology may be the cause of the difference in *RE* between the fatigue specimens and the plate specimens. These loading processes were similarly applied to both PICK treated and mechanically expanded specimens.

Table 5. Results for measured retained expansion (*RE*)

	Specimen #	Expansion		
		Top	**Bottom**	**AVE**
Mechanically Expanded Fatigue Specimens	P-6	7.64	12.64	10.14
	P-7	-2.9	10.28	3.69
	P-8	6.43	0.45	3.44
	P-9	4.16	7.95	6.06
			AVE	5.83
Mechanically Expanded and Ultrasonically Treated (PICK) Fatigue Specimens	P-3	-0.48	3.6	1.56
	P-4	6.32	7.07	6.70
	P-10	7.18	7.04	7.11
	P-11	15.83	8.51	12.17
	P-12	4.36	6.7	5.53
	P-13	9.06	8.26	8.66
	P-14M	8.12	8.39	8.26
	P-15M	8.69	5.96	7.33
			AVE	7.16
Mechanically Expanded and PICK Treated Plates	PL-2 P			15.18
	PL-3 P			19.54
	PL-4 P			14.13
			AVE	16.28
Mechanically Expanded Plates	PL-10 D			9.76

المنارة للاستشارات
www.manaraa.com

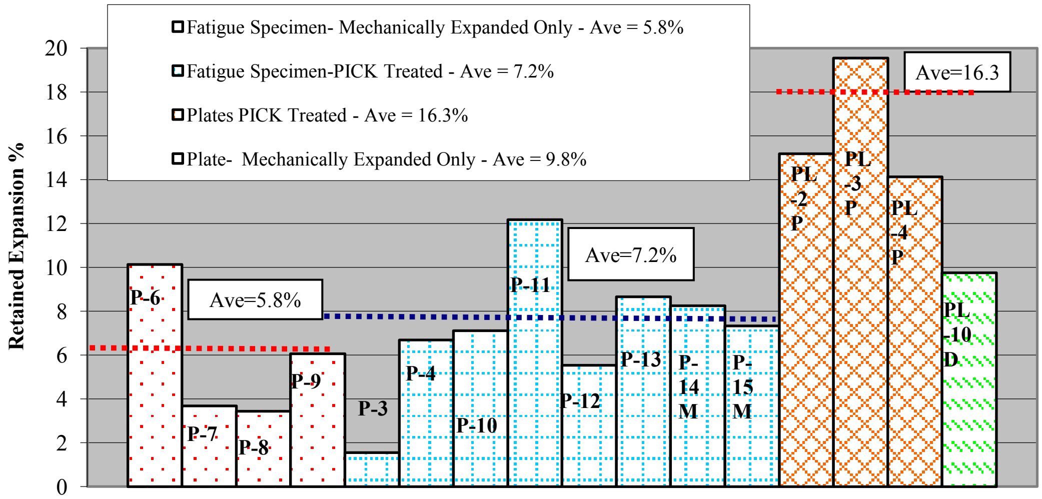

Figure 19. Retained expansion of crack-arrest holes

The results from the RE measurements of the hole diameters before and after treatment were plotted on the stress-strain curve from the tension testing (Crain 2010) used to establish the material properties of the plate used in the fatigue testing (Fig. 20). It appears that stain hardening occurred with both mechanical expansion only and the PICK treatment regardless of the loading protocol. However, the strain hardening was higher in the PICK-treated specimens, both fatigue and plate specimens, that in the mechanically expanded specimens.

المنارة للاستشارات
www.manaraa.com

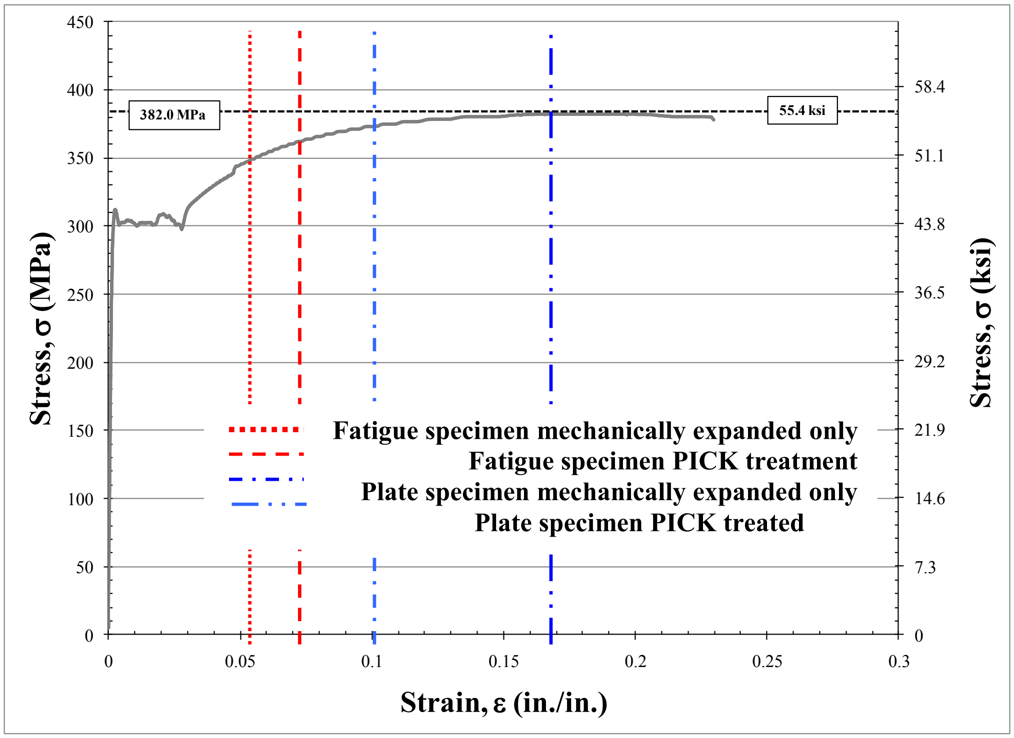

Figure 20. Retained Expansion Plotted on Material Stress-Strain Curve from Tension Testing (Crain 2010)

Load Decay

During the treatment of the fatigue specimens, it was observed that the load / strain in the tool decayed with time. This observation was reinforced when the decision was made to keep the strain level at a constant 224 microstrain. Reviewing the lab notes, two fatigue specimens were found that provided some data of the load decay with time (Fig.21). Creep is defined as increasing strain with constant stress while relaxation is defined as decreasing load with constant strain (Dowling 2007). Rather than creep or relaxation, the behavior observed in the fatigue specimens is thought to be further evidence of acoustic softening.

المنارة للاستشارات
www.manaraa.com

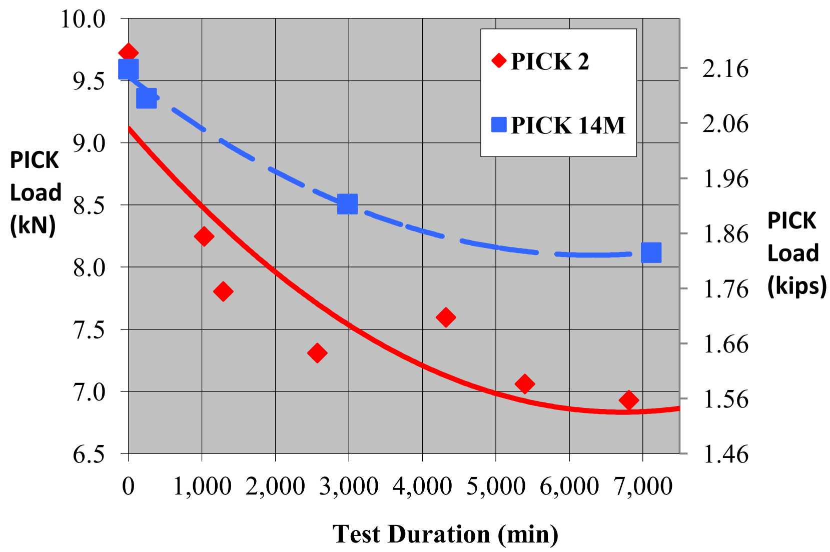

Figure 21. Decay of tool load with time

Power

Typically, when resonance was achieved, the signal frequency supplied to the piezoelectric elements was in the kilohertz range and, because this was above the capacity of the Extech RMS Multimeter, the voltage supplied to the piezoelectric elements was measured with the Telequipment Type D54 oscilloscope. A typical value for the voltage from the oscilloscope was approximately 46 volts RMS. Current through the piezoelectric elements was measured with the multimeter inserted into the circuit and a value of 0.0266 Amps was obtained. From these, the calculated power supplied to the piezoelectric elements during the PICK treatment was approximately 1.23 watts.

Discussion

The results of fatigue testing demonstrate that the PICK treatment process provides an improvement in preventing fatigue crack re-initiation in crack-arrest holes over that provided by

المنارة للاستشارات
www.manaraa.com

mechanical expansion only (Fig. 12). While the mechanical cold-expansion increased fatigue initiation life by approximately a factor of 2, combining the mechanical cold-expansion with ultrasonic vibration increased the fatigue initiation life by approximately a factor of 3. Evidence points to a combination of strain hardening, work-hardening, and ultrasonic vibration leading to an improvement in fatigue initiation life.

When the Retained Expansion averages are plotted on the material stress-strain plot (Fig 20), the intersections of the RE lines with the stress-strain curve seem to show that strain hardening may have occurred.

From the metallurgical analysis, the grain size analyses seem to show a change in the grain structure around the hole between the untreated, mechanically treated only and the fully PICK treated specimens (Figs. 14-18). The grain flattening and elongation seen in the PICK treated specimens may be the result of ultrasonic vibration and may be an indication of work-hardening; this seems to be supported by the increased hardness achieved between the untreated, mechanically treated, and the fully PICK treated specimens as shown in Fig. 13. Conversely, the higher hardness readings for the PICK treated specimens may also be an indication of acoustic hardening due to the PICK treatment.

The higher retained expansion (Fig 19) and the higher hardness values (Fig 13) also show an additional effect from the ultrasonic vibration beyond that achieved by the mechanically expansion only treatment. The load decay (Fig. 19) and the retained expansion (Fig 19) combined seem to indicate the existence of acoustic softening during the PICK treatment. If so,

www.manaraa.com

then the increase in hardness values shown in Fig 12 may be an indication of acoustic hardening rather than cold working. Further research is required to determine which or either of these is the case.

Additionally, increasing the radius of the hole and inducing residual compressive stresses around the hole also contributed to the enhanced resistance to fatigue initiation. These topics are further discussed in Simmons 2013.

CONCLUSIONS

This proof-of-concept study with testing of a reduced-scale, laboratory specimens has demonstrated that fatigue initiation life can be increased by mechanically cold-expanding a hole and subjecting the inside surface of that hole with treatment from ultrasonic vibration. This technique provides for an improved resistance for crack-arrest over that provided by only mechanically expanding the hole. In addition, the ultrasonic vibration input from the piezoelectric elements also resulted in the following behavior:

1. Increased Retained Expansion,
2. Raised ultimate strength of the steel,
3. Provided for additional work hardening,
4. And may have produced strain hardening.

On the basis of these conclusions, the PICK treatment may provide a method of improving the capacity of crack-arrest holes to stop fatigue crack growth. Expansion from the PICK treatment

المنارة للاستشارات
www.manaraa.com

may eventually be used to arrest fatigue crack growth in bridges and provide an economical, efficient repair for fatigue cracks in bridges.

REFERENCES

1. Akesson, Bjorn (2008). Understanding Bridge Collapses. Taylor & Francis Group, London, England, 79-88.

2. American Association of State Highway and Transportation Officials (AASHTO), (1983) "Standard Specification for Highway Bridges". 13th Edition, Washington, D.C.

3. American Association of State Highway and Transportation Officials (AASHTO), (1985) "Standard Specification for Highway Bridges Interim ". 13th Edition, Washington, D.C.

4. ASTM E 466-07 (2007) "Standard Practice for Conducting Force Controlled Constant Amplitude Axial Fatigue Tests of Metallic Materials" American Society for Testing and Materials, West Conshohocken, Pa.

5. ASTM E140 - 07 (2007) "Standard Hardness Conversion Tables for Metals Relationship Among Brinell Hardness, Vickers Hardness, Rockwell Hardness, Superficial Hardness, Knoop Hardness, and Scleroscope Hardness" American Society for Testing and Materials, West Conshohocken, Pa.

6. ASTM E8-04 (2004) "Standard Methods for Tension Testing of Metallic Materials" American Society for Testing and Materials, West Conshohocken, Pa.

7. Ball, D. L. and Lowry, D. R. (1998). "Experimental Investigation on the Effects of Cold Expansion of Fastener Holes". Fatigue and Fracture of Engineering Materials and Structures, vol 12, pp 17-33.

8. Barsom, John M. and Rolfe, S. T. (1999). Fracture and Fatigue Control in Structures: Applications of Fracture Mechanics. American Society of Testing Materials, Philadelphia, PA, 182-192.

9. Bontillo, Robert, PBFasteners, personal communications, Feb 28, 2011.

10. Boyer, H. E. Atlas of Stress Strain Curves (1987). ASM International, Materials Park, Ohio.

11. Crain, Josh S (2010). "Fatigue Enhancement of Undersized, Drilled Crack-Stop Holes" M.S. thesis, University of Kansas, Lawrence, KS.

المنارة للاستشارات

www.manaraa.com

12. Crain, Josh S., Simmons, Gary G., Bennett, Caroline R., Barrett-Gonzales, Ron, Matamoros, Adolfo B., and Rolfe, Stanley T. (2010) "Development of a Technique to Improve Fatigue Lives of Crack-Stop Holes in Steel Bridges" Transportation Research Record: Journal of the Transportation Research Board, No 2200, Transportation Research Board of the National Academies, Washington, DC.

13. Dexter, Robert J. (2004). "Signs, Signals, Light Support Structures and Manual for Repair of Fatigue and Fracture" Third Annual Bridge Workshop: Fatigue and Fracture. Available on the Internet.

14. Dieter, George (1989), Mechanical Metallurgy, McGraw-Hill, New York, New York, 229-236

15. Dowling, Norman E. (2007). Mechanical Behavior of Materials, 3rd edition, Pearson / Prentice Hall, New Jersey, 179.

16. Federal Highway Administration (FWHA) Bridge Program Group. (2001). Count of deficient bridges by state non-federal aid highway http://www.fhwa.dot.gov./bridges/britab/.htm (March 20,2002). The Office of Bridge Technology, Washington, D. C.

17. Fisher, John W. and Keating, P. B. (1989). "Distortion-Induced Fatigue Cracking of Bridge Details in Web Gaps". Journal of Construction Steel Research, 12, 215-228.

18. Fisher, John W., Barthelemy, B. M., Mertz, D. R., and Edinger, J. A. (1980). "Fatigue Behavior of Full-Scale Welded Bridge Attachments". National Cooperative Highway Research Program (NCHRP) Report 227, National Transportation Research Board, Washington, D. C.

19. Fisher, John W., Jin, Jain, Wagner, David C., and Yen, Ben T. (1990). "Distortion-Induced Fatigue Cracking in Steel Bridges". National Cooperative Highway Research Program (NCHRP) Report 336, National Transportation Research Board, Washington, D. C.

20. Hayes, B. (1996). "Classic Brittle Failures in Large Welded Structures". Engineering Failure Analysis, Vol 3 (2), 115-127.

21. Lanciotti, A. and Polese, C. (2005). "The effect of interference-fit fasteners on the fatigue life of central hole specimens". Fatigue and Fracture in Engineering Materials and Structures 28 (2005), 587-597.

22. Langenecker, Bertwin (1966) "Effects of Ultrasound on Deformation Characteristics of Metals", Transaction on Sonics and Ultrasound, vol su-13, no 1, 1-8.

23. Maranian, Peter (2010). Reducing Brittle and Fatigue Failures in Steel Structures. American Society of Civil Engineers, Reston, VA, 15-18.

المنارة للاستشارات

www.manaraa.com

24. McGuire, William (1968). Steel Structures. Prentice-Hall, Inc. Englewood Cliffs, NJ, 208-220, 771-772.

25. Merritt, Frederick S., Editor, (1972). Structural Steel Designers' Handbook. McGraw-Hill Book Company, New York, NY, 10-36.

26. Moniz, B. J. (1994), Metallurgy, Second Edition, American Technical Publishers, Inc., Homewood, Illinois, 493.

27. Nevill, G. F., Jr. and Brotzen, Franz R., (1957) "The Effect of Vibration on the Static Yield Strength of Low-Carbon Steel" Proceedings of American Society of Testing Materials, vol 57, 751-758.

28. Reid, Len, Fatigue Technology, personal communications, Feb 28, 2011

29. Richards, Cedric W. (1961) Engineering Materials Science, Wadsworth Publishing Co, Belmont, California, 405-406.

30. Roddis, W. M. Kim and Zhao, Yuan (2001). "Out-of-Plane Fatigue Cracking in Welding Steel Bridges". Welding Innovations, 27(2), 2-7.

31. Rolfe, S. T. and Barsom, John M. (1977). Fracture and Fatigue Control in Structures: Applications of Fracture Mechanics. First Edition. Prentice Hall.

32. Simmons, Gary G. (2013). "Fatigue Enhancement of Undersized, Drilled Crack-Arrest Holes" PhD thesis, presented to the University of Kansas, Lawrence, KS. , in partial fulfillment of the requirements for the degree of Doctor of Philosophy.

33. Sirnivasan, A. V. and McFarland, D. Michael, (2001) Smart Structures, Cambridge University Press, Cambridge, UK, 7-25.

34. Tavakkolizadeh, M. and Saadatmanesh, H. (2003). "Fatigue Strength of Steel Girders Strengthened with Carbon Fiber Reinforced Polymer Patch". American Society of Civil Engineers Journal of Structural Engineering, 129(2), 186.

المنارة للاستشارات
www.manaraa.com

CHAPTER 5: DEVELOPMENT OF A TECHNIQUE TO IMPROVE FATIGUE LIVES OF CRACK-ARREST HOLES IN STEEL BRIDGES – ANALYTICAL AND EXPERIMENTAL STRESS AND STRAIN

ABSTRACT

This paper presents a new technique to improve the performance of crack-arrest holes to arrest fatigue crack propagation. The historical background for one fatigue-susceptible detail is provided as an example of the seriousness of the problem. Repair options for fatigue cracks are discussed, including crack-arrest holes. The new technique, termed Piezoelectric Induced Compressive Kinetics (PICK), consists of cold expanding the inside of the crack-arrest hole and subjecting the inside of the hole to ultrasonic vibration using piezoelectric elements. The research performed to develop this new technique was conducted as a proof-of-concept, laboratory study using 3.2 mm (1/8-in) thick steel bar specimens. The effectiveness of this technique was evaluated by comparing the result of fatigue testing of control, partially treated, and fully treated specimens. In addition to the fatigue testing, physical changes caused by the PICK process were studied using metallurgical examination, measuring retained expansion (RE), and monitoring load decay. An analytical study is included; this study used closed-form solutions to evaluate stress and strain around the hole both during and after PICK treatment. The results were then compared to strains experimentally measured by both X-ray diffraction and neutron diffraction.

INTRODUCTION

The principal loads on bridges are dead loads from the weight of the bridge materials and live

www.manaraa.com

loads from traffic occurring on the bridge. Depending on span length (McGuire 1968), the ratio of live-to-dead loads varies from less than 1 to approximately 3. From the live-to-dead load ratios, the time-varying stresses for the higher ratio could approach 50-80% of the allowable stress in the steel and may cause fatigue cracks to initiate in welded-steel bridges if fatigue was not properly accounted for in the design. Fatigue cracks, in fact, currently exist or will form in numerous steel highway bridges in the United States. The Federal Highway Administration (FHWA) has governmental oversight responsibility for the maintenance for more than 120,000 steel highway bridges with welded details. According to the 2001 National Bridge Inventory, approximately 14% (16,800 bridges) may be structurally deficient (FHWA 2001). The major problems causing bridges to be labeled structurally deficient are the presence of fatigue-sensitive details, increasing service loads, corrosion, and lack of proper maintenance (Tavakkolizadeh and Saadatmanesh 2003).

Because of its simplicity, one of the first techniques often considered for arresting fatigue crack propagation is to drill a crack-arrest hole at each end of the fatigue crack. A crack-arrest hole increases the radius of the crack tip from infinitely small to the radius of the hole; the goal of this type of repair is to blunt the crack tip to an extent that crack growth is arrested. Experience has shown that if the diameter of the hole is not large enough, the crack will eventually grow through the hole and continue propagating. Large diameter holes may not be feasible because of interference or available spacing; therefore, techniques are needed to improve the performance of crack-arrest holes so that a reduced-sized hole will arrest crack propagation as well as a large diameter hole.

المنارة للاستشارات
www.manaraa.com

OBJECTIVE

The objective of this research was to develop a new technique to cold-expand and treat crack-arrest holes such that a hole with a smaller-than-required diameter would gain effectiveness in halting further crack propagation. The technique investigated to expand and treat the undersized hole has been termed Piezoelectric Induced Compressive Kinetics (referred to herein as PICK) and, in general, consists of the following steps in the laboratory:

1. Drilling a hole in a fatigue specimen made from steel plate,
2. Driving an oversized aluminum plug into the hole,
3. Compressively loading the aluminum plug to develop plastic stresses in the aluminum plug and in the adjacent steel specimen,
4. Using multiple piezoelectric elements to further load and deform the plug while subjecting the aluminum plug and the steel around the hole to ultrasonic vibration, and
5. Removing the aluminum plug from the steel specimen.

It was hypothesized that this process would produce three separate results, all of which would contribute to preventing crack reinitiation and propagation. First, the compressive force on the plug during cold-expansion would result in stress fields around the hole which would become compressive residual stresses when the force and aluminum plug were removed. Second, cold-expansion would cause strain hardening and cold-working to occur around the treated hole with a corresponding increase in the yield and ultimate strength of the steel. Third, ultrasonic vibration from the PICK treatment also would produce additional increases in the yield and ultimate

المنارة للاستشارات
www.manaraa.com

strengths of the steel.

This paper describes the design, fabrication, and operation of the PICK tool and presents analytical and experimental evaluations of the stresses and strain resulting from PICK treatment. A discussion and evaluation of the PICK process using fatigue testing, measured retained expansion (RE), hardness testing, and metallurgical examination have been summarized here and discussed in detail in Simmons (2013) and Simmons et al. (2013).

BACKGROUND

Distortion-Induced Fatigue Cracking

One reason that fatigue cracks are an issue with bridges is that some of the conditions which lead to fatigue cracks were not addressed by codes or adopted in practice until early mid 1980s. For example, one detail which produces a large percentage of the fatigue cracks in steel plate-girder bridges occurs at the gap left between a connection plate and adjacent girder flange when the connection plate is welded to the girder web but not to the flange. Asymmetric loads from normal traffic cause torsion to develop about the longitudinal axis of the girder, resulting in bending in the girder webs at these gaps. This bending results in distortion-induced fatigue cracking (DIFC) in the girder webs (Fig. 1), and this particular detail is often referred to as a web-gap.

www.manaraa.com

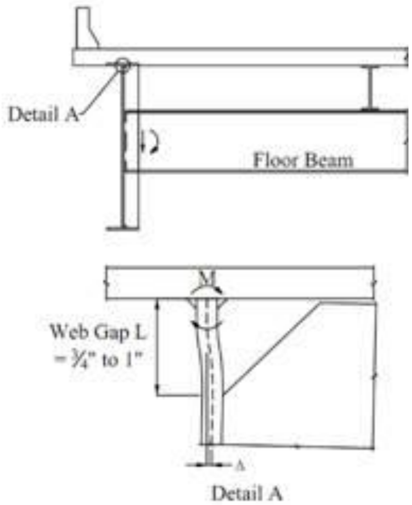

Figure 1. Distortion in the web gap

Fisher and Keating (1989) stated that the practice of leaving a gap between the connection plate and flanges was the result of bridge failures in Europe in the late 1930s and further cited as an example the Hasselt Bridge. The Hasselt Bridge was composed of Vierendeel trusses shaped like a tied arch, in that the top chords were arched and the bottom chords served as tie members (Akesson 2008). The vertical members between the top and bottom chords were welded to the respective chords instead of having pinned connections as in a true truss. The bridge was commissioned in January, 1937, and collapsed at 8:20 am on March 14, 1938, when the temperature was –20 ^{o}C (-4 ^{o}F) and while a tramcar and several pedestrians were on the bridge (Maranian 2010). The initial crack started in the tension flange of the lower chord at a butt weld between a vertical member and the lower chord (Hayes 1996). Shortly thereafter the bridge broke into three pieces and fell into the Albert Canal.

As a result of the failure of the Hasselt Bridge, it became standard practice in the United States to not weld connection plates to the tension flanges of the main girders. Steel design texts and design guides recommended leaving a gap between the connection plates and the tension flange

المنارة للاستشارات
www.manaraa.com

as late as 1972 (McGuire 1968; Merritt 1972). Roddis and Zhao (2001) presented a concise history of detailing of connection plates in which they stated that the *AASHTO Standard Specification for Highway Bridges* did not require welding connection plates to the girder flanges until the 1985 Interim (AASHTO 1985). Even with this change, it took several years for these details to become accepted practice; for example, the Kansas Department of Transportation (KDOT) did not begin to weld or bolt connection plates to both top and bottom flanges of plate girders until 1989 (Roddis and Zhao 2001). The result was that from approximately 1940-1990 a detail prone to distortion-induced fatigue cracking (DIFC) was often used in welded steel bridge girders, and as a result, these bridges were and are susceptible to fatigue cracking.

Once fatigue cracks occur, they must be repaired or closely monitored for crack growth. Numerous approaches have been used to repair fatigue cracks (Roddis and Zhao 2001), and the chosen repair generally depends on the type of fatigue loading (in-plane vs. out-of-plane) and the location and severity of the crack. Replacing a structural member may be difficult and cost-prohibitive, as the bridge may have to be taken out of service, the bridge deck removed, the member replaced, and the deck reinstalled. Re-welding or filling the fatigue crack with weld material requires grinding out the crack and any associated welds, filling the crack with weld material, and grinding the new weld surfaces smooth. Access and quality field welding often present difficult problems with welded solutions. Crack-arrest holes may be an appropriate solution if the holes are drilled large enough to effectively prevent crack reinitiation. At locations where cracking was caused by distortion-induced fatigue, techniques that have been used include stiffening web-gap regions, softening web-gap regions, removing or repositioning lateral bracing and diaphragms, or even loosening bolts at the cross frame to web connections

المنارة للاستشارات
www.manaraa.com

(Roddis and Zhao 2001).

Crack-Stop Hole Formulae

There are two formulae in the literature that may be used to determine the required radius for a crack-arrest hole to effectively stop crack growth. Both formulae relate the radius of the hole to the yield strength of the steel, the range of the stress intensity factor, and the half-length of the crack; however, the equations use a different constant. The basic equation was developed experimentally and was originally published in Rolfe and Barsom (1977) and is also found in Barsom and Rolfe (1999); this formula was the result of fatigue testing of flat plate under cyclical tension loads. Fisher et al. (1980; 1990) used the same equation as Rolfe and Barsom (1977) but developed a different constant based on testing of full-scale steel girders and rolled shapes configured and loaded to produce DIFC. Applying either of these two formulae to arrest fatigue cracking on an actual bridge may be difficult as it may not be possible to determine the in situ stresses used in the formulae. In addition some consideration needs to be given to hole placement, and this placement may affect the required hole diameter. A discussion of the development of the two formulae, development of the two values for the constant, and the significance of each of the terms have been presented in Simmons (2013). An extension to the formula to include the diameter of the crack-arrest hole in the in the definition of the crack length is also included in Simmons (2013).

Typical practice in Kansas is to drill a crack-arrest hole with a diameter from 19 mm (¾ in) to 38 mm (1½ in) (Fig. 2); unfortunately, these hole diameters are often not large enough to arrest crack propagation, and the fatigue crack eventually reinitiates and continues to propagate on the

المنارة للاستشارات
www.manaraa.com

other side of the hole (Fig. 3).

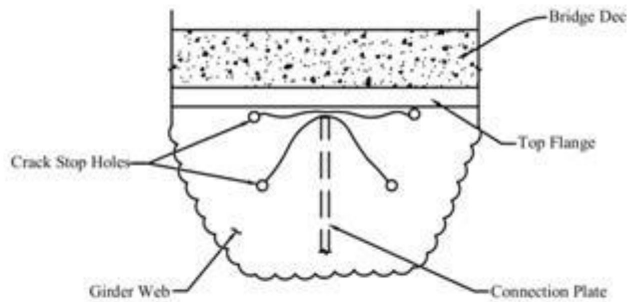

Figure 2. Crack-arrest holes at fatigue cracks (Roddis and Zhao 2001)

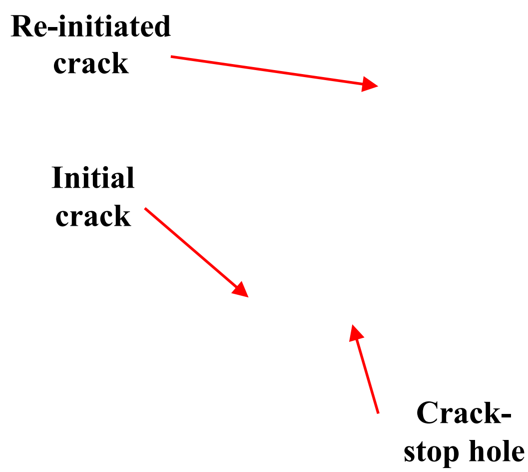

Figure 3. Fatigue crack reinitiating through crack-arrest hole (Dexter 2004)

Reinforcing Crack Stop Holes

Two techniques, cold- expansion of a crack-arrest hole and installation of interference fit fasteners, have been developed in the aerospace industry to improve the performance of crack-arrest holes. Cold- expansion is an accepted technique used to reinforce bolt and/or rivet holes in aluminum aircraft members during both manufacturing and maintenance to keep fatigue cracks from developing or to extend fatigue life in the presence of existing cracks. A literature review

www.manaraa.com

did not produce any examples in which cold- expansion has been used outside the aircraft industry but, from a personal conversation with L. Reid of Fatigue Technology, cold- expansion has recently been used on railroad tracks and bridges (Reid 2011). This technique is being used by railroads to improve the fatigue performance of the boltholes in connections joining rail sections and it has been used on one bridge structure, an elevated section of a highway in California (Reid 2011). The Fatigue Technology cold- expansion process utilizes a split-sleeve mandrel system that consists of a solid, tapered mandrel and an internally lubricated split sleeve. The split sleeve is placed on the small end of the tapered mandrel and the mandrel split-sleeve placed in the hole with the large end of the mandrel going in first. An external force is then applied to the small end of the mandrel and the large end of the mandrel is pulled through the split-sleeve causing the sleeve and hole to expand, plastically deforming the inside of the hole in both the radial and tangential directions. The sleeve is then withdrawn. This results in cold-working the inside diameter of the hole and induces residual, compressive stresses tangentially and radially around the hole. Both the cold-working and the residual compressive stresses act to retard crack initiation and crack propagation.

Use of interference fit fasteners is has been limited to the aircraft industry where they are applied to improve fatigue performance of drilled holes; their use has not translated to bridges or other civil structures (Bontillo 2011). Interference fit fasteners consist of a tapered bolt and an internally tapered and flanged outer-sleeve, which is ground straight externally for use in a straight-sided hole. The interference fit is achieved by tightening the bolt, forcing the taper of the bolt to work against the taper of the sleeve. Fatigue tests have shown an increase in fatigue life with interference fit fasteners by a factor of 10 (10^5 cycles to 10^6 cycles) (Lanciotti and Polese 2005).

المنارة للاستشارات
www.manaraa.com

Strain Hardening, Cold-working, and Hardness Testing

Cold-expanding a crack-arrest hole results in cold-working and strain hardening of the material around the hole. These effects have the potential to increase both the yield and tensile strengths of the material around the hole thereby improving the effectiveness of the crack-arrest hole. Strain hardening phenomena is depicted in Fig. 4, which represents a portion of an idealized stress-strain curve for a strain-hardening steel. If point σ_{yt} in Fig. 4 is the yield stress in tension, strain hardening occurs with increasing deformation and stress beyond σ_{yt}. If stress is reduced after the onset of strain hardening at σ_{yt}, the stress-strain relationship unloads with the same slope as the elastic portion of the stress-strain curve (Point A to Point B). If unloading does not progress beyond Point B to yielding in compression at Point C, reloading follows back along the same path as unloading until the previous high stress, Point A, is reached. Further loading beyond Point A continues with the same strain hardening behavior as previously. The stress at which strain hardening begins after unloading and reloading is approximately the same value that was reached before unloading occurred, Point A, and is higher than initial yielding, σ_{yt}.

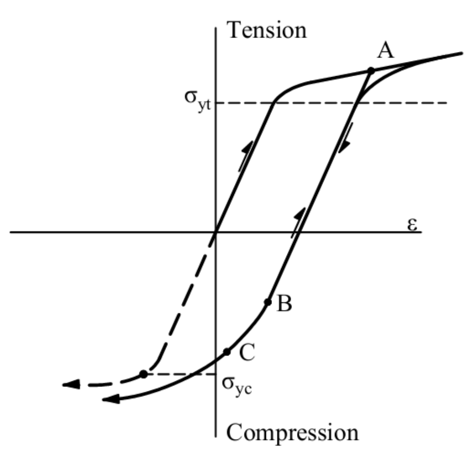

Figure 4. Stress / Strain with strain hardening for a strain hardening steel

www.manaraa.com

Cold-working is severe plastic deformation induced by a controlled mechanical operation (e.g. rolling or drawing) performed at ambient temperature for the purpose of shaping a product. Cold-working elongates the grains of the material in the direction of working, while flattening the grains perpendicular to the direction of working (see Fig. 5). Cold-working increases dislocation density, vacancies, stacking faults, and twin faults; however, most of the energy from cold-working appears to be expended in increasing the dislocation density (Dieter 1989). An annealed metal has a dislocation density of 10^6 – 10^8 dislocations per cm^2 (Dieter 1989); but, after cold-working with severe plastic deformation of ~10%, the dislocation density increases to 10^{12} dislocations per cm^2 (Dieter 1989). Cold-working with the grain deformation and increase in dislocation density raises the yield stress, ultimate stress, and hardness while reducing elongation and reduction in area (Dieter 1989), as depicted in Fig. 6. The plastic deformation associated with cold-working also produces strain hardening.

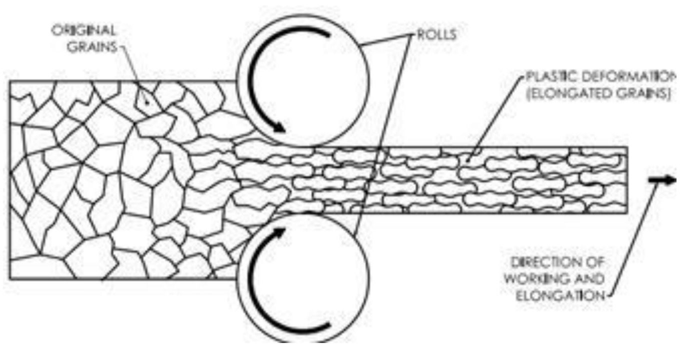

Figure 5. Cold-Working by rolling (Moniz 1994)

المنارة للاستشارات
www.manaraa.com

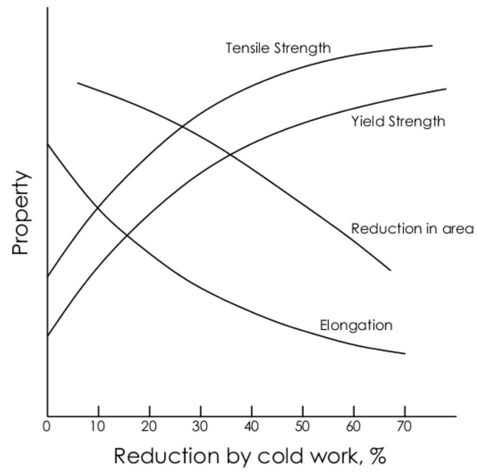

Figure 6. Variation of Tensile Properties with Amount of Cold-working (Dieter 1989)

Because of the small volume affected, measuring cold-working on the inside surface of a crack-arrest hole is not possible with standard testing techniques such as reduced-size tension tests. One method to qualitatively assess the existence and extent of any cold-working is with hardness measurements. Hardness can be measured by forcing an indenter into the surface of a material with a known load. Ball-, pyramid-, or diamond-shaped indenters are all used in hardness testing. In steel specimens, the indenter only disturbs the top few grain layers but, for these top few grain layers, the indentations impose a triaxial state of stress and plastic deformation with strains in the range of 30% or more (Richards 1961). Empirical relationships exist to relate the hardness values of the different indenters to each other (ASTM E140-07 2007) and to the ultimate strength (F_u) of the metal (Moniz 1994). Because the indenter readings are physically related to plastic deformation of the material, the hardness readings can only be related to the ultimate strength; no empirical relationship exists between the indenter hardness values and the yield stress.

Piezoelectric Material and the Effects of Ultrasonic Waves on Metals

Pierre and Jacques Curie first identified the direct piezoelectric effect in 1881 when they showed

www.manaraa.com

that a quartz crystal produced an electric current when subjected to pressure. The converse piezoelectric effect is when the application of a voltage to a material produces expansion in the crystal. This property can be induced into certain other materials containing dipole elements by ‘poling’. ‘Poling’ consists of raising the material above the Curie temperature, applying a strong electric field across it, and cooling the material below the Curie temperature while maintaining the electrical field. This process changes the dipoles which are arrayed in a random direction before poling and fixes them so that they are aligned in the direction of the electrical field. After poling to align and fix the dipoles, the material will act as a piezoelectric material and exhibit both the direct and converse piezoelectric effects (Srinivasan and McFarland 2001).

Various researchers have reported changes in yield strength and tensile strength when metals are subjected to ultrasonic vibration while under tensile loads. Langenecker (1966) reported that ultrasonic vibration can both soften and harden metals. He documented that softening, which he termed acoustic softening, occurred immediately when zinc crystals were subjected to ultrasonic vibration above certain minimum energy levels during static tension testing under deformation control. The tension stress required for continued straining dropped abruptly below the linear-elastic stress-strain curve when the ultrasonic vibration was applied and returned to original value when it was removed. Above higher energy inputs, the acoustic softening occurred during ultrasonic vibration but, when it was turned off, the stress required to produce additional strain was above the original elastic stress-strain curve. Langenecker labeled this effect acoustic hardening.

Nevill and Brotzen (1957) subjected low-carbon steel to ultrasonic vibration while testing the steel in tension. They used annealed, 0.9 mm (20-gage) (0.04-in) diameter wire in a small

المنارة للاستشارات
www.manaraa.com

tension-testing machine under deformation control. The wire was tensioned and ultrasonic vibration applied along the axis of the wire for short time intervals. Nevill and Brotzen (1957) reported that the stress necessary to initiate plastic deformation was reduced by the introduction of the ultrasonic vibration. The reduction in stress was proportional the amplitude of the vibration, but independent of frequency within the range of 15 kHz to 80 kHz, of temperature between 30^{0}C (86^{o}F) and 500^{0}C (932^{o}F), and of prior strain for values of average permanent elongation up to 15%.

Residual Stress and Strain around Cold-Expanded Holes

A substantial body of literature exists on determining the stress / strain resulting from cold-expanding bolt and rivet holes in aluminum members in aircraft and the residual stress / strain remaining at the end of cold-working. These papers discuss results from a range of techniques involving analytical (Nadai 1943; Hsu and Forman 1975; Rich and Impellizzeri 1977; Guo 1993; Ball 1995; Zhang et al. 2005), numerical (Forgues et al. 1993; Poussard et al. 1994; Poussard et al. 1995; Zhang et al. 2005; Nigrelli and Pasta 2008), and experimental procedures (Arora et al. 1992; Polosook and Sharp 1978; Gracia-Granda 2001). Ball and Lowery (1998) provide a comprehensive summary and evaluation of the different techniques. The analytical techniques report development of closed-form solutions that provide acceptable results with low computational effort and are amenable to parametric studies. The closed-form solutions were developed from the formulae for thick shells with different analysts using different yield criteria (i.e., Tresca or von Mises), different stress-state assumptions (i.e., plane stress or plane strain), different material models (varying between elastic-perfectly plastic to elastic with nonlinear strain-hardening), and different unloading models (from elastic to elastic with non-linear reverse yielding). Numerical techniques, primarily finite element analysis (FEA), are efficient for

www.manaraa.com

determining residual stresses after cold-working, modeling nonlinear material behavior, and accommodating large deflections. However, each FEA is limited to a unique geometric configuration and material model, and any change in initial geometry or material model requires a new FEA. In addition, a sophisticated FEA program and substantial computer capacity may be necessary for solving complicated problems such as the residual stress around a hole produced by cold-working. Several experimental techniques have been used to measure the strain in both circumferential and radial directions around the hole during and after cold-working. Because of the dimensions, strain gradients, and strain magnitudes involved, measuring these strains is a difficult task and requires skill, patience, and, sometimes, sophisticated equipment for success.

Analytical Solutions

Nadai (1943) reported the first analytical work concerning cold-working around a hole. He was concerned with copper boiler tubing which was pressed into holes in steel drums or steel head plates in industrial water heaters, steam boilers, and turbine condensers. These connections had to remain tight under high pressure and high temperatures; consequentially, high pressures need to be developed between the copper tubing and the steel boiler head / plate. The high pressure was achieved by expanding the tube and steel plate with rollers. When the expanding operation was completed and the rollers removed, residual stresses remained (compressive in both the circumferential and the radial direction) which kept the joint tight. Nadai (1943) used plane-stress assumptions with an elastic, perfectly-plastic stress-strain relationship for the steel during loading and with elastic behavior when the pressure was removed.

Later analytical work was primarily undertaken to understand the residual stresses around cold

المنارة للاستشارات
www.manaraa.com

worked holes in aluminum for the aerospace industry. Hsu and Forman (1975) extended the work from Nadai (1943) using a modified Ramberg-Osgood (1943) type strain hardening model but still using elastic unloading and applied this to an infinite plate. Rich and Impellizzeri (1977) used formulae for thick tubes from Hoffman and Sachs (1953) and developed different formulae using plane strain assumptions. They used von Mises yield criteria to predict compression yielding on unloading near the edge of the hole. Guo (1993) extended the Hsu and Forman (1975) analysis by including kinematic hardening (Bauschinger effect) and by investigating the effect of a finite thin plate. Ball (1995) also extended the Hsu and Forman (1975) analysis by including elastic–plastic unloading and providing an explicit solution for elastic, nonlinear-plastic unloading for residual stress that predicted a zone of reverse yielding in compression near the hole edge. Zhang et al. (2005) used Ball's (1995) approach but developed the solution for a finite-sized plate with appropriate boundary conditions. Table 1 presents a summary of these different analyses.

المنارة للاستشارات
www.manaraa.com

Table 1 Comparison of Assumptions for Various Closed-Form Analytical Methods

	Material	Plate Size	Stress State	Failure Criterion	Stress - Strain Curve for Loading	Stress – Strain Curve for Unloading	Compressive Yielding on Unloading
Nadai(1943)	Steel	Thin Infinite	Plane Stress	von Mises	Elastic – Perfectly plastic	Elastic	No
Hsu-Forman(1975)	Aluminum	Thin Infinite	Plane Stress	von Mises	Modified Ramberg-Osgood	Elastic	No
Rich / Impellizzeri(1977)	Aluminum	Thick Finite	Plane Strain	von Mises	Elastic - Perfectly Plastic	Elastic with approximation for reverse yielding	Yes
Guo(1993)	Aluminum and high strength steel	Thin Finite	Plane Stress	von Mises	Modified Ramberg-Osgood	Elastic non-linear strain hardening with Bauschinger parameter	Yes
Ball(1995)	Aluminum	Thin Infinite	Plane Stress	von Mises	Modified Ramberg-Osgood	Elastic non-linear strain hardening with Bauschinger parameter	Yes
Zhanget al. (2005)	Medium Carbon Steel	Thin Finite	Plane Stress	von Mises	Modified Ramberg-Osgood	Elastic non-linear strain hardening with Bauschinger parameter	Yes

Numerical Solutions (FEA)

Various papers report the details of FEA of cold-expanded holes (Forgues et al. 1993; Poussard et al. 1994; Poussard et al. 1995; Zhang et al. 2005; and Nigrelli and Pasta 2008). The FEA models in these analyses consisted of 2D, 3D, or axisymmetric models, with axisymmetric and 2D being the predominate approaches. The material properties were input mostly as the actual stress-strain curves developed from unixial tension testing. One paper (Nigrelli and Pasta 2008) used a power hardening law. The effects of plane stress and plane strain assumptions were investigated by using different element formulations. For example, Zhang et al. (2005) used

المنارة للاستشارات
www.manaraa.com

eight-node, biquadratic plane stress quadrilaterals and eight-node, biquadratic plane strain quadrilaterals to investigate the differences between plane stress and plane strain assumptions. The von Mises yield criteria was invoked to determine yielding. Yielding in tension during loading and compressive yielding with unloading were modeled with both isotropic (no Bauschinger effect) and kinematic behavior (full Bauschinger effect). The models were typically loaded with specified displacements being imposed in steps on the hole wall. Results from the FEA analysis were compared with results from closed-form solutions; both the closed-form solutions and the finite element analyses produced similar results when the same parameters were used (Zhang et al. 2005). Fig 7 shows a comparison between Zhang et al.'s implementation of Ball's approach (labeled Present model), Ball's method, and two FEAs – one based on plane stress and one based on plane strain.

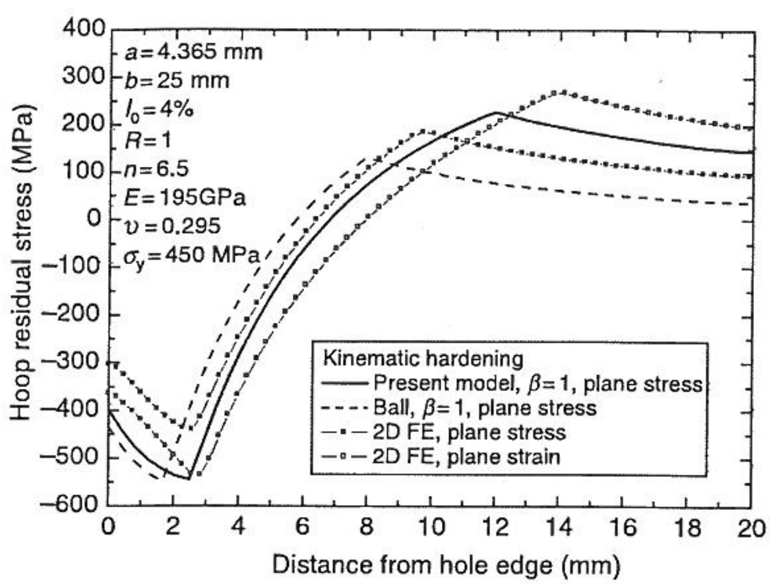

Figure 7. Comparison of FEA and Closed Form Analytical Solutions (Zhang et al. 2005)

Experimental Solutions

Accurate experimental determination of strain around a cold-expanded hole requires precise

المنارة للاستشارات
www.manaraa.com

measurements to obtain reliable results. Several techniques have been tried; these have included using strain gages, a micro-grid around the cold-worked hole, Sach's boring method, X-ray diffraction, and neutron diffraction.

Arora et al. (1992) and Polosook and Sharp (1978) both used strain gages to determine the boundary between the plastic and elastic regions- of a cold-worked hole. Arora et al. (1992) placed 12 gages in a spiral pattern around a hole with gages spaced from 1.5 mm (0.059 in) to 14.0 mm (0.551 in) and measured the strain both before and after cold-working.

Sharp (1978) used a Vickers hardness tester to place a micro-grid around a hole before cold-working. The Vickers hardness tester was used to form pyramidal indentions approximately 10μm (0.00039 in) square and in a pattern at 200 μm (0.00787 in) spacing. The distance between the indentations was measured both before and after cold-working and could be measured within 0.1μm (0.000004 in) allowing for accurate measurement of strain greater than 2%.

Sach's boring method was developed to determine axisymmetric residual stresses in autofrettaged tubes (Gracia-Granda 2001), where autofrettage describes the process in which an outer thick tube is heated, a thick inner tube inserted, and the outer tube allowed to cool. After cooling, compressive residual stresses exist in the inner tube and tensile residual stresses form in the outer tube. This method can be adapted to cold-worked holes by machining the specimen after cold-working into a disk with the hole at the center of the disk. The interior residual compressive stresses in the tangential direction are balanced by tension stress in the tangential

المنارة للاستشارات
www.manaraa.com

direction on the outer edge of the disk. Strain gages are placed in the circumferential direction on the outer edge of the disk (the edge along the thickness of the plate) to measure changes in tangential strain around the circumference of the disk. The inner hole is then bored out in small increments. The change in tangential strain on the outer edge is measured by the strain gages after each boring increment and used to quantify the change in residual strain at the hole edge. Further boring increments allow the strain field to be mapped, as shown in Figure 11.

X-Ray Diffraction

X-rays are waves in the electromagnetic spectrum and exhibit wave characteristics of refraction, diffraction, and constructive and destructive interference. X-ray diffraction (XRD) is an experimental technique for determining near-surface elastic strains in a polycrystalline sample. The generated X-rays consist of a few characteristic lines and a broad spectrum. Two higher energy characteristic lines are the most intense and, since they are very close in energy, these two effectively have a single wavelength of 0.15418 nm (6.094×10^{-9} in). With these short wavelengths they can penetrate from 1 μm (0.00004 in) up to 0.24 mm (0.01 in) depending on the material in the sample, the energy of the X-ray, and the angle of incidence (Hutchins et al. 2005). If the monochromatic (single wavelength) X-ray impinges on a sample with ordered-lattice spacing, constructive interference will occur at a diffraction angle, 2θ. Changes in strain produce a change in the diffraction angle 2θ, which can be measured by the X-ray detectors. From the strains, stresses can be determined within 20 - 35 MPa (3-5 ksi) compared to ~2 MPa (0.3 ksi) for strain gages on metal (Rowlands 1993). For ferritic steels about 60% of the diffracted beam is the result of diffraction in the top 5μm (0.0002 in) layer (Rowlands 1993). XRD utilizes interatomic spacing d and changes in this spacing for a specified hkl lattice plane as

www.manaraa.com

the gage length for strain determination (Fig 8), where *hkl* refers to the Miller indices which describe the specific set of crystalline planes being considered. X-rays from the incident beam are diffracted from the *hkl* planes in the sample surface according to Bragg's Law (Eqn 1) and the diffracted beam is recorded as intensity versus scattering angle by a detector.

Bragg's Law

$$\lambda = 2d_{hkl}\sin\theta_{hkl} \qquad \text{Equation 1}$$

where: λ = wavelength of X-ray beam
d_{hkl} = distance between *hkl* lattice planes inside the material
$2\theta_{hkl}$ = angle between the incident and the diffracted beams

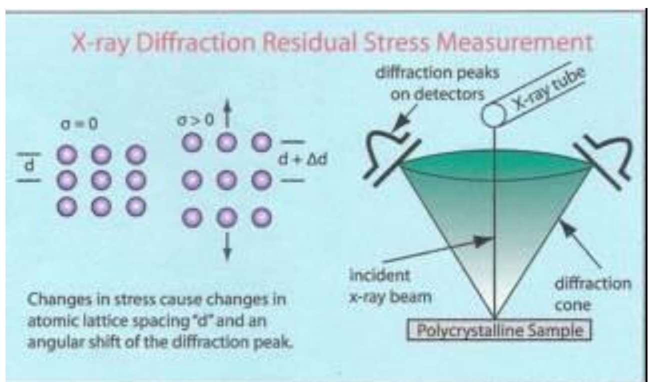

Figure 8. Schematic Showing XRD (PROTO 2013)

Residual and/or applied stress expands or contracts the *hkl* lattice spacing *d* and the residual strain can be determined by comparing the angle of diffraction of the deformed lattice with the angle of diffraction of the undeformed lattice. Equation 2 derived from Bragg's Law shows how the strain and angle change are related.

$$\varepsilon = \frac{\Delta d_{hkl}}{d_{hkl}} = -\left[\cot\left(\Theta_{hkl}\right)\right]\left(\frac{\Delta 2\Theta_{hkl}}{2}\right) \qquad \text{Equation 2 (Rowlands 1993)}$$

المنارة للاستشارات
www.manaraa.com

Where: ε = strain
d_{hkl} = spacing between *hkl* lattice planes
Δd_{hkl} = change in spacing
$2\Theta_{hkl}$ = Bragg's diffraction angle - angle between the beam incident on the *hkl* lattice planes and beam diffracted off the *hkl* lattice planes
$\Delta 2\Theta_{hkl}$ = change in angle

To measure the strain in one direction in the sample surface, the X-ray tube and detectors are tilted in a series of angles called Ψ-tilts where Ψ is the angle between the surface normal and the bisector of the incident and diffracted beams. Tilts on both sides of the surface normal are used. During each measurement at a given tilt angle, the incident beam and detectors oscillate about the tilt angle to improve the reliability of the strain measurement.

With the $sin^2\Psi$ technique, stress can be calculated directly from a single series of Ψ-tilts without first having to determine the strains in two directions (Prevely 1986, Fitzpatrick et al. 2005). The $sin^2\Psi$ technique uses Equation 3 from elasticity theory which defines the strain along an inclined plane in an isotropic material.

$$\varepsilon_{\varphi\psi} = \left(\frac{1+\nu}{E}\right)_{hkl}\left(\sigma_1 \cos^2\phi + \sigma_2 \sin^2\phi\right)\sin^2\psi - \frac{\nu}{E}(\sigma_1 + \sigma_2)$$

Equation 3 (Fitzpatrick et al. 2005)

Where: ν and E are the Poission's ratio and Young's Modulus of the lattice plane hkl being used for the measurements, not the bulk properties of the material,
$\sigma 1$ and $\sigma 2$ are principle stresses in the plane of the surface,
ϕ is the angle from a principle stress in the plane of the surface (Fig 9),
ψ is the tilt angle of the X-ray tube (Fig 9)

المنارة للاستشارات
www.manaraa.com

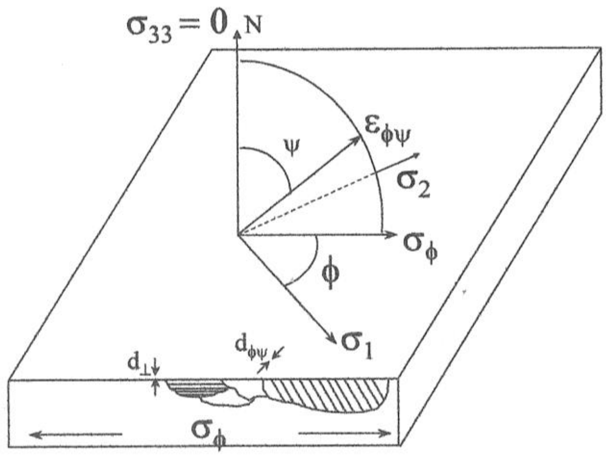

Figure 9. Schematic Showing Diffraction Planes Parallel to the Surface and at an Angles $\phi\psi$ (Firzpatrick et al. 2005)

This equation can be manipulated to derive an equation relating the stress to the slope of a plot of $d_{\phi\psi}$ versus $sin^2\,\Psi$ (Eqn 4).

$$\sigma_\phi = \left(\frac{E}{1+\nu}\right)_{hkl} \frac{1}{d_{\phi 0}} \left(\frac{\partial d_{\phi\psi}}{\partial \sin^2\psi}\right)$$ Equation 4 (Prevey 1986)

Where: E and ν are the same as in Eqn 3,

$\left(\frac{\partial d_{\phi\psi}}{\partial \sin^2\psi}\right)$ is the slope of the line of the measured d at the various ψ angles, and

$d_{\phi 0}$ is the measurement of d at $\psi = 0$

The unstrained lattice spacing d_0 is unknown but the value of $d_{\phi 0}$ differs from d_0 by less than 1%; therefore, $d_{\phi 0}$ may be used in lieu of d_0 with little error (Prevey 1986). In summary, a series of measurements of $d_{\phi\psi}$ is taken at various ψ angles and $d_{\phi\psi}$ plotted versus $sin^2\,\Psi$. The slope of the resulting line is used with the values of $d_{\phi 0}$ at $\psi = 0$ and with E and ν for the lattice plane being

المنارة للاستشارات
www.manaraa.com

considered to calculate the stress along the line formed by the intersection of the plane of the surface and the plane containing the ψ tilts. This allows the XRD process to measure stress directly from a sample under load or with residual stress without the need for comparison to a reference measurement of an unstrained sample.

One problem with X-ray diffraction is that it is sensitive to strains in the surface. Hence, all residual surface stresses from manufacturing processes such as rolling or forming must be removed in such a manner so as not to induce new residual surface stresses. This can typically be accomplished by electropolishing the surface. XRD has several advantages over neutron diffraction or other techniques to measure residual strain. Measurements at a given Ψ-angle can be taken in a matter of minutes; the complete data set for 10-30 different Ψ-angles may only take a couple of hours. Portable XRD equipment is available to make in-situ measurements. XRD has been successfully used to measure strains in the vicinity of a cold-expanded hole; Figure 10 shows a plot comparing tangential residual stress as calculated from Ball's closed-form solution with that calculated from strain measured by XRD (Ball 1995).

المنارة للاستشارات
www.manaraa.com

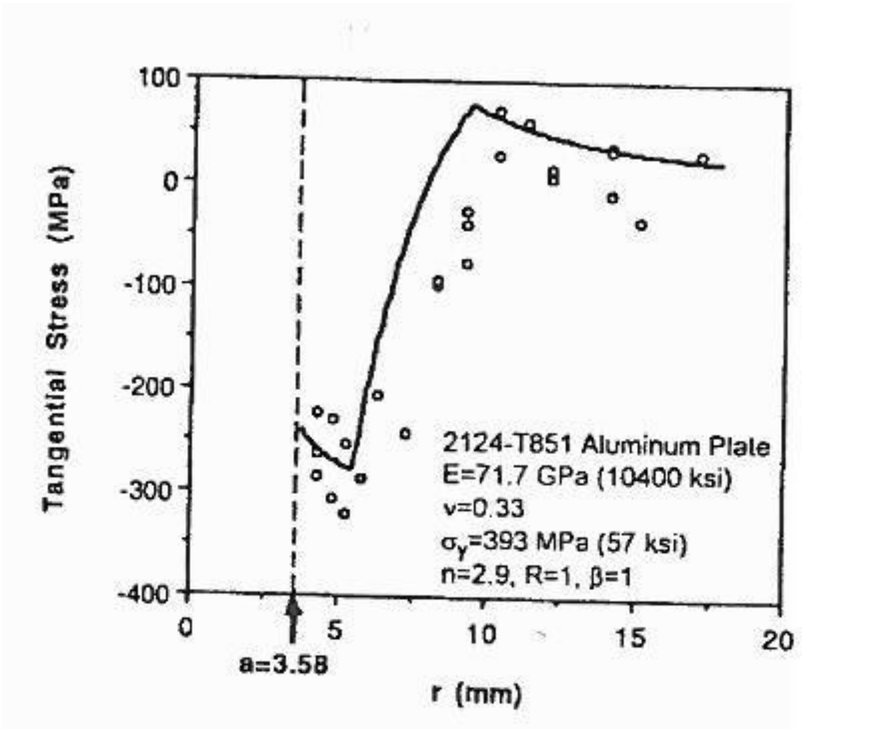

Figure 10. Comparison of Ball's Closed Form Solutions with Stress Calculated from XRD (Ball 1995)

<u>*Neutron Diffraction*</u>

Neutron diffraction (ND) is analogous to X-ray diffraction in that neutrons, like X-rays, interact with the material and are scattered from lattice planes in the crystalline materials according to Bragg's Law. Just as occurs with X-rays, the neutrons of a select wavelength diffract from a subset of grains with specific orientations relative to the scattering geometry. The measured *hkl* lattice spacing can be related to the angle between the incident and diffracted neutron beams and the wavelength of the radiation per Bragg's Law Eqn 1. Residual and/or applied stress change the *hkl* lattice spacing thereby changing the diffraction angle; this allows the computation of strain from the change in the diffraction angle. Unlike XRD, ND equipment cannot be rotated to make multiple ψ-tilts and the $\sin^2\psi$ technique cannot be used to calculate stress. Instead, strain must be measured along three orthogonal lines and stress calculated from these strains using

www.manaraa.com

equations from elasticity theory.

The penetration power of the neutrons is approximately several orders of magnitude greater than conventional X-rays and thus allows strain measurement in ferritic steels to a depth of 25 mm (0.98 in) (Hutchings et al. 2005). Neutron diffraction is a volumetric measurement in which strains are averaged within a volume defined by the intersection of the projection of the incident and diffracted beams through their corresponding apertures; these dimensions can be as small as 0.5 x 0.5 x 1.0 mm (0.0197 x 0.197 x 0.0394 in) in steel (Cheng et al. 2003). By using different orientations of the specimen, strains in all three orthogonal directions can be obtained. As in X-ray diffraction, strains in a specified direction can be measured along a line across the sample with spacing so close as to make the measurements almost continuous. Unlike X-ray diffraction, surface preparation to eliminate surface residual stresses is not required. However, ND requires a high flux neutron source. Even with this high flux source, an order of magnitude more time is typically required to obtain similar precision in data from ND as from XRD. Neutron sources are not portable as a high neutron flux is only available from a nuclear reactor or similarly complex facility such as the Spallation Neutron Source at Oak Ridge National Laboratory (ORVL). Only a few of the nuclear reactors in the United States have an instrument configured to measure residual strain: High Flux Isotope Reactor at ORNL; National Institute of Standards and Technology, Gaithersburg, Maryland; and the University of Missouri, Columbia, MO.

Comparison of XRD and ND

Figure 11 (Stefanescu et al. 2004) provides a comparison of several experimental techniques to determine residual strain around a cold expanded hole. Fig 11 shows the residual hoop (tangential) strain from cold-expansion of a 9.5 mm (3/8 in) diameter hole in a rectangular plate

المنارة للاستشارات
www.manaraa.com

specimen (180mm x 40 mm x 5mm) (7.09 in x 1.57 in x 0.20in) made from 7050-T76 aluminum alloy. The residual strains in this specimen were measured with high-energy X-rays, Synchrotron XRD. Fig 11 relates the residual hoop strain measured with the high-energy X-rays with those measured by ND and Sach's boring method on similar specimens (Edwards and Wang 1996). Figure 11 shows that all three experimental techniques yield similar results and, based on Figure 10 and Figure 11, it is clear that both XRD and ND are valuable tools for measuring the residual strains due to cold expanding a hole.

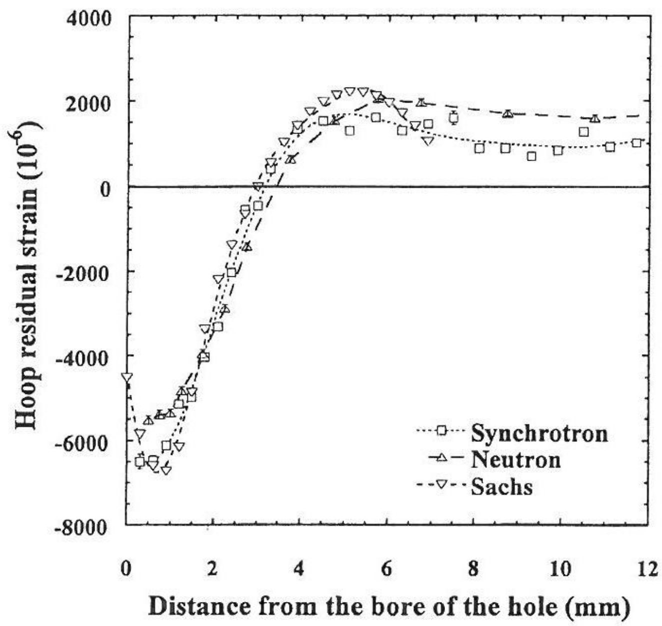

Figure 11. Comparison of Measured Tangential Strain After Cold-Working (Stefanescu et al. 2004)

TEST METHODOLOGY

It was decided to focus the current research on a proof-of-concept study using a reduced-scale, laboratory-compatible PICK tool and fatigue specimens. The hypothesis was that the PICK treatment would improve fatigue performance of the crack-arrest holes in fatigue specimens. While multiple techniques would be used to understand how the PICK treatment improved the fatigue performance, the most conclusive way to demonstrate an improved fatigue performance

المنارة للاستشارات
www.manaraa.com

from PICK treatment was by fatigue testing PICK treated specimens. Simulating a fatigue crack by inducing a controlled crack with specific dimension is a complex operation difficult to duplicate with precision required in laboratory testing of multiple specimens. Since the objective was to study crack initiation from a hole at the tip of an existing crack, it was decided that the same effect could be evaluated without inducing a crack but by drilling a hole in a location that would be designed to be susceptible to fatigue cracking and counting the load cycles for fatigue cracks to initiate at the either edge of the hole. This also eliminated the length of the crack as a variable. The specimen was designed with a hole at a location which would be subjected to the maximum cyclical stresses and to fit the universal testing machine (UTM) available for fatigue testing. When the details for the fatigue specimens were decided upon, the PICK tool was designed to be compatible.

Hardware Description

Fatigue Specimens

As the majority of plate girder bridges susceptible to fatigue cracking were built before the mid-1980s, it was decided to use Gr. A36 steel with yield strength of approximately 250 MPa (36 ksi) for the fatigue specimens. The actual material properties were determined for the steel per standard tension testing requirements for flat bars (ASTM E8-04), but the material properties used for the aluminum plug, which was 60601-T6, were taken from literature (Boyer 1987). Both were reported in Crain et al. (2010) and are reproduced in Table 2.

المنارة للاستشارات
www.manaraa.com

Table 2. Material Properties for A-36 Steel and 6061-T6 Aluminum (Crain et al. 2010)

Material	Modulus of Elasticity, MPa (ksi)	Yield Strength, MPa (ksi)	Ultimate Strength, MPa (ksi)	Poisson's Ratio
Aluminum	77,220 (11,200)	312 (45.2)	440 (63.8)	0.35
Mild Steel	200,000 (29,000)	319 (46.3)	463 (67.2)	0.30

The test specimens were fabricated from a 3.2 mm (1/8-in) thick steel bar and, to ensure that fatigue cracking occurred at the center of the specimen, the width of the specimens narrowed from 53 mm (2 in) at the ends to 32 mm (1-1/8 in) at the center (Fig. 12). Holes with diameters of 3.2 mm (1/8 in) were drilled and reamed at the center of each specimen at the minimum width with the expectation that fatigue cracking would initiate at this location first with the cracks oriented perpendicular to the long axis of the specimen and initiating at the inside edges of the hole.

Aluminum Plug

The aluminum plug was fabricated from aluminum dowel stock with a slightly larger diameter than the 3.2 mm (1/8-in) diameter holes with the length slightly longer than the 3.2 mm (1/8-in) thickness of the bar.

المنارة للاستشارات
www.manaraa.com

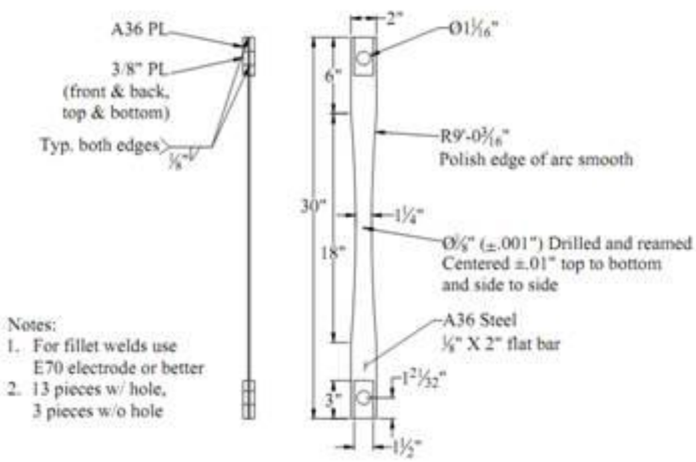

Figure 12. Fatigue test specimen

PICK Tool

The PICK tool was designed to compress the aluminum plug, hold this force on the plug, and provide a stiff reaction platform to direct the ultrasonic vibration into the aluminum plug and the steel fatigue specimen. The tool needed to be stiff to ensure that most of the energy went into the specimen and was not absorbed by the tool. The tool was bench mounted with its major features being the C-shaped base, threaded bolt, piezoelectric elements, and a round, load-transfer plate (Figs. 13 and 14). The base and the other steel components were machined from 4140 annealed steel with yield strength of 412 MPa (60 ksi) having dimensions as shown in Fig. 13. The end of the bolt was machined to form a 3.2 mm (1/8-in) diameter tip to match the 3.2 mm (1/8-in) plug; force was applied to the plug by tightening the bolt at the top of the tool thereby pressing the tip into the aluminum plug. The tip of the bolt proved to be too soft and deformed excessively; therefore, the tip was replaced with a hardened dowel pin which was pressed into a hole drilled into the tip of the bolt. The tip of the hardened dowel pin was machined into a truncated-cone with the smaller end fitting on the end of the aluminum plug. Underneath the fatigue specimen was a round, load-transfer plate, which was held in place by a nylon rod and assembled to fit

المنارة للاستشارات
www.manaraa.com

tight with the top of the piezoelectric stack beneath it. Another hardened dowel pin with a tip similarly machined to that in the tip of the bolt was pressed into the top of the round, load-transfer plate and completed the load path through the aluminum plug. The piezoelectric elements were stacked and held in place with the nylon rod. The load path for the ultrasonic force developed by the piezoelectric elements was through the round, load-transfer plate, directed by the aluminum plug into the steel fatigue specimen, and eventually resisted by the threaded bolt and the top portion of the tool.

A Micro-Measurements strain gage (EA-06-062AQ-350) and a small strip of piezoelectric material (7.5-mil thick strip of PZT-5A from Piezo Systems) were attached to the PICK tool. The strain gage was glued to the flat section on the inside surface of the vertical upright of the PICK tool so that the gage measured bending strain (Fig. 13). The piezoelectric strip was aligned vertically and glued to the vertical leg of the tool on the back surface opposite the strain gage, as shown in Fig. 13.

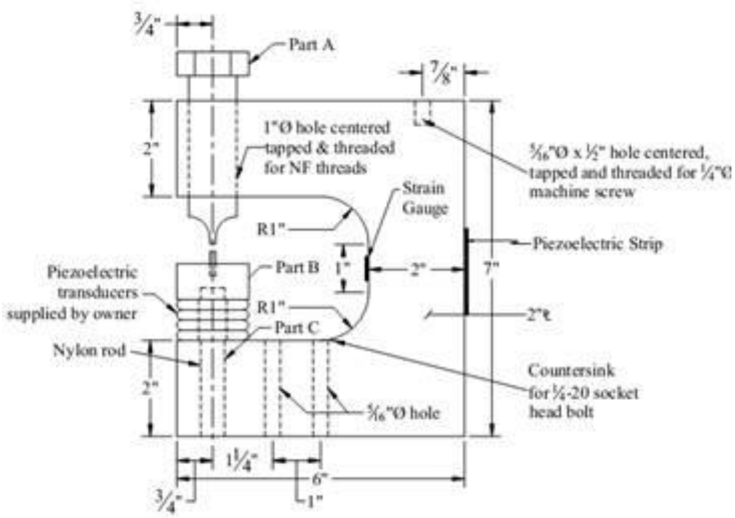

Figure 13. PICK tool schematic

المنارة للاستشارات
www.manaraa.com

Figure 14. Fatigue specimen during PICK treatment

Piezoelectric Elements

The piezoelectric elements were obtained by disassembling a commercial ultrasonic cleaner; the piezoelectric elements were assumed to be PZT-4 material, which is the commonly used piezoelectric element in these cleaners. The properties for PZT-4 are shown in Table 3.

Table 3. Assumed Properties for Piezoelectric Elements

Electromechanical coupling coefficient - □	Piezoelectric transfer efficiency - □	Activation constant for strain in the 3-direction for current in the 3-direction - d33	Short circuit Young's modulus of piezoelectric material - YE33
0.700	0.837	285x10-12 m/volt	6.6x1010 N/m2

Piezoelectric elements have a positive and a negative side; these can be identified by placing an element on a conductive surface and connecting a volt meter between the conductive surface and the upper face of the piezoelectric element. If the voltmeter shows positive when the positive probe is pressed against the surface of the piezoelectric element, that face of the piezoelectric

المنارة للاستشارات
www.manaraa.com

element is the positive side and the other side is the negative side. This can be checked by reversing the probes and the faces of the piezoelectric elements and applying force through the negative probe. Once the positive and negative faces were identified, the four piezoelectric elements were assembled as shown in Figs. 13 and 14 such that direction of current was the same across each element. With the piezoelectric elements stacked in this a manner, expansion and contraction deformations obtained by applying an electric field across the elements (converse effect) were additive in all the elements.

Electronics

Electronics powering the PICK tool consisted of a sine wave generator and an amplifier. The sine wave generator was a Hewlett Packard 3300A Function Generator with a variable-sweep-frequency capability and adjustable voltage output. The amplifier was a Piezo Systems Inc. Linear Amplifier Model EPA-104 with adjustable gain, as shown in Fig. 15.

Figure 15. Electronics Used with PICK Tool

المنارة للاستشارات
www.manaraa.com

Data Acquisition

While fatigue testing of the treated specimens was considered to be the most direct method to demonstrate any improvement in fatigue performance achieved by the PICK tool, multiple techniques besides fatigue testing were used to evaluate PICK tool performance.

Retained expansion (*RE*) as defined by Eqn. 5 is used by the aerospace industry as a measure of the amount of the expansion remaining after cold- expanding a hole (Ball and Lowery 1998).

$$RE = \left(\frac{R_{final} - R_{initial}}{R_{initial}} * 100 \right)\% \qquad \text{Equation 5}$$

Where: R_{final} = the final radius of the hole and
$R_{initial}$ = the initial radius before cold-expansion

RE was obtained for treated specimens by measuring the hole diameter with a digital caliper before and after treatment by the PICK tool. Ten measurements were taken at different diametric locations around the hole and the values averaged both before and after treatment. Retained expansion was then computed using Eqn. 5.

A brittle coating with a layer of undercoat was applied to the specimens after the plug was pressed into the hole but before treatment by the PICK tool. The brittle coating and undercoat were Stresscoat ST-70F/21C and Stresscoat ST-850 Undercoat; these products were applied following the manufacturer’s directions. These were applied to provide an immediate visual and quantative indication of whether the PICK tool was actually plastically deforming the steel in the vicinity of the hole. The brittle coating is formulated to crack at a specified level of elastic

المنارة للاستشارات
www.manaraa.com

strain; however, where the steel plastically deforms, the brittle coating debonds and flakes off. This flaking provides a clear delineation of the extent of plastic deformation and the location of the elastic-plastic boundary.

The strain gage that was installed on the vertical upright of the PICK tool was used to monitor static loading when the bolt was tightened on the aluminum plug; this was to ensure the loading on the plug from the PICK tool was consistent on every specimen treated. Another gage (MicroMeasurements WK-06-250BG-350) was glued to a piece of scrap steel that was separate from the tool but in close vicinity to the tool. This gage was used to monitor for signal drift and random electrical noise. A National Instruments (NI) NI ENET-9219 Ethernet DAQ device with a NI cDAQ 9172 USB Data Acquisition System was used to power both of these gages and to collect both of their output signals. NI LabView on a desktop computer was used to process the signals and to provide the results for real time monitoring and evaluation.

The piezoelectric elements of the PICK tool were excited with a sine wave from the signal generator through the amplifier. The converse effect of these piezoelectric elements subjected the aluminum plug and the surrounding steel to ultrasonic vibration and imposed a sine wave bending deformation mode on the PICK tool. The bending response of the PICK tool to this imposed deflection caused bending in the piezoelectric strip on the back of the PICK tool which generated another electrical signal by the direct effect. This signal was monitored with a Telequipment Type D54 oscilloscope (Fig.15), which provided a measurement of the strength and frequency of the PICK tool response.

www.manaraa.com

An Extech True RMS Multimeter was used to measure the frequency output from the signal generator to the amplifier and to measure current output from the amplifier to the piezoelectric elements in the PICK tool. As the input frequency to the piezoelectric elements was in the kilohertz range and the multimeter was not capable of measuring voltage output at this frequency range, the Telequipment Type D54 oscilloscope was used to measure voltage from the signal generator to the amplifier, from the amplifier to the piezoelectric elements, and the output from the piezoelectric strip on the back of the tool.

Fatigue specimens were also instrumented. Two Micro-Measurement strain gages (WK-06-250BG-350) were attached to opposite faces of each of the fatigue specimens. These two gages were aligned on the fatigue specimen to measure axial strain at corresponding locations on the opposite faces of the fatigue specimen for the purpose of monitoring bending of the specimen during fatigue testing. ASTM E 466-07 (2007) requires that the bending stress should be limited to 5% of the greater of the range, maximum, or minimum stress imposed during any fatigue-testing program. In addition, another strain gage was placed on an unrelated piece of scrap steel and used to monitor signal drift and electrical noise. These three gages were powered and the output signal collected by a NI ENET-9219 Ethernet DAQ device with a NI cDAQ 9172 USB Data Acquisition System, which provided results to a desktop computer. A MTS Model 312.31 Load Frame with a MTS Model 661.21, 345-MPa (50-kip) Load Cell was used to perform the fatigue testing. During fatigue testing, movement of the crosshead of the MTS and load from the load cell of the MTS were provided to the same NI data acquisition devices as the strain gage values. NI LabView was used to process and display in real time the crosshead movement and load from the UTS along with the strain gage data.

المنارة للاستشارات
www.manaraa.com

Other Evaluation Techniques

Metallurgical Evaluation

One fatigue specimen was sent to a metallurgical lab for evaluation after being treated by the PICK tool but before being subjected to fatigue testing. The metallurgical evaluation consisted of grain size analysis and hardness testing. After reviewing the results of the metallurgical analyses of the first specimen, three additional specimens from the same bar stock were sent to the metallurgical lab where grain size analysis and hardness testing were performed on them. One of these was a control specimen not treated by the PICK tool. The second was only cold-expanded by applying force with the PICK tool to plastically deform the steel in the vicinity around the hole but not using the piezoelectric elements to apply ultrasonic vibration. The third was fully PICK-treated. See Simmons (2013) for a complete description of this testing.

X-Ray Diffraction

Neutron diffraction and X-ray diffraction measurements of the residual strain distribution around the PICK treated holes were conducted at Oak Ridge National Laboratory (ORNL) in Oak Ridge, TN in May 2011. Two 51 mm x 51 mm (2 in x 2 in) plates were fabricated from the same bar stock with a hole as previously described and were treated with the PICK tool. Neutron diffraction was used to measure the value and distribution of the residual strain produced by the PICK tool on one of these plates and X-ray diffraction was used to measure the same on the other.

The X-ray diffraction was performed at the High Temperature Materials Laboratory at ORNL

المنارة للاستشارات
www.manaraa.com

using PROTO LXRD 2000 X-ray diffraction equipment (Figs. 16 and 17). The PROTO LXRD consists of the following major components (PROTO LXRD 2013):

1. X-ray tube
2. Detectors
3. Goniometer
4. XYZ-stages
5. Mapping function
6. Computer controls
7. Safety features

The X-ray tube was the PROTO MG2000L with a Cu target which operates at 40 Kv with 30ma and is water-cooled. The detectors consist of two Position Sensitive Scintillation Detectors (PSSD), which are mounted on the goniometer attached to the tube housing so as to detect diffracted x-rays at angles on either side of the incident beam. The goniometer accurately measures the detector positions and, in conjunction with the detector outputs, accurately measures the angles of the diffracted beam profiles. The xy-stages are intended to position the sample in the xy-plane and can be computer controlled to move the sample to successive positions to obtain a series of measurements. The accuracy of measurement requires carefully positioning of the goniometer height relative to the sample surface. To achieve this, a special touch probe is inserted into the X-ray tube and is used in conjunction with the Z-stage to map the

www.manaraa.com

elevation of the surface of the material. For mapping, the computer positions the sample so that each successive point of interest is positioned under the touch probe. Then the computer lowers the touch probe until it just touches the surface of the sample. With the touching the computer maps the elevation of the sample surface in the z (vertical) direction. This elevation is stored in the computer and is used to control the elevation of the X-ray tube with respect the surface of the sample so that the distance between the X-ray tube and the sample is correct for the X-ray diffraction measurement. With the vertical elevation from the mapping function and with a series of xy-locations programmed into the computer, the computer is used to successively position the points on the sample under the X-ray beam, to position the X-ray tube at the correct elevation, and then to take a series of diffraction measurements at a successive number of Ψ-tilts. The computer then processes these measurements into a residual stress value at each point using the $sin^2\psi$ analysis procedure. Safety features include tube shielding, computer controlled shutter on the X-ray beam, the X-ray tube's kilovolt and milliamp settings, an enclosure with shielding glass to absorb scattered X-rays, a light to show when the X-rays are being emitted, and an automatic shutoff if the enclosure doors are opened while the X-ray tube is in operation. The XRD equipment is shown in Fig. 16 and 17.

المنارة للاستشارات
www.manaraa.com

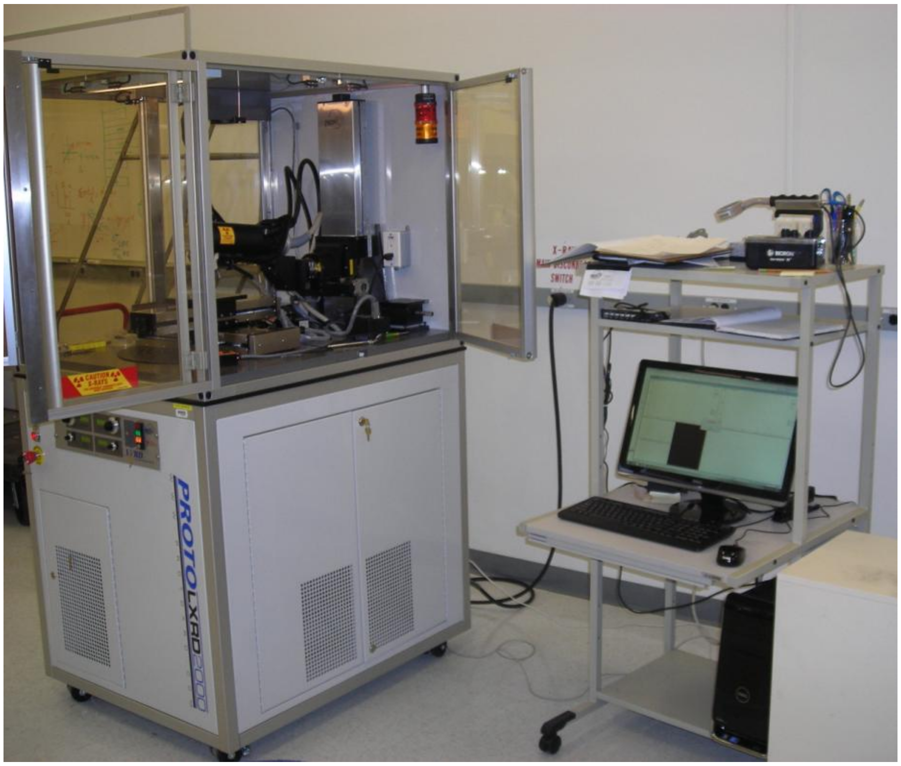

Figure 16. PROTO LXRD X-ray Diffraction System

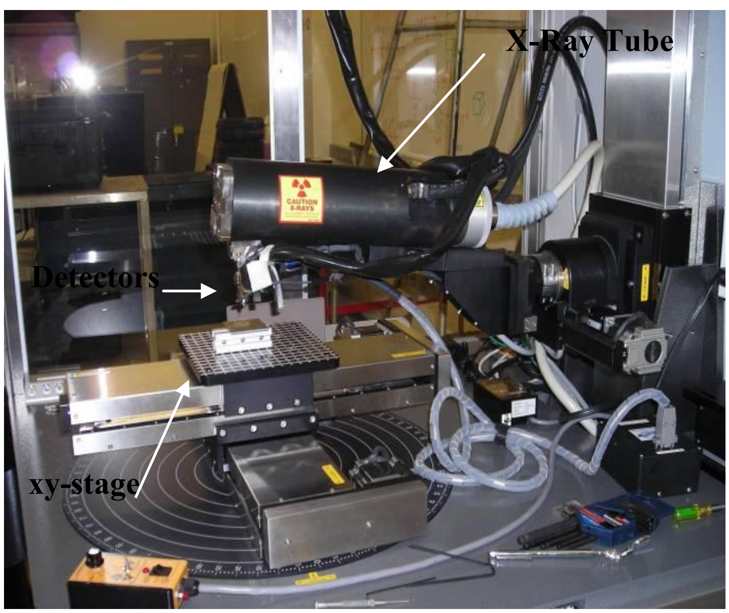

Figure 17. X-Ray Tube, Detectors, and X, Y, and Rotation Stages

www.manaraa.com

Neutron Diffraction

Neutron diffraction measurements were performed at the ORNL Second Generation Neutron Residual Stress Mapping Facility (NRSF2), which is located at the HB-2B beamline at the High Flux Isotope Reactor (HIFR). Components of NRSF2 are (Fig 18):

1. Reactor
2. Shielding
3. Beam tubes
4. Monochromator
5. Shutter
6. Apertures
7. X-Y-Z-Ω-2Θ goniometer
8. Detectors
9. Computer controls

The reactor at HFIR is a beryllium (Be) -reflected, light-water-cooled and -moderated, flux-trap type reactor that uses highly enriched uranium-235 as the fuel to provide a continuous source of neutrons (ORNL 2013). The beam tubes leading from the Be reflector provide the thermal neutron with an intensity of ~$3x10^{15}$ neutrons/(cm^2 sec) (Hutchings et al. 2005). The beam tubes transmit the neutrons to the monochromator and from the monochromator to the incident aperture (incident slit). The doubly bent stacked Si wafer monochromator at NRSF2 was designed to extract a narrow range of wavelengths and to provide a beam of neutrons which can

المنارة للاستشارات
www.manaraa.com

be diffracted off the chosen *hkl* lattice plane (Hubbard 2013). The monochromator for HB-2B beamline also serves to focus the neutron beam on the diffraction target or sample. A neutron beam of the selected cross section passes through the incident aperture (incident slit) before reaching the sample. The incident aperture establishes the height and one horizontal dimension of the gage volume over which the strain is averaged. The sample is mounted on the X-Y-Z-Ω manipulation table which is computer controlled and used to accurately place the gage volume at precise positions within the sample and at the correct angle to obtain a given strain component. The neutrons diffracted from the gage volume in the sample pass through the diffraction beam aperture and register on the detectors. The diffraction aperture fixes the other horizontal dimension of the gage volume. Both apertures are carefully machined from gadolinium, a neutron absorbing rare earth element (Hubbard 2013). The seven detectors at NRSF2 are He^3/Ar filled linear position sensitive detectors (PSD), which detect neutrons by measuring electric charge produced by the interaction of the neutrons with the He^3 (Hubbard 2013). The detectors and electronics determine the linear position of the neutron in the detector. The position and detector number are then recorded in a multichannel analyzer (MCA). The MCA reports to the NRSF2 data collection computer the number and position of all the neutrons detected for a single measurement. The data collection computer uses the diffraction profile to determine the diffraction angle via fitting a profile model. The results are peak position, peak intensity, and full width at half maximum of the diffraction profile. Strain is then calculated by comparing the diffracted angle for the target sample with the diffracted angle from an unstressed / unstrained sample (Fig. 18). Safety features at NRSF2 include beam stop, intrusion sensor, warning lights, and automatic shutter closure; all of which are activated if anything approaches closer than a set distance from the vicinity of the incident and diffracted beams when the shutter is open. The

المنارة للاستشارات
www.manaraa.com

safety features for the general experimental area of the reactor are extensive and include continuous air monitors (detects radioactive contamination in the air), gamma radiation detectors, fire detectors, and many sensors for safe operation of the reactor.

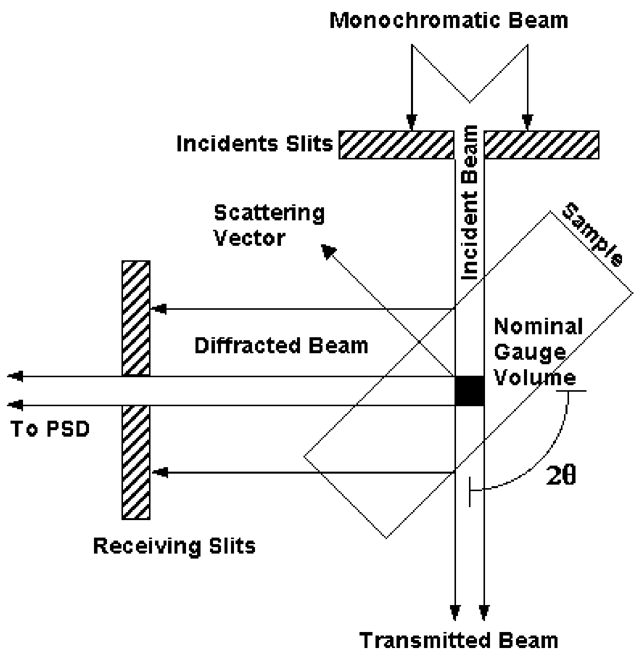

Figure 18. Schematic Diagram of Neutron Diffraction HB-2B Beamline (Watkins et al. to be published)

Testing Protocol

PICK Treatment

In preparing fatigue specimens for PICK treatment, an area approximately 51 mm (2 in) long and centered on the fatigue specimen was cleaned of mill scale. The width and thickness at the center as well as the hole diameter were measured with digital calipers. The alignment of the PICK tool was adjusted and the aluminum plug pressed into the hole. The undercoat and brittle coating were applied to the cleaned area and cured per manufacturer's instructions. The specimen was placed in the PICK tool, alignment re-checked, and bolt tightened until a strain value of 224 microstrain was read from the strain gage. This equated to a force of 9.2 kN (2.1

www.manaraa.com

kips), or an approximate stress of 1.2 GPa (170 ksi), on the aluminum plug. The electronics were energized and supplied power as a sine wave voltage to the piezoelectric elements in the PICK tool. A sweep of frequencies was conducted to identify the resonant frequency of the tool with the sine wave excitation from the piezoelectric elements. Resonant frequency, which was in the ultrasonic range and always at the upper end or above the audible range, was the input frequency to the tool that produced the largest output voltage from the piezoelectric strip on the back of the tool. Once the resonance frequency was determined, the strain gage for the tool was checked and the bolt tightened until the 224 microstrain was re-established. The treatment was left with the 224 microstrain and the frequency set at the resonance frequency for 114.5 hours. Both of these values, 224 microstrain and 114.5 hours, were arbitrary, but they were used on the first specimen and were therefore maintained to provide a consistent basis for comparing results. Once the time period was reached, the specimen was taken out of the tool, photographed, and the extent of the area where the brittle coating had flaked off measured with a circle template. The aluminum plug and the remnants of the brittle coating were then removed. Dimensions of the hole were measured along 10 different diametric locations and the diameters averaged and the retained expansion calculated using Eqn. 5.

Fatigue Testing

Due to several causes which could not be totally eliminated (slight misalignment of the grips of the UTS, slight initial imperfections in specimen straightness, the holes in the ends of the fatigue specimen not being entirely parallel, the holes in the ends not being perpendicular to the axis of the fatigue specimens, etc.), some bending was induced in the tensile fatigue specimen during fatigue testing. To eliminate or minimize this bending, cable ferrules were pressed on the ends

www.manaraa.com

of two small wire cables and one end of each cable threaded through the hole of the fatigue specimen. The other ends of the cables were attached to turnbuckles which were in turn attached through other small cables to the columns of the MTS (Fig. 19). The tension in the cables could be adjusted using the turnbuckles and the center of the fatigue specimen held in an aligned position to minimize induced bending strain. To measure the bending strain, strain from the two strain gages attached to the fatigue specimen were collected and processed with LabView to separate bending and tension strains. The wire cables connected to the center of the fatigue specimens were tightened or loosened as required to minimize bending strain as much as possible. This allowed minimization of bending strain, but it existed to some extent in all the fatigue specimens and it was difficult to limit the bending strain to less than 5% of the range or maximum stress as required by ASTM E 466-07 (2007).

After completing several fatigue tests to establish the testing protocol, a stress range was selected that provided a basis for comparison yet limit testing time to a reasonable value. A crack-initiation indicator was established by using a crosshead displacement several thousandths of an inch larger than the highest displacement being experienced and setting this value as a displacement limit for the test. Reaching this limit was an indication that a crack had initiated. Once this limit was reached, the test was immediately halted and the specimen checked to determine if a fatigue crack had actually initiated. If fatigue cracking had initiated, the stress range and the number of cycles were recorded. If not, the test was re-started with new displacement limits and was allowed to continue until the new displacement limit was reached. This cycle was repeated until a fatigue crack was observed.

المنارة للاستشارات
www.manaraa.com

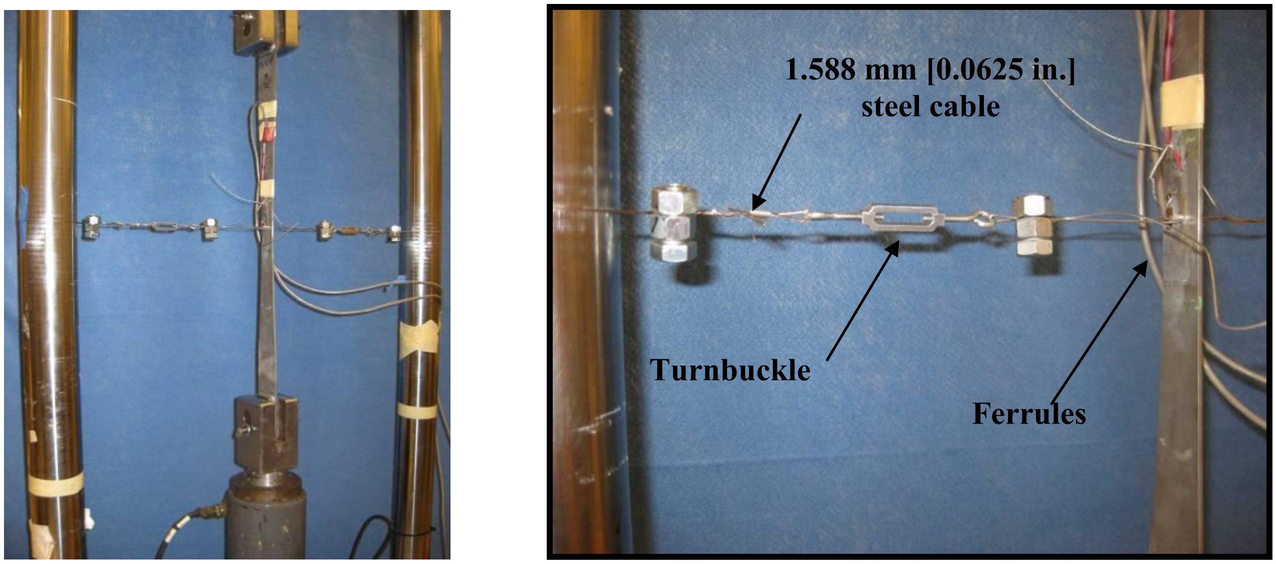

Figure 19. Fatigue specimen mounted in UTS (Crain 2010)

X-Ray Diffraction

From inspection of the plates selected for XRD, it was suspected that the surface of the plate contained residual stress from rolling during the manufacturing process. To check this, the LXRD was programmed to measure hoop strain along a radial line and the results differed from expected. To remove these surface residual strains from the rolling, an Electrolytical Polisher (Fig. 20) was used to polish the surface and remove a small layer of material. The Electrolytical Polisher is an electrochemical process to remove material from a metallic surface. The metallic surface was connected to the positive terminal of a DC power supply and served as the anode. The negative side was from the plate through a flowing electrolyte to the cathode. A current passed from the anode, where thin layers of metal on the surface were oxidized and dissolved in the electrolyte. This polisher used a super saturated salt solution as the electrolyte and an approximately 6.35 mm ($^{1}/_{4}$-in) diameter surface could be polished at one time (Fig 21). The line

المنارة للاستشارات
www.manaraa.com

of measurements was longer than this diameter; so polishing along the line was accomplished with the successive circles of polished area overlapping. XRD measurements were then taken along the polished line and the surface further polished until successive XRD measurements yielded similar strain values, indicating that the residual surface strains induced by rolling had been removed and just the macro strains from the PICK process remained. It took five cycles (cycles 4 and 5) of polishing before two successive sets of strain measurements were roughly equivalent.

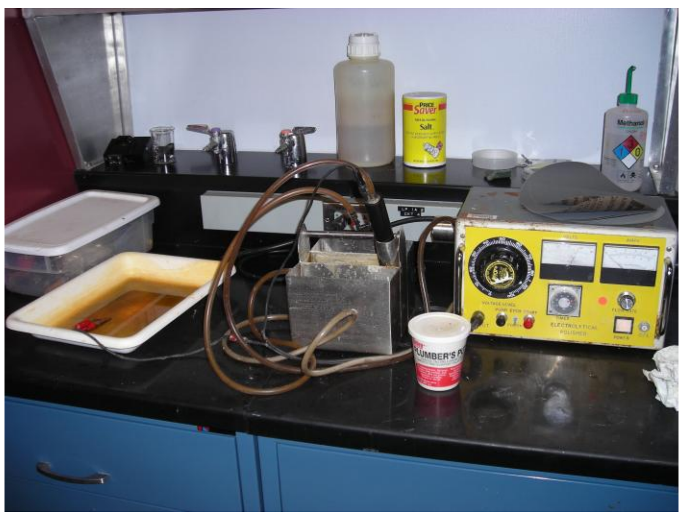

Figure 20. Electrolytical Polishing Equipment

المنارة للاستشارات
www.manaraa.com

Figure 21. Electrolytical Polishing Tip Working on the Surface of Specimen

Once the polishing procedure was established, two radial lines perpendicular to each other and parallel to the sides of the specimen were polished. When a polished line was accurately aligned with the axis of the X-ray tube and detectors, tangential strain could be measured and, when a polished line was accurately aligned perpendicular to the axis of the X-ray tube and detectors, radial strain could be measured. The appropriate coordinates, x and y, where the measurement were to be taken along the line were programmed into the computer and the mapping function used to locate the z elevation. Once this was done, the computer was programmed to take the measurements along the line. Two sets of measurements were taken for the tangential strain and one was taken for the hoop strain on each of Rows 1 and 2; for a total for four sets of tangential strain measurements along a radial line and two sets of radial strain measurements along a radial line. The ferritic 211 planes (where 211 are the *hkl*-Miller indices designating the crystalline planes being measured) were used for the XRD stress measurements. This plane was used because it exhibits the strongest diffraction of any of the planes in a ferritic material and its elastic constants provide the best match for the macro strain produced by tension testing

المنارة للاستشارات
www.manaraa.com

(Hubbard 2013). For CuKa the diffraction angle, 2θ, was approximately 156°. Measurements were made at Ψ-tilts from -40° to $+40^{\circ}$ with the X-ray tube tilting a total of eleven times yielding a total of 22 measurements of *d*-spacing versus Ψ angle. The measured *d*-spacing was plotted against the $sin^2\Psi$ for each of the 22 Ψ-tilts and the slope of the line calculated (Fig 22). With this slope, the nominal elastic properties for the 211 plane, and the $d_{\phi 0}$ which was measured perpendicular to the surface; the stress at this location could be determined using Eqn 4. Each set of measurements for either the tangential or radial stress along a line took roughly four hours from setup to finish.

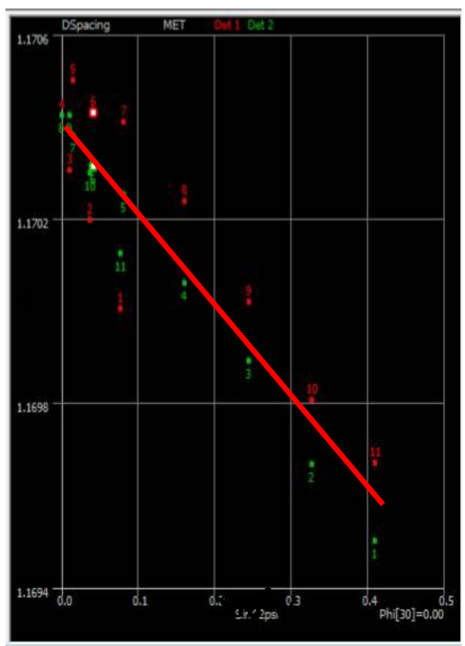

Figure 22. Computer Generated Plot of d vs $Sin^2\psi$ at One Measurement Point. Shows the Slope Used in the Stress Calculation Eqn. 4

Neutron Diffraction

A 3.2 mm (1/8 in) cube from the same A-36 steel plate as the treated specimens but which was in the same stress / strain condition as the original, untreated steel plate was mounted on one edge

www.manaraa.com

of the sample plate at a corner (Fig. 23) for use for reference measurement and for periodic test of the stability of the system during measurements. The specimen was mounted on the manipulation table (Fig. 24) and the table maneuvered until the center of the hole was centered in the neutron beam; this centering was optically controlled using three theodolites. Gadiolinium slits for the incident beam and diffracted beam produced a gage volume 0.5mm high x 1mm x 1mm for the tangential strain measurements and 1 mm high x 0.5mm x 1mm for the radial and normal strain measurements. Nominal gage volumes for tangential, radial, and normal ND measurement were therefore all 0.5 mm^3. The volume of the material over which the strain was actually averaged, instrumental gage volume, was slightly larger than the nominal gage volume because of widening of the incident beams and the diffracted beams due to divergence in the beams over the slit to sample distance of approximately 25 mm (1 in). Once the specimen was centered with the theodolites and the slits installed, the measurements were started and the plate moved through the beam in such a manner as to map the beam across the plate thickness. Evaluating the measured intensities of the diffracted beam as the gage volume traversed from one side of the plate to the other, the exact coordinates of the center of the plate were established. Starting with the hole center and the plate mid-thickness coordinates, three series of measurements were taken: one each for the radial, tangential, and normal directions. Each series (radial, tangential, or normal) consisted of measurements along the same three radial lines through the center of the plate; one was along the centerline of the plate and the others were at 0.5 mm (0.02 in) on each side of the centerline. For each series, a measurement was taken starting 1 mm (0.04 in) from the center of the hole and then taken along the radial line at 0.25 mm (0.01 in) intervals until 5 mm (0.20 in) from the center of the hole was reached. Then the intervals were increased to 0.5 mm (0.02 in) until 7.5 mm (0.30 in) was reached, increased to 1

المنارة للاستشارات
www.manaraa.com

mm (0.04 in) until 12.5 mm (0.49 in) was reached, and a final measurement was taken at a distance of 14 mm (0.55 in) from the center of the hole. The 211 planes were used as the lattice plane for measuring the strain by neutron diffraction - the same as was used in the XRD. Strains were reported along with the intensity of the neutrons impacting on the detectors in neutrons / sec.

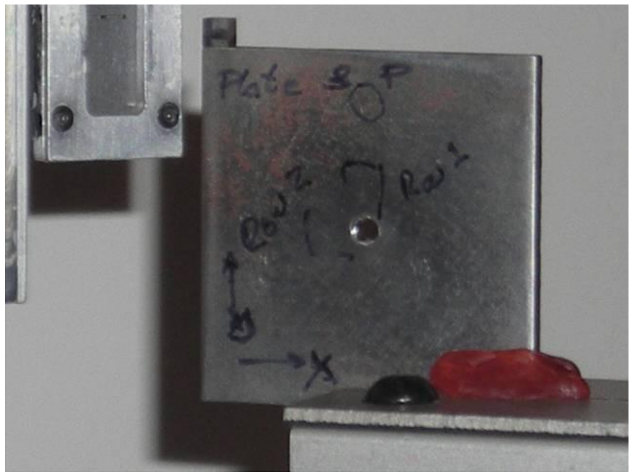

Figure 23. ND Specimen with Cube from the Original, Untreated Steel Plate Mounted on Top Left Corner

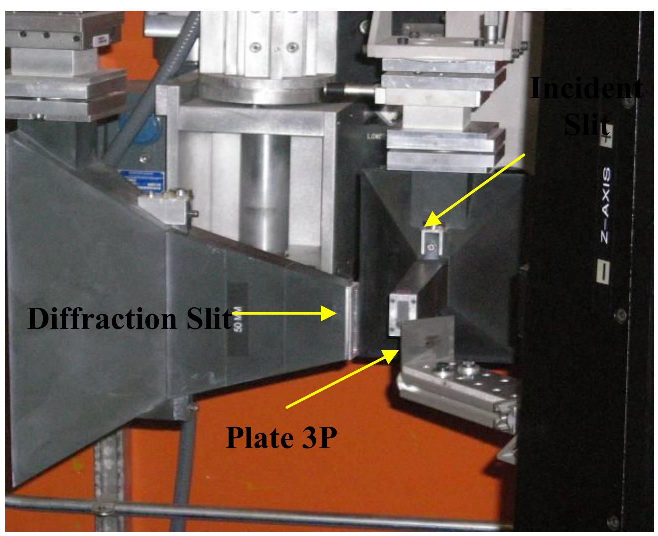

Figure 24. Incident and Diffraction Apertures with Plate 3P Mounted on XYZ-Stage

المنارة للاستشارات
www.manaraa.com

RESULTS AND DISCUSSION

The results of the test program including fatigue testing, hardness testing, grain size analysis, retained expansion, load decay, and power measurement are summarized here but discussed in detail in Simmons (2013) and Simmons et al. (2013). The focus of the results and discussion presented in this chapter are focused on the results from the XRD and ND measurements and comparing these results with those from analyses using close-form solution techniques.

Three sets of fatigue testing specimens were fabricated: the first set of five was used as control specimens with no cold-expansion of the aluminum plug or treatment by the PICK tool, the second set consisted of four specimens subjected only to cold-expansion with no PICK treatment, and the third set consisted of six specimens that were subject to cold- expansion and PICK treatment with ultrasonic vibration. Using a 95% confidence level, cold- expansion by itself increased fatigue life by 84% over those with no treatment; while treatment with the PICK tool showed an increase in fatigue live of 160% over those with no treatment.

From the metallurgical testing, shallow grain deformation was observed at the surface of the hole for the untreated specimen, which was only subjected to drilling and reaming of the hole. This deformation was limited to those grains immediately next to the hole surface. For the cold-expanded specimen, a layer around the surface of the hole exhibited grain deformations to a depth of approximately 0.008 to 0.009 mm (0.0003- 0.0035 in). For the PICK-treated specimen, a layer of grain deformation was revealed to a depth of approximately 0.01 mm (0.004 in) from the edge of the hole. The scanning electron microscope revealed grain deformation to a slightly greater extent in some locations; but, in general, the difference in the radial extent of the grain

المنارة للاستشارات
www.manaraa.com

deformation between the cold-expanded and the PICK-treated specimens was so slight that it appears that the cold-working of both the cold-expanded and the PICK-treated specimens was roughly equivalent.

Also from the metallurgical testing, the hardness readings from the cold-expanded specimen were roughly 15% higher than for the untreated specimen; this difference in hardness readings between untreated and cold-expanded specimens is thought to be the result of cold-working during the cold-expansion process. The hardness readings from the PICK-treated specimens were approximately 22% higher than those for the untreated specimens. The differences between the cold-expanded and the PICK treated specimens is thought to be the result of acoustic-hardening from the ultrasonic vibration during the PICK treatment.

Retained Expansion (*RE*) was calculated using the diametric measurements before and after treatment using Eqn 5. For fatigue specimens, the PICK treatment produced a *RE* ratio 24% higher than those cold-expanded. For the plate specimens, the PICK treatment produced a *RE* ratio 66.3% higher than specimens that were only cold-expanded.

Brittle Coating

Although applying the brittle coating according to the manufacturer's directions required care and attention to detail, it was an excellent means of immediately evaluating the effectiveness of the PICK tool by providing a visual indication that the PICK tool had plastically deformed the steel around the hole (Fig. 25). The limit of the plastic deformation, the elastic-plastic boundary, is clearly visible in Fig 25 as the area where the brittle coating disbonded. Note the

المنارة للاستشارات
www.manaraa.com

radial cracks in the remaining brittle coating in Fig 25 near the elastic-plastic boundary; these indicate elastic tension strain in the tangential direction.

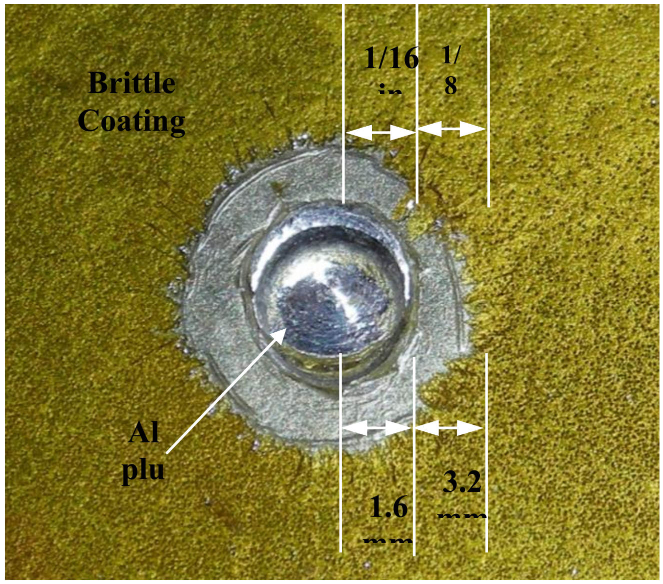

Figure 25. PICK Treated Specimen Showing Plastic Region

Analysis

To further evaluate the performance of the PICK tool, it was decided to compare the experimental results from the XRD and the ND with that predicted by analytical techniques. From the results shown in Figure 10 from Ball (1995), it was decided to use the closed-form solutions from Nadai (1943) and Ball (1995) with the material properties for the steel plate used in this research program (Table 2).

Nadai (1943)

As a first approximation it was decided to use Nadai (1943) approach, which assumes elastic, perfectly-plastic stress-strain relationship for the steel material and Von Mises failure criteria.

www.manaraa.com

Applying this method and using the material properties in Table 2, the results for both the stress at the end of the expansion process and after the removal of the expansion pressure are shown in Fig 26 as a normalized function (σ/σ_{yield}) of the normalized distance (*radius / initial radius*) from the center of the hole. The plot does not account for the deformation of the hole. Note that the peak of the tangential stress coincides with the elastic-plastic boundary at $r/r_{initial}$ equal to 1.75. Also at the end of expansion, the tangential stress near the hole is in compression and not tension. This is believed to be the result of Poission's ratio changing from an elastic value of 0.3 to a plastic value of 0.5 (Dowling 2007). The plot of residual tangential stress shows a minimum stress of 1.15σ_y in compression, that the tangential residual stress becomes tensile at $r/r_{initial}$ equal to 1.4, and becomes a maximum at 0.39σ_{yield}. Note that the radial residual stress is 0 at the hole edge which agrees with engineering mechanics. The radial residual stress is always compressive along the radial line with the maximum compressive stress equal to 0.24 σ_{yield} at $r/r_{initial}$ equal to 1.5.

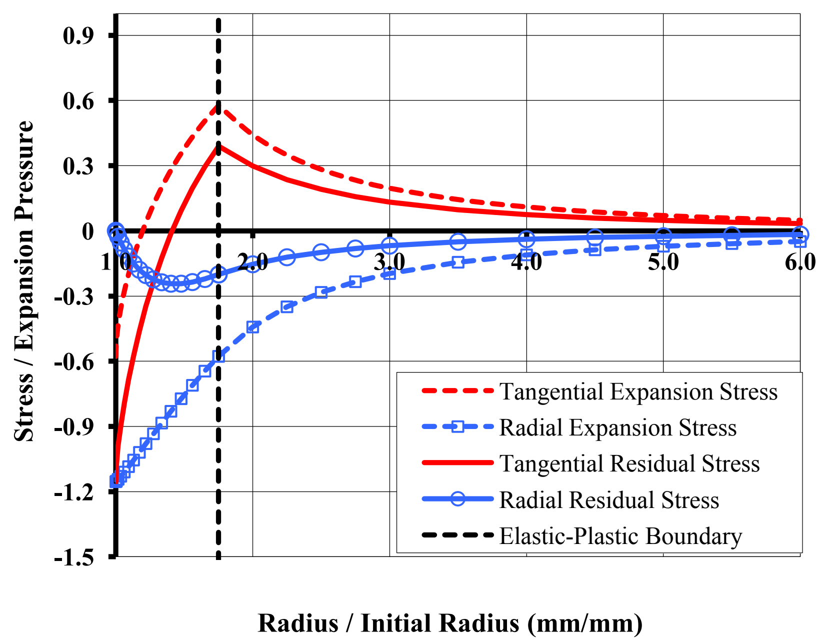

Figure 26. Expansion and Residual Stress from Nadia (1943)

المنارة للاستشارات
www.manaraa.com

Ball (1995)

It was apparent from the results achieved from the application of Nadai's approach (1943) that the elastic, perfectly-plastic modeling of the material properties in Table 2 was inadequate to evaluate the residual strain induced by the PICK tool. Ball (1995) approach uses a modified Ramberg-Osgood (1943) relationship to model the stain hardening behavior of the steel (Fig. 27) in the plastic portion of the stress-strain curve. It was thought that this relationship would more accurately modelt the imposed strains and residual stress from the PICK treatment. Equation 6 shows the modified Ramberg-Osgood (1943) equation. In the elastic region, stress and strain are related by Young's modulus; while in the plastic region, they are related with a power hardening relationship.

$$\sigma < \sigma_{yield} \qquad\qquad \varepsilon = \frac{\sigma}{E} \qquad \text{Equation 6a}$$

$$\sigma > \sigma_{yield} \qquad\qquad \varepsilon = \frac{\sigma}{E}\left(\frac{\sigma}{\sigma_{yield}}\right)^{n-1} \qquad \text{Equation 6b}$$

The behavior of Equation 6 with a stress-strain curve developed from testing of the steel plate used in this research (Crain 2010) was investigated with different values of n and is plotted in Figure 27. The Measured Stress-Strain curve in Fig 27 is a curve from a tension test conducted according to the requirements of ASTM E08-04 (2004). High values of n (n >1000) behave as an elastic, perfectly-plastic material. Because ε =0.06, i.e. 6%, was a typical value for the Retained Expansion at the end of the PICK treatment, σ_{yield} was adjusted for all values of n in Fig 27 so that the value of the modified Ramberg-Osgood (1943) curve matched the measured values of stress and strain for σ = 358.4 MPa (52.0 ksi) and ε = 0.06. n = *10* was selected as best

المنارة للاستشارات
www.manaraa.com

representing the strain hardening in the plastic region because the energy between the n = 10 curve and the Measured Stress-Strain curve less than about ε = 0.01 approximately equals the energy between the n = 10 curve and the Measured Stress-Strain curve beyond ε = 0.01. For n = 10, a yield stress of 241.6 MPa (35.04 ksi) was use compared to a measured yield stress of 319.2 MPa (46.3 ksi).

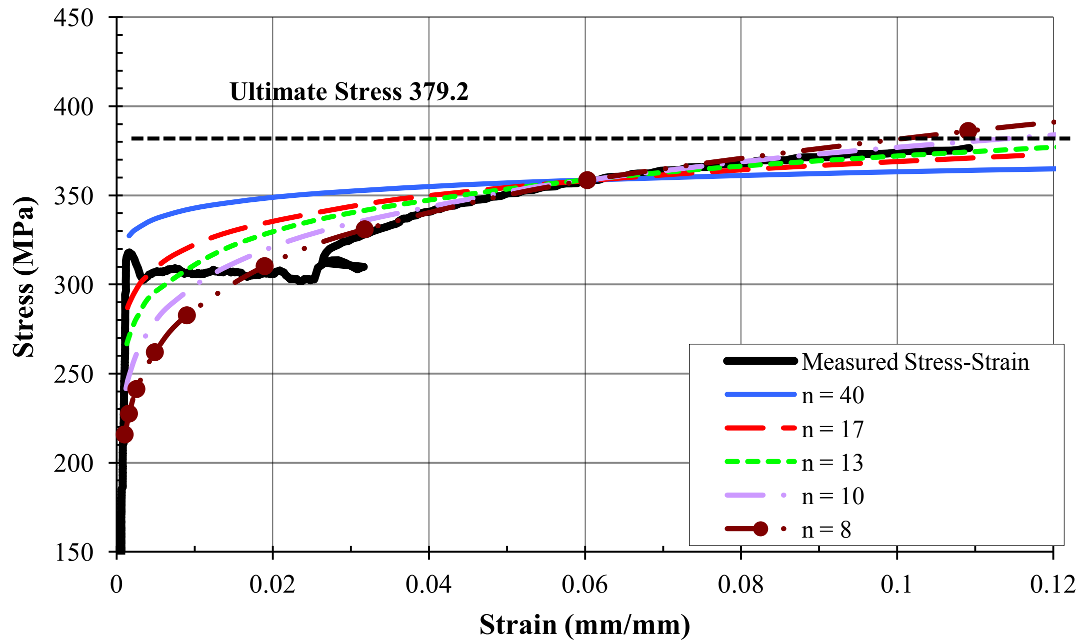

Figure 27. Modified Ramberg-Osgood (1943) Equation with Different Power Values Plotted on Measured Stress-Strain Curve

The residual stress from the procedures presented in Ball (1995) with n = 10 and n = 40 are plotted in Figs. 28 and 29 with the residual stresses from the analysis using Nadai's (1943) procedure. Ball's procedure shows that a region of compressive yielding exists next to the hole ($r/r_{initial}$ = 1) when the expansion pressure is removed (Fig 28). This effect is so small that it is not discernable at the scale used in Fig 28 for n = 40, but it is quite evident for n = 10. Note that the elastic-plastic boundaries (the peaks of the tangential stress) are roughly equal for Nadai

www.manaraa.com

(1943) and for Ball (1995) n = 40 (1.751) but it is at a larger $r/r_{initial}$ (2.57) for Ball (1995) n=10. For Ball (1995) n = 10, minimum tangential stress is -1.4 σ_y and the maximum tangential stress is 0.3 σ_y. For all the analyses, the radial residual stress is approximately equal to zero at the edge of the hole and always compressive along the radial line away from the hole (Fig. 29). Maximum compressive stress for the residual radial stress for Ball (1995) n = 10 is –0.45 σ_y.

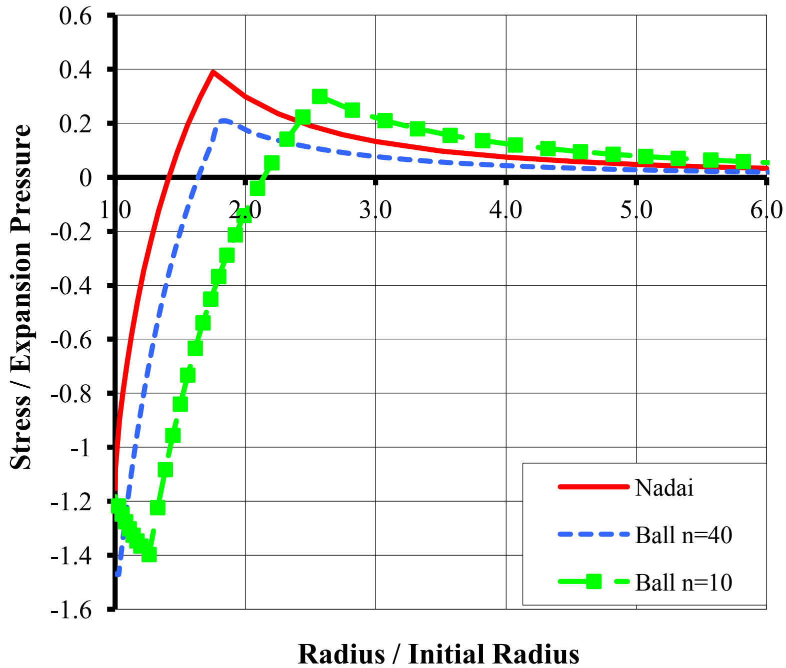

Figure 28. Analytical Determination of Tangential Residual Stress

المنارة للاستشارات
www.manaraa.com

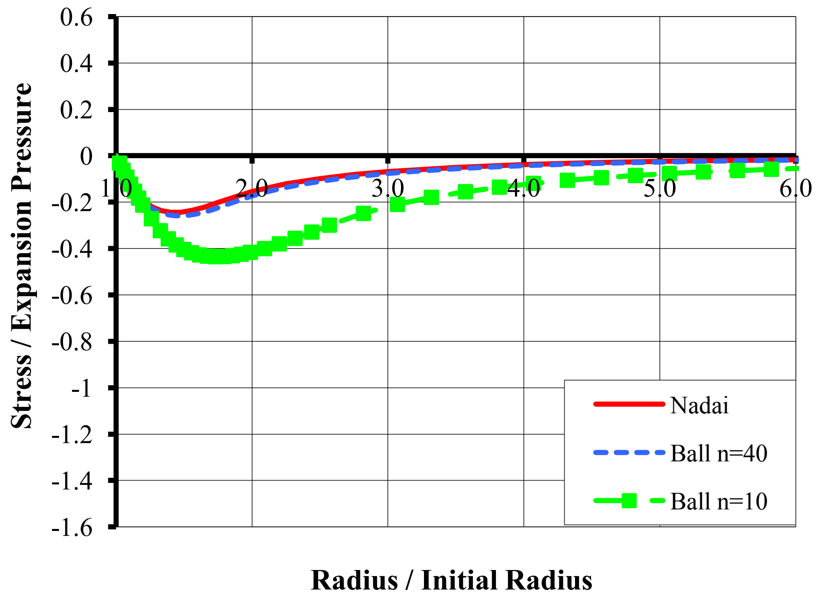

Figure 29. Analytical Determination of Radial Residual Stress

X-Ray Diffraction

The *sin*^{2} Ψ procedure was used along with the macro elastic properties of the material to derive both radial and tangential residual stress from the XRD strain measurements. These radial and tangential residual stresses are plotted in Figure 30 as a function of the normalized radius from the center of the hole. The tangent residual stress is an average of four different series of XRD measurements, two each from Row 1 and Row 2, while the radial residual stress is an average of two series of XRD measurements, one each from Row 1 and from 2. Neither the radial nor the tangential residual stresses from the XRD (Fig 30) agree well with the calculated radial and tangential residual stresses from Ball (1995) and Nadai (1943) in Figs. 28 and 29. This is thought to be a result of the surface residual stresses in the plate from the manufacturing processes and the electro-polishing which was used in an attempt to eliminate them. The mapping feature in the XRD equipment measured the elevation differences from the elevation

المنارة للاستشارات
www.manaraa.com

measured at the first point which was at the edge of the hole. Figure 31 shows the differences in elevations along Row 1 plotted in relation to the distance from the center of the hole and Figure 32 shows the same for Row 2. These two figures show maximum elevation differences of 0.1 for Row 1 and 0.15 for Row 2. The elevation differences have the same shape for each of the rows although within each graph there is some offset between each measurement; so it appears that the differences actually exist. If 60% of the diffracted beam is the result of diffraction in the top 5μm (0.0002 in) layer in the steel (Rowlands 1993), the measured strains are taken from different elevations with respect to the ideal layer being measured and are probably affected by the residual stress from the manufacturing processes that were not removed by the electrolytical polishing. Because of the elevation differences, it was thought that the XRD results were not accurate and they were not included in evaluating the PICK performance.

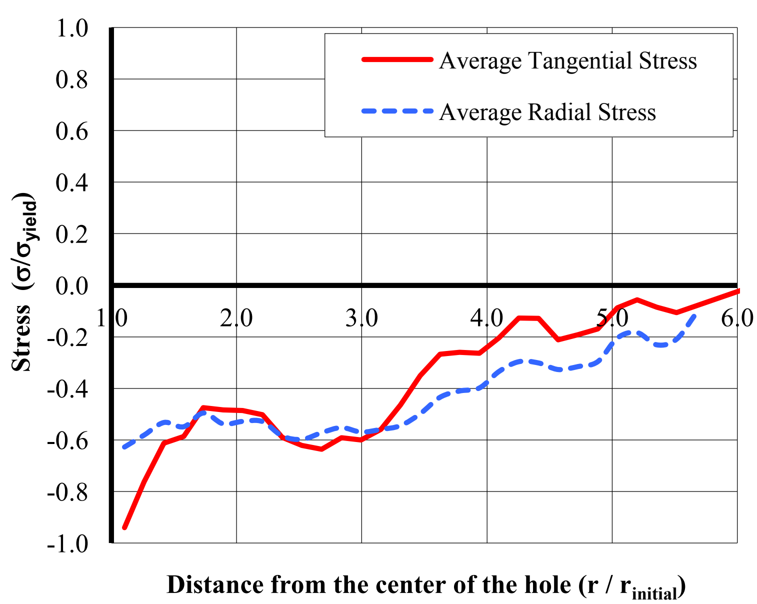

Figure 30. Normalized Stress vs Normalized Radius from X-Ray Diffraction

www.manaraa.com

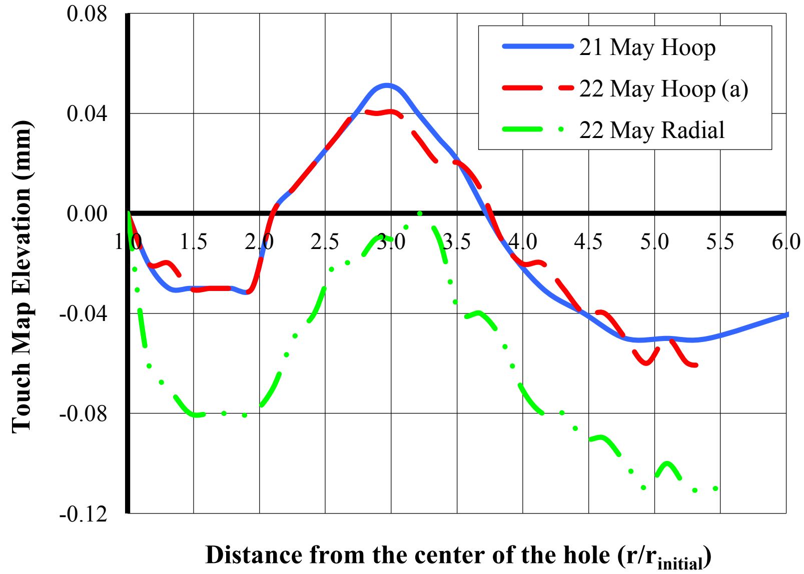

Figure 31. Elevation with Distance from the Hole Row 1

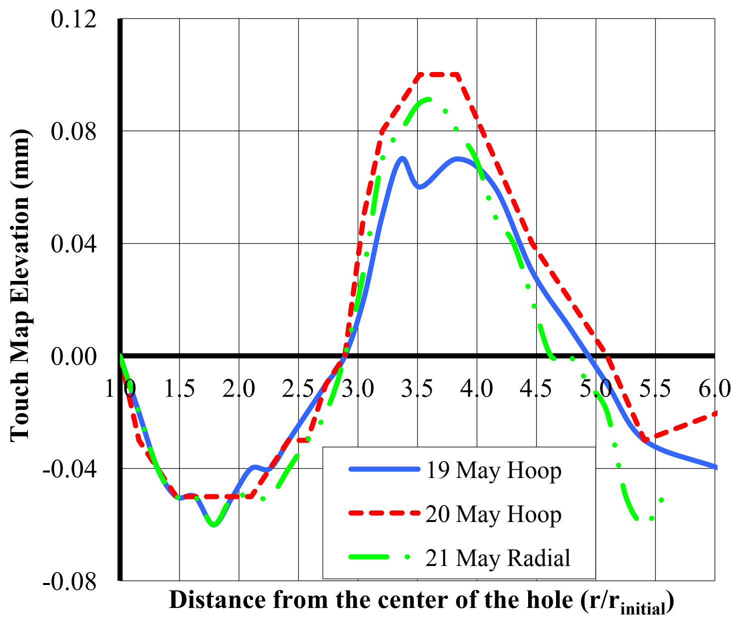

Figure 32. Elevation with Distance from the Hole Row 2

Neutron Diffraction

The tangential, radial, and normal strains measured from the ND are plotted in Figure 33. Each

www.manaraa.com

curve (average tangential, average radial, and average normal) in Figure 33 is the average of that strain component taken along same three different lines through the middle of the plate; one line was along the exact centerline of the plate and the other two lines were 0.5 mm on either side of the exact centerline of the plate. The ordinate on Figure 33 is in units of microstrain, i.e. length/length x 10^6; while the abscissa shows radius / the initial radius measured all from the center of the hole. For the tangential residual strain, the minimum strain is $-1553\mu\varepsilon$, the maximum is $396\mu\varepsilon$, while the elastic-plastic boundary is about $r/r_i = 5.6$. Note that the tangential strain near the hole edge ($r/r_i = 1$) appears to showed yielding in compression. The radial residual stress exhibited a minimum at $-597\mu\varepsilon$ and shows some tension near the hole edge but was compressive over most of the radial line along which the measurements were made. The normal strain had a maximum of $484\mu\varepsilon$ starting out in tension and becoming compressive along the radial line. The shapes of the radial and tangential residual strain, in general, matched the curves of stress calculated from procedures of Nadai (1943) and Ball (1995) in Figs. 28 and 29.

المنارة للاستشارات
www.manaraa.com

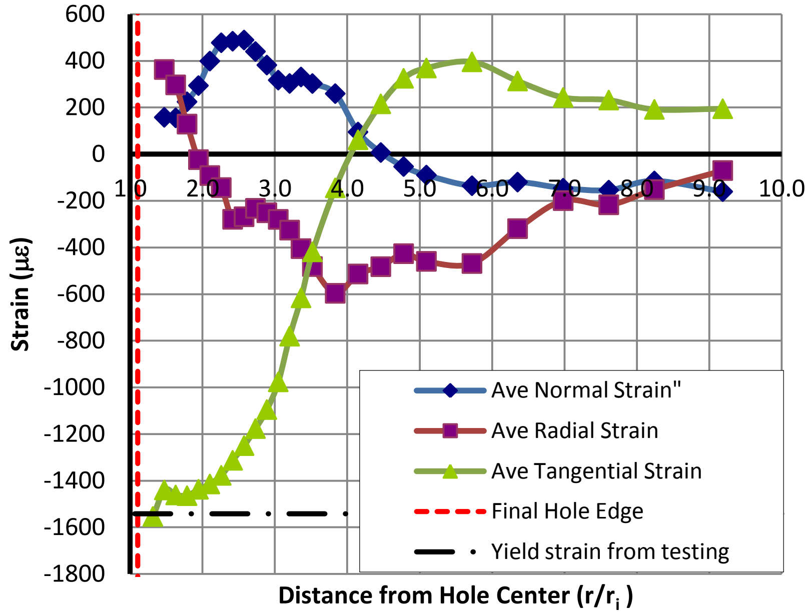

Figure 33. Strain Measured with ND

To provide a better comparison between the calculated stress from Ball (1995) and Nadia (1943) and the strain measured by the ND, the results from Nadia (1943) and Ball (1995) were converted from stress to strain. Ball (1995) provides a procedure to convert stress from his equations to strain; unfortunately this procedure is incorrect and also does not provide strain values which can be compared with the values measured by ND. Figure 34 is an idealized stress-strain curve constructed from the modified Ramberg-Osgood (1943) Equation 6 with a n value selected to fit the stress-strain with the values shown. The loading cycle for a cold-expansion starts at zero at A, linearly increasing with increasing pressure to yielding, and proceeds plastically to B where unloading begins with a decrease in the cold-expansion pressure. With decreasing pressure unloading recovers along a linear line with a slope equal to the original linear loading region. Yielding occurs at further decreasing pressure at a value equal to the stress at B minus twice the value of the stress at initial yielding. This behavior is kinematic hardening

المنارة للاستشارات
www.manaraa.com

(Dowling 2007). After yielding from unloading, unloading continues plastically to point C where the unloading is assumed to have removed all the expansion pressure. At C a residual stress of F and a total strain of D remain in the material. The total strain D can be calculated by using the modified Rambeg-Osgood (1943) equation (Eqn 6b) to calculate the strain at B; note that the modified Ramberg-Osgood (1943) equation for the plastic region provides total strain and it is not necessary to add the elastic strain from Eqn 6a to the strain calculated from Eqn 6b. The total strain at D can be calculated by subtracting the strain from B to C from the strain at B. The total strain value D is load path dependent.

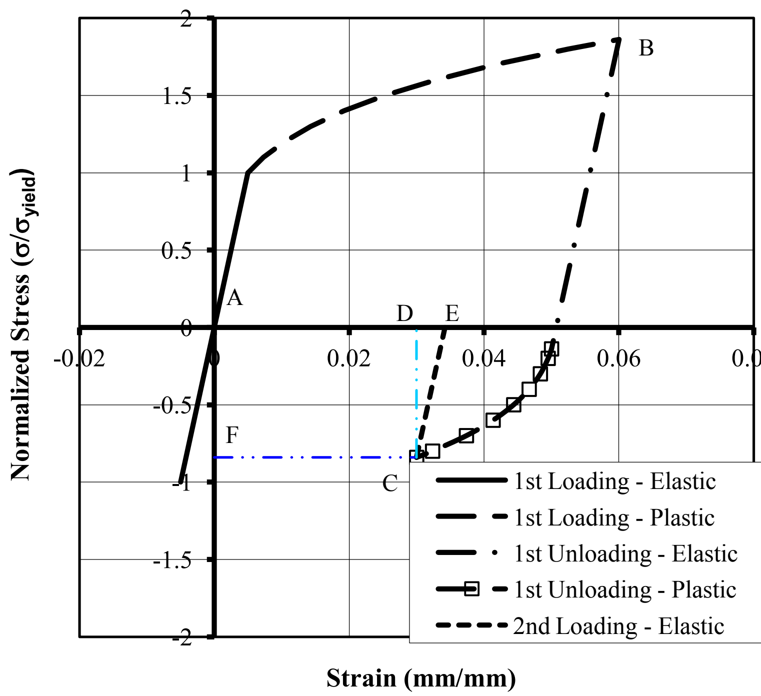

Figure 34. Tangential Stress Load Path

It should be noted that ND does not measure total strain; ND measures the elastic strain in a volume of the target material. It measures the strain which can be recovered when the residual stress goes to zero. The recovery of the residual stress and the strain associated with it proceed

www.manaraa.com

along the linear line from C to E. Therefore, the tangential and radial strain associated with the residual stress can be calculated from stresses from Nadai (1943) and Ball (1995) using standard calculations for converting elastic stresses to elastic strain in a biaxial state of stress. Figures 35 and 36 show the strain calculated from the stresses resulting from using Nadia's (1943) and Ball's (1995) closed-form techniques plotted with the measured strain from ND. Figure 35 shows the tangential residual strain and Figure 36 shows the radial residual strain. The shapes of the curves of the calculated strain from Nadai (1943) and Ball (1995) match roughly the curves of the measured strain from ND with the exception that the plots of the ND strain are broader than those from the closed-form solutions. The location of the elastic-plastic boundary from the ND measurements are not as distinct as those from the closed form solutions but appears to be at approximately $r/r_i = 5.7$, an increase of 250% over Nadai's (1943) 210%, over Ball's (1995) $n = 40$, and 120% over Ball's (1995) $n = 10$. It is believed that this increase is the result of acoustic softening from the ultrasonic vibration during the PICK treatment. This conclusion would be more conclusive if ND had also been used to measure the strain from a specimen which had undergone only cold-expansion from the PICK tool but had not been subjected to the ultrasonic vibration. However, this was not possible because of the financial and time constraints on using the ND facilities at ORNL.

المنارة للاستشارات
www.manaraa.com

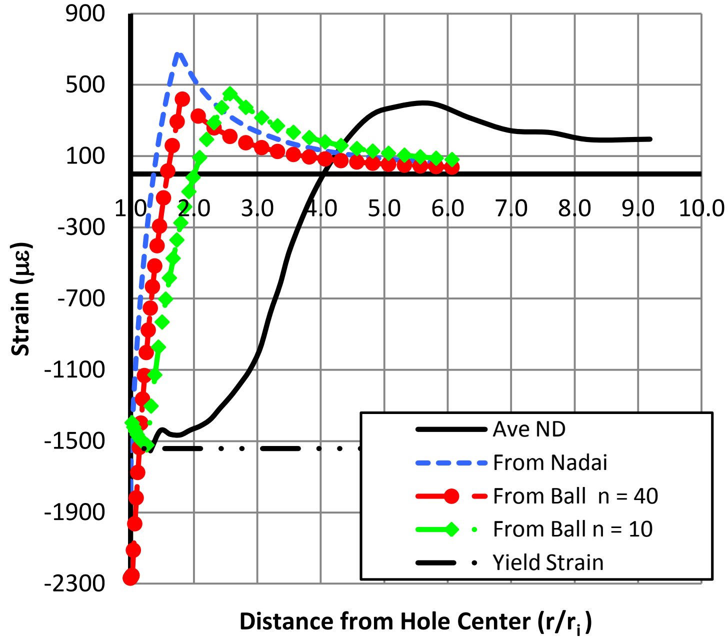

Figure 35. Comparison of Tangential Strain

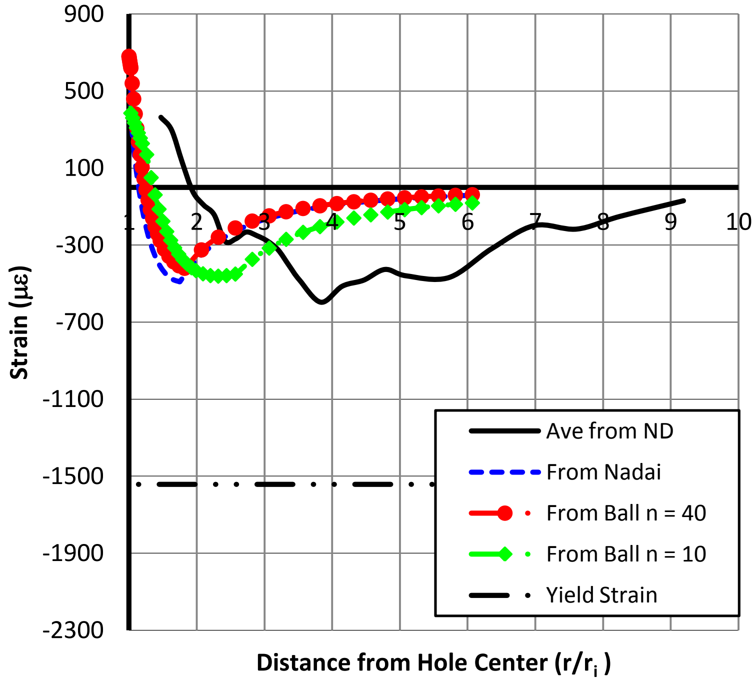

Figure 36. Comparison of Radial Strain

المنارة للاستشارات
www.manaraa.com

CONCLUSIONS

This proof-of-concept study with testing of a reduced-scale, laboratory model has demonstrated that fatigue initiation life can be increased by mechanically cold-expanding a hole and subjecting the inside surface of that hole with treatment from ultrasonic vibration. This paper provides an engineering mechanics basis which demonstrates how the ultrasonic vibration changed the internal stresses and strains in the vicinity hole to provide this increase in fatigue initiation life. The following conclusions are presented:

1. The brittle coating was an excellent and simple means of immediately evaluating the effectiveness of the PICK tool by providing a visual indication that the PICK tool had plastically deformed the steel around the hole. The limit of the plastic deformation, the elastic-plastic boundary, was clearly visible as the boundary of the area within which the brittle coating had disbonded.

2. Working through the closed-form techniques proposed by Nadai (1943) and expanded by Ball (1995) provided a detailed understanding of the engineering mechanics aspects and material behavior of the problem. Because the PICK treatment produced a large area with plastic deformation, Nadai's (1943) technique with its elastic, perfectly-plastic characterization of material behavior is not adequate to model PICK-induced stresses in a strain-hardening material. Ball's (1995) enhancement of Nadai's (1943) technique using a power-law type relationship for the stress-strain relationship in the plastic region is a better model of the behavior of the PICK tool treated material especially if the power of the equation is calibrated to the actual measured stress-strain curve.

المنارة للاستشارات
www.manaraa.com

3. Ball's (1995) recommended technique for converting residual stress to strain is incorrect.

4. X-Ray diffraction did not provide credible results for residual tangential and radial stress / strain produced by the PICK treatment. It is believed that this is a result of the existence of residual stresses in the plate from the manufacturing processes and the difficulty of removing these in such a manner that the XRD would measure stresses at the same elevation along the line of the measurements. This is important because 60% of the diffracted beam is the result of diffraction in the top 5μm (0.0002 in) layer of the material (Rowlands 1993).

5. Neutron diffraction provided an excellent method to measure the residual strain around the PICK treated hole; however, it is expensive and time consuming.

6. A comparison of the strain measured by ND and that calculated from the closed-form techniques reveals that the PICK treatment produced larger radial area of plasticity and compressive residual tangential stress around the hole than is predicted by the closed-form techniques. It is thought that this larger area of compressive tangential stress is a result of the ultrasonic vibration from the piezoelectric elements and is responsible for the increase in the number of cycles required to initiate a fatigue crack.

From these conclusions, it is apparent that the PICK treatment provides a method of improving the capacity of crack-arrest holes to stop fatigue crack growth in small scale specimens. Expansion from the PICK treatment may eventually be used to arrest fatigue crack growth in bridges and provide an economical, efficient repair for fatigue cracks in bridges.

المنارة للاستشارات
www.manaraa.com

REFERENCES

1. Akesson, Bjorn (2008). Understanding Bridge Collapses. Taylor & Francis Group, London, England, 79-88.

2. American Association of State Highway and Transportation Officials (AASHTO), (1985) "Standard Specification for Highway Bridges Interim ". 13th Edition, Washington, D.C.

3. Arora, P. R, Dattagaguru, B., and Subramanya Hande, H. S., (1992) "A Method of Estimation of the Radius of Elastic-Plastic Boundary Around Cold-Worked Holes" Journal of Testing and Evaluation vol 20, no. 5 Sept 1992.

4. ASTM E 8-04 (2004) "Standard Methods for Tension Testing of Metallic Materials" American Society for Testing and Materials, West Conshohocken, Pa.

5. ASTM E 140 - 07 (2007) "Standard Hardness Conversion Tables for Metals Relationship Among Brinell Hardness, Vickers Hardness, Rockwell Hardness, Superficial Hardness, Knoop Hardness, and Scleroscope Hardness" American Society for Testing and Materials, West Conshohocken, Pa.

6. ASTM E 466-07 (2007) "Standard Practice for Conducting Force Controlled Constant Amplitude Axial Fatigue Tests of Metallic Materials" American Society for Testing and Materials, West Conshohocken, Pa.

7. Ball, D. L. (1995) "Elastic-Plastic Stress Analysis of Cold Expanded Fastener Holes", Fatigue and Fracture of Engineering Materials and Structures, vol 18, issue 1

8. Ball, D. L. and Lowry, D. R. (1998). "Experimental Investigation on the Effects of Cold Expansion of Fastener Holes". Fatigue and Fracture of Engineering Materials and Structures, vol 12, pp 17-33.

9. Barsom, John M. and Rolfe, S. T. (1999). Fracture and Fatigue Control in Structures: Applications of Fracture Mechanics. American Society of Testing Materials, Philadelphia, PA, 182-192.

10. Bontillo, Robert, PBFasteners, personal communications, Feb 28, 2011.

11. Boyer, H. E. Atlas of Stress Strain Curves (1987). ASM International, Materials Park, Ohio.

12. Cheng, Xiaohua, Fisher, John W., Prask, Henry J., Gnaupel-Herold, Thomas, Yen, Ben T., and Roy, Saugata (2003) "Residual stress modification of post-weld treatment and its beneficial effect on fatigue strength of welded structures" International Journal of Fatigue 25.

المنارة للاستشارات

www.manaraa.com

13. Crain, Josh S (2010). "Fatigue Enhancement of Undersized, Drilled Crack-Stop Holes" M.S. thesis, University of Kansas, Lawrence, KS.

14. Crain, Josh S., Simmons, Gary G., Bennett, Caroline R., Barrett-Gonzales, Ron, Matamoros, Adolfo B., and Rolfe, Stanley T. (2010) "Development of a Technique to Improve Fatigue Lives of Crack-Stop Holes in Steel Bridges" Transportation Research Record: Journal of the Transportation Research Board, No 2200, Transportation Research Board of the National Academies, Washington, DC.

15. Dexter, Robert J. (2004). "Signs, Signals, Light Support Structures and Manual for Repair of Fatigue and Fracture" Third Annual Bridge Workshop: Fatigue and Fracture. Available on the Internet.

16. Dieter, George (1989), Mechanical Metallurgy, McGraw-Hill, New York, New York, 229-236

17. Dowling, Norman E. (2007). Mechanical Behavior of Materials, 3rd edition, Pearson / Prentice Hall, New Jersey.

18. Edwards, L. and Wang, D.Q. (1996). "Neutron diffraction determination of the complete 3D residual stress distribution surrounding a cold expanded hole" Proceedings of the Fourth European Conference on Residual Stress (ECRS4), Cluny en Bourgogne, France, vol 2.

19. Federal Highway Administration (FWHA) Bridge Program Group. (2001). Count of deficient bridges by state non-federal aid highway http://www.fhwa.dot.gov./bridges/britab/.htm (March 20,2002). The Office of Bridge Technology, Washington, D. C.

20. Fisher, John W. and Keating, P. B. (1989). "Distortion-Induced Fatigue Cracking of Bridge Details in Web Gaps". Journal of Construction Steel Research, 12, 215-228.

21. Fisher, John W., Barthelemy, B. M., Mertz, D. R., and Edinger, J. A. (1980). "Fatigue Behavior of Full-Scale Welded Bridge Attachments". National Cooperative Highway Research Program (NCHRP) Report 227, National Transportation Research Board, Washington, D. C.

22. Fisher, John W., Jin, Jain, Wagner, David C., and Yen, Ben T. (1990). "Distortion-Induced Fatigue Cracking in Steel Bridges". National Cooperative Highway Research Program (NCHRP) Report 336, National Transportation Research Board, Washington, D. C.

23. Fitzpatrick, M. E., Fry, A. T., Holdway, P., Kandil, F. A., Shackleton, J., and Suominen, L., (2005) "Determination of Residual Stresses by X-Ray Diffraction – Issue 2" A National Measurement Good Practice Guide No 52. National Physical Laboratory, Teddington, Middlesex, United Kingdom, TW11 0LW. 5-10.

المنارة للاستشارات
www.manaraa.com

24. Forgues, S. A., Bernard, M., and Bui-Quoc, T. (1993) “3-d axisymmetric numerical analysis and experimental study of the fastener hole coldworking process” Transactions of Engineering Sciences vol 2 WIT Press.

25. Garcia-Granda, A. A., Lacarac, V. D., Smith, D. J., and Parier, M. J., (2001) “A new procedure based on Sachs’ boring method for measuring non-axisymmetric residual stress: experimental application”, International Journal of Mechanical Application 43.

26. Guo, Wanlin (1993), “Elastic Plastic Analysis of a Finite Sheet with a Cold-Worked Hole”, Engineering Fracture Mechanics, vol 46, Issue 3.

27. Hayes, B. (1996). “Classic Brittle Failures in Large Welded Structures”. Engineering Failure Analysis, Vol 3 (2), 115-127.

28. Hoffman, Oscar and Sachs, George (1953), Introduction to the Theory of Plasticity for Engineers, McGraw-Hill, New York, New York.

29. Hsu, Y.C. and Forman, R. G. (1975), “Elastic-Plastic Analysis of an Infinite Sheet Having a Circular Hole Under Pressure”, The American Society of Mechanical Engineers Journal of Applied Mechanics 42.

30. Hubbard, Camden R., (2013), Applied Diffraction Corp. personal communications, 110 Crestview Lane, Oak Ridge TN 37830.

31. Hutchings, M. T., Withers, P. J., Holden, T. M., and Lorentzen, T., (2005). Introduction to the Characterization of Residual Stress by Neutron Diffraction, CRC Press, Tasylor & Francis Group, Boca Raton, FL.

32. Lanciotti, A. and Polese, C. (2005). “The effect of interference-fit fasteners on the fatigue life of central hole specimens”. Fatigue and Fracture in Engineering Materials and Structures 28 (2005), 587-597.

33. Langenecker, Bertwin (1966) “Effects of Ultrasound on Deformation Characteristics of Metals”, Transaction on Sonics and Ultrasound, vol su-13, no 1, 1-8.

34. Maranian, Peter (2010). Reducing Brittle and Fatigue Failures in Steel Structures. American Society of Civil Engineers, Reston, VA, 15-18.

35. McGuire, William (1968). Steel Structures. Prentice-Hall, Inc. Englewood Cliffs, NJ, 208-220, 771-772.

36. Merritt, Frederick S., Editor, (1972). Structural Steel Designers’ Handbook. McGraw-Hill Book Company, New York, NY, 10-36.

37. Moniz, B. J. (1994), Metallurgy, Second Edition, American Technical Publishers, Inc., Homewood, Illinois, 493.

المنارة للاستشارات
www.manaraa.com

38. Nadai, A. (1943) “Theory of Expanding of Boiler and Condenser Tube Joints Through Rolling”, Transaction of the American Society of Mechanical Engineers, vol 65, issue 8.

39. Nevill, G. F., Jr. and Brotzen, Franz R., (1957) “The Effect of Vibration on the Static Yield Strength of Low-Carbon Steel” Proceedings of American Society of Testing Materials, vol 57, 751-758.

40. Nigrelli, V. and Pasta, S. (2008) “Finite element simulation of residual stress induced by split-sleeve cold-expansion process of holes” Journal of Material Processing Technology 205.

41. Oak Ridge National Laboratory, “High Isotope Flux Reactor”, www.neutron.ornl.gov /facilities/HIFR/techparameters> (2013).

42. Poolsuk, S. and Sharpe, W. N., Jr., (1978) “Measurement of the Elastic Plastic Boundary and Coldworked Fastener Holes”, Winter Annual Meeting Dec 1978, American Society of Mechanical Engineers.

43. Poussard, C. G. C., Pavier, M. J., and Smith (1994) Prediction of Residual Stress in Clod Worked Fastener Holes Using the Finite Element Method” Proceedings of the 2nd Biennial European Joint Conference on Engineering System Design and Analysis vol 8, part A (American Society of Mechanical Engineers, New York).

44. Poussard, C., Pavier, M.J., and Smith, D. J. (1995) “Analytical and Finite Element Predictions of Residual Stress in Cold Worked Faster Holes” Journal of Strain Analysis vol 30 no 4.

45. Prevey, Paul S., (1986) “X-Ray Diffraction Residual Stress Techniques”, Metals Handbook 10. Metals Park, American Society for Metals, 380-392. 3-6.

46. PROTO LXRD, http://www.protoxrd.com, (2013), PROTO Manufacturing, Ltd., Oldcastle, Ontario, Canada.

47. Ramberg, W. and Osgood, W. R. (1943) “Description of Stress-Strain Curves by Three Parameters”, NCAA TN 902.

48. Reid, Len, Fatigue Technology, personal communications, Feb 28, 2011.

49. Rich, D. L. and Impellizzeri, L. F., (1977) “Fatigue Analysis of Cold-Worked and Interference Fit Fastener Holes”, Cyclic Stress-Strain and Plastic Deformation Aspects of Fatigue Crack Growth ASTM 637, American Society of Testing Materials Philadelphia, PA.

50. Richards, Cedric W. (1961) Engineering Materials Science, Wadsworth Publishing Co, Belmont, California, 405-406.

www.manaraa.com

51. Roddis, W. M. Kim and Zhao, Yuan (2001). "Out-of-Plane Fatigue Cracking in Welding Steel Bridges". Welding Innovations, 27(2), 2-7.

52. Rolfe, S. T. and Barsom, John M. (1977). Fracture and Fatigue Control in Structures: Applications of Fracture Mechanics. First Edition. Prentice Hall.

53. Rowlands, Robert E. (1993) "Residual Stress" Chap 18 Handbook on Experimental Mechanics, Kobayoshi, Albert S. ed, Society for Experimental Mechanics, Bethel CT.

54. Sharpe, W.N. Jr., (1978) "Residual Stress around Coldworked Fastener Holes", Journal of Engineering Materials and Technology, Vol 100, July 1978.

55. Simmons, G. G., Bennett, Caroline R., Barrett-Gonzales, Ron, Matamoros, Adolfo B., and Rolfe, Stanley T. (2013). "Design, modeling, and testing of a piezoelectric impact compressive kinetic (PICK) tool for crack-stop hole treatment", SPIE Smart Structures Conference 2013.

56. Simmons, Gary G. (2013). "Fatigue Enhancement of Undersized, Drilled Crack-Arrest Holes" PhD thesis, presented to the University of Kansas, Lawrence, KS., in partial fulfillment of the requirements for the degree of Doctor of Philosophy.

57. Sirnivasan, A. V. and McFarland, D. Michael, (2001) Smart Structures, Cambridge University Press, Cambridge, UK, 7-25.

58. Stefanescu, D., Steuwer, A., Owen, R. A., Nadri, B., Edwards, L., Fitzpatrick, M. E., and Withers, P. J. (2004). "Elastic strains around cracked cold-expanded fastener holes measured using synchroton X-rays diffraction technique", Journal of Strain Analysis, Vol 39 No 5.

59. Tavakkolizadeh, M. and Saadatmanesh, H. (2003). "Fatigue Strength of Steel Girders Strengthened with Carbon Fiber Reinforced Polymer Patch". American Society of Civil Engineers Journal of Structural Engineering, 129(2), 186.

60. Watkins, T. R., Schajer, G. S., and Lance, M. J. (to be published 2014). Chap 1.09 Residual Stress Measurement, "Comprehensive Material Processing" Elsevier Ltd.

61. Zhang, Y., Fitzpatrick, M. E., and Edwards, L., (2005) "Analysis of Residual Stress Around a Cold-Expanded Fastener Hole in a Finite Plate" Strain vol 41.

المنارة للاستشارات
www.manaraa.com

CHAPTER 6: SUMMARY, CONCLUSIONS AND RECOMMENDATIONS

OBJECTIVE

The objective of this research was to investigate the possible development of a new, cost-effective technique that could be used to arrest the growth of fatigue cracks before they develop to an extent that more expensive repairs are required. It is well known that drilling a hole (crack-arrest hole) at each end of a fatigue crack may stop the growth of the fatigue crack. The diameter of the hole required to arrest crack growth can be calculated from formulae developed by Rolfe and Barsom (1977) and by Fisher et al (1980, 1990). Unfortunately, the required diameter of the hole is usually so large that it is may be impractical or may not fit within the space available. This research was aimed at investigating a new technique to cold-expand and treat crack-arrest holes so that a practically sized hole would gain effectiveness in halting further crack propagation. This new technique consisted of two steps: cold-working the inside surface of an undersized hole and subjecting the cold-worked surface to ultrasonic vibration. It was hypothesized that this process might produce three separate results, all of which would enhance fatigue crack initiation life. First, the compressive force used to cold-expand the hole would result in residual compressive stress fields around the hole when the radial force was removed. Second, the cold-expansion would cause strain-hardening and cold-working with a concomitant increase in the yield and ultimate strengths of the steel. Third, the ultrasonic vibration from the Piezoelectric Induced Compressive Kinetic (PICK) treatment would further increase the resistance to fatigue propagation by increasing the yield strength and the ultimate strength. These expected results and their effects on fatigue crack initiation were investigated through both laboratory testing and mathematical modeling.

المنارة للاستشارات
www.manaraa.com

SUMMARY

Sizing Crack-Arrest Holes

1. The location of the crack-arrest hole with respect to the crack tip is an important consideration with regard to crack reinitiation. Depending on the spatial relationship between the crack-arrest hole and the crack tip, some portion of the radius of the crack-arrest hole needs to be added to the half-length of the crack when calculating the required radius of the crack-arrest hole from the formula from Rolfe and Barsom (1977) or Fisher et al (1980, 1990).

2. The stress range producing fatigue is the critical unknown quantity and dominates the calculation in the formula for determining the required diameter for the crack-arrest hole. When a crack results from distortion-induced fatigue, it is not clear what value should be used for the critical stress range. Aditionally, it is not clear whether the stress range should be determined in the flange or in the web. Determining the in situ value for this complex, 3D stress range on an actual bridge will be difficult.

3. The values for *C*, the constant used in the formula for determining the required radius of the crack-arrest hole, were determined experimentally by Rolfe and Barsom (1977) from tests on flat steel plates using cyclical tension and Fisher et al (1980,1990) from tests on full-scale steel rolled-shapes and girders configured and loaded to produce distortion induced fatigue (DIFC). The constants $C = 4$ from Fisher et al (1980, 1990) was a lower bound value and $C = 10$ from Role and Barsom (1977) was an average value. Both must be used within the limits of the experimental parameters from which they were developed, and in conjunction with reasonable estimates of stress range.

المنارة للاستشارات
www.manaraa.com

4. Crack-arrest hole diameters may become so large as to be impractical. It may not be physically possible to drill the size of hole indicated by the calculations because of interferences with stiffeners, flanges, etc.

Development of a Technique to Improve Fatigue Lives of Crack-Stop Holes in Steel Bridges

5. A 4 percent expansion of crack-arrest holes in steel plates was found to have a similar effect to that observed in aluminum plates. This conclusion is based on the similarity of normalized tangential residual stress for both materials. This was an important finding, because it helps to provide a meaningful link between existing research performed in the aerospace engineering literature and current needs within the field of bridge engineering. Results from the 2-D and 3-D uniform expansion modeling (Crain 2010) can be interpreted to be independent from the particular technique chosen to cold-expand undersized crack-arrest holes and can be used in future studies to corroborate detailed finite element analyses and experimental findings for specific techniques applicable to steel bridges.

Development of a Technique to Improve Fatigue Lives of Crack-Arrest Holes in Steel Bridges –Fatigue and Metallurgical Results

Fatigue Testing

6. The results of fatigue testing as part of this study demonstrate that the PICK treatment process provided an improvement in preventing fatigue crack re-initiation in crack-arrest holes over that provided only by cold-expansion. While the cold-expansion increased fatigue initiation life by a factor of 1.8 over specimens not cold-expanded, combining the cold-expansion with ultrasonic vibration from the PICK tool increased the fatigue initiation life by a factor of 2.6 over specimens not cold-expanded.

المنارة للاستشارات
www.manaraa.com

Metallurgical Testing Results

Grain Size Analysis

7. For the untreated specimen, which was only subjected to drilling and reaming of the hole, grain size analysis with the optical microscope revealed shallow deformation of the grains at the surface of the hole, as expected. For the cold-expanded specimens, cold-working produced a layer around the surface of the hole exhibiting flattened and elongated grains to a depth of approximately 0.008 to 0.009 mm (0.0003- 0.0035 in). For PICK-treated specimen, grain size analysis with the optical microscope revealed a similar layer of grain deformation to a depth of approximately 0.01 mm (0.004 in) from the edge of the hole. The difference in the radial extent of the grain deformation between the cold-expanded and the PICK-treated specimens was so slight that it appears that the cold-working of both the cold-expanded and the PICK treated specimens was roughly equivalent.

Hardness Testing

8. Hardness values for PICK-treated specimens were found to be consistently higher than those for the cold-expanded specimens. Hardness readings for cold-expanded specimens were approximately 15 percent higher than those for the untreated specimens; hardness values for the PICK-treated specimens were approximately 22 percent higher than those for the untreated specimens. The increase in hardness in the cold-expanded specimens over the untreated specimens was the result of cold-working during cold-expansion. The increase in hardness in the PICK treated specimens over the increase in hardness in the cold-expanded specimens was the result of acoustic-hardening from PICK treatment.

www.manaraa.com

Retained Expansion (RE)

9. *RE* was calculated from diametric measurements before and after treatment with cold-expansion and PICK-treatment. Different loading regimes were used for the fatigue specimens than for the plate specimens. For fatigue specimens, PICK treatment produced a *RE* ratio 24 percent higher than the *RE* achieved in the cold-expanded fatigue specimens. For plate specimens, PICK treatment produced a *RE* ratio 66 percent higher than the *RE* in the cold-expanded plate specimens. The RE obtained from the cold-expansion was from cold-working. The cold-working produced the same increase in *RE* in the PICK-treated specimens and the additional *RE* in the PICK-treated specimens above the *RE* from the cold-expanded specimens could have been the result of acoustic-softening.

Load Decay

10. During the PICK treatment of the fatigue specimens, the load / strain in the tool was observed to decay with time; another indication that acoustic softening was occurring.

Development of a Technique to Improve Fatigue Lives of Crack-Arrest Holes in Steel Bridges – Analytical and Experimental Stress and Strain

Brittle Coating

11. A brittle coating was an excellent and simple means of immediately evaluating the effectiveness of the PICK tool by providing a visual indication that the PICK tool had plastically deformed the steel around the hole. The limit of the plastic deformation, the elastic-plastic boundary, was clearly visible as the boundary of the area within which the brittle coating had disbonded.

المنارة للاستشارات
www.manaraa.com

Closed-Form Analysis

12. Nadai's (1943) technique with its elastic, perfectly-plastic characterization of material behavior is not adequate to model PICK-induced stresses in a strain-hardening material at the strain magnitude produced by the PICK process.

13. Ball's (1995) extension of Nadai's (1943) technique using a power-law type relationship to model the stress and strain in the plastic region is a better match of the behavior of the strain-hardening steel material especially if the power term, *n*, in the Ball's (1995) equations is calibrated to the actual measured stress-strain curve.

14. Ball's (1995) recommended technique for converting residual stresses to strains is incorrect as discussed in the text of this thesis.

X-Ray Diffraction

15. X-Ray diffraction did not provide credible results for residual tangential stress and strain or residual radial stress and strain produced by the PICK treatment. It is believed that this is a result of the difficulty in polishing the specimen to remove the surface residual stresses induced by rolling during manufacturing.

Neutron Diffraction (ND)

16. Neutron diffraction provided an excellent method to measure the residual strain around the PICK treated hole; however, it was both expensive and time consuming.

17. A comparison of the strain measured by ND and that calculated from the closed-form, mathematical techniques revealed that PICK treatment produced a larger area of plasticity and a more extensive area with residual compressive tangential stress than was

المنارة للاستشارات
www.manaraa.com

predicted by the closed-form techniques. It is thought that this larger area was the result of the ultrasonic vibration during the PICK treatment and was responsible for the increase in the number of cycles required to initiate a fatigue crack.

CONCLUSIONS

The technique of cold-expansion of holes in aluminum components has already been proven in the aerospace industry as an effective means to improve fatigue life. The research reported in this thesis was a proof-of-concept study using reduced-scale, laboratory models to investigate if the fatigue initiation life in steel specimens could be further increased not only by cold-expanding a hole in a but also by subjecting the inside surface of that cold-expanded hole to ultrasonic vibration (PICK treatment). Fatigue testing was the primary method of demonstrating the effectiveness of this PICK treatment, but analytical techniques and other experimental techniques were used to investigate how the PICK process modified the material to enhance the effectiveness of the crack-arrest holes.

The fatigue testing program demonstrated that the PICK process improved the fatigue initiation life of a small-scale, Grade A36 steel specimen. The brittle coating showed that a plastic region was formed as a result of the PICK treatment. Metallurgical testing, i.e., grain size analysis, indicated that cold-working modified the grain sizes of the steel in the cold-expanded specimens and in the PICK-treated specimens about the same. The increase in hardness between the mechanically expanded specimens and the PICK treated specimens was the result of acoustic hardening. Analyses using closed-form techniques by Nadai (1943) and Ball (1995) show that a compressive, residual stress field was imposed tangentially around the hole by cold-expansion. These closed-form analytical techniques were not capable of predicting the stress field caused by

المنارة للاستشارات
www.manaraa.com

the ultrasonic vibration during the PICK process. Neutron diffraction measurements of strain made evident that the PICK process produced a radial extent of the plastic strain and of the residual compressive stress which exceeded that predicted by the closed-form analyses. This increase in the extent of the tangential compressive stress field resulting from the PICK process contributed to the increase in fatigue initiation life. While the cold-expansion increased fatigue initiation life by a factor of 1.8 over specimens not cold-expanded, the total effect of PICK treatment was to improve the fatigue initiation life by a factor of 2.6 over specimens not cold-expanded. From these it is apparent that the PICK treatment was successful in providing a method of improving the capacity of crack-arrest holes to stop fatigue crack initiation in reduced-scale, laboratory models for the particular sized specimens employed.

The PICK process was so successful a patent was obtained (Barrett et al 2013).

SIGNIFICANCE

Although this study consisted of reduced-scale testing, results from this program lend confidence in the ability of the PICK tool to be scaled up to treat the thicker plate material and the larger diameter crack-arrest holes typically required to halt fatigue cracks in bridges or other structures. The study showed that PICK treatment might eventually be used to improve the efficiency of a commonly used repair technique for fatigue cracks in steel bridges. Other applications may exist in the automotive industry where the PICK process might be used in the manufacturing of car and truck bodies to improve the fatigue performance of bolt holes in frame members. A similar use might be in the railroad industry but with larger members. Certainly the PICK process could be used to improve the performance of crack-arrest holes in any structure susceptible to fatigue

المنارة للاستشارات
www.manaraa.com

cracking.

RECOMMENDATIONS

Neutron diffraction measurements should be made for the residual strain field around a hole in the same steel material which has been cold-expanded with the same pressure as was used in the PICK process but without ultrasonic vibration from the PICK treatment. A comparison of the results would provide further insight into the effectiveness of the PICK process with respect to cold-expansion only. Financial and time constraints prohibited this from being accomplished as part of this study.

The analytical solutions should be confirmed with numerical analysis methods (Finite Element Analysis). These Finite Element Analysis (FEA) analyses should start with duplicating the parameters used in the Nadai's (1943) analysis and Ball's (1995) analysis with (n = 10) to benchmark the FEA with the two closed-form solutions. The FEA should then be extended in steps to a pressure equal to that used in the PICK process. Comparing the results from the FEA analyses with the measured strain from the ND will provide further confidence that the radial extent of the compressive, tangential residual stress field measured by the ND is the result of the PICK process.

Further experimentation should be conducted to investigate the existence of acoustic softening and acoustic hardening in bridge steels and the frequency range where they occur.

Using steels with different yield strengths, additional experimentation needs to be performed focused on developing the optimum pressure range on the inside surface of the hole for the PICK

المنارة للاستشارات
www.manaraa.com

process and relating this pressure to the yield strengths of the steel.

Optimization of PICK treatment time is another area which needs further study.

The PICK process needs to be scaled up to match plate thickness and hole diameters used in real structures. During this process, the tool itself must be redesigned to be portable, practical, and useable in expected field conditions. In the process of scaling and redesigning the tool, different and possibly larger piezoelectric elements will be required necessitating further study to refine power requirements.

المنارة للاستشارات
www.manaraa.com

REFERENCES

1. Akesson, Bjorn (2008). Understanding Bridge Collapses. Taylor & Francis Group, London, England, 79-88.

2. American Association of State Highway and Transportation Officials (AASHTO), (1995) "Standard Specification for Highway Bridges". 16th Edition, Washington, D.C.

3. American Association of State Highway and Transportation Officials (AASHTO), (1983) "Standard Specification for Highway Bridges". 13th Edition, Washington, D.C.

4. American Association of State Highway and Transportation Officials (AASHTO), (1985) "Standard Specification for Highway Bridges Interim ". 13th Edition, Washington, D.C.

5. Amrouche, A., Ghfiri, R., Imad, A., & Mesmacque, G. (2000). "Fatigue life estimation after crack repair in 6005 A-T6 aluminum alloy using the cold expansion hole technique." Fatigue Fract. Engr. Mater. Struct., 23, 991-916.

6. Anderson, Benjamin, Rolfe, S. T., Matamoros, A. B., Bennett, C., and Bonetti, S. (2008). Post-Retrofit Analysis of the Tuttle Creek Bridge (Bridge NO 16-81-2.24). Report No. K-TRAN: KU-06-2, Final Report.

7. Arora, P. R, Dattagaguru, B., and Subramanya Hande, H. S., (1992) "A Method of Estimation of the Radius of Elastic-Plastic Boundary Around Cold-Worked Holes" Journal of Testing and Evaluation vol 20, no. 5 Sept 1992.

8. ASTM E 466-07 (2007) "Standard Practice for Conducting Force Controlled Constant Amplitude Axial Fatigue Tests of Metallic Materials" American Society for Testing and Materials, West Conshohocken, Pa.

9. ASTM E140 - 07 (2007) "Standard Hardness Conversion Tables for Metals Relationship Among Brinell Hardness, Vickers Hardness, Rockwell Hardness, Superficial Hardness, Knoop Hardness, and Scleroscope Hardness" American Society for Testing and Materials, West Conshohocken, Pa.

10. ASTM E8-04 (2004) "Standard Methods for Tension Testing of Metallic Materials" American Society for Testing and Materials, West Conshohocken, Pa.

11. Ball, D. L. (1995) "Elastic-Plastic Stress Analysis of Cold Expanded Fastener Holes", Fatigue and Fracture of Engineering Materials and Structures, vol 18, issue 1.

12. Ball, D. L. and Lowry, D. R. (1998). "Experimental Investigation on the Effects of Cold Expansion of Fastener Holes". Fatigue and Fracture of Engineering Materials and Structures, vol 12, pp 17-33.

المنارة للاستشارات
www.manaraa.com

13. Barrett, R., 25%; Bennett, C., 25%; Rolfe, S., 25%; and Matamoros, A., 25%. (2013). “Method of Enhancing the Fatigue Life of a Structure”, US Patent Application 13/687524,847, Filled 06/15/2012, Issued 01/01/2013.

14. Barsom, John M. and Rolfe, Stanley. T. (1999). Fracture and Fatigue Control in Structures: Applications of Fracture Mechanics. Third Edition American Society of Testing Materials, Philadelphia, PA, 182-192.

15. Blaha, F. and Langenecker, B. (1955). “Tensile Deformation of Zinc Crystals Under Ultrasonic Vibration”, Naturwissenschaften vol 42, p. 556.

16. Bontillo, Robert, PBFasteners, personal communications, 2011.

17. Boyer, H. E. Atlas of Stress Strain Curves (1987). ASM International, Materials Park, Ohio.

18. Brown, J.D., Lubitz, D.J., Cekov, Y.C., Frank, K.H., and Keating, P.B. (2007). “Evaluation of influence of hole making upon the performance of structural steel plates and connections.” Center for Transportation Research, Texas, Project: 0-4624, CTR Technical Report:0-4624-1. 236 p. Sponsored by the Texas Department of Transportation.

19. Cheng, Xiaohua, Fisher, John W., Prask, Henry J., Gnaupel-Herold, Thomas, Yen, Ben T., and Roy, Saugata (2003) “Residual stress modification of post-weld treatment and its beneficial effect on fatigue strength of welded structures” International Journal of Fatigue 25.

20. Crain, Josh S (2010). “Fatigue Enhancement of Undersized, Drilled Crack-Stop Holes” M.S. thesis, University of Kansas, Lawrence, KS.

21. Crain, Josh S., Simmons, Gary G., Bennett, Caroline R., Barrett-Gonzales, Ron, Matamoros, Adolfo B., and Rolfe, Stanley T. (2010) “Development of a Technique to Improve Fatigue Lives of Crack-Stop Holes in Steel Bridges” Transportation Research Record: Journal of the Transportation Research Board, No 2200, Transportation Research Board of the National Academies, Washington, DC.

22. Creager, M. (1966). "The elastic stress field near the tip of a blunt crack," Measter Science thesis, Lehigh University, Bethlehem, PA.

23. de Matos, P. F. P, Moreira, P. M. G. P., Camanho, P. P., and de Castro, P. M. S. T. (2005). "Numerical simulation of cold working of rivet holes." Finite Elements in Analysis and Design, 41(9-10), 989-1007.

24. de Matos, P. F. P., McEvily, A. J., Moreira, P. M. G. P., and de Castro, P. M. S. T. (2007). "Analysis of the effect of cold-working of rivet holes on the fatigue life of an aluminum alloy." International Journal of Fatigue, 29(3), 575-586.

المنارة للاستشارات
www.manaraa.com

25. Dexter, Robert J. (2004). "Signs, Signals, Light Support Structures and Manual for Repair of Fatigue and Fracture" Third Annual Bridge Workshop: Fatigue and Fracture. Available on the Internet.

26. Dieter, George (1989), Mechanical Metallurgy, McGraw-Hill, New York, New York, 229-236

27. Domazet, Z. (1996). "Comparison of fatigue crack retardation methods." Engineering Failure Analysis, 3(2), 137-147.

28. Dowling, Norman E. (2007). Mechanical Behavior of Materials, 3rd edition, Pearson / Prentice Hall, New Jersey, 179.

29. Edwards, L. and Wang, D.Q. (1996). "Neutron diffraction determination of the complete 3D residual stress distribution surrounding a cold expanded hole" Proceedings of the Fourth European Conference on Residual Stress (ECRS4), Cluny en Bourgogne, France, vol 2.

30. Fatigue Technology (2011). "Split Sleeve Cold Expansion", Fatigue Technology, <www.fatiguetech.com> (Feb. 27, 2011).

31. Federal Highway Administration (FWHA) Bridge Program Group. (2001). Count of deficient bridges by state non-federal aid highway http://www.fhwa.dot.gov./bridges/britab/.htm (March 20,2002). The Office of Bridge Technology, Washington, D. C.

32. Fisher, John (1984). Fatigue and Fracture in Steel Bridges. John Wiley and Sons, New York.

33. Fisher, John W. and Keating, P. B. (1989). "Distortion-Induced Fatigue Cracking of Bridge Details in Web Gaps". Journal of Construction Steel Research, 12.

34. Fisher, John W. and Keating, P. B. (1989). "Distortion-Induced Fatigue Cracking of Bridge Details in Web Gaps". Journal of Construction Steel Research, 12, 215-228.

35. Fisher, John W., Barthelemy, B. M., Mertz, D. R., and Edinger, J. A. (1980). "Fatigue Behavior of Full-Scale Welded Bridge Attachments". National Cooperative Highway Research Program (NCHRP) Report 227, National Transportation Research Board, Washington, D. C.

36. Fisher, John W., Jin, Jain, Wagner, David C., and Yen, Ben T. (1990). "Distortion-Induced Fatigue Cracking in Steel Bridges". National Cooperative Highway Research Program (NCHRP) Report 336, National Transportation Research Board, Washington, D. C.

37. Fisher, John W., Jin, Jain, Wagner, David C., and Yen, Ben T. (1990). "Distortion-Induced Fatigue Cracking in Steel Bridges". National Cooperative Highway

المنارة للاستشارات
www.manaraa.com

Research Program (NCHRP) Report 336, National Transportation Research Board, Washington, D. C.

38. Fitzpatrick, M. E., Fry, A. T., Holdway, P., Kandil, F. A., Shackleton, J., and Suominen, L., (2005) "Determination of Residual Stresses by X-Ray Diffraction – Issue 2" A National Measurement Good Practice Guide No 52. National Physical Laboratory, Teddington, Middlesex, United Kingdom, TW11 0LW. 5-10.

39. Forgues, S. A., Bernard, M., and Bui-Quoc, T. (1993) "3-d axisymmetric numerical analysis and experimental study of the fastener hole coldworking process" Transactions of Engineering Sciences vol 2 WIT Press.

40. Forgues, S. A., Bernard, M., and Bui-Quoc, T. (1993). "3-d axisymmetric numerical analysis and experimental study of the fastener hole coldworking process." Computer Methods and Experimental Measurements for Surface Treatments Effects, edited by C. A. Brebbia and M. H. Aliabadi, Engineering Sciences, (2), Computational Mechanics Publications, Southampton, UK, 61-70.

41. Garcia-Granda, A. A., Lacarac, V. D., Smith, D. J., and Parier, M. J., (2001) "A new procedure based on Sachs' boring method for measuring non-axisymmetric residual stress: experimental application", International Journal of Mechanical Application 43.

42. Guo, Wanlin (1993), "Elastic Plastic Analysis of a Finite Sheet with a Cold-Worked Hole", Engineering Fracture Mechanics, vol 46, Issue 3.

43. Hayes, B. (1996). "Classic Brittle Failures in Large Welded Structures". Engineering Failure Analysis, Vol 3 (2), 115-127.

44. Herman, R. & Ozdemir, A.T. (1999). "Effect of expansion techniques and plate thickness on near-hole residual stresses and fatigue life of cold expanded holes." Journal of Material Science. 34, 1243-1252.

45. Hoffman, Oscar and Sachs, George (1953), Introduction to the Theory of Plasticity for Engineers, McGraw-Hill, New York, New York.

46. Hsu, Y.C. and Forman, R. G. (1975), "Elastic-Plastic Analysis of an Infinite Sheet Having a Circular Hole Under Pressure", The American Society of Mechanical Engineers Journal of Applied Mechanics 42.

47. Hu, Y., Shield, C.K. and Dexter, R.J. (2005). "Use of adhesives to retrofit out-of-plane distortion at connection plates." Journal of the Transportation Research Board., CD 11-S, 419-427.

48. Hubbard, Camden R., (2013), Applied Diffraction Corp. personal communications, 110 Crestview Lane, Oak Ridge TN 37830.

49. Huhn, H. and Valtinat, G. (2004). "Bolted connections with hot dipped galvanized steel members with punched holes." Proceedings of the ECCS/AISC Workshop,

المنارة للاستشارات

www.manaraa.com

Connection in Steel Structures V: Innovative Steel Connections, June 3-5,2004. Amsterdam: European Convention for Construction Steelwork/American Institute of Steel Construction.

50. Hutchings, M. T., Withers, P. J., Holden, T. M., and Lorentzen, T., (2005). Introduction to the Characterization of Residual Stress by Neutron Diffraction, CRC Press, Tasylor & Francis Group, Boca Raton, FL.

51. Kuhn, B., Lukic, M., Naussbaumer, A., Gunther, H. P., Helmerich, R., Herion, S., Kolstein, M. H., Walbridge, S., Androic, B., Dijkstra, O., and Bucak O. (2008). "Assessment of Existing Steel Structures: Recommendations for Estimation of Remaining Fatigue Life". JRC Scientific and Technical Reports, EUR 23252EN-2008.

52. Lanciotti, A. and Polese, C. (2005). "The effect of interference-fit fasteners on the fatigue life of central hole specimens". Fatigue and Fracture in Engineering Materials and Structures 28 (2005), 587-597.

53. Landry, M. A., Armen, H. Jr., and Eidinoff, H. L. (1986). "Enhanced Stop-Drill Repair Procedure for Cracked Structures." Fatigue in Mechanically Fastened Composite and Metallic Joints, ASTM STP 927, edited by J. M. Potter, American Society for Testing and Materials, Philadelphia, PA, 190-220.

54. Langenecker, Bertwin (1966) "Effects of Ultrasound on Deformation Characteristics of Metals", Transaction on Sonics and Ultrasound, vol su-13, no 1.

55. Leon, A. (1998). "Benefits of split mandrel coldworking." International Journal of Fatigue, 20(1), 1-8.

56. Maranian, Peter (2010). Reducing Brittle and Fatigue Failures in Steel Structures. American Society of Civil Engineers, Reston, VA, 15-18.

57. McGuire, William (1968). Steel Structures. Prentice-Hall, Inc. Englewood Cliffs, NJ, 208-220, 771-772.

58. Merritt, Frederick S., Editor, (1972). Structural Steel Designers' Handbook. McGraw-Hill Book Company, New York, NY, 10-36.

59. Moniz, B. J. (1994), Metallurgy, Second Edition, American Technical Publishers, Inc., Homewood, Illinois, 493.

60. Nadai, A. (1931), Plasticity, McGraw-Hill, New York, New York.

61. Nadai, A. (1943) "Theory of Expanding of Boiler and Condenser Tube Joints Through Rolling", Transaction of the American Society of Mechanical Engineers, vol 65, issue 8.

المنارة للاستشارات
www.manaraa.com

62. Nadai, A. (1950) Theory of Flow and Fracture in Solids, McGraw-Hill, New York, New York.

63. Nevill, G. F., Jr. and Brotzen, Franz R., (1957) “The Effect of Vibration on the Static Yield Strength of Low-Carbon Steel” Proceedings of American Society of Testing Materials, vol 57, 751-758.

64. Nigrelli, V. and Pasta, S. (2008) “Finite element simulation of residual stress induced by split-sleeve cold-expansion process of holes” Journal of Material Processing Technology 205.

65. Oak Ridge National Laboratory, “High Isotope Flux Reactor”, www.neutron.ornl.gov /facilities/HIFR/techparameters> (2013).

66. Ozdemir, A. T. and Edwards, L. (2004). “An Assessment of the Complete Through Thickness Residual Stress Distribution after the Split Sleeve Cold Expansion of Fastener Holes” Canadian Metallurgical Quarterly, vol. 43, no. 2.

67. Ozelton, M. W., and Coyle, T. G. (1986). "Fatigue Life Improvement by Cold Working Fastener Holes in 7050 Aluminum." Fatigue in Mechanically Fastened Composite and Metallic Joints, ASTM STP 927, edited by J. M. Potter, American Society for Testing and Materials, Philadelphia, PA, 53-71.

68. Pavier, M. J., Poussard, C. G. C., and Smith, D. J. (1999). "Effect of residual stress around cold worked holes on fracture under superimposed mechanical load." Engineering Fracture Mechanics, 63(6), 751-773.

69. PBFasteners (2011). “SLEEvbolt Interference Fastening System” PBFasteners <www.pbfasteners.com> (Feb. 27, 2011).

70. Phillips, J.L. (1974). “Sleeve cold working fastener holes, Vol. 1.” AFML-TR-74-10, Air Force Materials Laboratory, Wright-Patterson AFB OH.

71. Poolsuk, S. and Sharpe, W. N., Jr, (1978) “Measurement of the Elastic Plastic Boundary and Coldworked Fastener Holes”, Winter Annual Meeting Dec 1978, American Society of Mechanical Engineers.

72. Poolsuk, Saravut. (1977). "Measurement of the elastic-plastic boundary around coldworked fastener holes," thesis, presented to Michigan State University at East Lancing, MI, in partial fulfillment of the requirements for the degree of Doctor of Applied Mechanics.

73. Poussard, C. G. C., Pavier, M. J., and Smith, D. J. (1994). "Prediction of residual stresses in cold worked fastener holes using the finite element method." Proceedings of the 2nd Biennial European Joint Conference on Engineering Systems Design and Analysis, 8(A) ASME, New York, N.Y., 47-53.

المنارة للاستشارات
www.manaraa.com

74. Poussard, C., Pavier, M. J., and Smith, D. J. (1995). "Analytical and finite element predictions of residual stresses in cold worked fastener holes." Journal of Strain Analysis for Engineering Design, 30(4), 291-304.

75. Prevey, Paul S., (1986) "X-Ray Diffraction Residual Stress Techniques", Metals Handbook 10. Metals Park, American Society for Metals, 380-392. 3-6.

76. PROTO LXRD, http://www.protoxrd.com, (2013), PROTO Manufacturing, Ltd., Oldcastle, Ontario, Canada.

77. Ramberg, W. and Osgood, W. R. (1943) "Description of Stress-Strain Curves by Three Parameters", NCAA TN 902.

78. Reemsnyder, H.S. (1975). "Fatigue life extension of riveted connections." ASCE Journal of the Structural Division, 101(12), 2591-2608.

79. Reeve, L. (1940). "Examination of Welded Steel Specimens from the Hasselt Bridge". Transaction of the Institute of Welding, vol 3 (1).

80. Reid, Len. Engineering manager. Fatigue Technology, Inc., Seattle, WA, 98188, personal communications, Feb 28, 2011.

81. Rich, D. L. and Impellizzeri, L. F., (1977) "Fatigue Analysis of Cold-Worked and Interference Fit Fastener Holes", Cyclic Stress-Strain and Plastic Deformation Aspects of Fatigue Crack Growth ASTM 637, American Society of Testing Materials Philadelphia, PA.

82. Richards, Cedric W. (1961) Engineering Materials Science, Wadsworth Publishing Co, Belmont, California, 405-406.

83. Roddis, W. M. Kim and Zhao, Yuan (2001). "Out-of-Plane Fatigue Cracking in Welding Steel Bridges". Welding Innovations, 27(2), 2-7.

84. Roddis, W.M. Kim and Zhao, Y. (2003). "Finite-element analysis of steel bridge distortion-induced fatigue." Journal of Bridge Engineering, 8(5), 259-266.

85. Rolfe, S. T. and Barsom, John M. (1977). Fracture and Fatigue Control in Structures: Applications of Fracture Mechanics. First Edition. Prentice Hall.

86. Rowlands, Robert E. (1993) "Residual Stress" Chap 18 Handbook on Experimental Mechanics, Kobayoshi, Albert S. ed, Society for Experimental Mechanics, Bethel CT.

87. Sharpe, W.N. Jr., (1978) "Residual Stress around Coldworked Fastener Holes", Journal of Engineering Materials and Technology, Vol 100, July 1978.

88. Shin, C.S., Song, P.S., & Wang, C.M. (1996). "Fatigue damage repair: a comparison of some possible methods." International Journal of Fatigue, 18(8), 535-546.

المنارة للاستشارات
www.manaraa.com

89. Simmons, G. G., Bennett, Caroline R., Barrett-Gonzales, Ron, Matamoros, Adolfo B., and Rolfe, Stanley T. (2013). "Design, modeling, and testing of a piezoelectric impact compressive kinetic (PICK) tool for crack-stop hole treatment", SPIE Smart Structures Conference 2013.

90. Simmons, Gary G. (2013). "Fatigue Enhancement of Undersized, Drilled Crack-Arrest Holes" PhD thesis, presented to the University of Kansas, Lawrence, KS. , in partial fulfillment of the requirements for the degree of Doctor of Philosophy.

91. Sirnivasan, A. V. and McFarland, D. Michael, (2001) Smart Structures, Cambridge University Press, Cambridge, UK, 7-25.

92. Statnikov, E.S. (2004). "Physics and mechanisms of ultrasonic impact treatment." IIV Document XIII-2004-04, International Institute of Welding, Paris, France.

93. Stefanescu, D., Steuwer, A., Owen, R. A., Nadri, B., Edwards, L., Fitzpatrick, M. E., and Withers, P. J. (2004). "Elastic strains around cracked cold-expanded fastener holes measured using synchroton X-rays diffraction technique", Journal of Strain Analysis, Vol 39 No 5.

94. Tavakkolizadeh, M. and Saadatmanesh, H. (2003). "Fatigue Strength of Steel Girders Strengthened with Carbon Fiber Reinforced Polymer Patch". American Society of Civil Engineers Journal of Structural Engineering, 129(2), 186.

95. Vulić, N., Jecić, S., and Grubišić, V. (1997). "Validation of crack arrest technique by numerical modeling." International Journal of Fatigue, 19(4), 283-291.

96. Wang, Z. and Zang, X. (2003) "Predicting Fatigue Crack Growth Life for Cold-Worked Holes Based on Existing Closed-Form Residual Stress Models" International Journal of Fatigue, vol 25 issue 9-11.

97. Watkins, T. R., Schajer, G. S., and Lance, M. J. (to be published 2014). Chap 1.09 Residual Stress Measurement, "Comprehensive Material Processing" Elsevier Ltd.

98. Zhang, Y., Fitzpatrick, M. E., and Edwards, L. (2005). "Analysis of the Residual Stress around a Cold-expanded Fastener Hole in a Finite Plate." Strain, 41(2), 59-70.

99. Zhao, Y. & Kim Roddis, W.M. (2007). "Fatigue behavior and retrofit investigation of distortion-induced web gap cracking." Journal of Bridge Engineering, 12(6), 737-745.

المنارة للاستشارات

www.manaraa.com

APPENDIX A METALLURGICAL TESTING

المنارة للاستشارات
www.manaraa.com

CONSULTING FOR GARY SIMMONS
LAB SERVICES

ESI Project #33944M

www.manaraa.com

923-A Terra Lane
O'Fallon, MO 63366

6603-F Royal St.
Liberty, MO 64068

Consulting for Gary Simmons – Lab Services

ESI Project #33944M

Report Submitted to:

Gary Simmons
University of Kansas, CEAE
1530 W. 15th St.
2150 Learned Hall
Lawrence, KS 66045

Report Submitted by:

Clifford C. Bigelow, P.E.
Senior Consultant

April 4, 2012
Date

Technical Review by:

Steven A. Sanders, M.S.
Staff Consultant

April 4, 2012
Date

This report and its contents are the Work Product of Engineering Systems Inc. (ESI). This report should only be duplicated or distributed in its entirety. This report may contain confidential or court protected information; please contact an authorized entity prior to distributing. Conclusions reached and opinions offered in this report are based upon the data and information available to ESI at the time of this report, and may be subject to revision as additional information or data becomes available after the date of publication.

Copyright 2011 Engineering Systems Inc.

St. Louis Phone (636) 240-6095 ▪ Fax (636) 281-9052 ▪ Kansas City Phone (816) 415-8340

MO Office www.esi-mo.com ▪ *Corporate* www.esi-website.com

www.manaraa.com

INTRODUCTION

Samples of 1/8-inch thick steel plate with machined fastener holes were submitted by Mr. Gary Simmons of the University of Kansas for characterization of experimental mechanical treatments applied to the hole bores. Samples were initially submitted in January of 2011 with additional samples submitted in November of 2011. Included for comparative analysis were samples with drilled and reamed holes, holes mechanically expanded with pressure, and holes mechanically expanded and then treated with piezoelectric impact compressive kinetics (PICK) to induce work hardening and compressive strains at the hole bores. ESI was requested to conduct a metallurgical study to characterize and document the effects of the mechanical treatment applied to the hole bores.

PROCEDURE

A total of four hole samples were submitted for analysis that were reportedly prepared as follows:

Sample 1-P	drilled, reamed, mechanically expanded and Pick treated, (submitted 01/2011)
Sample 4-P	drilled, reamed, mechanically expanded and PICK treated
Sample 10-D	drilled, reamed and mechanically expanded
Sample 9-U	drilled and reamed only

Characterization of the submitted samples was undertaken through the following destructive examinations and testing:

Sample 1-P:

A transverse cross sectional specimen was cut from the sample plate perpendicular to the plate rolling direction at a location approximately 1-inch from the treated hole for characterization of the base metal. The base metal is defined as the as-manufactured metal where hardness was unaffected by the mechanical treatment surrounding the hole. The cross section was mounted and polished for metallographic examination and microhardness testing.

A second, transverse cross sectional specimen was cut from the plate perpendicular to the plate rolling direction and intersecting the equator of the hole bore. The specimen was mounted and polished for metallographic examination and photo documentation. Two microhardness traverses were performed on the cross section with hardness readings initiating just below the inside cylindrical surface of the hole and extending into the base metal. One traverse was near the outer surface of the plate, and the other near mid-thickness.

Sample 4-P:

A transverse cross sectional specimen was cut from the plate perpendicular to the plate rolling direction and intersecting the equator of the hole bore. The specimen was mounted and polished for metallographic examination and documentation.

www.manaraa.com

A microhardness traverse was performed on the cross section near mid-thickness of the plate, initiating just below the inside cylindrical surface of the hole and extending into the base metal.

Additional metallographic examination was performed at magnification of 1000x to 4000X by scanning electron microscope (SEM).

Sample 10-D:

A transverse, cross sectional specimen was cut from the plate perpendicular to the plate rolling direction and intersecting the equator of the hole bore. The specimen was mounted and polished for metallographic examination and documentation.

A microhardness traverse was performed on the cross section near mid-thickness of the plate, initiating just below the inside cylindrical surface of the hole and extending into the base metal.

Additional SEM metallographic examination was performed at magnification of 1000x to 4000X.

Sample 9-U:

A transverse cross sectional specimen was cut from the plate perpendicular to the plate rolling direction and intersecting the equator of the hole. The specimen was mounted and polished for metallographic examination and documentation.

A microhardness traverse was performed on the cross section near mid-thickness of the plate, initiating just below the inside cylindrical surface of the hole and extending into the base metal.

Lab Notes:

Metallographic cross sections intersecting the inside cylindrical surface hole bores were cut utilizing a slow speed diamond saw to minimize effects of cold work during cutting. The samples were mounted in Bakelite material, as typically used for metallographic samples, and then ground and polished at progressively finer grits through one micron.

Microhardness readings were taken from the metallographic cross sections to assess the degree of work hardening imparted at the hole bores resulting from the mechanical treatments performed. Attempts were made to take readings as close to the inside cylindrical surface of holes as practical. Given the size of the hardness indents, valid readings could only be taken within approximately 0.13 - 0.15 mm (0.005 -0.006 inch) of the surfaces.

RESULTS

Base metal properties:

The submitted samples were reportedly machined from A36 steel plate. Typical microstructures of the plate base metal are shown in Photos 1–3 for Samples 1-P and 4-P. The

المنارة للاستشارات
www.manaraa.com

base metal exhibited light-etching ferrite grains with small islands of dark-etching pearlite, consistent with a low carbon steel such as grade A36. Grain size was mixed exhibiting apparent grain sizes ranging between ASTM grain size numbers 9.5-9.0, which have corresponding average grain diameters of 13.3 and 15.9 microns, respectively.

Hardness of the steel base metal from each sample was determined by Vickers microhardness testing and converted to Rockwell B (HRB), with results contained in Tables 1 - 6. Hardness readings from the base metal of Samples 1-P and 4-P are contained in Table 1 and 6, respectively, and ranged from 68 to 71 HRB. However, nominal hardness of the base metal of samples 9-U and 10-D (the base metal of 10D includes areas 0.09 inches or more from the hole) was somewhat lower, with nominal readings ranging from 63 to 66 HRB, as shown in Tables 4 and 5, respectively.

Drilled and Reamed Sample:

Sample 9-U was essential original base metal that contained a drilled and reamed hole without any mechanical treatment. A metallographic cross section was taken from the sample intersecting the inside surface of the hole bore. As expected, the drilling and reaming process resulted in shallow grain deformation along at the surface of the hole bore, which is indicated in the metallographic cross section shown in Photos 4 and 5.

A Vickers microhardness traverse was taken from the metallographic sample just below the inside cylindrical surface of the hole and extending into the base metal. No significant depth of work hardening resulted from the drill and ream machining process, as indicated from the hardness data contained in Table 4.

Mechanically Expanded Sample:

Sample 10-D was subjected to expansion by mechanical pressure only. The microstructure along the inside cylindrical surface of the hole of this sample is shown in Photos 6 and 7, exhibiting a shallow layer of grain deformation as pictured in Photo 7, and in the SEM images shown in Photo 8 and 9. A visibly apparent zone of grain deformation was evident to a depth of approximately 0.008-0.009 mm (.0003-.00035 inch) below the inside surface of the hole. Microscopic pits were also revealed in the zone of grain deformation, as shown in Photo 9.

Results of the microhardness traverse from the inside surface of the hole bore are contained in Table 5. The maximum hardness near the hole surface was approximately 15 HRB higher than the base metal, consistent with the effects of work hardening induced by the expansion process. The elevated hardness resulting from work hardening by the mechanical expansion process was measureable over a distance of approximately 2.26 mm (0.089 inches) from the inside surface of the hole. All material beyond 2.26 mm in depth from the hole was the original base metal.

PICK Treated Sample:

Samples 1-P and 4-P were subjected to expansion by mechanical pressure as well as the PICK treatment.

المنارة للاستشارات

www.manaraa.com

Typical microstructures along the inside surface of the hole of sample 1-P is shown in Photos 10 and 11. A shallow layer of grain deformation was revealed along the surface of the hole and extended a distance of approximately 0.01 mm (0.0004) inches from the surface.

Sample 4-P also exhibited a shallow zone of grain deformation at the inside surface of the hole measuring nominally 0.01 mm (0.0004 inch) in width, but also displayed semi-circular regions immediately below the surface of the hole where grain deformation was evident over a distance of 0.038 mm (0.0015 inch) from the surface of the hole, as shown in Photos 12 -14. Within these zones there appeared to be highly elongated and flattened grains that transitioned to a finer, unresolved microstructure. Small pits or porosity had also formed within the surface regions of grain deformation.

Additional examination was conducted by SEM with only a light etch applied to the sample to minimize grain boundary broadening from the chemical attack. SEM examination revealed the transition from the original, base metal grain size and shape to the highly elongated and flattened grains near the hole surface, and a further transition to an unresolved structure where grain size and shape could not be discerned, depicted in Photos 15-19. At one location, shown in Photo 15, a crack-like feature was revealed which may have been a cold lap formed during the pressure expansion or PICK treatment of the surface. It was noted that the deeper zones of grain deformation were discontinuous, occurring at localized areas under the surface of the hole, as depicted in Photo 17. A population of pits or porosity was also evident within the zone of grain deformation, as shown in Photos 16-19, that further masked the microstructural features.

Microhardness traverses on the cross sections from the hole bore to the base metal were conducted near the plate surface and at mid-thickness of sample 1-P. Results are contained in Tables 2 and 3, respectively. Hardness readings close to the surface of the hole measured 81 - 83 HRB, as converted from Vickers hardness, which was approximately 15 HRB higher hardness than the base metal readings away from the hole. The depth of work hardening, determined from the elevated hardness numbers, was approximately 2.0 to 2.2 mm (.078-.087 inches) below the surface of the hole.

Similar hardness results were observed from Sample 4-P, contained in Table 6, where hardness near the surface of the hole measured approximately 13 HRB higher than the base metal. Depth of work hardening determined by the hardness data was approximately 2.1 mm (.083 inches) below the surface of the hole.

DISCUSSION OF RESULTS

Studies [1] on the effects of ultrasound deformation (comparable in some respects to the PICK treatment) of some non-ferrous alloys have reported that recrystallization can occur during treatment that results in the formation of nano grain sizes. Recrystallization [2, 3,] is a mechanism driven by the internal energy resulting from grain deformation and applied thermal energy to nucleate and propagate recrystallization. The mechanism causing possible crystallization during PICK treatment is not addressed here.

The microstructure along the surface of hole in the PICK treated sample 1-P displayed a very shallow layer of apparent grain deformation evident to a maximum distance of approximately

المنارة للاستشارات
www.manaraa.com

0.01 mm (0.0004 inch) from the inside surface of the hole; however, there was no visible indication of recrystallization revealed by the optical metallography employed in this study. Hardness test results indicated that the effects of work hardening resulting from the mechanical treatments had affected the metal a greater distance from the surface of the hole than the visibly apparent depth of grain deformation.

The PICK treated sample 4-P exhibited a unique microstructural feature along the surface of the hole that consisted of a shallow region of highly elongated, flattened grains within localized, semicircular regions where grain deformation resulted deeper below the surface of the hole. The severely flattened grains in the deformation zone transitioned to a finer structure closer to the surface of the hole that could not be fully resolved by the metallographic technique employed in this study. Optical and SEM metallography could not verify whether or not recrystallization had occurred in the unresolved microstructure.

Porosity or pitting was also revealed within the grain deformation zones at the hole surfaces in sample 10-D and the PICK treated sample 4-P. The source of the pitting could not be determined from the described metallographic techniques. The microscopic pits could be the artifacts of inclusion particles inherent to the steel microstructure that have been concentrated in the zones of grain flattening, and then subsequently pulled out of the surface during polishing or etching. Alternatively, it is theorized that they could be etch pits [2, 3] formed at dislocation pileups resulting from the grain deformation that intersect the polished surface; however, they did not exhibit the typical geometric array and pit shape. The pitting is not particular evidence of a recrystallized microstructure.

<<End of Report Text>>

المنارة للاستشارات
www.manaraa.com

REFERENCES

1. X. An, et al, *Study of the Surface Nanocrystalliztion Induced by Esonix Ultrasonic Impact Treatment on the Near-Surface of 2024-T351 Aluminum Alloy.* J. of Materials Engineering and Performance, Vol. 15, ASM International, 2003.

2. *Physical Metallurgy Principles*, R.E. Reed-Hill, PWS-Kent Publishing Co. Boston, 1973.

3. *Modern Physical Metallurgy,* R.E. Smallman, Butterworth's & Co., London, 1985.

المنارة للاستشارات

www.manaraa.com

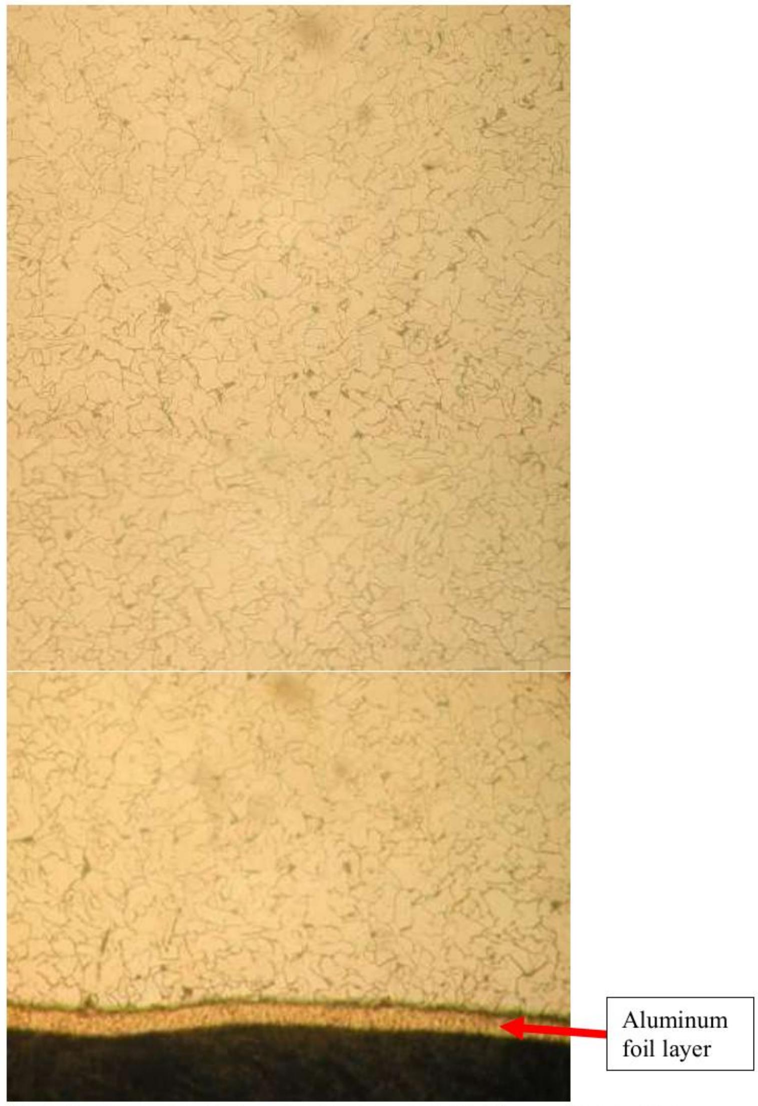

Photo 1. Sample 1-P; typical base metal microstructure near mid thickness of plate. Hole bore surface is shown at arrow at bottom. Note: a layer of aluminum foil overlays the surface, which was applied to aid in edge retention during polishing. (~214 x)

www.manaraa.com

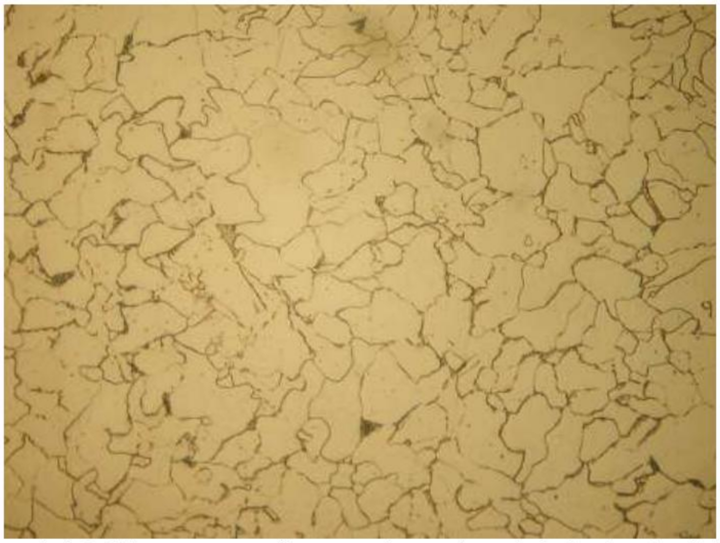

Photo 2. Sample 1-P. Microstructure of base metal away from the hole, showing light-etching ferrite matrix with small, dark-etching pearlite colonies. (~550x)

Photo 3. Sample 4-P. Microstructure of base metal away from the hole, exhibiting a ferrite matrix with dispersed pearlite colonies. (~500x)

المنارة للاستشارات

www.manaraa.com

Photo 4. Sample 9-U. Microstructure of base metal. Hole bore surface is edge at top of photo. (~100X)

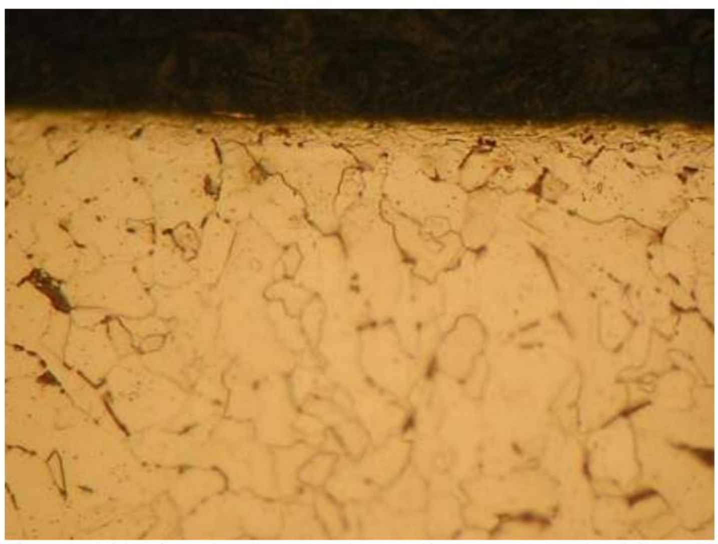

Photo 5. Sample 9-U. Microstructure, showing shallow depth of grain deformation at the surface of the hole, shown at top. (~500X)

المنارة للاستشارات
www.manaraa.com

Photo 6. Sample 10-D. Base metal microstructure. Surface of the hole is at top. (~100X)

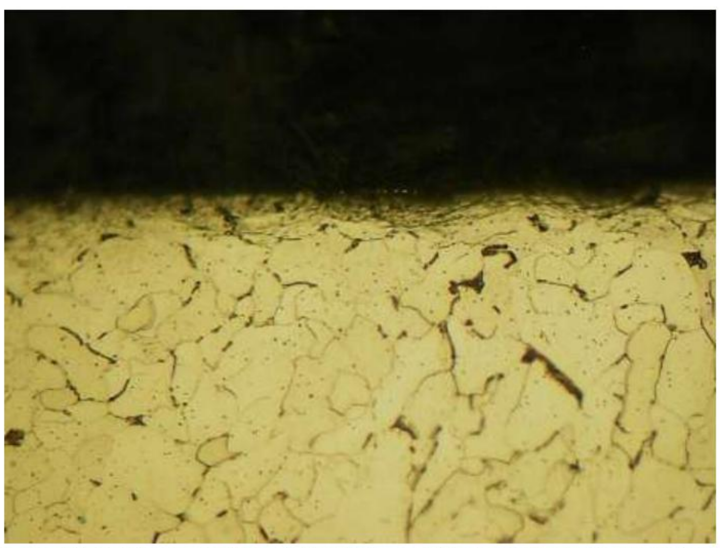

Photo 7. Sample 10-D. Microstructure at the surface of the hole (top), showing shallow zone of grain deformation. (~500X)

www.manaraa.com

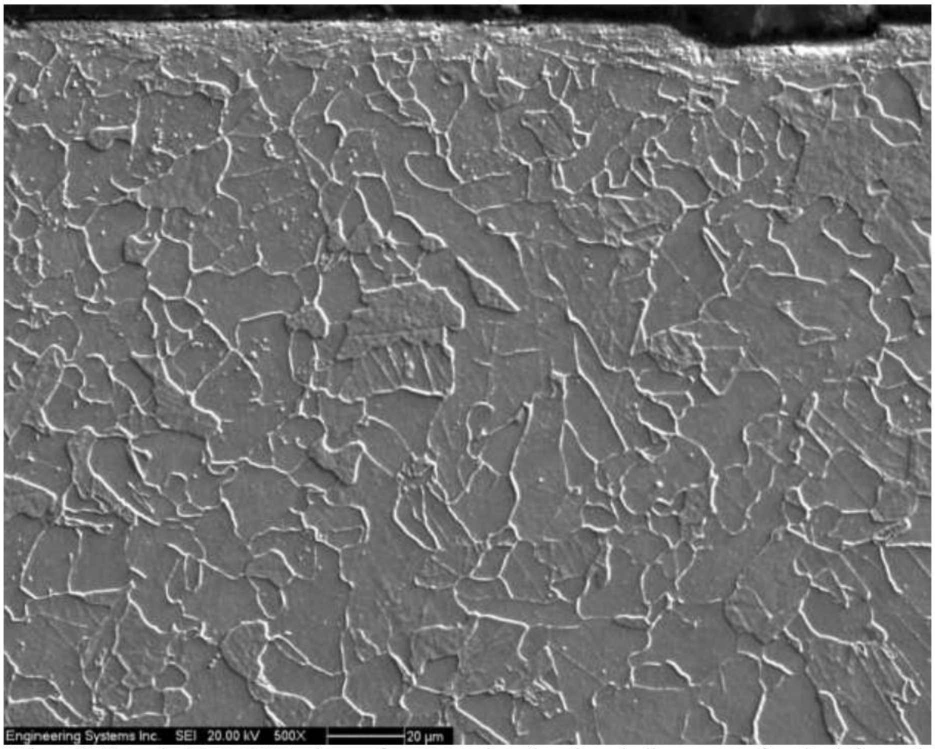

Photo 8. Sample 10-D, SEM photo of cross section showing shallow zone of grain deformation along the surface of the hole (top). (~500X)

المنارة للاستشارات
www.manaraa.com

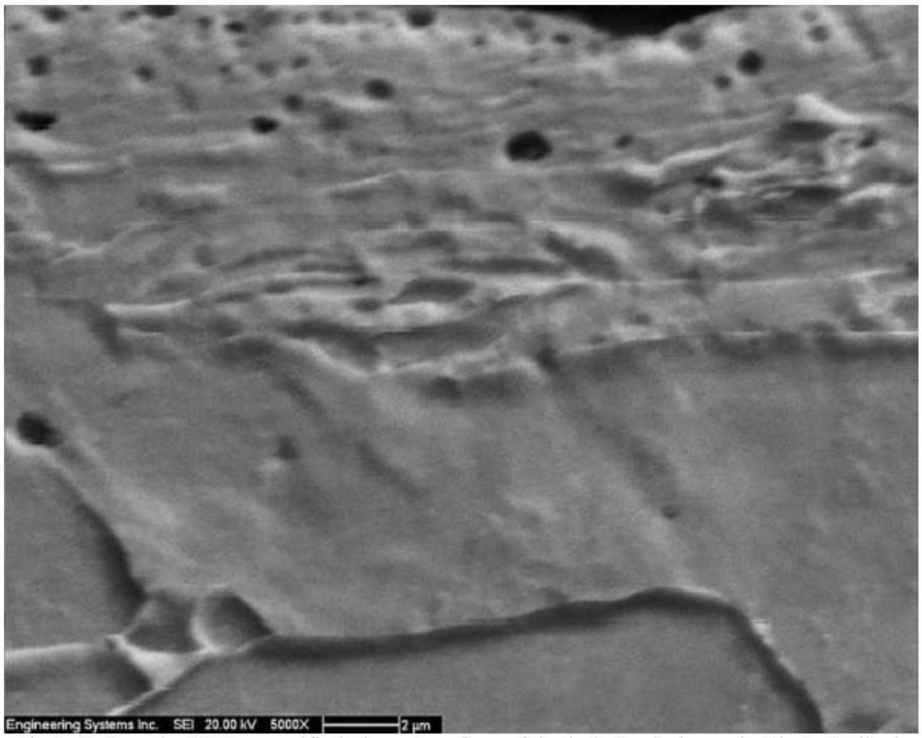

Photo 9. Sample 10-D, magnified view at surface of the hole (top) shown in Photo 8, displaying grain deformation and pitting. (~5000X)

المنارة للاستشارات
www.manaraa.com

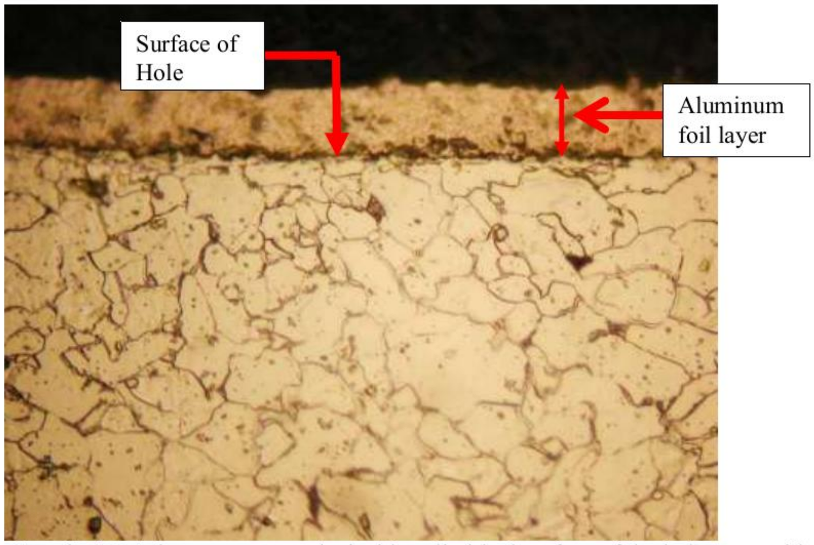

Photo 10. Sample 1-P. Microstructure at the inside cylindrical surface of the hole, near mid-thickness of plate, showing very shallow region of apparent grain deformation (arrow). (~560X)

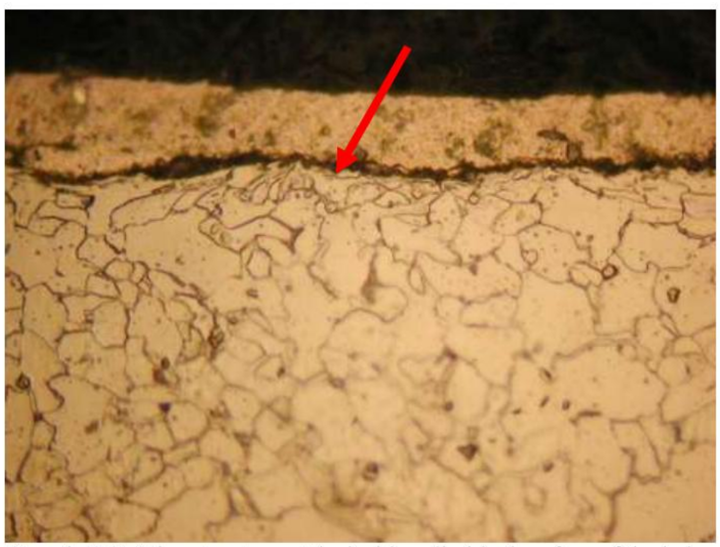

Photo 11. Sample 1-P. Microstructure at the inside cylindrical surface of the hole, near mid-thickness of plate showing shallow grain deformation (arrow). (~560X).

المنارة للاستشارات
www.manaraa.com

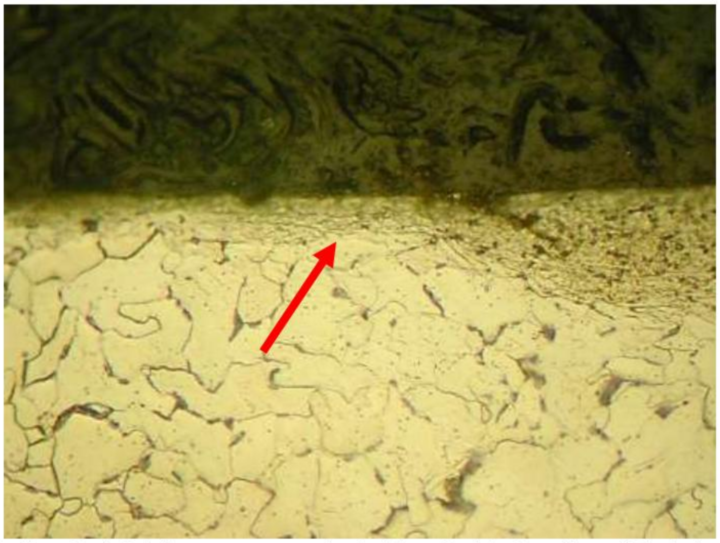

Photo 12. Sample 4-P. Microstructure at the inside cylindrical surface of the hole showing shallow zone of grain deformation (arrow). (~500 X).

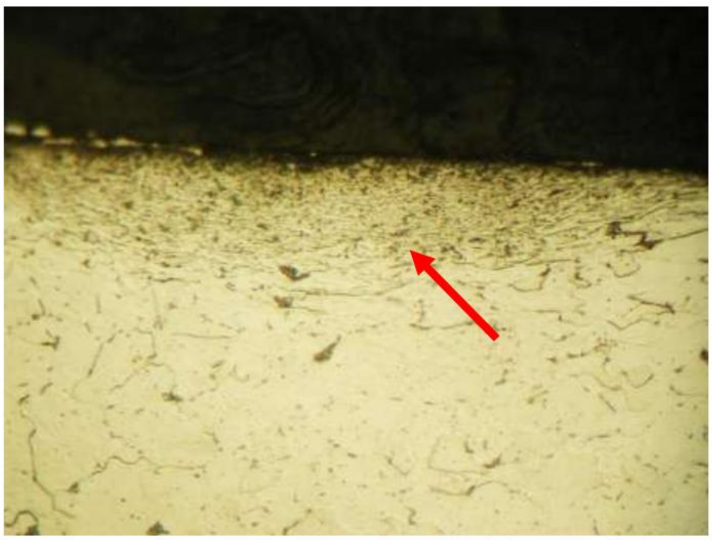

Photo 13. Sample 4-P. Microstructure at the surface of the hole, near mid-thickness of plate, showing a semi-circular zone of grain deformation and unresolved microstructure (arrow). (~500 X).

www.manaraa.com

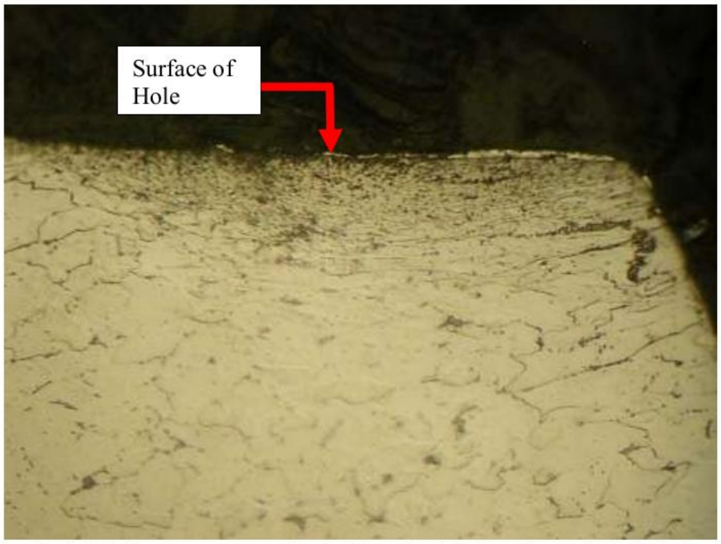

Photo 14. Sample 4-P. Microstructure at the inside cylindrical surface of the hole (top edge) near outer surface of plate (at right) displaying localized zone of grain deformation and unresolved microstructure (~500 X).

المنارة للاستشارات
www.manaraa.com

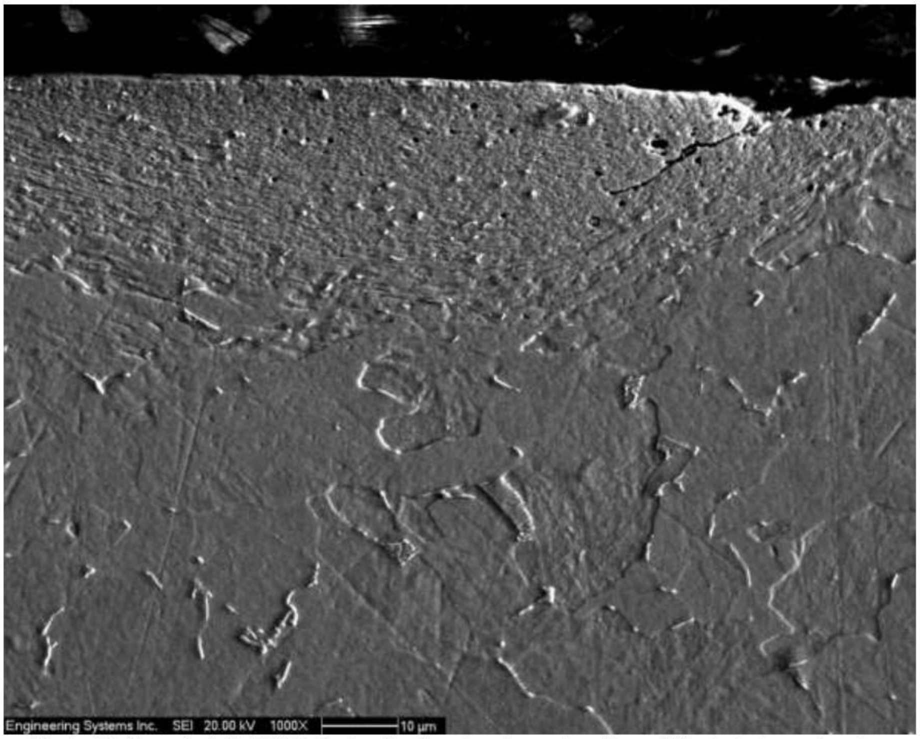

Photo 15. Sample 4-P. SEM photo of microstructure at surface of the hole bore showing localized region of grain deformation. (~1000 X).

المنارة للاستشارات
www.manaraa.com

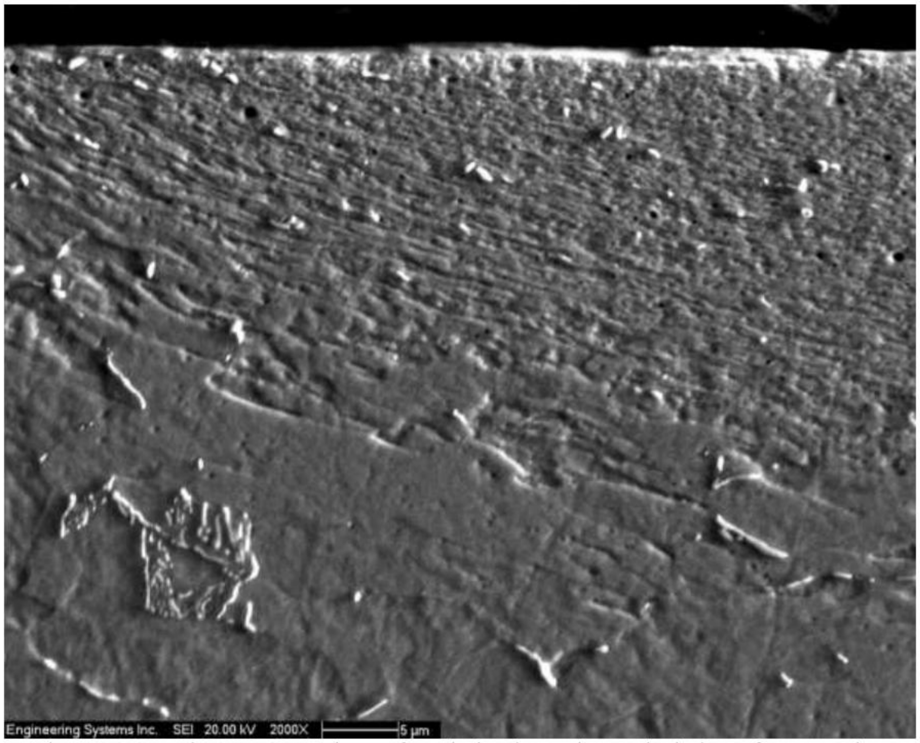

Photo 16. Sample 4-P. SEM photo of semi-circular region at the hole surface near the outer plate surface, showing localized grain deformation, and unresolved structure closer to the hole surface (top). Note small pits within this region (~2000 X).

www.manaraa.com

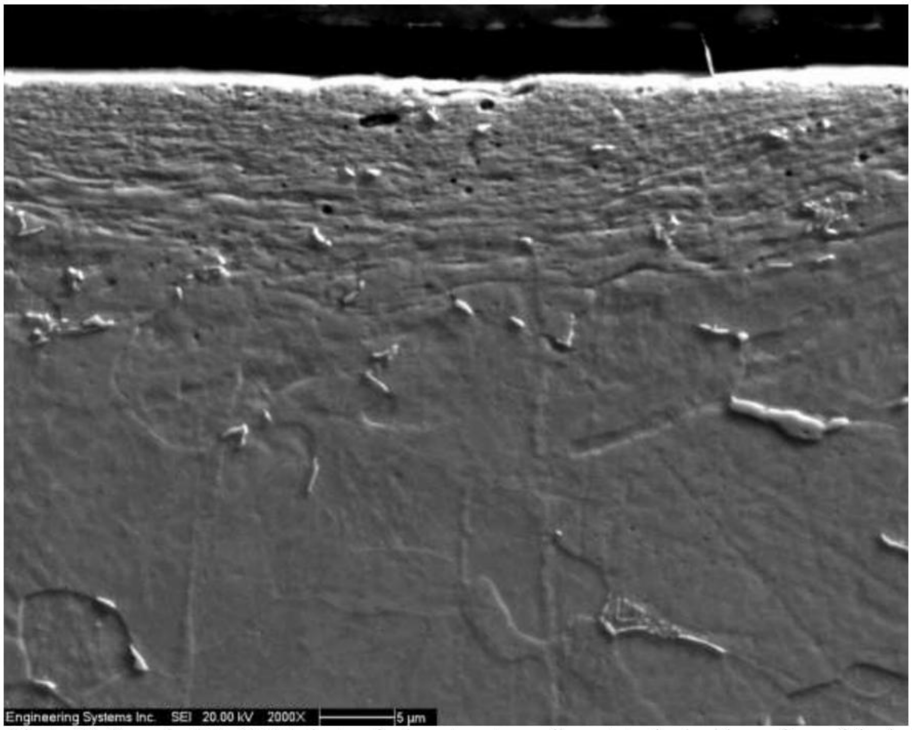

Photo 17. Sample 4-P. SEM photo of microstructure adjacent to the inside surface of the hole (top) near the outer surface of the plate, showing localized region of grain deformation and unresolved structure closer to the hole surface.
(~2000 X).

www.manaraa.com

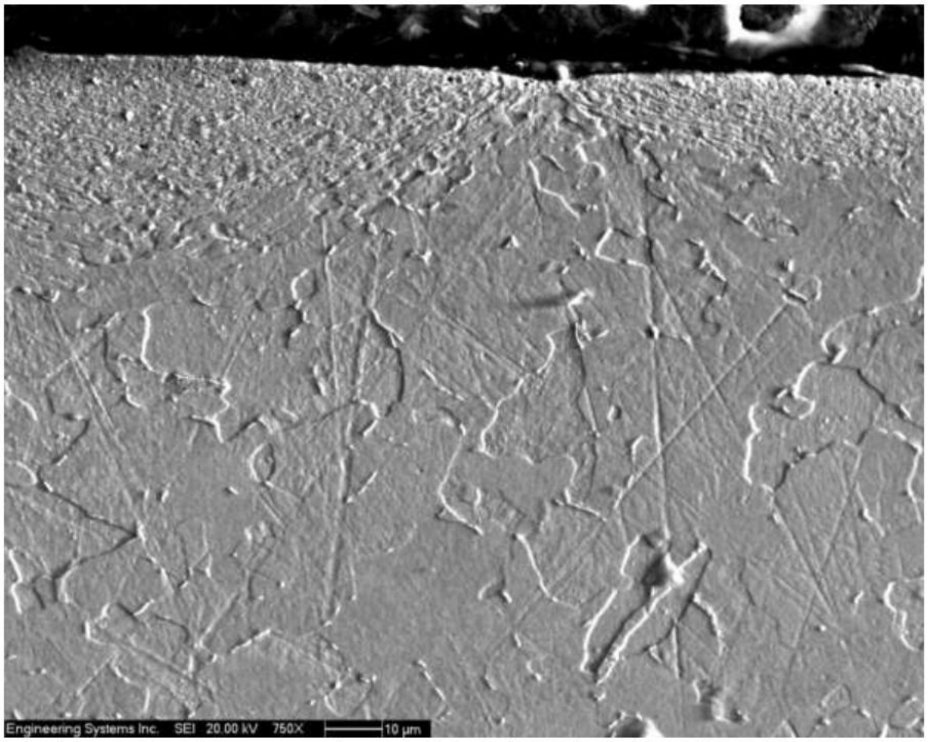

Photo 18. Sample 4-P. SEM photo of cross section at the inside surface of the hole, at top, showing discontinuous nature of the grain deformation zones. (~750X)

المنارة للاستشارات
www.manaraa.com

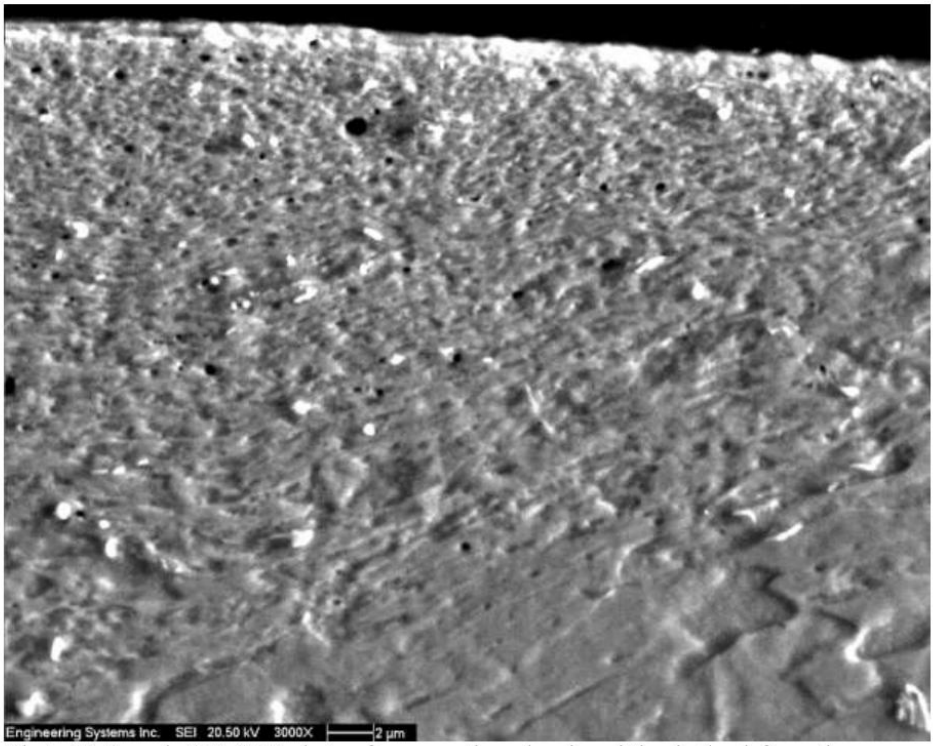

Photo 19. Sample 4-P. SEM photo of cross section, showing pitting in the deformation zone. (~3000X)

المنارة للاستشارات
www.manaraa.com

Table 1. Vickers Microhardness Readings

Sample 1-P
Base Metal

Dist. From Plate Outer Surface [mm]	Vickers Hardness (HV)	HRB (converted)[1]
9.35	126.3	71
9.10	120.6	68
8.85	122.6	69
8.60	122.8	69
8.35	122.8	69
AVERAGE HARDNESS		69

[1] ASTM E140 – NON-AUSTENITIC STEELS CONVERSION

www.manaraa.com

Table 2. Vickers Microhardness Readings

Sample 1-P
From surface of the hole, near outer surface of plate

Dist. from Hole Bore Surface [mm]	Vickers Hardness (HV)	Rockwell B Hardness (HRB) (converted)[(1)]
0.13	163.0	84
0.39	148.4	80
0.63	152.6	81
0.89	148.4	80
1.13	139.6	76
1.24	144.3	78
1.35	148.4	80
1.48	148.4	80
1.61	145.4	78
1.73	144.6	78
1.85	148.4	80
1.97	148.4	80
2.21	148.4	80
2.47	136.1	75
2.58	136.1	75
2.83	137.2	75
3.08	138.0	76
3.32	135.1	74
3.57	134.3	74
3.83	133.8	74
4.06	133.8	74
4.31	138.0	76
5.31	128.6	72
6.31	134.8	74

[1] ASTM E140 – NON-AUSTENITIC STEELS CONVERSION

المنارة للاستشارات
www.manaraa.com

Table 3. Vickers Microhardness Readings

Sample 1-P
From surface of the hole, near mid-thickness of plate

Dist. from Hole Bore Surface [mm]	Vickers Hardness (HV)	Rockwell B Hardness (HRB) (converted)[1]
0.15	153.8	81
0.20	160.0	83
0.25	148.4	80
0.32	155.1	82
0.45	157.0	82
0.52	150.1	80
0.58	157.7	83
0.64	148.4	80
0.70	152.9	81
0.77	146.6	79
0.82	152.9	81
0.96	150.5	80
1.10	149.8	80
1.23	152.0	81
1.36	141.5	77
1.50	135.6	75
1.63	136.1	75
1.80	139.0	76
1.93	140.1	76
2.05	135.1	74
2.17	131.0	73
2.43	128.9	72
2.68	122.2	69
2.92	122.8	69
3.18	122.8	69
3.42	122.6	69
4.42	127.4	71

[1] ASTM E140 – NON-AUSTENITIC STEELS CONVERSION

المنارة للاستشارات
www.manaraa.com

Table 4. Vickers Microhardness Readings

Sample 9-U

From surface of the hole, near mid-thickness of plate

Dist. from Hole Bore Surface [mm]	Vickers Hardness (HV)	Rockwell B Hardness (HRB) (converted)[(1)]
0.15	114.8	64.6
0.30	116.2	65.4
0.45	120.2	67.5
0.60	119.3	67.1
0.75	114.8	64.6
0.90	116.2	65.4
1.05	119.1	67.0
1.20	117.8	66.3
1.35	115.8	65.2
1.50	113.4	63.8
1.65	116.0	65.3
1.80	116.6	65.6
1.95	112.0	63.0
2.10	115.0	64.7
2.25	114.6	64.5
2.40	115.0	64.7
2.55	114.2	64.2
2.70	111.4	62.6
2.85	114.0	64.1
3.00	113.4	63.8
3.15	117.4	66.1
3.30	113.0	63.6
3.45	112.2	63.1
3.60	115.0	64.7
3.75	108.4	60.8

[1] ASTM E140 – NON-AUSTENITIC STEELS CONVERSION

www.manaraa.com

Table 5. Vickers Microhardness Readings

Sample 10-D
From surface of the hole, near mid-thickness of plate

Dist. from Hole Bore Surface [mm]	Vickers Hardness (HV)	Rockwell B Hardness (HRB) (converted)(1)
0.16	153.2	81.2
0.31	141.5	77.0
0.46	137.7	75.5
0.61	142.6	77.4
0.76	142.6	77.4
0.91	135.9	74.8
1.06	142.6	77.4
1.21	134.6	74.2
1.36	132.3	73.2
1.51	128.1	71.4
1.66	127.2	71.0
1.81	129.6	72.1
1.96	121.7	68.3
2.11	125.8	70.3
2.26	121.3	68.1
2.41	113.8	64.0
2.56	113.8	64.0
2.71	116.6	65.6
2.86	117.4	66.1
3.01	120.0	67.4
3.16	118.3	66.5
3.31	112.6	63.3
3.46	111.0	62.4
3.61	115.0	64.7
3.76	114.2	64.2

[1] ASTM E140 – NON-AUSTENITIC STEELS CONVERSION

www.manaraa.com

Table 6. Vickers Microhardness Readings

Sample 4-P
At hole bore near mid-thickness of plate

Dist. from Hole Bore Surface [mm]	Vickers Hardness (HV)	Rockwell B Hardness (HRB) (converted)(1)
0.15	156.4	82.2
0.28	156.1	82.1
0.40	158.3	82.8
0.53	153.8	81.4
0.65	146.0	78.7
0.78	152.6	81.0
0.90	151.4	80.5
1.03	149.5	79.9
1.15	155.1	81.8
1.28	143.2	77.6
1.40	150.8	80.3
1.53	138.8	75.9
1.65	143.7	77.8
1.78	132.5	73.4
1.90	138.2	75.7
2.03	129.1	71.8
2.15	137.7	75.5
2.28	129.1	71.8
2.40	125.8	70.3
2.53	125.8	70.3
2.65	128.6	71.6
2.78	121.7	68.3
2.90	121.3	68.1
3.03	126.3	70.5
3.15	125.8	70.3

[1]ASTM E140– NON-AUSTENITIC STEELS CONVERSION

المنارة للاستشارات
www.manaraa.com

APPENDIX B CALCULATIONS

Appendix B-1 Nadai's Closed-From Solution for Stress Around A Cold-Expanded Hole

Appendix B-2 Ball's Closed-From Solution for Stress Around A Cold-Expanded Hole

Appendix B-3 Modified Ramberg-Osgood Equations for Different *n* Values

Appendix B-4 Ball's Closed-From Solution for *n* = 40

Appendix B-5 Ball's Closed-From Solution for *n* = 10

www.manaraa.com

Appendix B-1 Nadai's Closed-From Solution for Stress Around A Cold-Expanded Hole

B-1. Investigation of the Technique and Formulae Presented in Nadai A., Theory of the Expanding of Boiler and Condenser Tube Joints Through Rolling, (1943), Americsan Society of Mechanical Engineers - Transactions vol 65 issue 8, p 865-880.

A. Assumptions:

1. Plane stress. The principle stresses are in the tangential and radial directions around the hole and perpendicular to the surface of the plate. The stress perpendicular to the plate is zero, leaving the material in a biaxial state of stress with only S_t, tangential stress and S_r, radial stress.

2. The steel has an elastic-perfectly plastic stress strain curve.

3. Von Mises ellipse controls yielding.

4. No Bauschinger effect upon unloading after cold expansion.

5. No friction between the surface of the hole and the tool used to impose the cold expansion.

6. After yielding, constant volume maintained. Results in Poisson's ratio μ = 0.5 after yielding.

B Calculations for stresses due to cold expansion

1. Check / determine max radius of plastic zone.

Let r_1 be the initial radius of the hole and c be the radius of the elastic-plastic interface. Nadai's Equation 10 provides the relationship between c/r as function of parameterization variable Θ 2. As Θ 2 varies from -90 deg to 0 deg, the ratio of c/r can be determine and reaches a maximum. Let C2 $=c^2/ r_1{}^2$, C2 can be determined by Nadai's Equation 10 and let C then is square root of

C2 and = c/r. c/r then:

Nadai Equation10

$i := 1, 2.. 19$

المنارة للاستشارات

www.manaraa.com

Convert Θ 2 from degrees to radians

$$\Theta 2 := \begin{pmatrix} -90 \\ -85 \\ -80 \\ -75 \\ -70 \\ -65 \\ -60 \\ -55 \\ -50 \\ -45 \\ -40 \\ -35 \\ -30 \\ -25 \\ -20 \\ -15 \\ -10 \\ -5 \\ 0 \end{pmatrix} \cdot \mathrm{deg}$$

$$(C2)_i := \left(e^{-\sqrt{3}\cdot\Theta 2_i}\right)\cdot\cos\left(\Theta 2_i\right)$$

$(C2)_i =$

	1
1	0
2	1.138
3	1.95
4	2.498
5	2.838
6	3.015
7	3.067
8	3.025
9	2.914
10	2.756
11	2.567
12	2.36
13	2.145
14	1.93
15	1.72
16	1.52
17	1.332
18	1.159
19	1

$$C_i := \sqrt{C2_i}$$

$\Theta 2 =$ (values $\cdot$ rad)

	1
1	-1.5708
2	-1.4835
3	-1.3963
4	-1.309
5	-1.2217
6	-1.1345
7	-1.0472
8	-0.9599
9	-0.8727
10	-0.7854
11	-0.6981
12	-0.6109
13	-0.5236
14	-0.4363
15	-0.3491
16	-0.2618
17	-0.1745
18	-0.0873
19	0

$\cdot$ rad

$\max(C) = 1.75124$

$C_i =$

	1
1	$3.05\cdot10^{-8}$
2	1.067
3	1.396
4	1.581
5	1.685
6	1.736
7	1.751
8	1.739
9	1.707
10	1.66
11	1.602
12	1.536
13	1.465
14	1.389
15	1.312
16	1.233
17	1.154
18	1.076
19	1

$\Theta\ 2_7$ corresponds to the max value of c/r at C_7

$\Theta 2_7 = -1.047$

www.manaraa.com

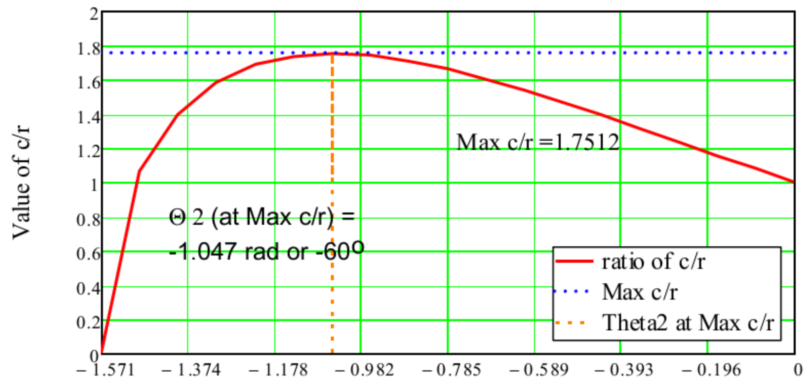

Fig. 1 Plastic zone radius as function of initial radius

For 1/8-in dia hole, the max radius of the elastic-plastic zone (R_{ep}) is Max (c/r) x (radius)

$Rep := 1.7512 \cdot \frac{.125 \cdot in}{2}$ $\quad Rep = 0.109 \cdot in \quad Dep := 2 \cdot Rep \quad Dep = 0.219 \cdot in$

0.219-in approximately equals $^{7}/_{32}$ -in << $^{3}/_{8}$ -in = 0.375 in which was measured after cold expansion by the PICK tool.

2. Determine the max ratio St of the tangential stress to yield stress and the max ratio Sr of radial stress to the yield stress at the end of cold expansion before the plug is removed.

To get max S_{tp} and max S_{rp} in the plastic zone from cold-expansion,

A. Use Θ_2 which provide the largest c/r_1 ratio from Equation 10 above. This occurs at Θ_2 = -60º or -1.0472 rad. See Fig 1. This also provides the pressure that produces the highest stresses, Equation 11. Because of the assumption of elastic-perfectly, plastic material properties in the steel, pressure above this will cause additional deformation but will not increase either tangential or radial stresses.

B. Let r = the radius of interest at which the stress is desired and r_1 = the original radius of the hole, then $R = r / r_1$ and R varies from 1, which is at the edge of the hole, to R = 1.7512 the location of the elastic-plastic interface, to 1,7512 into the elastic zone. Solve for R as function of Θ , using Equation 12 with the value of Θ_2 that provides for the highest stress Θ_2 = -60º.

المنارة للاستشارات
www.manaraa.com

C. Calculate the value of the stress ratios S_{tp}, plastic tangential stress, and S_{rp}, plastic radial stress, in the plastic range as functions of Θ using equations 9.

D. Plot S_{tp} and S_{rp} as functions of R using the corresponding values of Θ to link S_{rp} and S_{tp} to R. See Fig 2.

$$\Theta := \begin{pmatrix} 0 \\ -4 \\ -8 \\ -12 \\ -16 \\ -20 \\ -24 \\ -28 \\ -32 \\ -36 \\ -40 \\ -44 \\ -48 \\ -52 \\ -56 \\ -60 \end{pmatrix} \cdot deg$$

$i := 1,2..16$

$\Theta 2 := -60 \cdot deg$

Equation 12

$$R_i := \sqrt{\frac{\left(e^{-\sqrt{3}\cdot\Theta 2} \cdot \cos(\Theta 2)\right)}{e^{-\sqrt{3}\cdot\Theta_i} \cdot \cos\left(\Theta_i\right)}}$$

$R_i =$

	1
1	1.751
2	1.651
3	1.559
4	1.477
5	1.402
6	1.335
7	1.275
8	1.221
9	1.172
10	1.13
11	1.093
12	1.062
13	1.036
14	1.017
15	1.005
16	1

Equations 9

$$Srp_i := \frac{2}{\sqrt{3}} \cdot \sin\left(\Theta_i - \frac{\pi}{6}\right)$$

$$Stp_i := \frac{2}{\sqrt{3}} \cdot \sin\left(\Theta_i + \frac{\pi}{6}\right)$$

$Stp_i =$

0.577
0.506
0.433
0.357
0.279
0.201
0.121
0.04
-0.04
-0.121
-0.201
-0.279
-0.357
-0.433
-0.506
-0.577

$m := -2, -1..2$

$\max(C) = 1.751$

$Srp_i =$

	1
1	-0.577
2	-0.646
3	-0.711
4	-0.773
5	-0.831
6	-0.885
7	-0.934
8	-0.979
9	-1.02
10	-1.055
11	-1.085
12	-1.11
13	-1.129
14	-1.143
15	-1.152
16	-1.155

المنارة للاستشارات
www.manaraa.com

E. Pick radii for calculating elastic stress ratios S_{te}, elastic tangential stress, and S_{re}, elastic radial stress, Pick $R_{elastic}$ values above the radius of the elastic-plastic interface.

F. Calculate the ratio of c / $R_{elastic}$ and use this ratio in Equation 17 to calculate S_{te}. Since the
material is elastic, S_{re} = -S_{te}. Plot these as a function of $R_{elastic}$ in Fig 2.

Equation 17 for the elastic region r>c

$$\text{Relastic} := \begin{pmatrix} 1.751 \\ 2.0 \\ 2.25 \\ 2.5 \\ 2.75 \\ 3.0 \\ 3.5 \\ 4.0 \\ 4.5 \\ 5.0 \\ 5.5 \\ 6.0 \end{pmatrix} \qquad \text{RCelastic} := \frac{\max(C)}{\text{Relastic}} \qquad \text{Ste} := \frac{1}{\sqrt{3}} \cdot \text{RCelastic}^2 \qquad \text{Sre} := -\text{Ste}$$

RCelastic =

	1
1	1
2	0.876
3	0.778
4	0.7
5	0.637
6	0.584
7	0.5
8	0.438
9	0.389
10	0.35
11	0.318
12	0.292

Ste =

	1
1	0.578
2	0.443
3	0.35
4	0.283
5	0.234
6	0.197
7	0.145
8	0.111
9	0.087
10	0.071
11	0.059
12	0.049

Sre =

	1
1	-0.578
2	-0.443
3	-0.35
4	-0.283
5	-0.234
6	-0.197
7	-0.145
8	-0.111
9	-0.087
10	-0.071
11	-0.059
12	-0.049

المنارة للاستشارات
www.manaraa.com

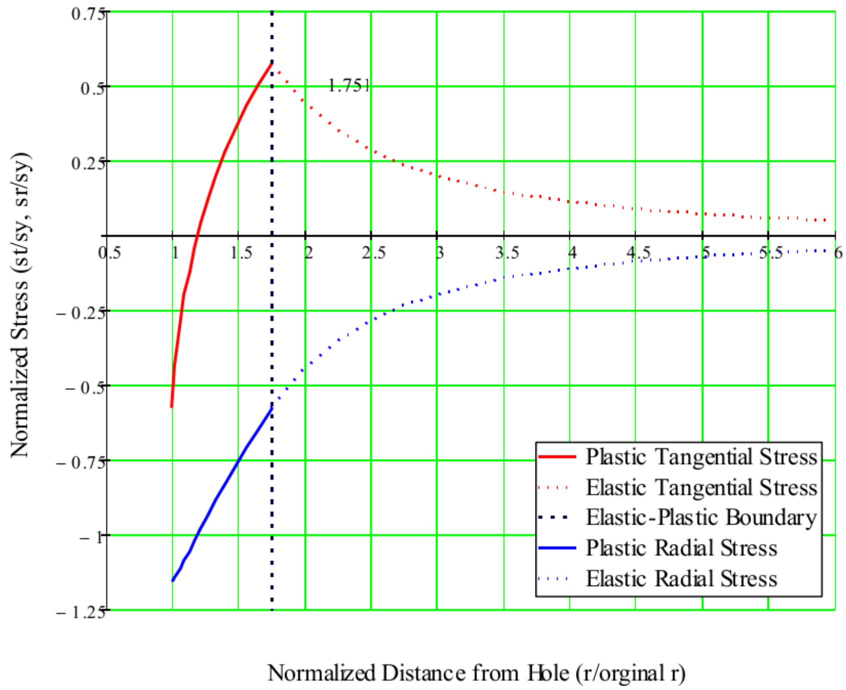

Fig 2 Stress from Cold Expansion before Plug Removed

3. Determine elastic stress which will be recovered with removal of work hardening process

A. At first yield, pressure =0.577σ_{yield} and Stu (the ratio of recovered elastic tangential stress / σ_{yield}) = 0.577 and Sru (the ratio of the recovered elastic radial stess / σ_{yield}) = -0.577.

As function of distance:

$l := 1..16$ $\qquad\qquad$ $h := 17..28$

$Ru_l := R_{17-l}$ $\qquad\qquad$ $Ru_h := Relastic_{h-16}$

$Stu := \left(\frac{1}{Ru}\right)^2 \cdot .577$ $\qquad\qquad$ $Sru := -\left(\frac{1}{Ru}\right)^2 \cdot (1.155)$

المنارة للاستشارات
www.manaraa.com

Stu =

	1
1	0.577
2	0.572
3	0.558
4	0.537
5	0.512
6	0.483
7	0.452
8	0.42
9	0.387
10	0.355
11	0.324
12	0.293
13	0.265
14	0.237
15	0.212
16	0.188
17	0.188
18	0.144
19	0.114
20	0.092
21	0.076
22	0.064
23	0.047
24	0.036
25	0.028
26	0.023
27	0.019
28	0.016

Ru =

	1
1	1
2	1.005
3	1.017
4	1.036
5	1.062
6	1.093
7	1.13
8	1.172
9	1.221
10	1.275
11	1.335
12	1.402
13	1.477
14	1.559
15	1.651
16	...

Sru =

	1
1	-1.155
2	-1.145
3	-1.117
4	-1.075
5	-1.024
6	-0.967
7	-0.905
8	-0.84
9	-0.775
10	-0.711
11	-0.648
12	-0.587
13	-0.529
14	-0.475
15	-0.424
16	-0.377
17	-0.377
18	-0.289
19	-0.228
20	-0.185
21	-0.153
22	-0.128
23	-0.094
24	-0.072
25	-0.057
26	-0.046
27	-0.038
28	-0.032

Ru =

	1
1	1
2	1.005
3	1.017
4	1.036
5	1.062
6	1.093
7	1.13
8	1.172
9	1.221
10	1.275
11	1.335
12	1.402
13	1.477
14	1.559
15	1.651
16	1.751
17	1.751
18	2
19	2.25
20	2.5
21	2.75
22	3
23	3.5
24	4
25	4.5
26	5
27	5.5
28	6

Note: The recoverable elastic stress for the tangential direction is 0.577 which is the limit of the tangential stress in tension. But the recoverable elastic stress for the radial stress is 1.155 which is the maximum radial stress in compression. See correspoonding points on the von Mises failure ellipse.

المنارة للاستشارات

www.manaraa.com

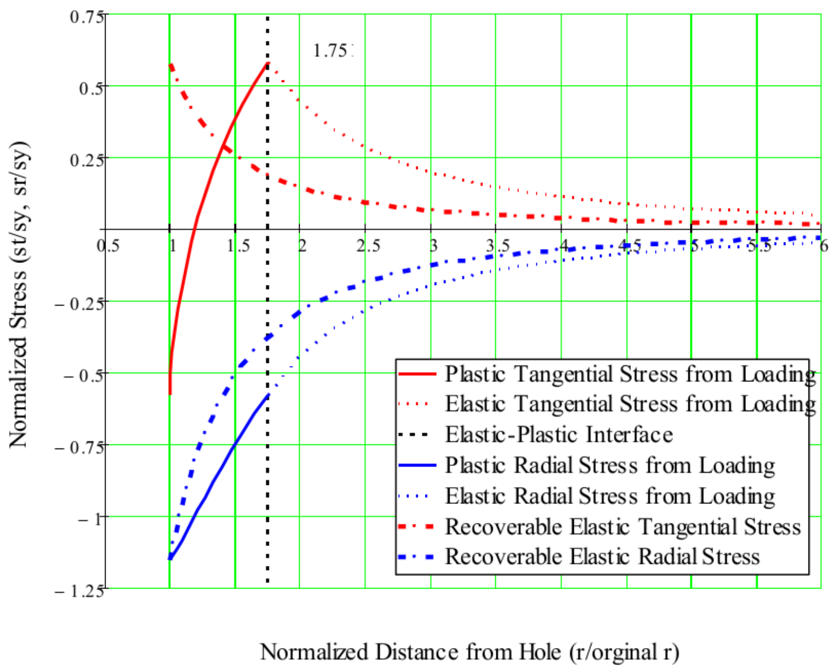

Fig 3 Stress Under Pressure and Pressure Removed

4. Determine Residual Stress

$StL_1 := Stp_{1\,7-1}$

$StL_h := Ste_{h-16}$

$SrL_1 := Srp_{1\,7-1}$

$SrL_h := Sre_{h-16}$

$StR := StL - Stu$

$SrR := SrL - Sru$

المنارة للاستشارات
www.manaraa.com

Ru =

	1
1	1
2	1.005
3	1.017
4	1.036
5	1.062
6	1.093
7	1.13
8	1.172
9	1.221
10	1.275
11	1.335
12	1.402
13	1.477
14	1.559
15	1.651
16	1.751
17	1.751
18	2
19	2.25
20	2.5
21	2.75
22	3
23	3.5
24	4
25	4.5
26	5
27	5.5
28	6

StL =

	1
1	-0.577
2	-0.506
3	-0.433
4	-0.357
5	-0.279
6	-0.201
7	-0.121
8	-0.04
9	0.04
10	0.121
11	0.201
12	0.279
13	0.357
14	0.433
15	0.506
16	0.577
17	0.578
18	0.443
19	0.35
20	0.283
21	0.234
22	0.197
23	0.145
24	0.111
25	0.087
26	0.071
27	0.059
28	0.049

SrL =

	1
1	-1.155
2	-1.152
3	-1.143
4	-1.129
5	-1.11
6	-1.085
7	-1.055
8	-1.02
9	-0.979
10	-0.934
11	-0.885
12	-0.831
13	-0.773
14	-0.711
15	-0.646
16	-0.577
17	-0.578
18	-0.443
19	-0.35
20	-0.283
21	-0.234
22	-0.197
23	-0.145
24	-0.111
25	-0.087
26	-0.071
27	-0.059
28	-0.049

www.manaraa.com

StR =

	1
1	-1.154
2	-1.078
3	-0.99
4	-0.894
5	-0.791
6	-0.683
7	-0.573
8	-0.46
9	-0.347
10	-0.234
11	-0.123
12	-0.014
13	0.092
14	0.195
15	0.294
16	0.389
17	0.389
18	0.298
19	0.236
20	0.191
21	0.158
22	0.133
23	0.097
24	0.075
25	0.059
26	0.048
27	0.039
28	0.033

SrR =

	1
1	$2.995 \cdot 10^{-4}$
2	$-7.275 \cdot 10^{-3}$
3	-0.027
4	-0.054
5	-0.086
6	-0.118
7	-0.15
8	-0.179
9	-0.204
10	-0.223
11	-0.237
12	-0.243
13	-0.243
14	-0.236
15	-0.222
16	-0.201
17	-0.201
18	-0.154
19	-0.122
20	-0.099
21	-0.081
22	-0.068
23	-0.05
24	-0.038
25	-0.03
26	-0.025
27	-0.02
28	-0.017

المنارة للاستشارات

www.manaraa.com

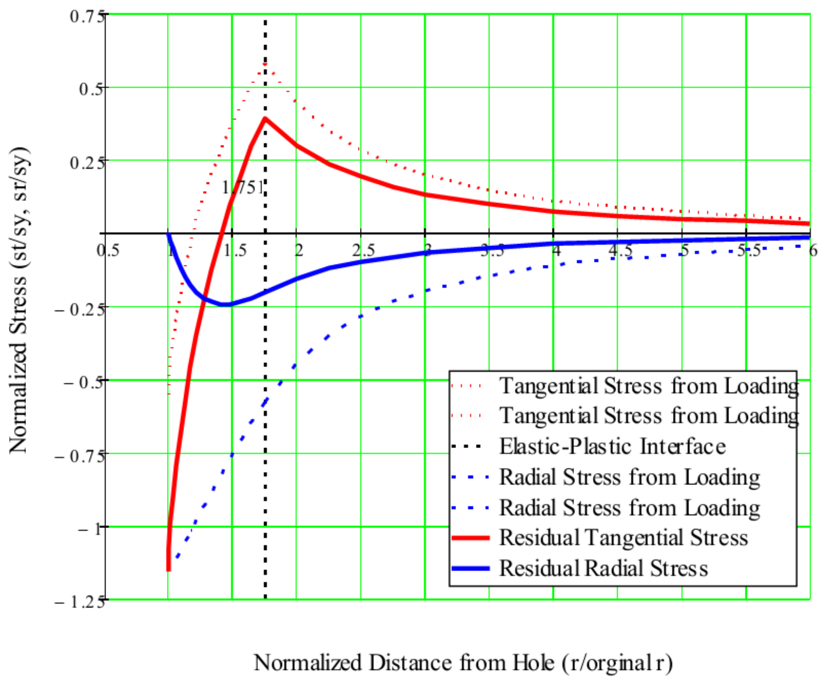

Fig 4 Residual Stress from Cold Expansion

www.manaraa.com

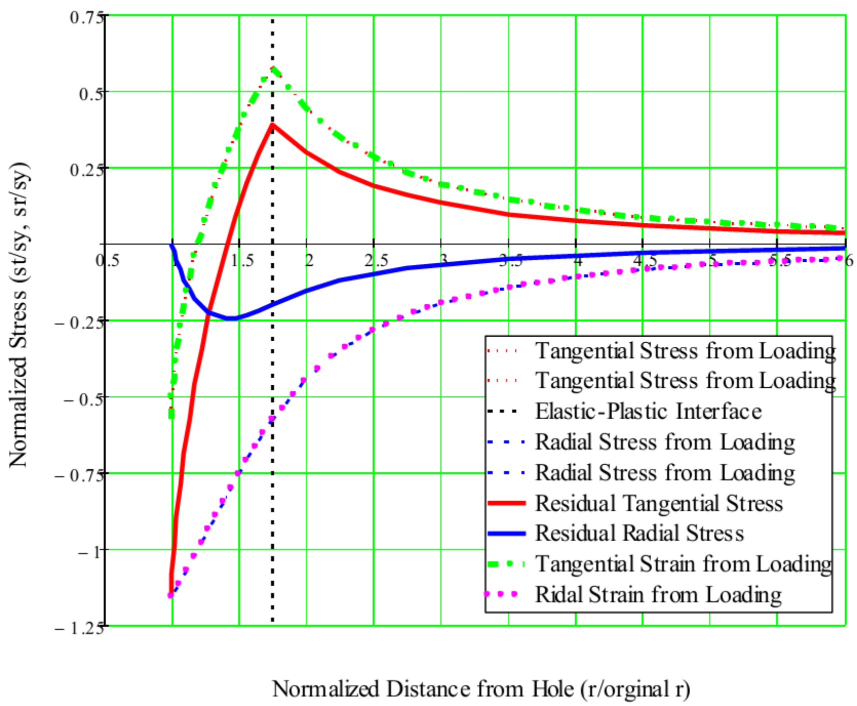

Fig 5 Residual Stress from Cold Expansion

المنارة للاستشارات
www.manaraa.com

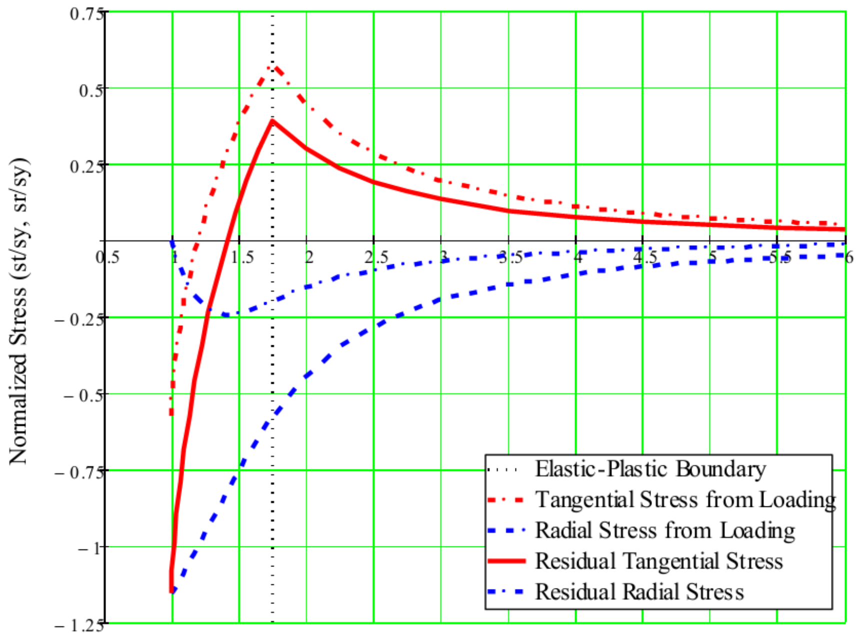

Normalized Distance from Hole (r/orginal r)

Fig 6 Residual Stress from Cold Expansion

www.manaraa.com

C. Calculation of Strains

1. Calculation of strains at the end of loading

$E := 30000 \cdot ksi \qquad \sigma yield := 46.3 \cdot ksi \qquad \mu := 0.3$

R =

	1
1	1.751
2	1.651
3	1.559
4	1.477
5	1.402
6	1.335
7	1.275
8	1.221
9	1.172
10	1.13
11	1.093
12	1.062
13	1.036
14	1.017
15	1.005
16	1

Stp =

	1
1	0.577
2	0.506
3	0.433
4	0.357
5	0.279
6	0.201
7	0.121
8	0.04
9	-0.04
10	-0.121
11	-0.201
12	-0.279
13	-0.357
14	-0.433
15	-0.506
16	-0.577

Srp =

	1
1	-0.577
2	-0.646
3	-0.711
4	-0.773
5	-0.831
6	-0.885
7	-0.934
8	-0.979
9	-1.02
10	-1.055
11	-1.085
12	-1.11
13	-1.129
14	-1.143
15	-1.152
16	-1.155

$i := 1..16$

$R1_i := R_{17-i}$

$Stp1_i := Stp_{17-i}$

$Srp1_i := Srp_{17-i}$

R1 =

	1
1	1
2	1.005
3	1.017
4	1.036
5	1.062
6	1.093
7	1.13
8	1.172
9	1.221
10	1.275
11	1.335
12	1.402
13	1.477
14	1.559
15	1.651
16	1.751

Stp1 =

	1
1	-0.577
2	-0.506
3	-0.433
4	-0.357
5	-0.279
6	-0.201
7	-0.121
8	-0.04
9	0.04
10	0.121
11	0.201
12	0.279
13	0.357
14	0.433
15	0.506
16	0.577

Srp1 =

	1
1	-1.155
2	-1.152
3	-1.143
4	-1.129
5	-1.11
6	-1.085
7	-1.055
8	-1.02
9	-0.979
10	-0.934
11	-0.885
12	-0.831
13	-0.773
14	-0.711
15	-0.646
16	-0.577

$j := 1..12$

www.manaraa.com

Relastic =

	1
1	1.751
2	2
3	2.25
4	2.5
5	2.75
6	3
7	3.5
8	4
9	4.5
10	5
11	5.5
12	6

Ste =

	1
1	0.578
2	0.443
3	0.35
4	0.283
5	0.234
6	0.197
7	0.145
8	0.111
9	0.087
10	0.071
11	0.059
12	0.049

Sre =

	1
1	-0.578
2	-0.443
3	-0.35
4	-0.283
5	-0.234
6	-0.197
7	-0.145
8	-0.111
9	-0.087
10	-0.071
11	-0.059
12	-0.049

$RAL_i := R1_i$

$RAL_{16+j} := Relastic_j$

$STL_i := Stp1_i$

$STL_{16+j} := Ste_j$

$SRL_i := Srp1_i$

$SRL_{16+j} := Sre_j$

RAL =

	1
1	1
2	1.005
3	1.017
4	1.036
5	1.062
6	1.093
7	1.13
8	1.172
9	1.221
10	1.275
11	1.335
12	1.402
13	1.477
14	1.559
15	1.651
16	1.751
17	1.751
18	2
19	2.25
20	2.5
21	2.75
22	...

STL =

	1
1	-0.577
2	-0.506
3	-0.433
4	-0.357
5	-0.279
6	-0.201
7	-0.121
8	-0.04
9	0.04
10	0.121
11	0.201
12	0.279
13	0.357
14	0.433
15	0.506
16	0.577
17	0.578
18	0.443
19	0.35
20	0.283
21	0.234
22	...

SRL =

	1
1	-1.155
2	-1.152
3	-1.143
4	-1.129
5	-1.11
6	-1.085
7	-1.055
8	-1.02
9	-0.979
10	-0.934
11	-0.885
12	-0.831
13	-0.773
14	-0.711
15	-0.646
16	-0.577
17	-0.578
18	-0.443
19	-0.35
20	-0.283
21	-0.234
22	...

$STU := Stu$

$RAU := Ru$

$SRU := Sru$

المنارة للاستشارات
www.manaraa.com

$\varepsilon TL := \frac{1}{E} \cdot (STL \cdot \sigma yield - \mu \cdot SRL \cdot \sigma yield)$ $\varepsilon RL := \frac{1}{E} \cdot (SRL \cdot \sigma yield - \mu \cdot STL \cdot \sigma yield)$

$\varepsilon NL := \frac{1}{E} \cdot (-\mu \cdot SRL \cdot \sigma yield - \mu \cdot STL \cdot \sigma yield)$

εTL =

	1
1	$-3.564 \cdot 10^{-4}$
2	$-2.479 \cdot 10^{-4}$
3	$-1.382 \cdot 10^{-4}$
4	$-2.775 \cdot 10^{-5}$
5	$8.279 \cdot 10^{-5}$
6	$1.929 \cdot 10^{-4}$
7	$3.021 \cdot 10^{-4}$
8	$4.099 \cdot 10^{-4}$
9	$5.156 \cdot 10^{-4}$
10	$6.188 \cdot 10^{-4}$
11	$7.19 \cdot 10^{-4}$
12	$8.157 \cdot 10^{-4}$
13	$9.084 \cdot 10^{-4}$
14	$9.967 \cdot 10^{-4}$
15	$1.08 \cdot 10^{-3}$
16	$1.158 \cdot 10^{-3}$
17	$1.159 \cdot 10^{-3}$
18	$8.881 \cdot 10^{-4}$
19	$7.017 \cdot 10^{-4}$
20	$5.684 \cdot 10^{-4}$
21	$4.698 \cdot 10^{-4}$
22	$3.947 \cdot 10^{-4}$
23	$2.9 \cdot 10^{-4}$
24	$2.22 \cdot 10^{-4}$
25	$1.754 \cdot 10^{-4}$
26	$1.421 \cdot 10^{-4}$
27	$1.174 \cdot 10^{-4}$
28	$9.868 \cdot 10^{-5}$

εRL =

	1
1	$-1.515 \cdot 10^{-3}$
2	$-1.543 \cdot 10^{-3}$
3	$-1.564 \cdot 10^{-3}$
4	$-1.578 \cdot 10^{-3}$
5	$-1.584 \cdot 10^{-3}$
6	$-1.582 \cdot 10^{-3}$
7	$-1.572 \cdot 10^{-3}$
8	$-1.555 \cdot 10^{-3}$
9	$-1.53 \cdot 10^{-3}$
10	$-1.498 \cdot 10^{-3}$
11	$-1.458 \cdot 10^{-3}$
12	$-1.411 \cdot 10^{-3}$
13	$-1.358 \cdot 10^{-3}$
14	$-1.297 \cdot 10^{-3}$
15	$-1.231 \cdot 10^{-3}$
16	$-1.158 \cdot 10^{-3}$
17	$-1.159 \cdot 10^{-3}$
18	$-8.881 \cdot 10^{-4}$
19	$-7.017 \cdot 10^{-4}$
20	$-5.684 \cdot 10^{-4}$
21	$-4.698 \cdot 10^{-4}$
22	$-3.947 \cdot 10^{-4}$
23	$-2.9 \cdot 10^{-4}$
24	$-2.22 \cdot 10^{-4}$
25	$-1.754 \cdot 10^{-4}$
26	$-1.421 \cdot 10^{-4}$
27	$-1.174 \cdot 10^{-4}$
28	$-9.868 \cdot 10^{-5}$

εNL =

	1
1	0.0008
2	0.00077
3	0.00073
4	0.00069
5	0.00064
6	0.0006
7	0.00054
8	0.00049
9	0.00043
10	0.00038
11	0.00032
12	0.00026
13	0.00019
14	0.00013
15	0.00006
16	0
17	0
18	0
19	0
20	0
21	0
22	0
23	0
24	0
25	0
26	0
27	0
28	0

www.manaraa.com

2. Calculation of strains at the end of unloading

	RAL	RAU	STU	SRU
1	1	1	0.577	-1.155
2	1.005	1.005	0.572	-1.145
3	1.017	1.017	0.558	-1.117
4	1.036	1.036	0.537	-1.075
5	1.062	1.062	0.512	-1.024
6	1.093	1.093	0.483	-0.967
7	1.13	1.13	0.452	-0.905
8	1.172	1.172	0.42	-0.84
9	1.221	1.221	0.387	-0.775
10	1.275	1.275	0.355	-0.711
11	1.335	1.335	0.324	-0.648
12	1.402	1.402	0.293	-0.587
13	1.477	1.477	0.265	-0.529
14	1.559	1.559	0.237	-0.475
15	1.651	1.651	0.212	-0.424
16	1.751	1.751	0.188	-0.377
17	1.751	1.751	0.188	-0.377
18	2	2	0.144	-0.289
19	2.25	2.25	0.114	-0.228
20	2.5	2.5	0.092	-0.185
21	2.75	2.75	0.076	-0.153
22	3	3	0.064	-0.128
23	3.5	3.5	0.047	-0.094
24	4	4	0.036	-0.072
25	4.5	4.5	0.028	-0.057
26	5	5	0.023	-0.046
27	5.5	5.5	0.019	-0.038
28	6	6	0.016	-0.032

$$\varepsilon TU := \frac{1}{E} \cdot (STU \cdot \sigma yield - \mu \cdot SRU \cdot \sigma yield)$$

$$\varepsilon RU := \frac{1}{E} \cdot (SRU \cdot \sigma yield - \mu \cdot STU \cdot \sigma yield)$$

$$\varepsilon NU := \frac{1}{E} \cdot (-\mu \cdot SRU \cdot \sigma yield - \mu \cdot STU \cdot \sigma yield)$$

www.manaraa.com

$\varepsilon TU =$

	1
1	$1.425\cdot10^{-3}$
2	$1.412\cdot10^{-3}$
3	$1.378\cdot10^{-3}$
4	$1.327\cdot10^{-3}$
5	$1.264\cdot10^{-3}$
6	$1.193\cdot10^{-3}$
7	$1.116\cdot10^{-3}$
8	$1.037\cdot10^{-3}$
9	$9.566\cdot10^{-4}$
10	$8.77\cdot10^{-4}$
11	$7.994\cdot10^{-4}$
12	$7.246\cdot10^{-4}$
13	$6.534\cdot10^{-4}$
14	$5.861\cdot10^{-4}$
15	$5.232\cdot10^{-4}$
16	$4.647\cdot10^{-4}$
17	$4.649\cdot10^{-4}$
18	$3.563\cdot10^{-4}$
19	$2.815\cdot10^{-4}$
20	$2.28\cdot10^{-4}$
21	$1.885\cdot10^{-4}$
22	$1.584\cdot10^{-4}$
23	$1.163\cdot10^{-4}$
24	$8.908\cdot10^{-5}$
25	$7.038\cdot10^{-5}$
26	$5.701\cdot10^{-5}$
27	$4.712\cdot10^{-5}$
28	$3.959\cdot10^{-5}$

$\varepsilon RU =$

	1
1	$-2.05\cdot10^{-3}$
2	$-2.031\cdot10^{-3}$
3	$-1.982\cdot10^{-3}$
4	$-1.908\cdot10^{-3}$
5	$-1.818\cdot10^{-3}$
6	$-1.716\cdot10^{-3}$
7	$-1.605\cdot10^{-3}$
8	$-1.491\cdot10^{-3}$
9	$-1.376\cdot10^{-3}$
10	$-1.261\cdot10^{-3}$
11	$-1.15\cdot10^{-3}$
12	$-1.042\cdot10^{-3}$
13	$-9.396\cdot10^{-4}$
14	$-8.429\cdot10^{-4}$
15	$-7.524\cdot10^{-4}$
16	$-6.683\cdot10^{-4}$
17	$-6.685\cdot10^{-4}$
18	$-5.124\cdot10^{-4}$
19	$-4.049\cdot10^{-4}$
20	$-3.28\cdot10^{-4}$
21	$-2.71\cdot10^{-4}$
22	$-2.277\cdot10^{-4}$
23	$-1.673\cdot10^{-4}$
24	$-1.281\cdot10^{-4}$
25	$-1.012\cdot10^{-4}$
26	$-8.199\cdot10^{-5}$
27	$-6.776\cdot10^{-5}$
28	$-5.694\cdot10^{-5}$

$\varepsilon NU =$

	1
1	$2.676\cdot10^{-4}$
2	$2.652\cdot10^{-4}$
3	$2.587\cdot10^{-4}$
4	$2.492\cdot10^{-4}$
5	$2.374\cdot10^{-4}$
6	$2.24\cdot10^{-4}$
7	$2.096\cdot10^{-4}$
8	$1.947\cdot10^{-4}$
9	$1.796\cdot10^{-4}$
10	$1.647\cdot10^{-4}$
11	$1.501\cdot10^{-4}$
12	$1.361\cdot10^{-4}$
13	$1.227\cdot10^{-4}$
14	$1.101\cdot10^{-4}$
15	$9.824\cdot10^{-5}$
16	$8.726\cdot10^{-5}$
17	$8.728\cdot10^{-5}$
18	$6.69\cdot10^{-5}$
19	$5.286\cdot10^{-5}$
20	$4.282\cdot10^{-5}$
21	$3.539\cdot10^{-5}$
22	$2.973\cdot10^{-5}$
23	$2.185\cdot10^{-5}$
24	$1.673\cdot10^{-5}$
25	$1.322\cdot10^{-5}$
26	$1.07\cdot10^{-5}$
27	$8.847\cdot10^{-6}$
28	$7.434\cdot10^{-6}$

www.manaraa.com

3. Calculation of residual strains

$\varepsilon TR := \varepsilon TL - \varepsilon TU \quad \varepsilon RR := \varepsilon RL - \varepsilon RU \quad \varepsilon NR := \varepsilon NL - \varepsilon NU$

$\varepsilon TR =$

	1
1	$-1.782\cdot10^{-3}$
2	$-1.66\cdot10^{-3}$
3	$-1.516\cdot10^{-3}$
4	$-1.355\cdot10^{-3}$
5	$-1.181\cdot10^{-3}$
6	$-10\cdot10^{-4}$
7	$-8.142\cdot10^{-4}$
8	$-6.271\cdot10^{-4}$
9	$-4.41\cdot10^{-4}$
10	$-2.582\cdot10^{-4}$
11	$-8.04\cdot10^{-5}$
12	$9.109\cdot10^{-5}$
13	$2.551\cdot10^{-4}$
14	$4.106\cdot10^{-4}$
15	$5.57\cdot10^{-4}$
16	$6.936\cdot10^{-4}$
17	$6.938\cdot10^{-4}$
18	$5.318\cdot10^{-4}$
19	$4.202\cdot10^{-4}$
20	$3.404\cdot10^{-4}$
21	$2.813\cdot10^{-4}$
22	$2.364\cdot10^{-4}$
23	$1.737\cdot10^{-4}$
24	$1.33\cdot10^{-4}$
25	$1.05\cdot10^{-4}$
26	$8.509\cdot10^{-5}$
27	$7.032\cdot10^{-5}$
28	$5.909\cdot10^{-5}$

$\varepsilon RR =$

	1
1	$5.349\cdot10^{-4}$
2	$4.879\cdot10^{-4}$
3	$4.172\cdot10^{-4}$
4	$3.305\cdot10^{-4}$
5	$2.343\cdot10^{-4}$
6	$1.338\cdot10^{-4}$
7	$3.329\cdot10^{-5}$
8	$-6.363\cdot10^{-5}$
9	$-1.542\cdot10^{-4}$
10	$-2.363\cdot10^{-4}$
11	$-3.084\cdot10^{-4}$
12	$-3.692\cdot10^{-4}$
13	$-4.181\cdot10^{-4}$
14	$-4.545\cdot10^{-4}$
15	$-4.785\cdot10^{-4}$
16	$-4.9\cdot10^{-4}$
17	$-4.902\cdot10^{-4}$
18	$-3.757\cdot10^{-4}$
19	$-2.969\cdot10^{-4}$
20	$-2.404\cdot10^{-4}$
21	$-1.987\cdot10^{-4}$
22	$-1.67\cdot10^{-4}$
23	$-1.227\cdot10^{-4}$
24	$-9.393\cdot10^{-5}$
25	$-7.421\cdot10^{-5}$
26	$-6.011\cdot10^{-5}$
27	$-4.968\cdot10^{-5}$
28	$-4.174\cdot10^{-5}$

$\varepsilon NR =$

	1
1	$5.343\cdot10^{-4}$
2	$5.025\cdot10^{-4}$
3	$4.71\cdot10^{-4}$
4	$4.39\cdot10^{-4}$
5	$4.059\cdot10^{-4}$
6	$3.712\cdot10^{-4}$
7	$3.347\cdot10^{-4}$
8	$2.96\cdot10^{-4}$
9	$2.551\cdot10^{-4}$
10	$2.12\cdot10^{-4}$
11	$1.666\cdot10^{-4}$
12	$1.192\cdot10^{-4}$
13	$6.985\cdot10^{-5}$
14	$1.882\cdot10^{-5}$
15	$-3.364\cdot10^{-5}$
16	$-8.726\cdot10^{-5}$
17	$-8.728\cdot10^{-5}$
18	$-6.69\cdot10^{-5}$
19	$-5.286\cdot10^{-5}$
20	$-4.282\cdot10^{-5}$
21	$-3.539\cdot10^{-5}$
22	$-2.973\cdot10^{-5}$
23	$-2.185\cdot10^{-5}$
24	$-1.673\cdot10^{-5}$
25	$-1.322\cdot10^{-5}$
26	$-1.07\cdot10^{-5}$
27	$-8.847\cdot10^{-6}$
28	$-7.434\cdot10^{-6}$

المنارة للاستشارات
www.manaraa.com

StR =

	1
1	-1.154
2	-1.078
3	-0.99
4	-0.894
5	-0.791
6	-0.683
7	-0.573
8	-0.46
9	-0.347
10	-0.234
11	-0.123
12	-0.014
13	0.092
14	0.195
15	0.294
16	...

SrR =

	1
1	$2.995 \cdot 10^{-4}$
2	$-7.275 \cdot 10^{-3}$
3	-0.027
4	-0.054
5	-0.086
6	-0.118
7	-0.15
8	-0.179
9	-0.204
10	-0.223
11	-0.237
12	-0.243
13	-0.243
14	-0.236
15	-0.222
16	...

$n := -.004, -0.003.. .002$

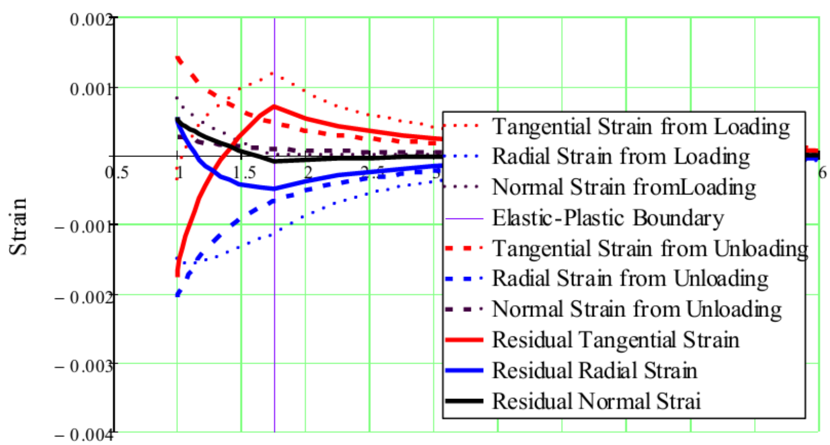

Fig 7. Strain from Expansion, Unloading, and Residual

www.manaraa.com

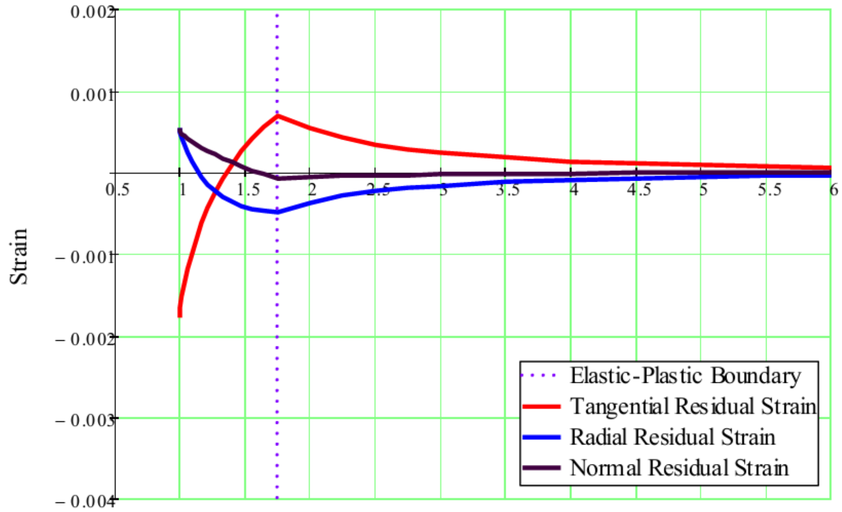

Normalized Distance from Hole (r/orginal r)

Fig 8. Residual Strain from Cold Expansion

4. Calculate residual strain directly from Residual Stress

$\varepsilon TR1 := \frac{1}{E} \cdot (StR \cdot \sigma yield - \mu \cdot SrR \cdot \sigma yield)$

$\varepsilon RR1 := \frac{1}{E} \cdot (SrR \cdot \sigma yield - \mu \cdot StR \cdot \sigma yield)$

$\varepsilon NR1 := \frac{1}{E} \cdot (-\mu \cdot SrR \cdot \sigma yield - \mu \cdot StR \cdot \sigma yield)$

εTR1 =

	1
1	$-1.782 \cdot 10^{-3}$
2	$-1.66 \cdot 10^{-3}$
3	$-1.516 \cdot 10^{-3}$
4	$-1.355 \cdot 10^{-3}$
5	$-1.181 \cdot 10^{-3}$
6	$-10 \cdot 10^{-4}$
7	$-8.142 \cdot 10^{-4}$
8	$-6.271 \cdot 10^{-4}$
9	$-4.41 \cdot 10^{-4}$
10	$-2.582 \cdot 10^{-4}$
11	$-8.04 \cdot 10^{-5}$
12	...

εRR1 =

	1
1	$5.349 \cdot 10^{-4}$
2	$4.879 \cdot 10^{-4}$
3	$4.172 \cdot 10^{-4}$
4	$3.305 \cdot 10^{-4}$
5	$2.343 \cdot 10^{-4}$
6	$1.338 \cdot 10^{-4}$
7	$3.329 \cdot 10^{-5}$
8	$-6.363 \cdot 10^{-5}$
9	$-1.542 \cdot 10^{-4}$
10	$-2.363 \cdot 10^{-4}$
11	$-3.084 \cdot 10^{-4}$
12	...

εNR1 =

	1
1	$5.343 \cdot 10^{-4}$
2	$5.025 \cdot 10^{-4}$
3	$4.71 \cdot 10^{-4}$
4	$4.39 \cdot 10^{-4}$
5	$4.059 \cdot 10^{-4}$
6	$3.712 \cdot 10^{-4}$
7	$3.347 \cdot 10^{-4}$
8	$2.96 \cdot 10^{-4}$
9	$2.551 \cdot 10^{-4}$
10	$2.12 \cdot 10^{-4}$
11	$1.666 \cdot 10^{-4}$
12	...

المنارة للاستشارات
www.manaraa.com

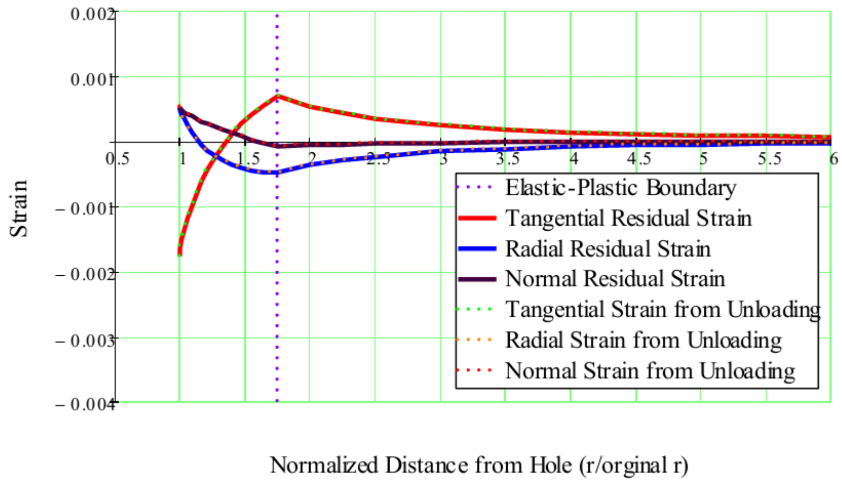

Fig 9. Residual Strain from Cold Expansion

www.manaraa.com

Appendix B-2 Ball's Closed-From Solution for Stress Around A Cold-Expanded Hole

Appendix B 2. BALL'S CLOSED-FORM SOLUTION TO COLD-EXPANDED HOLES on Aluminum Plate (Ball Fig 6)

A. Constants Defined

constants chosen to attempt to match Ball's result in Fig 6

yield stress is 414 MPa (60 ksi) E= 69 GPa (10,000 ksi) $ksi := 1000 \cdot psi$

Poisson's ratio μ $\mu := .33$ $\sigma yield := 60 \cdot ksi$

n is strain hardening exponent $n := 10$

Bauschinger parameter β is a measure of the change yield stress from reverse yielding

$\beta := 1$ $\beta = 1$ implies kinetic strain hardening model

R is used to model implicitly the degree of plastic anisotropy and is defined as the ratio of in-plane transverse plastic strain to through thickness plastic strain

$R := 1$

Constants used in calculations

$$\mu := \frac{n + 1 + 2 \cdot R}{n^2 + 1 + 2 \cdot R} \qquad \mu = 0.126$$

$$\gamma := \frac{n \cdot (1 + R)}{n^2 + 1 + 2 \cdot R} \qquad \gamma = 0.194$$

Constants defined to make equations fit on single page

$$A := (n - 1) \cdot \sqrt{1 + 2 \cdot R} \qquad A = 15.588$$

$$B := n + 1 + 2 \cdot R \qquad B = 13$$

$$C := n^2 + 1 + 2 \cdot R \qquad C = 103$$

$$D := \left(n^2 - 1\right) \cdot \sqrt{1 + 2 \cdot R} \qquad D = 171.473$$

B. Result at the end of Cold Expansion

Note: **L** is used to denote the loading phase

1. Determination of α ***aL for*** $^{P}/_{\sigma\ yield}$

α a is the parameterization variable and can vary between $\pi /2$ to α max

define α aL

$$\alpha maxL := atan\left[-\frac{(n + 1 + 2 \cdot R)}{(n - 1) \cdot \sqrt{1 + 2 \cdot R}}\right] \qquad \alpha maxL = -39.826 \cdot deg$$

has to be in the 2nd quadrant $\alpha maxL := \alpha maxL + 180 \cdot deg$

$$\alpha maxL = 140.174 \cdot deg$$

المنارة للاستشارات

www.manaraa.com

Define α_{bL} which ranges from 90 deg to α_{maxL}

$i := 1..14$

$$\alpha bL := \begin{pmatrix} 140 \\ 136 \\ 133 \\ 130 \\ 127 \\ 124 \\ 121 \\ 118 \\ 115 \\ 112 \\ 109 \\ 106 \\ 103 \\ 90 \end{pmatrix} \cdot \mathrm{deg}$$

$\alpha bL =$

	1
1	2.443
2	2.374
3	2.321
4	2.269
5	2.217
6	2.164
7	2.112
8	2.059
9	2.007
10	1.955
11	1.902
12	1.85
13	1.798
14	1.571

$\cdot$ rad

Determine the ratio of the pressure to the effective stress. The effective stress during loading is equal to yield stress. Try to match the same elastic plastic boundary in Ball's Fig 6 for n = 10. Vary R/σ yield until radius of the elastic-plastic boundary ~ 2.2. Then use this value to determine the value of α aL, the value of α at the edge of the hole during loading.

$$P\sigma yL_i := \sqrt{\frac{1+R}{2}} \cdot \left(\frac{\sin\left(\alpha bL_i\right)}{\sqrt{1+2\cdot R}} - \cos\left(\alpha bL_i\right) \right) \cdot \left(\frac{A}{A\cdot\sin\left(\alpha bL_i\right) + B\cdot\cos\left(\alpha bL_i\right)} \right)^{\mu} \cdot e^{\left(\frac{A}{C}\right)\cdot\left(\alpha bL_i - \frac{\pi}{2}\cdot \mathrm{rad}\right)}$$

Solve for α aL. α aL is the value of α at the edge of the hole while α = 90 deg at the elastic-plastic boundary. Use the root function from Mathcad to solve the above equation fordifferent values of Pσ yL until the elastic plastic boundary = 2.2

$$\mathrm{Function}(\alpha cL) := \sqrt{\frac{1+R}{2}} \cdot \left(\frac{\sin(\alpha cL)}{\sqrt{1+2\cdot R}} - \cos(\alpha cL) \right) \cdot \left(\frac{A}{A\cdot\sin(\alpha cL) \ldots + B\cdot\cos(\alpha cL)} \right)^{\mu} \cdot e^{\left(\frac{A}{C}\right)\cdot\left(\alpha cL\cdot \mathrm{rad} - \frac{\pi}{2}\cdot \mathrm{rad}\right)} - 1.53$$

$\alpha aL := \mathrm{root}(\mathrm{Function}(\alpha cL), \alpha cL, 1.57\cdot \mathrm{rad}, 2.4\cdot \mathrm{rad})$ $\qquad \alpha aL = 2.309512 \qquad \alpha aL = 132.325\cdot \mathrm{deg}$

2. Calculate the radius of the elastic-plastic interface

Ratio of the radius of the elastic-plastic interface to radius of the hole is b_1/a in Ball. Labeled B1L in the following calculation and is only a function of α_a.

$$B1L := \sqrt{\sin(\alpha aL)} \cdot \left(\frac{A}{A\cdot\sin(\alpha aL) + B\cdot\cos(\alpha aL)} \right)^{\gamma} \cdot e^{\left(\frac{D}{2\cdot C}\right)\cdot\left(\alpha aL - \frac{\pi}{2}\cdot \mathrm{rad}\right)}$$

$B1L = 2.224$

Use P/σ y = 1.53

www.manaraa.com

3. Calculate r/a as a function of α as $\pi/2 < \alpha < \alpha_{aL}$ **r/a in calcs as raL**

r/a = 1- initial edge of the hole

$i := 1..22$

$$\alpha L := \begin{pmatrix} 132.352 \\ 130 \\ 128 \\ 126 \\ 124 \\ 122 \\ 120 \\ 118 \\ 116 \\ 114 \\ 112 \\ 110 \\ 108 \\ 106 \\ 104 \\ 102 \\ 100 \\ 98 \\ 96 \\ 94 \\ 92 \\ 90 \end{pmatrix} \cdot deg \qquad \alpha L_i = \begin{array}{|c|} \hline 2.31 \\ \hline 2.269 \\ \hline 2.234 \\ \hline 2.199 \\ \hline 2.164 \\ \hline 2.129 \\ \hline 2.094 \\ \hline 2.059 \\ \hline 2.025 \\ \hline 1.99 \\ \hline 1.955 \\ \hline 1.92 \\ \hline 1.885 \\ \hline 1.85 \\ \hline 1.815 \\ \hline 1.78 \\ \hline 1.745 \\ \hline 1.71 \\ \hline 1.676 \\ \hline 1.641 \\ \hline 1.606 \\ \hline 1.571 \\ \hline \end{array} \cdot rad$$

r/a =2.224 - the radius of the elastic-plastic boundary

$$raL_i := \sqrt{\frac{\sin(\alpha aL)}{\sin(\alpha L_i)}} \cdot \left(\frac{A \cdot \sin(\alpha L_i) + B \cdot \cos(\alpha L_i)}{A \cdot \sin(\alpha aL) + B \cdot \cos(\alpha aL)} \right)^{\gamma} \cdot e^{\left(\frac{D}{2 \cdot C}\right) \cdot (\alpha aL - \alpha L_i)}$$

α = 2.309 rad (132.325 deg) edge of the hole

raL =

	1
1	0.999
2	1.068
3	1.122
4	1.174
5	1.224
6	1.274
7	1.323
8	1.373
9	1.423
10	1.474
11	1.526
12	1.58
13	1.635
14	1.692
15	1.75
16	1.811
17	1.873
18	1.938
19	2.006
20	2.076
21	...

www.manaraa.com

$\alpha = 1.571$ rad (90 deg)   elastic-plastic boundary

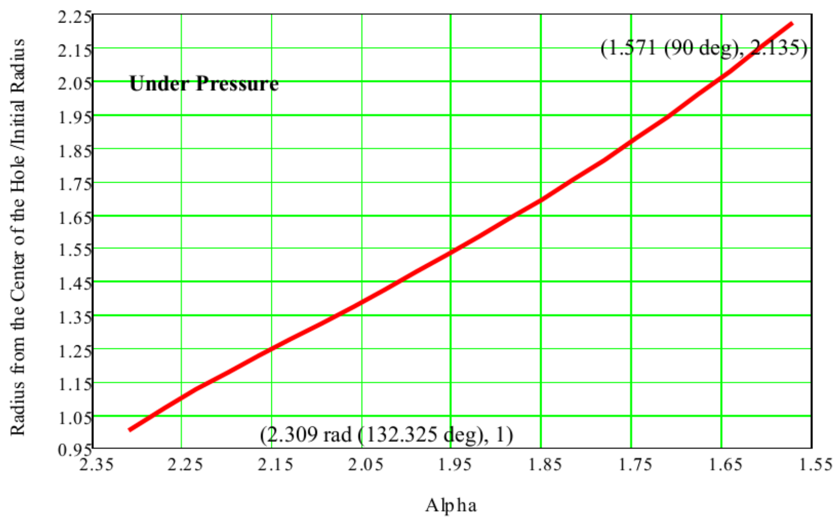

Fig. 1 Radius from the Center of the Hole Versus Parameterization Angle Alpha

4. Calculate ratio of effective stress / yield stress as a function of α

Ratio of effective stress / yield stress labeled Rσ eL in calculations

$$R\sigma eL_i := \left(\frac{A}{A\cdot\sin(\alpha L_i) + B\cdot\cos(\alpha L_i)}\right)^{\mu}\cdot e^{\left(\frac{A}{C}\right)\cdot\left(\alpha L_i - \frac{\pi}{2}\cdot rad\right)}$$

$\alpha = 2.309$ rad (132.35 deg), $r/a = 1$

www.manaraa.com

$R\sigma eL_i =$

	1
1	1.391
2	1.338
3	1.301
4	1.27
5	1.243
6	1.219
7	1.198
8	1.178
9	1.16
10	1.143
11	1.127
12	1.112
13	1.098
14	1.085
15	1.073
16	1.061
17	1.05
18	1.039
19	1.029
20	1.019
21	1.009
22	1

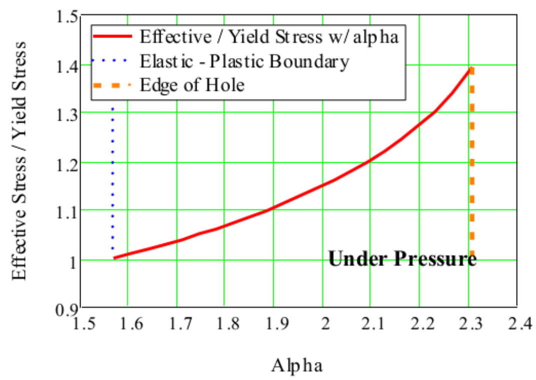

Fig 2. Normalized Effective Stress vs Alpha

α = 1.571 (90 deg),
r/a =2.135

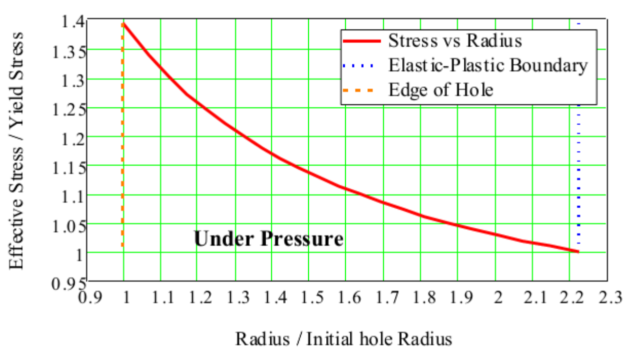

Fig 3. Normalized Effective Stress vs Normalized Radius

www.manaraa.com

5. Calculate ratio of tangential and radial plastic stress in the plastic region between the edge of the hole and the elastic-plastic boundary

Let ratio for tangential plastic stress to yield stress be SptL and and ratio for plastic radial stress to yield stress be SprL and both are functions of ratio of effective stress to yield stress (Rσ e) and α

$$SptL_i := \frac{R\sigma eL_i}{2} \cdot \sqrt{2 + 2 \cdot R} \cdot \left(\cos\left(\alpha L_i\right) + \frac{1}{\sqrt{1 + 2 \cdot R}} \cdot \sin\left(\alpha L_i\right) \right)$$

$q := -2..\,.1.6$

$$SprL_i := \frac{R\sigma eL_i}{2} \cdot \sqrt{2 + 2 \cdot R} \cdot \left(\cos\left(\alpha L_i\right) - \frac{1}{\sqrt{1 + 2 \cdot R}} \cdot \sin\left(\alpha L_i\right) \right)$$

SptL =

	1
1	-0.344
2	-0.268
3	-0.209
4	-0.153
5	-0.1
6	-0.049
7	0
8	0.047
9	0.093
10	0.138
11	0.181
12	0.223
13	0.264
14	0.303
15	0.341
16	0.379
17	0.415
18	0.449
19	0.483
20	0.516
21	0.547
22	0.577

SprL =

	1
1	-1.531
2	-1.452
3	-1.393
4	-1.34
5	-1.29
6	-1.243
7	-1.198
8	-1.153
9	-1.11
10	-1.067
11	-1.025
12	-0.984
13	-0.942
14	-0.901
15	-0.86
16	-0.82
17	-0.779
18	-0.739
19	-0.698
20	-0.658
21	-0.617
22	-0.577

6. Calculate ratio of elastic tangential to yield stress and ratio of elastic radial stresses to yield stress

Use SetL for the ratio of elastic tangential to yield stress and SerL for the ratio of elastic radial stress to yield stress

$BIL = 2.224$ $\quad a := 2.224, 2.474..\, 6.474$ $\quad j := 1..\,17$

المنارة للاستشارات
www.manaraa.com

$rL_1 := 2.224$

$rL_{j+1} := rL_j + 0.25$

$j := 1..18$

$$SetL_j := \sqrt{\frac{1+R}{2(1+2\cdot R)}\cdot\left(\frac{B1L}{rL_j}\right)^2}$$

$SerL := -SetL$

rL =

	1
1	2.224
2	2.474
3	2.724
4	2.974
5	3.224
6	3.474
7	3.724
8	3.974
9	4.224
10	4.474
11	4.724
12	4.974
13	5.224
14	5.474
15	5.724
16	5.974
17	6.224
18	6.474

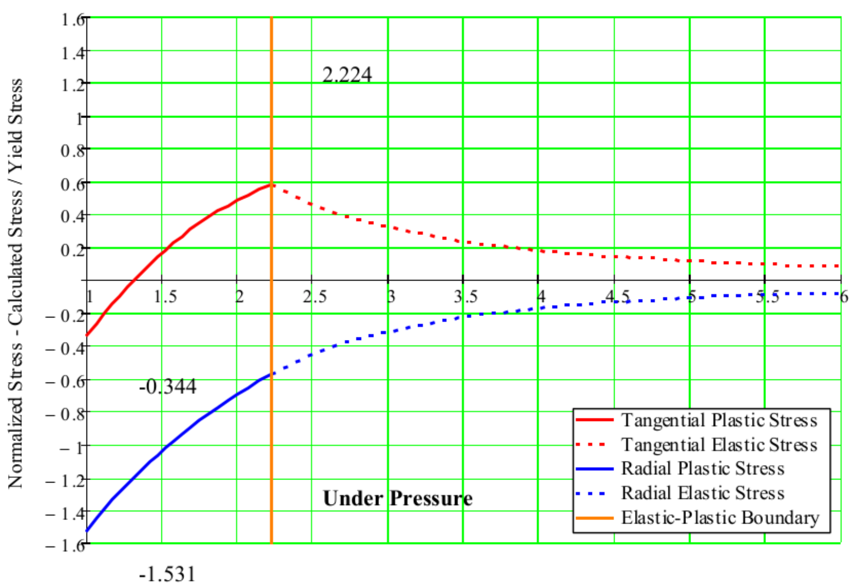

Fig 4. Radial and Tangential Stresses Adjacent to Expanded Hole Under Pressure

المنارة للاستشارات
www.manaraa.com

C. Results after removal of expansion

1. Constants defined

β is Bauschinger's parameter and is a measure of the reduction in yield stress in compression due to strain be yield strain in tension. $\beta = 0$ is for isotropic behavior while $\beta = 1$ implies kinematic hardening

Note: U is used to denote the unloading phase

from expansion calculation, use $\sigma_{yield} = 60$ ksi and $P/\sigma_{yield} = 1.53$

$$P := 1.53 \cdot \sigma yield \qquad P = 91.8 \cdot ksi$$

2. Determination of new α_a *(α_{aU})*

α_{aU} is the parameterization variable and can vary between $\pi/2$ to α max. α_{aU} is for the region in the plastic

annulus in which the unloading causes reverse yielding. α_{aU} is new value at the edge of the hole while

$\alpha = 90deg$ is the value at the new elastic-plastic boundary. α max as determine above.

new yield stress σ_{o2}

$P\sigma$ yL is ratio of the pressure/new yield stress and varies with α_b where α_b is α bL from the original calculation for the plastic region in 1 above

Using $\beta = 0$ $\qquad \sigma o2 := (1+\beta)\cdot \sigma yield + (1-\beta)\cdot \sigma yield \qquad \sigma o2 = 120 \cdot ksi$

$$i := 1..14 \qquad \frac{P}{\sigma o2} = 0.765$$

$$P\sigma yU_i := \sqrt{\frac{1+R}{2}} \cdot \left(\frac{\sin(\alpha bL_i)}{\sqrt{1+2\cdot R}} - \cos(\alpha bL_i) \right) \cdot \left(\frac{A}{A\cdot \sin(\alpha bL_i) + B \cdot \cos(\alpha bL_i)} \right)^{\mu} \cdot e^{\left(\frac{A}{C}\right)\cdot\left(\alpha bL_i - \frac{\pi}{2}\cdot rad\right)}$$

Solve for α bU. α aU is the value of α at the edge of the hole while $\alpha = 90$ deg at the elastic-plastic boundary. Use the root function from Mathcad to solve the above equation for $P\sigma$ yL = 1.5.

$$\text{Function}(\alpha bL) := \sqrt{\frac{1+R}{2}} \cdot \left(\frac{\sin(\alpha bL)}{\sqrt{1+2\cdot R}} - \cos(\alpha bL) \right) \cdot \left(\frac{A}{A\cdot \sin(\alpha bL)\ ... + B \cdot \cos(\alpha bL)} \right)^{\mu} \cdot e^{\left(\frac{A}{C}\right)\cdot\left(\alpha bL - \frac{\pi}{2}\cdot rad\right)} - 0.765$$

$$\alpha aU := root(\text{Function}(\alpha bL), \alpha bL, 1.57\cdot rad, 2.5\cdot rad) \qquad \alpha aU = 1.73324 \qquad \alpha aU = 99.307\cdot deg$$

3. Calculate the radius of the region experiencing reverse yielding after unloading

Ratio of the radius of material experiencing reverse yielding to hole radius is b_2/a. Labeled B2U in the following calculation and is only a function of new α_{aU}. γ from 1 above.

www.manaraa.com

$$B2U := \sqrt{\sin(\alpha aU)} \cdot \left(\frac{A}{A \cdot \sin(\alpha aU) + B \cdot \cos(\alpha aU)}\right)^{\gamma} \cdot e^{\left(\frac{D}{2 \cdot C}\right) \cdot \left(\alpha aU - \frac{\pi}{2} \cdot rad\right)}$$

$B2U = 1.17316$ **Looks approximately correct from Fig 6a**

4. Calculate r/a as a function of new α as π /2 < α < α aU.

$k := 1..9$

$$\alpha U := \begin{pmatrix} 99.307 \\ 97.2791 \\ 96.2393 \\ 95.1994 \\ 94.1595 \\ 93.1196 \\ 92.0798 \\ 91.039 \\ 90 \end{pmatrix} \cdot deg \qquad \alpha U_k = \begin{array}{|c|} \hline 1.733 \\ \hline 1.698 \\ \hline 1.68 \\ \hline 1.662 \\ \hline 1.643 \\ \hline 1.625 \\ \hline 1.607 \\ \hline 1.589 \\ \hline 1.571 \\ \hline \end{array} \cdot rad$$

edge of the hole

elastic-plastic boundary on unloading

r/a for unloading as in calcs as labeled - rb

$$rb_k := \sqrt{\frac{\sin(\alpha aU)}{\sin(\alpha U_k)}} \cdot \left(\frac{A \cdot \sin(\alpha U_k) + B \cdot \cos(\alpha U_k)}{A \cdot \sin(\alpha aU) + B \cdot \cos(\alpha aU)}\right)^{\gamma} \cdot e^{\left(\frac{D}{2 \cdot C}\right) \cdot (\alpha aU - \alpha U_k)}$$

$$rb = \begin{pmatrix} 1.0000058 \\ 1.0351579 \\ 1.0537018 \\ 1.0726159 \\ 1.091911 \\ 1.1115999 \\ 1.1316938 \\ 1.1522277 \\ 1.1731597 \end{pmatrix}$$

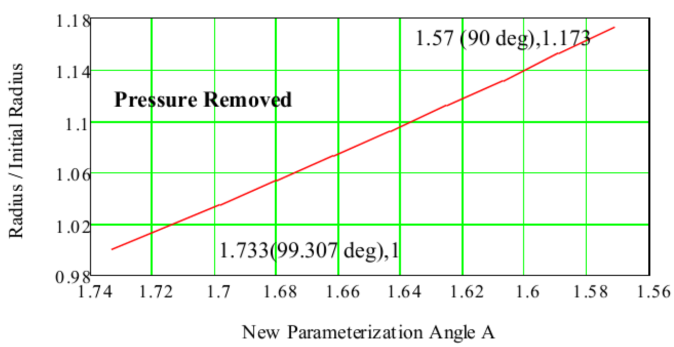

Fig 5. Radius versus Alpha for Unloading

$rb_9 = 1.1731597$

المنارة للاستشارات
www.manaraa.com

5. Calculate ratio of effective stress / new yield stress as a function of α

Ratio of effective stress / yield stress. Ratio labeled Rσ eU in calculations

$$R\sigma eU_k := -\left[\left(\frac{A}{A\cdot\sin\left(\alpha U_k\right)+B\cdot\cos\left(\alpha U_k\right)}\right)^{\mu}\cdot e^{\left(\frac{A}{C}\right)\cdot\left(\alpha U_k-\frac{\pi}{2}\mathrm{rad}\right)}\right]$$

α = 1.716 (98.319 deg),
rb=1

edge of hole

$$R\sigma eU = \begin{pmatrix} -1.046 \\ -1.035 \\ -1.03 \\ -1.025 \\ -1.019 \\ -1.014 \\ -1.01 \\ -1.005 \\ -1 \end{pmatrix}$$

α = 1.571 (90 deg),
rb = 1.1581

elastic-plastic
boundary on
unloading

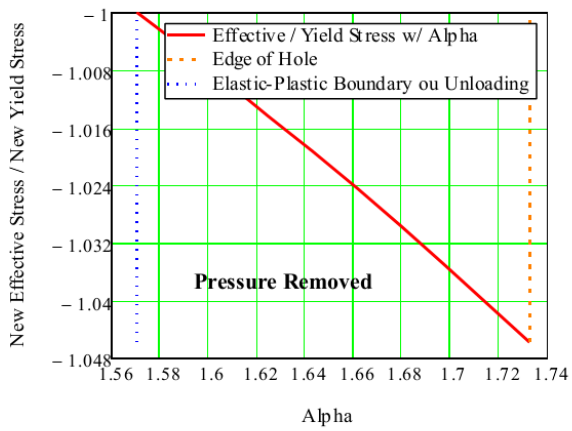

Fig 6. Normalized Effective Stress vs Alpha

www.manaraa.com

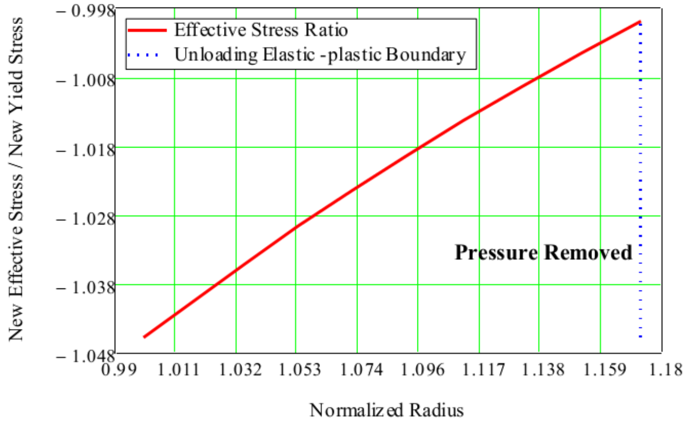

Fig 7. Normalized Effective Stress vs Normalized Radius

6. Calculate ratio of tangential and radial plastic stress

Let ratio for tangential plastic stress to yield stress be SptU and and ratio for plastic radial stress to yield stress be SprU and both are functions of ratio of new effective stress to new yield stress (Rσ eU) and α U

$$SptU_k := 2\left[\frac{R\sigma eU_k}{2}\cdot\sqrt{2+2\cdot R}\cdot\left(\cos\left(\alpha U_k\right)+\frac{1}{\sqrt{1+2\cdot R}}\cdot\sin\left(\alpha U_k\right)\right)\right]$$

$$SprU_k := 2\cdot\left[\frac{R\sigma eU_k}{2}\cdot\sqrt{2+2\cdot R}\cdot\left(\cos\left(\alpha U_k\right)-\frac{1}{\sqrt{1+2\cdot R}}\cdot\sin\left(\alpha U_k\right)\right)\right]$$

$$SptU = \begin{pmatrix}-0.853\\-0.923\\-0.958\\-0.992\\-1.026\\-1.059\\-1.092\\-1.124\\-1.155\end{pmatrix} \qquad SprU = \begin{pmatrix}1.53\\1.448\\1.406\\1.364\\1.322\\1.28\\1.238\\1.196\\1.155\end{pmatrix}$$

q is to plot elastic-plastic boundary

$$q := -2..2$$

المنارة للاستشارات
www.manaraa.com

7. Calculate ratio of the change in elastic tangential to yield stress due to unloading and the ratio of the change in elastic radial stresses to yield stress from unloading

Use 'Setu' for the ratio of the change in elastic tangential to yield stress and 'Seru' for the ratio of elastic radial stress to yield stress

$B2U = 1.173$ $\quad a := 1.173, 1.423 .. 6.173$ $\quad j := 1 .. 21$ $\quad J_j := j$ $\quad ru_j := B2U + 0.25 \cdot J_j - 0.25$

j =

	1
1	1
2	2
3	3
4	4
5	5
6	6
7	7
8	8
9	9
10	10
11	11
12	12
13	13
14	14
15	15
16	16
17	17
18	18
19	19
20	20
21	21

J =

	1
1	1
2	2
3	3
4	4
5	5
6	6
7	7
8	8
9	9
10	10
11	11
12	12
13	13
14	14
15	15
16	16
17	17
18	18
19	19
20	20
21	21

a =

	1
1	1.173
2	1.423
3	1.673
4	1.923
5	2.173
6	2.423
7	2.673
8	2.923
9	3.173
10	3.423
11	3.673
12	3.923
13	4.173
14	4.423
15	4.673
16	4.923
17	5.173
18	5.423
19	5.673
20	5.923
21	6.173

ru_j =

	1
1	1.173
2	1.423
3	1.673
4	1.923
5	2.173
6	2.423
7	2.673
8	2.923
9	3.173
10	3.423
11	3.673
12	3.923
13	4.173
14	4.423
15	4.673
16	4.923
17	5.173
18	5.423
19	5.673
20	5.923
21	6.173

$$SerU_j := 2 \cdot \left[\sqrt{\frac{1 + R}{2(1 + 2 \cdot R)}} \cdot \left(\frac{B2U}{ru_j} \right)^2 \right]$$

$$SetU_j := -SerU_j$$

www.manaraa.com

$SerU =$

	1
1	1.155
2	0.785
3	0.568
4	0.43
5	0.337
6	0.271
7	0.222
8	0.186
9	0.158
10	0.136
11	0.118
12	0.103
13	0.091
14	0.081
15	0.073
16	0.066
17	0.059
18	0.054
19	0.049
20	0.045
21	0.042

$SetU =$

	1
1	-1.155
2	-0.785
3	-0.568
4	-0.43
5	-0.337
6	-0.271
7	-0.222
8	-0.186
9	-0.158
10	-0.136
11	-0.118
12	-0.103
13	-0.091
14	-0.081
15	-0.073
16	-0.066
17	-0.059
18	-0.054
19	-0.049
20	-0.045
21	-0.042

Plot Δ stress from unloading

$i := 1 .. 22$

المنارة للاستشارات
www.manaraa.com

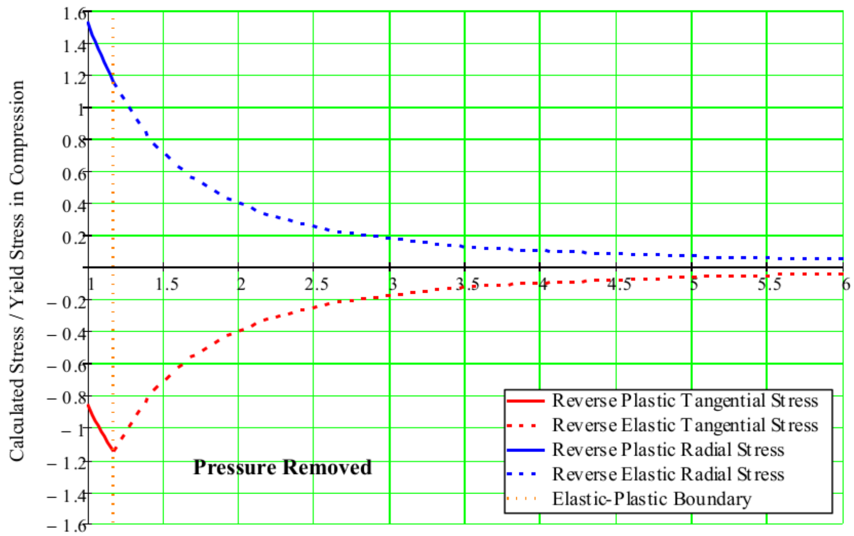

Normalized Distance from the Center of the Hole - Radius / Initial Radius

Fig 8. Changes in Radial and Tangential Stress due to Unloading

raL =

	1
1	0.999
2	1.068
3	1.122
4	1.174
5	1.224
6	1.274
7	1.323
8	1.373
9	1.423
10	1.474
11	1.526
12	1.58
13	1.635
14	1.692
15	1.75
16	...

$$rb = \begin{pmatrix} 1 \\ 1.035 \\ 1.054 \\ 1.073 \\ 1.092 \\ 1.112 \\ 1.132 \\ 1.152 \\ 1.173 \end{pmatrix}$$

www.manaraa.com

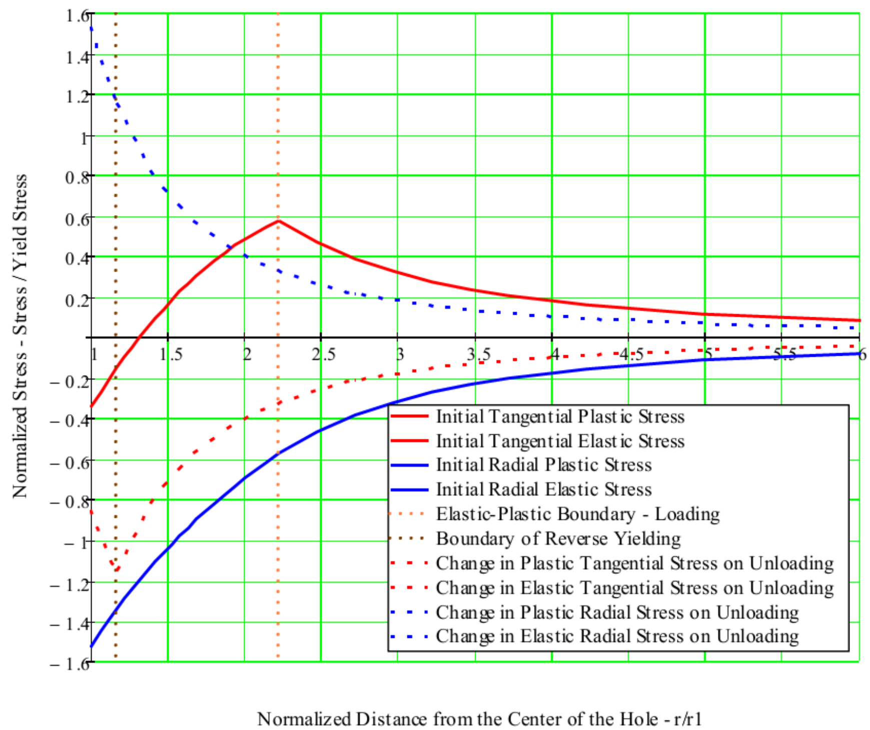

Fig 9. Stresses from Expansion Pressure and from Removing the Expansion Pressure

D. Combine Results 2 and 3 to Obtain Residual Stress

Revise calculations to determine results for 3 separate regions

1. Region 1 from edge of hole to elastic-plastic boundary from unloading
   ra = 1 to ra =1.1581
2. From elastic-boundary from unloading to the elastic-plastic boundary from loading
   ra = 1.1581 to ra = 2.138
3. From elastic-plastic boundary from loading to infinite ~ ra = 6

1. For Region 1 where r/a = 1.17316

Calculate the alpha angle for the loading stress in this region between r/a =1 and r/a = 1.1581 at the same interval as was done for the unloading step

www.manaraa.com

$\alpha aL = 2.31$ r/a for the unloading step

$$rb = \begin{pmatrix} 1.000006 \\ 1.035158 \\ 1.053702 \\ 1.072616 \\ 1.091911 \\ 1.1116 \\ 1.131694 \\ 1.152228 \\ 1.17316 \end{pmatrix}$$

Radius 1

$$\text{function}(\alpha) := \sqrt{\frac{\sin(\alpha aL)}{\sin(\alpha)}} \cdot \left[\frac{(n-1)\cdot\sqrt{1+2\cdot R}\cdot\sin(\alpha)\ ... \ +(n+1+2\cdot R)\cdot\cos(\alpha)}{(n-1)\cdot\sqrt{1+2\cdot R}\cdot\sin(\alpha aL)\ ... \ +(n+1+2\cdot R)\cdot\cos(\alpha aL)}\right]^{\gamma} \cdot e^{\left[\frac{\left(n^2-1\right)\cdot\sqrt{1+2\cdot R}}{2\cdot\left(n^2+1+2\cdot R\right)}\right]\cdot(\alpha aL-\alpha)} - rb_1$$

$\alpha_1 := \text{root}(\text{function}(\alpha), \alpha, 1.57\cdot\text{rad}, 2.5\cdot\text{rad})$ $\alpha_1 = 132.325\cdot\text{deg}$ $\alpha_1 = 2.31$

Radius 2

$$\text{function}(\alpha) := \sqrt{\frac{\sin(\alpha aL)}{\sin(\alpha)}} \cdot \left[\frac{(n-1)\cdot\sqrt{1+2\cdot R}\cdot\sin(\alpha)\ ... \ +(n+1+2\cdot R)\cdot\cos(\alpha)}{(n-1)\cdot\sqrt{1+2\cdot R}\cdot\sin(\alpha aL)\ ... \ +(n+1+2\cdot R)\cdot\cos(\alpha aL)}\right]^{\gamma} \cdot e^{\left[\frac{\left(n^2-1\right)\cdot\sqrt{1+2\cdot R}}{2\cdot\left(n^2+1+2\cdot R\right)}\right]\cdot(\alpha aL-\alpha)} - rb_2$$

$\alpha_2 := \text{root}(\text{function}(\alpha), \alpha, 2.1\cdot\text{rad}, 2.3\cdot\text{rad})$ $\alpha_2 = 131.16\cdot\text{deg}$ $\alpha_2 = 2.289$

Radius 3

$$\text{function}(\alpha) := \sqrt{\frac{\sin(\alpha aL)}{\sin(\alpha)}} \cdot \left[\frac{(n-1)\cdot\sqrt{1+2\cdot R}\cdot\sin(\alpha)\ ... \ +(n+1+2\cdot R)\cdot\cos(\alpha)}{(n-1)\cdot\sqrt{1+2\cdot R}\cdot\sin(\alpha aL)\ ... \ +(n+1+2\cdot R)\cdot\cos(\alpha aL)}\right]^{\gamma} \cdot e^{\left[\frac{\left(n^2-1\right)\cdot\sqrt{1+2\cdot R}}{2\cdot\left(n^2+1+2\cdot R\right)}\right]\cdot(\alpha aL-\alpha)} - rb_3$$

$\alpha_3 := \text{root}(\text{function}(\alpha), \alpha, 2.1\cdot\text{rad}, 2.3\cdot\text{rad})$ $\alpha_3 = 130.517\cdot\text{deg}$ $\alpha_3 = 2.278$

Radius 4

$$\text{function}(\alpha) := \sqrt{\frac{\sin(\alpha aL)}{\sin(\alpha)}} \cdot \left[\frac{(n-1)\cdot\sqrt{1+2\cdot R}\cdot\sin(\alpha)\ ... \ +(n+1+2\cdot R)\cdot\cos(\alpha)}{(n-1)\cdot\sqrt{1+2\cdot R}\cdot\sin(\alpha aL)\ ... \ +(n+1+2\cdot R)\cdot\cos(\alpha aL)}\right]^{\gamma} \cdot e^{\left[\frac{\left(n^2-1\right)\cdot\sqrt{1+2\cdot R}}{2\cdot\left(n^2+1+2\cdot R\right)}\right]\cdot(\alpha aL-\alpha)} - rb_4$$

المنارة للاستشارات
www.manaraa.com

$\alpha_4 := \mathrm{root}(\mathrm{function}(\alpha), \alpha, 2.1 \cdot \mathrm{rad}, 2.3 \cdot \mathrm{rad})$ $\alpha_4 = 129.843 \cdot \mathrm{deg}$ $\alpha_4 = 2.266$

Radius 5

$$\mathrm{function}(\alpha) := \sqrt{\frac{\sin(\alpha L)}{\sin(\alpha)}} \cdot \left[\frac{(n-1)\cdot\sqrt{1+2\cdot R}\cdot\sin(\alpha) + (n+1+2\cdot R)\cdot\cos(\alpha)}{(n-1)\cdot\sqrt{1+2\cdot R}\cdot\sin(\alpha L) + (n+1+2\cdot R)\cdot\cos(\alpha L)}\right]^{\gamma} \cdot e^{\left[\frac{(n^2-1)\cdot\sqrt{1+2\cdot R}}{2\cdot(n^2+1+2\cdot R)}\right]\cdot(\alpha L-\alpha)} - rb_5$$

$\alpha_5 := \mathrm{root}(\mathrm{function}(\alpha), \alpha, 2.1 \cdot \mathrm{rad}, 2.3 \cdot \mathrm{rad})$ $\alpha_5 = 129.138 \cdot \mathrm{deg}$ $\alpha_5 = 2.254$

Radius 6

$$\mathrm{function}(\alpha) := \sqrt{\frac{\sin(\alpha L)}{\sin(\alpha)}} \cdot \left[\frac{(n-1)\cdot\sqrt{1+2\cdot R}\cdot\sin(\alpha) + (n+1+2\cdot R)\cdot\cos(\alpha)}{(n-1)\cdot\sqrt{1+2\cdot R}\cdot\sin(\alpha L) + (n+1+2\cdot R)\cdot\cos(\alpha L)}\right]^{\gamma} \cdot e^{\left[\frac{(n^2-1)\cdot\sqrt{1+2\cdot R}}{2\cdot(n^2+1+2\cdot R)}\right]\cdot(\alpha L-\alpha)} - rb_6$$

$\alpha_6 := \mathrm{root}(\mathrm{function}(\alpha), \alpha, 2.1 \cdot \mathrm{rad}, 2.3 \cdot \mathrm{rad})$ $\alpha_6 = 128.404 \cdot \mathrm{deg}$ $\alpha_6 = 2.241$

Radius 7

$$\mathrm{function}(\alpha) := \sqrt{\frac{\sin(\alpha L)}{\sin(\alpha)}} \cdot \left[\frac{(n-1)\cdot\sqrt{1+2\cdot R}\cdot\sin(\alpha) + (n+1+2\cdot R)\cdot\cos(\alpha)}{(n-1)\cdot\sqrt{1+2\cdot R}\cdot\sin(\alpha L) + (n+1+2\cdot R)\cdot\cos(\alpha L)}\right]^{\gamma} \cdot e^{\left[\frac{(n^2-1)\cdot\sqrt{1+2\cdot R}}{2\cdot(n^2+1+2\cdot R)}\right]\cdot(\alpha L-\alpha)} - rb_7$$

$\alpha_7 := \mathrm{root}(\mathrm{function}(\alpha), \alpha, 2.1 \cdot \mathrm{rad}, 2.3 \cdot \mathrm{rad})$ $\alpha_7 = 127.64 \cdot \mathrm{deg}$ $\alpha_7 = 2.228$

Radius 8

$$\mathrm{function}(\alpha) := \sqrt{\frac{\sin(\alpha L)}{\sin(\alpha)}} \cdot \left[\frac{(n-1)\cdot\sqrt{1+2\cdot R}\cdot\sin(\alpha) + (n+1+2\cdot R)\cdot\cos(\alpha)}{(n-1)\cdot\sqrt{1+2\cdot R}\cdot\sin(\alpha L) + (n+1+2\cdot R)\cdot\cos(\alpha L)}\right]^{\gamma} \cdot e^{\left[\frac{(n^2-1)\cdot\sqrt{1+2\cdot R}}{2\cdot(n^2+1+2\cdot R)}\right]\cdot(\alpha L-\alpha)} - rb_8$$

$\alpha_8 := \mathrm{root}(\mathrm{function}(\alpha), \alpha, 2.1 \cdot \mathrm{rad}, 2.3 \cdot \mathrm{rad})$ $\alpha_8 = 126.846 \cdot \mathrm{deg}$ $\alpha_8 = 2.214$

www.manaraa.com

Radius 9

$$\text{function}(\alpha) := \sqrt{\frac{\sin(\alpha aL)}{\sin(\alpha)}} \cdot \left[\frac{(n-1)\cdot\sqrt{1+2\cdot R}\cdot\sin(\alpha)\ ... \\ +(n+1+2\cdot R)\cdot\cos(\alpha)}{(n-1)\cdot\sqrt{1+2\cdot R}\cdot\sin(\alpha aL)\ ... \\ +(n+1+2\cdot R)\cdot\cos(\alpha aL)}\right]^{\gamma} \cdot e^{\left[\frac{\left(n^2-1\right)\cdot\sqrt{1+2\cdot R}}{2\cdot\left(n^2+1+2\cdot R\right)}\right]\cdot(\alpha aL-\alpha)} - rb_9$$

$\alpha_9 := \text{root}(\text{function}(\alpha), \alpha, 2.1\cdot \text{rad}, 2.3\cdot \text{rad})$ $\qquad \alpha_9 = 126.026\ \text{deg} \qquad \alpha_9 = 2.2$

$$\alpha = \begin{pmatrix} 2.31 \\ 2.289 \\ 2.278 \\ 2.266 \\ 2.254 \\ 2.241 \\ 2.228 \\ 2.214 \\ 2.2 \end{pmatrix} \qquad \alpha 1R := \alpha \qquad \alpha 1R = \begin{pmatrix} 2.31 \\ 2.289 \\ 2.278 \\ 2.266 \\ 2.254 \\ 2.241 \\ 2.228 \\ 2.214 \\ 2.2 \end{pmatrix} \qquad \alpha 1R = \begin{pmatrix} 132.325 \\ 131.16 \\ 130.517 \\ 129.843 \\ 129.138 \\ 128.404 \\ 127.64 \\ 126.846 \\ 126.026 \end{pmatrix}\cdot \text{deg}$$

looks reasonable

Calculate the ratio of effective stress / yield stress as function of α . Ratio is Rσ r

$o := 1..9$

$$R\sigma r_o := \left(\frac{A}{A\cdot\sin\left(\alpha 1R_o\right) + B\cdot\cos\left(\alpha 1R_o\right)}\right)^{\mu} \cdot e^{\left(\frac{A}{C}\right)\cdot\left(\alpha 1R_o - \frac{\pi}{2}\cdot \text{rad}\right)}$$

$$R\sigma r = \begin{pmatrix} 1.391 \\ 1.363 \\ 1.349 \\ 1.335 \\ 1.321 \\ 1.308 \\ 1.296 \\ 1.283 \\ 1.271 \end{pmatrix}$$

Calculate ratio of tangential and radial plastic stress in the plastic region between the edge of the hole and the elastic-plastic boundary

Let ratio for tangential plastic stress to yield stress be SptR and and ratio for plastic radial stress to yield stress be SprR and both are functions of ratio of effective stress to yield stress (Rσ r) and α 1R

$$SptR_o := \frac{R\sigma r_o}{2}\cdot\sqrt{2+2\cdot R}\cdot\left(\cos\left(\alpha 1R_o\right) + \frac{1}{\sqrt{1+2\cdot R}}\cdot\sin\left(\alpha 1R_o\right)\right)$$

المنارة للاستشارات
www.manaraa.com

$$SprR_o := \frac{R\sigma r_o}{2} \cdot \sqrt{2 + 2 \cdot R} \cdot \left(\cos\left(\alpha 1R_o\right) - \frac{1}{\sqrt{1 + 2 \cdot R}} \cdot \sin\left(\alpha 1R_o\right) \right)$$

$$SptR = \begin{pmatrix} -0.343 \\ -0.305 \\ -0.284 \\ -0.263 \\ -0.242 \\ -0.221 \\ -0.199 \\ -0.177 \\ -0.154 \end{pmatrix} \qquad SprR = \begin{pmatrix} -1.53 \\ -1.489 \\ -1.468 \\ -1.447 \\ -1.426 \\ -1.405 \\ -1.383 \\ -1.362 \\ -1.341 \end{pmatrix}$$

2. For Region 2, calculate the change in elastic stress between r/a = 1.17316 and r/a = 2.224

raL =

	1
1	0.999
2	1.068
3	1.122
4	1.174
5	1.224
6	1.274
7	1.323
8	1.373
9	1.423
10	1.474
11	1.526
12	1.58
13	1.635
14	1.692
15	1.75
16	1.811
17	1.873
18	1.938
19	2.006
20	2.076
21	2.148
22	2.224

$raR_1 := 1.1731$

$m := 2..19$

$n := 1..19$

$raR_m := raL_{m+3}$

$$SerU1_n := 2\sqrt{\frac{1 + R}{2(1 + 2 \cdot R)}} \cdot \left(\frac{B2U}{raR_n}\right)^2$$

$$SetU1_n := -SerU1_n$$

raR =

	1
1	1.173
2	1.224
3	1.274
4	1.323
5	1.373
6	1.423
7	1.474
8	1.526
9	1.58
10	1.635
11	1.692
12	1.75
13	1.811
14	1.873
15	1.938
16	2.006
17	2.076
18	2.148
19	2.224

المنارة للاستشارات
www.manaraa.com

3. For Region 3, calculate the change in elastic stress between r/a = 2.224 to r/a = 6.338

$rR := rL$

$rR =$

	1
1	2.224
2	2.474
3	2.724
4	2.974
5	3.224
6	3.474
7	3.724
8	3.974
9	4.224
10	4.474
11	4.724
12	4.974
13	5.224
14	5.474
15	5.724
16	5.974
17	6.224
18	6.474

$p := 1..18$

$$SerR_p := 2\sqrt{\frac{1+R}{2(1+2\cdot R)}}\cdot\left(\frac{B2U}{rR_p}\right)^2$$

$$SetR_p := -SerR_p$$

$SerR =$

	1
1	0.321
2	0.26
3	0.214
4	0.18
5	0.153
6	0.132
7	0.115
8	0.101
9	0.089
10	0.079
11	0.071
12	0.064
13	0.058
14	0.053
15	0.049
16	...

$SetR =$

	1
1	-0.321
2	-0.26
3	-0.214
4	-0.18
5	-0.153
6	-0.132
7	-0.115
8	-0.101
9	-0.089
10	-0.079
11	-0.071
12	-0.064
13	-0.058
14	-0.053
15	-0.049
16	...

www.manaraa.com

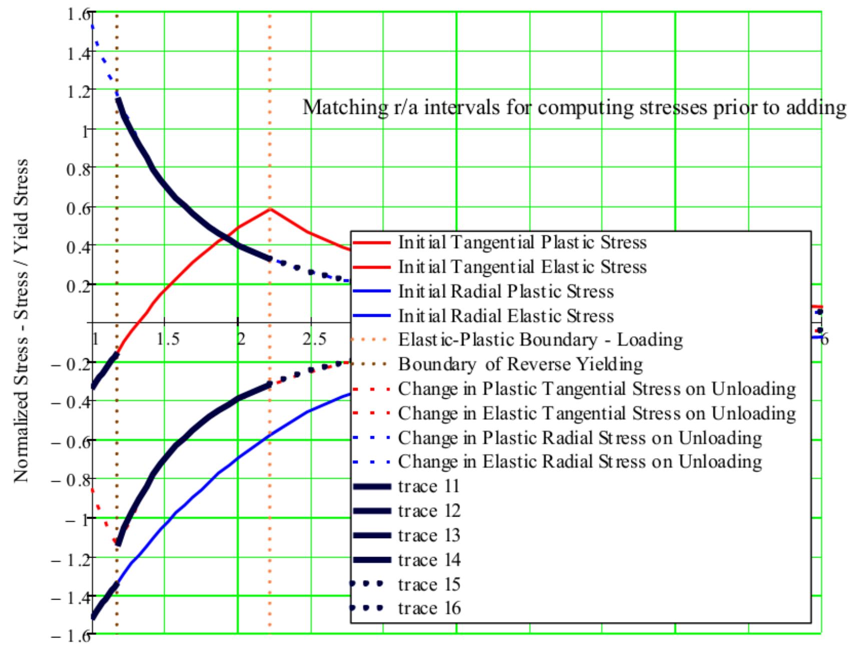

Fig 10. Stresses from Pressure and Changes from Removing the Pressure

4. For Region 1, calculate the residual stress between r/a = 1 to r/a = 1.17316

$RSt1_o := SptU_o + SptR_o$

$RSp1 := SprR + SprU$

$SptU_o =$	$SptR_o =$	$RSt1_o =$
-0.853	-0.343	-1.196
-0.923	-0.305	-1.228
-0.958	-0.284	-1.242
-0.992	-0.263	-1.256
-1.026	-0.242	-1.268
-1.059	-0.221	-1.28
-1.092	-0.199	-1.291
-1.124	-0.177	-1.3
-1.155	-0.154	-1.309

www.manaraa.com

$rb_o =$

1
1.035
1.054
1.073
1.092
1.112
1.132
1.152
1.173

$$SprR = \begin{pmatrix} -1.53 \\ -1.489 \\ -1.468 \\ -1.447 \\ -1.426 \\ -1.405 \\ -1.383 \\ -1.362 \\ -1.341 \end{pmatrix} \qquad SprU = \begin{pmatrix} 1.53 \\ 1.448 \\ 1.406 \\ 1.364 \\ 1.322 \\ 1.28 \\ 1.238 \\ 1.196 \\ 1.155 \end{pmatrix} \qquad RSp1 = \begin{pmatrix} -6.776\times 10^{-6} \\ -0.041 \\ -0.062 \\ -0.083 \\ -0.104 \\ -0.125 \\ -0.145 \\ -0.166 \\ -0.186 \end{pmatrix}$$

5. For Region 2, calculate the residual stress between r/a = 1.17316 to r/a = 2.224

$SetU1 =$

-1.155
-1.061
-0.98
-0.908
-0.843
-0.785
-0.731
-0.682
-0.637
-0.594
-0.555
-0.519
-0.485
-0.453
-0.423
-0.395
-0.369
...

$raR =$

1.173
1.224
1.274
1.323
1.373
1.423
1.474
1.526
1.58
1.635
1.692
1.75
1.811
1.873
1.938
2.006
2.076
...

$SptL =$

-0.344
-0.268
-0.209
-0.153
-0.1
-0.049
0
0.047
0.093
0.138
0.181
0.223
0.264
0.303
0.341
0.379
0.415
0.449
0.483
0.516
...

$raL =$

0.999
1.068
1.122
1.174
1.224
1.274
1.323
1.373
1.423
1.474
1.526
1.58
1.635
1.692
1.75
1.811
1.873
1.938
2.006
2.076
...

$v := 2..19$

$raL2_1 := 1.158$ $\quad SptL1_1 := SptR_9$ $\quad SprL1_1 := SprR_9$ $\quad SprL1_v := SprL_{v+3}$

$raL2_v := raL_{v+3}$ $\quad SptL1_v := SptL_{v+3}$ $\quad RSt2 := SetU1 + SptL1$ $\quad RSr2 := SerU1 + SprL1$

المنارة للاستشارات
www.manaraa.com

raL2 =

	1
1	1.158
2	1.224
3	1.274
4	1.323
5	1.373
6	1.423
7	1.474
8	1.526
9	1.58
10	1.635
11	1.692
12	1.75
13	1.811
14	1.873
15	1.938
16	2.006
17	2.076
18	...

SetU1 =

	1
1	-1.155
2	-1.061
3	-0.98
4	-0.908
5	-0.843
6	-0.785
7	-0.731
8	-0.682
9	-0.637
10	-0.594
11	-0.555
12	-0.519
13	-0.485
14	-0.453
15	-0.423
16	-0.395
17	-0.369
18	...

SptL1 =

	1
1	-0.154
2	-0.1
3	-0.049
4	0
5	0.047
6	0.093
7	0.138
8	0.181
9	0.223
10	0.264
11	0.303
12	0.341
13	0.379
14	0.415
15	0.449
16	0.483
17	0.516
18	...

RSt2 =

	1
1	-1.3087
2	-1.1609
3	-1.029
4	-0.908
5	-0.796
6	-0.6914
7	-0.5933
8	-0.5009
9	-0.4135
10	-0.3307
11	-0.2521
12	-0.1773
13	-0.1061
14	-0.0383
15	0.0264
16	0.088
17	0.1467
18	...

SprL =

	1
1	-1.531
2	-1.452
3	-1.393
4	-1.34
5	-1.29
6	-1.243
7	-1.198
8	-1.153
9	-1.11
10	-1.067
11	-1.025
12	-0.984
13	-0.942
14	-0.901
15	-0.86
16	-0.82
17	-0.779
18	...

SprL1 =

	1
1	-1.341
2	-1.29
3	-1.243
4	-1.198
5	-1.153
6	-1.11
7	-1.067
8	-1.025
9	-0.984
10	-0.942
11	-0.901
12	-0.86
13	-0.82
14	-0.779
15	-0.739
16	-0.698
17	-0.658
18	...

SerU1 =

	1
1	1.155
2	1.061
3	0.98
4	0.908
5	0.843
6	0.785
7	0.731
8	0.682
9	0.637
10	0.594
11	0.555
12	0.519
13	0.485
14	0.453
15	0.423
16	0.395
17	0.369
18	...

RSr2 =

	1
1	-0.186
2	-0.23
3	-0.263
4	-0.29
5	-0.31
6	-0.325
7	-0.336
8	-0.343
9	-0.347
10	-0.348
11	-0.346
12	-0.342
13	-0.335
14	-0.326
15	-0.316
16	-0.303
17	-0.289
18	...

المنارة للاستشارات
www.manaraa.com

6. For Region 3, calculate the residual stress between r/a = 2.224 to r/a = 6.338

SetR =

	1
1	-0.321
2	-0.26
3	-0.214
4	-0.18
5	-0.153
6	-0.132
7	-0.115
8	-0.101
9	-0.089
10	-0.079
11	-0.071
12	-0.064
13	-0.058
14	-0.053
15	-0.049
16	-0.045
17	-0.041
18	-0.038

SetL =

	1
1	0.577
2	0.467
3	0.385
4	0.323
5	0.275
6	0.237
7	0.206
8	0.181
9	0.16
10	0.143
11	0.128
12	0.115
13	0.105
14	0.095
15	0.087
16	0.08
17	0.074
18	0.068

rR =

	1
1	2.224
2	2.474
3	2.724
4	2.974
5	3.224
6	3.474
7	3.724
8	3.974
9	4.224
10	4.474
11	4.724
12	4.974
13	5.224
14	5.474
15	5.724
16	5.974
17	6.224
18	6.474

rL =

	1
1	2.224
2	2.474
3	2.724
4	2.974
5	3.224
6	3.474
7	3.724
8	3.974
9	4.224
10	4.474
11	4.724
12	4.974
13	5.224
14	5.474
15	5.724
16	5.974
17	6.224
18	6.474

RSet3 := SetR + SetL

RSer3 := SerR + SerL

RSet3 =

	1
1	0.256
2	0.207
3	0.171
4	0.143
5	0.122
6	0.105
7	0.091
8	0.08
9	0.071
10	0.063
11	0.057
12	0.051
13	0.046
14	0.042
15	...

SerR =

	1
1	0.321
2	0.26
3	0.214
4	0.18
5	0.153
6	0.132
7	0.115
8	0.101
9	0.089
10	0.079
11	0.071
12	0.064
13	0.058
14	0.053
15	...

SerL =

	1
1	-0.577
2	-0.467
3	-0.385
4	-0.323
5	-0.275
6	-0.237
7	-0.206
8	-0.181
9	-0.16
10	-0.143
11	-0.128
12	-0.115
13	-0.105
14	-0.095
15	...

RSer3 =

	1
1	-0.256
2	-0.207
3	-0.171
4	-0.143
5	-0.122
6	-0.105
7	-0.091
8	-0.08
9	-0.071
10	-0.063
11	-0.057
12	-0.051
13	-0.046
14	-0.042
15	...

المنارة للاستشارات
www.manaraa.com

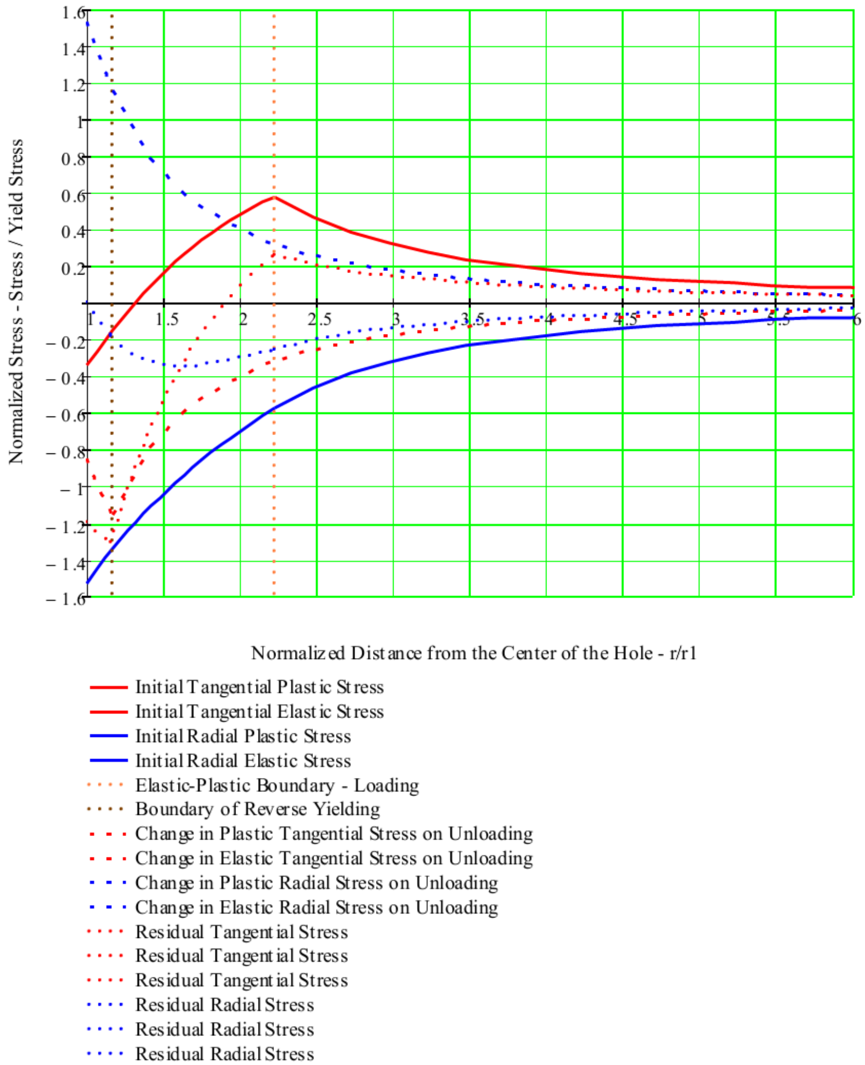

Fig 11. Stresses from Pressure,Removing the Pressure, and Residual Stress

www.manaraa.com

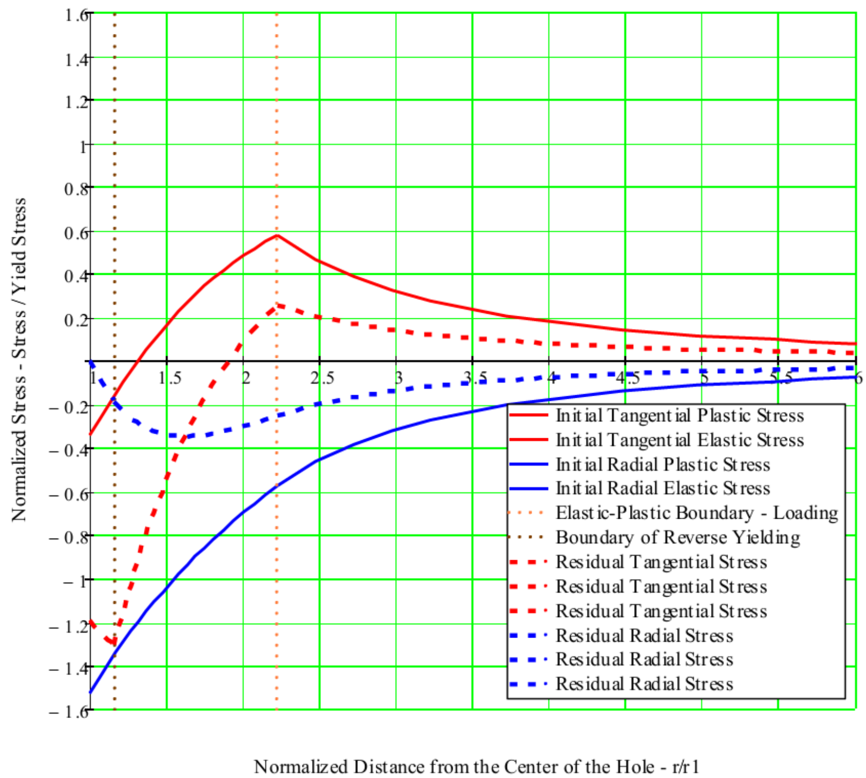

Fig 12. Expansion Stress and Residual Stress

www.manaraa.com

Appendix B-3 Modified Ramberg-Osgood Equations for Different *n* Values

Appendix B 3 Modified Ramberg-Osgood Equation

1 Assumptions

A. Isotropic behavior in all directions. From this isotropic parameter R = 1.
B. Yield strength of steel is 45.3 ksi.
C. Strain hardening exponent n = 13 from other calculations

2. Calculations

A. Calculations for Maximum Pressure and Corresponding Load

Let α_a range between $\pi/2$ and α_{max}. Where α_{max} is:

n = 13

$R := 1 \qquad n := 13 \qquad \sigma yield := 45.3$

$$\alpha max := atan\left[\frac{-(n+1+2\cdot R)}{(n-1)\cdot\sqrt{1+2\cdot R}}\right]$$

$\alpha max = -0.6560534 \quad \alpha max = -37.5890895 deg$

$\alpha max1 := \pi + \alpha max \qquad \alpha max1 = 2.4855393 \quad \alpha max1 = 142.4109105 deg$

$i := 1..15$

$$\alpha := \begin{pmatrix} 90 \\ 94 \\ 98 \\ 102 \\ 106 \\ 110 \\ 114 \\ 118 \\ 122 \\ 126 \\ 130 \\ 134 \\ 138 \\ 142 \\ 142.4 \end{pmatrix}\cdot deg$$

$$\mu := \frac{n+1+2\cdot R}{n^2+1+2\cdot R} \qquad \mu = 0.0930233$$

$$S_i := \left[\frac{(n-1)\cdot\sqrt{1+2\cdot R}}{n^2+1+2\cdot R}\right]\cdot\left(\alpha_i - \frac{\pi}{2}\right)$$

$$Sratio_i := \sqrt{\frac{1+R}{2}}\cdot\left(\frac{\sin(\alpha_i)}{\sqrt{1+2\cdot R}} - \cos(\alpha_i)\right)\cdot\left[\frac{(n-1)\cdot\sqrt{1+2\cdot R}}{(n-1)\cdot\sqrt{1+2\cdot R}\cdot\sin(\alpha_i) + (n+1+2\cdot R)\cdot\cos(\alpha_i)}\right]^{\mu}\cdot\left(e^{S_i}\right)$$

المنارة للاستشارات
www.manaraa.com

$pressure_i := Sratio_i \cdot \sigma yield$

Sratio =

	1
1	0.5773503
2	0.6546796
3	0.7314082
4	0.8073892
5	0.8825327
6	0.9568353
7	1.0304276
8	1.1036588
9	1.1772575
10	1.2526749
11	1.3329283
12	1.4251891
13	1.5526357
14	1.9766456
15	2.7752727

$pressure_i =$

26.1539672
29.6569847
33.1327934
36.5747298
39.9787293
43.344637
46.6783718
49.9957446
53.3297639
56.7461718
60.3816516
64.561065
70.3343977
89.5420468
125.7198513

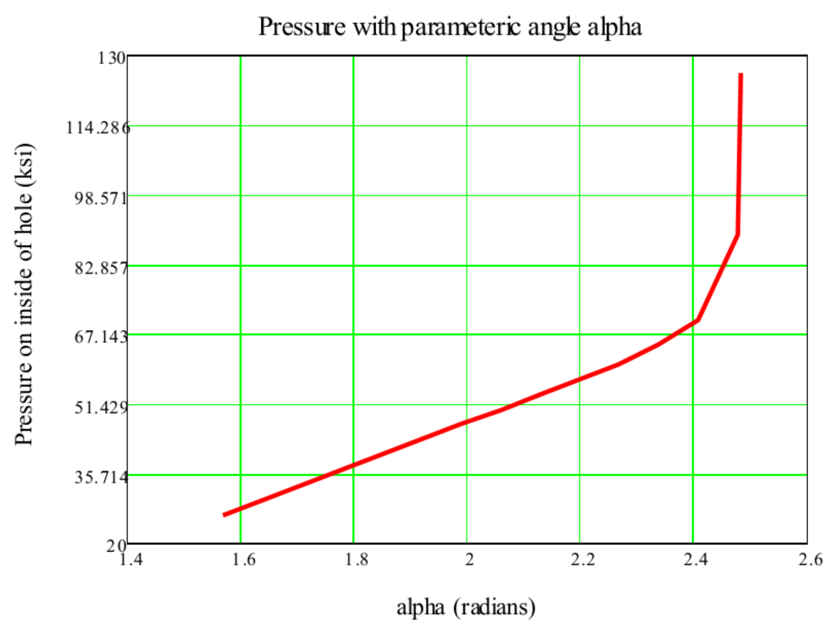

المنارة للاستشارات
www.manaraa.com

$$load_i := pressure_i \cdot \pi \cdot \left(\frac{0.125}{2}\right)^2$$

$load_i =$

	1
1	0.3209575
2	0.363946
3	0.4066005
4	0.4488395
5	0.4906128
6	0.5319187
7	0.5728298
8	0.6135401
9	0.6544547
10	0.6963803
11	0.7409943
12	0.7922835
13	0.8631329
14	1.0988462
15	1.5428147

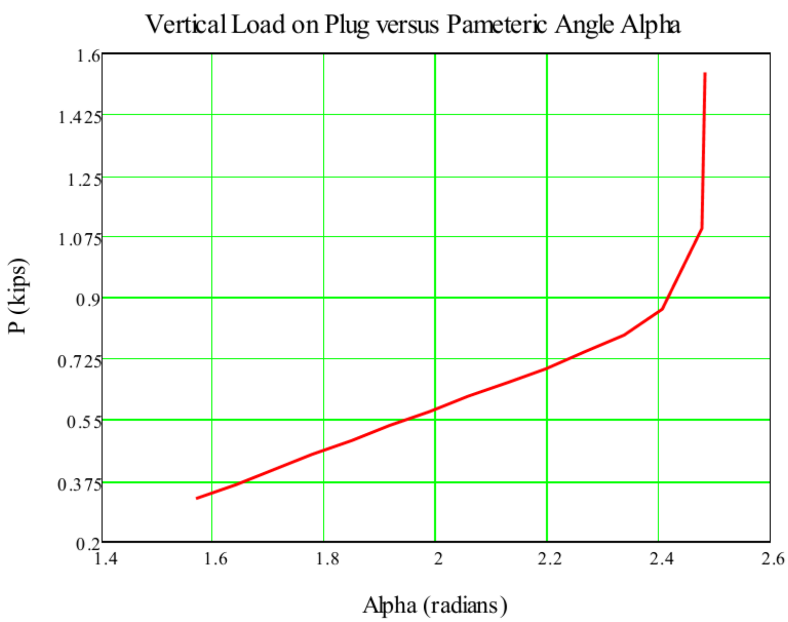

www.manaraa.com

Try n=5 $n := 5$

$$\alpha max2 := atan\left[\frac{-(n+1+2\cdot R)}{(n-1)\cdot\sqrt{1+2\cdot R}}\right]$$

$\alpha max2 = -0.8570719$ $\alpha max2 = -49.1066054 deg$

$\alpha max3 := \pi + \alpha max2$ $\alpha max3 = 2.2845207$ $\alpha max3 = 130.8933946 deg$

$j := 1..12$

$$\alpha := \begin{pmatrix} 90 \\ 94 \\ 98 \\ 102 \\ 106 \\ 110 \\ 114 \\ 118 \\ 122 \\ 126 \\ 130 \\ 130.8 \end{pmatrix}\cdot deg$$

$$\mu := \frac{n+1+2\cdot R}{n^2+1+2\cdot R} \qquad \mu = 0.2857143$$

$$S_j := \left[\frac{(n-1)\cdot\sqrt{1+2\cdot R}}{n^2+1+2\cdot R}\right]\cdot\left(\alpha_j - \frac{\pi}{2}\right)$$

$$Sratio1_j := \sqrt{\frac{1+R}{2}}\cdot\left(\frac{\sin(\alpha_j)}{\sqrt{1+2\cdot R}} - \cos(\alpha_j)\right)\cdot\left[\frac{(n-1)\cdot\sqrt{1+2\cdot R}}{(n-1)\cdot\sqrt{1+2\cdot R}\cdot\sin(\alpha_j) + (n+1+2\cdot R)\cdot\cos(\alpha_j)}\right]^{\mu}\cdot\left(e^{S_j}\right)$$

$pressure1_j := Sratio1_j\cdot\sigma yield$ $pressure1_j =$

Sratio1 =

	1
1	0.5773503
2	0.6734147
3	0.7762493
4	0.8875089
5	1.0097459
6	1.1471058
7	1.3068304
8	1.5029987
9	1.7681147
10	2.2059247
11	3.7516448
12	7.2124457

26.1539672
30.5056842
35.164093
40.2041551
45.7414877
51.9638946
59.1994164
68.0858406
80.0955946
99.9283874
169.9495087
326.7237921

www.manaraa.com

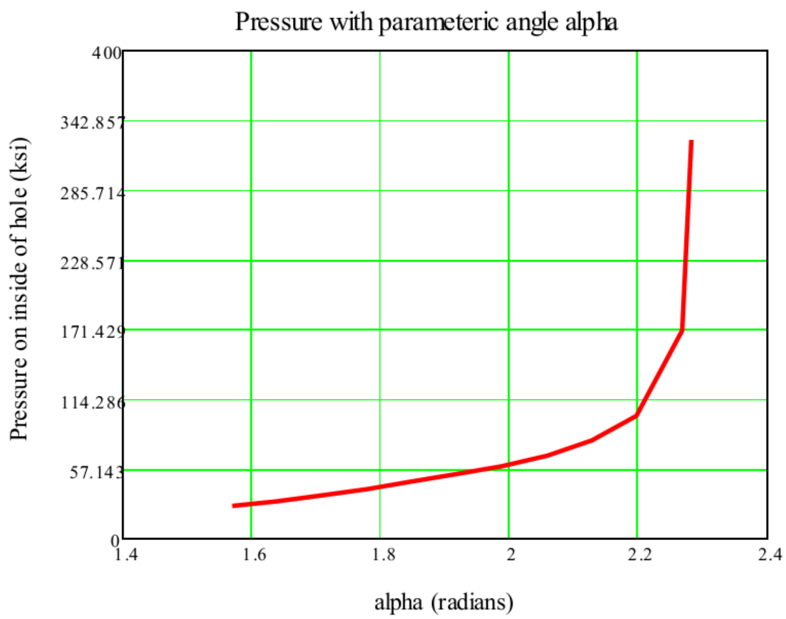

$\text{load1}_j := \text{pressure1}_j \cdot \pi \cdot \left(\frac{0.125}{2}\right)^2$

$\text{load1}_j =$

0.3209575
0.3743611
0.4315283
0.4933792
0.5613325
0.6376929
0.7264861
0.835539
0.9829208
1.2263058
2.0855942
4.0095042

www.manaraa.com

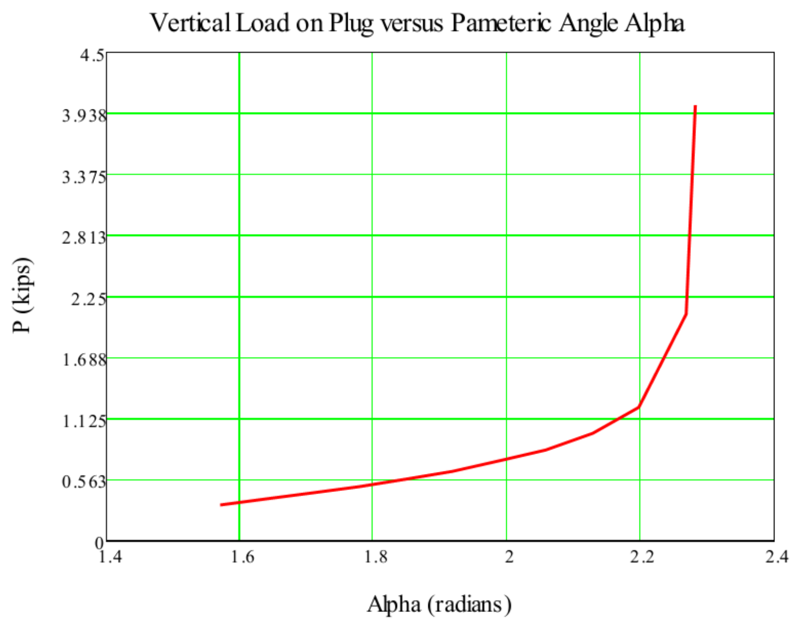

Try n = 805

$n := 805$ $\qquad \alpha max4 := \operatorname{atan}\left[\frac{-(n+1+2\cdot R)}{(n-1)\cdot\sqrt{1+2\cdot R}}\right]$

$\alpha max4 = -0.5257504$ $\alpha max4 = -30.1232783 deg$

$\alpha max5 := \pi + \alpha max4$ $\qquad \alpha max5 = 2.6158423$ $\qquad \alpha max5 = 149.8767217 deg$

$k := 1..18$

$$\alpha := \begin{pmatrix} 90 \\ 94 \\ 98 \\ 102 \\ 106 \\ 110 \\ 114 \\ 118 \\ 122 \\ 126 \\ 130 \\ 134 \\ 138 \\ 142 \\ 146 \\ 148 \\ 149 \\ 149.98 \end{pmatrix} \cdot deg$$

$$\mu := \frac{n+1+2\cdot R}{n^2+1+2\cdot R} \qquad \mu = 0.0012469$$

$$S_k := \left[\frac{(n-1)\cdot\sqrt{1+2\cdot R}}{n^2+1+2\cdot R}\right]\cdot\left(\alpha_k - \frac{\pi}{2}\right)$$

المنارة للاستشارات
www.manaraa.com

$$Sratio2_k := \sqrt{\frac{1+R}{2}} \cdot \left(\frac{\sin(\alpha_k)}{\sqrt{1+2 \cdot R}} - \cos(\alpha_k) \right) \cdot \left[\frac{(n-1) \cdot \sqrt{1+2 \cdot R}}{(n-1) \cdot \sqrt{1+2 \cdot R} \cdot \sin(\alpha_k) + (n+1+2 \cdot R) \cdot \cos(\alpha_k)} \right]^{\mu} \cdot \left(e^{S_k} \right)$$

$$pressure2_k := Sratio2_k \cdot \sigma yield$$

Elastic-plastic p_{max} from Nadia

Sratio2 =

	1
1	0.5773503
2	0.6458325
3	0.7112021
4	0.7731415
5	0.8313502
6	0.8855462
7	0.9354676
8	0.9808737
9	1.0215476
10	1.0572973
11	1.0879585
12	1.1133995
13	1.1335301
14	1.1483303
15	1.157984
16	...

$pressure2_k =$

26.1539672
29.2562141
32.2174539
35.0233084
37.6601644
40.115245
42.3766807
44.4335806
46.2761076
47.8955665
49.2845223
50.4369994
51.3489153
52.0193608
52.4566765
...

$$pmax := \frac{2}{\sqrt{3}} \cdot \sigma yield$$

$$pmax = 52.3079344$$

$$pactual := \frac{2.132}{\left[\pi \cdot \left(\frac{0.125}{2}\right)^2\right]}$$

$$pactual = 173.7309894$$

www.manaraa.com

Pressure w/ parameteric angle alpha

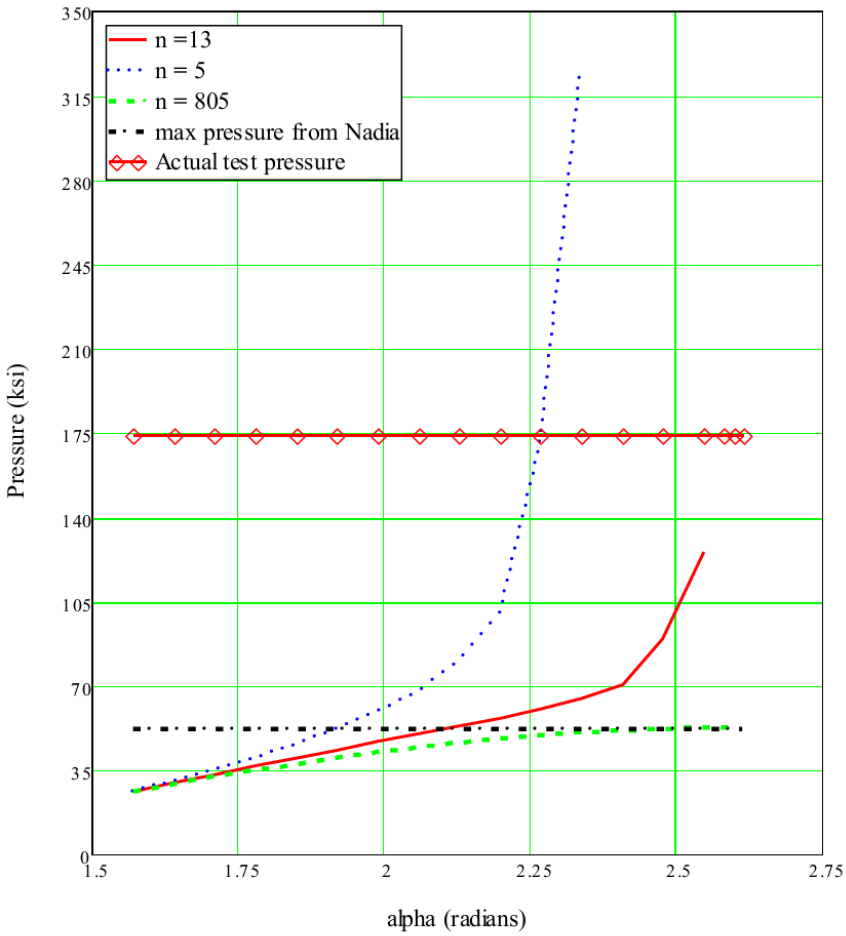

www.manaraa.com

$$load2_k := pressure2_k \cdot \pi \cdot \left(\frac{0.125}{2}\right)^2$$

$load2_k =$

0.3209575
0.3590278
0.3953676
0.4298007
0.4621597
0.4922881
0.5200401
0.5452821
0.5678933
0.587767
0.6048121
0.6189551
0.630146
0.6383736
0.6437403
...

$Pmax := pmax\left[\pi \cdot \left(\frac{0.125}{2}\right)^2\right]$ $Pmax = 0.6419149$ $Pactual := \frac{9.2282224 + 64.6378}{1000}$ $Pactual = 2.1317546$

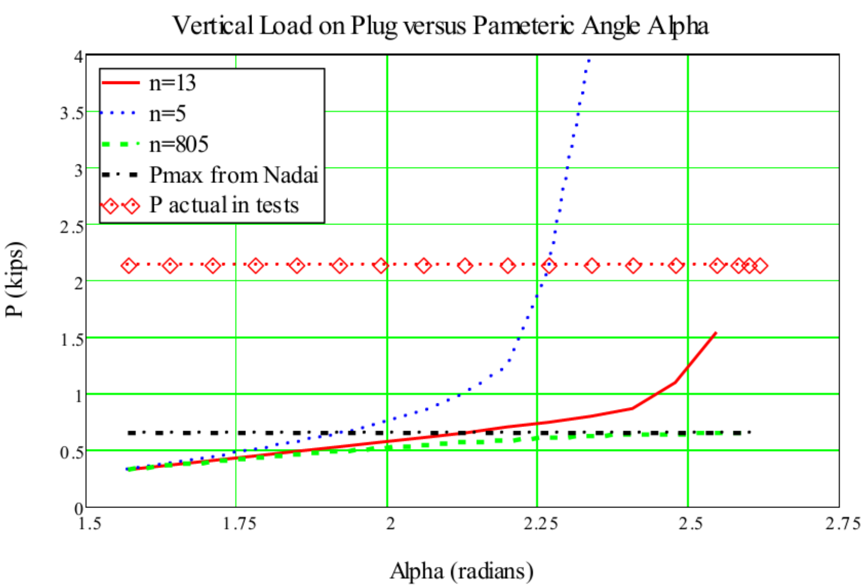

www.manaraa.com

B. Calculations for Max Radius of Plastic - Elastic Boundary

$$n := \begin{pmatrix} 5 \\ 10 \\ 15 \\ 20 \\ 40 \\ 100 \\ 201 \\ 400 \\ 805 \\ 5000 \end{pmatrix} \qquad i := 1..10$$

$$\text{Amax} := \operatorname{atan}\left[\frac{-(n+1+2\cdot R)}{(n-1)\cdot\sqrt{1+2\cdot R}}\right]$$

Amax =

	1
1	-0.8570719
2	-0.6951023
3	-0.6385597
4	-0.6099858
5	-0.566873
6	-0.5409176
7	-0.5322157
8	-0.5279289
9	-0.5257504
10	-0.5239452

Amax = ·deg

	1
1	-49.1066054
2	-39.8264298
3	-36.5867756
4	-34.9496107
5	-32.4794312
6	-30.9922928
7	-30.4937151
8	-30.2480965
9	-30.1232783
10	-30.0198478

$$\alpha_i := \pi + \text{Amax}_i$$

$\alpha_i =$

1.5707963
1.6406095
1.7104227
1.7802358
1.850049
1.9198622
1.9896753
2.0594885
2.1293017
2.1991149

$\alpha_i =$ ·deg

90
94
98
102
106
110
114
118
122
126

$$\gamma_i := \frac{n_i\cdot(1+2\cdot R)}{\left[(n_i)^2+1+2\cdot R\right]}$$

$\gamma =$

	1
1	0.5357143
2	0.2912621
3	0.1973684
4	0.1488834
5	0.0748596
6	0.029991
7	0.0149243
8	0.0074999
9	0.0037267
10	0.0006

B = ratio of radius of elastic plastic boundary to initial radius

$$\text{exp}_i := \frac{\left[(n_i)^2-1\right]\cdot\sqrt{1+2\cdot R}}{2\cdot\left[(n_i)^2+1+2\cdot R\right]}\cdot\left(\alpha_i-\frac{\pi}{2}\right)$$

www.manaraa.com

$$B_i := \left(\sqrt{\sin(\alpha_i)}\right)\cdot\left[\frac{(n_i - 1)\cdot\sqrt{1+2\cdot R}}{(n_i - 1)\cdot\sqrt{1+2\cdot R}\cdot\sin(\alpha_i) + (n_i + 1 + 2\cdot R)\cdot\cos(\alpha_i)}\right]^{\gamma_i}\cdot e^{exp_i}$$

$B_i =$

	1
1	267526152.4507625
2	53029.6161038
3	2101.4153485
4	411.1408062
5	25.2360919
6	5.2040122
7	2.9938227
8	2.2810076
9	2.0104695
10	1.7895877

$\log(B_i) =$

	1
1	8.4273662
2	4.7245185
3	3.3225119
4	2.6139906
5	1.4020221
6	0.7163383
7	0.4762261
8	0.3581267
9	0.3032975
10	0.252753

$A_i := 1.75$

$m := 30$

$D_i := 3$

$A_i =$

	1
1	1.75
2	1.75
3	1.75
4	1.75
5	1.75
6	1.75
7	1.75
8	1.75
9	1.75
10	1.75

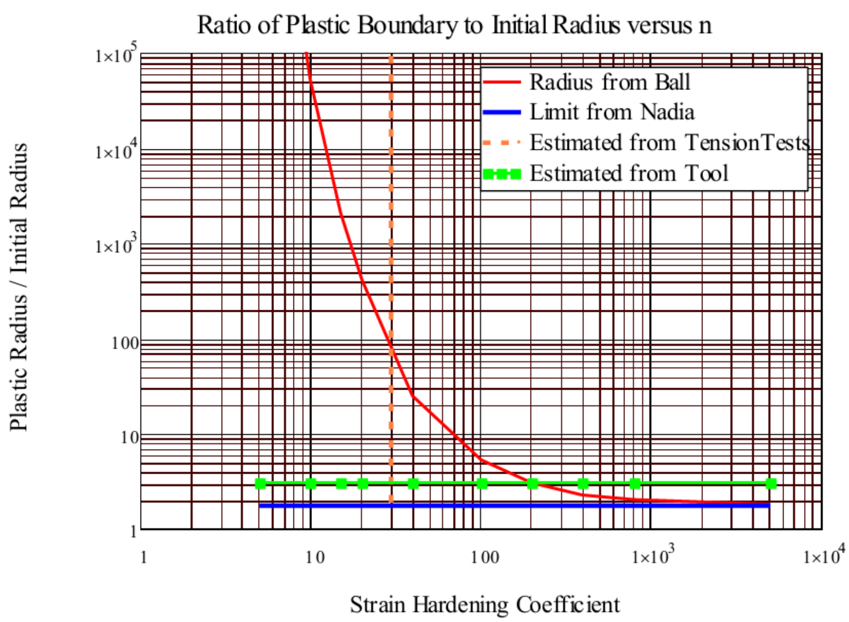

www.manaraa.com

$E := 3000($ $\sigma y := 45.3$

$\sigma e := \begin{pmatrix} 0 \\ 45.3 \end{pmatrix}$ $\varepsilon e := \begin{pmatrix} 0 \\ .001510 \end{pmatrix}$

for n =9

$n := 9$ $i := 1..10$

$\sigma := \begin{pmatrix} 0 \\ 25 \\ 35 \\ 46.3 \\ 55 \\ 60 \\ 65 \\ 70 \\ 75 \\ 80 \end{pmatrix}$

$\varepsilon_i := \frac{\sigma_i}{E} \cdot \left(\frac{\sigma_i}{\sigma y} \right)^{n-1}$

$\varepsilon_i =$

0
0.0000072
0.0001482
0.0018379
0.0086568
0.0189432
0.0389326
0.0758535
0.1411382
0.2522917

for n =13

$n := 13$ $i := 1..15$

$\sigma 1 := \begin{pmatrix} 46.3 \\ 47 \\ 49 \\ 51 \\ 53 \\ 56 \\ 59 \\ 61 \\ 64 \\ 67 \\ 70 \\ 73 \\ 76 \\ 79 \\ 82 \end{pmatrix}$

$\varepsilon 1_i := \frac{\sigma 1_i}{E} \cdot \left(\frac{\sigma 1_i}{\sigma y} \right)^{n-1}$

$\varepsilon 1_i =$

0.0020056
0.0024377
0.0041903
0.0070488
0.0116222
0.0237763
0.0468572
0.072275
0.1349087
0.2447219
0.4324888
0.7462726
1.2597287
2.0837831
3.3828318

for n = 15

$\sigma 2 := \begin{pmatrix} 0 \\ 20 \\ 35 \\ 45.3 \\ 46 \\ 47 \\ 48 \\ 49 \\ 50 \\ 51 \\ 52 \\ 53 \\ 54 \\ 60 \\ 65 \end{pmatrix}$

$n := 15$ $i := 1..15$

$\varepsilon 2_i := \frac{\sigma 2_i}{E} \cdot \left(\frac{\sigma 2_i}{\sigma y} \right)^{n-1}$

$\varepsilon 2_i =$

0
0
0.0000315
0.00151
0.0019005
0.002624
0.0035985
0.0049028
0.0066383
0.0089342
0.0119551
0.015909
0.0210577
0.1022757
0.3397851

المنارة للاستشارات
www.manaraa.com

for n =17 $\quad n := 17 \quad i := 1..8$

$$\sigma 3 := \begin{pmatrix} 40 \\ 46.3 \\ 47 \\ 49 \\ 52 \\ 55 \\ 60 \\ 65 \end{pmatrix} \qquad \varepsilon 3_i := \frac{\sigma 3_i}{E} \cdot \left(\frac{\sigma 3_i}{\sigma y}\right)^{n-1}$$

$\varepsilon 3_i =$

0.0001821
0.0021887
0.0028247
0.0057364
0.015753
0.0408765
0.1794233
0.6995755

for n =30 $\quad n := 30 \quad i := 1..9$

$$\sigma 4 := \begin{pmatrix} 46.3 \\ 47 \\ 48 \\ 49 \\ 50 \\ 51 \\ 53 \\ 55 \\ 55.31 \end{pmatrix} \qquad \varepsilon 4_i := \frac{\sigma 4_i}{E} \cdot \left(\frac{\sigma 4_i}{\sigma y}\right)^{n-1}$$

$\varepsilon 4_i =$

0.0029071
0.00456
0.0085757
0.0159189
0.0291831
0.0528611
0.1676127
0.5092272
0.6027547

for n =40 $\quad n := 40 \quad i := 1..8$

$$\sigma 5 := \begin{pmatrix} 45 \\ 46.3 \\ 47 \\ 48 \\ 49 \\ 50 \\ 51 \\ 52 \end{pmatrix} \qquad \varepsilon 5_i := \frac{\sigma 5_i}{E} \cdot \left(\frac{\sigma 5_i}{\sigma y}\right)^{n-1}$$

$\varepsilon 5_i =$

0.0011576
0.0036165
0.0065912
0.0153002
0.0349054
0.0783157
0.1729243
0.3759955

المنارة للاستشارات
www.manaraa.com

New σ yield

for n =17

$\sigma y := 41.23$

$n := 17$ $\qquad i := 1 .. 11$

$$\sigma 6 := \begin{pmatrix} 41.23 \\ 43 \\ 42 \\ 45 \\ 47 \\ 50 \\ 51 \\ 51.4858 \\ 52 \\ 53 \\ 54 \end{pmatrix} \qquad \varepsilon 6_i := \frac{\sigma 6_i}{E} \cdot \left(\frac{\sigma 6_i}{\sigma y} \right)^{n-1} \qquad \varepsilon 6_i =$$

0.0013743
0.0028082
0.0018824
0.0060824
0.0127388
0.0364717
0.0510691
0.0600001
0.0710432
0.0982099
0.1349458

New σ yield

for n =13

$\sigma y := 38.3$

$n := 13$ $\qquad i := 1 .. 11$

$$\sigma 7 := \begin{pmatrix} 38.23 \\ 40 \\ 42 \\ 44 \\ 46 \\ 48 \\ 50 \\ 51.486 \\ 55 \\ 60 \\ 65 \end{pmatrix} \qquad \varepsilon 7_i := \frac{\sigma 7_i}{E} \cdot \left(\frac{\sigma 7_i}{\sigma y} \right)^{n-1} \qquad \varepsilon 7_i =$$

0.0012467
0.0022453
0.0042338
0.0077514
0.0138148
0.0240231
0.0408417
0.0597658
0.1409965
0.4369781
1.2369926

المنارة للاستشارات
www.manaraa.com

New σ yield

for n =12

$\sigma y := 37.27$

$n := 12$ $\quad i := 1..11$

$$\sigma 8 := \begin{pmatrix} 37.273 \\ 39 \\ 41 \\ 43 \\ 45 \\ 47 \\ 49 \\ 51 \\ 55 \\ 60 \\ 65 \end{pmatrix}$$

$$\varepsilon 8_i := \frac{\sigma 8_i}{E} \cdot \left(\frac{\sigma 8_i}{\sigma y}\right)^{n-1}$$

$\varepsilon 8_i =$

0.0012424
0.0021395
0.0038989
0.006905
0.0119149
0.0200778
0.033105
0.0535036
0.1324016
0.3761455
0.9828815

New σ yield

for n =11

$\sigma y := 36.($

$n := 11$ $\quad i := 1..11$

$$\sigma 9 := \begin{pmatrix} 36.0 \\ 39 \\ 41 \\ 43 \\ 45 \\ 47 \\ 49 \\ 51 \\ 55 \\ 60 \\ 65 \end{pmatrix}$$

$$\varepsilon 9_i := \frac{\sigma 9_i}{E} \cdot \left(\frac{\sigma 9_i}{\sigma y}\right)^{n-1}$$

$\varepsilon 9_i =$

0.0012
0.0028944
0.0050174
0.0084724
0.0139698
0.0225388
0.035646
0.055351
0.1270116
0.3307634
0.7978122

المنارة للاستشارات

www.manaraa.com

New σ yield

for n =10

$\sigma y := 34.69$

$n := 10$ $\quad i := 1..11$

$$\sigma 10 := \begin{pmatrix} 34.69 \\ 36 \\ 38 \\ 40 \\ 42 \\ 45 \\ 48 \\ 51 \\ 55 \\ 60 \\ 65 \end{pmatrix} \qquad \varepsilon 10_i := \frac{\sigma 10_i}{E} \cdot \left(\frac{\sigma 10_i}{\sigma y}\right)^{n-1} \qquad \varepsilon 10_i =$$

0.0011563
0.0016752
0.0028766
0.0048044
0.0078259
0.0156015
0.0297476
0.0545433
0.1160558
0.2770464
0.6168415

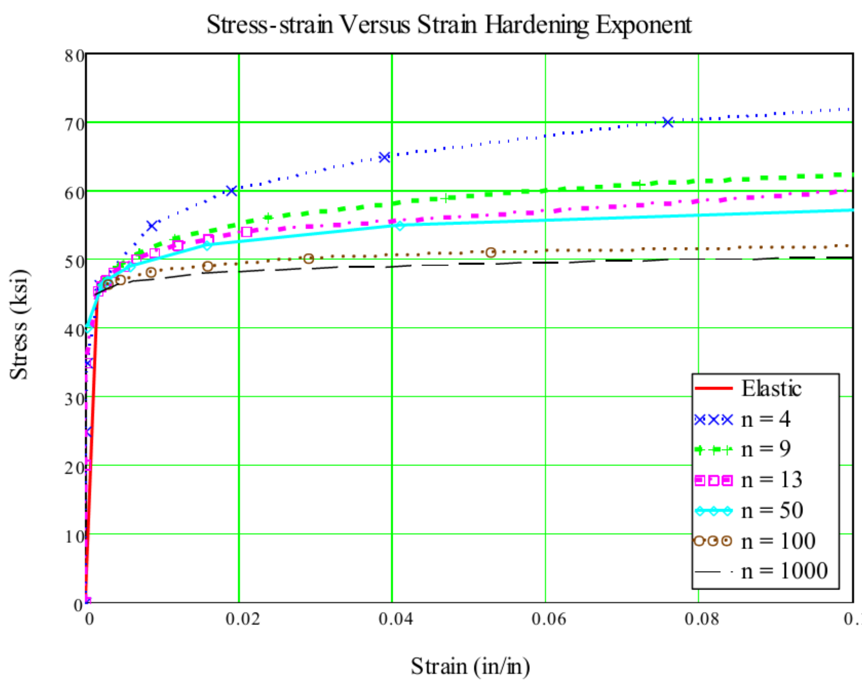

المنارة للاستشارات
www.manaraa.com

Load and Plastic Radius as Function of n (strain hardening exponent)

1. Assumptions:

A. Plane stress

B. Deformation theory of plasticity applies. This means:

1). A single curve relates effective stress to effective strain for all states of stress

2). Principal stresses maintain proportional magnitudes and constant directions through entire loading range

3). Monotonic loading - no unloading

C. Material is isotropic

D. Small strains

E. Except in certain regions, only applies for n < 17.

2. Development of Equations

A. From thick shell formulas

$\sigma_r = C_1 + \frac{C_2}{r^2}$ $\sigma_r = C_1 + \frac{C_2}{r^2}$

Characterization of stress-strain in the plastic regions
Ramberg-Osgood formulation
modified Ramberg-Osgood

$\varepsilon = \varepsilon_e + (\sigma/H)^{1/n'}$

$\varepsilon = \varepsilon_e + (\sigma/E)^{n''-1}$

n - strain hardening exponent
H - strength coefficient

$\varepsilon_e = \sigma/E$

for $\sigma < \sigma_{yield}$

$\varepsilon = \sigma/E\,(\sigma/\sigma_y)^{n''-1}$

for $\sigma > \sigma_{yield}$

n' does not equal n"

www.manaraa.com

Max Pressure and Load as Function of n - strain hardening exponent

$$n := \begin{pmatrix} 4 \\ 9 \\ 13 \\ 20 \\ 30 \\ 40 \\ 60 \\ 100 \\ 150 \\ 200 \end{pmatrix}$$

$\sigma yield := 45.3$ $\quad R := 1$ $\quad i := 1..10$

$$\alpha max_i := atan\left[\frac{-(n_i + 1 + 2\cdot R)}{(n_i - 1)\cdot\sqrt{1 + 2\cdot R}}\right]$$

$$\alpha maxl_i := \pi + \alpha max_i - 0.005 deg$$

$\alpha max_i =$

-0.9322366
-0.7137244
-0.6560534
-0.6099858
-0.5812698
-0.566873
-0.5524583
-0.5409176
-0.5351453
-0.5322588

$\alpha max_i =$ (·deg)

-53.4132244
-40.8933946
-37.5890895
-34.9496107
-33.3043052
-32.4794312
-31.6535275
-30.9922928
-30.6615653
-30.4961836

$\alpha maxl =$

	1
1	2.2092688
2	2.427781
3	2.485452
4	2.5315196
5	2.5602356
6	2.5746324
7	2.5890471
8	2.6005878
9	2.6063601
10	2.6092466

$\alpha maxl_i =$ (·deg)

126.5817756
139.1016054
142.4059105
145.0453893
146.6906948
147.5155688
148.3414725
149.0027072
149.3334347
149.4988164

$$\mu_i := \frac{n_i + 1 + 2\cdot R}{(n_i)^2 + 1 + 2\cdot R}$$

$\mu_i =$

0.3684211
0.1428571
0.0930233
0.057072
0.0365449
0.0268247
0.0174854
0.0102969
0.0067991
0.0050746

$$S_i := \left[\frac{(n_i - 1)\cdot\sqrt{1 + 2\cdot R}}{(n_i)^2 + 1 + 2\cdot R}\right]\cdot\left(\alpha maxl_i - \frac{\pi}{2}\right)$$

$S_i =$

0.1746105
0.1413658
0.1105277
0.0784526
0.0550377
0.0423014
0.0288804
0.0176529
0.0118764
0.0089476

المنارة للاستشارات
www.manaraa.com

$$\mathrm{Sratio}_i := \sqrt{\frac{1+R}{2}}\cdot\left(\frac{\sin\left(\alpha\mathrm{max1}_i\right)}{\sqrt{1+2\cdot R}} \ldots + -\cos\left(\alpha\mathrm{max1}_i\right)\right)\cdot\left[\frac{\left(n_i-1\right)\cdot\sqrt{1+2\cdot R}}{\left(n_i-1\right)\cdot\sqrt{1+2\cdot R}\cdot\sin\left(\alpha\mathrm{max1}_i\right)+\left(n_i+1+2\cdot R\right)\cdot\cos\left(\alpha\mathrm{max1}_i\right)}\right]^{\mu_i}\cdot\left(e^{S_i}\right)$$

$\mathrm{Sratio}_i =$

32.6326566
4.7695611
2.9842856
2.0972475
1.7027106
1.5393458
1.395028
1.2917486
1.2438033
1.2207006

$$\mathrm{pressure}_i := \mathrm{Sratio}_i\cdot\sigma\mathrm{yield}$$

$$\mathrm{pmax} := \frac{2}{\sqrt{3}}\cdot\sigma\mathrm{yield}$$

$\mathrm{pmax} = 52.3079344$

$$\mathrm{pactual} := \frac{2.132}{\left[\pi\cdot\left(\frac{0.125}{2}\right)^2\right]}$$

$\mathrm{pactual} = 173.7309894$

$\mathrm{pressure}_i =$

1478.2593433
216.061118
135.1881378
95.0053129
77.13279
69.7323653
63.1947671
58.5162101
56.3442876
55.2977381

$$\mathrm{Pmax} := \mathrm{pmax}\cdot\left[\pi\cdot\left(\frac{0.125}{2}\right)^2\right]$$

$\mathrm{Pmax} = 0.6419149$

$$\mathrm{Pactual} := \frac{9.2282224 + 64.637}{1000}$$

$\mathrm{Pactual} = 2.1317546$

$$P_i := \mathrm{pressure}_i\cdot\left[\pi\cdot\left(\frac{0.125}{2}\right)^2\right]$$

$P_i =$

18.1409715
2.6514688
1.659008
1.1658906
0.9465617
0.8557449
0.7755165
0.7181019
0.6914484
0.6786053

www.manaraa.com

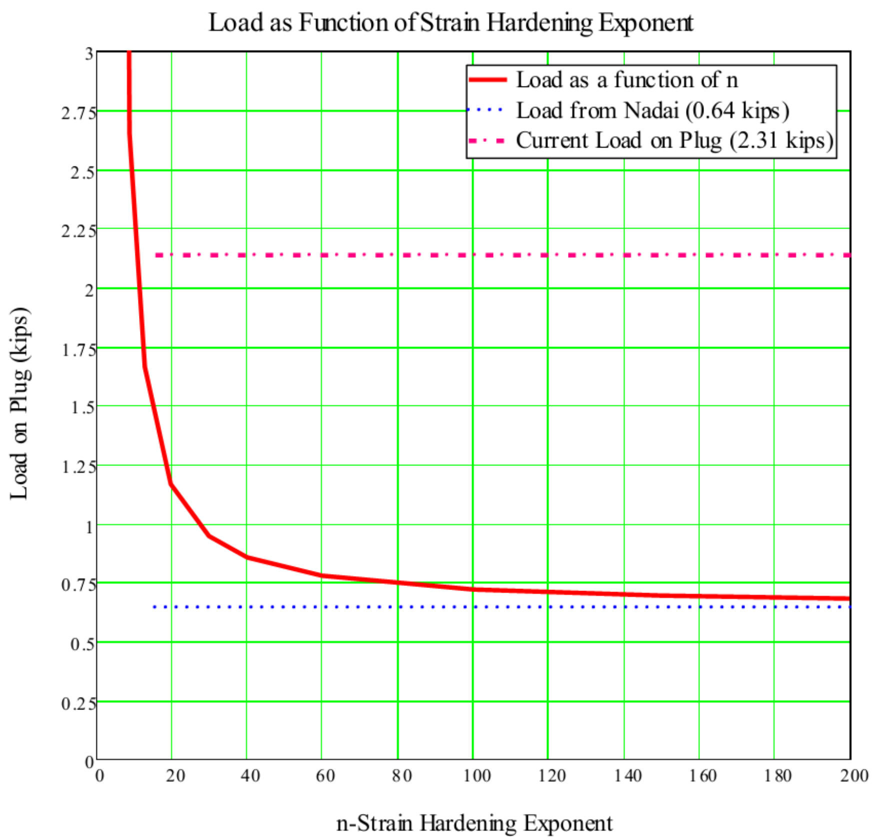

المنارة للاستشارات
www.manaraa.com

Appendix B-4 Ball's Closed-From Solution for *n* = 40

Appendix B -4. BALL'S CLOSED-FORM SOLUTION TO COLD-EXPANDED HOLES APPLIED TO PICK TOOL SPECIMENS n = 40

A. Constants Defined

constants chosen to attempt to match Ball's result in Fig 6

yield stress is 319 MPa (46.3 ksi), E= 207 GPa (30,000 ksi) $ksi := 1000 \cdot psi$

Poisson's ratio ν elastic $\nu e := .3($

plastic $\nu p := 0.5$

$\sigma yield := 46.3 \cdot ksi$

n is strain hardening exponent from measured stress-strain curve, it appears that 10<n<17 $n := 4($

$E := 30000 \cdot ksi$

Bauschinger parameter β is a measure of the change yield stress from reverse yielding

$\beta := 1$ β = 1 implies kinematic strain hardening rule while β =0 results in an isotropic model

R is used to model implicitly the degree of plastic anisotropy and is defined as the ratio of in-plane transverse plastic strain to through thickness plastic strain $R := 1$

Constants used in calculations

$$\mu := \frac{n+1+2\cdot R}{n^2+1+2\cdot R} \qquad \mu = 0.027$$

$$\gamma := \frac{n\cdot(1+R)}{n^2+1+2\cdot R} \qquad \gamma = 0.05$$

Constants defined to make equations fit on single page

$$A := (n-1)\cdot\sqrt{1+2\cdot R} \qquad A = 67.55$$

$$B := n+1+2\cdot R \qquad B = 43$$

$$C := n^2+1+2\cdot R \qquad C = 1.603\times 10^3$$

$$D := \left(n^2-1\right)\cdot\sqrt{1+2\cdot R} \qquad D = 2.77\times 10^3$$

B. Result at the end of Cold Expansion

Note: L is used to denote the cold expansion loading

1. Determination of α ***aL for*** $^{P}/_{\sigma\ yield}$

α a is the parameterization variable and can vary between π /2 to α max

define α aL

$$\alpha maxL := atan\left[-\frac{(n+1+2\cdot R)}{(n-1)\cdot\sqrt{1+2\cdot R}}\right] \qquad \alpha maxL = -32.479\cdot deg$$

has to be in the 2nd quadrant $\alpha maxL := \alpha maxL + 180\cdot deg$

المنارة للاستشارات
www.manaraa.com

Define α_{bL} which ranges from 90 deg to α_{maxL}

$i := 1..16$

$$\alpha := \begin{pmatrix} 147.21 \\ 144 \\ 140 \\ 136 \\ 133 \\ 130 \\ 127 \\ 124 \\ 121 \\ 118 \\ 115 \\ 112 \\ 109 \\ 106 \\ 103 \\ 90 \end{pmatrix} \cdot deg$$

$\alpha maxL = 147.521 \cdot deg$

$\alpha =$ (· rad)

	1
1	2.569
2	2.513
3	2.443
4	2.374
5	2.321
6	2.269
7	2.217
8	2.164
9	2.112
10	2.059
11	2.007
12	1.955
13	1.902
14	1.85
15	1.798
16	1.571

Determine the ratio of the pressure to the effective stress. The effective stress during loading is equal to yield stress. Let α aL be the value of α at the edge of the hole during loading. Use n=40 and vary the pressure to obtain the maximum elastic-plastic radius.

$$P\sigma y L_i := \sqrt{\frac{1+R}{2}} \cdot \left(\frac{\sin(\alpha_i)}{\sqrt{1+2 \cdot R}} - \cos(\alpha_i) \right) \cdot \left(\frac{A}{A \cdot \sin(\alpha_i) + B \cdot \cos(\alpha_i)} \right)^{\mu} \cdot e^{\left(\frac{A}{C}\right) \cdot \left(\alpha_i - \frac{\pi}{2} \cdot rad\right)}$$

Solve for α aL. α aL is the value of α at the edge of the hole while α = 90 deg at the elastic-plastic boundary. Use the root function from Mathcad to solve the above equation fordifferent values of Pσ yL until the elastic plastic boundary = 2.2

$$\text{Function}(\alpha cL) := \sqrt{\frac{1+R}{2}} \cdot \left(\frac{\sin(\alpha cL)}{\sqrt{1+2 \cdot R}} - \cos(\alpha cL) \right) \cdot \left(\frac{A}{A \cdot \sin(\alpha cL) \ldots + B \cdot \cos(\alpha cL)} \right)^{\mu} \cdot e^{\left(\frac{A}{C}\right) \cdot \left(\alpha cL rad - \frac{\pi}{2} rad\right)} - 1.2179$$

$\alpha aL := \text{root}(\text{Function}(\alpha cL), \alpha cL, 1.57 \cdot rad, 2.4 \cdot rad)$ $\qquad \alpha aL = 2.399996 \qquad \alpha aL = 137.51 \cdot deg$

2. Calculate the radius of the elastic-plastic interface

Ratio of the radius of the elastic-plastic interface to radius of the hole is b_1/a in Ball. Labeled B1L in the following calculation and is only a function of α_a.

$$B1L := \sqrt{\sin(\alpha aL)} \cdot \left(\frac{A}{A \cdot \sin(\alpha aL) + B \cdot \cos(\alpha aL)} \right)^{\gamma} \cdot e^{\left(\frac{D}{2 \cdot C}\right) \cdot \left(\alpha aL - \frac{\pi}{2} \cdot rad\right)} \qquad B1L = 1.82024$$

www.manaraa.com

Use P/σ y = 1.218

actual mesured radius for the elastic-plastic boundary was from ~2.5 to ~3; but may have incresed by the ultrasonic vibration

3. Calculate r/a as a function of α as $\pi/2 < \alpha < \alpha_{aL}$

r/a in calcs as raL

r/a = 1- initial edge of the hole

$i := 1..22$

$$\alpha L := \begin{pmatrix} 137.51 \\ 135 \\ 133 \\ 131 \\ 129 \\ 127 \\ 125 \\ 123 \\ 121 \\ 119 \\ 117 \\ 115 \\ 113 \\ 111 \\ 109 \\ 107 \\ 105 \\ 102 \\ 99 \\ 96 \\ 93 \\ 90 \end{pmatrix} \cdot deg \qquad \alpha L_i = \begin{array}{|c|} \hline 2.4 \\ \hline 2.356 \\ \hline 2.321 \\ \hline 2.286 \\ \hline 2.251 \\ \hline 2.217 \\ \hline 2.182 \\ \hline 2.147 \\ \hline 2.112 \\ \hline 2.077 \\ \hline 2.042 \\ \hline 2.007 \\ \hline 1.972 \\ \hline 1.937 \\ \hline 1.902 \\ \hline 1.868 \\ \hline 1.833 \\ \hline 1.78 \\ \hline 1.728 \\ \hline 1.676 \\ \hline 1.623 \\ \hline 1.571 \\ \hline \end{array} \cdot rad$$

r/a =1.82024 - the radius of the elastic-plastic boundary

$$rpL_i := \sqrt{\frac{\sin(\alpha aL)}{\sin(\alpha L_i)}} \cdot \left(\frac{A \cdot \sin(\alpha L_i) + B \cdot \cos(\alpha L_i)}{A \cdot \sin(\alpha aL) + B \cdot \cos(\alpha aL)} \right)^{\gamma} \cdot e^{\left(\frac{D}{2 \cdot C}\right) \cdot (\alpha aL - \alpha L_i)}$$

edge of the hole

α = 2.4 rad (137.51 deg)

www.manaraa.com

rpL =

	1
1	1
2	1.026
3	1.048
4	1.07
5	1.092
6	1.116
7	1.141
8	1.166
9	1.193
10	1.222
11	1.251
12	1.282
13	1.315
14	1.349
15	1.385
16	1.422
17	1.461
18	1.523
19	1.59
20	1.661
21	1.738
22	1.82

elastic-plastic boundary
α = 1.571 rad (90 deg)

المنارة للاستشارات
www.manaraa.com

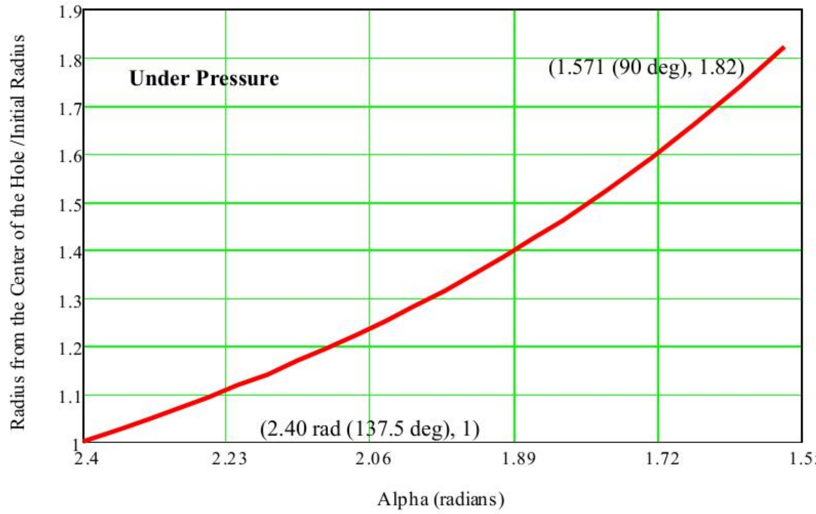

Fig. 1 Radius from the Center of the Hole Versus Parameterization Angle Alpha

4. Calculate ratio of effective stress / yield stress as a function of α

Ratio of effective stress / yield stress labeled Rσ eL in calculations

$$R\sigma eL_i := \left(\frac{A}{A \cdot \sin(\alpha L_i) + B \cdot \cos(\alpha L_i)}\right)^{\mu} \cdot e^{\left(\frac{A}{C}\right)\cdot\left(\alpha L_i - \frac{\pi}{2}\cdot rad\right)}$$

المنارة للاستشارات
www.manaraa.com

$R\sigma L_i =$

	1
1	1.08
2	1.072
3	1.066
4	1.061
5	1.056
6	1.052
7	1.048
8	1.044
9	1.041
10	1.037
11	1.034
12	1.031
13	1.028
14	1.025
15	1.022
16	1.02
17	1.017
18	1.013
19	1.01
20	1.006
21	1.003
22	1

α = 2.40 rad (137.5 deg), r/a = 1

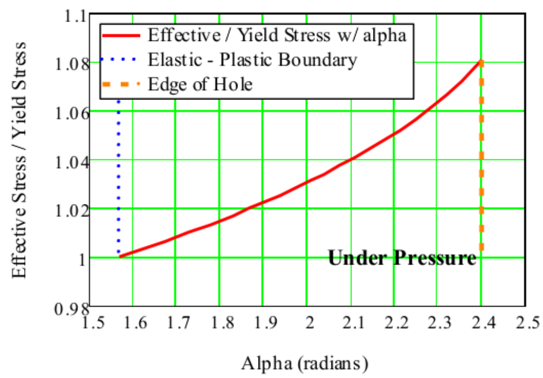

Fig 2. Normalized Effective Stress vs Alpha

α = 1.571 (90 deg),
r/a =1.82024

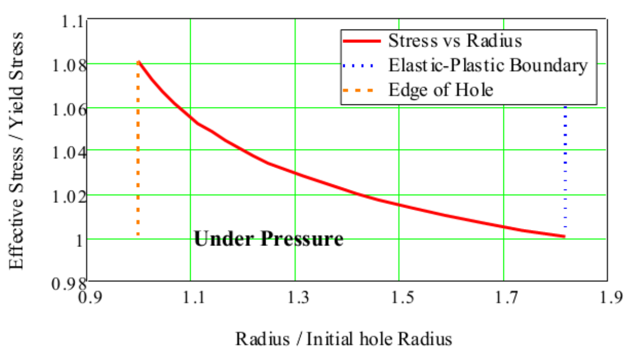

Fig 3. Normalized Effective Stress vs Normalized Radius

www.manaraa.com

5. Calculate ratio of tangential and radial plastic stress in the plastic region between the edge of the hole and the elastic-plastic boundary

Let ratio for tangential plastic stress to yield stress be SptL and and ratio for plastic radial stress to yield stress be SprL and both are functions of ratio of effective stress to yield stress (Rσ e) and α

$$SptL_i := \frac{R\sigma eL_i}{2} \cdot \sqrt{2 + 2 \cdot R} \cdot \left(\cos\left(\alpha L_i\right) + \frac{1}{\sqrt{1 + 2 \cdot R}} \cdot \sin\left(\alpha L_i\right) \right) \qquad q := -2..\,.1.6$$

$$SprL_i := \frac{R\sigma eL_i}{2} \cdot \sqrt{2 + 2 \cdot R} \cdot \left(\cos\left(\alpha L_i\right) - \frac{1}{\sqrt{1 + 2 \cdot R}} \cdot \sin\left(\alpha L_i\right) \right)$$

SptL =

	1
1	-0.375
2	-0.32
3	-0.277
4	-0.234
5	-0.191
6	-0.148
7	-0.105
8	-0.063
9	-0.021
10	0.021
11	0.062
12	0.104
13	0.145
14	0.185
15	0.225
16	0.265
17	0.304
18	0.362
19	0.418
20	0.473
21	0.526
22	0.577

SprL =

	1
1	-1.218
2	-1.196
3	-1.177
4	-1.159
5	-1.139
6	-1.118
7	-1.097
8	-1.074
9	-1.051
10	-1.027
11	-1.001
12	-0.975
13	-0.948
14	-0.92
15	-0.891
16	-0.861
17	-0.83
18	-0.783
19	-0.734
20	-0.683
21	-0.631
22	-0.577

6. Calculate ratio of elastic tangential to yield stress and ratio of elastic radial stresses to yield stress

Use SetL for the ratio of elastic tangential to yield stress and SerL for the ratio of elastic radial stress to yield stress

www.manaraa.com

$B1L = 1.82$ $a := 1.820, 2.07 .. 6.070$ $j := 1 .. 17$

$reL_1 := 1.820$

$reL_{j+1} := reL_j + 0.25$

$j := 1 .. 18$

$$SetL_j := \sqrt{\frac{1 + R}{2(1 + 2 \cdot R)}} \cdot \left(\frac{B1L}{reL_j}\right)^2$$

$SerL := -SetL$

reL =

	1
1	1.82
2	2.07
3	2.32
4	2.57
5	2.82
6	3.07
7	3.32
8	3.57
9	3.82
10	4.07
11	4.32
12	4.57
13	4.82
14	5.07
15	5.32
16	5.57
17	5.82
18	6.07

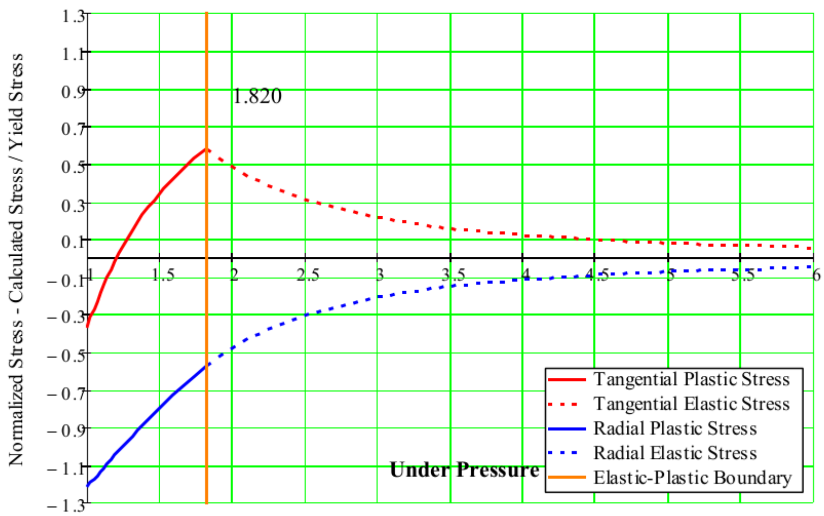

Normalized Distance from the Center of the Hole - Radius / Initial Radius

Fig 4. Radial and Tangential Stresses Adjacent to Expanded Hole Under Pressure

المنارة للاستشارات
www.manaraa.com

7. Combine into 1 matrix of distance and 1 each for Tangential and Radial Stress

$RAL_i := rpL_i \quad RAL_{j+22} := reL_j \qquad TSL_i := SptL_i \quad TSL_{j+22} := SetL_j \qquad RSL_i := SprL_i \qquad RSL_{j+22} := SerL_j$

RAL =

	1
1	1
2	1.026
3	1.048
4	1.07
5	1.092
6	1.116
7	1.141
8	1.166
9	1.193
10	1.222
11	1.251
12	1.282
13	1.315
14	1.349
15	1.385
16	...

TSL =

	1
1	-0.375
2	-0.32
3	-0.277
4	-0.234
5	-0.191
6	-0.148
7	-0.105
8	-0.063
9	-0.021
10	0.021
11	0.062
12	0.104
13	0.145
14	0.185
15	0.225
16	...

RSL =

	1
1	-1.218
2	-1.196
3	-1.177
4	-1.159
5	-1.139
6	-1.118
7	-1.097
8	-1.074
9	-1.051
10	-1.027
11	-1.001
12	-0.975
13	-0.948
14	-0.92
15	-0.891
16	...

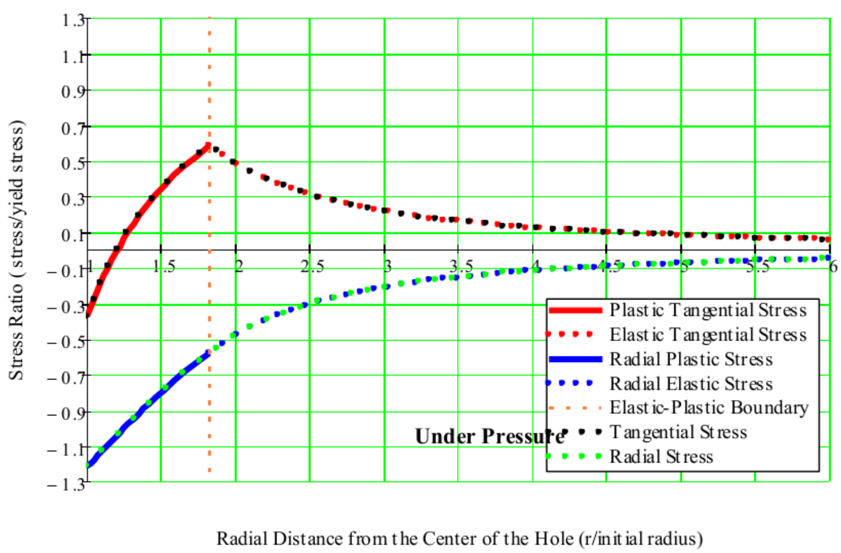

Fig 5. Tangential and Radial Stress Under Pressure

المنارة للاستشارات
www.manaraa.com

C. Results after removal of expansion

1. Constants defined

β is Bauschinger's parameter and is a measure of the reduction in yield stress in compression due to strain be yield strain in tension. $\beta = 0$ is for isotropic behavior while $\beta = 1$ implies kinematic hardening

Note: U is used to denote the unloading phase

from Section 1 expansion calculation, use $\sigma_{yield} = 46.3$ ksi and $P/\sigma_{yield} = 1.218$

$P := 1.21799 \cdot \sigma yield \qquad P = 56.393 \cdot ksi$

2. Determination of new α_a *(α_{aU})*

α_{aU} is the parameterization variable and can vary between $\pi/2$ to α max. α_{aU} is for the region in the plastic

annulus in which the unloading causes reverse yielding. α_{aU} is new value at the edge of the hole while

$\alpha = 90deg$ is the value at the new elastic-plastic boundary. α max as determine above.

new yield stress σ_{o2}

$P\sigma$ yL is ratio of the pressure/new yield stress and varies with α_b where α_b is α bL from the original calculation for the plastic region in 2 above

Using $\beta = 1 \qquad \sigma o2 := (1+\beta)\cdot \sigma yield + (1-\beta)\cdot \sigma yield \qquad \sigma o2 = 92.6 \cdot ksi$

$i := 1..14 \qquad \frac{P}{\sigma o2} = 0.609$

$$P\sigma yU_i := \sqrt{\frac{1+R}{2}} \cdot \left(\frac{\sin(\alpha L_i)}{\sqrt{1+2\cdot R}} - \cos(\alpha L_i) \right) \cdot \left(\frac{A}{A\cdot \sin(\alpha L_i) + B\cdot \cos(\alpha L_i)} \right)^{\mu} \cdot e^{\left(\frac{A}{C}\right)\cdot\left(\alpha L_i - \frac{\pi}{2} rad\right)}$$

Solve for α aU. α aU is the value of α at the edge of the hole while $\alpha = 90$ deg at the elastic-plastic boundary. Use the root function from Mathcad to solve the above equation for $P\sigma$ yL = .609.

$$\text{Function}(\alpha bL) := \sqrt{\frac{1+R}{2}} \cdot \left(\frac{\sin(\alpha bL)}{\sqrt{1+2\cdot R}} - \cos(\alpha bL) \right) \cdot \left(\frac{A}{A\cdot \sin(\alpha bL) \ ... + B\cdot \cos(\alpha bL)} \right)^{\mu} \cdot e^{\left(\frac{A}{C}\right)\cdot\left(\alpha bL - \frac{\pi}{2} rad\right)} - \frac{P}{\sigma o2}$$

$\alpha aU := \text{root}(\text{Function}(\alpha bL), \alpha bL, 1.57 \cdot rad, 2.5 \cdot rad) \qquad \alpha aU = 1.601599 \qquad \alpha aU = 91.76486 \cdot deg$

المنارة للاستشارات
www.manaraa.com

3. Calculate the radius of the region experiencing reverse yielding after unloading

Ratio of the radius of material experiencing reverse yielding to hole radius is b_2/a. Labeled B2U in the following calculation and is only a function of new α_{aU}. γ from Section 1 CONSTANTS above.

$$B2U := \sqrt{\sin(\alpha aU)} \cdot \left(\frac{A}{A \cdot \sin(\alpha aU) + B \cdot \cos(\alpha aU)} \right)^{\gamma} \cdot e^{\left(\frac{D}{2 \cdot C}\right) \cdot \left(\alpha aU - \frac{\pi}{2} \cdot rad\right)}$$

$$B2U = 1.02776$$

4. Calculate r/a as a function of new α as π /2 < α < α aU.

$k := 1 .. 9$

$$\alpha U := \begin{pmatrix} 91.76486 \\ 91.75 \\ 91.5 \\ 91.25 \\ 91 \\ 90.75 \\ 90.5 \\ 90.25 \\ 90 \end{pmatrix} \cdot deg \qquad \alpha U_k = \begin{array}{|c|} \hline 1.602 \\ \hline 1.601 \\ \hline 1.597 \\ \hline 1.593 \\ \hline 1.588 \\ \hline 1.584 \\ \hline 1.58 \\ \hline 1.575 \\ \hline 1.571 \\ \hline \end{array} \cdot rad$$

edge of the hole

elastic-plastic boundary on unloading

r/a for unloading as in calcs as labeled - rb

$$rpU_k := \sqrt{\frac{\sin(\alpha aU)}{\sin(\alpha U_k)}} \cdot \left(\frac{A \cdot \sin(\alpha U_k) + B \cdot \cos(\alpha U_k)}{A \cdot \sin(\alpha aU) + B \cdot \cos(\alpha aU)} \right)^{\gamma} \cdot e^{\left(\frac{D}{2 \cdot C}\right) \cdot (\alpha aU - \alpha U_k)}$$

$$rpU = \begin{pmatrix} 1 \\ 1.000229 \\ 1.0040922 \\ 1.0079785 \\ 1.0118881 \\ 1.0158212 \\ 1.0197779 \\ 1.0237584 \\ 1.0277628 \end{pmatrix}$$

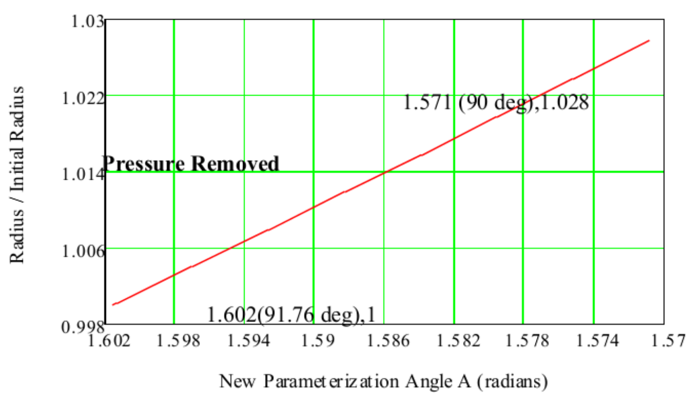

$$rpU_9 = 1.0277628$$

Fig 6. Radius versus Alpha for Unloading

www.manaraa.com

5. *Calculate ratio of effective stress / new yield stress as a function of α*

Ratio of effective stress / yield stress. Ratio labeled Rσ eU in calculations

$$R\sigma eU_k := -\left[\left(\frac{A}{A \cdot \sin\left(\alpha U_k\right) + B \cdot \cos\left(\alpha U_k\right)}\right)^{\mu} \cdot e^{\left(\frac{A}{C}\right)\cdot\left(\alpha U_k - \frac{\pi}{2} \mathrm{rad}\right)}\right]$$

α = 1.602 (91.76 deg),rb=1 edge of hole

√

$R\sigma eU_k =$

-1.00184
-1.00183
-1.00156
-1.0013
-1.00104
-1.00078
-1.00052
-1.00026
-1

α = 1.571 (90 deg),
rb = 1.028

elastic-plastic boundary on unloading

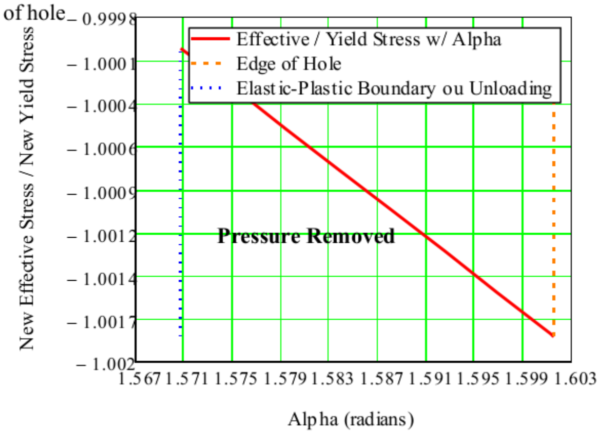

Fig 7. Normalized Effective Stress vs Alpha

www.manaraa.com

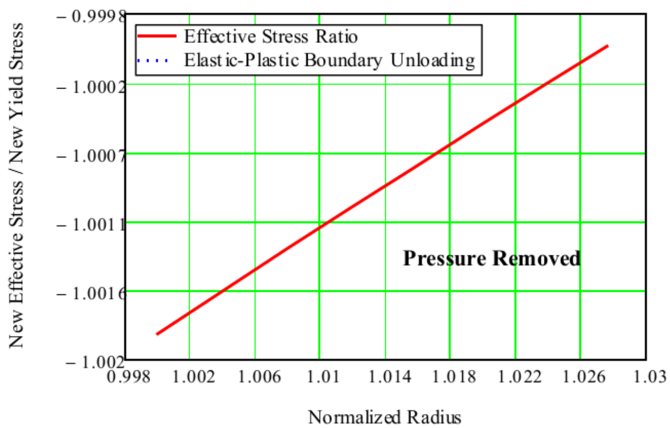

Fig 8. Normalized Effective Stress vs Normalized Radius

6. Calculate ratio of tangential and radial plastic stress

Let ratio for tangential plastic stress to yield stress be SptU and and ratio for plastic radial stress to yield stress be SprU and both are functions of ratio of new effective stress to new yield stress (Rσ eU) and α U

$$SptU_k := 2\left[\frac{R\sigma eU_k}{2}\cdot\sqrt{2+2\cdot R}\cdot\left(\cos\left(\alpha U_k\right)+\frac{1}{\sqrt{1+2\cdot R}}\cdot\sin\left(\alpha U_k\right)\right)\right]$$

$$SprU_k := 2\cdot\left[\frac{R\sigma eU_k}{2}\cdot\sqrt{2+2\cdot R}\cdot\left(\cos\left(\alpha U_k\right)-\frac{1}{\sqrt{1+2\cdot R}}\cdot\sin\left(\alpha U_k\right)\right)\right]$$

$$SptU = \begin{pmatrix}-1.095\\-1.095\\-1.104\\-1.112\\-1.121\\-1.129\\-1.138\\-1.146\\-1.155\end{pmatrix} \qquad SprU = \begin{pmatrix}1.218\\1.217\\1.209\\1.2\\1.191\\1.182\\1.173\\1.164\\1.155\end{pmatrix}$$

q is to plot elastic-plastic boundary

$$q := -2..2$$

www.manaraa.com

7. Calculate ratio of the change in elastic tangential to yield stress due to unloading and the ratio of the change in elastic radial stresses to yield stress from unloading

Use 'Setu' for the ratio of the change in elastic tangential to yield stress and 'Seru' for the ratio of elastic radial stress to yield stress

$B2U = 1.028$ $\quad a := 1.02776, 1.27776 .. 6.0277$ $\quad j := 1 .. 21$ $\quad J_j := j$ $\quad reU_j := B2U + 0.25 \cdot J_j - 0.2$

$j =$

	1
1	1
2	2
3	3
4	4
5	5
6	6
7	7
8	8
9	9
10	10
11	11
12	12
13	13
14	14
15	15
16	16
17	17
18	18
19	19
20	20
21	21

$J =$

	1
1	1
2	2
3	3
4	4
5	5
6	6
7	7
8	8
9	9
10	10
11	11
12	12
13	13
14	14
15	15
16	16
17	17
18	18
19	19
20	20
21	21

$a =$

	1
1	1.028
2	1.278
3	1.528
4	1.778
5	2.028
6	2.278
7	2.528
8	2.778
9	3.028
10	3.278
11	3.528
12	3.778
13	4.028
14	4.278
15	4.528
16	4.778
17	5.028
18	5.278
19	5.528
20	5.778
21	6.028

$reU_j =$

	1
1	1.028
2	1.278
3	1.528
4	1.778
5	2.028
6	2.278
7	2.528
8	2.778
9	3.028
10	3.278
11	3.528
12	3.778
13	4.028
14	4.278
15	4.528
16	4.778
17	5.028
18	5.278
19	5.528
20	5.778
21	6.028

$$SerU_j := 2 \cdot \left[\sqrt{\frac{1 + R}{2(1 + 2 \cdot R)}} \cdot \left(\frac{B2U}{reU_j} \right)^2 \right]$$

$$SetU_j := -SerU_j$$

www.manaraa.com

SerU =

	1
1	1.155
2	0.747
3	0.523
4	0.386
5	0.297
6	0.235
7	0.191
8	0.158
9	0.133
10	0.114
11	0.098
12	0.085
13	0.075
14	0.067
15	0.059
16	0.053
17	0.048
18	0.044
19	0.04
20	0.037
21	0.034

SetU =

	1
1	-1.155
2	-0.747
3	-0.523
4	-0.386
5	-0.297
6	-0.235
7	-0.191
8	-0.158
9	-0.133
10	-0.114
11	-0.098
12	-0.085
13	-0.075
14	-0.067
15	-0.059
16	-0.053
17	-0.048
18	-0.044
19	-0.04
20	-0.037
21	-0.034

Plot Δ stress from unloading

$i := 1..22$

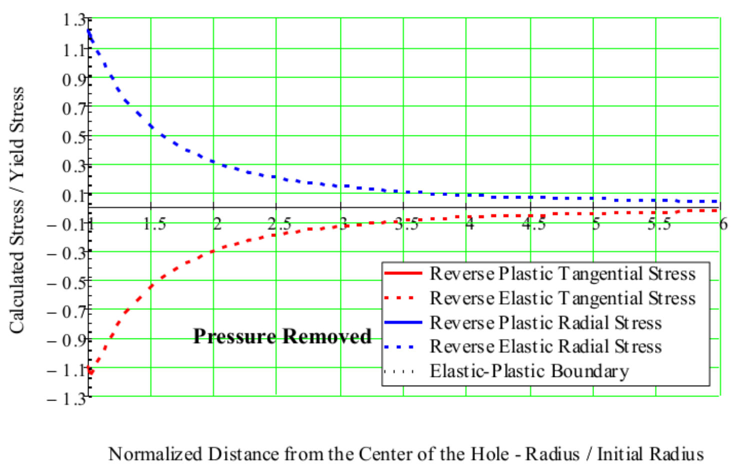

Fig 9. Changes in Radial and Tangential Stress due to Unloading

www.manaraa.com

8. Combine into 1 matrix of distance and 1 each for Tangential and Radial Stress

$rpL =$

	1
1	1
2	1.026
3	1.048
4	1.07
5	1.092
6	1.116
7	1.141
8	1.166
9	1.193
10	1.222
11	1.251
12	1.282
13	1.315
14	1.349
15	1.385
16	1.422
17	1.461
18	1.523
19	1.59
20	1.661
21	1.738
22	1.82

$$rpU = \begin{pmatrix} 1 \\ 1.000229 \\ 1.004092 \\ 1.007978 \\ 1.011888 \\ 1.015821 \\ 1.019778 \\ 1.023758 \\ 1.027763 \end{pmatrix}$$

$reU =$

	1
1	1.028
2	1.278
3	1.528
4	1.778
5	2.028
6	2.278
7	2.528
8	2.778
9	3.028
10	3.278
11	3.528
12	3.778
13	4.028
14	4.278
15	4.528
16	4.778
17	5.028
18	5.278
19	5.528
20	5.778
21	6.028

$$RAU_k := rpU_k$$

$$RAU_{j+8} := reU_j$$

$$TSU_k := SptU_k$$

$$TSU_{j+8} := SetU_j$$

$$RSU_k := SprU_k$$

$$RSU_{j+8} := SerU_j$$

www.manaraa.com

RAU =

	1
1	1
2	1.000229
3	1.004092
4	1.007978
5	1.011888
6	1.015821
7	1.019778
8	1.023758
9	1.027763
10	1.277763
11	1.527763
12	1.777763
13	2.027763
14	2.277763
15	2.527763
16	2.777763
17	3.027763
18	3.277763
19	3.527763
20	3.777763
21	4.027763
22	4.277763
23	4.527763
24	4.777763
25	5.027763
26	5.277763
27	5.527763
28	5.777763
29	6.027763

TSU =

	1
1	-1.095
2	-1.095
3	-1.104
4	-1.112
5	-1.121
6	-1.129
7	-1.138
8	-1.146
9	-1.155
10	-0.747
11	-0.523
12	-0.386
13	-0.297
14	-0.235
15	-0.191
16	-0.158
17	-0.133
18	-0.114
19	-0.098
20	-0.085
21	-0.075
22	-0.067
23	-0.059
24	-0.053
25	-0.048
26	-0.044
27	-0.04
28	-0.037
29	-0.034

RSU =

	1
1	1.218
2	1.217
3	1.209
4	1.2
5	1.191
6	1.182
7	1.173
8	1.164
9	1.155
10	0.747
11	0.523
12	0.386
13	0.297
14	0.235
15	0.191
16	0.158
17	0.133
18	0.114
19	0.098
20	0.085
21	0.075
22	0.067
23	0.059
24	0.053
25	0.048
26	0.044
27	0.04
28	0.037
29	0.034

$z := 1..29$

المنارة للاستشارات
www.manaraa.com

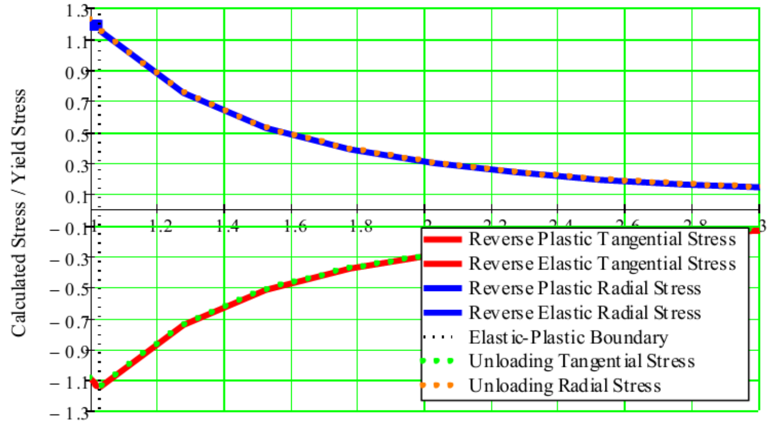

Normalized Distance from the Center of the Hole - Radius / Initial Radius

Fig 10. Changes in Radial and Tangential Stress due to Unloading

9. Plot combined matrices of distance and Tangential and Radial Stress

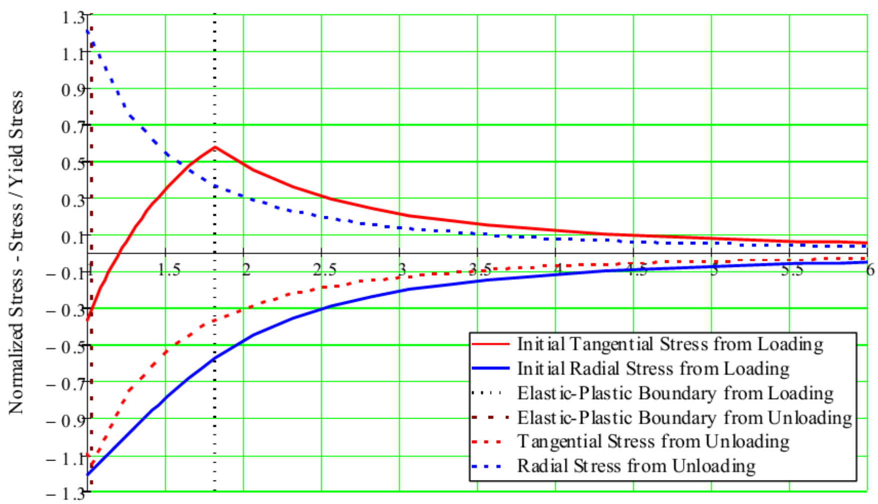

Normalized Distance from the Center of the Hole - r/r1

Fig 11. Stresses from Expansion Pressure and from Removing the Expansion Pressure

www.manaraa.com

D. Combine Results 2 and 3 to Obtain Residual Stress

Revise calculations to determine results for 3 separate regions

1. Region 1 from edge of hole to elastic-plastic boundary from unloading
   ra = 1 to ra =1.0278
2. From elastic-boundary from unloading to the elastic-plastic boundary from loading
   ra = 1.0278 to ra = 1.820
3. From elastic-plastic boundary (ra=1.820) from loading to infinite ~ ra = 6

1. For Region 1 where 0< r/a < 1.0278

Calculate the alpha angle for the loading stress in this region between r/a =1 and r/a = 1.174 at the same interval as was done for the unloading step

$\alpha aL = 2.399996$ r/a for the unloading step

$raR1 := rpU$

$$rpU = \begin{pmatrix} 1 \\ 1.000229 \\ 1.004092 \\ 1.007978 \\ 1.011888 \\ 1.015821 \\ 1.019778 \\ 1.023758 \\ 1.027763 \end{pmatrix} \qquad raR1 = \begin{pmatrix} 1 \\ 1.00023 \\ 1.00409 \\ 1.00798 \\ 1.01189 \\ 1.01582 \\ 1.01978 \\ 1.02376 \\ 1.02776 \end{pmatrix}$$

Radius 1

$$\text{function}(\alpha) := \sqrt{\frac{\sin(\alpha aL)}{\sin(\alpha)}} \cdot \left[\frac{(n-1)\cdot\sqrt{1+2\cdot R}\cdot\sin(\alpha)\ ... \\ +(n+1+2\cdot R)\cdot\cos(\alpha)}{(n-1)\cdot\sqrt{1+2\cdot R}\cdot\sin(\alpha aL)\ ... \\ +(n+1+2\cdot R)\cdot\cos(\alpha aL)}\right]^{\gamma} \cdot e^{\left[\frac{\left(n^2-1\right)\cdot\sqrt{1+2\cdot R}}{2\cdot\left(n^2+1+2\cdot R\right)}\right]\cdot(\alpha aL-\alpha)} - raR1_1$$

$\alpha 1R_1 := \text{root}(\text{function}(\alpha), \alpha, 1.57\cdot \text{rad}, 2.5\cdot \text{rad})$ $\qquad \alpha 1R_1 = 137.51\cdot \text{deg}$ $\qquad \alpha 1R_1 = 2.40000$

Radius 2

$$\text{function}(\alpha) := \sqrt{\frac{\sin(\alpha aL)}{\sin(\alpha)}} \cdot \left[\frac{(n-1)\cdot\sqrt{1+2\cdot R}\cdot\sin(\alpha)\ ... \\ +(n+1+2\cdot R)\cdot\cos(\alpha)}{(n-1)\cdot\sqrt{1+2\cdot R}\cdot\sin(\alpha aL)\ ... \\ +(n+1+2\cdot R)\cdot\cos(\alpha aL)}\right]^{\gamma} \cdot e^{\left[\frac{\left(n^2-1\right)\cdot\sqrt{1+2\cdot R}}{2\cdot\left(n^2+1+2\cdot R\right)}\right]\cdot(\alpha aL-\alpha)} - raR1_2$$

$\alpha 1R_2 := \text{root}(\text{function}(\alpha), \alpha, 2.1\cdot \text{rad}, 2.4\cdot \text{rad})$ $\qquad \alpha 1R_2 = 137.487\cdot \text{deg}$ $\qquad \alpha 1R_2 = 2.4$

Radius 3

$$\text{function}(\alpha) := \sqrt{\frac{\sin(\alpha aL)}{\sin(\alpha)}} \cdot \left[\frac{(n-1)\cdot\sqrt{1+2\cdot R}\cdot\sin(\alpha)\ ... \\ +(n+1+2\cdot R)\cdot\cos(\alpha)}{(n-1)\cdot\sqrt{1+2\cdot R}\cdot\sin(\alpha aL)\ ... \\ +(n+1+2\cdot R)\cdot\cos(\alpha aL)}\right]^{\gamma} \cdot e^{\left[\frac{\left(n^2-1\right)\cdot\sqrt{1+2\cdot R}}{2\cdot\left(n^2+1+2\cdot R\right)}\right]\cdot(\alpha aL-\alpha)} - raR1_3$$

المنارة للاستشارات
www.manaraa.com

$\alpha 1R_3 := \text{root}(\text{function}(\alpha), \alpha, 2.1 \cdot \text{rad}, 2.4 \cdot \text{rad})$ $\alpha 1R_3 = 137.119 \cdot \text{deg}$ $\alpha 1R_3 = 2.393$

Radius 4

$$\text{function}(\alpha) := \sqrt{\frac{\sin(\alpha aL)}{\sin(\alpha)}} \cdot \left[\frac{(n-1)\cdot\sqrt{1+2\cdot R}\cdot\sin(\alpha)\ ...\ +(n+1+2\cdot R)\cdot\cos(\alpha)}{(n-1)\cdot\sqrt{1+2\cdot R}\cdot\sin(\alpha aL)\ ...\ +(n+1+2\cdot R)\cdot\cos(\alpha aL)}\right]^{\gamma} \cdot e^{\left[\frac{(n^2-1)\cdot\sqrt{1+2\cdot R}}{2\cdot(n^2+1+2\cdot R)}\right]\cdot(\alpha aL-\alpha)} - raR1_4$$

$\alpha 1R_4 := \text{root}(\text{function}(\alpha), \alpha, 2.1 \cdot \text{rad}, 2.4 \cdot \text{rad})$ $\alpha 1R_4 = 136.748 \cdot \text{deg}$ $\alpha 1R_4 = 2.387$

Radius 5

$$\text{function}(\alpha) := \sqrt{\frac{\sin(\alpha aL)}{\sin(\alpha)}} \cdot \left[\frac{(n-1)\cdot\sqrt{1+2\cdot R}\cdot\sin(\alpha)\ ...\ +(n+1+2\cdot R)\cdot\cos(\alpha)}{(n-1)\cdot\sqrt{1+2\cdot R}\cdot\sin(\alpha aL)\ ...\ +(n+1+2\cdot R)\cdot\cos(\alpha aL)}\right]^{\gamma} \cdot e^{\left[\frac{(n^2-1)\cdot\sqrt{1+2\cdot R}}{2\cdot(n^2+1+2\cdot R)}\right]\cdot(\alpha aL-\alpha)} - raR1_5$$

$\alpha 1R_5 := \text{root}(\text{function}(\alpha), \alpha, 2.1 \cdot \text{rad}, 2.4 \cdot \text{rad})$ $\alpha 1R_5 = 136.374 \cdot \text{deg}$ $\alpha 1R_5 = 2.38$

Radius 6

$$\text{function}(\alpha) := \sqrt{\frac{\sin(\alpha aL)}{\sin(\alpha)}} \cdot \left[\frac{(n-1)\cdot\sqrt{1+2\cdot R}\cdot\sin(\alpha)\ ...\ +(n+1+2\cdot R)\cdot\cos(\alpha)}{(n-1)\cdot\sqrt{1+2\cdot R}\cdot\sin(\alpha aL)\ ...\ +(n+1+2\cdot R)\cdot\cos(\alpha aL)}\right]^{\gamma} \cdot e^{\left[\frac{(n^2-1)\cdot\sqrt{1+2\cdot R}}{2\cdot(n^2+1+2\cdot R)}\right]\cdot(\alpha aL-\alpha)} - raR1_6$$

$\alpha 1R_6 := \text{root}(\text{function}(\alpha), \alpha, 2.1 \cdot \text{rad}, 2.4 \cdot \text{rad})$ $\alpha 1R_6 = 135.998 \cdot \text{deg}$ $\alpha 1R_6 = 2.374$

Radius 7

$$\text{function}(\alpha) := \sqrt{\frac{\sin(\alpha aL)}{\sin(\alpha)}} \cdot \left[\frac{(n-1)\cdot\sqrt{1+2\cdot R}\cdot\sin(\alpha)\ ...\ +(n+1+2\cdot R)\cdot\cos(\alpha)}{(n-1)\cdot\sqrt{1+2\cdot R}\cdot\sin(\alpha aL)\ ...\ +(n+1+2\cdot R)\cdot\cos(\alpha aL)}\right]^{\gamma} \cdot e^{\left[\frac{(n^2-1)\cdot\sqrt{1+2\cdot R}}{2\cdot(n^2+1+2\cdot R)}\right]\cdot(\alpha aL-\alpha)} - raR1_7$$

$\alpha 1R_7 := \text{root}(\text{function}(\alpha), \alpha, 2.1 \cdot \text{rad}, 2.4 \cdot \text{rad})$ $\alpha 1R_7 = 135.621 \cdot \text{deg}$ $\alpha 1R_7 = 2.367$

Radius 8

$$\text{function}(\alpha) := \sqrt{\frac{\sin(\alpha aL)}{\sin(\alpha)}} \cdot \left[\frac{(n-1)\cdot\sqrt{1+2\cdot R}\cdot\sin(\alpha)\ ...\ +(n+1+2\cdot R)\cdot\cos(\alpha)}{(n-1)\cdot\sqrt{1+2\cdot R}\cdot\sin(\alpha aL)\ ...\ +(n+1+2\cdot R)\cdot\cos(\alpha aL)}\right]^{\gamma} \cdot e^{\left[\frac{(n^2-1)\cdot\sqrt{1+2\cdot R}}{2\cdot(n^2+1+2\cdot R)}\right]\cdot(\alpha aL-\alpha)} - raR1_8$$

$\alpha 1R_8 := \text{root}(\text{function}(\alpha), \alpha, 2.1 \cdot \text{rad}, 2.4 \cdot \text{rad})$ $\alpha 1R_8 = 135.242 \cdot \text{deg}$ $\alpha 1R_8 = 2.36$

المنارة للاستشارات
www.manaraa.com

Radius 9

$$\text{function}(\alpha) := \sqrt{\frac{\sin(\alpha L)}{\sin(\alpha)}}\cdot\left[\frac{(n-1)\cdot\sqrt{1+2\cdot R}\cdot\sin(\alpha)\ \ldots \\ +(n+1+2\cdot R)\cdot\cos(\alpha)}{(n-1)\cdot\sqrt{1+2\cdot R}\cdot\sin(\alpha L)\ \ldots \\ +(n+1+2\cdot R)\cdot\cos(\alpha L)}\right]^{\gamma}\cdot e^{\left[\frac{\left(n^2-1\right)\cdot\sqrt{1+2\cdot R}}{2\cdot\left(n^2+1+2\cdot R\right)}\right]\cdot(\alpha L-\alpha)} - raR1_9$$

$\alpha 1R_9 := \text{root}(\text{function}(\alpha), \alpha, 2.1\cdot \text{rad}, 2.5\cdot \text{rad})$ $\qquad \alpha 1R_9 = 134.862\cdot \text{deg}$ $\qquad \alpha 1R_9 = 2.354$

$\alpha L =$

	1
1	2.4
2	2.356
3	2.321
4	2.286
5	2.251
6	2.217
7	2.182
8	2.147
9	2.112
10	2.077
11	2.042
12	2.007
13	1.972
14	1.937
15	1.902
16	...

$\alpha L =$

	1
1	137.51
2	135
3	133
4	131
5	129
6	127
7	125
8	123
9	121
10	119
11	117
12	115
13	113
14	111
15	109
16	...

$\cdot$ deg

α for Loading at the same interval as Unloading between the edge of the hole and the elastic-plastic boundary in Unloading

$$\alpha 1R = \begin{pmatrix} 137.51 \\ 137.487 \\ 137.119 \\ 136.748 \\ 136.374 \\ 135.998 \\ 135.621 \\ 135.242 \\ 134.862 \end{pmatrix}\cdot \text{deg} \qquad \alpha 1R = \begin{pmatrix} 2.399995 \\ 2.399595 \\ 2.393178 \\ 2.386696 \\ 2.380175 \\ 2.373619 \\ 2.367034 \\ 2.360424 \\ 2.353790 \end{pmatrix}$$

looks reasonable

Calculate the ratio of effective stress / yield stress as function of α 1R. Ratio is Rσ eL1

$o := 1..9$

$$R\sigma eL1_o := \left(\frac{A}{A\cdot\sin\left(\alpha 1R_o\right)+B\cdot\cos\left(\alpha 1R_o\right)}\right)^{\mu}\cdot e^{\left(\frac{A}{C}\right)\cdot\left(\alpha 1R_o-\frac{\pi}{2}\cdot \text{rad}\right)}$$

$$R\sigma eL1 = \begin{pmatrix} 1.08 \\ 1.08 \\ 1.079 \\ 1.078 \\ 1.076 \\ 1.075 \\ 1.074 \\ 1.073 \\ 1.072 \end{pmatrix}$$

Calculate ratio of tangential and radial plastic stress in the plastic region between the edge of the hole and the elastic-plastic boundary

المنارة للاستشارات
www.manaraa.com

In the first region, let ratio for tangential plastic stress to yield stress be SptR1 and the ratio for plastic radial stress to yield stress be SprR1 and both are functions of ratio of effective stress to yield stress (Rσ r) and α 1R

$$SptLR1_o := \frac{R\sigma eL1_o}{2} \cdot \sqrt{2+2\cdot R} \cdot \left(\cos\left(\alpha 1R_o\right) + \frac{1}{\sqrt{1+2\cdot R}} \cdot \sin\left(\alpha 1R_o\right) \right)$$

$$SprLR1_o := \frac{R\sigma eL1_o}{2} \cdot \sqrt{2+2\cdot R} \cdot \left(\cos\left(\alpha 1R_o\right) - \frac{1}{\sqrt{1+2\cdot R}} \cdot \sin\left(\alpha 1R_o\right) \right)$$

$$SptLR1 = \begin{pmatrix} -0.375 \\ -0.375 \\ -0.367 \\ -0.359 \\ -0.35 \\ -0.342 \\ -0.334 \\ -0.326 \\ -0.317 \end{pmatrix} \qquad SprLR1 = \begin{pmatrix} -1.218 \\ -1.218 \\ -1.215 \\ -1.211 \\ -1.208 \\ -1.205 \\ -1.201 \\ -1.198 \\ -1.194 \end{pmatrix}$$

2. For Region 2, calculate the change in elastic stress from Unloading between r/a = 1.0277 and r/a = 1.82024 at the same locations as the plastic stress were calculated for Loading

Use radius from Loading between r=1 to r=1.82024, subtract the region between r=1 and r=1.02776. Then calculate the elastic Unloading stress in this region for the same radii as for Loading

المنارة للاستشارات

www.manaraa.com

rpL =

	1
1	1
2	1.026
3	1.048
4	1.07
5	1.092
6	1.116
7	1.141
8	1.166
9	1.193
10	1.222
11	1.251
12	1.282
13	1.315
14	1.349
15	1.385
16	1.422
17	1.461
18	1.523
19	1.59
20	1.661
21	1.738
22	1.82

$raR2_1 := 1.0277($

$m := 2..21 \qquad n := 1..21$

$raR2_m := rpL_{m+1}$

$$SerUR2_n := 2\sqrt{\frac{1+R}{2(1+2\cdot R)}\cdot\left(\frac{B2U}{raR2_n}\right)^2}$$

$SetUR2_n := -SerUR2_n$

raR2 =

	1
1	1.028
2	1.048
3	1.07
4	1.092
5	1.116
6	1.141
7	1.166
8	1.193
9	1.222
10	1.251
11	1.282
12	1.315
13	1.349
14	1.385
15	1.422
16	1.461
17	1.523
18	1.59
19	1.661
20	1.738
21	1.82

www.manaraa.com

3. For Region 3, calculate the change in elastic stress for Unloading between r/a = 1.8024 to r/a = 6.07 at the same loactions as the stresses were calculated for Loading

$p := 1..18$

$raR3 := reL$

$$SerUR3_p := 2\sqrt{\frac{1+R}{2(1+2\cdot R)}}\cdot\left(\frac{B2U}{raR3_p}\right)^2$$

$$SetUR3_p := -SerUR3_p$$

raR3 =

	1
1	1.82
2	2.07
3	2.32
4	2.57
5	2.82
6	3.07
7	3.32
8	3.57
9	3.82
10	4.07
11	4.32
12	4.57
13	4.82
14	5.07
15	5.32
16	5.57
17	5.82
18	6.07

SetUR3 =

	1
1	-0.368
2	-0.285
3	-0.227
4	-0.185
5	-0.153
6	-0.129
7	-0.111
8	-0.096
9	-0.084
10	-0.074
11	-0.065
12	-0.058
13	-0.053
14	-0.047
15	-0.043
16	-0.039
17	-0.036
18	-0.033

SerUR3 =

	1
1	0.368
2	0.285
3	0.227
4	0.185
5	0.153
6	0.129
7	0.111
8	0.096
9	0.084
10	0.074
11	0.065
12	0.058
13	0.053
14	0.047
15	0.043
16	0.039
17	0.036
18	0.033

Ensure intervals in the 3 Regions matching r/a intervals for computing stresses prior to adding

المنارة للاستشارات
www.manaraa.com

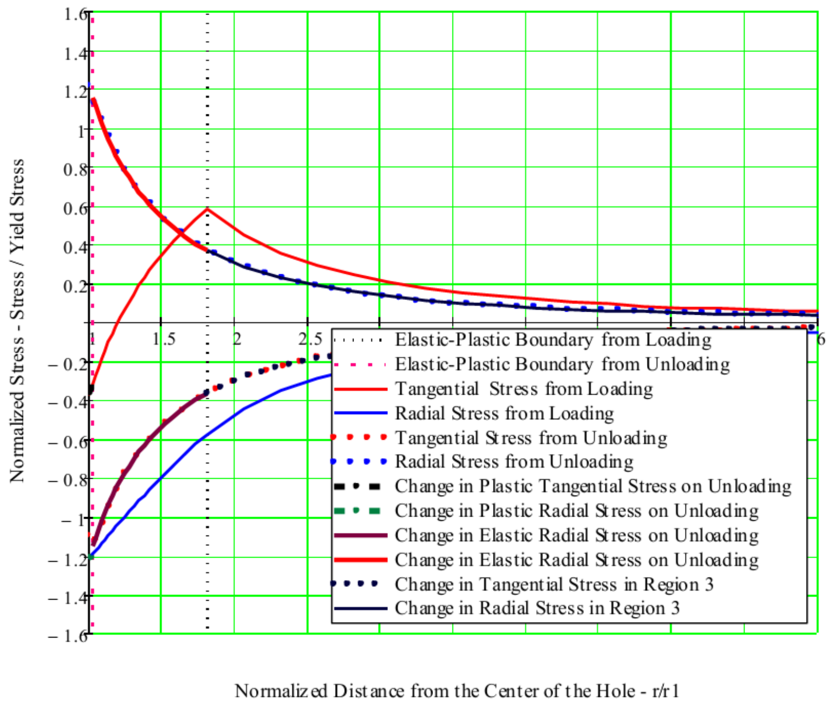

Fig 12. Check of Increments for Calculating Residual Stresses

4. For Region 1, calculate the residual stress between r/a = 1 to r/a = 1.024

$RStR1_o := SptU_o + SptLR1_o$

$RSrR1 := SprU + SprLR1$

$SptU_o =$

-1.095
-1.095
-1.104
-1.112
-1.121
-1.129
-1.138
-1.146
-1.155

$SptLR1_o =$

-0.375
-0.375
-0.367
-0.359
-0.35
-0.342
-0.334
-0.326
-0.317

$RStR1_o =$

-1.47
-1.47
-1.47
-1.471
-1.471
-1.471
-1.472
-1.472
-1.472

المنارة للاستشارات
www.manaraa.com

$raR1_o =$

1
1
1.004
1.008
1.012
1.016
1.02
1.024
1.028

$$SprU = \begin{pmatrix} 1.218 \\ 1.217 \\ 1.209 \\ 1.2 \\ 1.191 \\ 1.182 \\ 1.173 \\ 1.164 \\ 1.155 \end{pmatrix} \quad SprLR1 = \begin{pmatrix} -1.218 \\ -1.218 \\ -1.215 \\ -1.211 \\ -1.208 \\ -1.205 \\ -1.201 \\ -1.198 \\ -1.194 \end{pmatrix} \quad RSrR1 = \begin{pmatrix} 1.776\times 10^{-7} \\ -3.265\times 10^{-4} \\ -5.992\times 10^{-3} \\ -0.012 \\ -0.017 \\ -0.023 \\ -0.029 \\ -0.034 \\ -0.04 \end{pmatrix}$$

5. For Region 2, calculate the residual stress between r/a = 1.0278 to r/a = 1.8202

Loading Values of radius and tangential stress

$rpL =$

	1
1	1
2	1.02631
3	1.04762
4	1.06956
5	1.09229
6	1.11595
7	1.14065
8	1.16648
9	1.19349
10	1.22178
11	1.25139
12	1.28241
13	1.31489
14	1.34891
15	1.38454
16	1.42186
17	1.46094
18	1.52308
19	1.5897
20	1.66117
21	1.73787
22	1.82024

$SptL =$

	1
1	-0.375
2	-0.32
3	-0.277
4	-0.234
5	-0.191
6	-0.148
7	-0.105
8	-0.063
9	-0.021
10	0.021
11	0.062
12	0.104
13	0.145
14	0.185
15	0.225
16	0.265
17	0.304
18	0.362
19	0.418
20	0.473
21	0.526
22	0.577

Unloading values of radius and tangential stress at the same radius as the loading values from

$raR2 =$

	1
1	1.02776
2	1.04762
3	1.06956
4	1.09229
5	1.11595
6	1.14065
7	1.16648
8	1.19349
9	1.22178
10	1.25139
11	1.28241
12	1.31489
13	1.34891
14	1.38454
15	1.42186
16	1.46094
17	1.52308
18	1.5897
19	1.66117
20	1.73787
21	1.82024

$SetUR2 =$

	1
1	-1.155
2	-1.111
3	-1.066
4	-1.022
5	-0.979
6	-0.937
7	-0.896
8	-0.856
9	-0.817
10	-0.779
11	-0.742
12	-0.705
13	-0.67
14	-0.636
15	-0.603
16	-0.571
17	-0.526
18	-0.483
19	-0.442
20	-0.404
21	-0.368

$v := 2..21$

www.manaraa.com

$SptL2 =$

	1
1	-0.317
2	-0.277
3	-0.234
4	-0.191
5	-0.148
6	-0.105
7	-0.063
8	-0.021
9	0.021
10	0.062
11	0.104
12	0.145
13	0.185
14	0.225
15	0.265
16	0.304
17	0.362
18	0.418
19	0.473
20	0.526
21	0.577

$RStR2 =$

	1
1	-1.4721
2	-1.3883
3	-1.3
4	-1.2131
5	-1.1275
6	-1.0429
7	-0.9595
8	-0.8772
9	-0.7962
10	-0.7164
11	-0.6379
12	-0.5608
13	-0.4852
14	-0.411
15	-0.3384
16	-0.2675
17	-0.1642
18	-0.0648
19	0.0307
20	0.122
21	0.2092

$SprL2_1 := SprLR1_9$

$SprL2_v := SprL_{v+1}$

$RSrR2 := SerUR2 + SprL2$

$SptL2_1 := SptLR1_9$

$SptL2_v := SptL_{v+1}$

$RStR2 := SetUR2 + SptL2$

المنارة للاستشارات
www.manaraa.com

SprL =

	1
1	-1.218
2	-1.196
3	-1.177
4	-1.159
5	-1.139
6	-1.118
7	-1.097
8	-1.074
9	-1.051
10	-1.027
11	-1.001
12	-0.975
13	-0.948
14	-0.92
15	-0.891
16	-0.861
17	-0.83
18	-0.783
19	-0.734
20	-0.683
21	-0.631
22	-0.577

SprL2 =

	1
1	-1.194
2	-1.177
3	-1.159
4	-1.139
5	-1.118
6	-1.097
7	-1.074
8	-1.051
9	-1.027
10	-1.001
11	-0.975
12	-0.948
13	-0.92
14	-0.891
15	-0.861
16	-0.83
17	-0.783
18	-0.734
19	-0.683
20	-0.631
21	-0.577

SerUR2 =

	1
1	1.155
2	1.111
3	1.066
4	1.022
5	0.979
6	0.937
7	0.896
8	0.856
9	0.817
10	0.779
11	0.742
12	0.705
13	0.67
14	0.636
15	0.603
16	0.571
17	0.526
18	0.483
19	0.442
20	0.404
21	0.368

RSrR2 =

	1
1	-0.04
2	-0.066
3	-0.092
4	-0.117
5	-0.139
6	-0.159
7	-0.178
8	-0.195
9	-0.21
10	-0.223
11	-0.233
12	-0.243
13	-0.25
14	-0.255
15	-0.258
16	-0.259
17	-0.257
18	-0.251
19	-0.241
20	-0.227
21	-0.209

المنارة للاستشارات
www.manaraa.com

6. For Region 3, calculate the residual stress between r/a = 1.8202 to r/a = 6.07

Unloading radius

raR3 =

	1
1	1.82
2	2.07
3	2.32
4	2.57
5	2.82
6	3.07
7	3.32
8	3.57
9	3.82
10	4.07
11	4.32
12	4.57
13	4.82
14	5.07
15	5.32
16	5.57
17	5.82
18	6.07

reL =

	1
1	1.82
2	2.07
3	2.32
4	2.57
5	2.82
6	3.07
7	3.32
8	3.57
9	3.82
10	4.07
11	4.32
12	4.57
13	4.82
14	5.07
15	5.32
16	5.57
17	5.82
18	6.07

SetUR3 =

	1
1	-0.368
2	-0.285
3	-0.227
4	-0.185
5	-0.153
6	-0.129
7	-0.111
8	-0.096
9	-0.084
10	-0.074
11	-0.065
12	-0.058
13	-0.053
14	-0.047
15	-0.043
16	-0.039
17	-0.036
18	-0.033

SetL =

	1
1	0.578
2	0.446
3	0.355
4	0.29
5	0.241
6	0.203
7	0.174
8	0.15
9	0.131
10	0.115
11	0.103
12	0.092
13	0.082
14	0.074
15	0.068
16	0.062
17	0.056
18	0.052

RSetR3 := SetUR3 + SetL   RSerR3 := SerUR3 + SerL

المنارة للاستشارات
www.manaraa.com

RSetR3 =

	1
1	0.209
2	0.162
3	0.129
4	0.105
5	0.087
6	0.074
7	0.063
8	0.054
9	0.048
10	0.042
11	0.037
12	0.033
13	0.03
14	0.027
15	0.024
16	0.022
17	0.02
18	0.019

SerUR3 =

	1
1	0.368
2	0.285
3	0.227
4	0.185
5	0.153
6	0.129
7	0.111
8	0.096
9	0.084
10	0.074
11	0.065
12	0.058
13	0.053
14	0.047
15	0.043
16	0.039
17	0.036
18	0.033

SerL =

	1
1	-0.578
2	-0.446
3	-0.355
4	-0.29
5	-0.241
6	-0.203
7	-0.174
8	-0.15
9	-0.131
10	-0.115
11	-0.103
12	-0.092
13	-0.082
14	-0.074
15	-0.068
16	-0.062
17	-0.056
18	-0.052

RSerR3 =

	1
1	-0.209
2	-0.162
3	-0.129
4	-0.105
5	-0.087
6	-0.074
7	-0.063
8	-0.054
9	-0.048
10	-0.042
11	-0.037
12	-0.033
13	-0.03
14	-0.027
15	-0.024
16	-0.022
17	-0.02
18	-0.019

المنارة للاستشارات
www.manaraa.com

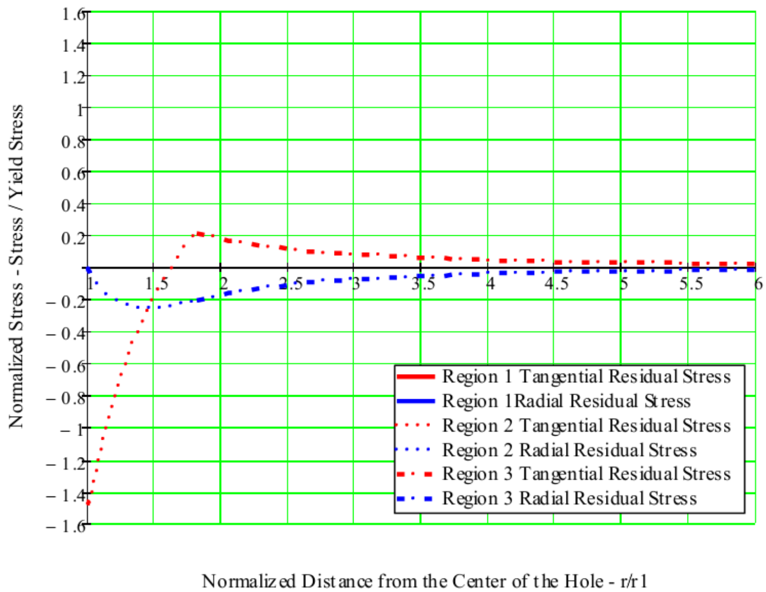

Fig 13. Residual Stresses

7. Combine into 1 matrix of radius and 1 matrix each of tangential and radial residual stress

المنارة للاستشارات
www.manaraa.com

$j := 1..9 \quad l := 2..18 \quad k := 2..21$

$RAR_j := raR1_j \qquad RAR_{k+8} := raR2_k$

$RAR_{l+28} := raR3_l$

$RSTC_j := RStR1_j$

$RSTC_{k+8} := RStR2_k$

$RSTC_{l+28} := RSetR3_l$

$$raR1 = \begin{pmatrix} 1 \\ 1.00023 \\ 1.00409 \\ 1.00798 \\ 1.01189 \\ 1.01582 \\ 1.01978 \\ 1.02376 \\ 1.02776 \end{pmatrix}$$

raR2 =

	1
1	1.028
2	1.048
3	1.07
4	1.092
5	1.116
6	1.141
7	1.166
8	1.193
9	1.222
10	1.251
11	1.282
12	1.315
13	1.349
14	1.385
15	1.422
16	...

raR3 =

	1
1	1.82
2	2.07
3	2.32
4	2.57
5	2.82
6	3.07
7	3.32
8	3.57
9	3.82
10	4.07
11	4.32
12	4.57
13	4.82
14	5.07
15	...

$$RStR1 = \begin{pmatrix} -1.46991 \\ -1.46991 \\ -1.47041 \\ -1.47082 \\ -1.47117 \\ -1.47147 \\ -1.47172 \\ -1.47192 \\ -1.47208 \end{pmatrix}$$

RStR2 =

	1
1	-1.472
2	-1.388
3	-1.3
4	-1.213
5	-1.127
6	-1.043
7	-0.96
8	-0.877
9	-0.796
10	...

RSetR3 =

	1
1	0.209
2	0.162
3	0.129
4	0.105
5	0.087
6	0.074
7	0.063
8	0.054
9	0.048
10	0.042
11	0.037
12	0.033
13	0.03
14	0.027
15	...

$RSRC_j := RSrR1_j \qquad RSRC_{k+8} := RSrR2_k \qquad RSRC_{l+28} := RSerR3_l$

المنارة للاستشارات
www.manaraa.com

$$RSrR1 = \begin{pmatrix} 1.77633\times 10^{-7} \\ -0.00033 \\ -0.00599 \\ -0.01164 \\ -0.01728 \\ -0.02291 \\ -0.02853 \\ -0.03414 \\ -0.03974 \end{pmatrix}$$

RSrR2 =

	1
1	-0.04
2	-0.066
3	-0.092
4	-0.117
5	-0.139
6	-0.159
7	-0.178
8	-0.195
9	-0.21
10	-0.223
11	-0.233
12	-0.243
13	-0.25
14	-0.255
15	...

RSerR3 =

	1
1	-0.209
2	-0.162
3	-0.129
4	-0.105
5	-0.087
6	-0.074
7	-0.063
8	-0.054
9	-0.048
10	-0.042
11	-0.037
12	-0.033
13	-0.03
14	-0.027
15	-0.024
16	...

RAR =

	1
1	1
2	1
3	1.004
4	1.008
5	1.012
6	1.016
7	1.02
8	1.024
9	1.028
10	1.048
11	1.07
12	...

RSTC =

	1
1	-1.46991
2	-1.46991
3	-1.47041
4	-1.47082
5	-1.47117
6	-1.47147
7	-1.47172
8	-1.47192
9	-1.47208
10	-1.3883
11	-1.30002
12	...

RSRC =

	1
1	$1.776\cdot10^{-7}$
2	$-3.265\cdot10^{-4}$
3	$-5.992\cdot10^{-3}$
4	-0.012
5	-0.017
6	-0.023
7	-0.029
8	-0.034
9	-0.04
10	-0.066
11	-0.092
12	...

www.manaraa.com

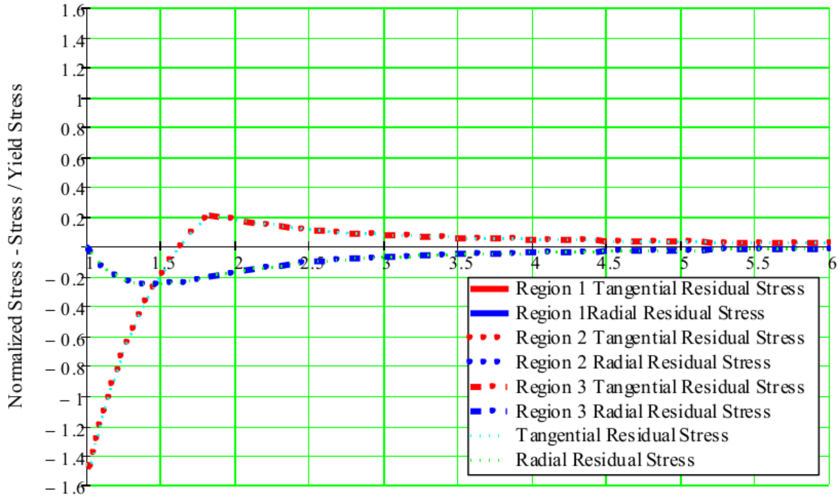

Normalized Distance from the Center of the Hole - r/r1

Fig 14. Check of Combining Residual Stresses in the 3 Regions

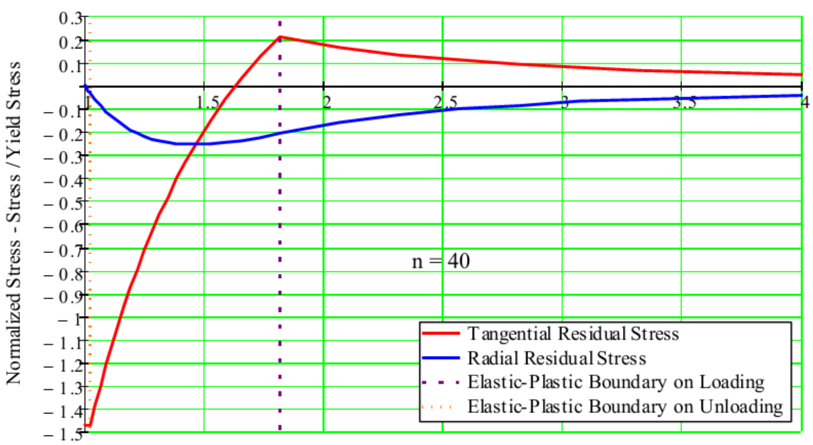

Normalized Distance from the Center of the Hole - r/r1

Fig 15. Residual Stress

www.manaraa.com

E. Convert Stresses into Strain

1. Total Residual Strain- (Loading Strain -Unloading strain)

A. For Region 1, calculate the residual strain between r/a = 1 to r/a = 1.17316

When the ratio of stress over effective stress is less than 1, use the elastic formulation for converting from stress to strain for that stress component. When the ratio of effective stress over seffective stress is greater than 1, use the modified Ramberg-Osgood equation for converting stress to total strain

$\sigma yield = 46.3 \cdot ksi$ $\quad i := 1..9$ $\quad n := 40$ $\quad E = 3 \times 10^4 \cdot ksi$ $\quad ve = 0.3$ $\quad vp = 0.5$

$$raR1 = \begin{pmatrix} 1 \\ 1.00023 \\ 1.00409 \\ 1.00798 \\ 1.01189 \\ 1.01582 \\ 1.01978 \\ 1.02376 \\ 1.02776 \end{pmatrix} \quad SptLR1 = \begin{pmatrix} -0.375 \\ -0.375 \\ -0.367 \\ -0.359 \\ -0.35 \\ -0.342 \\ -0.334 \\ -0.326 \\ -0.317 \end{pmatrix} \quad SprLR1 = \begin{pmatrix} -1.218 \\ -1.218 \\ -1.215 \\ -1.211 \\ -1.208 \\ -1.205 \\ -1.201 \\ -1.198 \\ -1.194 \end{pmatrix} \quad SptU = \begin{pmatrix} -1.095 \\ -1.095 \\ -1.104 \\ -1.112 \\ -1.121 \\ -1.129 \\ -1.138 \\ -1.146 \\ -1.155 \end{pmatrix} \quad SprU = \begin{pmatrix} 1.218 \\ 1.217 \\ 1.209 \\ 1.2 \\ 1.191 \\ 1.182 \\ 1.173 \\ 1.164 \\ 1.155 \end{pmatrix}$$

from Loading

$$\varepsilon rL1_i := \frac{1}{E} \cdot \left[\left(\left| SprLR1_i \right| \right)^{(n-1)} \cdot SprLR1_i \cdot \sigma yield - (ve) \cdot SptLR1_i \cdot \sigma yield \right]$$

$$\varepsilon tL1_i := \frac{1}{E} \cdot \left[SptLR1_i \cdot \sigma yield - \left(\left| SprLR1_i \right| \right)^{n-1} \cdot vp \cdot SprLR1_i \cdot \sigma yield \right]$$

from Unloading

$$\varepsilon rU1_i := \frac{1}{E} \cdot \left[\left(\left| SprU_i \right| \right)^{n-1} \cdot SprU_i \cdot \sigma yield - \left(\left| SptU_i \right| \right)^{n-1} \cdot vp \cdot SptU_i \cdot \sigma yield \right]$$

$$\varepsilon tU1_i := \frac{1}{E} \cdot \left[\left(\left| SptU_i \right| \right)^{n-1} \cdot SptU_i \cdot \sigma yield - \left(\left| SprU_i \right| \right)^{n-1} \cdot vp \cdot SprU_i \cdot \sigma yield \right]$$

$$\varepsilon rL1 = \begin{pmatrix} -4.113 \\ -4.086 \\ -3.672 \\ -3.295 \\ -2.953 \\ -2.644 \\ -2.364 \\ -2.112 \\ -1.884 \end{pmatrix} \quad \varepsilon tL1 = \begin{pmatrix} 2.056 \\ 2.043 \\ 1.835 \\ 1.647 \\ 1.476 \\ 1.322 \\ 1.182 \\ 1.055 \\ 0.941 \end{pmatrix} \quad \varepsilon rU1 = \begin{pmatrix} 4.142 \\ 4.072 \\ 3.053 \\ 2.294 \\ 1.734 \\ 1.327 \\ 1.039 \\ 0.846 \\ 0.73 \end{pmatrix} \quad \varepsilon tU1 = \begin{pmatrix} -2.114 \\ -2.08 \\ -1.586 \\ -1.228 \\ -0.978 \\ -0.813 \\ -0.722 \\ -0.695 \\ -0.73 \end{pmatrix}$$

www.manaraa.com

Total Residual Strain

$\varepsilon tR1 := \varepsilon tL1 + \varepsilon tU1$ $\varepsilon rR1 := \varepsilon rL1 + \varepsilon rU1$

$$\varepsilon tR1 = \begin{pmatrix} -0.058 \\ -0.037 \\ 0.249 \\ 0.419 \\ 0.499 \\ 0.508 \\ 0.46 \\ 0.36 \\ 0.211 \end{pmatrix} \quad \varepsilon rR1 = \begin{pmatrix} 0.029 \\ -0.014 \\ -0.619 \\ -1.001 \\ -1.22 \\ -1.317 \\ -1.325 \\ -1.266 \\ -1.154 \end{pmatrix} \quad RSrR1 = \begin{pmatrix} 1.77633\times 10^{-7} \\ -0.00033 \\ -0.00599 \\ -0.01164 \\ -0.01728 \\ -0.02291 \\ -0.02853 \\ -0.03414 \\ -0.03974 \end{pmatrix} \quad RStR1 = \begin{pmatrix} -1.46991 \\ -1.46991 \\ -1.47041 \\ -1.47082 \\ -1.47117 \\ -1.47147 \\ -1.47172 \\ -1.47192 \\ -1.47208 \end{pmatrix}$$

Calculate elastic residual strain from residual stress

$$R\varepsilon rR1_i := \frac{1}{E}\cdot\left(RSrR1_i\cdot\sigma yield - ve\cdot RStR1_i\cdot\sigma yield\right)$$

$$R\varepsilon tR1_i := \frac{1}{E}\cdot\left(RStR1_i\cdot\sigma yield - ve\cdot RSrR1_i\cdot\sigma yield\right)$$

$E = 3\times 10^4\cdot ksi$

$\sigma yield = 46.3\cdot ksi$

$n = 40$ $RStR1_9 = -1.47208$

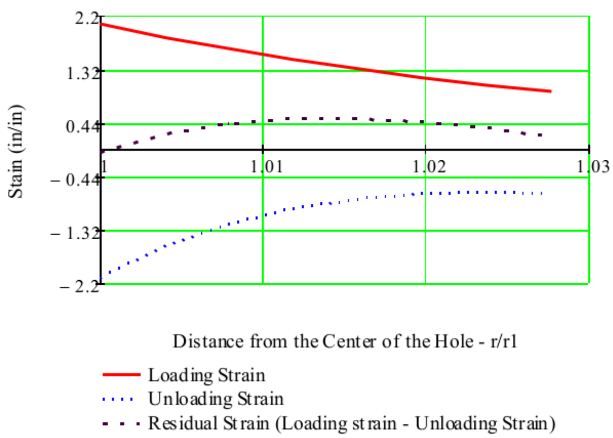

Fig 16. Tangential Strain in Region 1

www.manaraa.com

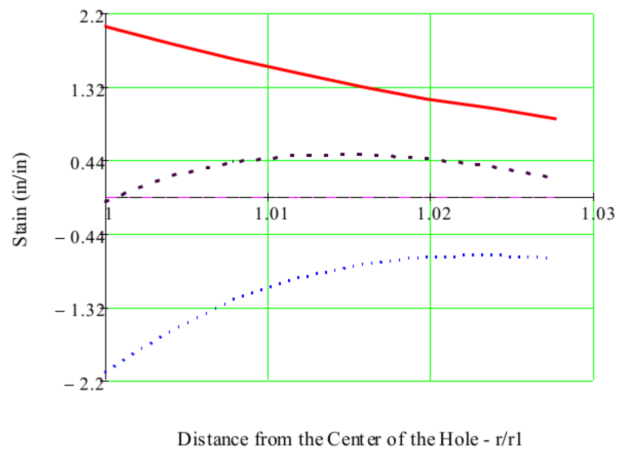

$$RatR1 = \begin{pmatrix} -0.002269 \\ -0.002268 \\ -0.002267 \\ -0.002265 \\ -0.002263 \\ -0.00226 \\ -0.002258 \\ -0.002256 \\ -0.002254 \end{pmatrix}$$

Fig 17 Tangential Strain in Region 1

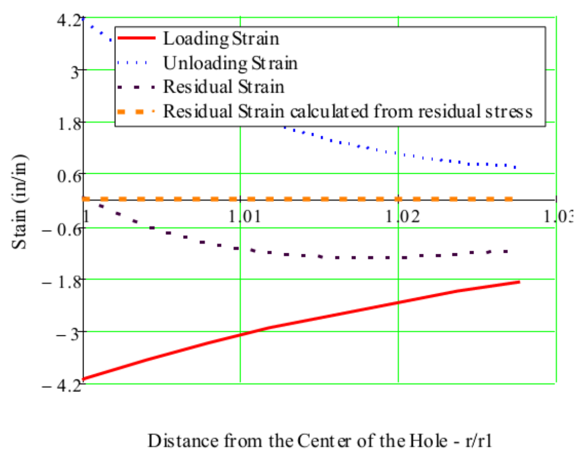

Fig 18. Radial Strain in Region 1

www.manaraa.com

2. For Region 2, calculate the residual strain between r/a = 1.17316 to r/a = 2.224

from Loading

$j := 1..10$

$k := 11..21$

raR2 =

	1
1	1.028
2	1.048
3	1.07
4	1.092
5	1.116
6	1.141
7	1.166
8	1.193
9	1.222
10	1.251
11	1.282
12	1.315
13	1.349
14	1.385
15	1.422
16	1.461
17	1.523
18	1.59
19	1.661
20	1.738
21	1.82

SptL2 =

	1
1	-0.317
2	-0.277
3	-0.234
4	-0.191
5	-0.148
6	-0.105
7	-0.063
8	-0.021
9	0.021
10	0.062
11	0.104
12	0.145
13	0.185
14	0.225
15	0.265
16	0.304
17	0.362
18	0.418
19	0.473
20	0.526
21	0.577

SprL2 =

	1
1	-1.194
2	-1.177
3	-1.159
4	-1.139
5	-1.118
6	-1.097
7	-1.074
8	-1.051
9	-1.027
10	-1.001
11	-0.975
12	-0.948
13	-0.92
14	-0.891
15	-0.861
16	-0.83
17	-0.783
18	-0.734
19	-0.683
20	-0.631
21	-0.577

$$\varepsilon rL2_j := \frac{1}{E}\cdot\left[\left(\left|SprL2_j\right|\right)^{n-1}\cdot SprL2_j\cdot\sigma yield-(\nu e)\cdot SptL2_j\cdot\sigma yield\right]$$

$$\varepsilon tL2_j := \frac{1}{E}\cdot\left[SptL2_j\cdot\sigma yield-\left(\left|SprL2_j\right|\right)^{n-1}\cdot\nu p\cdot SprL2_j\cdot\sigma yield\right]$$

$$\varepsilon rL2_k := \frac{1}{E}\cdot\left[SprL2_k\cdot\sigma yield-(\nu e)\cdot SptL2_k\cdot\sigma yield\right]$$

$$\varepsilon tL2_k := \frac{1}{E}\cdot\left[SptL2_k\cdot\sigma yield-(\nu e)\cdot SprL2_k\cdot\sigma yield\right]$$

www.manaraa.com

$\varepsilon tL2 =$

	1
1	0.94148
2	0.53025
3	0.27734
4	0.13957
5	0.06726
6	0.03091
7	0.0135
8	0.00561
9	0.00224
10	0.00091
11	0.00061
12	0.00066
13	0.00071
14	0.00076
15	0.00081
16	0.00085
17	0.00092
18	0.00098
19	0.00105
20	0.0011
21	0.00116

$\varepsilon rL2 =$

	1
1	-1.88379
2	-1.06124
3	-0.55529
4	-0.27964
5	-0.1349
6	-0.06209
7	-0.02718
8	-0.01128
9	-0.00443
10	-0.00166
11	-0.00155
12	-0.00153
13	-0.00151
14	-0.00148
15	-0.00145
16	-0.00142
17	-0.00138
18	-0.00133
19	-0.00127
20	-0.00122
21	-0.00116

$l := 1..4 \qquad m := 5..21$

from Unloading

$SetUR2 =$

	1
1	-1.155
2	-1.111
3	-1.066
4	-1.022
5	-0.979
6	-0.937
7	-0.896
8	-0.856
9	-0.817
10	-0.779
11	-0.742
12	-0.705
13	-0.67
14	-0.636
15	-0.603
16	-0.571
17	-0.526
18	-0.483
19	-0.442
20	-0.404
21	-0.368

$SerUR2 =$

	1
1	1.155
2	1.111
3	1.066
4	1.022
5	0.979
6	0.937
7	0.896
8	0.856
9	0.817
10	0.779
11	0.742
12	0.705
13	0.67
14	0.636
15	0.603
16	0.571
17	0.526
18	0.483
19	0.442
20	0.404
21	0.368

$$\varepsilon tU2_l := \frac{1}{E} \cdot \left[\left(\left| SetUR2_l \right| \right)^{n-1} \cdot SetUR2_l \cdot \sigma yield - \left(\left| SerUR2_l \right| \right)^{n-1} \cdot \nu p \cdot SerUR2_l \cdot \sigma yield \right]$$

$$\varepsilon rU2_l := \frac{1}{E} \cdot \left[\left(\left| SerUR2_l \right| \right)^{n-1} \cdot SerUR2_l \cdot \sigma yield - \left(\left| SetUR2_l \right| \right)^{n-1} \cdot \nu p \cdot SetUR2_l \cdot \sigma yield \right]$$

$$\varepsilon tU2_m := \frac{1}{E} \cdot \left(SetUR2_m \cdot \sigma yield - \nu e \cdot SerUR2_m \cdot \sigma yield \right)$$

$$\varepsilon rU2_m := \frac{1}{E} \cdot \left(SerUR2_m \cdot \sigma yield - \nu e \cdot SetUR2_m \cdot \sigma yield \right)$$

www.manaraa.com

$\varepsilon tL2 =$

	1
1	0.941
2	0.53
3	0.277
4	0.14
5	0.067
6	0.031
7	0.014
8	$5.611 \cdot 10^{-3}$
9	$2.243 \cdot 10^{-3}$
10	$9.117 \cdot 10^{-4}$
11	$6.116 \cdot 10^{-4}$
12	$6.622 \cdot 10^{-4}$
13	$7.117 \cdot 10^{-4}$
14	$7.602 \cdot 10^{-4}$
15	$8.075 \cdot 10^{-4}$
16	$8.536 \cdot 10^{-4}$
17	$9.206 \cdot 10^{-4}$
18	$9.847 \cdot 10^{-4}$
19	$1.046 \cdot 10^{-3}$
20	$1.104 \cdot 10^{-3}$
21	$1.158 \cdot 10^{-3}$

$\varepsilon rL2 =$

	1
1	-1.884
2	-1.061
3	-0.555
4	-0.28
5	-0.135
6	-0.062
7	-0.027
8	-0.011
9	$-4.431 \cdot 10^{-3}$
10	$-1.659 \cdot 10^{-3}$
11	$-1.553 \cdot 10^{-3}$
12	$-1.53 \cdot 10^{-3}$
13	$-1.505 \cdot 10^{-3}$
14	$-1.479 \cdot 10^{-3}$
15	$-1.452 \cdot 10^{-3}$
16	$-1.422 \cdot 10^{-3}$
17	$-1.376 \cdot 10^{-3}$
18	$-1.326 \cdot 10^{-3}$
19	$-1.273 \cdot 10^{-3}$
20	$-1.217 \cdot 10^{-3}$
21	$-1.158 \cdot 10^{-3}$

$\varepsilon tU2 =$

	1
1	-0.73016
2	-0.15788
3	-0.0301
4	-0.00559
5	-0.00197
6	-0.00188
7	-0.0018
8	-0.00172
9	-0.00164
10	-0.00156
11	-0.00149
12	-0.00142
13	-0.00134
14	-0.00128
15	-0.00121
16	...

Total Residual Strain

$$\varepsilon tR2 := \varepsilon tL2 + \varepsilon tU2$$

$$\varepsilon rR2 := \varepsilon rL2 + \varepsilon rU2$$

www.manaraa.com

$\varepsilon rU2 =$

	1
1	0.73
2	0.158
3	0.03
4	$5.595 \cdot 10^{-3}$
5	$1.965 \cdot 10^{-3}$
6	$1.881 \cdot 10^{-3}$
7	$1.798 \cdot 10^{-3}$
8	$1.718 \cdot 10^{-3}$
9	$1.639 \cdot 10^{-3}$
10	$1.563 \cdot 10^{-3}$
11	$1.488 \cdot 10^{-3}$
12	$1.415 \cdot 10^{-3}$
13	$1.345 \cdot 10^{-3}$
14	$1.277 \cdot 10^{-3}$
15	$1.21 \cdot 10^{-3}$
16	...

$\varepsilon tR2 =$

	1
1	0.21132
2	0.37237
3	0.24724
4	0.13397
5	0.06529
6	0.02903
7	0.01171
8	0.00389
9	0.0006
10	-0.00065
11	-0.00088
12	-0.00075
13	-0.00063
14	-0.00052
15	-0.0004
16	-0.00029
17	-0.00013
18	$1.63609 \cdot 10^{-5}$
19	0.00016
20	0.00029
21	0.00042

$\varepsilon rR2 =$

	1
1	-1.154
2	-0.903
3	-0.525
4	-0.274
5	-0.133
6	-0.06
7	-0.025
8	$-9.558 \cdot 10^{-3}$
9	$-2.792 \cdot 10^{-3}$
10	$-9.682 \cdot 10^{-5}$
11	$-6.5 \cdot 10^{-5}$
12	$-1.146 \cdot 10^{-4}$
13	$-1.606 \cdot 10^{-4}$
14	$-2.027 \cdot 10^{-4}$
15	$-2.412 \cdot 10^{-4}$
16	$-2.759 \cdot 10^{-4}$
17	$-3.21 \cdot 10^{-4}$
18	$-3.577 \cdot 10^{-4}$
19	$-3.863 \cdot 10^{-4}$
20	$-4.069 \cdot 10^{-4}$
21	$-4.198 \cdot 10^{-4}$

Calculate elastic residual strain
from residual stress

$RSrR2 =$

	1
1	-0.04
2	-0.066
3	-0.092
4	-0.117
5	-0.139
6	-0.159
7	-0.178
8	-0.195
9	-0.21
10	-0.223
11	-0.233
12	-0.243
13	...

$RStR2 =$

	1
1	-1.472
2	-1.388
3	-1.3
4	-1.213
5	-1.127
6	-1.043
7	-0.96
8	-0.877
9	-0.796
10	-0.716
11	-0.638
12	-0.561
13	...

$$R\varepsilon tR2 := \frac{1}{E} \cdot (RStR2 \cdot \sigma yield - ve \cdot RSrR2 \cdot \sigma yield)$$

$$R\varepsilon rR2 := \frac{1}{E} \cdot (RSrR2 \cdot \sigma yield - ve \cdot RStR2 \cdot \sigma yield)$$

www.manaraa.com

$R\varepsilon tR2 =$

	1
1	-0.002254
2	-0.002112
3	-0.001964
4	-0.001818
5	-0.001676
6	-0.001536
7	-0.001398
8	-0.001264
9	-0.001132
10	-0.001003
11	-0.000876
12	-0.000753
13	-0.000633
14	-0.000516
15	-0.000403
16	...

$R\varepsilon rR2 =$

	1
1	0.00062
2	0.000541
3	0.000459
4	0.000382
5	0.000308
6	0.000237
7	0.00017
8	0.000106
9	0.000045
10	-0.000012
11	-0.000065
12	-0.000115
13	-0.000161
14	-0.000203
15	-0.000241
16	...

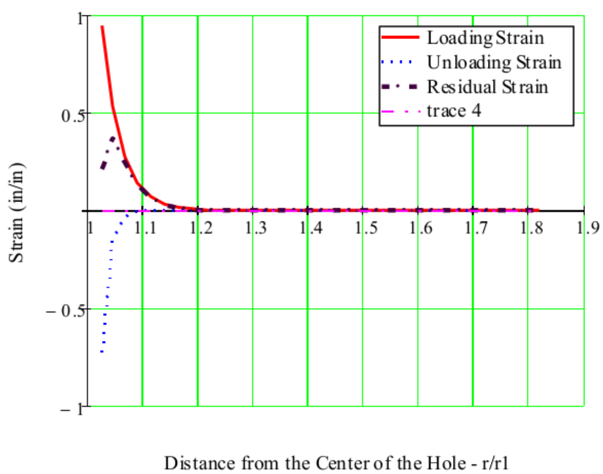

Fig 19 Tangential Strain Regions 2

www.manaraa.com

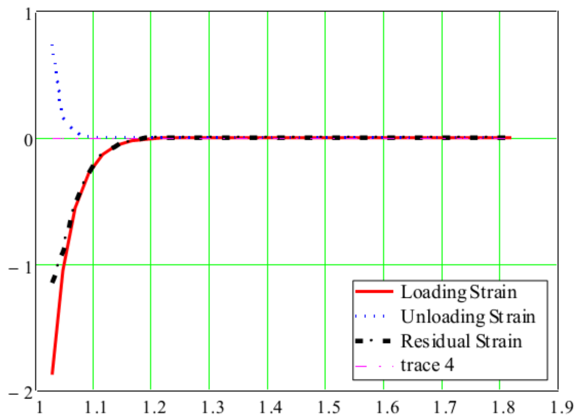

Fig 20. Radial Strain Region 2

3. For Region 3, calculate the residual stress between r/a = 2.224 to r/a >6 $k := 1..18$

from Loading

	raR3 =	SetL =	SerL =	SetUR3 =
	1	1	1	1
1	1.82	0.578	-0.578	-0.368
2	2.07	0.446	-0.446	-0.285
3	2.32	0.355	-0.355	-0.227
4	2.57	0.29	-0.29	-0.185
5	2.82	0.241	-0.241	-0.153
6	3.07	0.203	-0.203	-0.129
7	3.32	0.174	-0.174	-0.111
8	3.57	0.15	-0.15	-0.096
9	3.82	0.131	-0.131	-0.084
10	4.07	0.115	-0.115	-0.074
11	4.32	0.103	-0.103	-0.065
12	4.57	0.092	-0.092	-0.058
13	4.82	0.082	-0.082	-0.053
14	5.07	0.074	-0.074	-0.047
15	5.32	0.068	-0.068	-0.043
16	5.57	0.062	-0.062	-0.039
17	5.82	0.056	-0.056	-0.036
18	6.07	0.052	-0.052	-0.033

المنارة للاستشارات
www.manaraa.com

$$\varepsilon tL3_k := \frac{1}{E} \cdot \left(SetL_k \cdot \sigma yield - ve \cdot SerL_k \cdot \sigma yield\right)$$

$$\varepsilon rL3_k := \frac{1}{E} \cdot \left(SerL_k \cdot \sigma yield - ve \cdot SetL_k \cdot \sigma yield\right)$$

SerUR3 =

	1
1	0.368
2	0.285
3	0.227
4	0.185
5	0.153
6	0.129
7	0.111
8	0.096
9	0.084
10	0.074
11	0.065
12	0.058
13	0.053
14	0.047
15	0.043
16	0.039
17	0.036
18	0.033

εtL3 =

	1
1	0.00116
2	0.0009
3	0.00071
4	0.00058
5	0.00048
6	0.00041
7	0.00035
8	0.0003
9	0.00026
10	0.00023
11	0.00021
12	0.00018
13	0.00017
14	0.00015
15	0.00014
16	0.00012
17	0.00011
18	0.0001

εrL3 =

	1
1	-0.00116
2	-0.0009
3	-0.00071
4	-0.00058
5	-0.00048
6	-0.00041
7	-0.00035
8	-0.0003
9	-0.00026
10	-0.00023
11	-0.00021
12	-0.00018
13	-0.00017
14	-0.00015
15	-0.00014
16	-0.00012
17	-0.00011
18	-0.0001

from Unloading

$$\varepsilon tU3_k := \frac{1}{E} \cdot \left(SetUR3_k \cdot \sigma yield - ve \cdot SerUR3_k \cdot \sigma yield\right)$$

$$\varepsilon rU3_k := \frac{1}{E} \cdot \left(SerUR3_k \cdot \sigma yield - ve \cdot SetUR3_k \cdot \sigma yield\right)$$

www.manaraa.com

$\varepsilon tU3 =$

	1
1	-0.00074
2	-0.00057
3	-0.00045
4	-0.00037
5	-0.00031
6	-0.00026
7	-0.00022
8	-0.00019
9	-0.00017
10	-0.00015
11	-0.00013
12	-0.00012
13	-0.00011
14	$-9.52012\cdot10^{-5}$
15	$-8.64639\cdot10^{-5}$
16	$-7.88765\cdot10^{-5}$
17	$-7.22457\cdot10^{-5}$
18	$-6.64172\cdot10^{-5}$

$\varepsilon rU3 =$

	1
1	0.00074
2	0.00057
3	0.00045
4	0.00037
5	0.00031
6	0.00026
7	0.00022
8	0.00019
9	0.00017
10	0.00015
11	0.00013
12	0.00012
13	0.00011
14	$9.52012\cdot10^{-5}$
15	$8.64639\cdot10^{-5}$
16	$7.88765\cdot10^{-5}$
17	$7.22457\cdot10^{-5}$
18	$6.64172\cdot10^{-5}$

Total Residual Strain

$\varepsilon tR3 := \varepsilon tL3 + \varepsilon tU3$

$\varepsilon rR3 := \varepsilon rL3 + \varepsilon rU3$

$\varepsilon tR3 =$

	1
1	$4.199\cdot10^{-4}$
2	$3.246\cdot10^{-4}$
3	$2.584\cdot10^{-4}$
4	$2.106\cdot10^{-4}$
5	$1.749\cdot10^{-4}$
6	$1.476\cdot10^{-4}$
7	$1.262\cdot10^{-4}$
8	$1.091\cdot10^{-4}$
9	$9.531\cdot10^{-5}$
10	$8.396\cdot10^{-5}$
11	$7.453\cdot10^{-5}$
12	$6.659\cdot10^{-5}$
13	$5.987\cdot10^{-5}$
14	$5.411\cdot10^{-5}$
15	$4.914\cdot10^{-5}$
16	...

$\varepsilon rR3 =$

	1
1	$-4.199\cdot10^{-4}$
2	$-3.246\cdot10^{-4}$
3	$-2.584\cdot10^{-4}$
4	$-2.106\cdot10^{-4}$
5	$-1.749\cdot10^{-4}$
6	$-1.476\cdot10^{-4}$
7	$-1.262\cdot10^{-4}$
8	$-1.091\cdot10^{-4}$
9	$-9.531\cdot10^{-5}$
10	$-8.396\cdot10^{-5}$
11	$-7.453\cdot10^{-5}$
12	$-6.659\cdot10^{-5}$
13	$-5.987\cdot10^{-5}$
14	$-5.411\cdot10^{-5}$
15	$-4.914\cdot10^{-5}$
16	$-4.483\cdot10^{-5}$
17	$-4.106\cdot10^{-5}$
18	$-3.775\cdot10^{-5}$

المنارة للاستشارات
www.manaraa.com

Calculate elastic residual strain from residual stress

$$R\varepsilon rR3 := \frac{1}{E} \cdot (RSerR3 \cdot \sigma yield - \nu e \cdot RSetR3 \cdot \sigma yield)$$

$$R\varepsilon tR3 := \frac{1}{E} \cdot (RSetR3 \cdot \sigma yield - \nu e \cdot RSerR3 \cdot \sigma yield)$$

$R\varepsilon tR3 =$

	1
1	$4.199 \cdot 10^{-4}$
2	$3.246 \cdot 10^{-4}$
3	$2.584 \cdot 10^{-4}$
4	$2.106 \cdot 10^{-4}$
5	$1.749 \cdot 10^{-4}$
6	$1.476 \cdot 10^{-4}$
7	$1.262 \cdot 10^{-4}$
8	$1.091 \cdot 10^{-4}$
9	$9.531 \cdot 10^{-5}$
10	$8.396 \cdot 10^{-5}$
11	$7.453 \cdot 10^{-5}$
12	$6.659 \cdot 10^{-5}$
13	$5.987 \cdot 10^{-5}$
14	$5.411 \cdot 10^{-5}$
15	$4.914 \cdot 10^{-5}$
16	...

$R\varepsilon rR3 =$

	1
1	$-4.199 \cdot 10^{-4}$
2	$-3.246 \cdot 10^{-4}$
3	$-2.584 \cdot 10^{-4}$
4	$-2.106 \cdot 10^{-4}$
5	$-1.749 \cdot 10^{-4}$
6	$-1.476 \cdot 10^{-4}$
7	$-1.262 \cdot 10^{-4}$
8	$-1.091 \cdot 10^{-4}$
9	$-9.531 \cdot 10^{-5}$
10	$-8.396 \cdot 10^{-5}$
11	$-7.453 \cdot 10^{-5}$
12	$-6.659 \cdot 10^{-5}$
13	$-5.987 \cdot 10^{-5}$
14	$-5.411 \cdot 10^{-5}$
15	$-4.914 \cdot 10^{-5}$
16	...

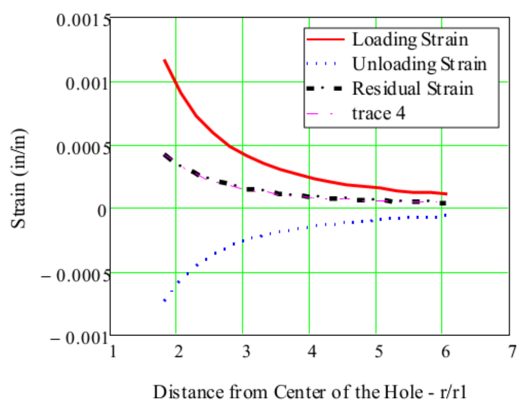

Fig 21. Tangential Strain Region 3

المنارة للاستشارات
www.manaraa.com

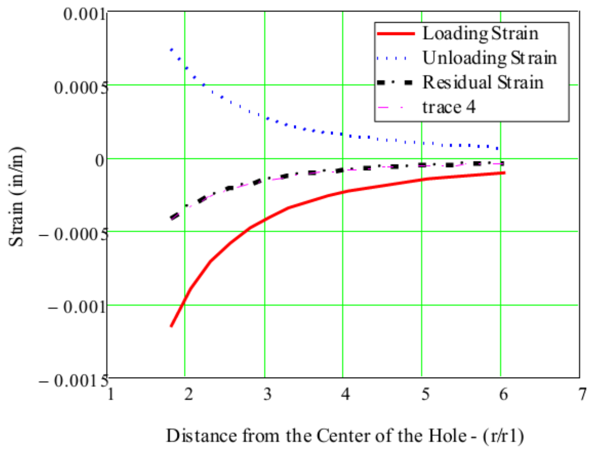

$q := -4.2, -3.2 .. 4.2$

Fig 22. Radial Strain Region 3

4. Plot all Regions together review results in different Regions

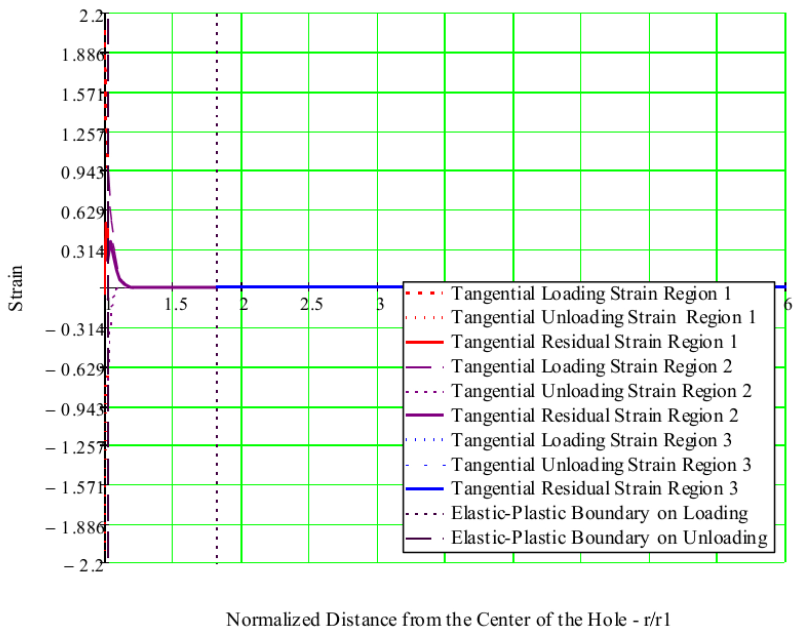

Fig 23. Total Tangential Residual Strain

www.manaraa.com

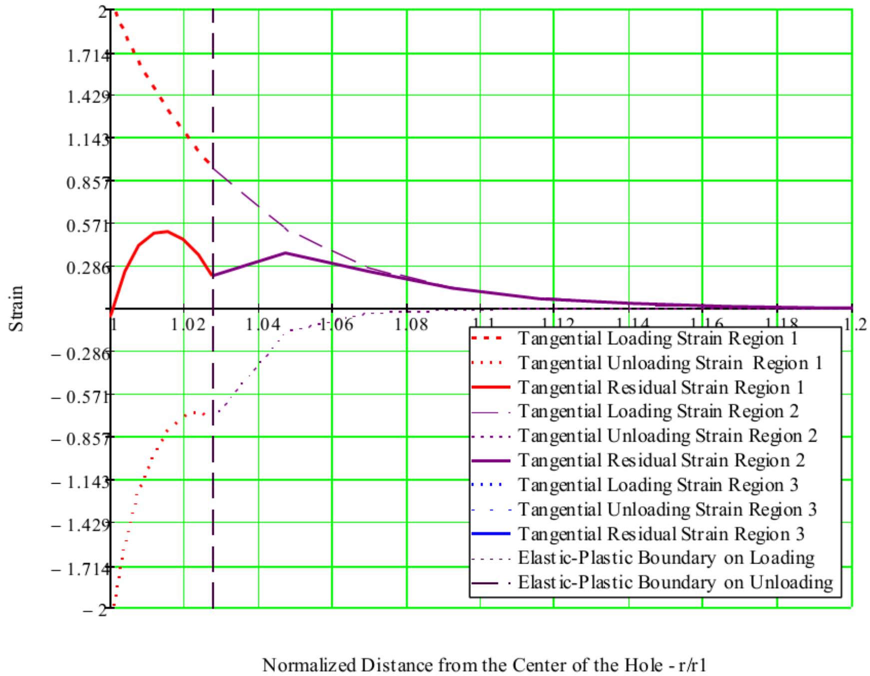

Fig 24. Total Tangential Residual Strain

$pY\varepsilon_m := .00154$ $nY\varepsilon_m := -.00154$ $pY\varepsilon_k := .00154$ $nY\varepsilon_k := -.00154$

المنارة للاستشارات
www.manaraa.com

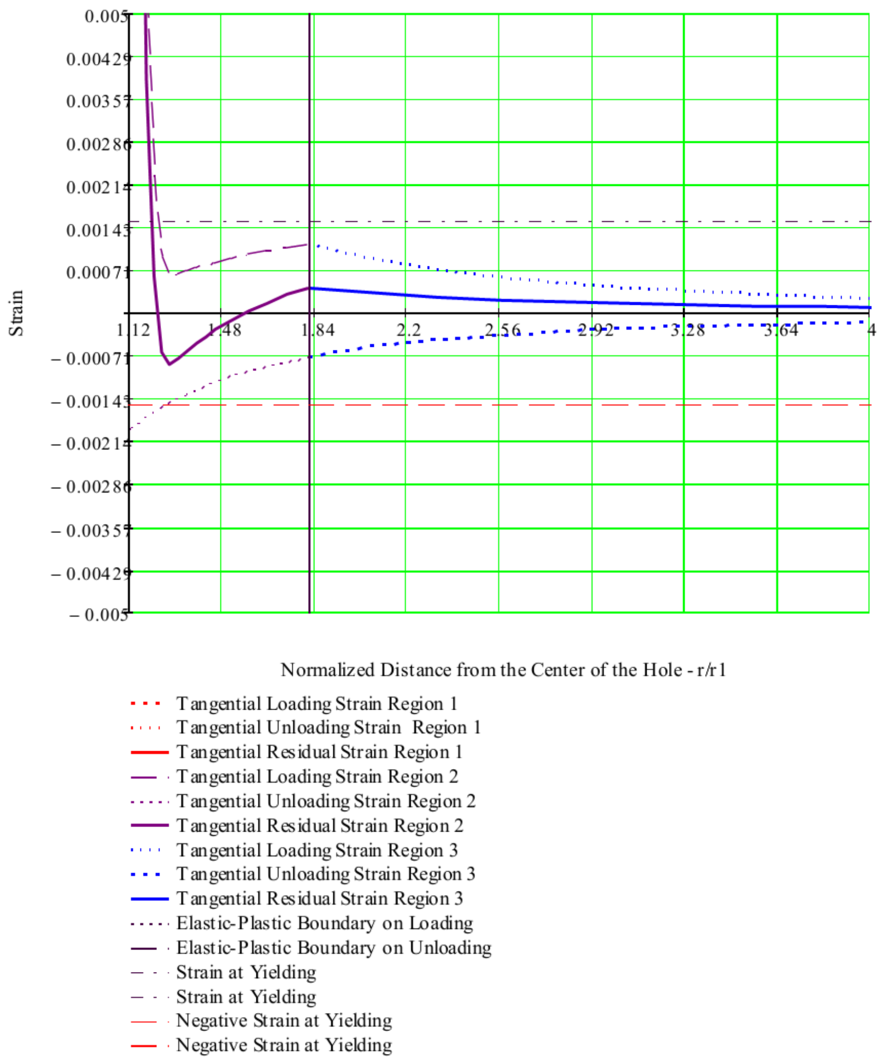

Fig 25. Total Tangential Residual Strain

www.manaraa.com

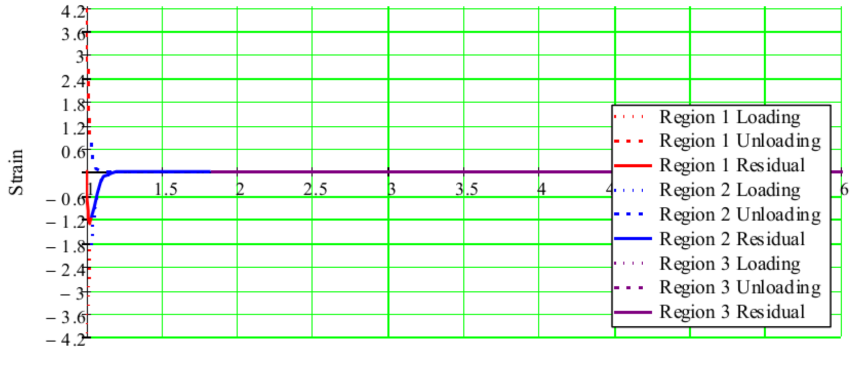

Normalized Distance from the Center of the Hole - r/r1

Fig 26. Total Radial Residual Strain

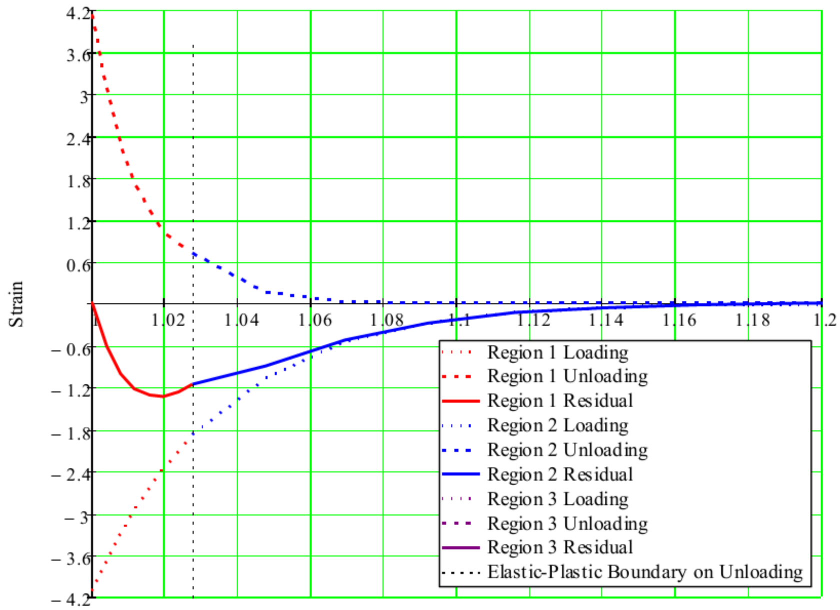

Normalized Distance from the Center of the Hole - r/r1

Fig 27. Total Radial Residual Strain

www.manaraa.com

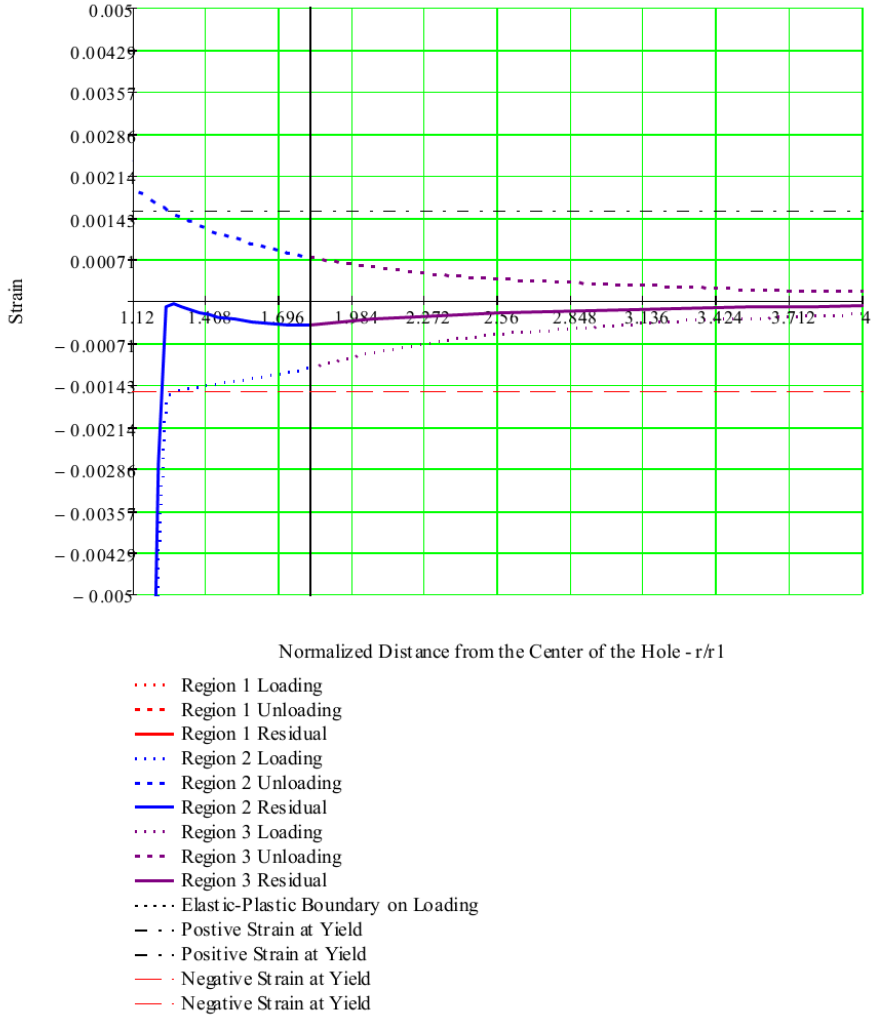

Fig 28. Total Radial Residual Strain

www.manaraa.com

5. Combine into one array for total tangential strain and one for total radial strain

$j := 1..9 \qquad l := 2..18 \qquad k := 2..21$

$R\varepsilon TC_j := \varepsilon tR1_j \qquad R\varepsilon RC_j := \varepsilon rR1_j$

$R\varepsilon TC_{k+8} := \varepsilon tR2_k \qquad R\varepsilon RC_{k+8} := \varepsilon rR2_k$

$R\varepsilon TC_{l+28} := \varepsilon tR3_l \qquad R\varepsilon RC_{l+28} := \varepsilon rR3_l$

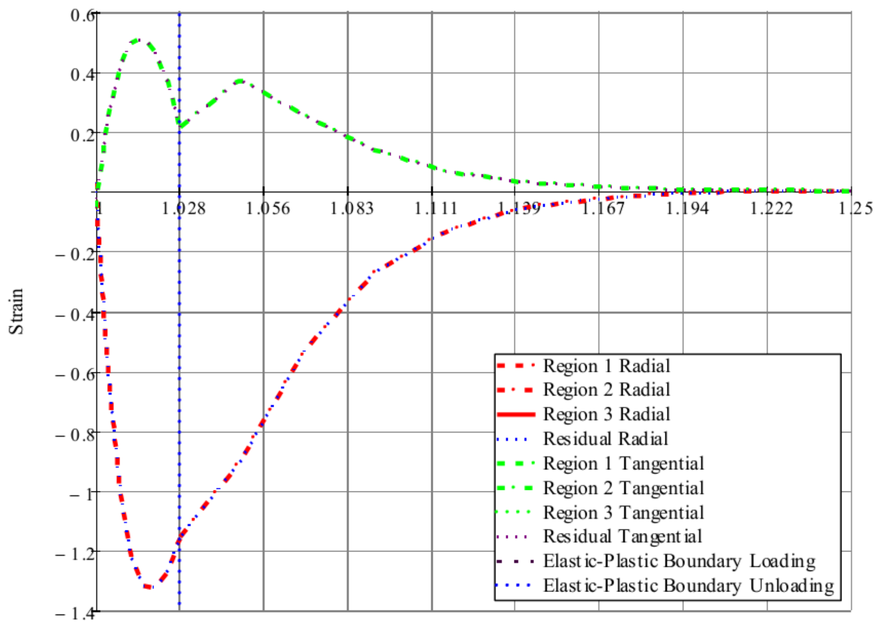

Normalized Distance from the Center of the Hole - r/r1

Fig 29. Total Residual Strain

www.manaraa.com

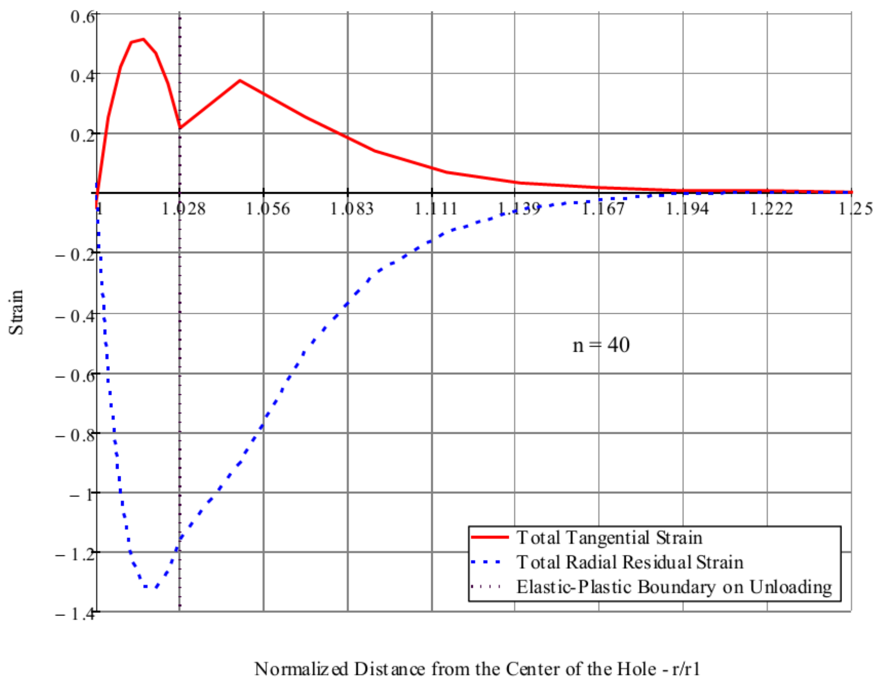

Fig 30. Total Residual Strain

B1L = 1.82

www.manaraa.com

$RAR =$

	1
1	1
2	1.00023
3	1.00409
4	1.00798
5	1.01189
6	1.01582
7	1.01978
8	1.02376
9	1.02776
10	1.04762
11	1.06956
12	1.09229
13	1.11595
14	1.14065
15	1.16648
16	1.19349
17	1.22178
18	1.25139
19	1.28241
20	1.31489
21	1.34891
22	1.38454
23	1.42186
24	1.46094
25	1.52308
26	1.5897
27	1.66117
28	1.73787
29	1.82024
30	...

$R\varepsilon RC =$

	1
1	0.029
2	-0.014
3	-0.619
4	-1.001
5	-1.22
6	-1.317
7	-1.325
8	-1.266
9	-1.154
10	-0.903
11	-0.525
12	-0.274
13	-0.133
14	-0.06
15	-0.025
16	$-9.558\cdot10^{-3}$
17	$-2.792\cdot10^{-3}$
18	$-9.682\cdot10^{-5}$
19	$-6.5\cdot10^{-5}$
20	$-1.146\cdot10^{-4}$
21	$-1.606\cdot10^{-4}$
22	$-2.027\cdot10^{-4}$
23	$-2.412\cdot10^{-4}$
24	$-2.759\cdot10^{-4}$
25	$-3.21\cdot10^{-4}$
26	$-3.577\cdot10^{-4}$
27	$-3.863\cdot10^{-4}$
28	$-4.069\cdot10^{-4}$
29	$-4.198\cdot10^{-4}$
30	...

$R\varepsilon TC =$

	1
1	-0.058
2	-0.037
3	0.249
4	0.419
5	0.499
6	0.508
7	0.46
8	0.36
9	0.211
10	0.372
11	0.247
12	0.134
13	0.065
14	0.029
15	0.012
16	0.004
17	0.001
18	-0.001
19	-0.001
20	-0.001
21	-0.001
22	-0.001
23	-0
24	-0
25	-0
26	$1.636\cdot10^{-5}$
27	0
28	0
29	0
30	...

Eε TC - Combined array of Elastic Residual Tangential Strain
Eε TC - Combined array of Elastic Residual Radial Strain

$E\varepsilon TC_j := R\varepsilon tR1_j \qquad E\varepsilon RC_j := R\varepsilon rR1_j$

$E\varepsilon TC_{k+8} := R\varepsilon tR2_k \qquad E\varepsilon RC_{k+8} := R\varepsilon rR2_k$

$E\varepsilon TC_{l+28} := R\varepsilon tR3_l \qquad E\varepsilon RC_{l+28} := R\varepsilon rR3_l$

المنارة للاستشارات
www.manaraa.com

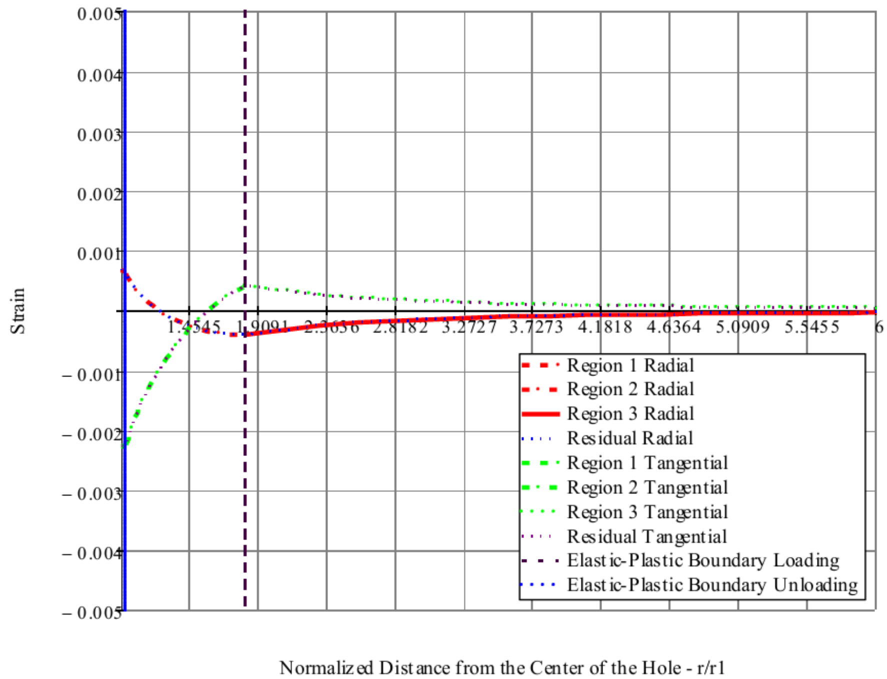

Fig 31. Elastic Residual Strain

RAR =

	1
1	1
2	1
3	1.004
4	1.008
5	1.012
6	1.016
7	1.02
8	1.024
9	1.028
10	1.048
11	1.07
12	1.092
13	1.116
14	...

EεTC =

	1
1	$-2.269 \cdot 10^{-3}$
2	$-2.268 \cdot 10^{-3}$
3	$-2.267 \cdot 10^{-3}$
4	$-2.265 \cdot 10^{-3}$
5	$-2.263 \cdot 10^{-3}$
6	$-2.26 \cdot 10^{-3}$
7	$-2.258 \cdot 10^{-3}$
8	$-2.256 \cdot 10^{-3}$
9	$-2.254 \cdot 10^{-3}$
10	$-2.112 \cdot 10^{-3}$
11	$-1.964 \cdot 10^{-3}$
12	...

EεRC =

	1
1	$6.806 \cdot 10^{-4}$
2	$6.801 \cdot 10^{-4}$
3	$6.716 \cdot 10^{-4}$
4	$6.63 \cdot 10^{-4}$
5	$6.545 \cdot 10^{-4}$
6	$6.459 \cdot 10^{-4}$
7	$6.374 \cdot 10^{-4}$
8	$6.288 \cdot 10^{-4}$
9	$6.202 \cdot 10^{-4}$
10	$5.408 \cdot 10^{-4}$
11	$4.595 \cdot 10^{-4}$
12	...

المنارة للاستشارات
www.manaraa.com

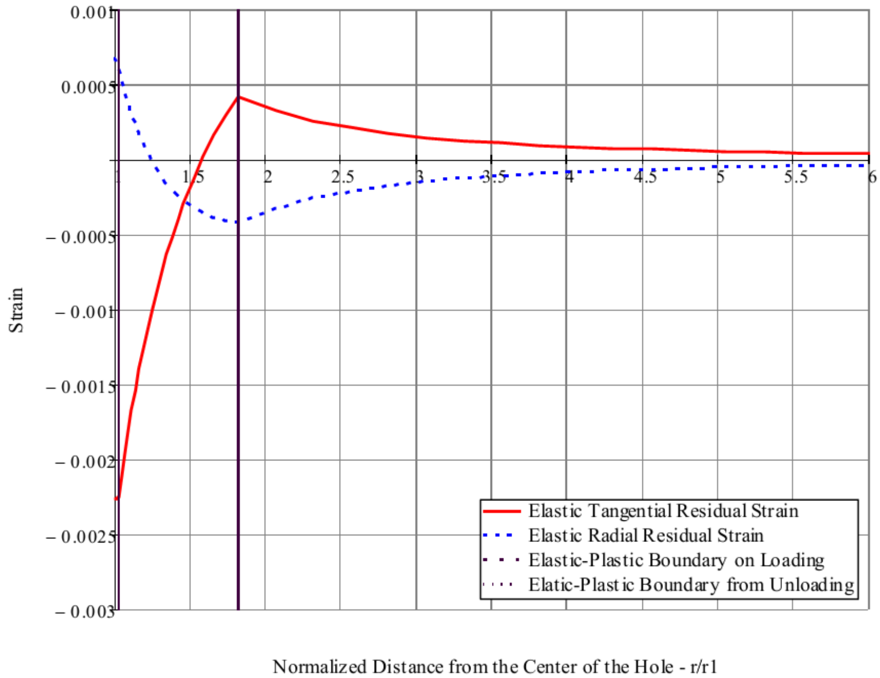

Fig 32. Elastic Residual Strain

المنارة للاستشارات
www.manaraa.com

Appendix B-5 Ball's Closed-From Solution for *n* = 10

Appendix 5. BALL'S CLOSED-FORM SOLUTION TO COLD-EXPANDED HOLES APPLIED TO PICK TOOL SPECIMENS with n = 10

A. Constants Defined

constants chosen to attempt to match Ball's result in Fig 6

yield stress is 414 MPa (60 ksi) E= 207 GPa (30,000 ksi) $ksi := 1000 \cdot psi$

Poisson's ratio ν elastic = .3 $\nu e := 0.3($
ν plastic =.5 $\nu p := 0.5$

$\sigma yield := 34.69 \cdot ksi$

Actual yield stress is 46.3 ksi. Yield stress used (34.69 ksi) calculated from actual stress strain curve to achieve 51.49 ksi at 6% strain.

n is strain hardening exponent from measured stress-strain curve, it appears that 10<n<17 $n := 1($ $E := 30000 \cdot ksi$

Bauschinger parameter β is a measure of the change yield stress from reverse yielding

$\beta := 1$ β = 1 implies kinematic strain hardening rule while β =0 results in an isotropic model

R is used to model implicitly the degree of plastic anisotropy and is defined as the ratio of in-plane transverse plastic strain to through thickness plastic strain $R := 1$

Constants used in calculations

$$\mu := \frac{n + 1 + 2 \cdot R}{n^2 + 1 + 2 \cdot R} \qquad \mu = 0.126$$

$$\gamma := \frac{n \cdot (1 + R)}{n^2 + 1 + 2 \cdot R} \qquad \gamma = 0.194$$

Constants defined to make equations fit on single page

$$A := (n - 1) \cdot \sqrt{1 + 2 \cdot R} \qquad A = 15.588$$

$$B := n + 1 + 2 \cdot R \qquad B = 13$$

$$C := n^2 + 1 + 2 \cdot R \qquad C = 103$$

$$D := \left(n^2 - 1\right) \cdot \sqrt{1 + 2 \cdot R} \qquad D = 171.473$$

B. Result at the end of Cold Expansion

Note: L is used to denote the cold expansion loading

1. Determination of α $_{aL}$ ***for*** $^{P}/_{\sigma}$ ***yield***

α a is the parameterization variable and can vary between π /2 to α max

define α aL
$$\alpha maxL := atan\left[-\frac{(n + 1 + 2 \cdot R)}{(n - 1) \cdot \sqrt{1 + 2 \cdot R}}\right] \qquad \alpha maxL = -39.826 \cdot deg$$

has to be in the 2nd quadrant $\alpha maxL := \alpha maxL + 180 \cdot deg$

www.manaraa.com

Define α_{bL} which ranges from 90 deg to α_{maxL}

$i := 1..16$

$$\alpha := \begin{pmatrix} 140.174 \\ 139 \\ 137 \\ 135 \\ 133 \\ 130 \\ 127 \\ 124 \\ 121 \\ 118 \\ 115 \\ 112 \\ 109 \\ 106 \\ 103 \\ 90 \end{pmatrix} \cdot deg$$

$\alpha maxL = 140.174 \cdot deg$

$\alpha =$

	1
1	2.446
2	2.426
3	2.391
4	2.356
5	2.321
6	2.269
7	2.217
8	2.164
9	2.112
10	2.059
11	2.007
12	1.955
13	1.902
14	1.85
15	1.798
16	1.571

$\cdot$ rad

Determine the ratio of the pressure to the effective stress. The effective stress during loading is equal to yield stress. Let α aL be the value of α at the edge of the hole during loading. Use n=40 and vary the pressure to obtain the maximum elastic-plastic radius.

$$P\sigma y L_i := \sqrt{\frac{1+R}{2}} \cdot \left(\frac{\sin(\alpha_i)}{\sqrt{1+2\cdot R}} - \cos(\alpha_i) \right) \cdot \left(\frac{A}{A\cdot \sin(\alpha_i) + B\cdot \cos(\alpha_i)} \right)^{\mu} \cdot e^{\left(\frac{A}{C}\right)\cdot\left(\alpha_i - \frac{\pi}{2}\cdot rad\right)}$$

Solve for α aL. α aL is the value of α at the edge of the hole while α = 90 deg at the elastic-plastic boundary. Use the root function from Mathcad to solve the above equation for different values of Pσ yL until the elastic plastic boundary = 2.2

$$\mathrm{Function}(\alpha cL) := \sqrt{\frac{1+R}{2}} \cdot \left(\frac{\sin(\alpha cL)}{\sqrt{1+2\cdot R}} - \cos(\alpha cL) \right) \cdot \left(\frac{A}{A\cdot \sin(\alpha cL) \ldots + B\cdot \cos(\alpha cL)} \right)^{\mu} \cdot e^{\left(\frac{A}{C}\right)\cdot\left(\alpha cL \cdot rad - \frac{\pi}{2}\cdot rad\right)} - 1.7040$$

$\alpha aL := \mathrm{root}(\mathrm{Function}(\alpha cL), \alpha cL, 1.57\cdot rad, 2.5\cdot rad)$ $\alpha aL = 2.373842$ $\alpha aL = 136.011\cdot deg$

2. Calculate the radius of the elastic-plastic interface

Ratio of the radius of the elastic-plastic interface to radius of the hole is b_1/a in Ball. Labeled B1L in the following calculation and is only a function of α_a.

المنارة للاستشارات
www.manaraa.com

$$B1L := \sqrt{\sin(\alpha aL)} \cdot \left(\frac{A}{A \cdot \sin(\alpha aL) + B \cdot \cos(\alpha aL)}\right)^{\gamma} \cdot e^{\left(\frac{D}{2 \cdot C}\right)\cdot\left(\alpha aL - \frac{\pi}{2} \cdot rad\right)}$$

B1L = 2.57087

Use P/σ y = 1.704

Good agrement with experimental results. Actual mesured radius for the elastic-plastic boundary was from ~2.5 to ~3; but may have been incresed by the ultrasonic vibration

3. Calculate r/a as a function of α as π /2 < α < α ***aL***

r/a in calcs as raL

r/a = 1- initial edge of the hole

$i := 1..22$

$$\alpha L := \begin{pmatrix} 136.011 \\ 135 \\ 133 \\ 131 \\ 129.1586 \\ 127 \\ 125 \\ 123 \\ 121 \\ 119 \\ 117 \\ 115 \\ 113 \\ 111 \\ 109 \\ 107 \\ 105 \\ 102 \\ 99 \\ 96 \\ 93 \\ 90 \end{pmatrix} \cdot deg \qquad \alpha L_i = \begin{array}{|c|} \hline 2.374 \\ \hline 2.356 \\ \hline 2.321 \\ \hline 2.286 \\ \hline 2.254 \\ \hline 2.217 \\ \hline 2.182 \\ \hline 2.147 \\ \hline 2.112 \\ \hline 2.077 \\ \hline 2.042 \\ \hline 2.007 \\ \hline 1.972 \\ \hline 1.937 \\ \hline 1.902 \\ \hline 1.868 \\ \hline 1.833 \\ \hline 1.78 \\ \hline 1.728 \\ \hline 1.676 \\ \hline 1.623 \\ \hline 1.571 \\ \hline \end{array} \cdot rad$$

r/a =1.82024 - the radius of the elastic-plastic boundary

$$rpL_i := \sqrt{\frac{\sin(\alpha aL)}{\sin(\alpha L_i)}} \cdot \left(\frac{A \cdot \sin(\alpha L_i) + B \cdot \cos(\alpha L_i)}{A \cdot \sin(\alpha aL) + B \cdot \cos(\alpha aL)}\right)^{\gamma} \cdot e^{\left(\frac{D}{2 \cdot C}\right)\cdot(\alpha aL - \alpha L_i)}$$

α = 2.4 rad (136.011 deg) edge of the hole

المنارة للاستشارات
www.manaraa.com

rpL =

	1
1	1.00001
2	1.049
3	1.13118
4	1.20205
5	1.26163
6	1.32742
7	1.3861
8	1.44366
9	1.5008
10	1.55805
11	1.61584
12	1.67449
13	1.73428
14	1.79545
15	1.85822
16	1.9228
17	1.98937
18	2.09338
19	2.2029
20	2.31855
21	2.44099
22	2.57087

α = 1.571 rad (90 deg)   elastic-plastic boundary

www.manaraa.com

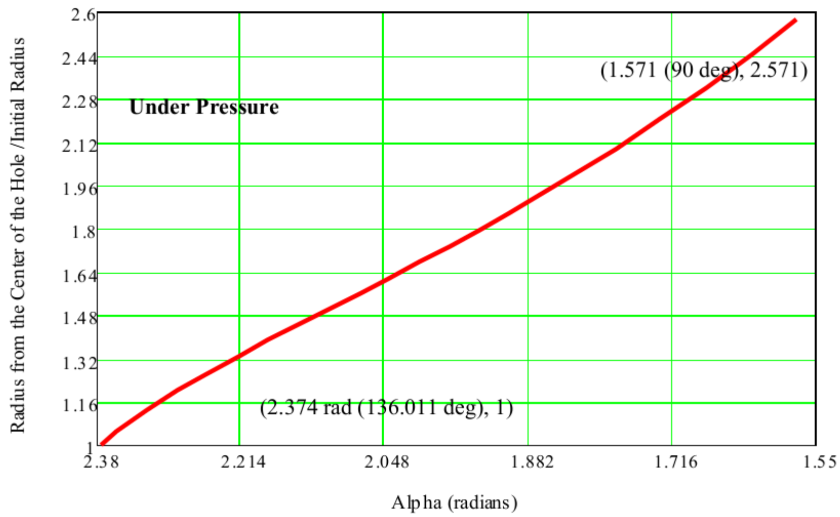

Fig. 1 Radius from the Center of the Hole Versus Parameterization Angle Alpha

4. Calculate ratio of effective stress / yield stress as a function of α

Ratio of effective stress / yield stress labeled Rσ eL in calculations

$$R\sigma eL_i := \left(\frac{A}{A \cdot \sin\left(\alpha L_i\right) + B \cdot \cos\left(\alpha L_i\right)} \right)^{\mu} \cdot e^{\left(\frac{A}{C}\right) \cdot \left(\alpha L_i - \frac{\pi}{2} \cdot rad\right)}$$

www.manaraa.com

$R\sigma eL_i =$

	1
1	1.521
2	1.476
3	1.409
4	1.359
5	1.322
6	1.285
7	1.256
8	1.231
9	1.208
10	1.187
11	1.168
12	1.151
13	1.135
14	1.119
15	1.105
16	1.092
17	1.079
18	1.061
19	1.044
20	1.029
21	1.014
22	1

α = 2.374 rad (136.011 deg), r/a = 1

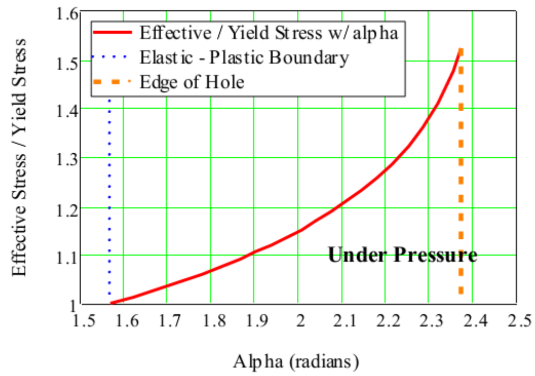

Fig 2. Normalized Effective Stress vs Alpha

α = 1.571 (90 deg),
r/a =2.57

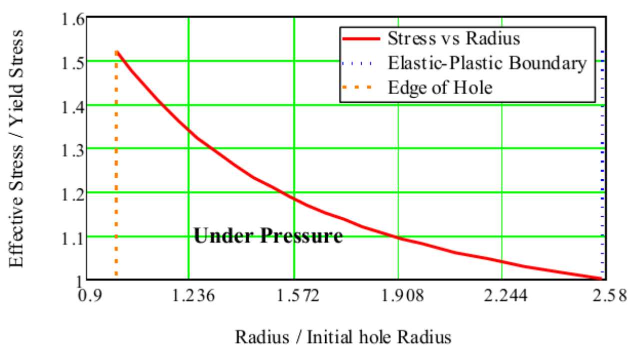

Fig 3. Normalized Effective Stress vs Normalized Radius

www.manaraa.com

5. Calculate ratio of tangential and radial plastic stress in the plastic region between the edge of the hole and the elastic-plastic boundary

Let ratio for tangential plastic stress to yield stress be SptL and and ratio for plastic radial stress to yield stress be SprL and both are functions of ratio of effective stress to yield stress (Rσ e) and α

$$SptL_i := \frac{R\sigma eL_i}{2} \cdot \sqrt{2 + 2 \cdot R} \cdot \left(\cos\left(\alpha L_i\right) + \frac{1}{\sqrt{1 + 2 \cdot R}} \cdot \sin\left(\alpha L_i\right) \right)$$

$q := -2.. .1.6$

$$SprL_i := \frac{R\sigma eL_i}{2} \cdot \sqrt{2 + 2 \cdot R} \cdot \left(\cos\left(\alpha L_i\right) - \frac{1}{\sqrt{1 + 2 \cdot R}} \cdot \sin\left(\alpha L_i\right) \right)$$

SptL =

	1
1	-0.484
2	-0.441
3	-0.366
4	-0.299
5	-0.243
6	-0.181
7	-0.126
8	-0.074
9	-0.024
10	0.024
11	0.071
12	0.116
13	0.16
14	0.202
15	0.243
16	0.284
17	0.322
18	0.379
19	0.432
20	0.483
21	0.531
22	0.577

SprL =

	1
1	-1.704
2	-1.646
3	-1.556
4	-1.484
5	-1.426
6	-1.366
7	-1.315
8	-1.266
9	-1.22
10	-1.175
11	-1.132
12	-1.089
13	-1.046
14	-1.005
15	-0.963
16	-0.922
17	-0.881
18	-0.82
19	-0.759
20	-0.698
21	-0.638
22	-0.577

6. Calculate ratio of elastic tangential to yield stress and ratio of elastic radial stresses to yield stress

Use SetL for the ratio of elastic tangential to yield stress and SerL for the ratio of elastic radial stress to yield stress

www.manaraa.com

$B1L = 2.571$

$j := 1..14$

$reL_1 := 2.571$

$reL_{j+1} := reL_j + 0.25$

$j := 1..15$

$$SetL_j := \sqrt{\frac{1+R}{2(1+2\cdot R)}} \cdot \left(\frac{B1L}{reL_j}\right)^2$$

$SerL := -SetL$

reL =

	1
1	2.571
2	2.821
3	3.071
4	3.321
5	3.571
6	3.821
7	4.071
8	4.321
9	4.571
10	4.821
11	5.071
12	5.321
13	5.571
14	5.821
15	6.071

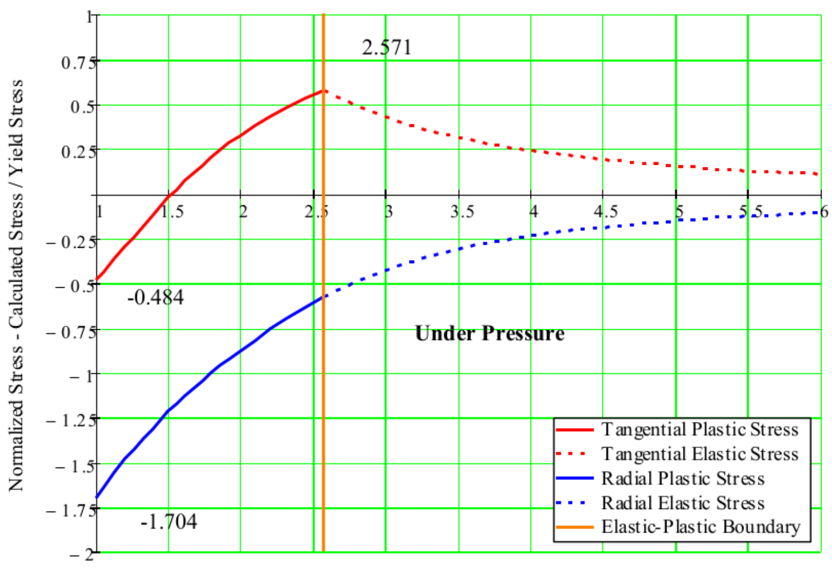

Fig 4. Radial and Tangential Stresses Adjacent to Expanded Hole Under Pressure

www.manaraa.com

7. Combine into 1 matrix of distance and 1 each for Tangential and Radial Stress

$RAL_i := rpL_i \quad RAL_{j+22} := reL_j \quad TSL_i := SptL_i \quad TSL_{j+22} := SetL_j \quad RSL_i := SprL_i \quad RSL_{j+22} := SerL_j$

RAL =

	1
1	1
2	1.049
3	1.131
4	1.202
5	1.262
6	1.327
7	1.386
8	1.444
9	1.501
10	1.558
11	1.616
12	1.674
13	1.734
14	1.795
15	1.858
16	...

TSL =

	1
1	-0.484
2	-0.441
3	-0.366
4	-0.299
5	-0.243
6	-0.181
7	-0.126
8	-0.074
9	-0.024
10	0.024
11	0.071
12	0.116
13	0.16
14	0.202
15	0.243
16	...

RSL =

	1
1	-1.704
2	-1.646
3	-1.556
4	-1.484
5	-1.426
6	-1.366
7	-1.315
8	-1.266
9	-1.22
10	-1.175
11	-1.132
12	-1.089
13	-1.046
14	-1.005
15	-0.963
16	...

www.manaraa.com

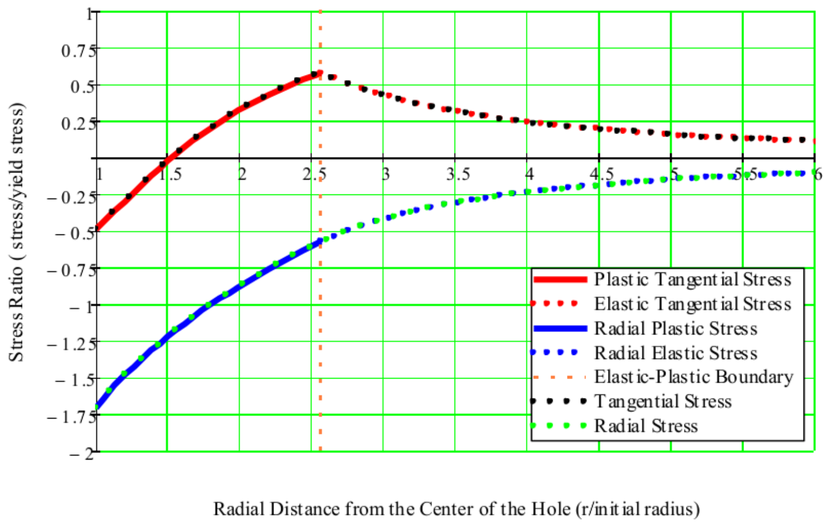

Fig 5. Tangential and Radial Stress Under Pressure

C. Results after removal of expansion

1. Constants defined

β is Bauschinger's parameter and is a measure of the reduction in yield stress in compression due to strain be yield strain in tension. $\beta = 0$ is for isotropic behavior while $\beta = 1$ implies kinematic hardening

Note: U is used to denote the unloading phase

from Section 1 expansion calculation, use $\sigma_{yield} = 34.69$ ksi and $P/\sigma_{yield} = 1.7040$

$$P := 1.70405\cdot \sigma yield \qquad P = 59.113\cdot \text{ksi}$$

2. Determination of new α_{a} *(α_{aU})*

α_{aU} is the parameterization variable and can vary between $\pi/2$ to α max. α_{aU} is for the region in the plastic

annulus in which the unloading causes reverse yielding. α_{aU} is new value at the edge of the hole while

$\alpha = 90deg$ is the value at the new elastic-plastic boundary. α max as determine above.

new yield stress σ_{o2}

$P\sigma yL$ is ratio of the pressure/new yield stress and varies with α_{b} where α_{b} is α bL from the original calculation for the plastic region in 2 above

Using $\beta = 1$ $\qquad \sigma o2 := (1+\beta)\cdot \sigma yield + (1-\beta)\cdot \sigma yield \qquad \sigma o2 = 69.38\cdot \text{ksi}$

www.manaraa.com

$i := 1..14$ $\qquad \dfrac{P}{\sigma o2} = 0.852$

$$P\sigma y U_i := \sqrt{\frac{1+R}{2}} \cdot \left(\frac{\sin(\alpha L_i)}{\sqrt{1+2 \cdot R}} - \cos(\alpha L_i) \right) \cdot \left(\frac{A}{A \cdot \sin(\alpha L_i) + B \cdot \cos(\alpha L_i)} \right)^{\mu} \cdot e^{\left(\frac{A}{C}\right)\cdot\left(\alpha L_i - \frac{\pi}{2}\cdot rad\right)}$$

Solve for α aU. α aU is the value of α at the edge of the hole while α = 90 deg at the elastic-plastic boundary. Use the root function from Mathcad to solve the above equation for Pσ yL = 0.852.

$$Function(\alpha bL) := \sqrt{\frac{1+R}{2}} \cdot \left(\frac{\sin(\alpha bL)}{\sqrt{1+2 \cdot R}} - \cos(\alpha bL) \right) \cdot \left(\frac{A}{A \cdot \sin(\alpha bL) \ ... \ + B \cdot \cos(\alpha bL)} \right)^{\mu} \cdot e^{\left(\frac{A}{C}\right)\cdot\left(\alpha bL - \frac{\pi}{2}\cdot rad\right)} - \frac{P}{\sigma o2}$$

$\alpha aU := root(Function(\alpha bL), \alpha bL, 1.57 \cdot rad, 2.5 \cdot rad)$ $\qquad \alpha aU = 1.807928$ $\qquad \alpha aU = 103.58666\ deg$

3. Calculate the radius of the region experiencing reverse yielding after unloading

Ratio of the radius of material experiencing reverse yielding to hole radius is b_2/a. Labeled B2U in the following calculation and is only a function of new α_{aU}. γ from Section 1 CONSTANTS above.

$$B2U := \sqrt{\sin(\alpha aU)} \cdot \left(\frac{A}{A \cdot \sin(\alpha aU) + B \cdot \cos(\alpha aU)} \right)^{\gamma} \cdot e^{\left(\frac{D}{2 \cdot C}\right)\cdot\left(\alpha aU - \frac{\pi}{2}\cdot rad\right)}$$

$B2U = 1.26164$

4. Calculate r/a as a function of new α as π /2 < α < α aU.

$k := 1..9$

$$\alpha U := \begin{pmatrix} 103.587 \\ 102 \\ 100.5 \\ 99 \\ 97.5 \\ 96 \\ 94.5 \\ 93 \\ 90 \end{pmatrix} \cdot deg \qquad \alpha U_k = \begin{array}{|c|} \hline 1.808 \\ \hline 1.78 \\ \hline 1.754 \\ \hline 1.728 \\ \hline 1.702 \\ \hline 1.676 \\ \hline 1.649 \\ \hline 1.623 \\ \hline 1.571 \\ \hline \end{array} \cdot rad$$

edge of the hole

elastic-plastic boundary on unloading

المنارة للاستشارات
www.manaraa.com

r/a for unloading as in calcs as labeled - rb

$$rpU_k := \sqrt{\frac{\sin(\alpha aU)}{\sin(\alpha U_k)}} \cdot \left(\frac{A \cdot \sin(\alpha U_k) + B \cdot \cos(\alpha U_k)}{A \cdot \sin(\alpha aU) + B \cdot \cos(\alpha aU)}\right)^{\gamma} \cdot e^{\left(\frac{D}{2 \cdot C}\right) \cdot (\alpha aU - \alpha U_k)}$$

$$rpU = \begin{pmatrix} 0.9999942 \\ 1.0273123 \\ 1.0538285 \\ 1.0810591 \\ 1.1090423 \\ 1.1378168 \\ 1.1674222 \\ 1.1978995 \\ 1.2616391 \end{pmatrix}$$

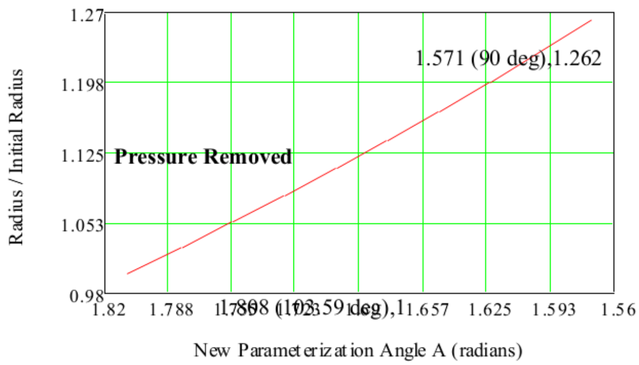

Fig 6. Radius versus Alpha for Unloading

$$rpU_9 = 1.2616391$$

5. Calculate ratio of effective stress / new yield stress as a function of α

Ratio of effective stress / yield stress. Ratio labeled Rσ eU in calculations

$$R\sigma eU_k := -\left[\left(\frac{A}{A \cdot \sin(\alpha U_k) + B \cdot \cos(\alpha U_k)}\right)^{\mu} \cdot e^{\left(\frac{A}{C}\right) \cdot \left(\alpha U_k - \frac{\pi}{2} \cdot rad\right)}\right]$$

المنارة للاستشارات
www.manaraa.com

edge of hole

α = 1.808 (103.59deg), rb=1

$$R\sigma eU_k = \begin{array}{|r|}\hline -1.07024 \\ \hline -1.06089 \\ \hline -1.05238 \\ \hline -1.04416 \\ \hline -1.03621 \\ \hline -1.02852 \\ \hline -1.02106 \\ \hline -1.01383 \\ \hline -1 \\ \hline \end{array}$$

elastic-plastic boundary on unloading

α = 1.571 (90 deg), rb = 1.262

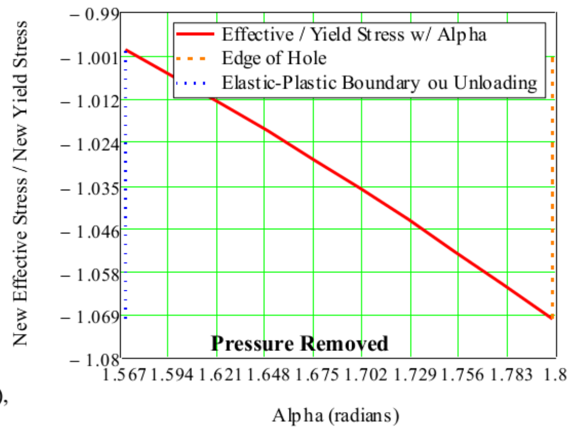

Fig 7. Normalized Effective Stress vs Alpha

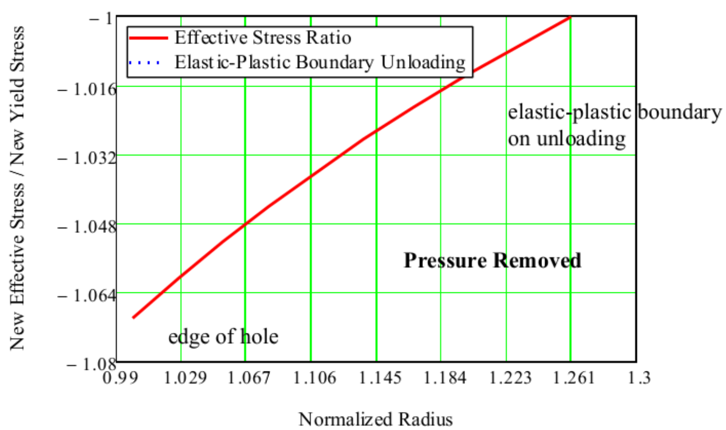

Fig 8. Normalized Effective Stress vs Normalized Radius

6. Calculate ratio of tangential and radial plastic stress

Let ratio for tangential plastic stress to yield stress be SptU and and ratio for plastic radial stress to yield stress be SprU and both are functions of ratio of new effective stress to new yield stress (Rσ eU) and α U

$$SptU_k := 2\left[\frac{R\sigma eU_k}{2}\cdot\sqrt{2+2\cdot R}\cdot\left(\cos\left(\alpha U_k\right)+\frac{1}{\sqrt{1+2\cdot R}}\cdot\sin\left(\alpha U_k\right)\right)\right]$$

المنارة للاستشارات
www.manaraa.com

$$SprU_k := 2 \cdot \left[\frac{R\sigma eU_k}{2} \cdot \sqrt{2 + 2 \cdot R} \cdot \left(\cos\left(\alpha U_k\right) - \frac{1}{\sqrt{1 + 2 \cdot R}} \cdot \sin\left(\alpha U_k\right) \right) \right]$$

$$SptU = \begin{pmatrix} -0.698 \\ -0.757 \\ -0.811 \\ -0.864 \\ -0.916 \\ -0.966 \\ -1.015 \\ -1.063 \\ -1.155 \end{pmatrix} \qquad SprU = \begin{pmatrix} 1.704 \\ 1.639 \\ 1.578 \\ 1.518 \\ 1.457 \\ 1.396 \\ 1.336 \\ 1.275 \\ 1.155 \end{pmatrix}$$

q is to plot elastic-plastic boundary

$q := -2 .. 2$

7. Calculate ratio of the change in elastic tangential to yield stress due to unloading and the ratio of the change in elastic radial stresses to yield stress from unloading

Use 'Setu' for the ratio of the change in elastic tangential to yield stress and 'Seru' for the ratio of elastic radial stress to yield stress

$B2U = 1.262$

$j := 1 .. 21 \quad J_j := j \quad reU_j := B2U + 0.25 \cdot J_j - 0.2$

j =

	1
1	1
2	2
3	3
4	4
5	5
6	6
7	7
8	8
9	9
10	10
11	11
12	12
13	13
14	14
15	15
16	16
17	17
18	18
19	...

J =

	1
1	1
2	2
3	3
4	4
5	5
6	6
7	7
8	8
9	9
10	10
11	11
12	12
13	13
14	14
15	15
16	16
17	17
18	18
19	...

reU_j =

	1
1	1.262
2	1.512
3	1.762
4	2.012
5	2.262
6	2.512
7	2.762
8	3.012
9	3.262
10	3.512
11	3.762
12	4.012
13	4.262
14	4.512
15	4.762
16	5.012
17	5.262
18	5.512
19	...

المنارة للاستشارات
www.manaraa.com

$$SerU_j := 2 \cdot \left[\sqrt{\frac{1+R}{2(1+2 \cdot R)}} \cdot \left(\frac{B2U}{reU_j} \right)^2 \right]$$

$$SetU_j := -SerU_j$$

SerU =

	1
1	1.155
2	0.804
3	0.592
4	0.454
5	0.359
6	0.291
7	0.241
8	0.203
9	0.173
10	0.149
11	0.13
12	0.114
13	0.101
14	0.09
15	0.081
16	0.073
17	0.066
18	0.061
19	0.055
20	0.051
21	0.047

SetU =

	1
1	-1.155
2	-0.804
3	-0.592
4	-0.454
5	-0.359
6	-0.291
7	-0.241
8	-0.203
9	-0.173
10	-0.149
11	-0.13
12	-0.114
13	-0.101
14	-0.09
15	-0.081
16	-0.073
17	-0.066
18	-0.061
19	-0.055
20	-0.051
21	-0.047

Plot Δ stress from unloading

$i := 1 .. 22$

المنارة للاستشارات

www.manaraa.com

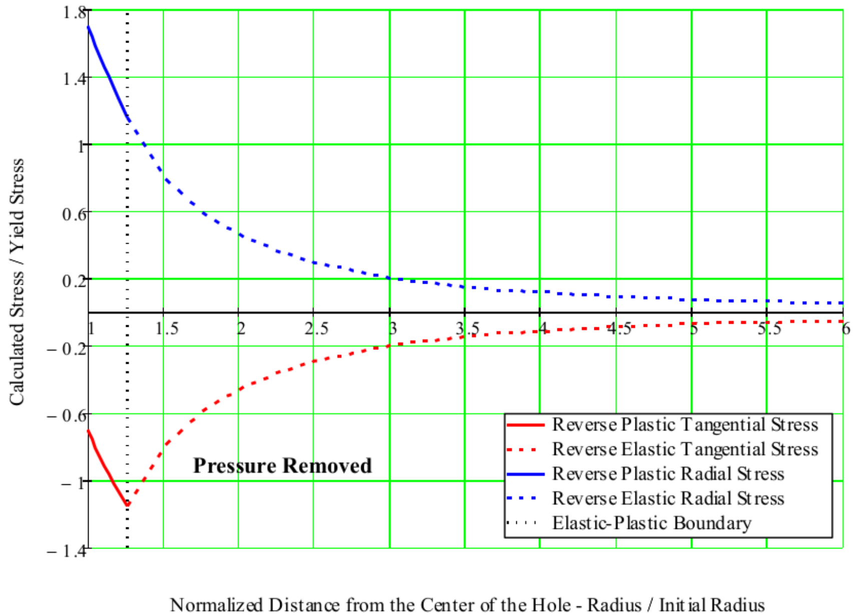

Fig 9. Changes in Radial and Tangential Stress due to Unloading

www.manaraa.com

8. Combine into 1 matrix of distance and 1 each for Tangential and Radial Stress

rpL =

	1
1	1
2	1.049
3	1.131
4	1.202
5	1.262
6	1.327
7	1.386
8	1.444
9	1.501
10	1.558
11	1.616
12	1.674
13	1.734
14	1.795
15	1.858
16	1.923
17	1.989
18	2.093
19	2.203
20	2.319
21	2.441
22	2.571

$$rpU = \begin{pmatrix} 0.999994 \\ 1.027312 \\ 1.053829 \\ 1.081059 \\ 1.109042 \\ 1.137817 \\ 1.167422 \\ 1.197899 \\ 1.261639 \end{pmatrix}$$

reU =

	1
1	1.262
2	1.512
3	1.762
4	2.012
5	2.262
6	2.512
7	2.762
8	3.012
9	3.262
10	3.512
11	3.762
12	4.012
13	4.262
14	4.512
15	4.762
16	5.012
17	5.262
18	5.512
19	5.762
20	6.012
21	6.262

$RAU_k := rpU_k$

$RAU_{j+8} := reU_j$

$TSU_k := SptU_k$

$TSU_{j+8} := SetU_j$

$RSU_k := SprU_k$

$RSU_{j+8} := SerU_j$

المنارة للاستشارات
www.manaraa.com

RAU =

	1
1	0.999994
2	1.027312
3	1.053829
4	1.081059
5	1.109042
6	1.137817
7	1.167422
8	1.197899
9	1.261639
10	1.511639
11	1.761639
12	2.011639
13	2.261639
14	2.511639
15	2.761639
16	3.011639
17	3.261639
18	3.511639
19	3.761639
20	4.011639
21	4.261639
22	4.511639
23	4.761639
24	5.011639
25	5.261639
26	5.511639
27	5.761639
28	6.011639
29	6.261639

TSU =

	1
1	-0.698
2	-0.757
3	-0.811
4	-0.864
5	-0.916
6	-0.966
7	-1.015
8	-1.063
9	-1.155
10	-0.804
11	-0.592
12	-0.454
13	-0.359
14	-0.291
15	-0.241
16	-0.203
17	-0.173
18	-0.149
19	-0.13
20	-0.114
21	-0.101
22	-0.09
23	-0.081
24	-0.073
25	-0.066
26	-0.061
27	-0.055
28	-0.051
29	-0.047

RSU =

	1
1	1.704
2	1.639
3	1.578
4	1.518
5	1.457
6	1.396
7	1.336
8	1.275
9	1.155
10	0.804
11	0.592
12	0.454
13	0.359
14	0.291
15	0.241
16	0.203
17	0.173
18	0.149
19	0.13
20	0.114
21	0.101
22	0.09
23	0.081
24	0.073
25	0.066
26	0.061
27	0.055
28	0.051
29	0.047

$z := 1 .. 29$

المنارة للاستشارات
www.manaraa.com

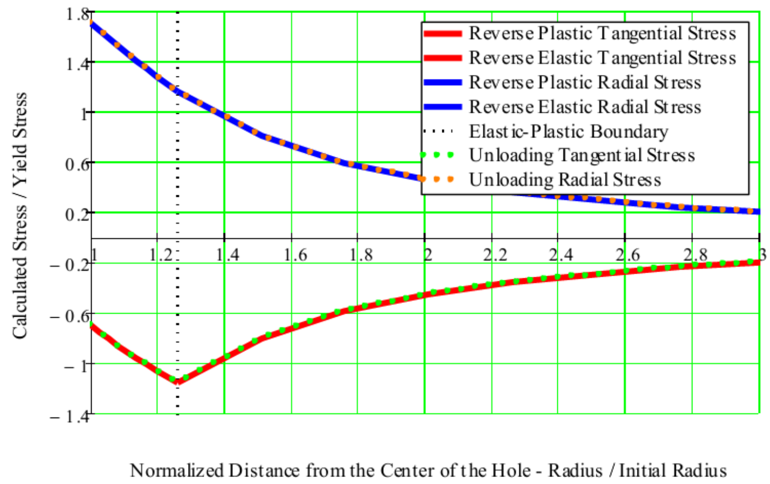

Fig 10. Changes in Radial and Tangential Stress due to Unloading

9. Plot combined matrices of distance and Tangential and Radial Stress

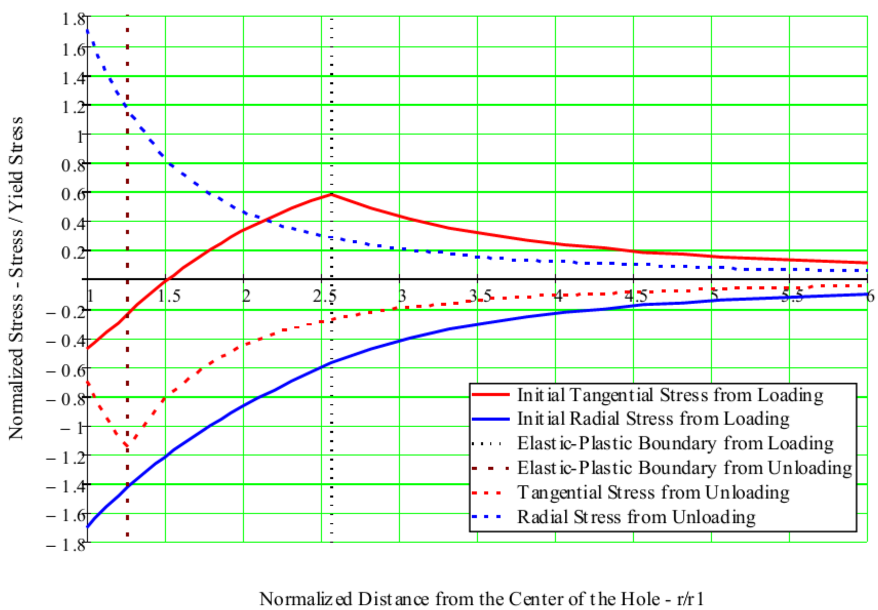

Fig 11. Stresses from Expansion Pressure and from Removing the Expansion Pressure

www.manaraa.com

D. Combine Results 2 and 3 to Obtain Residual Stress

Revise calculations to determine results for 3 separate regions

1. Region 1 from edge of hole to elastic-plastic boundary from unloading
   ra = 1 to ra =1.262
2. From elastic-boundary from unloading to the elastic-plastic boundary from loading
   ra = 1.262 to ra = 2.571
3. From elastic-plastic boundary (ra=2.571) from loading to infinite ~ ra = 6

1. For Region 1 where 0< r/a < 1.26164

Calculate the alpha angle for the loading stress in this region between r/a =1 and r/a = 1.174 at the same interval as was done for the unloading step

$\alpha aL = 2.373842$ r/a for the unloading step

$$raR1 := rpU \qquad rpU = \begin{pmatrix} 0.999994 \\ 1.027312 \\ 1.053829 \\ 1.081059 \\ 1.109042 \\ 1.137817 \\ 1.167422 \\ 1.197899 \\ 1.261639 \end{pmatrix} \qquad raR1 = \begin{pmatrix} 0.99999 \\ 1.02731 \\ 1.05383 \\ 1.08106 \\ 1.10904 \\ 1.13782 \\ 1.16742 \\ 1.1979 \\ 1.26164 \end{pmatrix}$$

Radius 1

$$\text{function}(\alpha) := \sqrt{\frac{\sin(\alpha aL)}{\sin(\alpha)}} \cdot \left[\frac{(n-1)\cdot\sqrt{1+2\cdot R}\cdot\sin(\alpha) + (n+1+2\cdot R)\cdot\cos(\alpha)}{(n-1)\cdot\sqrt{1+2\cdot R}\cdot\sin(\alpha aL) + (n+1+2\cdot R)\cdot\cos(\alpha aL)}\right]^{\gamma} \cdot e^{\left[\frac{(n^2-1)\cdot\sqrt{1+2\cdot R}}{2\cdot(n^2+1+2\cdot R)}\right]\cdot(\alpha aL-\alpha)} - raR1_1$$

$\alpha 1R_1 := \text{root}(\text{function}(\alpha), \alpha, 1.57\cdot\text{rad}, 2.5\cdot\text{rad})$ $\alpha 1R_1 = 136.011\cdot\text{deg}$ $\alpha 1R_1 = 2.37384$

Radius 2

$$\text{function}(\alpha) := \sqrt{\frac{\sin(\alpha aL)}{\sin(\alpha)}} \cdot \left[\frac{(n-1)\cdot\sqrt{1+2\cdot R}\cdot\sin(\alpha) + (n+1+2\cdot R)\cdot\cos(\alpha)}{(n-1)\cdot\sqrt{1+2\cdot R}\cdot\sin(\alpha aL) + (n+1+2\cdot R)\cdot\cos(\alpha aL)}\right]^{\gamma} \cdot e^{\left[\frac{(n^2-1)\cdot\sqrt{1+2\cdot R}}{2\cdot(n^2+1+2\cdot R)}\right]\cdot(\alpha aL-\alpha)} - raR1_2$$

$\alpha 1R_2 := \text{root}(\text{function}(\alpha), \alpha, 2.1\cdot\text{rad}, 2.4\cdot\text{rad})$ $\alpha 1R_2 = 135.465\cdot\text{deg}$ $\alpha 1R_2 = 2.364$

Radius 3

$$\text{function}(\alpha) := \sqrt{\frac{\sin(\alpha aL)}{\sin(\alpha)}} \cdot \left[\frac{(n-1)\cdot\sqrt{1+2\cdot R}\cdot\sin(\alpha) + (n+1+2\cdot R)\cdot\cos(\alpha)}{(n-1)\cdot\sqrt{1+2\cdot R}\cdot\sin(\alpha aL) + (n+1+2\cdot R)\cdot\cos(\alpha aL)}\right]^{\gamma} \cdot e^{\left[\frac{(n^2-1)\cdot\sqrt{1+2\cdot R}}{2\cdot(n^2+1+2\cdot R)}\right]\cdot(\alpha aL-\alpha)} - raR1_3$$

www.manaraa.com

$\alpha 1R_3 := \mathrm{root}(\mathrm{function}(\alpha), \alpha, 2.1 \cdot \mathrm{rad}, 2.4 \cdot \mathrm{rad})$ $\alpha 1R_3 = 134.893 \cdot \mathrm{deg}$ $\alpha 1R_3 = 2.354$

Radius 4

$$\mathrm{function}(\alpha) := \sqrt{\frac{\sin(\alpha aL)}{\sin(\alpha)}} \cdot \left[\frac{(n-1)\cdot\sqrt{1+2\cdot R}\cdot\sin(\alpha) \ldots + (n+1+2\cdot R)\cdot\cos(\alpha)}{(n-1)\cdot\sqrt{1+2\cdot R}\cdot\sin(\alpha aL) \ldots + (n+1+2\cdot R)\cdot\cos(\alpha aL)}\right]^{\gamma} \cdot e^{\left[\frac{(n^2-1)\cdot\sqrt{1+2\cdot R}}{2\cdot(n^2+1+2\cdot R)}\right]\cdot(\alpha aL-\alpha)} - raR1_4$$

$\alpha 1R_4 := \mathrm{root}(\mathrm{function}(\alpha), \alpha, 2.1 \cdot \mathrm{rad}, 2.4 \cdot \mathrm{rad})$ $\alpha 1R_4 = 134.264 \cdot \mathrm{deg}$ $\alpha 1R_4 = 2.343$

Radius 5

$$\mathrm{function}(\alpha) := \sqrt{\frac{\sin(\alpha aL)}{\sin(\alpha)}} \cdot \left[\frac{(n-1)\cdot\sqrt{1+2\cdot R}\cdot\sin(\alpha) \ldots + (n+1+2\cdot R)\cdot\cos(\alpha)}{(n-1)\cdot\sqrt{1+2\cdot R}\cdot\sin(\alpha aL) \ldots + (n+1+2\cdot R)\cdot\cos(\alpha aL)}\right]^{\gamma} \cdot e^{\left[\frac{(n^2-1)\cdot\sqrt{1+2\cdot R}}{2\cdot(n^2+1+2\cdot R)}\right]\cdot(\alpha aL-\alpha)} - raR1_5$$

$\alpha 1R_5 := \mathrm{root}(\mathrm{function}(\alpha), \alpha, 2.1 \cdot \mathrm{rad}, 2.4 \cdot \mathrm{rad})$ $\alpha 1R_5 = 133.575 \cdot \mathrm{deg}$ $\alpha 1R_5 = 2.331$

Radius 6

$$\mathrm{function}(\alpha) := \sqrt{\frac{\sin(\alpha aL)}{\sin(\alpha)}} \cdot \left[\frac{(n-1)\cdot\sqrt{1+2\cdot R}\cdot\sin(\alpha) \ldots + (n+1+2\cdot R)\cdot\cos(\alpha)}{(n-1)\cdot\sqrt{1+2\cdot R}\cdot\sin(\alpha aL) \ldots + (n+1+2\cdot R)\cdot\cos(\alpha aL)}\right]^{\gamma} \cdot e^{\left[\frac{(n^2-1)\cdot\sqrt{1+2\cdot R}}{2\cdot(n^2+1+2\cdot R)}\right]\cdot(\alpha aL-\alpha)} - raR1_6$$

$\alpha 1R_6 := \mathrm{root}(\mathrm{function}(\alpha), \alpha, 2.1 \cdot \mathrm{rad}, 2.4 \cdot \mathrm{rad})$ $\alpha 1R_6 = 132.823 \cdot \mathrm{deg}$ $\alpha 1R_6 = 2.318$

Radius 7

$$\mathrm{function}(\alpha) := \sqrt{\frac{\sin(\alpha aL)}{\sin(\alpha)}} \cdot \left[\frac{(n-1)\cdot\sqrt{1+2\cdot R}\cdot\sin(\alpha) \ldots + (n+1+2\cdot R)\cdot\cos(\alpha)}{(n-1)\cdot\sqrt{1+2\cdot R}\cdot\sin(\alpha aL) \ldots + (n+1+2\cdot R)\cdot\cos(\alpha aL)}\right]^{\gamma} \cdot e^{\left[\frac{(n^2-1)\cdot\sqrt{1+2\cdot R}}{2\cdot(n^2+1+2\cdot R)}\right]\cdot(\alpha aL-\alpha)} - raR1_7$$

$\alpha 1R_7 := \mathrm{root}(\mathrm{function}(\alpha), \alpha, 2.1 \cdot \mathrm{rad}, 2.4 \cdot \mathrm{rad})$ $\alpha 1R_7 = 132.006 \cdot \mathrm{deg}$ $\alpha 1R_7 = 2.304$

Radius 8

$$\mathrm{function}(\alpha) := \sqrt{\frac{\sin(\alpha aL)}{\sin(\alpha)}} \cdot \left[\frac{(n-1)\cdot\sqrt{1+2\cdot R}\cdot\sin(\alpha) \ldots + (n+1+2\cdot R)\cdot\cos(\alpha)}{(n-1)\cdot\sqrt{1+2\cdot R}\cdot\sin(\alpha aL) \ldots + (n+1+2\cdot R)\cdot\cos(\alpha aL)}\right]^{\gamma} \cdot e^{\left[\frac{(n^2-1)\cdot\sqrt{1+2\cdot R}}{2\cdot(n^2+1+2\cdot R)}\right]\cdot(\alpha aL-\alpha)} - raR1_8$$

$\alpha 1R_8 := \mathrm{root}(\mathrm{function}(\alpha), \alpha, 2.1 \cdot \mathrm{rad}, 2.4 \cdot \mathrm{rad})$ $\alpha 1R_8 = 131.123 \cdot \mathrm{deg}$ $\alpha 1R_8 = 2.289$

المنارة للاستشارات
www.manaraa.com

Radius 9

$$\text{function}(\alpha) := \sqrt{\frac{\sin(\alpha aL)}{\sin(\alpha)}} \cdot \left[\frac{(n-1)\cdot\sqrt{1+2\cdot R}\cdot\sin(\alpha)\ \ldots \\ +(n+1+2\cdot R)\cdot\cos(\alpha)}{(n-1)\cdot\sqrt{1+2\cdot R}\cdot\sin(\alpha aL)\ \ldots \\ +(n+1+2\cdot R)\cdot\cos(\alpha aL)}\right]^{\gamma} \cdot e^{\left[\frac{(n^2-1)\cdot\sqrt{1+2\cdot R}}{2\cdot(n^2+1+2\cdot R)}\right]\cdot(\alpha aL-\alpha)} - raR1_9$$

$\alpha 1R_9 := \text{root}(\text{function}(\alpha), \alpha, 2.1\cdot \text{rad}, 2.5\cdot \text{rad})$ $\alpha 1R_9 = 129.159\cdot \text{deg}$ $\alpha 1R_9 = 2.254$

$\alpha L =$

	1
1	2.374
2	2.356
3	2.321
4	2.286
5	2.254
6	2.217
7	2.182
8	2.147
9	2.112
10	2.077
11	2.042
12	2.007
13	1.972
14	1.937
15	1.902
16	...

$\alpha L =$ $\cdot$ deg

	1
1	136.011
2	135
3	133
4	131
5	129.159
6	127
7	125
8	123
9	121
10	119
11	117
12	115
13	113
14	111
15	109
16	...

α for Loading at the same interval as Unloading between the edge of the hole and the elastic-plastic boundary in Unloading

$$\alpha 1R = \begin{pmatrix}136.011\\135.465\\134.893\\134.264\\133.575\\132.823\\132.006\\131.123\\129.159\end{pmatrix}\cdot \text{deg} \qquad \alpha 1R = \begin{pmatrix}2.373843\\2.364306\\2.354326\\2.343348\\2.331319\\2.318194\\2.303939\\2.288532\\2.254242\end{pmatrix}$$

looks reasonable

Calculate the ratio of effective stress / yield stress for loading as function of α 1R. Ratio is Rσ eL1

$o := 1..9$

$$R\sigma eL1_o := \left(\frac{A}{A\cdot\sin(\alpha 1R_o)+B\cdot\cos(\alpha 1R_o)}\right)^{\mu}\cdot e^{\left(\frac{A}{C}\right)\cdot\left(\alpha 1R_o-\frac{\pi}{2}\cdot \text{rad}\right)}$$

$$R\sigma eL1 = \begin{pmatrix}1.521\\1.495\\1.472\\1.449\\1.426\\1.404\\1.383\\1.362\\1.322\end{pmatrix}$$

edge of hole (first value); elastic-plastic boundary on unloading (last value)

Calculate ratio of tangential and radial plastic stress in the plastic region between the edge of the hole and the elastic-plastic boundary

المنارة للاستشارات
www.manaraa.com

In the first region, let ratio for tangential plastic stress to yield stress be SptR1 and the ratio for plastic radial stress to yield stress be SprR1 and both are functions of ratio of effective stress to yield stress (Rσ rL1) and α 1R

$$SptLR1_o := \frac{R\sigma eL1_o}{2} \cdot \sqrt{2+2\cdot R} \cdot \left(\cos\left(\alpha 1R_o\right) + \frac{1}{\sqrt{1+2\cdot R}} \cdot \sin\left(\alpha 1R_o\right) \right)$$

$$SprLR1_o := \frac{R\sigma eL1_o}{2} \cdot \sqrt{2+2\cdot R} \cdot \left(\cos\left(\alpha 1R_o\right) - \frac{1}{\sqrt{1+2\cdot R}} \cdot \sin\left(\alpha 1R_o\right) \right)$$

$$SptLR1 = \begin{pmatrix} -0.484 \\ -0.46 \\ -0.437 \\ -0.412 \\ -0.386 \\ -0.36 \\ -0.332 \\ -0.303 \\ -0.243 \end{pmatrix} \qquad SprLR1 = \begin{pmatrix} -1.704 \\ -1.671 \\ -1.641 \\ -1.61 \\ -1.579 \\ -1.549 \\ -1.518 \\ -1.488 \\ -1.426 \end{pmatrix}$$

2. For Region 2, calculate the change in elastic stress from Unloading between r/a = 1.26164 and r/a = 2.5709 at the same locations as the plastic stress were calculated for Loading

Use radius from Loading between r=1 to r=2.5709, subtract the region between r=1 and r=1.2616. Then calculate the elastic Unloading stress in this region for the same radii as for Loading

المنارة للاستشارات
www.manaraa.com

$rpL =$

	1
1	1
2	1.049
3	1.131
4	1.202
5	1.262
6	1.327
7	1.386
8	1.444
9	1.501
10	1.558
11	1.616
12	1.674
13	1.734
14	1.795
15	1.858
16	1.923
17	1.989
18	2.093
19	2.203
20	2.319
21	2.441
22	2.571

$raR2_1 := 1.2616$

$m := 2..18$ $\quad n := 1..18$

$raR2_m := rpL_{m+4}$

$$SerUR2_n := 2\sqrt{\frac{1+R}{2(1+2\cdot R)}}\cdot\left(\frac{B2U}{raR2_n}\right)^2$$

$SetUR2_n := -SerUR2_n$

$raR2 =$

	1
1	1.262
2	1.327
3	1.386
4	1.444
5	1.501
6	1.558
7	1.616
8	1.674
9	1.734
10	1.795
11	1.858
12	1.923
13	1.989
14	2.093
15	2.203
16	2.319
17	2.441
18	2.571

3. For Region 3, calculate the change in elastic stress for Unloading between r/a = 2.5709 to r/a = 6.07 at the same loactions as the stresses were calculated for Loading

$p := 1..15$

www.manaraa.com

$raR3 := reL$

$$SerUR3_p := 2\sqrt{\frac{1+R}{2(1+2\cdot R)}}\cdot\left(\frac{B2U}{raR3_p}\right)^2$$

$$SetUR3_p := -SerUR3_p$$

raR3 =

	1
1	2.571
2	2.821
3	3.071
4	3.321
5	3.571
6	3.821
7	4.071
8	4.321
9	4.571
10	4.821
11	5.071
12	5.321
13	5.571
14	5.821
15	6.071

SetUR3 =

	1
1	-0.278
2	-0.231
3	-0.195
4	-0.167
5	-0.144
6	-0.126
7	-0.111
8	-0.098
9	-0.088
10	-0.079
11	-0.071
12	-0.065
13	-0.059
14	-0.054
15	-0.05

SerUR3 =

	1
1	0.278
2	0.231
3	0.195
4	0.167
5	0.144
6	0.126
7	0.111
8	0.098
9	0.088
10	0.079
11	0.071
12	0.065
13	0.059
14	0.054
15	0.05

Ensure intervals in the 3 Regions matching r/a intervals for computing stresses prior to adding

المنارة للاستشارات

www.manaraa.com

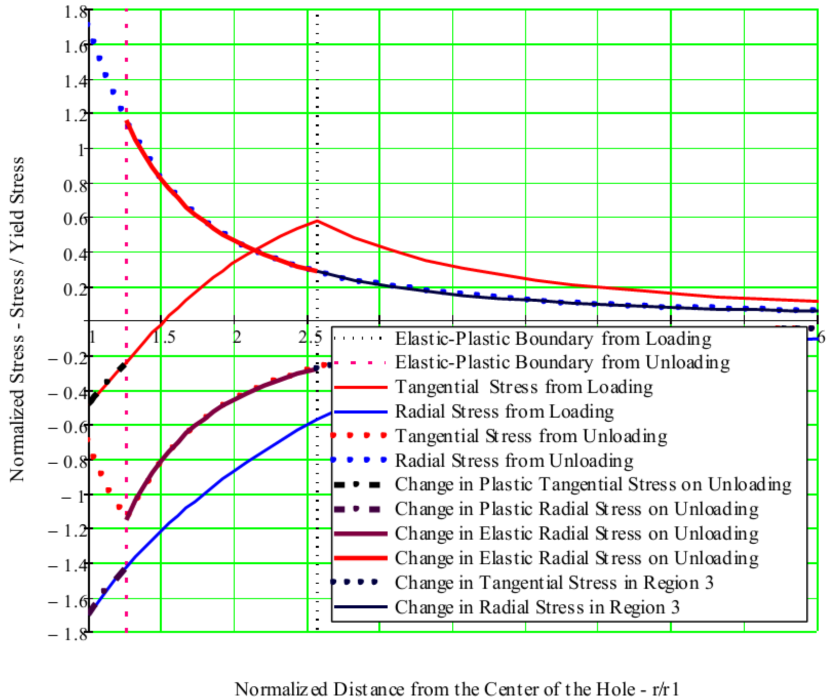

Fig 12. Check of Increments for Calculating Residual Stresses

4. For Region 1, calculate the residual stress between r/a = 1 to r/a = 1.26164

$RStR1_o := SptU_o + SptLR1_o$

$RSrR1 := SprU + SprLR1$

$SptU_o =$	$SptLR1_o =$	$RStR1_o =$
-0.698	-0.484	-1.183
-0.757	-0.46	-1.217
-0.811	-0.437	-1.248
-0.864	-0.412	-1.276
-0.916	-0.386	-1.302
-0.966	-0.36	-1.326
-1.015	-0.332	-1.347
-1.063	-0.303	-1.366
-1.155	-0.243	-1.398

www.manaraa.com

$$raR1_o = \begin{array}{|r|}\hline 1 \\ \hline 1.027 \\ \hline 1.054 \\ \hline 1.081 \\ \hline 1.109 \\ \hline 1.138 \\ \hline 1.167 \\ \hline 1.198 \\ \hline 1.262 \\ \hline \end{array} \qquad SprU = \begin{pmatrix} 1.704 \\ 1.639 \\ 1.578 \\ 1.518 \\ 1.457 \\ 1.396 \\ 1.336 \\ 1.275 \\ 1.155 \end{pmatrix} \qquad SprLR1 = \begin{pmatrix} -1.704 \\ -1.671 \\ -1.641 \\ -1.61 \\ -1.579 \\ -1.549 \\ -1.518 \\ -1.488 \\ -1.426 \end{pmatrix} \qquad RSrR1 = \begin{pmatrix} 1.103\times 10^{-6} \\ -0.032 \\ -0.062 \\ -0.092 \\ -0.123 \\ -0.153 \\ -0.183 \\ -0.213 \\ -0.272 \end{pmatrix}$$

5. For Region 2, calculate the residual stress between r/a = 1.26164 to r/a = 2.5709

Loading Values of radius and tangential stress

rpL =

	1
1	1.00001
2	1.049
3	1.13118
4	1.20205
5	1.26163
6	1.32742
7	1.3861
8	1.44366
9	1.5008
10	1.55805
11	1.61584
12	1.67449
13	1.73428
14	1.79545
15	1.85822
16	1.9228
17	1.98937
18	2.09338
19	2.2029
20	2.31855
21	2.44099
22	2.57087

SptL =

	1
1	-0.484
2	-0.441
3	-0.366
4	-0.299
5	-0.243
6	-0.181
7	-0.126
8	-0.074
9	-0.024
10	0.024
11	0.071
12	0.116
13	0.16
14	0.202
15	0.243
16	0.284
17	0.322
18	0.379
19	0.432
20	0.483
21	0.531
22	0.577

Unloading values of radius and tangential stress at the same radius as the loading values from

raR2 =

	1
1	1.26164
2	1.32742
3	1.3861
4	1.44366
5	1.5008
6	1.55805
7	1.61584
8	1.67449
9	1.73428
10	1.79545
11	1.85822
12	1.9228
13	1.98937
14	2.09338
15	2.2029
16	2.31855
17	2.44099
18	2.57087

SetUR2 =

	1
1	-1.155
2	-1.043
3	-0.957
4	-0.882
5	-0.816
6	-0.757
7	-0.704
8	-0.656
9	-0.611
10	-0.57
11	-0.532
12	-0.497
13	-0.464
14	-0.419
15	-0.379
16	-0.342
17	-0.308
18	-0.278

$v := 2..18$

$SptL2_1 := SptLR1_9 \qquad SprL2_1 := SprLR1_9$

$SptL2_v := SptL_{v+4} \qquad SprL2_v := SprL_{v+4}$

$RStR2 := SetUR2 + SptL2$

$RSrR2 := SerUR2 + SprL2$

المنارة للاستشارات
www.manaraa.com

SptL2 =

	1
1	-0.243
2	-0.181
3	-0.126
4	-0.074
5	-0.024
6	0.024
7	0.071
8	0.116
9	0.16
10	0.202
11	0.243
12	0.284
13	0.322
14	0.379
15	0.432
16	0.483
17	0.531
18	0.577

RStR2 =

	1
1	-1.3976
2	-1.224
3	-1.0831
4	-0.9563
5	-0.8404
6	-0.7332
7	-0.6333
8	-0.5397
9	-0.4514
10	-0.3679
11	-0.2888
12	-0.2136
13	-0.142
14	-0.0409
15	0.0533
16	0.1411
17	0.223
18	0.2993

www.manaraa.com

SprL =

	1
1	-1.704
2	-1.646
3	-1.556
4	-1.484
5	-1.426
6	-1.366
7	-1.315
8	-1.266
9	-1.22
10	-1.175
11	-1.132
12	-1.089
13	-1.046
14	-1.005
15	-0.963
16	-0.922
17	-0.881
18	-0.82
19	-0.759
20	-0.698
21	-0.638
22	-0.577

SprL2 =

	1
1	-1.426
2	-1.366
3	-1.315
4	-1.266
5	-1.22
6	-1.175
7	-1.132
8	-1.089
9	-1.046
10	-1.005
11	-0.963
12	-0.922
13	-0.881
14	-0.82
15	-0.759
16	-0.698
17	-0.638
18	-0.577

SerUR2 =

	1
1	1.155
2	1.043
3	0.957
4	0.882
5	0.816
6	0.757
7	0.704
8	0.656
9	0.611
10	0.57
11	0.532
12	0.497
13	0.464
14	0.419
15	0.379
16	0.342
17	0.308
18	0.278

RSrR2 =

	1
1	-0.272
2	-0.323
3	-0.358
4	-0.385
5	-0.404
6	-0.418
7	-0.428
8	-0.433
9	-0.435
10	-0.434
11	-0.431
12	-0.425
13	-0.416
14	-0.4
15	-0.38
16	-0.356
17	-0.329
18	-0.299

6. For Region 3, calculate the residual stress between r/a = 2.5709 to r/a = 6.07

Unloading radius

المنارة للاستشارات
www.manaraa.com

raR3 =

	1
1	2.571
2	2.821
3	3.071
4	3.321
5	3.571
6	3.821
7	4.071
8	4.321
9	4.571
10	4.821
11	5.071
12	5.321
13	5.571
14	5.821
15	6.071

reL =

	1
1	2.571
2	2.821
3	3.071
4	3.321
5	3.571
6	3.821
7	4.071
8	4.321
9	4.571
10	4.821
11	5.071
12	5.321
13	5.571
14	5.821
15	6.071

SetUR3 =

	1
1	-0.278
2	-0.231
3	-0.195
4	-0.167
5	-0.144
6	-0.126
7	-0.111
8	-0.098
9	-0.088
10	-0.079
11	-0.071
12	-0.065
13	-0.059
14	-0.054
15	-0.05

SetL =

	1
1	0.577
2	0.48
3	0.405
4	0.346
5	0.299
6	0.261
7	0.23
8	0.204
9	0.183
10	0.164
11	0.148
12	0.135
13	0.123
14	0.113
15	0.104

RSetR3 := SetUR3 + SetL   RSerR3 := SerUR3 + SerL

RSetR3 =

	1
1	0.299
2	0.249
3	0.21
4	0.179
5	0.155
6	0.135
7	0.119
8	0.106
9	0.095
10	0.085
11	0.077
12	0.07
13	0.064
14	0.058
15	0.054

SerUR3 =

	1
1	0.278
2	0.231
3	0.195
4	0.167
5	0.144
6	0.126
7	0.111
8	0.098
9	0.088
10	0.079
11	0.071
12	0.065
13	0.059
14	0.054
15	0.05

SerL =

	1
1	-0.577
2	-0.48
3	-0.405
4	-0.346
5	-0.299
6	-0.261
7	-0.23
8	-0.204
9	-0.183
10	-0.164
11	-0.148
12	-0.135
13	-0.123
14	-0.113
15	-0.104

RSerR3 =

	1
1	-0.299
2	-0.249
3	-0.21
4	-0.179
5	-0.155
6	-0.135
7	-0.119
8	-0.106
9	-0.095
10	-0.085
11	-0.077
12	-0.07
13	-0.064
14	-0.058
15	-0.054

المنارة للاستشارات

www.manaraa.com

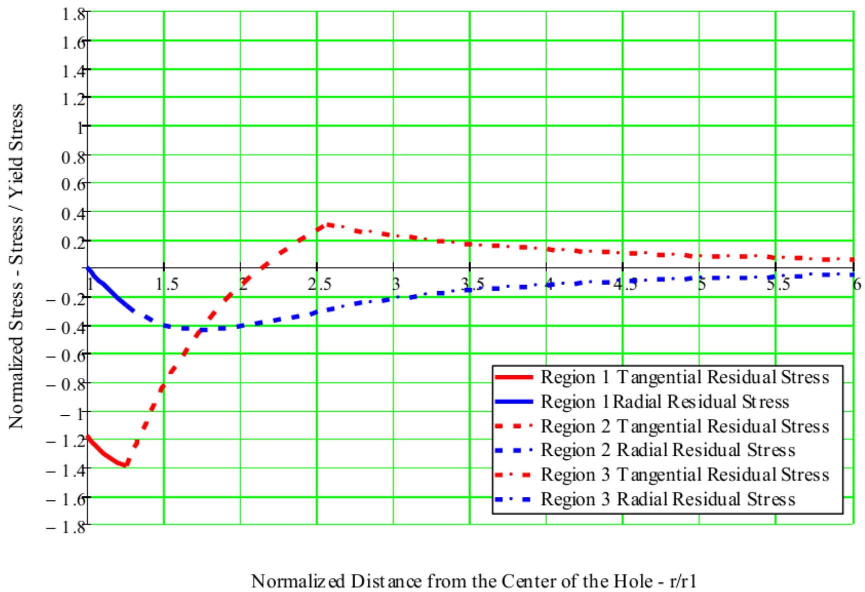

Fig 13. Residual Stresses

7. Combine into 1 matrix of radius and 1 matrix each of tangential and radial residual stress

$k := 2..18$

$j := 1..9 \qquad l := 2..15$

$RAR_j := raR1_j$

$RAR_{k+8} := raR2_k$

$RAR_{l+25} := raR3_l$

www.manaraa.com

$$raR1 = \begin{pmatrix} 0.99999 \\ 1.02731 \\ 1.05383 \\ 1.08106 \\ 1.10904 \\ 1.13782 \\ 1.16742 \\ 1.1979 \\ 1.26164 \end{pmatrix}$$

$$RSTC_j := RStR1_j$$

$$RSTC_{k+8} := RStR2_k$$

$$RSTC_{l+25} := RSetR3_l$$

raR2 =

	1
1	1.262
2	1.327
3	1.386
4	1.444
5	1.501
6	1.558
7	1.616
8	1.674
9	1.734
10	1.795
11	1.858
12	1.923
13	1.989
14	2.093
15	2.203
16	2.319
17	2.441
18	2.571

raR3 =

	1
1	2.571
2	2.821
3	3.071
4	3.321
5	3.571
6	3.821
7	4.071
8	4.321
9	4.571
10	4.821
11	5.071
12	5.321
13	5.571
14	5.821
15	6.071

RAR =

	1
1	1
2	1.0273
3	1.0538
4	1.0811
5	1.109
6	1.1378
7	1.1674
8	1.1979
9	1.2616
10	1.3274
11	1.3861
12	1.4437
13	1.5008
14	1.5581
15	1.6158
16	1.6745
17	1.7343
18	1.7954
19	...

www.manaraa.com

$$RStR1 = \begin{pmatrix} -1.18276 \\ -1.21748 \\ -1.24801 \\ -1.27628 \\ -1.30225 \\ -1.3259 \\ -1.34725 \\ -1.36629 \\ -1.39764 \end{pmatrix}$$

RStR2 =

	1
1	-1.398
2	-1.224
3	-1.083
4	-0.956
5	-0.84
6	-0.733
7	-0.633
8	-0.54
9	-0.451
10	-0.368
11	-0.289
12	-0.214
13	-0.142
14	-0.041
15	0.053
16	0.141
17	0.223
18	0.299

RSetR3 =

	1
1	0.299
2	0.249
3	0.21
4	0.179
5	0.155
6	0.135
7	0.119
8	0.106
9	0.095
10	0.085
11	0.077
12	0.07
13	0.064
14	0.058
15	0.054

RSTC =

	1
1	-1.183
2	-1.217
3	-1.248
4	-1.276
5	-1.302
6	-1.326
7	-1.347
8	-1.366
9	-1.398
10	-1.224
11	-1.083
12	-0.956
13	-0.84
14	-0.733
15	-0.633
16	...

$$RSRC_j := RSrR1_j$$

$$RSRC_{k+8} := RSrR2_k$$

$$RSRC_{l+25} := RSerR3_l$$

$$RSrR1 = \begin{pmatrix} 1.10271 \times 10^{-6} \\ -0.03192 \\ -0.06214 \\ -0.09238 \\ -0.12258 \\ -0.15272 \\ -0.18275 \\ -0.21262 \\ -0.27175 \end{pmatrix}$$

RSrR2 =

	1
1	-0.272
2	-0.323
3	-0.358
4	-0.385
5	-0.404
6	-0.418
7	-0.428
8	-0.433
9	-0.435
10	-0.434
11	-0.431
12	-0.425
13	...

RSerR3 =

	1
1	-0.299
2	-0.249
3	-0.21
4	-0.179
5	-0.155
6	-0.135
7	-0.119
8	-0.106
9	-0.095
10	-0.085
11	-0.077
12	-0.07
13	-0.064
14	-0.058
15	-0.054

RSRC =

	1
1	$1.103 \cdot 10^{-6}$
2	-0.032
3	-0.062
4	-0.092
5	-0.123
6	-0.153
7	-0.183
8	-0.213
9	-0.272
10	-0.323
11	-0.358
12	-0.385
13	...

المنارة للاستشارات
www.manaraa.com

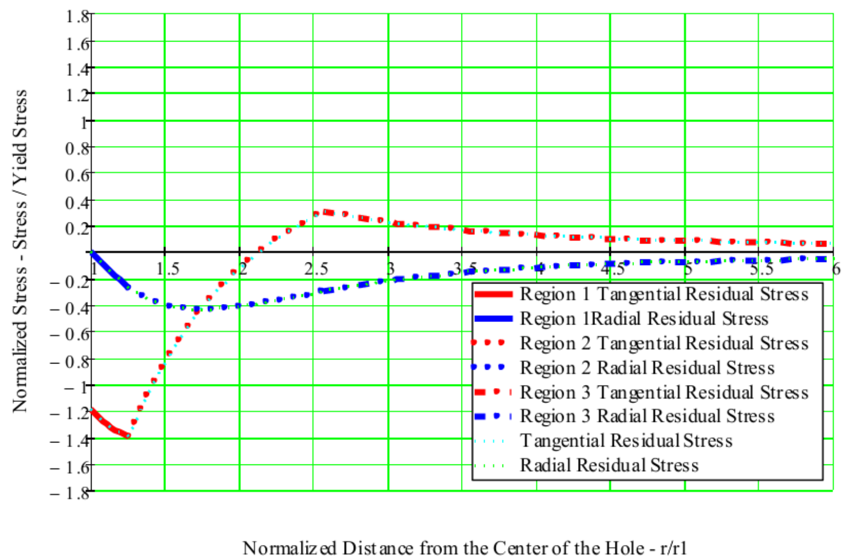

Fig 14. Check of Combining Residual Stresses in the 3 Regions

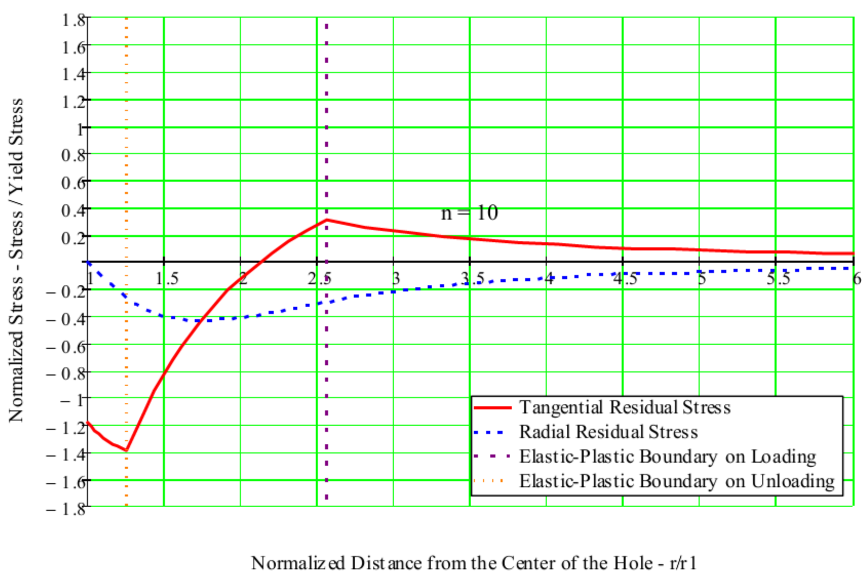

Fig 15. Residual Stress

www.manaraa.com

E. Convert Stresses into Strain

1. Total Residual Strain (Loading strain - Unloading strain

A. For Region 1, calculate the residual strain between r/a = 1 to r/a = 1.2616

When the ratio of stress over effective stress is less than 1, use the elastic formulation for converting from stress to strain for that stress component. When the ratio of effective stress over effective stress is greater than 1, use the modified Ramberg-Osgood equation for converting stress to total strain

$i := 1..9 \qquad n := 10 \qquad E = 3\times 10^4 \cdot ksi \qquad ve = 0.3 \qquad vp = 0.5$

$\sigma yield = 34.69 \cdot ksi$

$$raR1 = \begin{pmatrix} 0.99999 \\ 1.02731 \\ 1.05383 \\ 1.08106 \\ 1.10904 \\ 1.13782 \\ 1.16742 \\ 1.1979 \\ 1.26164 \end{pmatrix} \quad SptLR1 = \begin{pmatrix} -0.484 \\ -0.46 \\ -0.437 \\ -0.412 \\ -0.386 \\ -0.36 \\ -0.332 \\ -0.303 \\ -0.243 \end{pmatrix} \quad SprLR1 = \begin{pmatrix} -1.70406 \\ -1.67131 \\ -1.64055 \\ -1.60991 \\ -1.57937 \\ -1.54886 \\ -1.51836 \\ -1.48781 \\ -1.42645 \end{pmatrix} \quad SptU = \begin{pmatrix} -0.698 \\ -0.757 \\ -0.811 \\ -0.864 \\ -0.916 \\ -0.966 \\ -1.015 \\ -1.063 \\ -1.155 \end{pmatrix} \quad SprU = \begin{pmatrix} 1.70406 \\ 1.63939 \\ 1.5784 \\ 1.51754 \\ 1.45679 \\ 1.39614 \\ 1.33561 \\ 1.27519 \\ 1.1547 \end{pmatrix}$$

from Loading

$j := 1..6 \qquad k := 7..9$

$$\varepsilon rL1_i := \frac{1}{E}\cdot\left[\left(\left|SprLR1_i\right|\right)^{(n-1)}\cdot SprLR1_i\cdot\sigma yield - (ve)\cdot SptLR1_i\cdot\sigma yield\right]$$

$SptLR1_1 = -0.484$

$$\varepsilon tL1_i := \frac{1}{E}\cdot\left[SptLR1_i\cdot\sigma yield - vp\cdot\left(\left|SprLR1_i\right|\right)^{n-1}\cdot SprLR1_i\cdot\sigma yield\right]$$

$\varepsilon rL1_1 = -0.239$

from Unloading

$SptU_1 = -0.698$

$$\varepsilon rU1_j := \frac{1}{E}\cdot\left[\left(\left|SprU_j\right|\right)^{n-1}\cdot SprU_j\cdot\sigma yield - ve\cdot SptU_j\cdot\sigma yield\right]$$

$\varepsilon rU1_1 = 0.239$

$$\varepsilon tU1_j := \frac{1}{E}\cdot\left[SptU_j\cdot\sigma yield - vp\cdot\left(\left|SprU_j\right|\right)^{(n-1)}\cdot SprU_j\cdot\sigma yield\right]$$

$$\varepsilon rU1_k := \frac{1}{E}\cdot\left[\left(\left|SprU_k\right|\right)^{n-1}\cdot SprU_k\cdot\sigma yield - vp\cdot\left(\left|SptU_k\right|\right)^{(n-1)}\cdot SptU_k\cdot\sigma yield\right]$$

$$\varepsilon tU1_k := \frac{1}{E}\cdot\left[\left(\left|SptU_k\right|\right)^{(n-1)}\cdot SptU_k\cdot\sigma yield - vp\cdot\left(\left|SprU_k\right|\right)^{(n-1)}\cdot SprU_k\cdot\sigma yield\right]$$

المنارة للاستشارات
www.manaraa.com

$$\varepsilon rL1 = \begin{pmatrix} -0.239 \\ -0.196 \\ -0.163 \\ -0.135 \\ -0.112 \\ -0.092 \\ -0.075 \\ -0.061 \\ -0.04 \end{pmatrix} \quad \varepsilon tL1 = \begin{pmatrix} 0.119 \\ 0.098 \\ 0.081 \\ 0.067 \\ 0.055 \\ 0.046 \\ 0.037 \\ 0.03 \\ 0.02 \end{pmatrix} \quad \varepsilon rU1 = \begin{pmatrix} 0.239 \\ 0.162 \\ 0.111 \\ 0.075 \\ 0.05 \\ 0.033 \\ 0.022 \\ 0.014 \\ 0.007 \end{pmatrix} \quad \varepsilon tU1 = \begin{pmatrix} -0.12 \\ -0.082 \\ -0.056 \\ -0.038 \\ -0.026 \\ -0.017 \\ -0.012 \\ -0.009 \\ -0.007 \end{pmatrix}$$

$$\varepsilon tR1 := \varepsilon tL1 + \varepsilon tU1$$

$$\varepsilon rR1 := \varepsilon rL1 + \varepsilon rU1$$

Total Residual Strain

$$\varepsilon tR1 = \begin{pmatrix} -0.001 \\ 0.016 \\ 0.025 \\ 0.029 \\ 0.029 \\ 0.028 \\ 0.025 \\ 0.022 \\ 0.013 \end{pmatrix} \quad \varepsilon rR1 = \begin{pmatrix} 0 \\ -0.034 \\ -0.052 \\ -0.06 \\ -0.061 \\ -0.059 \\ -0.054 \\ -0.047 \\ -0.033 \end{pmatrix} \quad RSrR1 = \begin{pmatrix} 1.10271\times 10^{-6} \\ -0.03192 \\ -0.06214 \\ -0.09238 \\ -0.12258 \\ -0.15272 \\ -0.18275 \\ -0.21262 \\ -0.27175 \end{pmatrix} \quad RStR1 = \begin{pmatrix} -1.18276 \\ -1.21748 \\ -1.24801 \\ -1.27628 \\ -1.30225 \\ -1.3259 \\ -1.34725 \\ -1.36629 \\ -1.39764 \end{pmatrix}$$

Calculate elastic residual strain from residual stress

$$R\varepsilon rR1_i := \frac{1}{E} \cdot \left(RSrR1_i \cdot \sigma yield - ve \cdot RStR1_i \cdot \sigma yield \right)$$

$$R\varepsilon tR1_i := \frac{1}{E} \cdot \left(RStR1_i \cdot \sigma yield - ve \cdot RSrR1_i \cdot \sigma yield \right)$$

$$R\varepsilon rR1 = \begin{pmatrix} 0.00041 \\ 0.00039 \\ 0.00036 \\ 0.00034 \\ 0.00031 \\ 0.00028 \\ 0.00026 \\ 0.00023 \\ 0.00017 \end{pmatrix} \quad R\varepsilon tR1 = \begin{pmatrix} -0.00137 \\ -0.0014 \\ -0.00142 \\ -0.00144 \\ -0.00146 \\ -0.00148 \\ -0.00149 \\ -0.00151 \\ -0.00152 \end{pmatrix}$$

المنارة للاستشارات
www.manaraa.com

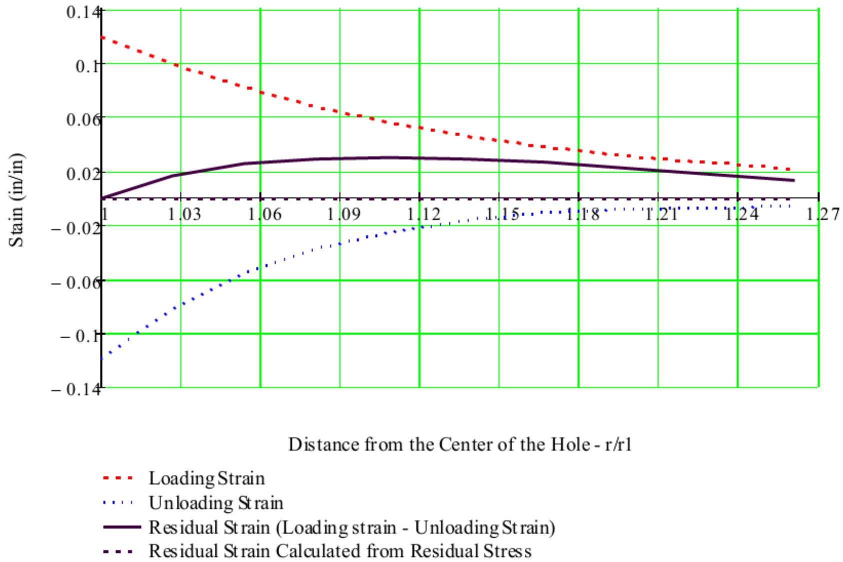

Fig 16. Tangential Strain in Region 1

www.manaraa.com

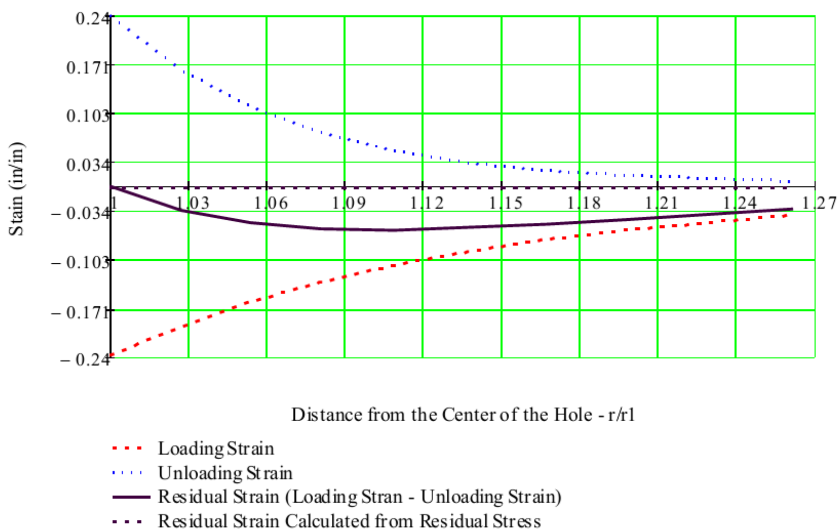

Fig 17. Radial Strain in Region 1

B. For Region 2, calculate the residual strain between r/a = 1.2616 to r/a = 2.5709

from Loading

k := 11.. 18

j := 1.. 10

raR2 =

	1
1	1.262
2	1.327
3	1.386
4	1.444
5	1.501
6	1.558
7	1.616
8	1.674
9	1.734
10	1.795
11	1.858
12	1.923
13	1.989
14	2.093
15	2.203
16	2.319
17	2.441
18	2.571

SptL2 =

	1
1	-0.243
2	-0.181
3	-0.126
4	-0.074
5	-0.024
6	0.024
7	0.071
8	0.116
9	0.16
10	0.202
11	0.243
12	0.284
13	0.322
14	0.379
15	0.432
16	0.483
17	0.531
18	0.577

SprL2 =

	1
1	-1.426
2	-1.366
3	-1.315
4	-1.266
5	-1.22
6	-1.175
7	-1.132
8	-1.089
9	-1.046
10	-1.005
11	-0.963
12	-0.922
13	-0.881
14	-0.82
15	-0.759
16	-0.698
17	-0.638
18	-0.577

المنارة للاستشارات
www.manaraa.com

$$\varepsilon rL2_j := \frac{1}{E} \cdot \left[\left(\left| SprL2_j \right| \right)^{n-1} \cdot SprL2_j \cdot \sigma yield - \nu e \cdot SptL2_j \cdot \sigma yield \right]$$

$$\varepsilon tL2_j := \frac{1}{E} \cdot \left[SptL2_j \cdot \sigma yield - \nu p \cdot \left(\left| SprL2_j \right| \right)^{(n-1)} \cdot SprL2_j \cdot \sigma yield \right]$$

$$\varepsilon rL2_k := \frac{1}{E} \cdot \left[SprL2_k \cdot \sigma yield - (\nu e) \cdot SptL2_k \cdot \sigma yield \right]$$

$$\varepsilon tL2_k := \frac{1}{E} \cdot \left[SptL2_k \cdot \sigma yield - (\nu e) \cdot SprL2_k \cdot \sigma yield \right]$$

$\varepsilon tL2 =$

	1
1	0.01989
2	0.01289
3	0.00879
4	0.00605
5	0.0042
6	0.00294
7	0.00207
8	0.00149
9	0.00109
10	0.00084
11	0.00062
12	0.00065
13	0.00068
14	0.00072
15	0.00076
16	0.0008
17	0.00084
18	0.00087

$\varepsilon rL2 =$

	1
1	-0.04025
2	-0.02614
3	-0.01782
4	-0.01225
5	-0.00845
6	-0.00582
7	-0.00401
8	-0.00274
9	-0.00188
10	-0.00128
11	-0.0012
12	-0.00116
13	-0.00113
14	-0.00108
15	-0.00103
16	-0.00097
17	-0.00092
18	-0.00087

www.manaraa.com

from Unloading

$l := 1..2$ $\qquad m := 3..18$

SetUR2 =

	1
1	-1.155
2	-1.043
3	-0.957
4	-0.882
5	-0.816
6	-0.757
7	-0.704
8	-0.656
9	-0.611
10	-0.57
11	-0.532
12	-0.497
13	-0.464
14	-0.419
15	-0.379
16	-0.342
17	-0.308
18	-0.278

SerUR2 =

	1
1	1.155
2	1.043
3	0.957
4	0.882
5	0.816
6	0.757
7	0.704
8	0.656
9	0.611
10	0.57
11	0.532
12	0.497
13	0.464
14	0.419
15	0.379
16	0.342
17	0.308
18	0.278

$$\varepsilon tU2_l := \frac{1}{E} \cdot \left[\left(\left| SetUR2_l \right| \right)^{n-1} \cdot SetUR2_l \cdot \sigma yield - \nu p \cdot \left(\left| SerUR2_l \right| \right)^{(n-1)} \cdot SerUR2_l \cdot \sigma yield \right]$$

$$\varepsilon rU2_l := \frac{1}{E} \cdot \left[\left(\left| SerUR2_l \right| \right)^{n-1} \cdot SerUR2_l \cdot \sigma yield - \nu p \cdot \left(\left| SetUR2_l \right| \right)^{n-1} \cdot SetUR2_l \cdot \sigma yield \right]$$

$$\varepsilon tU2_m := \frac{1}{E} \cdot \left(SetUR2_m \cdot \sigma yield - \nu e \cdot SerUR2_m \cdot \sigma yield \right)$$

$$\varepsilon rU2_m := \frac{1}{E} \cdot \left(SerUR2_m \cdot \sigma yield - \nu e \cdot SetUR2_m \cdot \sigma yield \right)$$

www.manaraa.com

$\varepsilon tL2 =$

	1
1	0.02
2	0.013
3	0.009
4	0.006
5	0.004
6	0.003
7	0.002
8	0.001
9	0.001
10	$8.39\cdot10^{-4}$
11	$6.157\cdot10^{-4}$
12	$6.477\cdot10^{-4}$
13	$6.784\cdot10^{-4}$
14	$7.221\cdot10^{-4}$
15	$7.628\cdot10^{-4}$
16	$8.007\cdot10^{-4}$
17	$8.357\cdot10^{-4}$
18	$8.679\cdot10^{-4}$

$\varepsilon rL2 =$

	1
1	-0.04
2	-0.026
3	-0.018
4	-0.012
5	-0.008
6	-0.006
7	-0.004
8	-0.003
9	-0.002
10	-0.001
11	-0.001
12	-0.001
13	-0.001
14	-0.001
15	-0.001
16	$-9.748\cdot10^{-4}$
17	$-9.216\cdot10^{-4}$
18	$-8.679\cdot10^{-4}$

$\varepsilon tU2 =$

	1
1	-0.00731
2	-0.00264
3	-0.00144
4	-0.00133
5	-0.00123
6	-0.00114
7	-0.00106
8	-0.00099
9	-0.00092
10	-0.00086
11	-0.0008
12	-0.00075
13	-0.0007
14	-0.00063
15	-0.00057
16	-0.00051
17	-0.00046
18	-0.00042

Total Residual Strain $\quad \varepsilon tR2 := \varepsilon tL2 + \varepsilon tU2 \quad \varepsilon rR2 := \varepsilon rL2 + \varepsilon rU2$

$\varepsilon rU2 =$

	1
1	0.00731
2	0.00264
3	0.00144
4	0.00133
5	0.00123
6	0.00114
7	0.00106
8	0.00099
9	0.00092
10	0.00086
11	0.0008
12	0.00075
13	0.0007
14	0.00063
15	0.00057
16	...

$\varepsilon tR2 =$

	1
1	0.01258
2	0.01025
3	0.00735
4	0.00473
5	0.00297
6	0.0018
7	0.00101
8	0.0005
9	0.00018
10	$-1.81258\cdot10^{-5}$
11	-0.00018
12	$-9.96134\cdot10^{-5}$
13	$-1.97057\cdot10^{-5}$
14	$9.16035\cdot10^{-5}$
15	0.00019
16	...

$\varepsilon rR2 =$

	1
1	-0.033
2	-0.023
3	-0.016
4	-0.011
5	-0.007
6	-0.005
7	-0.003
8	-0.002
9	$-9.566\cdot10^{-4}$
10	$-4.233\cdot10^{-4}$
11	$-3.98\cdot10^{-4}$
12	$-4.171\cdot10^{-4}$
13	$-4.323\cdot10^{-4}$
14	$-4.487\cdot10^{-4}$
15	$-4.579\cdot10^{-4}$
16	...

www.manaraa.com

Calculate elastic residual strain from residual stress

$i := 1..3$

$j := 4..18$

RSrR2 =

	1
1	-0.27175
2	-0.32317
3	-0.35828
4	-0.38461
5	-0.40414
6	-0.41817
7	-0.42763
8	-0.43317
9	-0.4353
10	-0.43441
11	-0.43081
12	-0.42476
13	-0.41648
14	-0.40028
15	-0.38002
16	...

RStR2 =

	1
1	-1.39764
2	-1.22397
3	-1.08309
4	-0.95628
5	-0.84036
6	-0.73321
7	-0.63334
8	-0.53967
9	-0.45141
10	-0.36794
11	-0.28879
12	-0.21357
13	-0.14199
14	-0.04086
15	0.05333
16	...

$$R\varepsilon rR2_i := \frac{1}{E}\cdot\left(RSrR2_i\cdot\sigma yield - ve\cdot RStR2_i\cdot\sigma yield\right)$$

$$R\varepsilon tR2_i := \frac{1}{E}\cdot\left(RStR2_i\cdot\sigma yield - ve\cdot RSrR2_i\cdot\sigma yield\right)$$

$$R\varepsilon rR2_j := \frac{1}{E}\cdot\left(RSrR2_j\cdot\sigma yield - ve\cdot RStR2_j\cdot\sigma yield\right)$$

$$R\varepsilon tR2_j := \frac{1}{E}\cdot\left(RStR2_j\cdot\sigma yield - ve\cdot RSrR2_j\cdot\sigma yield\right)$$

المنارة للاستشارات
www.manaraa.com

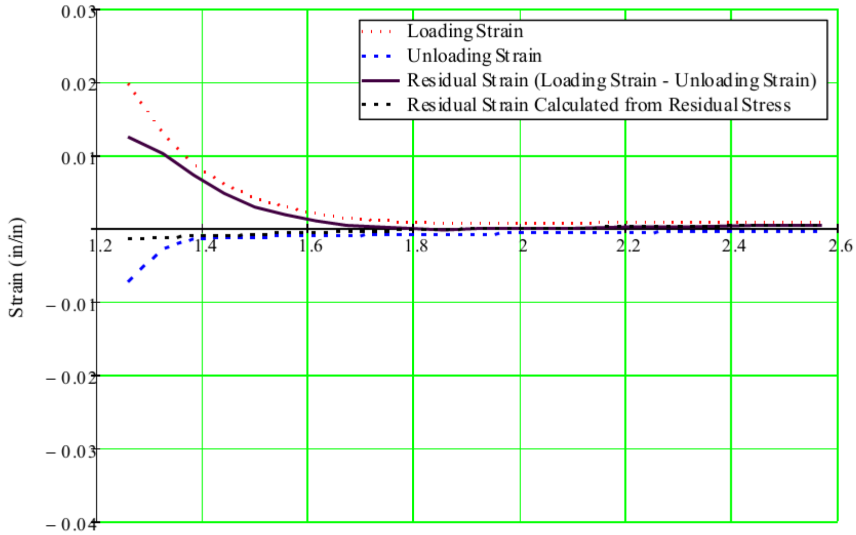

Distance from the Center of the Hole - r/r1

Fig 18. Tangential Strain Regions 2

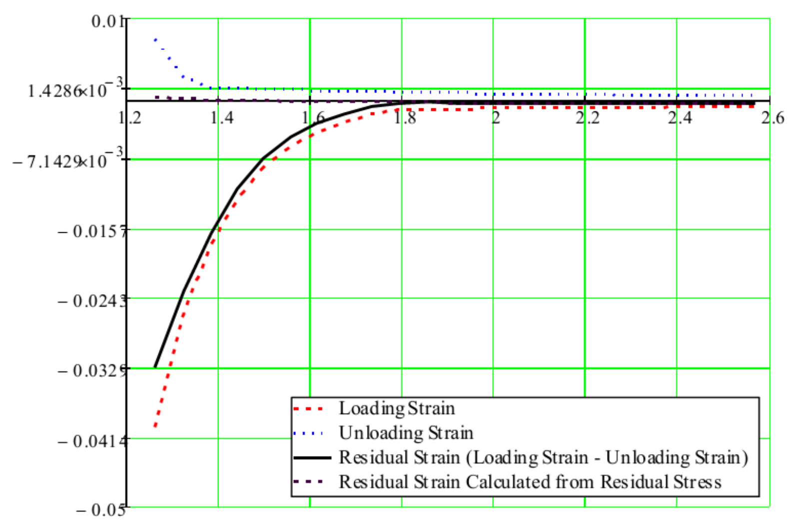

Fig 19. Radial Strain Region 2

www.manaraa.com

C. For Region 3, calculate the residual strain between r/a = 2.5709 to r/a >6

$k := 1..15$

from Loading

raR3 =

	1
1	2.571
2	2.821
3	3.071
4	3.321
5	3.571
6	3.821
7	4.071
8	4.321
9	4.571
10	4.821
11	5.071
12	5.321
13	5.571
14	5.821
15	6.071

SetL =

	1
1	0.577
2	0.48
3	0.405
4	0.346
5	0.299
6	0.261
7	0.23
8	0.204
9	0.183
10	0.164
11	0.148
12	0.135
13	0.123
14	0.113
15	0.104

SerL =

	1
1	-0.577
2	-0.48
3	-0.405
4	-0.346
5	-0.299
6	-0.261
7	-0.23
8	-0.204
9	-0.183
10	-0.164
11	-0.148
12	-0.135
13	-0.123
14	-0.113
15	-0.104

SetUR3 =

	1
1	-0.278
2	-0.231
3	-0.195
4	-0.167
5	-0.144
6	-0.126
7	-0.111
8	-0.098
9	-0.088
10	-0.079
11	-0.071
12	-0.065
13	-0.059
14	-0.054
15	-0.05

$$\varepsilon tL3_k := \frac{1}{E}\cdot\left(SetL_k\cdot\sigma yield - \nu e\cdot SerL_k\cdot\sigma yield\right)$$

$$\varepsilon rL3_k := \frac{1}{E}\cdot\left(SerL_k\cdot\sigma yield - \nu e\cdot SetL_k\cdot\sigma yield\right)$$

SerUR3 =

	1
1	0.278
2	0.231
3	0.195
4	0.167
5	0.144
6	0.126
7	0.111
8	0.098
9	0.088
10	0.079
11	0.071
12	0.065
13	0.059
14	0.054
15	0.05

$\varepsilon tL3$ =

	1
1	0.00087
2	0.00072
3	0.00061
4	0.00052
5	0.00045
6	0.00039
7	0.00035
8	0.00031
9	0.00027
10	0.00025
11	0.00022
12	0.0002
13	0.00018
14	0.00017
15	0.00016

$\varepsilon rL3$ =

	1
1	-0.00087
2	-0.00072
3	-0.00061
4	-0.00052
5	-0.00045
6	-0.00039
7	-0.00035
8	-0.00031
9	-0.00027
10	-0.00025
11	-0.00022
12	-0.0002
13	-0.00018
14	-0.00017
15	-0.00016

www.manaraa.com

from Unloading

$$\varepsilon tU3_k := \frac{1}{E}\cdot\left(SetUR3_k\cdot\sigma yield - \nu e\cdot SerUR3_k\cdot\sigma yield\right)$$

$$\varepsilon rU3_k := \frac{1}{E}\cdot\left(SerUR3_k\cdot\sigma yield - \nu e\cdot SetUR3_k\cdot\sigma yield\right)$$

$\varepsilon tU3 =$

	1
1	-0.00042
2	-0.00035
3	-0.00029
4	-0.00025
5	-0.00022
6	-0.00019
7	-0.00017
8	-0.00015
9	-0.00013
10	-0.00012
11	-0.00011
12	$-9.75842\cdot10^{-5}$
13	$-8.90225\cdot10^{-5}$
14	$-8.154\cdot10^{-5}$
15	$-7.49628\cdot10^{-5}$

$\varepsilon rU3 =$

	1
1	0.00042
2	0.00035
3	0.00029
4	0.00025
5	0.00022
6	0.00019
7	0.00017
8	0.00015
9	0.00013
10	0.00012
11	0.00011
12	$9.75842\cdot10^{-5}$
13	$8.90225\cdot10^{-5}$
14	$8.154\cdot10^{-5}$
15	$7.49628\cdot10^{-5}$

$RSerR3 =$

	1
1	-0.299
2	-0.249
3	-0.21
4	-0.179
5	-0.155
6	-0.135
7	-0.119
8	-0.106
9	-0.095
10	-0.085
11	-0.077
12	-0.07
13	-0.064
14	-0.058
15	-0.054

Total Residual Strain

$$\varepsilon tR3 := \varepsilon tL3 + \varepsilon tU3$$

$$\varepsilon rR3 := \varepsilon rL3 + \varepsilon rU3$$

المنارة للاستشارات
www.manaraa.com

$\varepsilon tR3 =$

	1
1	$4.498 \cdot 10^{-4}$
2	$3.736 \cdot 10^{-4}$
3	$3.153 \cdot 10^{-4}$
4	$2.696 \cdot 10^{-4}$
5	$2.332 \cdot 10^{-4}$
6	$2.037 \cdot 10^{-4}$
7	$1.794 \cdot 10^{-4}$
8	$1.592 \cdot 10^{-4}$
9	$1.423 \cdot 10^{-4}$
10	$1.279 \cdot 10^{-4}$
11	$1.156 \cdot 10^{-4}$
12	$1.05 \cdot 10^{-4}$
13	$9.58 \cdot 10^{-5}$
14	$8.775 \cdot 10^{-5}$
15	$8.067 \cdot 10^{-5}$

$\varepsilon rR3 =$

	1
1	$-4.498 \cdot 10^{-4}$
2	$-3.736 \cdot 10^{-4}$
3	$-3.153 \cdot 10^{-4}$
4	$-2.696 \cdot 10^{-4}$
5	$-2.332 \cdot 10^{-4}$
6	$-2.037 \cdot 10^{-4}$
7	$-1.794 \cdot 10^{-4}$
8	$-1.592 \cdot 10^{-4}$
9	$-1.423 \cdot 10^{-4}$
10	$-1.279 \cdot 10^{-4}$
11	$-1.156 \cdot 10^{-4}$
12	$-1.05 \cdot 10^{-4}$
13	$-9.58 \cdot 10^{-5}$
14	$-8.775 \cdot 10^{-5}$
15	$-8.067 \cdot 10^{-5}$

$RSetR3 =$

	1
1	0.299
2	0.249
3	0.21
4	0.179
5	0.155
6	0.135
7	0.119
8	0.106
9	0.095
10	0.085
11	0.077
12	0.07
13	0.064
14	0.058
15	0.054

Calculate elastic residual strain from residual stress

$$R\varepsilon rR3_k := \frac{1}{E} \cdot \left(RSerR3_k \cdot \sigma yield - ve \cdot RSetR3_k \cdot \sigma yield\right)$$

$$R\varepsilon tR3_k := \frac{1}{E} \cdot \left(RSetR3_k \cdot \sigma yield - ve \cdot RSerR3_k \cdot \sigma yield\right)$$

$R\varepsilon rR3 =$

	1
1	-0.00045
2	-0.00037
3	-0.00032
4	-0.00027
5	-0.00023
6	-0.0002
7	-0.00018
8	-0.00016
9	-0.00014
10	-0.00013
11	-0.00012
12	-0.00011
13	-0.0001
14	-0.00009
15	-0.00008

$R\varepsilon tR3 =$

	1
1	0.00045
2	0.00037
3	0.00032
4	0.00027
5	0.00023
6	0.0002
7	0.00018
8	0.00016
9	0.00014
10	0.00013
11	0.00012
12	0.00011
13	0.0001
14	0.00009
15	0.00008

المنارة للاستشارات
www.manaraa.com

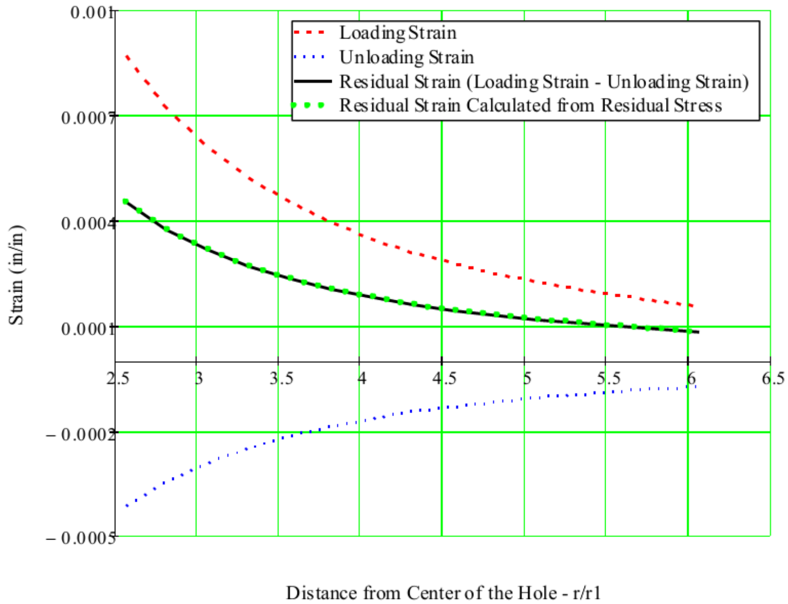

Fig 20. Tangential Strain Region 3

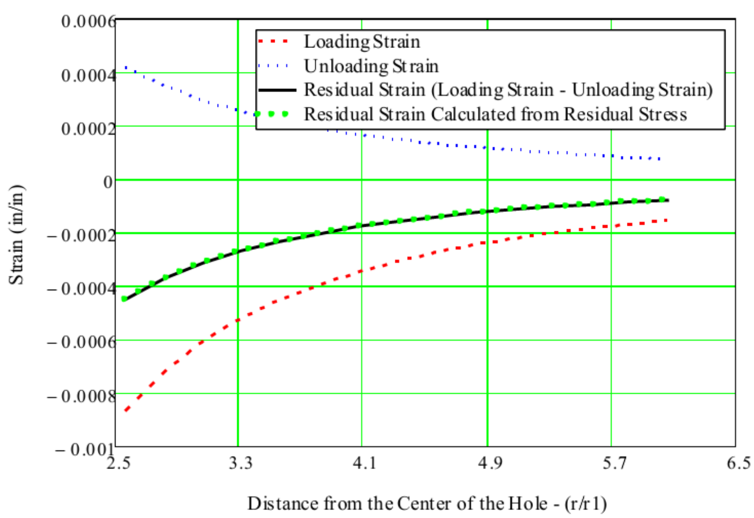

Fig 21. Radial Strain Region 3

المنارة للاستشارات
www.manaraa.com

D. Plot all Regions together review results in different Regions

$q := -4.2, -3.2 .. 4.2$

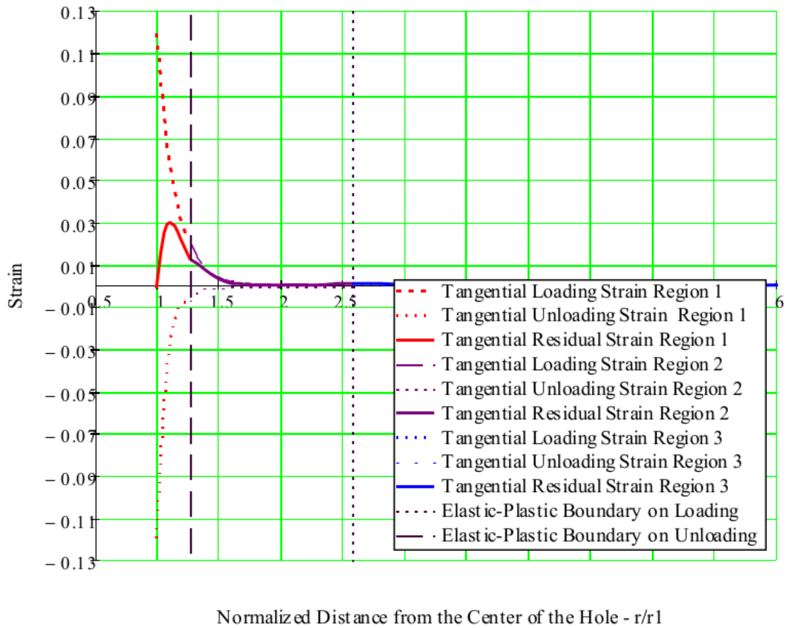

Fig 22. Total Tangential Residual Strain

www.manaraa.com

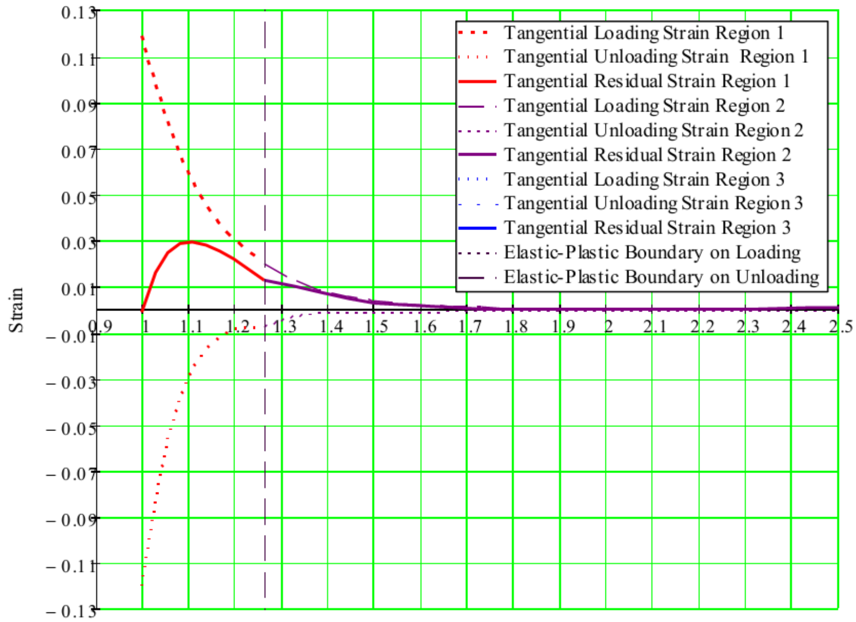

Fig 23. Total Tangential Residual Strain

$pY\varepsilon_m := .00154$ $\quad nY\varepsilon_m := -.00154$ $\quad pY\varepsilon_k := .00154$ $\quad nY\varepsilon_k := -.00154$

www.manaraa.com

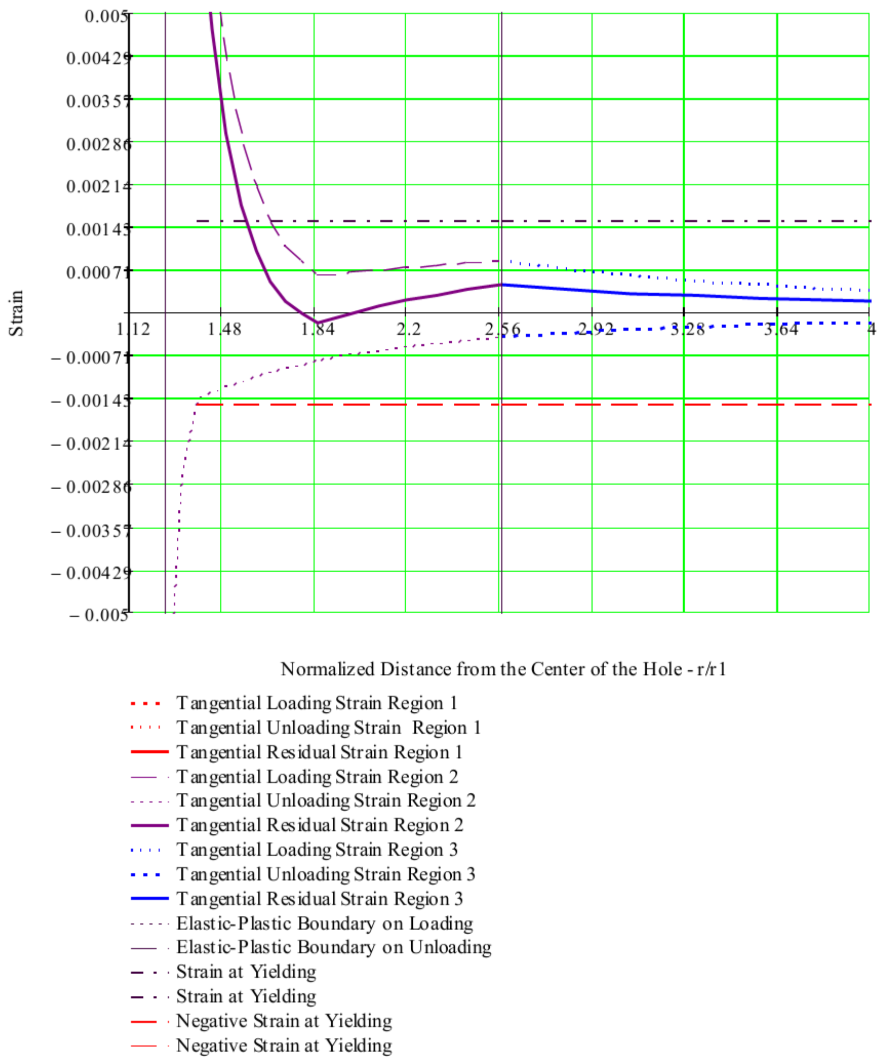

Fig 24. Total Tangential Residual Strain

www.manaraa.com

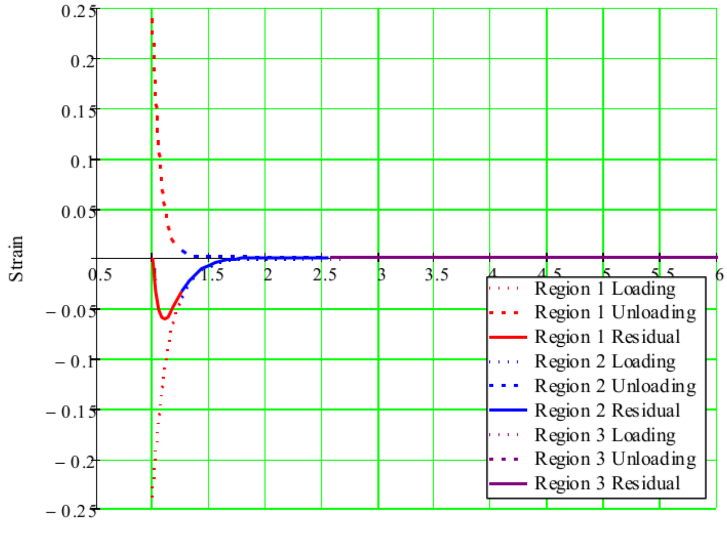

Normalized Distance from the Center of the Hole - r/r1

Fig 25. Total Radial Residual Strain

المنارة للاستشارات
www.manaraa.com

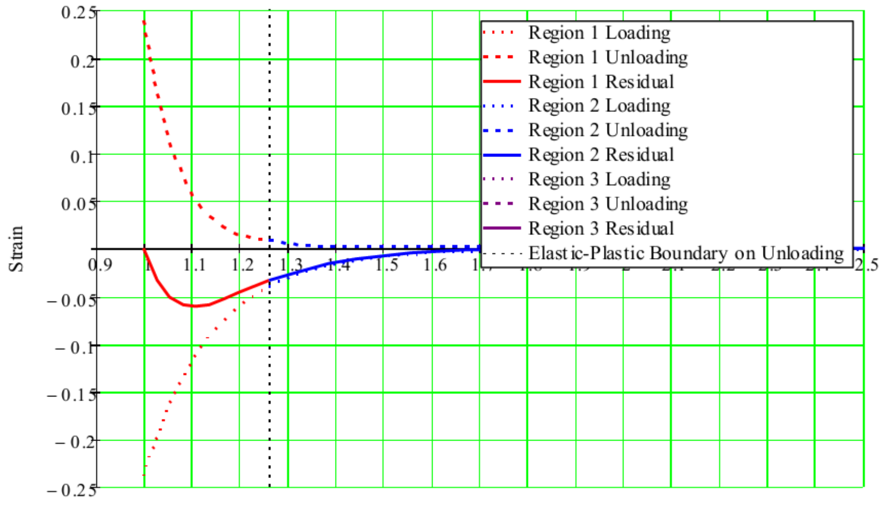

Fig 26. Total Radial Residual Strain

www.manaraa.com

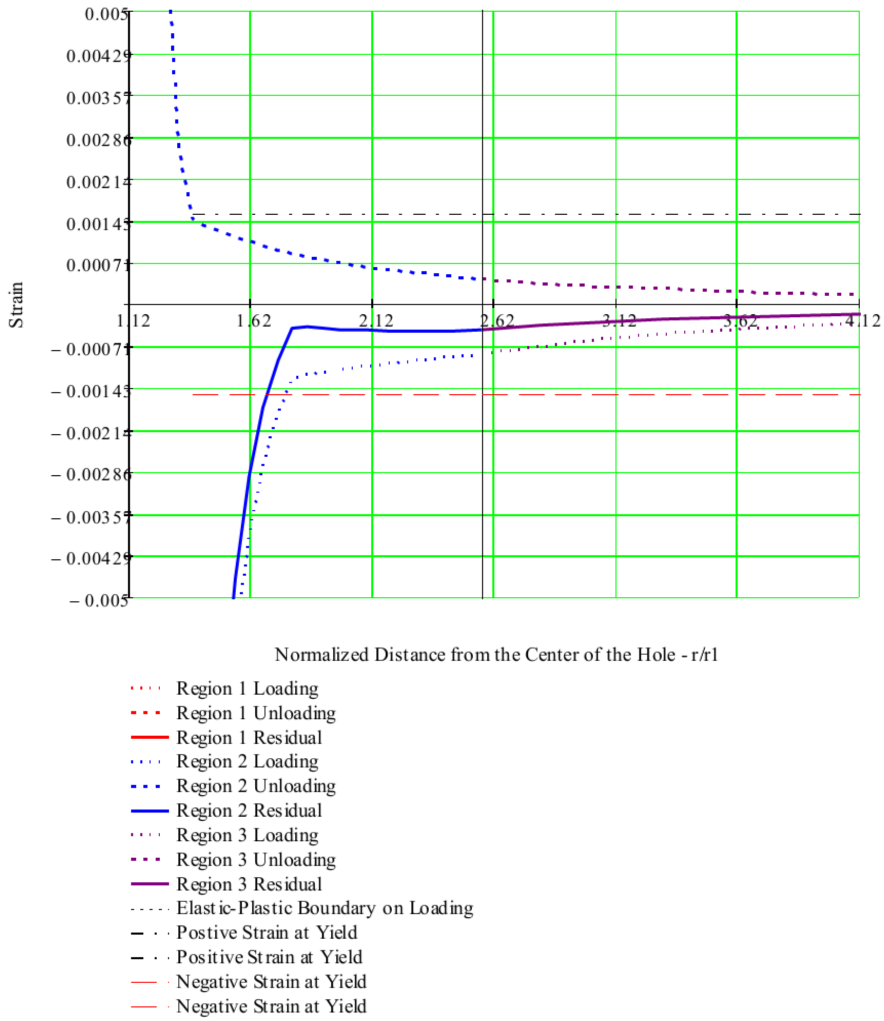

Fig 27. Total Radial Residual Strain

www.manaraa.com

E. Combine into one array for tangential strain and one for radial strain

$j := 1..9 \qquad l := 2..15 \qquad k := 2..18$

Rε TC - Combined array of Total Residual Tangential Strain
Rε RC - Combined array of Total Residual Radial Strain

$R\varepsilon TC_j := \varepsilon tR1_j \qquad R\varepsilon RC_j := \varepsilon rR1_j$

$R\varepsilon TC_{k+8} := \varepsilon tR2_k \qquad R\varepsilon RC_{k+8} := \varepsilon rR2_k$

$R\varepsilon TC_{l+25} := \varepsilon tR3_l \qquad R\varepsilon RC_{l+25} := \varepsilon rR3_l$

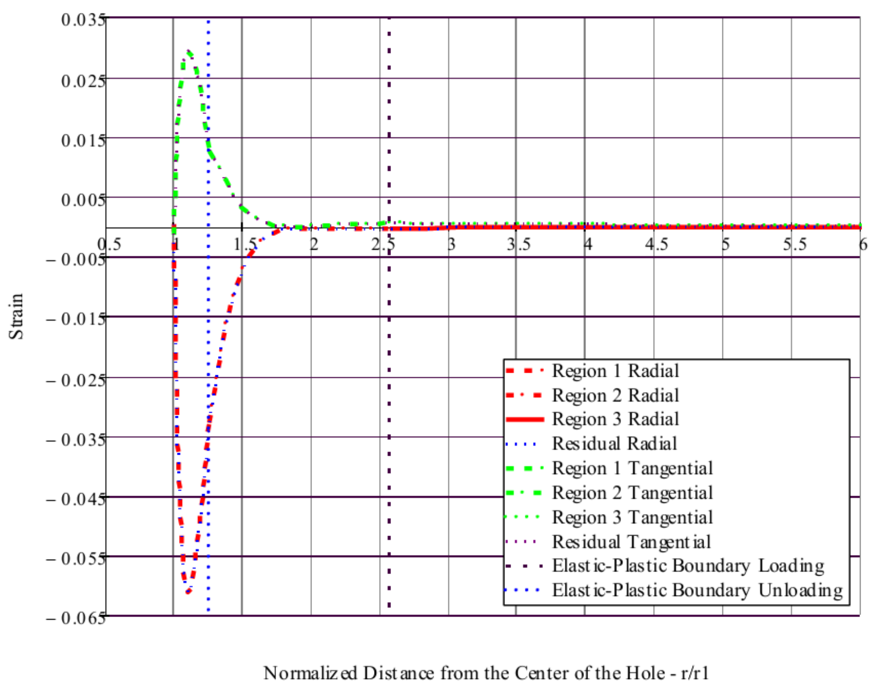

Fig 28. Total Residual Strain

www.manaraa.com

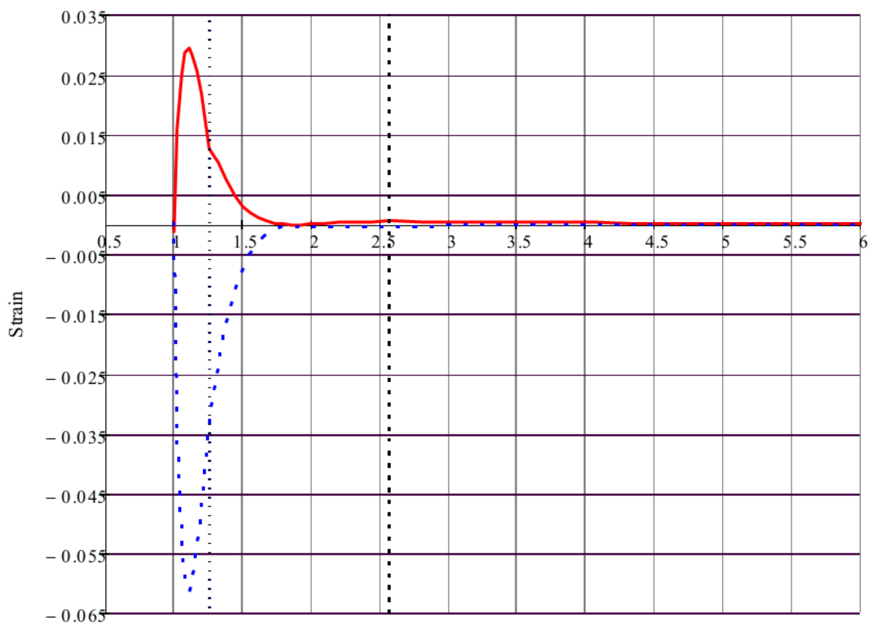

Normalized Distance from the Center of the Hole - r/r1

Fig 29. Total Residual Strain

المنارة للاستشارات
www.manaraa.com

RAR =

	1
1	1
2	1.027
3	1.054
4	1.081
5	1.109
6	1.138
7	1.167
8	1.198
9	1.262
10	1.327
11	1.386
12	1.444
13	1.501
14	1.558
15	1.616
16	...

RεTC =

	1
1	-0.001
2	0.016
3	0.025
4	0.029
5	0.029
6	0.028
7	0.025
8	0.022
9	0.013
10	0.01
11	0.007
12	0.005
13	0.003
14	0.002
15	0.001
16	...

RεRC =

	1
1	$4.118 \cdot 10^{-4}$
2	-0.034
3	-0.052
4	-0.06
5	-0.061
6	-0.059
7	-0.054
8	-0.047
9	-0.033
10	-0.023
11	-0.016
12	-0.011
13	-0.007
14	-0.005
15	-0.003
16	...

Eε TC - Combined array of Elastic Residual Tangential Strain
Eε TC - Combined array of Elastic Residual Radial Strain

$E\varepsilon TC_j := R\varepsilon tR1_j$ $\qquad E\varepsilon RC_j := R\varepsilon rR1_j$

$E\varepsilon TC_{k+8} := R\varepsilon tR2_k$ $\qquad E\varepsilon RC_{k+8} := R\varepsilon rR2_k$

$E\varepsilon TC_{l+25} := R\varepsilon tR3_l$ $\qquad E\varepsilon RC_{l+25} := R\varepsilon rR3_l$

www.manaraa.com

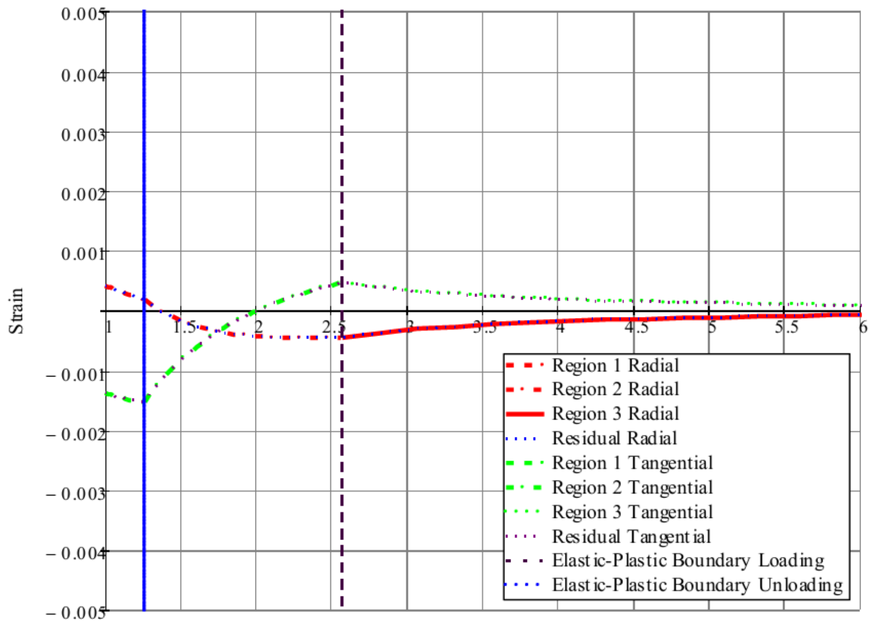

Normalized Distance from the Center of the Hole - r/r1

Fig 30. Elastic Residual Strain

RAR =

	1
1	1
2	1.027
3	1.054
4	1.081
5	1.109
6	1.138
7	1.167
8	1.198
9	1.262
10	1.327
11	1.386
12	1.444
13	1.501
14	...

EεTC =

	1
1	-0.001
2	-0.001
3	-0.001
4	-0.001
5	-0.001
6	-0.001
7	-0.001
8	-0.002
9	-0.002
10	-0.001
11	-0.001
12	$-9.724\cdot10^{-4}$
13	$-8.315\cdot10^{-4}$
14	...

EεRC =

	1
1	$4.103\cdot10^{-4}$
2	$3.854\cdot10^{-4}$
3	$3.611\cdot10^{-4}$
4	$3.359\cdot10^{-4}$
5	$3.1\cdot10^{-4}$
6	$2.834\cdot10^{-4}$
7	$2.56\cdot10^{-4}$
8	$2.281\cdot10^{-4}$
9	$1.706\cdot10^{-4}$
10	$5.091\cdot10^{-5}$
11	$-3.856\cdot10^{-5}$
12	$-1.13\cdot10^{-4}$
13	$-1.758\cdot10^{-4}$
14	...

www.manaraa.com

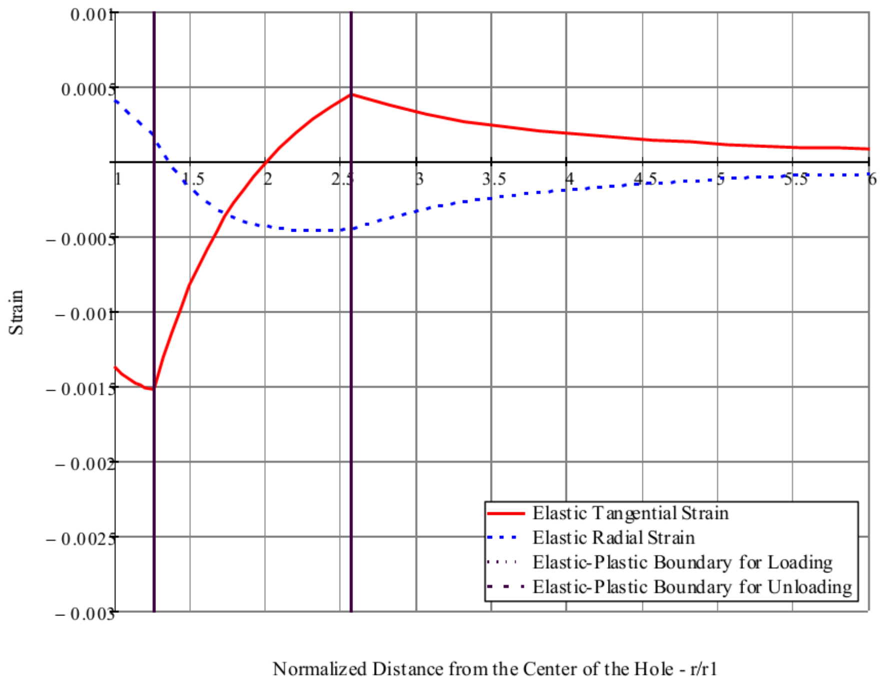

Fig 31. Elastic Residual Strain

www.manaraa.com

APPENDIX C PICK AND FATIGUE SPECIMENS DESIGN DRAWINGS

Appendix C-1 PICK Tool Design Drawings

Appendix C-2 Fatigue Specimens Design Drawings

المنارة للاستشارات
www.manaraa.com

Appendix C-1 PICK Tool Design Drawings

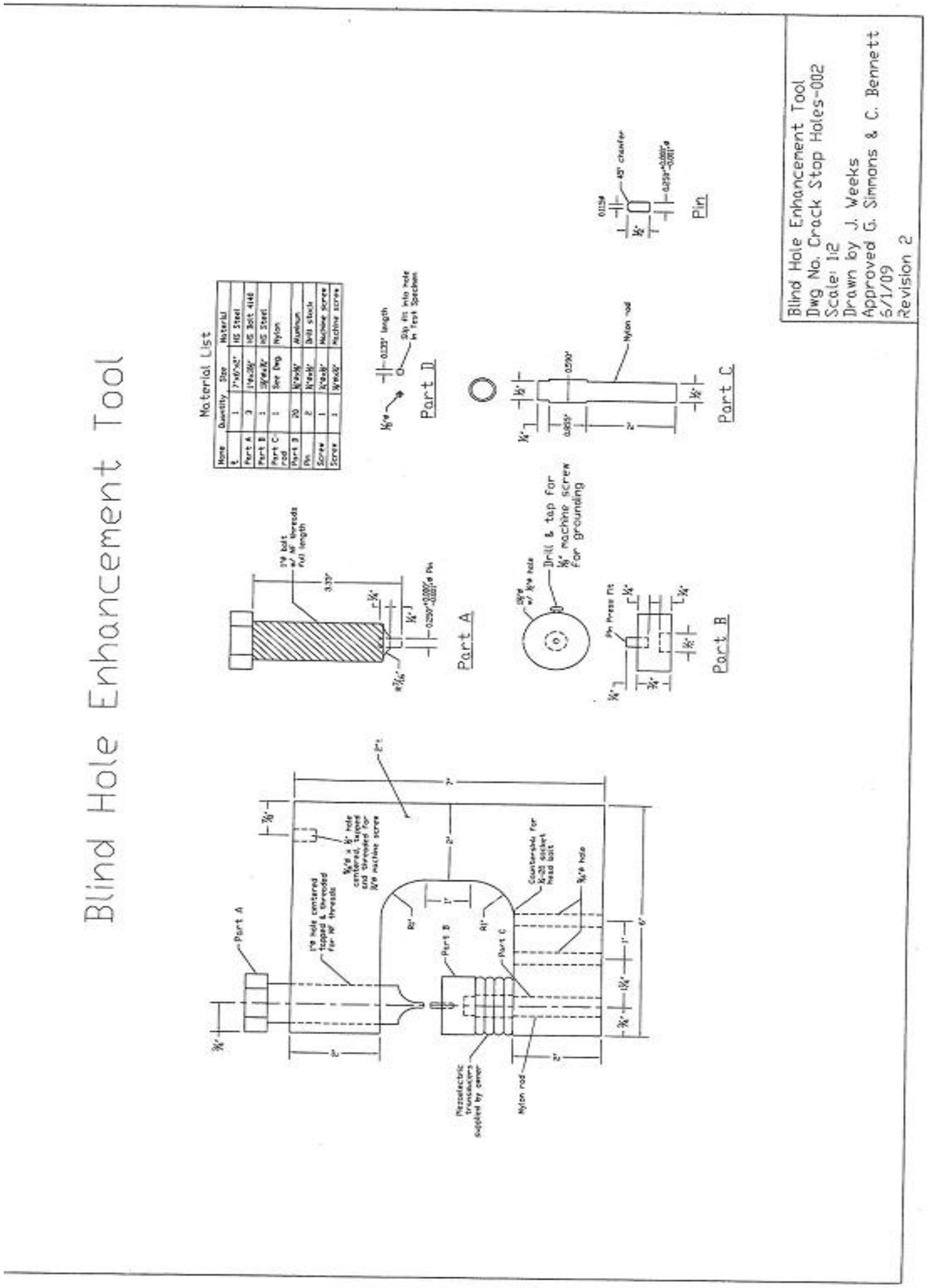

Figure C-1 PICK Tool Design Drawing

المنارة للاستشارات
www.manaraa.com

Appendix C-2 Fatigue Specimens Design Drawings

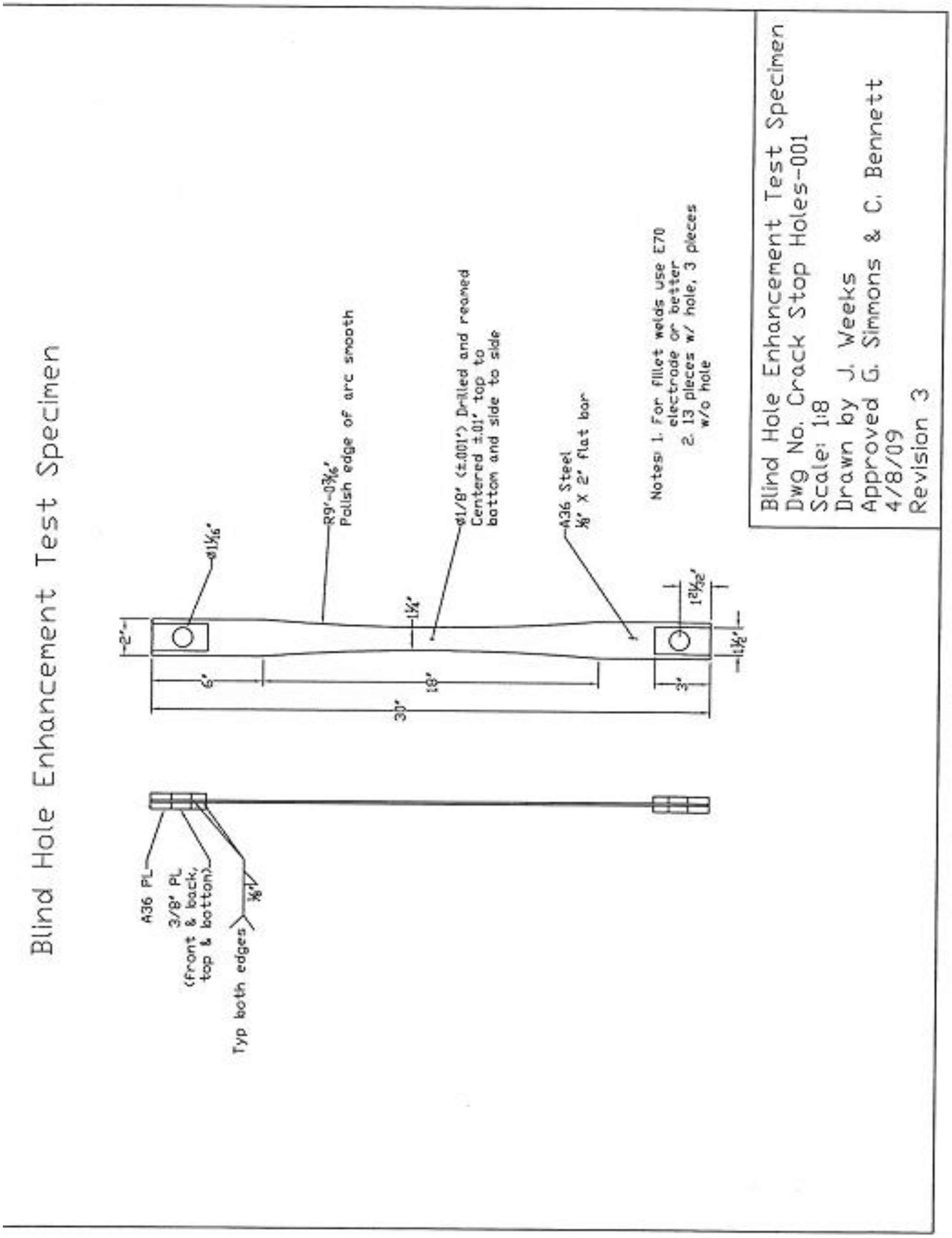

Figure C-2 Fatigue Specimen Design Drawings

www.manaraa.com

APPENDIX D CALIBRATION CURVES

Appendix D-1 Pick Tool

Appendix D-2 MTS Universal Testing Machine

Appendix D-3 10-kip Load Cell

www.manaraa.com

Appendix D-1 Pick Tool Calibration

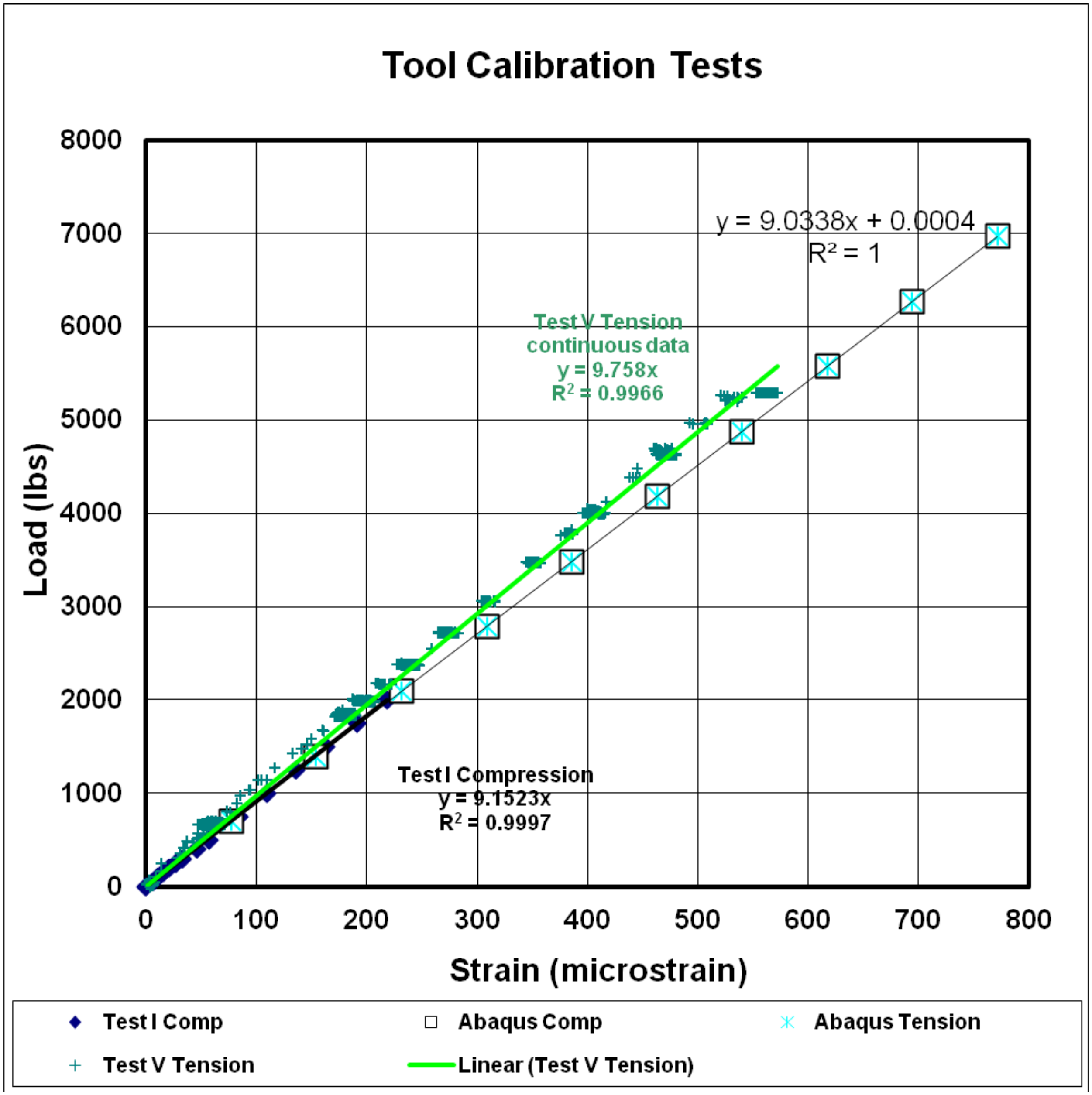

Figure D-1 Pick Tool Calibration

المنارة للاستشارات

www.manaraa.com

Appendix D-2 MTS Universal Testing Machine

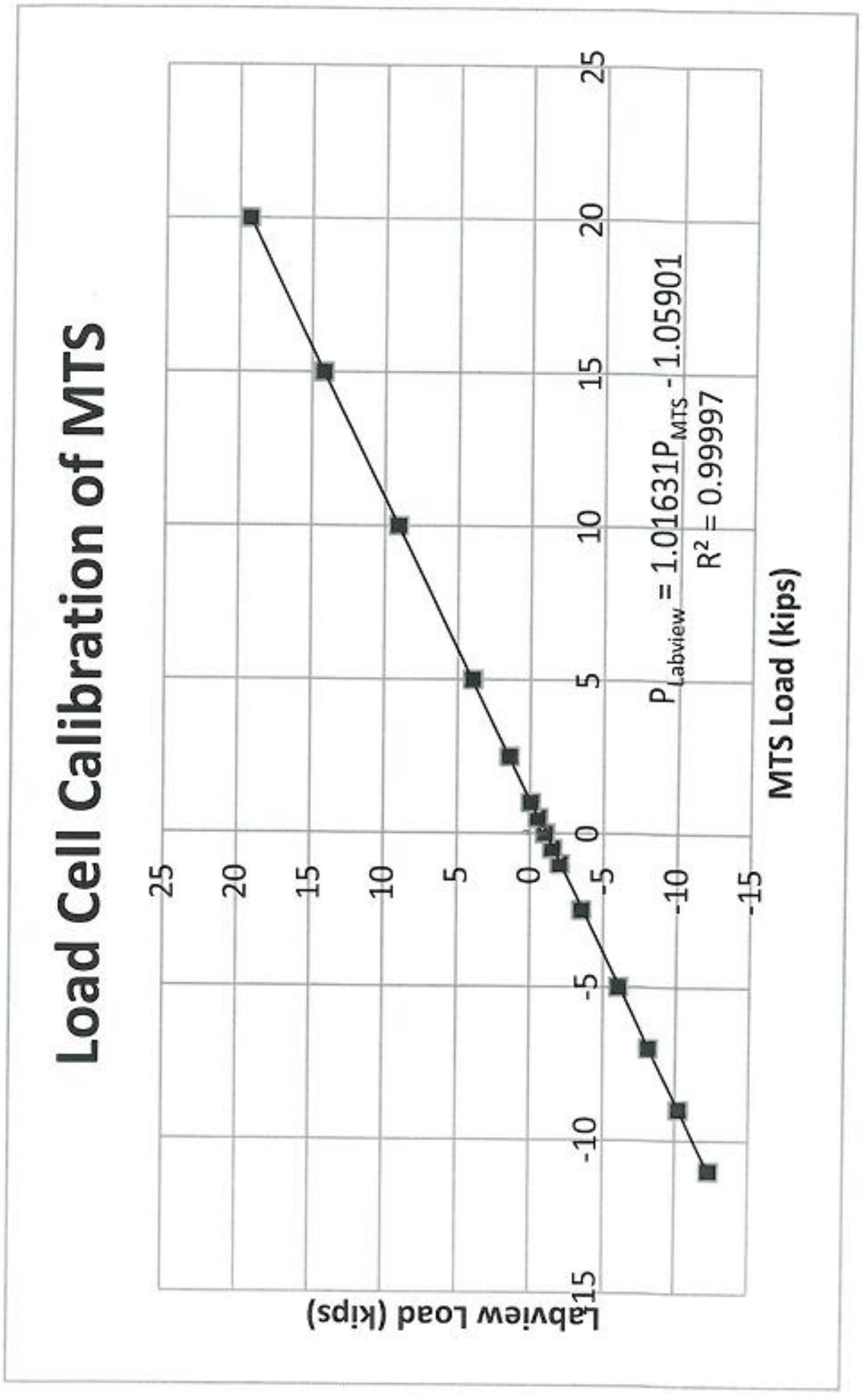

Figure D-2 Load Calibration Curve of MTS

www.manaraa.com

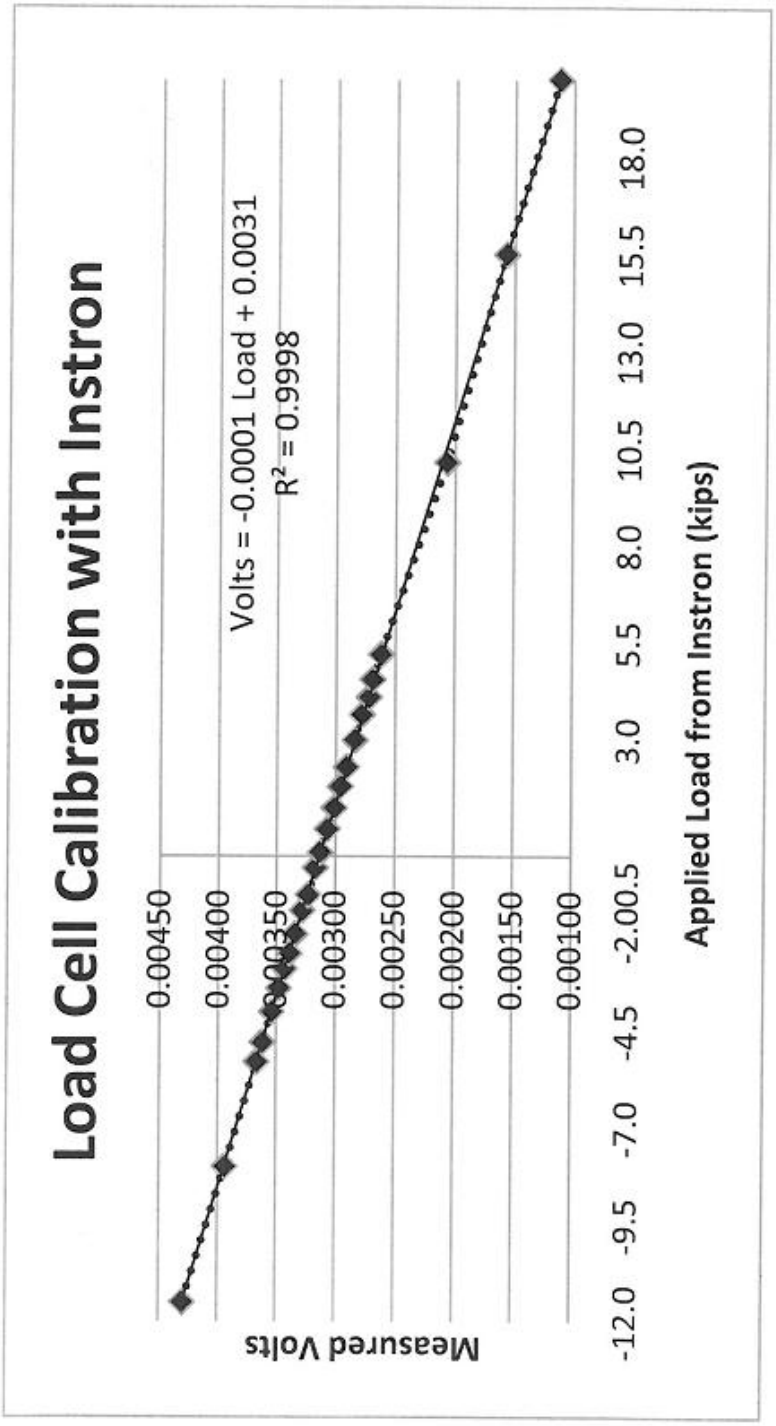

Figure D-3 Load Calibration of 50-kip Load Cell used on MTS

www.manaraa.com

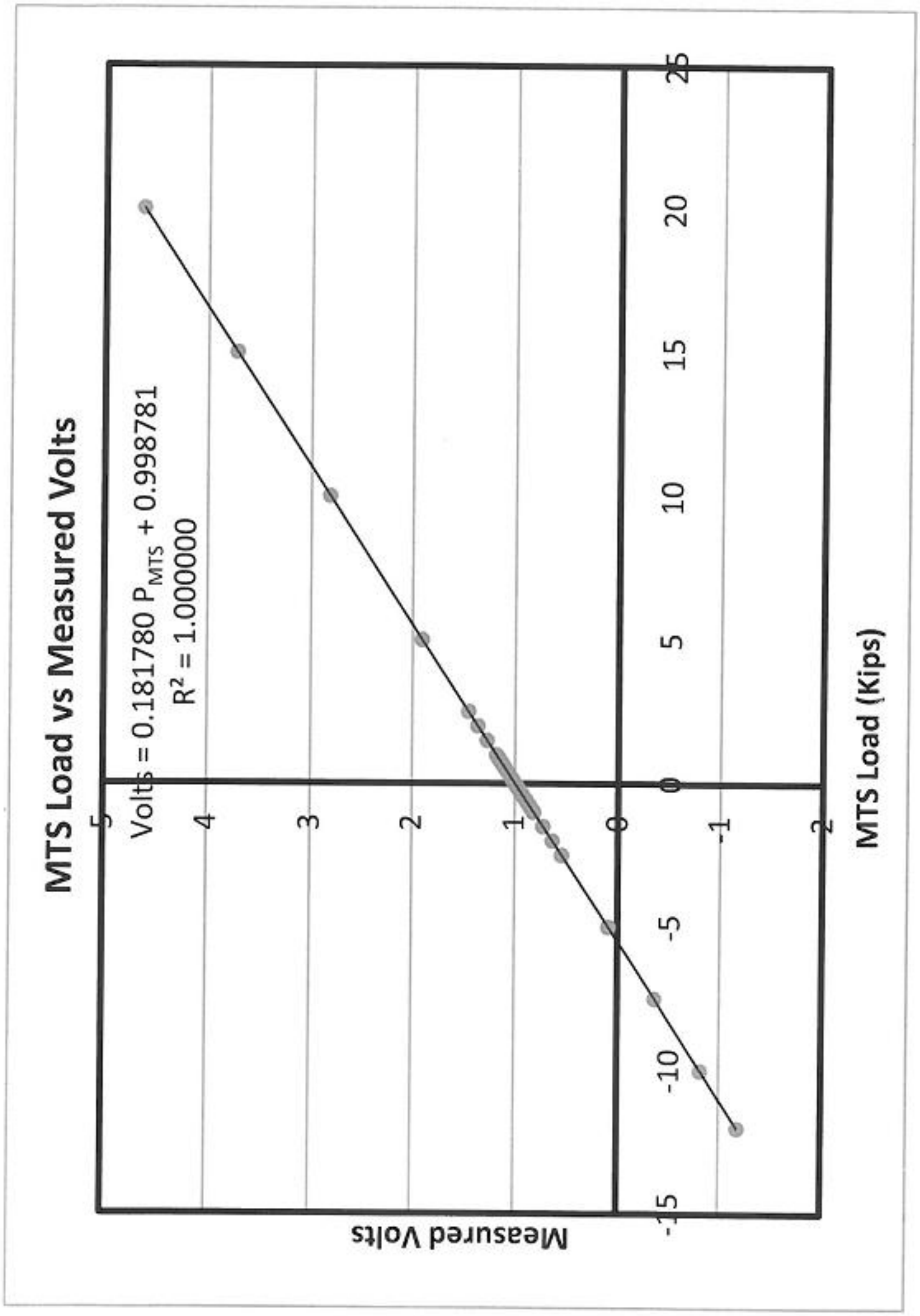

Figure D-4 Load from MTS with Volts Output

www.manaraa.com

Appendix D-3 10-kip Load Cell

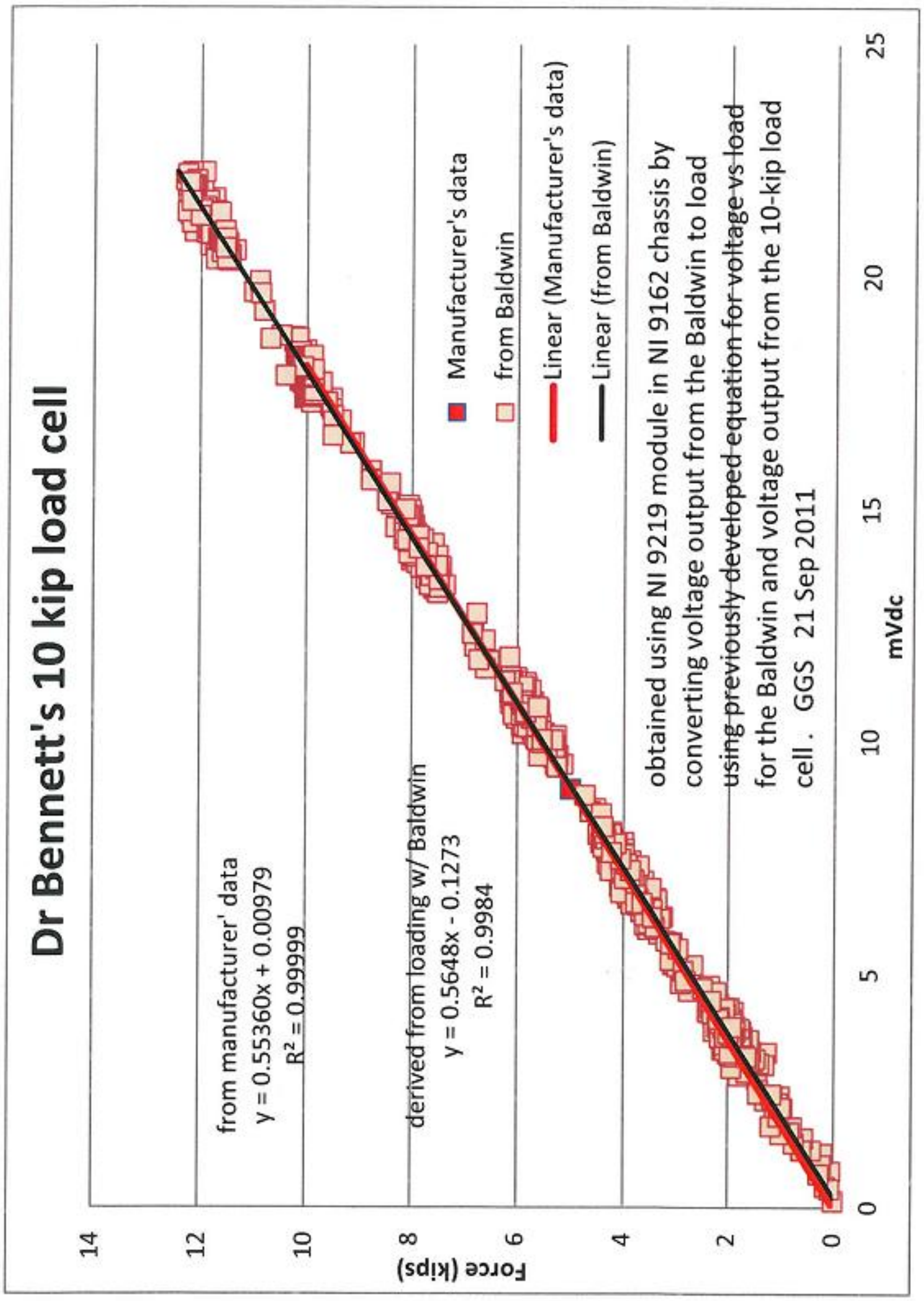

Figure D-5 Calibration of Small 10-kip Load Cell

www.manaraa.com

APPENDIX E PICK WIRING DIAGRAM

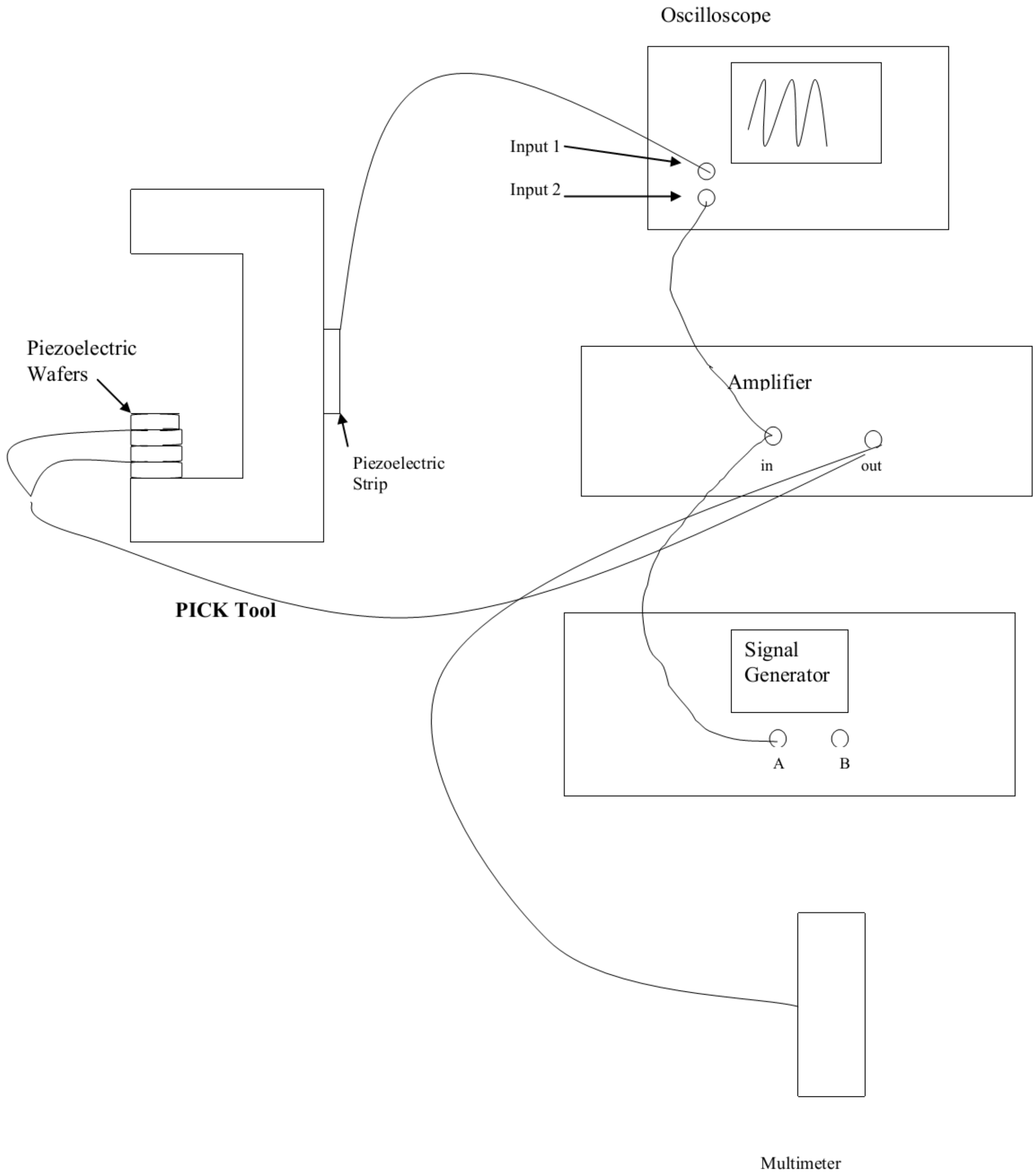

www.manaraa.com

APPENDIX F X-RAY DIFFRACTION DATA

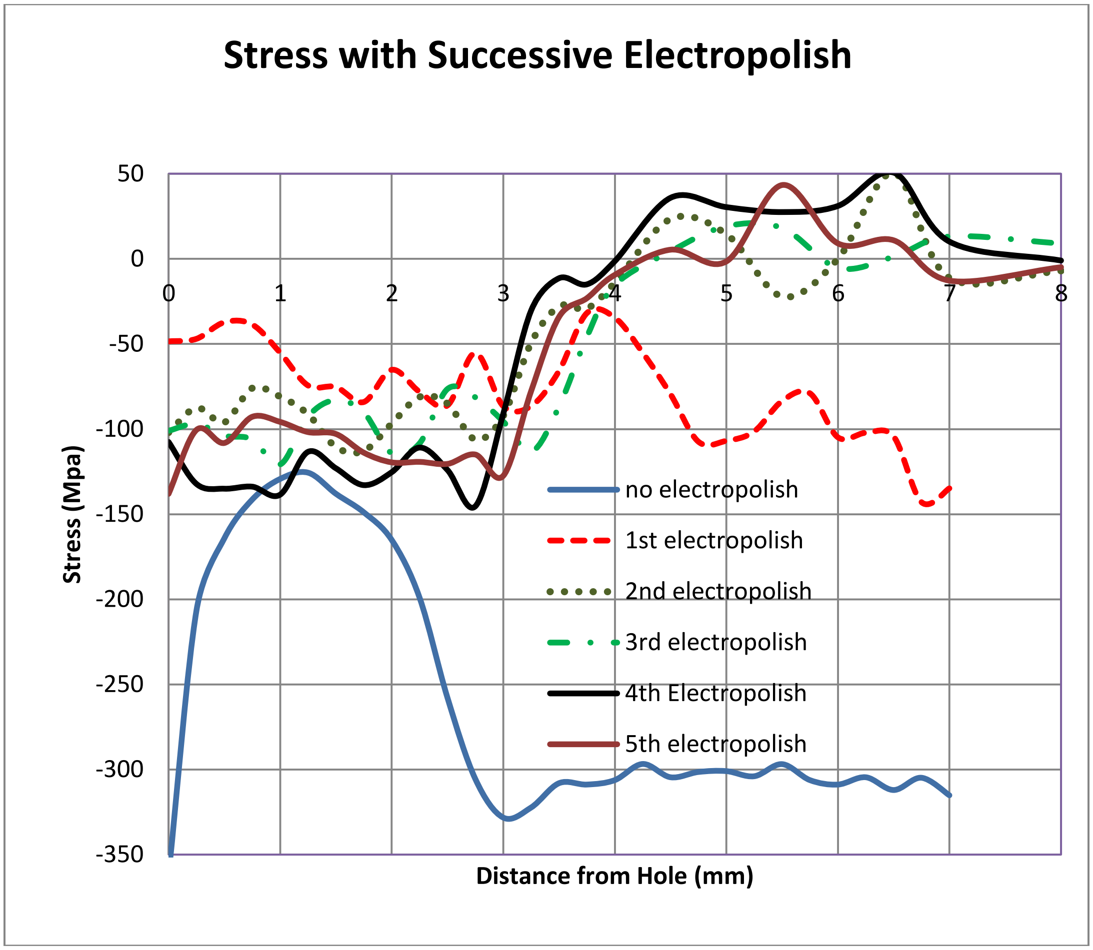

Fig F-1. Stress from X-Ray Diffraction over the Same Row with Successive Electropolishing

www.manaraa.com

Hoop Stress Averages (MPa)								
y-pos from edge of hole (mm)	19may row 2	20 may row 2	21 may row 1	y-pos from edge of hole (mm)	Averages of three rows	y-pos from edge of hole (mm)	22 may row 1(a)	Stress Average of Four rows (MPa)
0	-107.6	-121.6	-182.3	0	-137.17	0	-299.9	-218.53
0.2	-132.3	-100.5	-213.5	0.2	-148.77	0.25	-243.5	-196.13
0.5	-135.1	-108.2	-204.9	0.5	-149.40	0.5	-195.6	-172.50
0.75	-133.9	-92.8	-177.4	0.75	-134.70	0.75	-187	-160.85
1	-138.6	-98.8	-165.1	1	-134.17	1	-151.5	-142.83
1.25	-113.4	-101.8	-171.5	1.25	-128.90	1.25	-154.1	-141.50
1.5	-123.1	-102.9	-170.5	1.5	-132.17	1.5	-155	-143.58
1.75	-133	-113.9	-158.5	1.75	-135.13	1.75	-160.1	-147.62
2	-125.4	-119.6	-155.9	2	-133.63	2	-188.2	-160.92
2.25	-110.9	-119.3	-184.3	2.25	-138.17	2.25	-198.4	-168.28
2.5	-124.1	-120.5	-193.9	2.5	-146.17	2.5	-202.8	-174.48
2.75	-145.4	-115	-173.5	2.75	-144.63	2.75	-188.8	-166.72
3	-91	-127.5	-165.9	3	-128.13	3	-191.6	-159.87
3.25	-30.3	-77.7	-124.3	3.25	-77.43	3.25	-178.3	-127.87
3.5	-11.3	-34.1	-96	3.5	-47.13	3.5	-148.3	-97.72
3.75	-14.9	-23.1	-117.9	3.75	-51.97	3.75	-111.8	-81.88
4	-1.3	-9.4	-120.2	4	-43.63	4	-85.4	-64.52
4.5	36	5.4	-40			4.25	-82.8	-82.80
5	30.5	-1.5	-1.4	4.5	0.47	4.5	-84.1	-41.82
5.5	27.6	43.4	23.5			4.75	-65.3	-65.30
6	31.2	9.1	29.9	5	9.20	5	-40.6	-15.70
6.5	50.8	10.9	30.4			5.25	-41.1	-41.10
7	10.2	-12.8	2.2	5.5	31.50	5.5	-67.6	-18.05
8	-0.9	-4.9	23.6			5.75	-61.2	-61.20
				6	23.40	6	-53.9	-15.25
						6.25	-27.7	-27.70
				6.5	30.70	6.5	-17.8	6.45
						6.75	-27	-27.00
				7	-0.13	7	-34	-17.07
				8	5.93	8		5.93

www.manaraa.com

Hoop Stress Averages (ksi)		Radial Stress Averages (ksi)	
y-pos from center of hole (in)	Stress Averages of Four Rows (ksi)	y-pos from center of hole (in)	Stress Averages of Four Rows (ksi)
0.0691	-43.50	0.0691	-29.04
0.0789	-35.32	0.0789	-26.89
0.0887	-28.37	0.0887	-24.64
0.0986	-27.12	0.0986	-25.40
0.1084	-21.97	0.1084	-22.94
0.1183	-22.35	0.1183	-24.89
0.1281	-22.48	0.1281	-24.44
0.1379	-23.22	0.1379	-24.48
0.1478	-27.30	0.1478	-27.07
0.1576	-28.77	0.1576	-27.67
0.1675	-29.41	0.1675	-26.46
0.1773	-27.38	0.1773	-25.56
0.1872	-27.79	0.1872	-26.36
0.1970	-25.86	0.1970	-25.89
0.2068	-21.51	0.2068	-25.20
0.2167	-16.21	0.2167	-23.06
0.2265	-12.39	0.2265	-20.12
0.2364	-12.01	0.2364	-18.98
0.2462	-12.20	0.2462	-18.44
0.2561	-9.47	0.2561	-15.46
0.2659	-5.89	0.2659	-13.73
0.2757	-5.96	0.2757	-13.96
0.2856	-9.80	0.2856	-15.14
0.2954	-8.88	0.2954	-14.60
0.3053	-7.82	0.3053	-13.72
0.3151	-4.02	0.3151	-9.47
0.3250	-2.58	0.3250	-8.52
0.3348	-3.92	0.3348	-10.71
0.3446	-4.93	0.3446	-9.68
0.3840	0.00	0.3545	-4.98

المنارة للاستشارات
www.manaraa.com

APPENDIX G. NEUTRON DIFFRACTION DATA

inc slit	offset	diff slit	snout	offset
1 wide 0.5 high	35mm	1	50 mm	35 mm
A36 (211)				
Hole center	129.29	-11.33	245.60	by SCAN
ref cube center	152.66	-11.36	218.05	by SCAN
total time (hr)	20.5			
Measuring Hoop Strains	Line is vertical, along GS's X-axis			
Gary's Sample#	3P			
Row 1 hoops				
Face 1 (labels)	diffracted slit side, more negative Y(SPS)			

المنارة للاستشارات
www.manaraa.com

Time	MONO	2THETA	OMEGA	range omega	steps omega	X	Y	Z	MEMO	increments in Z	increments in Y	Sample thru thickness from mid plane
14	Si331AF	95.10	-42.45	5.00	11	152.66	-11.36	218.05	0	ref cube	ref cube	
14	Si331AF	95.10	-42.45	5.00	11	129.29	-11.83	244.60	1	1.00	-0.5	-0.5
14	Si331AF	95.10	-42.45	5.00	11	129.29	-11.83	244.35	2	1.25	0	-0.5
14	Si331AF	95.10	-42.45	5.00	11	129.29	-11.83	244.10	3	1.50	0.5	-0.5
14	Si331AF	95.10	-42.45	5.00	11	129.29	-11.83	243.85	4	1.75		-0.5
14	Si331AF	95.10	-42.45	5.00	11	129.29	-11.83	243.60	5	2.00		-0.5
14	Si331AF	95.10	-42.45	5.00	11	129.29	-11.83	243.35	6	2.25		-0.5
14	Si331AF	95.10	-42.45	5.00	11	129.29	-11.83	243.10	7	2.50		-0.5
14	Si331AF	95.10	-42.45	5.00	11	129.29	-11.83	242.85	8	2.75		-0.5
14	Si331AF	95.10	-42.45	5.00	11	129.29	-11.83	242.60	9	3.00		-0.5
14	Si331AF	95.10	-42.45	5.00	11	129.29	-11.83	242.35	10	3.25		-0.5
14	Si331AF	95.10	-42.45	5.00	11	129.29	-11.83	242.10	11	3.50		-0.5
14	Si331AF	95.10	-42.45	5.00	11	129.29	-11.83	241.85	12	3.75		-0.5
14	Si331AF	95.10	-42.45	5.00	11	129.29	-11.83	241.60	13	4.00		-0.5
14	Si331AF	95.10	-42.45	5.00	11	129.29	-11.83	241.35	14	4.25		-0.5
14	Si331AF	95.10	-42.45	5.00	11	129.29	-11.83	241.10	15	4.50		-0.5
14	Si331AF	95.10	-42.45	5.00	11	129.29	-11.83	240.85	16	4.75		-0.5
14	Si331AF	95.10	-42.45	5.00	11	129.29	-11.83	240.60	17	5.00		-0.5
14	Si331AF	95.10	-42.45	5.00	11	129.29	-11.83	240.10	18	5.50		-0.5
14	Si331AF	95.10	-42.45	5.00	11	129.29	-11.83	239.60	19	6.00		-0.5
14	Si331AF	95.10	-42.45	5.00	11	129.29	-11.83	239.10	20	6.50		-0.5
14	Si331AF	95.10	-42.45	5.00	11	129.29	-11.83	238.60	21	7.00		-0.5
14	Si331AF	95.10	-42.45	5.00	11	129.29	-11.83	238.10	22	7.50		-0.5
14	Si331AF	95.10	-42.45	5.00	11	129.29	-11.83	237.10	23	8.50		-0.5
14	Si331AF	95.10	-42.45	5.00	11	129.29	-11.83	236.10	24	9.50		-0.5
14	Si331AF	95.10	-42.45	5.00	11	129.29	-11.83	235.10	25	10.50		-0.5
14	Si331AF	95.10	-42.45	5.00	11	129.29	-11.83	234.10	26	11.50		-0.5
14	Si331AF	95.10	-42.45	5.00	11	129.29	-11.83	233.10	27	12.50		-0.5
14	Si331AF	95.10	-42.45	5.00	11	129.29	-11.83	231.60	28	14.00		-0.5
14	Si331AF	95.10	-42.45	5.00	11	152.66	-11.36	218.05	29	ref cube		
14	Si331AF	95.10	-42.45	5.00	11	129.29	-11.33	244.60	30	1.00		0.0
14	Si331AF	95.10	-42.45	5.00	11	129.29	-11.33	244.35	31	1.25		0.0
14	Si331AF	95.10	-42.45	5.00	11	129.29	-11.33	244.10	32	1.50		0.0
14	Si331AF	95.10	-42.45	5.00	11	129.29	-11.33	243.85	33	1.75		0.0
14	Si331AF	95.10	-42.45	5.00	11	129.29	-11.33	243.60	34	2.00		0.0
14	Si331AF	95.10	-42.45	5.00	11	129.29	-11.33	243.35	35	2.25		0.0
14	Si331AF	95.10	-42.45	5.00	11	129.29	-11.33	243.10	36	2.50		0.0
14	Si331AF	95.10	-42.45	5.00	11	129.29	-11.33	242.85	37	2.75		0.0
14	Si331AF	95.10	-42.45	5.00	11	129.29	-11.33	242.60	38	3.00		0.0
14	Si331AF	95.10	-42.45	5.00	11	129.29	-11.33	242.35	39	3.25		0.0
14	Si331AF	95.10	-42.45	5.00	11	129.29	-11.33	242.10	40	3.50		0.0
14	Si331AF	95.10	-42.45	5.00	11	129.29	-11.33	241.85	41	3.75		0.0
14	Si331AF	95.10	-42.45	5.00	11	129.29	-11.33	241.60	42	4.00		0.0
14	Si331AF	95.10	-42.45	5.00	11	129.29	-11.33	241.35	43	4.25		0.0
14	Si331AF	95.10	-42.45	5.00	11	129.29	-11.33	241.10	44	4.50		0.0
14	Si331AF	95.10	-42.45	5.00	11	129.29	-11.33	240.85	45	4.75		0.0
14	Si331AF	95.10	-42.45	5.00	11	129.29	-11.33	240.60	46	5.00		0.0
14	Si331AF	95.10	-42.45	5.00	11	129.29	-11.33	240.10	47	5.50		0.0
14	Si331AF	95.10	-42.45	5.00	11	129.29	-11.33	239.60	48	6.00		0.0
14	Si331AF	95.10	-42.45	5.00	11	129.29	-11.33	239.10	49	6.50		0.0
14	Si331AF	95.10	-42.45	5.00	11	129.29	-11.33	238.60	50	7.00		0.0
14	Si331AF	95.10	-42.45	5.00	11	129.29	-11.33	238.10	51	7.50		0.0
14	Si331AF	95.10	-42.45	5.00	11	129.29	-11.33	237.10	52	8.50		0.0
14	Si331AF	95.10	-42.45	5.00	11	129.29	-11.33	236.10	53	9.50		0.0
14	Si331AF	95.10	-42.45	5.00	11	129.29	-11.33	235.10	54	10.50		0.0
14	Si331AF	95.10	-42.45	5.00	11	129.29	-11.33	234.10	55	11.50		0.0
14	Si331AF	95.10	-42.45	5.00	11	129.29	-11.33	233.10	56	12.50		0.0
14	Si331AF	95.10	-42.45	5.00	11	129.29	-11.33	231.60	57	14.00		0.0
14	Si331AF	95.10	-42.45	5.00	11	152.66	-11.36	218.05	58	ref cube		
14	Si331AF	95.10	-42.45	5.00	11	129.29	-10.83	244.60	59	1.00		0.5
14	Si331AF	95.10	-42.45	5.00	11	129.29	-10.83	244.35	60	1.25		0.5
14	Si331AF	95.10	-42.45	5.00	11	129.29	-10.83	244.10	61	1.50		0.5
14	Si331AF	95.10	-42.45	5.00	11	129.29	-10.83	243.85	62	1.75		0.5
14	Si331AF	95.10	-42.45	5.00	11	129.29	-10.83	243.60	63	2.00		0.5
14	Si331AF	95.10	-42.45	5.00	11	129.29	-10.83	243.35	64	2.25		0.5
14	Si331AF	95.10	-42.45	5.00	11	129.29	-10.83	243.10	65	2.50		0.5
14	Si331AF	95.10	-42.45	5.00	11	129.29	-10.83	242.85	66	2.75		0.5
14	Si331AF	95.10	-42.45	5.00	11	129.29	-10.83	242.60	67	3.00		0.5
14	Si331AF	95.10	-42.45	5.00	11	129.29	-10.83	242.35	68	3.25		0.5
14	Si331AF	95.10	-42.45	5.00	11	129.29	-10.83	242.10	69	3.50		0.5

www.manaraa.com

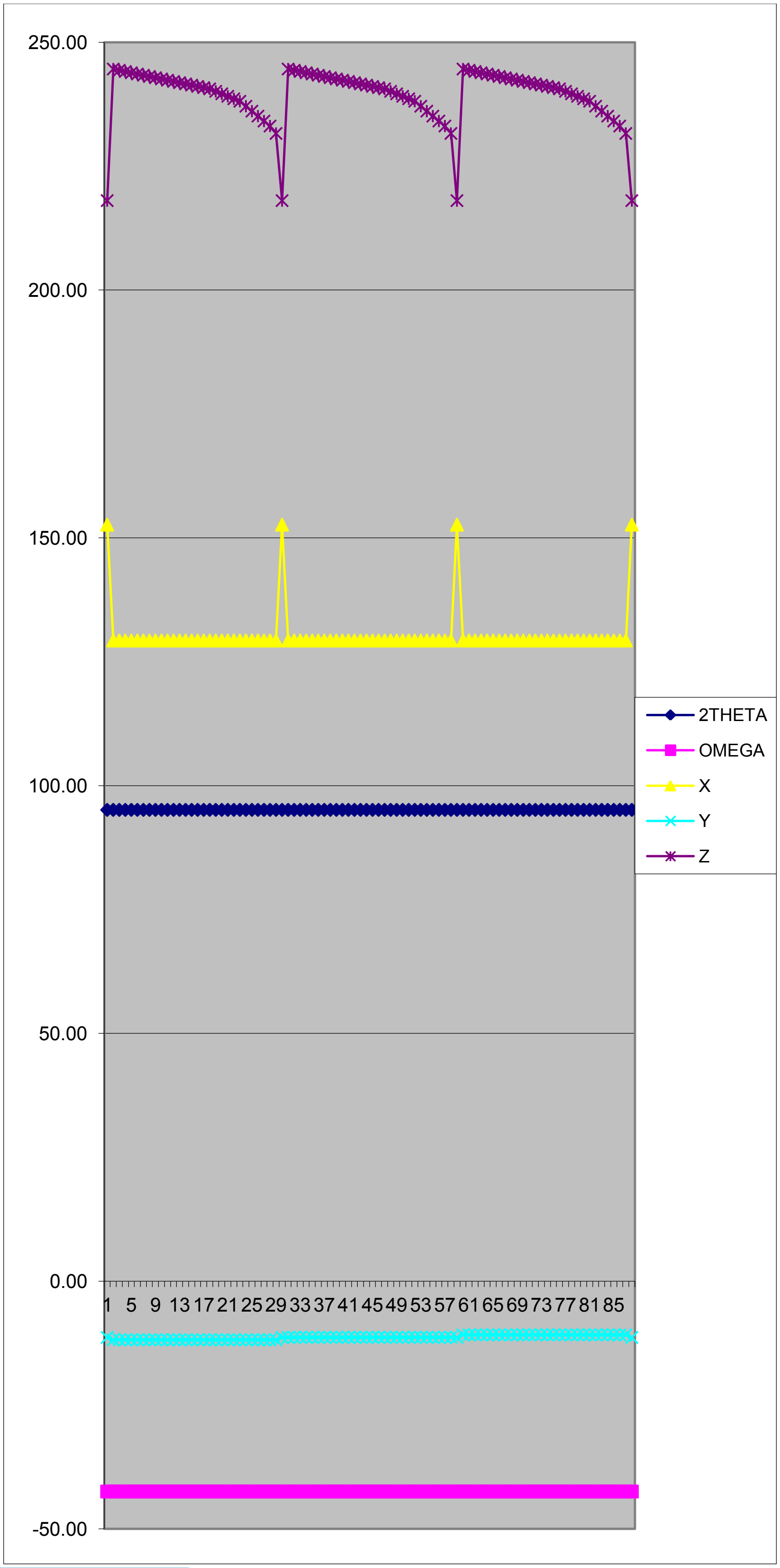

المنارة للاستشارات
www.manaraa.com

inc slit	offset	diff slit	snout	offset
1 wide 0.5 high	35mm	1	50 mm	35 mm
A36 (211)				
Hole center	90.53	-9.595	201.69	by SCAN
ref cube center	117.73	-10.21	225.23	by SCAN
total time (hr)	36.7			
Measuring Hoop Strains	Line is vertical, along GS's X-axis			
Gary's Sample#	3P			

steps omega	X	Y	Z	MEMO	increments in X	Distance from plate mid plane	increments in Y
11	117.73	-10.21	225.23	0	ref cube		ref cube
11	90.53	-9.095	202.690	1	1.00	-0.50	-0.5
11	90.53	-9.095	202.940	2	1.25	-0.50	0
11	90.53	-9.095	203.190	3	1.50	-0.50	0.5
11	90.53	-9.095	203.440	4	1.75	-0.50	
11	90.53	-9.095	203.690	5	2.00	-0.50	
11	90.53	-9.095	203.940	6	2.25	-0.50	
11	90.53	-9.095	204.190	7	2.50	-0.50	
11	90.53	-9.095	204.440	8	2.75	-0.50	
11	90.53	-9.095	204.690	9	3.00	-0.50	
11	90.53	-9.095	204.940	10	3.25	-0.50	
11	90.53	-9.095	205.190	11	3.50	-0.50	
11	90.53	-9.095	205.440	12	3.75	-0.50	
11	90.53	-9.095	205.690	13	4.00	-0.50	
11	90.53	-9.095	205.940	14	4.25	-0.50	
11	90.53	-9.095	206.190	15	4.50	-0.50	
11	90.53	-9.095	206.440	16	4.75	-0.50	
11	90.53	-9.095	206.690	17	5.00	-0.50	
11	90.53	-9.095	207.190	18	5.50	-0.50	
11	90.53	-9.095	207.690	19	6.00	-0.50	
11	90.53	-9.095	208.190	20	6.50	-0.50	
11	90.53	-9.095	208.690	21	7.00	-0.50	
11	90.53	-9.095	209.190	22	7.50	-0.50	
11	90.53	-9.095	210.190	23	8.50	-0.50	
11	90.53	-9.095	211.190	24	9.50	-0.50	
11	90.53	-9.095	212.190	25	10.50	-0.50	

المنارة للاستشارات
www.manaraa.com

11	90.53	-9.095	213.190	26	11.50	-0.50
11	90.53	-9.095	214.190	27	12.50	-0.50
11	90.53	-9.095	215.690	28	14.00	-0.50
11	117.73	-10.21	225.23	29	ref cube	
11	90.53	-9.595	202.690	30	1.00	0.00
11	90.53	-9.595	202.940	31	1.25	0.00
11	90.53	-9.595	203.190	32	1.50	0.00
11	90.53	-9.595	203.440	33	1.75	0.00
11	90.53	-9.595	203.690	34	2.00	0.00
11	90.53	-9.595	203.940	35	2.25	0.00
11	90.53	-9.595	204.190	36	2.50	0.00
11	90.53	-9.595	204.440	37	2.75	0.00
11	90.53	-9.595	204.690	38	3.00	0.00
11	90.53	-9.595	204.940	39	3.25	0.00
11	90.53	-9.595	205.190	40	3.50	0.00
11	90.53	-9.595	205.440	41	3.75	0.00
11	90.53	-9.595	205.690	42	4.00	0.00
11	90.53	-9.595	205.940	43	4.25	0.00
11	90.53	-9.595	206.190	44	4.50	0.00
11	90.53	-9.595	206.440	45	4.75	0.00
11	90.53	-9.595	206.690	46	5.00	0.00
11	90.53	-9.595	207.190	47	5.50	0.00
11	90.53	-9.595	207.690	48	6.00	0.00
11	90.53	-9.595	208.190	49	6.50	0.00
11	90.53	-9.595	208.690	50	7.00	0.00
11	90.53	-9.595	209.190	51	7.50	0.00
11	90.53	-9.595	210.190	52	8.50	0.00
11	90.53	-9.595	211.190	53	9.50	0.00
11	90.53	-9.595	212.190	54	10.50	0.00
11	90.53	-9.595	213.190	55	11.50	0.00
11	90.53	-9.595	214.190	56	12.50	0.00
11	90.53	-9.595	215.690	57	14.00	0.00
11	117.73	-10.21	225.23	58	ref cube	
11	90.53	-10.095	202.690	59	1.00	0.50
11	90.53	-10.095	202.940	60	1.25	0.50
11	90.53	-10.095	203.190	61	1.50	0.50
11	90.53	-10.095	203.440	62	1.75	0.50
11	90.53	-10.095	203.690	63	2.00	0.50
11	90.53	-10.095	203.940	64	2.25	0.50
11	90.53	-10.095	204.190	65	2.50	0.50
11	90.53	-10.095	204.440	66	2.75	0.50
11	90.53	-10.095	204.690	67	3.00	0.50
11	90.53	-10.095	204.940	68	3.25	0.50
11	90.53	-10.095	205.190	69	3.50	0.50
11	90.53	-10.095	205.440	70	3.75	0.50
11	90.53	-10.095	205.690	71	4.00	0.50

المنارة للاستشارات
www.manaraa.com

11	90.53	-10.095	205.940	72	4.25	0.50
11	90.53	-10.095	206.190	73	4.50	0.50
11	90.53	-10.095	206.440	74	4.75	0.50
11	90.53	-10.095	206.690	75	5.00	0.50
11	90.53	-10.095	207.190	76	5.50	0.50
11	90.53	-10.095	207.690	77	6.00	0.50
11	90.53	-10.095	208.190	78	6.50	0.50
11	90.53	-10.095	208.690	79	7.00	0.50
11	90.53	-10.095	209.190	80	7.50	0.50
11	90.53	-10.095	210.190	81	8.50	0.50
11	90.53	-10.095	211.190	82	9.50	0.50
11	90.53	-10.095	212.190	83	10.50	0.50
11	90.53	-10.095	213.190	84	11.50	0.50
11	90.53	-10.095	214.190	85	12.50	0.50
11	90.53	-10.095	215.690	86	14.00	0.50
11	117.73	-10.21	225.23	87	ref cube	

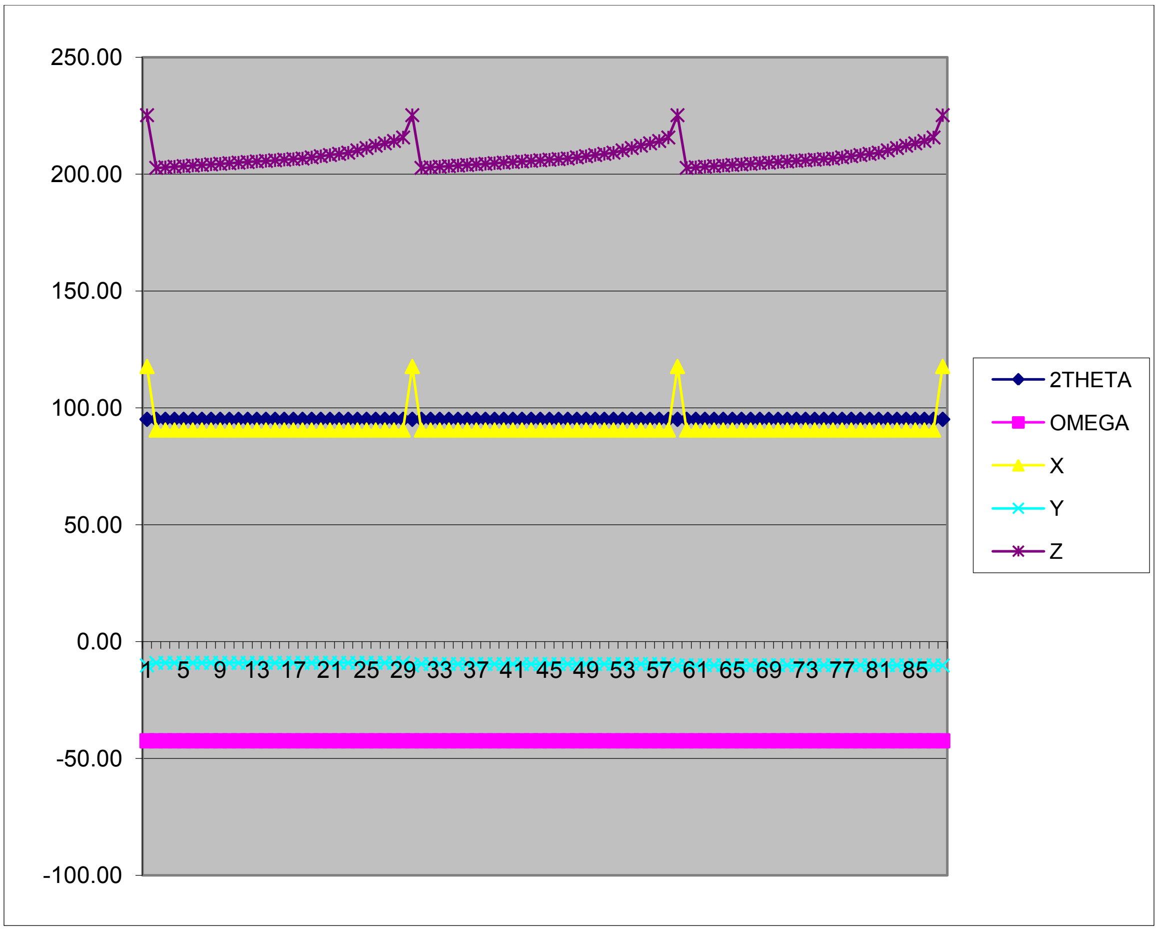

www.manaraa.com

inc slit	offset	diff slit	snout	offset
0.5 wide 1 high	35mm	0.5	50 mm	35 mm
A36 (211)				
Hole center	159.80	-10.75	237.12	by SCAN
ref cube center	182.93	-11.36	209.48	by SCAN

total time (min) 36.7

Measuring Radial Strains   Line is horizontal, along GS's X-axis

Gary's Sample# 3P

Y	Z	MEMO	distance from hole edge, increments in X	distance from plate center, move in Y	increments in Y
-11.36	209.48	0	ref cube		ref cube
-11.25	237.12	1	1.00	-0.50	-0.5
-11.25	237.12	2	1.25	-0.50	0
-11.25	237.12	3	1.50	-0.50	0.5
-11.25	237.12	4	1.75	-0.50	
-11.25	237.12	5	2.00	-0.50	
-11.25	237.12	6	2.25	-0.50	
-11.25	237.12	7	2.50	-0.50	
-11.25	237.12	8	2.75	-0.50	
-11.25	237.12	9	3.00	-0.50	
-11.25	237.12	10	3.25	-0.50	
-11.25	237.12	11	3.50	-0.50	
-11.25	237.12	12	3.75	-0.50	
-11.25	237.12	13	4.00	-0.50	
-11.25	237.12	14	4.25	-0.50	
-11.25	237.12	15	4.50	-0.50	
-11.25	237.12	16	4.75	-0.50	
-11.25	237.12	17	5.00	-0.50	
-11.25	237.12	18	5.50	-0.50	
-11.25	237.12	19	6.00	-0.50	

www.manaraa.com

-11.25	**237.12**	**20**	**6.50**	**-0.50**
-11.25	**237.12**	**21**	**7.00**	**-0.50**
-11.25	**237.12**	**22**	**7.50**	**-0.50**
-11.25	**237.12**	**23**	**8.50**	**-0.50**
-11.25	**237.12**	**24**	**9.50**	**-0.50**
-11.25	**237.12**	**25**	**10.50**	**-0.50**
-11.25	**237.12**	**26**	**11.50**	**-0.50**
-11.25	**237.12**	**27**	**12.50**	**-0.50**
-11.25	**237.12**	**28**	**14.00**	**-0.50**
-11.36	**209.48**	**29**	**ref cube**	
-10.75	**237.12**	**30**	**1.00**	**0.00**
-10.75	**237.12**	**31**	**1.25**	**0.00**
-10.75	**237.12**	**32**	**1.50**	**0.00**
-10.75	**237.12**	**33**	**1.75**	**0.00**
-10.75	**237.12**	**34**	**2.00**	**0.00**
-10.75	**237.12**	**35**	**2.25**	**0.00**
-10.75	**237.12**	**36**	**2.50**	**0.00**
-10.75	**237.12**	**37**	**2.75**	**0.00**
-10.75	**237.12**	**38**	**3.00**	**0.00**
-10.75	**237.12**	**39**	**3.25**	**0.00**
-10.75	**237.12**	**40**	**3.50**	**0.00**
-10.75	**237.12**	**41**	**3.75**	**0.00**
-10.75	**237.12**	**42**	**4.00**	**0.00**
-10.75	**237.12**	**43**	**4.25**	**0.00**
-10.75	**237.12**	**44**	**4.50**	**0.00**
-10.75	**237.12**	**45**	**4.75**	**0.00**
-10.75	**237.12**	**46**	**5.00**	**0.00**
-10.75	**237.12**	**47**	**5.50**	**0.00**
-10.75	**237.12**	**48**	**6.00**	**0.00**
-10.75	**237.12**	**49**	**6.50**	**0.00**
-10.75	**237.12**	**50**	**7.00**	**0.00**
-10.75	**237.12**	**51**	**7.50**	**0.00**
-10.75	**237.12**	**52**	**8.50**	**0.00**
-10.75	**237.12**	**53**	**9.50**	**0.00**
-10.75	**237.12**	**54**	**10.50**	**0.00**
-10.75	**237.12**	**55**	**11.50**	**0.00**
-10.75	**237.12**	**56**	**12.50**	**0.00**
-10.75	**237.12**	**57**	**14.00**	**0.00**
-11.36	**209.48**	**58**	**ref cube**	
-10.25	**237.12**	**59**	**1.00**	**0.50**
-10.25	**237.12**	**60**	**1.25**	**0.50**
-10.25	**237.12**	**61**	**1.50**	**0.50**
-10.25	**237.12**	**62**	**1.75**	**0.50**
-10.25	**237.12**	**63**	**2.00**	**0.50**
-10.25	**237.12**	**64**	**2.25**	**0.50**
-10.25	**237.12**	**65**	**2.50**	**0.50**

المنارة للاستشارات
www.manaraa.com

-10.25	**237.12**	**66**	**2.75**	**0.50**
-10.25	**237.12**	**67**	**3.00**	**0.50**
-10.25	**237.12**	**68**	**3.25**	**0.50**
-10.25	**237.12**	**69**	**3.50**	**0.50**
-10.25	**237.12**	**70**	**3.75**	**0.50**
-10.25	**237.12**	**71**	**4.00**	**0.50**
-10.25	**237.12**	**72**	**4.25**	**0.50**
-10.25	**237.12**	**73**	**4.50**	**0.50**
-10.25	**237.12**	**74**	**4.75**	**0.50**
-10.25	**237.12**	**75**	**5.00**	**0.50**
-10.25	**237.12**	**76**	**5.50**	**0.50**
-10.25	**237.12**	**77**	**6.00**	**0.50**
-10.25	**237.12**	**78**	**6.50**	**0.50**
-10.25	**237.12**	**79**	**7.00**	**0.50**
-10.25	**237.12**	**80**	**7.50**	**0.50**
-10.25	**237.12**	**81**	**8.50**	**0.50**
-10.25	**237.12**	**82**	**9.50**	**0.50**
-10.25	**237.12**	**83**	**10.50**	**0.50**
-10.25	**237.12**	**84**	**11.50**	**0.50**
-10.25	**237.12**	**85**	**12.50**	**0.50**
-10.25	**237.12**	**86**	**14.00**	**0.50**
-11.36	**209.48**	**87**	**ref cube**	

المنارة للاستشارات
www.manaraa.com

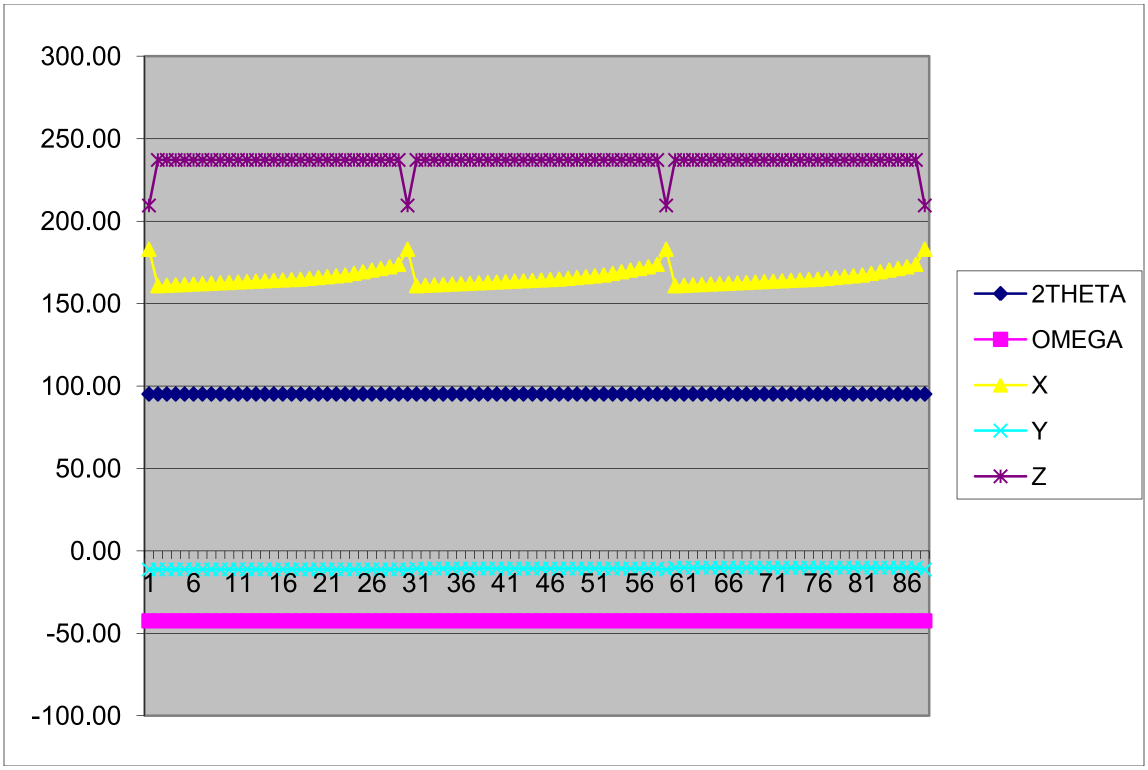

inc slit	offset	diff slit	snout	offset
1 wide 0.5 high	35mm	1	50 mm	35 mm
A36 (211)				
Hole center	90.53	-9.595	201.69	by SCAN
ref cube center	117.73	-10.21	225.23	by SCAN
total time (hr)	36.7			
Measuring Hoop Strains	Line is vertical, along GS's X-axis			
Gary's Sample#	3P			

Y	Z	MEMO	increments in X	increments in Y
-10.21	225.23	0	ref cube	ref cube
-9.095	202.690	1	1.00	-0.5
-9.095	202.940	2	1.25	0
-9.095	203.190	3	1.50	0.5

المنارة للاستشارات
www.manaraa.com

-9.095	203.440	4	1.75
-9.095	203.690	5	2.00
-9.095	203.940	6	2.25
-9.095	204.190	7	2.50
-9.095	204.440	8	2.75
-9.095	204.690	9	3.00
-9.095	204.940	10	3.25
-9.095	205.190	11	3.50
-9.095	205.440	12	3.75
-9.095	205.690	13	4.00
-9.095	205.940	14	4.25
-9.095	206.190	15	4.50
-9.095	206.440	16	4.75
-9.095	206.690	17	5.00
-9.095	207.190	18	5.50
-9.095	207.690	19	6.00
-9.095	208.190	20	6.50
-9.095	208.690	21	7.00
-9.095	209.190	22	7.50
-9.095	210.190	23	8.50
-9.095	211.190	24	9.50
-9.095	212.190	25	10.50
-9.095	213.190	26	11.50
-9.095	214.190	27	12.50
-9.095	215.690	28	14.00
-10.21	225.23	29	ref cube
-9.595	202.690	30	1.00
-9.595	202.940	31	1.25
-9.595	203.190	32	1.50
-9.595	203.440	33	1.75
-9.595	203.690	34	2.00
-9.595	203.940	35	2.25
-9.595	204.190	36	2.50
-9.595	204.440	37	2.75
-9.595	204.690	38	3.00
-9.595	204.940	39	3.25
-9.595	205.190	40	3.50
-9.595	205.440	41	3.75
-9.595	205.690	42	4.00
-9.595	205.940	43	4.25
-9.595	206.190	44	4.50
-9.595	206.440	45	4.75
-9.595	206.690	46	5.00
-9.595	207.190	47	5.50
-9.595	207.690	48	6.00
-9.595	208.190	49	6.50

المنارة للاستشارات
www.manaraa.com

-9.595	208.690	50	7.00
-9.595	209.190	51	7.50
-9.595	210.190	52	8.50
-9.595	211.190	53	9.50
-9.595	212.190	54	10.50
-9.595	213.190	55	11.50
-9.595	214.190	56	12.50
-9.595	215.690	57	14.00
-10.21	225.23	58	ref cube
-10.095	202.690	59	1.00
-10.095	202.940	60	1.25
-10.095	203.190	61	1.50
-10.095	203.440	62	1.75
-10.095	203.690	63	2.00
-10.095	203.940	64	2.25
-10.095	204.190	65	2.50
-10.095	204.440	66	2.75
-10.095	204.690	67	3.00
-10.095	204.940	68	3.25
-10.095	205.190	69	3.50
-10.095	205.440	70	3.75
-10.095	205.690	71	4.00
-10.095	205.940	72	4.25
-10.095	206.190	73	4.50
-10.095	206.440	74	4.75
-10.095	206.690	75	5.00
-10.095	207.190	76	5.50
-10.095	207.690	77	6.00
-10.095	208.190	78	6.50
-10.095	208.690	79	7.00
-10.095	209.190	80	7.50
-10.095	210.190	81	8.50
-10.095	211.190	82	9.50
-10.095	212.190	83	10.50
-10.095	213.190	84	11.50
-10.095	214.190	85	12.50
-10.095	215.690	86	14.00
-10.21	225.23	87	ref cube

المنارة للاستشارات
www.manaraa.com

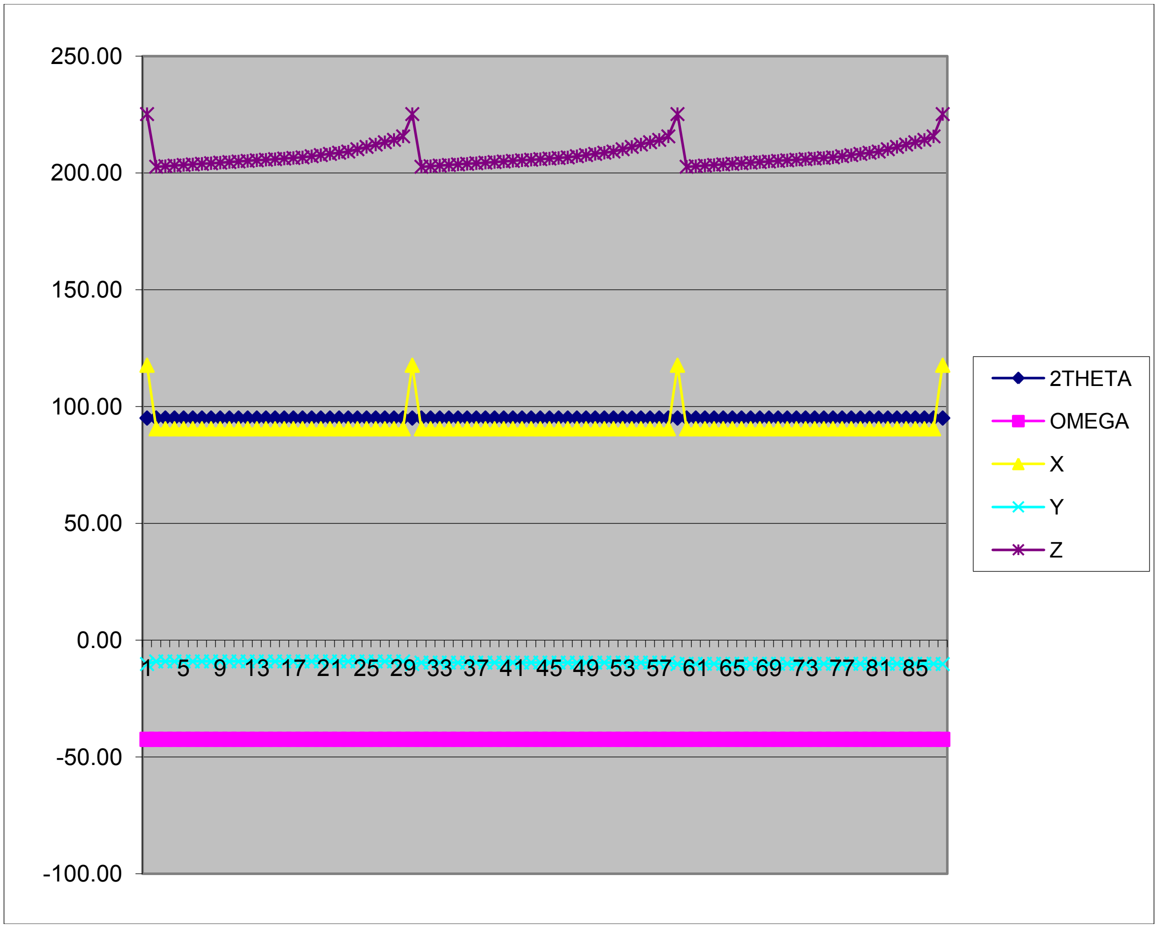

www.manaraa.com